

**A NOVEL IMAGE ANALYSIS APPROACH TO CHARACTERISE
THE EFFECTS OF DIETARY COMPONENTS ON INTESTINAL
MORPHOLOGY AND IMMUNE SYSTEM IN ATLANTIC SALMON**

**THESIS SUBMITTED TO THE UNIVERSITY OF STIRLING
FOR THE DEGREE OF DOCTOR OF PHILOSOPHY**

POLYANA FERREIRA DA SILVA

DECEMBER 2013

INSTITUTE OF AQUACULTURE



**UNIVERSITY OF
STIRLING**

*This thesis is dedicated to my parents, without whom
none of this would have been possible...*

DECLARATION

This thesis was compiled and written in full by the author, with thorough proofreading by the supervisors. Unless otherwise indicated in the text or references therein, this thesis is entirely the product of the author's research work and it has never been submitted, either in part or as a whole, for an academic degree at this or any other university or equivalent institution.

No authorisation is required for the reproduction of the material in this thesis for personal or educational use. Reproduction of this thesis, in part or as a whole, for publication purposes, is prohibited, without the written permission of the author.

Author: Polyana F. da Silva

Principal supervisor: Prof. James E. Bron

Professor of Aquatic Animal Health
Head of the Parasitology Research Group

Additional supervisors: Dr. Kim D. Thompson

Senior Research Fellow
Aquatic Vaccine Unit Group

Prof. Alexandra Adams

Research Professor in Aquatic Diseases & Immunology
Head of the Aquatic Vaccine Unit Group

ACKNOWLEDGMENTS

Although this thesis bears on its cover only the author's name, none of this work would even have been possible to accomplish without the hefty support of quite a large number of people. I am actually indebted to so many, that I fear I may have unintentionally omitted someone's name. If that was the case, please accept my sincere apologies. I do hope that, anyone who contributed in any way and helped me get so far, will share with me this particular moment of fulfilment that I am now enjoying!

First, I wish to mention my supervisors: Prof. James Bron, Dr. Kim Thompson and Prof. Alexandra Adams from whose advice and guidance I benefited. I am especially grateful for their continuous support, and for the insightful discussions and comments we had during the entire process.

Acknowledgements are also due to the role played by Dr. Charles McGurk and Mrs. Julia Mullins, co-promoters of this project. Their expertise and understanding added considerably to my research experience. Moreover, I would like to express my appreciation to Skretting's Aquaculture Research Centre (Skretting ARC, Stavanger, Norway), who financially supported this project. I would also like to acknowledge the staff at both Skretting's fish trial station and ARC for their technical assistance during the collection of the samples.

Special thanks are also extended to the Institute of Aquaculture elements, both academics and technicians, for their advice and guidance throughout the entire period. To Mr. Niall Auchinachie, Mrs. Deborah Faichney, Dr. John Taggart and Mr. Linton Brown, I owe a special word of thanks for their invaluable assistance and support in solving near infinite issues. Thanks also to those who provided me with statistical advice at times when it was most needed, namely Dr. Darren Green and Prof. George Gettinby.

I would like to express my sincere appreciation for the service and support provided by the Veterinary Diagnostics Services from the University of Glasgow, in particular to Mr. Iain MacMillan and Ms. Lynn Stevenson, for their personal commitment, advice and guidance from which I have benefited immensely. Moreover, I would like to thank the pathologists who took time to partake in this study, for the many valuable discussions on routine assessment of gastrointestinal samples as well as the useful validation process sessions

and constructive feedback. In special to Prof. Randolph Richards, Dr. David Knudsen, Dr. Marianne Pearson, Dr. Dave Cox and Dr. Jorge Del-Pozo.

The successful completion of this project has in no small measure been due to the outstanding efforts and commitment from a colleague and good friend, who has unflinchingly encouraged and helped me through all. Nilantha Jayasuriya, few lines are too short to show my appreciation for everything you and your family have done for me. I cannot thank you enough for that!

Life away from home can be very hard! Fortunately most of the hardships were overcome by a very effective, friendly and supportive atmosphere surrounding me. Special thanks are due to my "Stirling & Stavanger fellowship": Sofia Morais, Silvia Soares, Laura Martinez, Gilta Jackel, Thi Luu, Sean Monaghan, Christian Delannoy, Phuoc Nguyen Ngoc, Christoforos Metochis, Wanna Sirimanapong, Zinan Xu, Juliet Nattabi, Beatrix Berdal, Nafiha Usman and Seong-Chea Chua for the attention, encouragement and support provided during these last years. Particular thanks are also extended to my beloved "Africa / Mozambique": to my entire clan of friends living there who since the very beginning provided a warm encouragement to keep going. Natacha Melo, thanks once again for being such a good friend!

Finally and foremost, I am forever indebted to my family for the unconditional support they have provided throughout my entire life, and without whose love, motivation and encouragement I would not have reached so far! Especially, to my grandmother M^a Soledade and my parents Suzana & Carlos who were always there for me in spite of the distance! To them: *"Mwine, mi nga ni nhica a vutomi ni ti dondro a ku va ni pswi hanya hi ntsima ntsima, a pswi fanelanga ntsena a ku khensa. Mwine, mi nga vaningaa tindlela ta k uva ti mphmile, hi li randro ni hi ntsima ntsima a k uva ni nga tali hi ku tchava kamba na ni ni ku rindrela, a pswi fanelanga ntsena ku khensa. Ku mwine, va tatana hi xi hena ni li randro a pswi nga fanelanga ku lhaia pswako, a ni na marhito ya ku tlanguela kinkwapsho lepswi me nga yentchela mine. Ntsena hi pipswi yentchekaka, loku ni djuletela hi stsima ntsima a ma vonela ya ku komba a ku nyoxa ka ku kala ku nga heli. Kumwe ku nyoxa ka ku kala ku ngue te lhaiua hi ma ritu. Na mui randra ngopfu!"*

Kanimambo / Obrigada / Thanks to you all!

TABLE OF CONTENTS

DECLARATION.....	i
ACKNOWLEDGMENTS	ii
TABLE OF CONTENTS	iv
LIST OF FIGURES.....	ix
LIST OF TABLES	xiii
ABBREVIATIONS LIST.....	xiv
ABSTRACT	xx
LIST OF PUBLICATIONS AND PRESENTATIONS	xxiv
1. GENERAL INTRODUCTION	
1.1. Nutrition, feed and fish health	1
1.2. Diet and the gastrointestinal tract of fish.....	3
1.3. Gastrointestinal tract structure in salmonids.....	4
1.3.1. Intestinal macroscopic anatomy.....	6
1.3.2. Intestinal microscopic anatomy	8
1.3.3. Intestinal surface area	11
1.3.4. Anatomical homeostasis of the intestine.....	12
1.4. Multifunctional properties of salmonid intestine	12
1.4.1. Nutrient processing and absorption	13
1.4.2. Enteric barrier function	16
1.4.2.1. Extrinsic supra-epithelial barrier	16
1.4.2.2. Enteric epithelial barrier	17
1.4.2.3. Intrinsic sub-epithelial barrier.....	17
1.4.3. Osmoregulation and epithelial water transport.....	20
1.5. Diet mediated modulation and enteric integrity	21
1.5.1. Evaluation of the effects of nutritional modulation on fish intestinal health.....	21
1.5.1.1. Enteritis model in Atlantic salmon.....	26
1.6. Projects' contextual background.....	27
1.7. Project aims and outline.....	28
2. DESCRIPTION AND DEVELOPMENT OF A SEMI-AUTOMATED SYSTEM TO ASSESS INTESTINAL MORPHOLOGY OF ATLANTIC SALMON, BASED ON ADVANCED IMAGE ANALYSIS	
2.1. Introduction	33
2.2. Material and methods	37
2.2.1. Histological tissue samples	37
2.2.2. Digital image acquisition.....	38
2.2.3. Development tools – Image analysis hardware and software	40
2.2.4. Image processing and segmentation	41
2.2.4.1. Edge detection.....	41
2.2.4.2. Noise removal.....	42
2.2.4.3. Colour thresholding.....	42

2.2.4.4. Morphological filtering	42
2.2.4.5. Intensity thresholding	42
2.2.4.6. Size scrapping and filling	42
2.2.4.7. Intensity thresholding of inverted images.....	42
2.2.4.8. Manual object delineation	43
2.2.5. Histological identification and post-processing overlays	43
2.2.5.1. Mucosal and submucosal tissues	43
2.2.5.2. Mucous cells.....	43
2.2.5.3. Tissue vacuolisation	43
2.2.5.4. Mask overlays	43
2.2.6. Feature extraction and output generation.....	45
2.2.6.1. Geometric features.....	45
2.2.6.2. Shape features	46
2.2.6.3. Position and orientation features.....	47
2.2.6.4. Output generation.....	47
2.2.7. System performance.....	47
2.2.7.1. Efficiency	47
2.2.7.2. Accuracy.....	47
2.2.7.3. Reproducibility.....	48
2.2.7.4. Statistical analysis	48
2.3. Results and discussion.....	48
2.3.1. Standardisation of staining	49
2.3.2. Image acquisition and pre-processing	50
2.3.3. Development, training and evaluation	52
2.3.3.1. Feature selection.....	53
2.3.4. System performance.....	54
2.3.4.1. Efficiency	55
2.3.4.2. Accuracy.....	56
2.3.4.3. Reproducibility.....	59
2.4. General conclusions	62
TECHNICAL NOTE A1	64
3. INTESTINAL RESPONSES TO DIETARY ADDITIVES – APPLICATION OF TOOLS FOR RAPID SCREENING OF NOVEL DIETARY COMPONENTS	
3.1. Introduction.....	85
3.2. Materials and methods	89
3.2.1. Experimental fish and fish husbandry.....	89
3.2.2. Diets and feeding regime.....	90
3.2.3. Feed composition.....	90
3.2.4. Sampling procedure.....	91
3.2.5. Growth performance and feed efficiencies	92
3.2.6. Haematology and blood biochemistry	92

3.2.7. Respiratory burst activity and phagocytic activity assays	94
3.2.8. Histological staining and digital image acquisition	96
3.2.9. Quantitative image analysis	96
3.2.10. Statistical analysis	101
3.3. Results	102
3.3.1. Fish behaviour and feed intake	102
3.3.2. Feed chemical composition.....	103
3.3.3. Growth performance and feed efficiencies.....	103
3.3.4. Haematology and blood biochemistry.....	104
3.3.5. Respiratory burst activity and phagocytic activity assays	106
3.3.6. Image analysis performance	109
3.3.7. Quantitative variables from image analysis.....	110
3.4. Discussion.....	118
3.4.1. Growth performance and nutrient intake.....	118
3.4.2. Haematology and blood biochemistry.....	121
3.4.3. Respiratory burst and phagocytic activity assays	125
3.4.4. Image analysis performance	127
3.4.5. Quantitative variables from image analysis.....	128
3.5. General conclusions	131
4. HISTOLOGICAL EVALUATION OF ENTERITIS IN ATLANTIC SALMON: QUANTITATIVE IMAGE ANALYSIS VS SEMI-QUANTITATIVE SCORES	
4.1. Introduction	135
4.2. Materials and methods.....	137
4.2.1. Fish and rearing conditions	137
4.2.2. Diets and feeding regime	137
4.2.3. Feed composition	139
4.2.4. Sampling procedure	139
4.2.5. Histological staining and evaluation.....	140
4.2.5.1. Semi-quantitative scoring histological assessment	140
4.2.5.2. Quantitative image analysis histological assessment	140
4.2.6. Statistical analysis	144
4.2.6.1. Semi-quantitative histological data	144
4.2.6.2. Quantitative image analysis histological data.....	145
4.2.6.3. Comparison of the quantitative and semi-quantitative systems	145
4.3. Results	146
4.3.1. Semi-quantitative histological assessment	146
4.3.2. Quantitative histological assessment.....	148
4.3.3. Comparison of the quantitative and semi-quantitative systems.....	158
4.4. Discussion.....	159
4.5. General conclusions	167
TECHNICAL NOTE A2.....	168

5. QUANTITATIVE IMMUNOSTAINING: DEVELOPMENT OF A BIOMARKER PANEL FOR ASSESSMENT OF IMMUNE RESPONSE IN THE INTESTINAL TRACT OF ATLANTIC SALMON PARR FED DIFFERENT DIETS	
5.1. Introduction	175
5.2. Material and methods	179
5.2.1. Experimental fish and fish husbandry	179
5.2.2. Diets and feeding regime	179
5.2.3. Sampling procedure	180
5.2.4. Histology	180
5.2.5. Immunostaining assays – Immunolabelling of biomarkers	180
5.2.5.1. Cell proliferation and regeneration (PCNA)	181
5.2.5.2. Programmed cell death or apoptosis (TUNEL)	182
5.2.5.3. Eosinophilic granule cells (Active Caspase-3)	183
5.2.5.4. T-cell-like cells (CD3ε)	184
5.2.5.5. Mobilisation of stress related proteins for regenerative processes (HSP 70)	185
5.2.5.6. Facilitation of nutrient uptake and ion transport (Na ⁺ K ⁺ -ATPase)	185
5.2.6. Digital image acquisition	187
5.2.7. Quantitative image analysis of immunological labelling	187
5.2.8. Statistical analysis	190
5.3. Results	190
5.3.1. Intestinal histomorphology	190
5.3.2. Biomarker immunolabelling – visual observations of labelling pattern	191
5.3.2.1. Cell proliferation and regeneration (PCNA)	191
5.3.2.2. Programmed cell death or apoptosis (TUNEL)	194
5.3.2.3. Eosinophilic granule cells (Active Caspase-3)	194
5.3.2.4. T-cell-like cells (CD3ε)	197
5.3.2.5. Mobilisation of stress related proteins for regenerative processes (HSP 70)	199
5.3.2.6. Facilitation of nutrient uptake and ion transport (Na ⁺ K ⁺ -ATPase)	200
5.3.3. Quantitative image analysis of immunohistological labelling	201
5.3.3.1. Cell proliferation and regeneration (PCNA)	201
5.3.3.2. Programmed cell death or apoptosis (TUNEL)	203
5.3.3.3. Eosinophilic granule cells (Active Caspase-3)	205
5.3.3.4. T-cell-like cells (CD3ε)	206
5.4. Discussion	206
5.4.1. Cell proliferation and regeneration (PCNA)	208
5.4.2. Programmed cell death or apoptosis (TUNEL)	209
5.4.3. Eosinophilic granule cells (Active Caspase-3)	210
5.4.4. T-cell-like cells (CD3ε)	213
5.4.5. Mobilisation of stress-related proteins for regenerative processes (HSP 70)	213
5.4.6. Facilitation of nutrient uptake and ion transport (Na ⁺ K ⁺ -ATPase)	215
5.4.7. Technical pitfalls potentially affecting the immunolabelling	216
5.4.8. Quantification of immunohistolabelling	218

5.4.9. Perspectives	220
5.5. General conclusions	221
TECHNICAL NOTE B	222
6. CHARACTERISATION OF MAST CELLS / EOSINOPHILIC GRANULE CELLS IN THE ATLANTIC SALMON INTESTINE	
6.1. Introduction	229
6.2. Material and methods	232
6.2.1. Histochemical and ultrastructural features of intestinal MCs / EGCs	232
6.2.1.1. Histology tissue samples	232
6.2.1.2. Histochemical staining	233
6.2.1.3. Immunohistochemical labelling.....	233
6.2.1.4. Light microscopy examination	237
6.2.1.5. Immunofluorescent Antibody Test (IFAT).....	237
6.2.1.6. Confocal laser scanning microscopy (CLSM).....	238
6.2.1.7. Transmission electron microscopy (TEM)	239
6.2.1.8. Immunogold labelling (IGL).....	240
6.2.2. Isolation and characterisation of intestinal MCs / EGCs	241
6.2.2.1. Tissue sample collection.....	241
6.2.2.2. Isolation of MCs / EGCs	241
6.2.2.3. Electrophoresis and western blot	243
6.3. Results	245
6.3.1. Anatomical distribution of MCs / EGCs	245
6.3.2. Histochemical contents	246
6.3.3. Ultrastructure morphology and cytochemistry.....	249
6.3.3.1. Isolation of intestinal granulocytes and immunoblotting characterisation	256
6.4. Discussion.....	257
6.5. General conclusions	268
7. GENERAL SYNTHESIS	
7.1. Introduction	273
7.2. General study aim.....	274
7.3. Research approach.....	275
7.4. Summary of study outcomes	276
7.5. Future considerations	281
7.6. Adoption of the developed technology.....	282
7.7. Concluding remarks	284
BIBLIOGRAPHIC REFERENCES.....	287
APPENDIX 1	337
Stock solutions and buffers	337
Histochemical staining protocols.....	350
APPENDIX 2	361
Image sequence generated by the image processing and analysis semi-automates system.....	361

LIST OF FIGURES

Figure 1.1.	Gastrointestinal tract of Atlantic salmon illustrating the different intestinal segments.....	4
Figure 1.2.	The organisation of the tissue layers in the teleosts' gastrointestinal tract	6
Figure 1.3.	Scanning electron microscope (SEM) micrographs of the midgut from Atlantic salmon, showing the luminal appearance of the mucosal folds.....	7
Figure 1.4.	Photomicrographs of the Atlantic salmon distal intestine illustrating the general tissue organisation and the morphological tissue variations encountered across two different histological grades: normal morphology, moderate inflammation to severe enteritis.....	9
Figure 1.5.	Digital-scan photomicrographs of transverse sections of the intestinal tract of Atlantic salmon, stained with haematoxylin-eosin and with a combination of haematoxylin-eosin and Alcian blue 8 G	10
Figure 1.6.	Transmission electron microscope micrographs of the midgut from Atlantic salmon, showing apical cytoplasm of absorptive cells	11
Figure 1.7.	Schematic diagram showing the intestinal transepithelial transport occurring in fish intestines.....	15
Figure 2.1.	Images from Atlantic salmon distal intestine specimens showing the morphological tissue variations encountered across three different histological grades: normal morphology, mild to moderate inflammation and severe enteritis.....	39
Figure 2.2.	Digitised histological image of distal intestine tissue from Atlantic salmon, at successively higher magnification.....	40
Figure 2.3.	Flow diagram illustrating the sequence of image processing, for the proposed image analysis system	41
Figure 2.4.	Images generated by the described image analysis algorithms, from which morphometric features were extracted and employed to quantify the phenotypic appearance of the specimen's distal intestine.....	44
Figure 2.5.	Images generated by the described image analysis algorithms, from which morphometric features were extracted and employed to quantify the phenotypic appearance of the specimen's distal intestine.....	45
Figure 2.6.	Geometric and shape feature measurements employed in the study.....	46
Figure 2.7.	Schematic diagram of the box-counting method used to estimate fractal dimensions ...	47
Figure 2.8.	Images from Atlantic salmon distal intestine sections used in the comparison of results derived from the automatic algorithm system, against the manual measurements obtained by an expert histopathologist.....	58
Figure 2.9.	Scatter plots for the performance analysis results obtained by the proposed interactive image analysis system and an open source image analysis software.....	60
Figure 3.1.	Flow chart illustrating the sequence of image processing algorithms	98

Figure 3.2. Image outputs generated by the described image analysis algorithms, from which morphometric features were extracted and employed to quantify aspects of the specimen's distal intestine	100
Figure 3.3. Effect of feeding the different experimental diets to Atlantic salmon on the mean differential leucocyte cell percentage	106
Figure 3.4. Respiratory burst activity of head kidney macrophages from Atlantic salmon stimulated with 1 mg.mL ⁻¹ NBT containing 1 µg.mL ⁻¹ PMA, that were fed the different experimental diets	107
Figure 3.5. Light micrograph of Atlantic salmon head kidney macrophage cells	107
Figure 3.6. Phagocytic ability of macrophages from head kidneys of Atlantic salmon fed different experimental diets	108
Figure 3.7. Phagocytic activity and the phagocytic index of macrophages from head kidneys of Atlantic salmon fed different experimental diets	109
Figure 3.8. Representative images of morphological variations encountered across the distal intestine of Atlantic salmon fed different experimental diets	109
Figure 3.9. Component plot of the multivariate principal component analysis for the intestinal morphological features measured in Atlantic salmon fed different treatment diets	115
Figure 4.1. Chart of the main components involved in image analysis of the distal intestine morphometrics of Atlantic salmon	144
Figure 4.2. Images of morphological variations encountered across the distal intestine of Atlantic salmon fed different experimental diets	147
Figure 4.3. Correlations between the different morphological parameters detailed for the quantitative assessment analysis.....	151
Figure 4.4. Correlations between the different morphological parameters detailed for the quantitative assessment analysis.....	152
Figure 4.5. Component plot of the multivariate principal component analysis and corresponding loading weights, for the intestinal morphological features measured in Atlantic salmon fed different treatment diets	154
Figure 4.6. Factor plots of the multivariate principal components analysis for the intestinal morphology of Atlantic salmon fed different treatment diets	156
Figure 4.7. Scatterplot of the canonical scores and corresponding dietary group centroids, for a pair of discriminant functions, based on 9 morphometric features	157
Figure 4.8. Correlations between the different morphological parameters detailed for the quantitative image analysis and the semi-quantitative scoring assessments.....	160
Figure 5.1. Image outputs generated by the described image analysis algorithms, from which morphometric features were extracted and employed to quantify and characterise specific immunohistochemical biomarkers in the specimen's distal gut	189

Figure 5.2. Representative images of morphological variations encountered across the distal intestine of Atlantic salmon fed different experimental diets	191
Figure 5.3. Immunohistochemical detection of proliferating cell nuclear antigen in distal intestinal tissue sections of Atlantic salmon fed either a fish meal based control diet, a diet containing 25 % defatted soybean meal or a diet with inclusion of immunostimulant ingredients	193
Figure 5.4. Apoptosis labelled by a TUNEL assay in distal intestinal tissue sections of Atlantic salmon fed either a fish meal based control diet, a diet containing 25 % defatted soybean meal or a diet with inclusion of immunostimulant ingredients.....	195
Figure 5.5. Immunostained eosinophilic granule cells in distal intestinal tissue sections of Atlantic salmon fed either a fish meal based control diet, a diet with inclusion of immunostimulant ingredients or diet containing 25 % defatted soybean meal.....	195
Figure 5.6. Immunoreactivity to the antibody directed against a CD3 ϵ epitope. Immunoreactive cells exhibit a pattern suggestive of cell membrane or cytoplasmic staining	198
Figure 5.7. Immunohistochemical localisation of heat shock protein 70 immunoreactive cells recognised by an antibody, which labels both the constitutive and inducible forms of HSP 70 in various tissues.....	199
Figure 5.8. Immunohistochemical detection of Na ⁺ K ⁺ -ATPase immunoreactive cells recognised by an antibody against the conserved α -subunit region, in seawater-adapted Atlantic salmon gill, kidney and intestinal tissue sections	200
Figure 5.9. Immunoreactive indices of the histolabelling with four distinct biomarkers, performed in distal intestinal histological sections from Atlantic salmon fed different experimental diets	202
Figure 5.10. Immunoreactive indices and relative staining intensity of histolabelling with four distinct biomarkers, performed in distal intestinal histological sections from Atlantic salmon fed different experimental diets.....	203
Figure 5.11. Schematic description of a TMA slide	220
Figure 6.1. Granule cells resembling mammalian MCs / EGCs, found in the distal intestine of Atlantic salmon between the circular muscle layer and the stratum compactum, but also scattered in the lamina propria and in connective tissue strands of the mucosal folds. Transverse intestinal sections were stained with either haematoxylin and eosin or a combination of haematoxylin-eosin and Alcian blue	245
Figure 6.2. The granules of MCs / EGCs in the distal intestine of Atlantic salmon stained with different dyes and chromogens	246
Figure 6.3. Photomicrographs of normal distal intestine of Atlantic salmon, showing MCs / EGCs lying along the <i>stratum granulosum</i> adjacent to the <i>stratum compactum</i> . Transverse sections were stained with haematoxylin and eosin, haematoxylin-erythrosin-safran, thionin and Azur A	247

Figure 6.4. Photomicrographs of normal distal intestine of Atlantic salmon, showing MCs / EGCs lying along the <i>stratum granulosum</i> adjacent to the <i>stratum compactum</i> . Transverse sections were stained with May-Grünwald-Giemsa, toluidine blue, periodic acid Schiff and haematoxylin, periodic acid Schiff and Alcian blue, haematoxylin-eosin-Alcian blue and Astra blue	248
Figure 6.5. Photomicrographs showing immunohistochemical labelling of MCs / EGCs using different antibodies, either in distal intestinal tissue sections of Atlantic salmon or in mammalian positive control tissue sections known to express the antigens of interest	249
Figure 6.6. Atlantic salmon distal intestine MCs / EGCs, staining positively for an antibody directed against a peptide from the p17 fragment of human caspase-3	252
Figure 6.7. Electron micrograph of MCs / EGCs from the distal intestine of Atlantic salmon	253
Figure 6.8. Confocal micrographs showing the immunolocalisation of MC / EGC granules from the distal intestine of Atlantic salmon, incubated with a caspase-3 FITC-conjugated antibody and counterstained with a red nuclear stain	254
Figure 6.9. Ultrastructural immunogold labelling of Atlantic salmon intestinal MC / EGC granules, using a gold-covalently-conjugated antibody directed against a peptide from the p17 fragment of human caspase-3	255
Figure 6.10. Photomicrographs representative of each of the cell fractions recovered from the distal intestine of Atlantic salmon by means of a Percoll [®] step gradient centrifugation using densities of 1.060, 1.070, 1.085, 1.108 and 1.118 g.mL ⁻¹	256

LIST OF TABLES

Table 1.1.	Types of assessment employed in nutritional studies of fish, and their level of suitability	22
Table 2.1.	Image size and resulting image file size of 24-bit digital TIFF images, captured at different magnifications.....	51
Table 2.2.	List of measured morphological parameters and computed morphometric ratios used in the analysis	54
Table 2.3.	Total mean processing time required to accomplish the intended assessment tasks, by means of manual, interactive or automated threshold methods for mucous cell assessment.....	56
Table 2.4.	Correlations between measurements derived by using manual, interactive or automated threshold methods, for mucous cell assessment.....	57
Table 2.5.	Reproducibility of the semi-automated image analysis system, accounting for intra- and inter-operator variation.....	62
Table 3.1.	Formulation and proximate chemical composition of the feeds used in this experimental study	92
Table 3.2.	Growth response and feed efficiencies for Atlantic salmon fed the experimental diets.	103
Table 3.3.	Haematological profiles for Atlantic salmon fed the experimental diets	105
Table 3.4.	Morphometric assessment of the distal intestine from Atlantic salmon fed the experimental diets.....	112
Table 3.5.	Factor loading weights and component score coefficients derived from principal component analysis, regarding morphometric features measured in the distal intestine of Atlantic salmon fed with the experimental diets.....	114
Table 4.1.	Formulation and proximate chemical composition of the feeds used in this experimental study	138
Table 4.2.	Semi-quantitative scoring system according to Knudsen <i>et al.</i> (2008), using different parameters to assess the degree of histomorphological changes induced by soybean meal in the distal intestine of Atlantic salmon.....	141
Table 4.3.	List of measured morphological parameters and computed morphometric ratios used in the quantitative image analysis approach	143
Table 4.4.	Semi-quantitative histological assessment of the intestinal sections and schematic overlapping-ranges of averaged summary scores, for fish fed the different experimental diets	146
Table 4.5.	Quantitative image analysis histological assessment of the intestinal sections	149
Table 4.6.	Percentage of predicted classifications based on the discriminant function scores given to each individual fish fed the distinct experimental diets.....	158
Table 5.1.	Summary of immunostaining protocols used in this study	186
Table 6.1.	Histochemical methods employed in the evaluation of intestinal mast cells / eosinophilic granule cells from Atlantic salmon	233
Table 6.2.	Summary of immunohistochemical staining protocols employed in the evaluation of intestinal mast cells / eosinophilic granule cells from Atlantic salmon.....	234

ABBREVIATIONS LIST

%	Percent sign
Af	Main axis of an ellipse
AI	Anterior intestine sample
Alb	Albumin
AMPs	Antimicrobial peptides
ANFs	Anti-nutritional factors
ANOVA	Analysis of variance
ARC	Aquaculture research centre
BBM	Brush border membrane
Bf	Minor axis of an ellipse
BLM	Basolateral membrane
BSA	Bovine serum albumin
CD	Cluster of differentiation
CD3ε	T-cell surface glycoprotein cluster of differentiation epsilon chain
c-kit	Transmembrane tyrosine kinase receptor kit
CLSM	Confocal laser scanning microscope
cm	Centimetre
CRP	C-reactive protein
CT (or) Ct	Thickness of the connective tissue between the base of the mucosal folds and the <i>stratum compactum</i>
CTb	Collecting tubules
d	Day
dg	decigram
DAB	3,3'-Diaminobenzidine
DI	Distal intestine sample
dL	Decilitre
DNA	Deoxyribonucleic acid
DT	Distal tubule
DTT	Dithiothreitol
<i>e.g.</i>	<i>Exempli gratia</i> : "for example"
EDTA	Ethylenediaminetetraacetic acid
EGCs	Eosinophilic granule cells
ELISA	Enzyme linked immune-sorbent assay
En	Intestinal enterocytes
Epi	Epidermis
Epub	Electronic publication
<i>et al.</i>	<i>Et alia</i> : "and others"
<i>etc.</i>	<i>Et cetera</i> : "and other things"
F	Statistical F-value

FAO	Food and agricultural organisation
FCR	Feed conversion rate
FcRs	Cellular receptors for immunoglobulins
FI	Feed intake
FITC	Fluorescein isothiocyanate
fL	Femtolitre
FL	Fork length
FR	Fractal dimension of the perimeter line from the luminal surface
g	Gram
GALT	Gut associated lymphoid tissue
GB	Gigabytes
GI	Gastrointestinal
GILT	Interferon-gamma-inducible lysosomal thiol reductase
GL	Glomerulus
GLM	General linear model
GLMM	General linear mixed model
h	Hours
H&E	Haematoxylin and eosin
HES	Haematoxylin-erythrosin-safran
H ₂ O	Water
H ₂ O ₂	Hydrogen peroxidase
Hb	Haemoglobin
HBSS	Hank's balanced salt solution
Hct	Haematocrit
HIER	Heat induced epitope retrieval
HLS	Hue, lightness and saturation colour model
HRP	Horseradish peroxidase
HSC	Heat shock cognate protein (a constitutively expressed molecular chaperone)
HSP	Heat shock protein
<i>i.a.</i>	<i>Inter alia</i> : "among other things"
<i>i.e.</i>	<i>Id est</i> : "that is to say"
IFAT	Indirect fluorescent antibody test
IFN	Interferon
Ig	Immunoglobulin
IGL	Immunogold labelling
IHC	Immunohistochemistry
IL	Interleukin
Imm	Immunostimulants
IoA	Institute of Aquaculture
K	Condition factor
kg	Kilogram

kv	Kilovolts
L	Litre
LB	Lobule of epithelial cells from cutaneous tumour
LM	Lumen
Log	Logarithm
LP (or) Lp	<i>Lamina propria</i>
LW	Factor loading weight
Lys	Lysozyme
M	Molar
Mab	Monoclonal antibody
MB	Megabytes
MC	Mucous cell
MC Ellipse Af	Length of the main axis of an ellipse with the same geometric moment of inertia as the mucous cell
MC Ellipse Bf	Length of the secondary axis of an ellipse with the same geometric moment of inertia as the mucous cell
MC Ellipse Ratio	Ratio of the elliptical lengths Af and Bf for the mucous cell
MC Feret Max	Mucous cell maximum Feret length
MC Feret Min	Mucous cell minimum Feret length
MC Feret Ratio	Ratio of the mucous cell Feret lengths
MCA	Mucous cell total area
MCA / [MTA-Vac]	Ratio between mucous cell total area and the MTA without the vacuolisation area
MCA / MTA	Ratio between the mucous cell area and the mucosal tissue area
MCH	Mean corpuscular haemoglobin
MCirc	Mucous cell mean circularity index
MCMC	Markov Chain Monte Carlo
MCN	Mucous cell number
MCN / [MTA-Vac]	Ratio between mucous cell number and the MTA without the vacuolisation area
MCN / MTA	Ratio between the mucous cell number and the mucosal tissue area
MCs	Mast cells
MCT	Mast cell tryptase
MCV	Mean corpuscular volume
MF	Mucosal fold
MF Area	Total mean area of four simple mucosal folds
MF Ellipse Af	Mean length of the main axis of the ellipses with the same geometric moment of inertia as four of the simple mucosal folds
MF Ellipse Bf	Mean length of the secondary axis of the ellipses with the same geometric moment of inertia as the four of the simple mucosal folds
MF Ellipse Ratio	Mean ratio of the elliptical lengths Af and Bf for four simple mucosal folds
MF Feret Max	Maximum Feret lengths mean of four simple mucosal folds

MF Feret Min	Minimum Feret lengths mean of four simple mucosal folds
MF Feret Ratio	Mean ratio of the Feret lengths of four simple mucosal folds
MF Perimeter	Total mean perimeter length of four simple mucosal folds
mg	Milligram
MGG	May-Grünwald-Giemsa
MHz	Megahertz
Mi	Mitochondria
MI	Mid intestine sample
Min	Minute
mL	Millilitre
ML	Mucosal tissue layer
mM	Millimolar
MMCA	Mean mucous cell area
mRNA	Messenger ribonucleic acid
MRXS	Image file created by MIRAX-compatible microscope digital slide scanners such as the Carl Zeiss MIRAX series; multi-file JPEG with proprietary metadata and indexes.
MTA	Mucosal tissue area
MTA / STA	Ratio between the mucosal tissue area and the submucosal tissue area
MTA-Vac	MTA without the vacuolisation area
MUC	Remaining mucosal area
MV	Microvilli
MyD	Myeloid differentiation primary response gene
<i>n</i> (or) N ^o (or) No.	Number
N.A.	Non applicable
Na ⁺ K ⁺ -ATPase	Sodium-potassium adenosine triphosphatase
NBT	Nitro blue tetrazolium
NCR	National research council
NGS	Normal goat serum
NIRS	Near infrared reflectance spectroscopy
nm	Nanometer
°C	Degree Celsius
OD	Optical density
P	Total perimeter length of the luminal surface
P / MTA	Ratio between total perimeter length of the luminal surface and mucosal tissue area
PA	Phagocytic activity
Pab	Polyclonal antibody
PAR	Protease-activated receptor
PAS	Periodic-Acid-Schiff
PBS	Phosphate buffered saline solution

PC	Phagocytic capacity
PCA	Principal component analysis
PCNA	Proliferating cell nuclear antigen
PCR	Polymerase chain reaction
PF	Primary gill lamellae
pg	Picograms
pH	In chemistry is a measure of the acidity or basicity of an aqueous solution
PI	Phagocytic index
pi	Mean pixel intensity
PMA	Phorbol-12-myristate 13-acetate
PT	Proximal convoluted tubules
px	Pixel
<i>r</i>	Correlation co-efficient
R^2	Square of the correlation coefficients
RAM	Random access memory
RAPD	Random amplified polymorphic deoxyribonucleic acid
RBC	Red blood cells
RFLP	Restriction fragment length polymorphism
RGB	Red, green and blue colour model
RNA	Ribonucleic acid
ROI	Region of interest
RT	Room temperature
SB (or) SBM	Soybean (or) Soybean meal
SC	Component score coefficient
Sc	<i>Stratum compactum</i>
SD	Standard deviation
SDS-PAGE	Sodium dodecyl sulphate – polyacrylamide gel electroforesis
sec	Seconds
SEM	Scanning electron microscopy
Sg	<i>Stratum granulosum</i>
SG	Sweat glands
SGR	Specific growth rate
SL	Primary gill lamellae
SML	Submucosa tissue layer
SS	Soya saponin
STA	Submucosal tissue area
SUB	Submucosal area
SUP	Above the <i>stratum compactum</i>
TBS	Tris(hydroxymethyl)aminomethane buffered saline solution
TCR	T-cell receptor
TEM	Transmission electron microscopy

TGF	Transforming growth factor
TGGE	Temperature gradient gel electrophoresis
TIFF	Tagged image file format
TJs	Tight junctions
TMA	Tissue microarrays
TN	Trypsin neutraliser buffered saline solution
TNPI	TN buffer containing a protease inhibitor cocktail
TP	Total protein
Tris-HCl	Tris(hydroxymethyl)aminomethane hydrochloride buffered saline solution
TUNEL	Terminal deoxynucleotidyl transferase dUTP nick end labelling
U	Unit
UK	United Kingdom
USA	United States of America
V	Volts
v / v	Volume / volume
Vac	Supranuclear vacuoles
VC	Vacuolisation total area
VC / MTA	Ratio between the total vacuolisation area and the mucosal tissue area
vs.	<i>Versus</i> : “as oppose to; opposite”
w / v	Weight / volume
WBC	White blood cells
Wt	Weight gain
mg	Microgram
μL	Microliter
Mm	Micrometre
μM	Micromolar
ρ	Rho, symbol for density
X ²	Statistical test using chi-squared distribution

ABSTRACT

The intestinal tract of salmonids provides a dynamic interface that not only mediates nutrient uptake but also functions as the first line of defence against ingested pathogens. Exposure of the immune system to beneficial microorganisms and different dietary immunostimulants via the intestine has been shown to prime the immune system and help in the development of immune competence. Furthermore, the morphology and function of teleostean intestines are known to respond to feed components and to ingested and resident bacterial communities. Histological appraisal is still generally considered to be the gold standard for sensitive assessment of the effects of such dietary modulation.

The aim of the present study was to improve understanding of salmonid intestinal function, structure and dynamics and to use the knowledge gained to develop a model for analysis, which would allow intestinal health to be assessed with respect to different intestinal communities and feed components. Virtual histology, the process of assessing digital images of histological slides, is gaining momentum as an approach to supplement traditional histological evaluation methodologies and at the same time, image analysis of digitised histological sections provides a practical means for quantifiable assessment of structural and functional changes in tissues, being both objective and reproducible. This project focused on the development of a rapid, practical analytical methodology based on advanced image analysis, that was able to measure and characterise a range of features of the intestinal histology of Atlantic salmon in a quantitative manner.

In the first research chapter, the development of a novel histological assessment system based upon advanced image analysis was described, this being developed with the help of a soybean feed model known to induce enteropathy in Atlantic salmon. This tool targeted the evaluation of the extent of morphological changes occurring in the distal intestine of Atlantic salmon following dietary modulation. The final analytical methodology arrived at, could be conducted with minimal user-interaction, allowing rapid and objective assessment of 12 continuous variables per histological frame analysed. The processing time required for each histological frame was roughly 20-25 min, which greatly improved the

efficiency of conducting such a quantitative assessment with respect to the time taken for a subjective semi-quantitative alternative approach. Significant agreement between the fully automated and the manual morphometric image segmentation was achieved, however, the strength of this quantitative approach was enhanced by the employment of interactive procedures, which enabled the operator / observer to rectify preceding automated segmentation steps, and account for the specimen's variations. Results indicated that image analysis provided a viable alternative to a pathologist's manual scoring, being more practical and time-efficient.

In the second research chapter, feeding Atlantic salmon a high inclusion level of unrefined SBM (25 %) produced an inflammatory response in the distal intestine as previously described by other authors. The model feed trial successfully generated differentiable states, although these were not, for the most part, systemically differentiable through the majority of standard immunological procedures used, being only detectable morphologically. Quantitation of morphometric parameters associated with histological sections using the newly developed image analysis tool successfully allowed identification of major morphological changes. Image analysis was thus shown to provide a powerful tool for describing the histomorphological structure of Atlantic salmon distal intestine. In turn, the semi-automated image analysis methods were able to distinguish normal intestinal mucosa from those affected by enteritis. While individual parameters were less discriminatory, use of multivariate techniques allowed better discrimination of states and is likely to prove the most productive approach in further studies.

Work described in the third research chapter sought to validate the semi-automated image analysis system to establish that it was measuring the parameters it was purported to be measuring, and to provide reassurance that it could reliably measure pre-determined features. This study, using the same sections for semi-quantitative and quantitative analyses, demonstrated that the quantitative indices performed well when compared to analogous semi-quantitative descriptive parameters of assessment for enteritis prognosis. The excellent reproducibility and accuracy performance levels indicated that the image

analysis system was a useful and reliable morphometric method for the quantification of SB-induced enteritis in salmon. Other characteristics such as rapidity, simplicity and adaptability favour this method for image analysis, and are particularly useful where less experienced interpreters are performing the analysis.

The work described in the fourth research chapter characterised changes in the morphology of the intestinal epithelial cells occurring as a result of dietary modulation and aspects of inflammatory infiltration, using a selected panel of enzyme and IHC markers. To accomplish this, image analysis techniques were used to evaluate and systematically optimise a quantitative immunolabelling assessment protocol. Digital computer-assisted quantification of labelling for cell proliferation and regeneration (*i.e.* PCNA); programmed cell death or apoptosis (*i.e.* TUNEL); EGCs and t-cell like infiltrates (*i.e.* active caspase-3 and CD3 respectively); mobilisation of stress-related protein regenerative processes (*i.e.* HSP 70) and facilitation of nutrient uptake and ion transport (*i.e.* Na⁺K⁺-ATPase) provided encouraging results. Through the description of the intestinal cellular responses at a molecular level, such IHC expression profiling further characterised the inflammatory reaction generated by the enteropathic diet. In addition, a number of potential diagnostic parameters were described for fish intestinal health *e.g.* the relative levels of antigenicity and the spatial distribution of antigens in tissues.

Work described in the final research chapter focused on detailed characterisation of intestinal MCs / EGCs in order to try to elucidate their functional role in the intestinal immune responses. Through an understanding of their distribution, composition and ultrastructure, the intention was to better characterise these cells and their functional properties. The general morphology, histochemical characteristics and tissue distribution of these cells were explored in detail using histochemical, IHC and immunogold staining / labelling, visualised using light, confocal and TEM microscopy. Despite these extensive investigations, their physiological function and the content of their granules still remain somewhat obscure, although a role as immunodulatory cells reacting to various exogeneous signals through a finely regulated process and comparable to that causing the

degranulation of mammalian MCs is suggested. The histochemical staining properties demonstrated for salmonid MCs / EGCs seem to resemble those of mammalian mucosal mast cells, with both acidophilic and basophilic components in their granules, and a granule content containing neuromodulator / neurotransmitter-peptides such as serotonin, met-enkephalin and substance-p. Consequently, distinguishable bio-chromogenic markers have been identified that are of utility in generating a discriminatory profile for image analysis of such cells. Haematoxylin-erythrosin-safran (HES) and May-Grünwald-Giemsa (MGG) histochemical stains, and immunolabelling with anti-serotonin, met-enkephalin, substance-p and caspases-3 / -7 antibodies proved informative.

LIST OF PUBLICATIONS

Da Silva, P., McGurk, C., Bron, J.E. (2014). “Description and development of a semi-automated system to assess intestinal morphology of Atlantic salmon, based on advanced image analysis” – *Manuscript in Preparation*.

Da Silva, P., McGurk, C., Jayasurya, N., Knudsen, D., Bron, J.E. (2014). “Histological evaluation of enteritis in Atlantic salmon: quantitative image analysis vs semi-quantitative scores” – *Manuscript in Preparation*.

Da Silva, P., McGurk, C., Thompson, K.D., Adams, A., Mullins, J.E., Bron, J.E. (2014). “Characterisation of mast cells / eosinophilic granule cells in the Atlantic salmon intestine” – *Short Communication in Preparation*.

LIST OF CONFERENCE PROCEEDINGS

Da Silva, P. (26th-28th November 2013). “Quantitative analysis approach to characterise the effects of dietary components on intestinal morphology in Atlantic salmon”. Nutreco R&D Science Conference, Cuijk, Netherlands – *Poster Presentation*.

Da Silva, P., McGurk, C., Thompson, K.D., Adams, A., Mullins, J.E., Bron, J.E. (14th September 2013). “Development and validation of a semi-automated classification system, involving advanced image analysis, for assessment of the effects of dietary components on intestinal morphology of Atlantic salmon”. 16th International Conference on Diseases of Fish and Shellfish, Tampere, Finland – *Oral Presentation*.

Da Silva, P., McGurk, C., Thompson, K.D., Adams, A., Mullins, J.E., Bron, J.E. (17th April 2013). “Semi-automated classification system based on image analysis advanced image analysis, for assessment of the effects of dietary components on intestinal morphology of Atlantic salmon”. Skretting’s Nutrition and Fish Health Network Annual Meeting, Verona, Italy – *Oral Presentation*.

Da Silva, P., McGurk, C., Thompson, K.D., Adams, A., Mullins, J.E., Bron, J.E. (13th March 2013). “Histopathological evaluation of enteritis in Atlantic salmon: Quantitative analysis VS Semi-quantitative scores”. Fish Veterinary Society Spring Meeting, Edinburgh, UK – *Oral Presentation*.

Da Silva, P., McGurk, C., Thompson, K.D., Adams, A., Mullins, J.E., Bron, J.E. (24th October 2012). "Semi-automated classification system based on image analysis to assess the gut morphology of Atlantic salmon". 3rd Biennial Postgraduate Research Conference, Institute of Aquaculture University of Stirling, Scotland, UK – *Oral Presentation*.

Da Silva, P., McGurk, C., Thompson, K.D., Adams, A., Mullins, J.E., Bron, J.E. (14th June 2012). "Semi-automated classification system based on image analysis to assess the gut morphology of Atlantic salmon". Skretting's Aquaculture Research Centre, Stavanger, Norway – *Oral Presentation*.

Da Silva, P., Thompson, K.D., Adams, A., Bron, J.E. (9th May 2012). "A novel image analysis approach to characterise the effects of dietary components on intestinal morphology and immune system in Atlantic salmon". Institute of Aquaculture Lunchtime Seminar Series, University of Stirling, Scotland, UK – *Oral Presentation*.

Da Silva, P., McGurk, C., Thompson, K.D., Adams, A., Mullins, J.E., Bron, J.E. (15th Sept 2011). "Semi-automated classification system based on image analysis to assess the gut morphology of Atlantic salmon". 15th International Conference on Diseases of Fish and Shellfish, Split, Croatia – *Oral Presentation*.

Da Silva, P. (16th Feb 2011). "Development of a gut model to examine the effect of dietary components on Atlantic salmon". Skretting's Aquaculture Research Centre, Stavanger, Norway – *Oral Presentation*.

Da Silva, P., Thompson, K.D., Adams, A., Bron, J.E. (28th June 2010). "Development of a gut model to examine the effect of dietary components on Atlantic salmon". PhD Research Conference, Institute of Aquaculture, University of Stirling, Scotland, UK – *Poster Presentation*.

Da Silva, P., Thompson, K.D., McGurk, C., Bron, J.E. (11-15th April 2010). "Development of a gut model to examine the effect of dietary components on Atlantic salmon". 11th Fish Immunology Workshop, Wageningen Institute of Animal Sciences, Netherlands – *Poster Presentation*.

GENERAL INTRODUCTION

The global aquaculture industry sector is developing rapidly (FAO, 2012), and its major economic losses have, to date, been primarily due to disease, which thus remains a key constraint to its continued growth (Oliva-Teles, 2012). As the industry's rate of expansion intensifies, the benefits of high quality feeds, which offer enhanced fish growth and improved disease resistance, become more apparent (Trichet, 2010). Hence, over the past two decades there has been increased attention focusing on understanding the relationships between dietary formulation, growth efficiency, the immune system, and prevention / control of disease (Landolt, 1989; Lovell, 1998; Good, 2004; Bricknell & Dalmo, 2005; Ringø *et al.*, 2012; *inter alia*). It is widely recognised that nutritional modulation can enhance the fish's immune system and have a profound effect on their growth (*e.g.* Zhou *et al.*, 2010; Dong *et al.*, 2013). It is also accepted that besides satisfying the dietary nutrient requirements for maximum growth, certain feed additives can provide increased immunocompetence and in turn increased resistance to disease (*e.g.* Chang *et al.*, 2012; Awad *et al.*, 2013; Bui *et al.*, 2014). This highlights the complex interaction between fish nutrition and fish health (Lim & Webster, 2001; Kiron, 2012).

1.1. Nutrition, feed and fish health

The role of dietary ingredients and selective additives on the function of the immune system in fish has been investigated since the 1960s, and scientific evidence supports a direct role for nutrients in providing important cofactors and regulators / augmentation of the immune response (Blazer, 1992; Waagbø, 1994). Some of the dietary components that have been investigated include ingredients aimed at enhancing the fish immune response (*e.g.* yeast derived, β -glucans, ω -3 fatty acids), stimulating the establishment of beneficial gut microbes (*e.g.* probiotics and some types of prebiotics), stimulating digestive function (*e.g.* butyric acid, glucuronic acid, lactic acid, glutamine, threonine, cysteine, and

nucleotides) and reducing pathogen load in the gut (e.g. organic and inorganic acids, essential oils, high levels of zinc oxide, herbs and spices, some types of prebiotics, bacteriophages, and anti-microbial peptides) – Galeotti, 1998; Sakai, 1999; Gannam & Schrock, 1999; Sahoo, 2007; Govind & Madhuri, 2012; *inter alia*. Overall, there are good indications that changes in current dietary formulations, such as fortification of fish diets with antioxidant vitamins, various protein and amino acids, lipids and essential fatty acids, carbohydrates, minerals and dietary supplementation with non-nutritive immunostimulant compounds, can increase immune function and disease resistance in fish, and may be a cost effective means for reducing the levels of mortality in aquaculture due to disease (Lovell, 1998; Sealey & Gatlin, 1999; Oliva-Teles, 2012). Therefore, by definition, such dietary supplements can be considered as immunostimulants or otherwise functional ingredients (*i.e.* products from natural or synthetic origin with different chemical characteristics and mechanisms of action), that can be employed to enhance innate or non-specific immune responses by interacting directly with cells and tissues mediating immunity and activating them (Galindo-Villegas & Hosokawa, 2004).

The specific mode of action in fish of many of these ingredients is often difficult to fully elucidate, partly due to the complex synergy and multi-factorial relationships between these and other ingredients in the diet (Barker, 2000). Thus, much of our understanding of the mechanisms behind functional ingredients comes from mammalian and avian studies. Some of the modes of action suggested for functional ingredients in teleost fish include: provision of a source of macro and / or micronutrients and enzymatic contribution to digestion, action to improve gastric morphology, activities enhancing the immune response, provision of inhibitory compounds (e.g. chemical substances that have a bactericidal or bacteriostatic effect on microbial populations, which can alter interpopulation relationships by influencing the outcome of competition for chemicals or available energy), inhibition of virulence gene expression or disruption of quorum sensing (Galindo-Villegas & Hosokawa, 2004; Bricknell & Dalmo, 2005; Merrifield *et al.*, 2010; Trichet, 2010). Extensive research is nevertheless required to provide better comprehensive understanding of the mode of action

of such dietary factors, and to measure and confirm the benefits accruing from their use in fish. As better tools and biomarkers are developed, it should be feasible to assess the benefits of use of these ingredients in a structured manner. Given increased knowledge concerning mechanisms of action and improved techniques for assessing positive (and negative) effects, the rational formulation of diets that modulate the immune system and intestinal microflora, increasingly provides tools that may be employed in the implementation of preventative health care strategies involving novel feeding practices (Kiron, 2012).

1.2. Diet and the gastrointestinal tract of fish

The gastrointestinal tract is generally regarded in terms of its function as an organ of digestion and absorption of nutrients, however, there is currently a great interest in this organ with respect to its role as a physical and biochemical barrier to the exterior environment, particularly in preventing attachment and invasion by pathogens, and as an important immune organ (Urzúa, 2013). The nutritional composition of the fish's diet and the intestine's commensal microflora are closely linked to the development and maintenance of gastrointestinal structural integrity. One of the unintended consequences of dietary modulation and the feeding strategies followed, can be the loss of intestinal integrity (Domeneghini *et al.*, 2006), causing enhanced epithelial permeability that may lead to enhanced uptake of macromolecules, bacterial products and antigens across the epithelium. The presence of potentially pathogenic enteric bacteria, the proliferation and metabolic activity of which may perturb the digestive function, can in turn lead to reduced performance and susceptibility to disease (Montagne *et al.*, 2003). In addition, enteritis and poor gut morphology can lead to inefficient feed conversion and at the same time the repair of damaged enterocytes is an energy-consuming activity, which in turn directs valuable resources from growth to more urgent tissue repair and maintenance (Sweetman *et al.*, 2008). Thus the interactions between nutrient uptake, intestinal microflora, gut morphology and the immune system will have a major influence on the animal's health and performance. Therefore, diet formulation to support intestinal health is fast becoming an

important consideration for the aquaculture industry, because improvement of intestinal health is essential for the welfare and growth efficiency of fish, especially when suitable chemotherapeutants are not available or are not permitted by local guidelines or legal frameworks (Choct, 2009).

Although Atlantic salmon (*Salmo salar*, Linnaeus, 1758) is one of the major high-value fish species produced in aquaculture, knowledge of its gastrointestinal responses is far from adequate, especially given the potential such knowledge has for understanding diet-induced pathophysiology, which leads to various intestinal disorders (Chikwati *et al.*, 2013a). Understanding the effects that dietary manipulation has on the intestine's structure and function should increase our knowledge concerning the mechanisms of action involved in dietary manipulation.

1.3. Gastrointestinal tract structure in salmonids

The gastrointestinal tract (GI) of teleosts consists of several distinct regions that differ morphologically and histologically, as well as having distinct physiological functions. The GI tract can be divided into four distinct anatomical regions: the headgut, foregut, midgut and hindgut (Harder, 1975; Wilson & Castro, 2011; Figure 1.1).

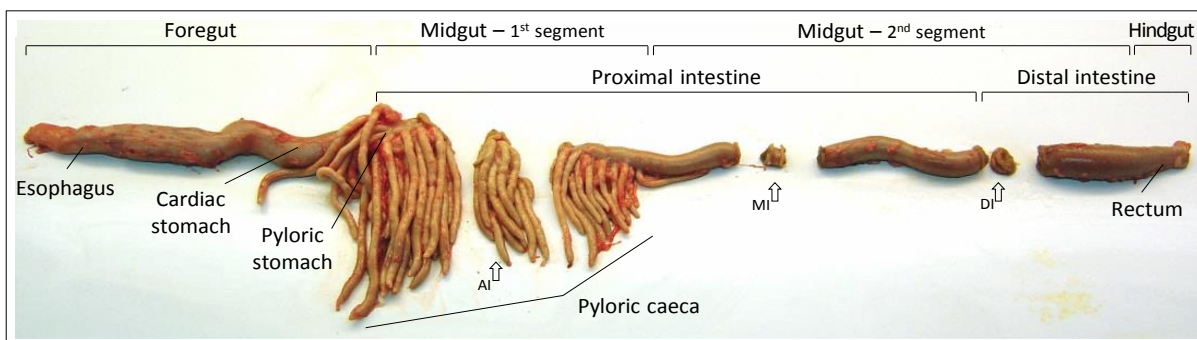


Figure 1.1. Gastrointestinal tract of Atlantic salmon illustrating the different intestinal segments (see Figure 1.5 for respective micrograph sections). (AI) Anterior intestine sample. (MI) Mid intestine sample. (DI) Distal intestine sample.

In most carnivorous fishes, including salmon, the GI is a relatively short and simple tube extending from the headgut. The function of the headgut, is to acquire food and mechanically process it. The food subsequently passes into the foregut, which comprises a

short muscular oesophagus leading into a large U-shaped cardiac stomach, where digestion occurs through chemical and mechanical breakdown of the food. The cardiac sphincter defines the anterior limits of the stomach in the same way that the pyloric sphincter defines the posterior extremity, both controlling the rate at which the *digesta* are released into the next segment, located just posterior to the stomach. This segment is the midgut or intestine, beginning with a cluster of finger-like projections called the pyloric caeca, which provide additional surface area for absorption and may also perform more specialised functions. The midgut displays a short bend at its anterior end and accounts for the greatest proportion of the GI length, being the principal site of chemical digestion and absorption. The final section of the GI is the hindgut, which includes the *rectum*, a straight tube to the vent or anus (Burnstock, 1959; Yasutake & Wales, 1983; Guillaume & Choubert, 2001; Rust, 2002; Løkka *et al.*, 2013).

Despite the various specialised regions of the GI tract, cross-sectional tissue organisation remains fairly similar throughout the tract (Jutfelt, 2006). The teleost's GI wall from foregut to hindgut consists of four concentric tissue layers: (1) the *tunica mucosa*, comprising the epithelium and the *lamina propria*, vascularised connective tissue containing nerves and leucocytes. The epithelium serves as a selectively permeable membrane that separates the body from the external environment (lumen). Additionally, the capillaries present in the *lamina propria* allow the exchange of materials between the host and the outside environment, using the former epithelium as the site of exchange. (2) The *submucosa*, an additional connective tissue layer penetrated by nerves and blood vessels that supports the mucosa. (3) The *tunica muscularis* consisting of circular and longitudinal layers of either striated or smooth muscle, vital for the segmental contractions that mix food items and the peristaltic contractions that propel the chyme in a distal direction. (4) The *tunica serosa* corresponds to an assemblage of mesothelial cells and loose connective tissue containing blood vessels that cover the alimentary canal and other viscera lying within the peritoneal cavity (Buddington & Kuz'mina, 2000; Good, 2004; Wilson & Castro, 2011; Urzúa, 2013; Figures 1.2 and 1.4).

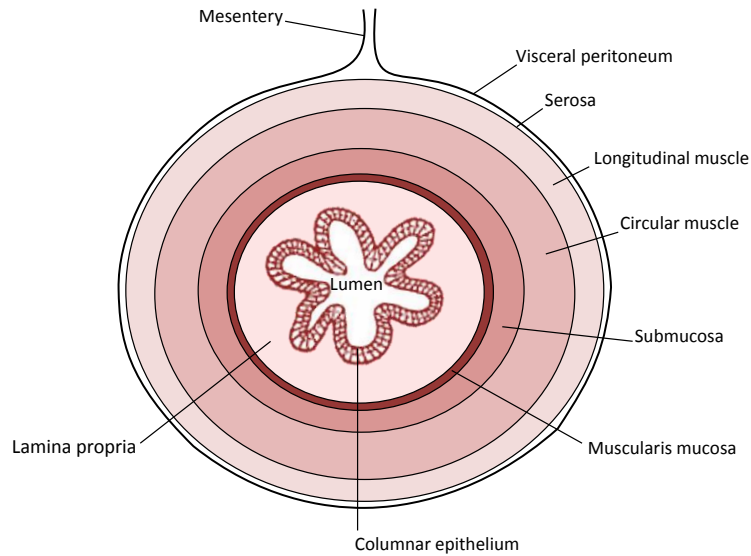


Figure 1.2. The organisation of the tissue layers in the teleosts' gastrointestinal tract (adapted from Buddington & Kuz'mina, 2000).

1.3.1. Intestinal macroscopic anatomy

The intestine of salmonid species is generally divided into two main regions: the upper anterior portion (also called the small, ascending, ileum, midgut or proximal intestine), and the lower posterior portion (also called the large, descending, rectum, hindgut or distal intestine) (Hibiya *et al.*, 1982; Yasutake & Wales, 1983; Rust, 2002). The terminology used by fish anatomists to describe the intestine segments is therefore inconsistent (Guillaume & Choubert, 2001). As a result, sections described as anterior, middle and posterior intestine; duodenum, jejunum and ileum often have different meanings depending on the author. This confusion arises mainly from the absence of obvious external anatomical landmarks, which makes the interpretation from different publications challenging. Nevertheless, for this study authors such as Van den Ingh *et al.* (1991), Baeverfjord & Krogdahl (1996), Krogdahl *et al.* (2003), Sanden *et al.* (2005), Bakke-McKellep *et al.* (2007a), Knudsen *et al.* (2008) and Penn *et al.* (2011) were followed, in naming the anterior portion the “proximal” and the posterior portion the “distal” intestine. Based on the external gross anatomy, the proximal region is more slender and its anterior part has generally 50-70 pyloric caeca, while the distal region is radially larger,

darker and with externally visible transverse blood vessels (Burnstock, 1959; Sundh, 2009; Løkka *et al.*, 2013; Figure 1.1). Internally, the surface area of the intestinal mucosa is arranged and expanded through a series of folds. However, due to the lack of the typical crypt structure in comparison to the mammalian intestine, the terms mucosal or villous folds are currently used to refer to teleosts' epithelial folding (Jutfelt, 2006). The innumerable mucosal folds impart a velvety appearance to the mucosa (Figure 1.3).

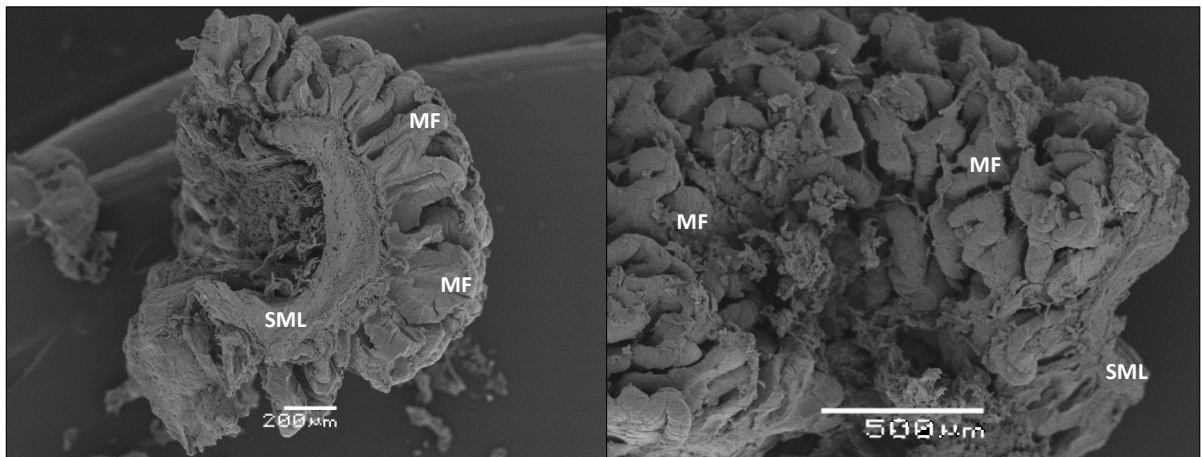


Figure 1.3. Scanning electron microscope (SEM) micrographs of the midgut from Atlantic salmon, showing the luminal appearance of the mucosal folds (MF). Note that intestine samples have an attached *muscularis mucosa* and so when in fixative solution they tend to curl up with their luminal mucosa outwards (ML, Mucosa tissue layer). (SML) Submucosal tissue layer.

The depth and complexity of the folds varies across the different regions of the intestine (Bruno & Poppe, 1996; Buddington & Kuz'mina, 2000). In the first segment of the proximal intestine the folds are irregular and are longitudinally orientated, and where caeca are present, small parallel folds can be seen longitudinally orientated along the length of the caecum. In the same intestinal region, where it is devoid of caeca, the folds have no particular direction of orientation. In most of the anterior region of the distal intestine, large circular and complex folds can be seen oriented transversely with respect to the tract (asterisk in Figure 1.5 C), with simple folds lying in between those oriented longitudinally with respect to the tract (arrow in Figure 1.5 C). In the posterior region of the tract, there is a gradual transition from the large circular folds, similar to those seen in the previous region, to smaller folds with an irregular pattern of folding (Løkka *et al.*, 2013).

1.3.2. Intestinal microscopic anatomy

The basic histology of the Atlantic salmon was first described in detail by Gulland (1898) and has recently been comprehensively reviewed by Løkka *et al.* (2013). The intestinal epithelium of salmonids consists of a single-cell layer of columnar absorptive cells (enterocytes) with a distinctive apical brush border (BBM, Figure 1.6), which greatly extends the surface of the apical membrane, increasing the area available for absorption and exposure of membrane-bound digestive and absorptive enzymes (Jutfelt, 2006; Rust, 2002). The enterocytes are generally tall and narrow, with an elongated nucleus located just below the middle of the cell and are attached to the connective tissue layer of the basement membrane. Although relatively homogeneous in appearance, they show regional differentiation, and in the distal intestine, absorptive cells with larger vacuoles in the apical region are observed (Yamamoto, 1966; Ezeasor & Stokoe, 1981).

Interspersed among the enterocytes are goblet-type mucous cells (Figure 1.4 [4]), which are filled with secretory granules mainly comprising acidic sialomucin mucosubstances, although they also contain smaller amounts of sulfomucins (Wilson & Castro, 2011). The mucus secreted by these cells and other digestive secretions forms a boundary layer that covers the epithelium and is referred to as a glycocalyx (Buddington & Kuz'mina, 2000; Figure 1.6). Other cell types present in between the absorptive enterocytes, especially in the basal region, include immune-associated cells (e.g. lymphocytes and macrophages), and cells containing cytoplasmic granules which appear to have secretory functions *i.e.* eosinophilic granule cells (Holmgren & Olsson, 2009).

Underlying the simple columnar epithelium is the *lamina propria*, a layer that is largely comprised of a capillary network embedded in connective tissue (Sundh, 2009; Figure 1.4 [8]). Embedded in the *lamina propria* is the prominent *stratum compactum* (Figure 1.4 [5]), a thick, often folded, layer of non-cellular fibrous material. Under this, is a layer of granule cells (*stratum granulosum*; Figure 1.4 [6]), which can vary in thickness within the same section (Jutfelt, 2006). The remainder of the *lamina propria* is composed of collagenous tissue which merges with the inner region of the muscular layer (Figure 1.4 [7 and 8]),

consisting of a thick inner circular region separated from a thin, outer longitudinal region by a layer of connective tissue of varying thickness (Bullock, 1963; Figure 1.2).

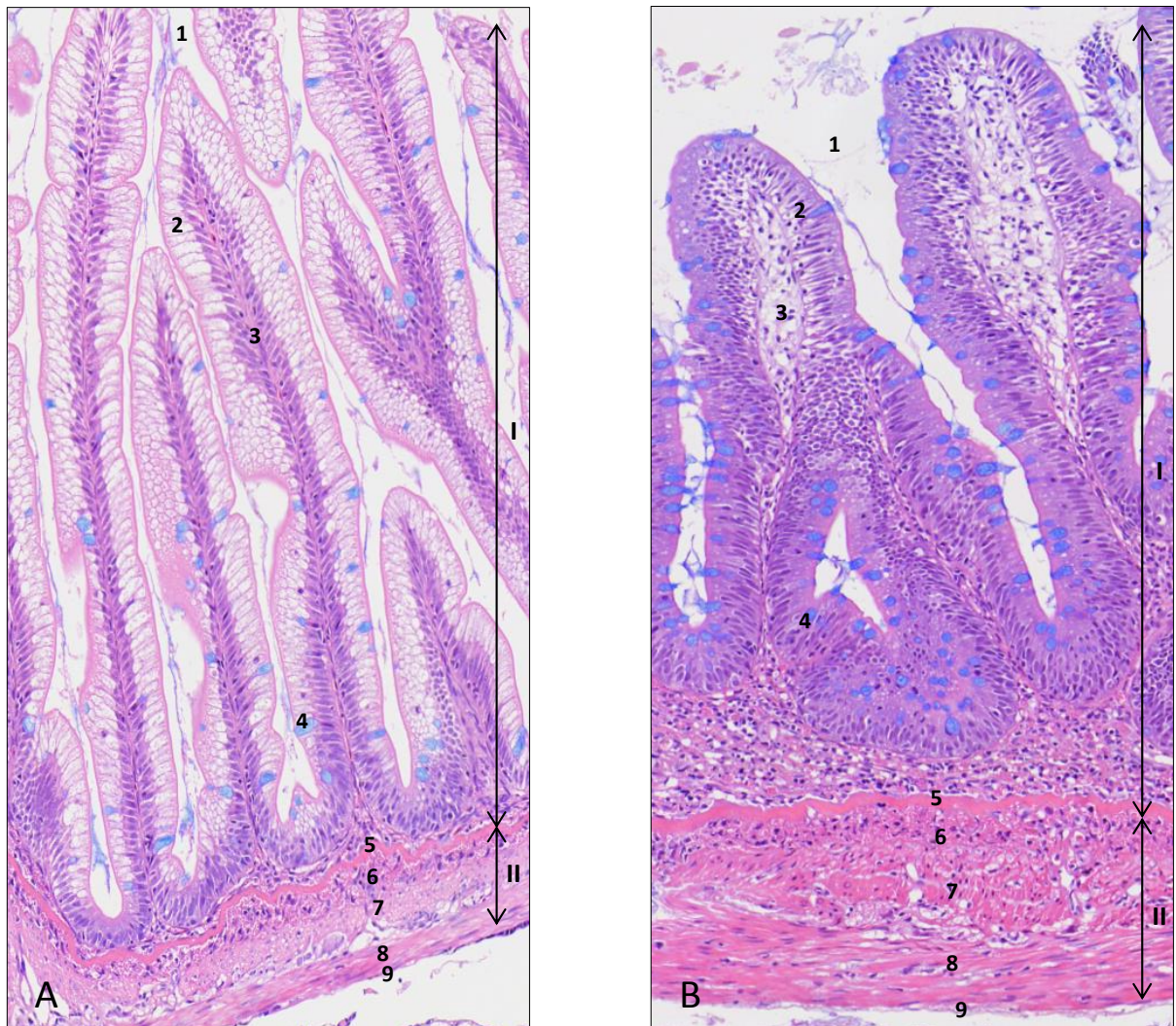


Figure 1.4 Photomicrographs of the Atlantic salmon distal intestine illustrating the general tissue organisation and the morphological tissue variations encountered across two different histological grades: (A) normal morphology, (B) moderate inflammation to severe enteritis. (I) Mucosa (II) Submucosa¹ (1) Lumen (2) Columnar epithelium (3) *Lamina propria* (4) Mucous cell (5) *Stratum compactum* (6) *Stratum granulosum* (7) Circular muscle (8) Longitudinal muscle (9) Serosa. Transverse intestinal sections were stained with a combination of haematoxylin-eosin and Alcian blue 8 GX.

¹ Term commonly used in all fishes, although technically a submucosa is only present in the groups with a mucosal smooth muscle layer, which excludes the teleost fish (Burnstock, 1959; Wilson & Castro, 2011). However, throughout this thesis, the muscle layer contributing to the longitudinal primary folds has been described as *muscularis mucosa*, whereas the layer of connective tissue separating this musculature from the *muscularis* has been designated submucosa, as recently described in the review of Løkka *et al.* (2013).

In the proximal intestine, the epithelium and the *lamina propria* are organised into small folds, which have a tendency to branch. The *stratum compactum* and *stratum granulosum* are not part of the folds but rather organised underneath them (Figure 1.5 A). Along the anterior region of the distal segment, complex circular folds comprise the epithelium, *lamina propria*, and a core of circularly-arranged smooth musculature, whereas the *stratum compactum* extends a short distance into the base of such folds. The secondary folds of the complex folds and the simple folds (triangles and arrow in Figure 1.5 C, respectively) are comprised of epithelium and *lamina propria* (Figure 1.5 C). The folds at the end of this segment have the same histological arrangement as in the proximal intestine, although they are a bit more irregular in appearance (Løkka *et al.*, 2013).

Lastly, the perimeter of the intestine is covered by the serosa, which is a thin layer of connective tissue continuous with the mesenteric tissue, and may contain adipose tissue and blood vessels (Bullock, 1963; Figure 1.4 [9]).

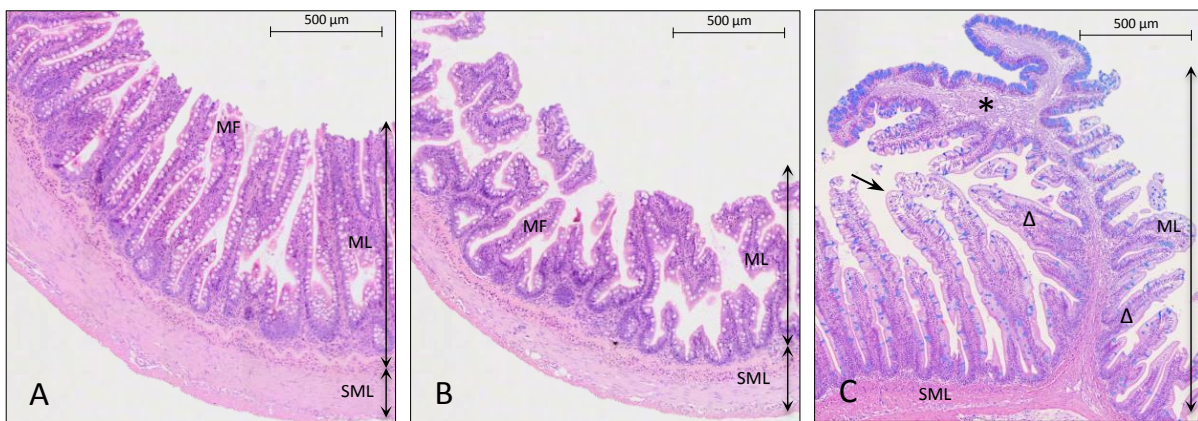


Figure 1.5. Digital-scan photomicrographs of transverse sections of the intestinal tract of Atlantic salmon, stained with haematoxylin-eosin (A & B) and with a combination of haematoxylin-eosin and Alcian blue 8 GX (C). (A) Section from the anterior region of the proximal intestine, with pyloric caeca. (B) Section from the posterior region of the proximal intestine. (C) Section from anterior region of the distal intestine with complex (asterisk) and simple mucosal folds (arrow). The complex folds are organised into simple secondary folds (triangles). (ML) Mucosal tissue layer. (SML) Submusocol tissue layer. (MF) Mucosal folds.

1.3.3. Intestinal surface area

Salmonids and some other teleost fish have specialised anatomical structures called pyloric caeca (Figure 1.1) that are blind diverticuli of the most anterior (proximal) part of the intestine, and are considered to be an extension to the surface area of intestine, the purpose of which is to increase the absorptive surface area of the digestive tract (Guillaume & Choubert, 2001). Similarly, the mucosa of the intestine is arranged into complex folds, which greatly increase the total intestinal surface area, compared to that of a smooth bore layer (Buddington & Kuz'mina, 2000). Additionally, the enterocyte cellular membrane that borders the lumen is highly folded into thousands of microvilli (Figure 1.6) forming an apical brush border that increases the exposed area, relative to areas with unfolded membranes (Buddington *et al.*, 1997; Rust, 2002). The stated consequence of these distinctive structural arrangements is that they can accommodate much more membrane than flat surfaces and have much greater capacity for accommodating various cell types, membrane-bound transporters and channels that endow the intestinal epithelium with its multifunctional properties.

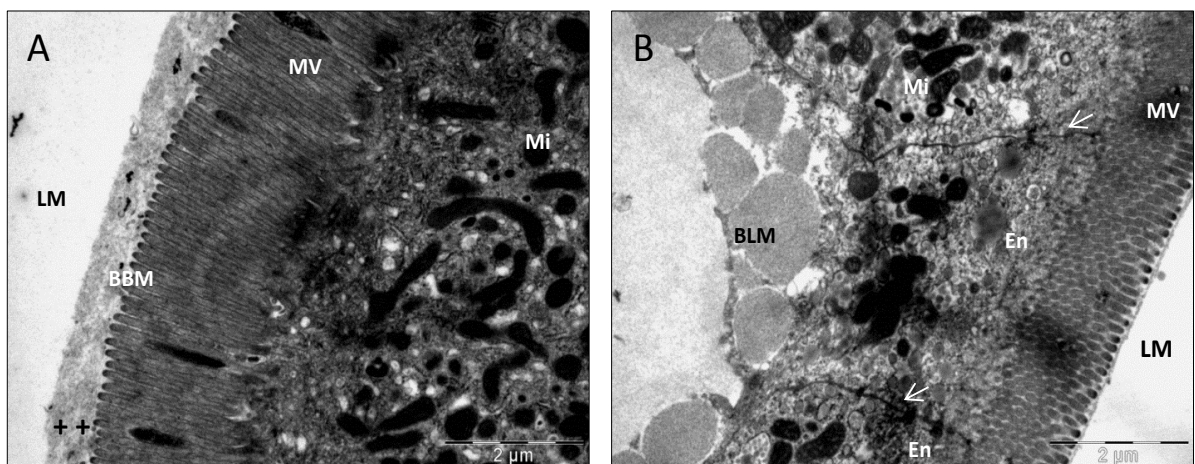


Figure 1.6. Transmission electron microscope (TEM) micrographs of the midgut from Atlantic salmon, showing apical cytoplasm of absorptive cells. (A) Section from fish fed a fish meal based control diet. (B) Fish fed a diet with inclusion of immunostimulant ingredients. (LM) Lumen (Mi) Mitochondria (MV) Microvilli (BBM) Brush border membrane (BLM) Basolateral membrane (En) Enterocyte (arrows) Junctional complex (++) Glycolyx.

1.3.4. Anatomical homeostasis of the intestine

Under normal homeostatic regulation of the intestinal epithelium, cells that constitute the epithelium are constantly being replaced, with controlled cell proliferation and regulated cell death (apoptosis) being central features in maintaining intestinal integrity (Ronza *et al.*, 2011). The intestinal epithelium includes three basic cell types (*i.e.* the enterocytes, mucous secreting goblet cells and enterochromaffin cells with distinct endocrine functions), all of which are formed at the base of the mucosal folds from pluripotent stem cells. As they migrate out from this region, they differentiate and become functionally competent (Buddington *et al.*, 1997). The fully differentiated cells migrate to the tips of the folds where they are subsequently shed (Hall *et al.*, 1994a, 1994b; Sanden & Olsvik, 2009). Consequently, when rates of cell proliferation exceed the rate of shedding, the mucosal folds grow in length, whereas when the rate of shedding is greater than that of cell replacement, they shorten.

Perturbation of intestinal homeostasis and damage to the intestinal epithelium has been suggested to result from apoptosis or necrosis following pathogen entry into the epithelial cells, but has also been demonstrated to be instigated by anti-nutritional dietary products such as dietary inulin and copper (*e.g.* Berntssen *et al.*, 1999; Olsen *et al.*, 2001; Olsvik *et al.*, 2007; Ringø *et al.*, 2007). Furthermore, it has been shown that a disruption of the epithelial layer may trigger deregulated inflammatory responses against foreign antigens, which may eventually lead to chronic intestinal inflammation. These observations emphasise the importance of preserving the integrity of the intestinal epithelium (Urzúa, 2013). Thus, although the continuous epithelial cell turnover is costly in terms of energy and nutrient expenditure, it is justified by the need to remove impaired / compromised cells and maintain tissue integrity through the proliferation of new cells and remodelling of connective tissue.

1.4. Multifunctional properties of salmonid intestine

The salmonid intestine is a complex, multifunctional organ. In addition to providing digestive enzymes and other components necessary to ensure optimal digestion of the

chyme and delivery of nutrients for absorption by the intestinal mucosa, the intestine is critical for protecting the intestinal mucosa from harmful dietary components as well as from the alimentary tract's own acid, alkaline and enzyme secretions. The intestine plays an important role in protecting the organism against microbes and chemicals that may be detrimental to the animal's health and well-being, and in maintaining water and electrolyte balance (Bakke *et al.*, 2011). Furthermore, it also functions in the elimination of toxins, waste and other metabolic products. A further aspect that might impact the intestine as much as any of the previously mentioned properties, is the resident microbiological flora (*e.g.* Nayak, 2010; Abid *et al.*, 2013), which was found to stimulate epithelial proliferation, the promotion of nutrient metabolism and the innate immune response (Navarrete *et al.*, 2013). Amongst the properties described, three distinct functions *i.e.* intestinal nutrient absorption, enteric barrier function and osmoregulation / water uptake, have been highlighted as areas of interest for investigation in the current thesis.

1.4.1. Nutrient processing and absorption

The intestinal tract is the main site of nutrient absorption in the gastrointestinal system of teleosts, and it follows that many of the morphological features described reflect the function of tissues in this process. The outer, apical membrane of the intestinal epithelium, which is exposed to the luminal contents, contains many different enzymes that complete the final stages of hydrolyzing water-soluble nutrients, and a set of proteins known as co-transporters that are responsible for absorbing the constituent building blocks. The other domain, known as the basolateral membrane (BLM, Figure 1.6 and 1.7), contains another set of functional proteins, including a different group of carrier proteins involved in the transport of absorbed nutrients across the basement membrane from whence it reaches the blood (Buddington & Diamond, 1987; Collie & Ferraris, 1995; Buddington & Kuz'mina, 2000). Ultimately, the ability of the intestine to hydrolyse and absorb dietary protein is, to a large extent, related to the total amount of surface area and rates of absorption per unit area. Therefore, the elegant structure of the intestine (*i.e.* presence of pyloric caeca, more complex mucosal architecture together with the microvilli of the epithelial cells), greatly

extends the surface area of the intestinal epithelium, increasing the interface available for absorption and quantities of membrane-bound enzymes, both important for enzymatic breakdown and absorption of feed constituents (Harder, 1975; McLean *et al.*, 1999; Bakke-McKellep *et al.*, 2000a; Denstadli *et al.*, 2004; Løkka *et al.*, 2013; *inter alia*).

The mechanisms of nutrient-uptake across the brush border membrane (BBM, Figure 1.7) of the intestinal epithelial cells in fish have been extensively reviewed by Collie & Ferraris (1995) and more recently by Jutfelt (2006) – Figure 1.7 A and B. In brief, besides endocytosis² and paracellular movement³, there are three basic mechanisms of nutrient absorption by enterocytes. These include: (1) passive diffusion independent of carriers, (2) transport by carriers that are independent of ion gradients, and (3) transport by energy dependent carriers that are coupled to ion gradients (Bakke-McKellep *et al.*, 2000a). The diffusion rate of nutrient molecules increases linearly with their concentration, whereas transport by membrane transporters becomes saturated at higher concentrations. Additionally, the energy for nutrient uptake against a charged gradient can be harnessed from ions (usually Na⁺) moving within an electrochemical gradient (Jutfelt, 2006).

In carnivorous fish, the intestinal portions of the digestive tract show histological features that reflect differentiation in nutrient absorption (Abaurrea-Equisoain & Ostos-Garrido, 1996). The first segment of the proximal intestine is believed to be the main site for nutrient uptake, whereas the distal region has less nutrient absorptive capacity and more endocytic activity (Buddington & Diamond, 1987; Hart *et al.*, 1988; Fanning *et al.*, 1999; Nordrum *et al.*, 2000b). Accordingly, the proximal portion has extensive elongated mucosal folds that are not apparent in the distal regions, and the mucosal folding further extends the absorptive surface area (Schep *et al.*, 1997). In addition, the abundance of mitochondria, well-developed basal folds, and the thickness and complexity of the basal lamina in the absorptive cells from the anterior region are consistent with proposed active absorption of

² **Endocytosis** is the process by which substrates enter a cell through the invagination of the cell membrane and the formation of intracellular vesicles, all of which takes place without passage through the plasma membrane.

³ **Paracellular transport**, refers to the transfer of substances across an epithelium by passage through the intercellular space between the cells. This contrasts to the trans-cellular transport route, where the substances are transferred through the cell, passing across the apical and basolateral membranes.

lipids, glucose, amino acids and small peptides by diffusion (Sire & Vernier, 1981; Ferraris & Ahearn, 1984; Abaurrea-Equisoain & Ostos-Garrido, 1996; Figure 1.7 B). In contrast, enterocytes from the posterior segment (distal intestine), display large numbers of apical pinocytotic vesicles, numerous vacuoles and lysosomes indicative of the fact that this region of the intestine is specialised for the uptake, through phagocytosis, of intact larger peptides and protein macromolecules (Ezeasor & Stokoe, 1981; Georgopoulou *et al.*, 1988; McLean & Donaldson, 1990; Vernier & Mellinger, 1990; Sire & Vernier, 1992; Abaurrea *et al.*, 1993; Bakke *et al.*, 2011; Figure 1.7 A). Similarly, the activities of various brush border proteases that perform the final stages of hydrolysis, vary along the length of the intestine, with activity tending to be highest in the mid regions where concentrations of substrates could be greater (Buddington *et al.*, 1997).

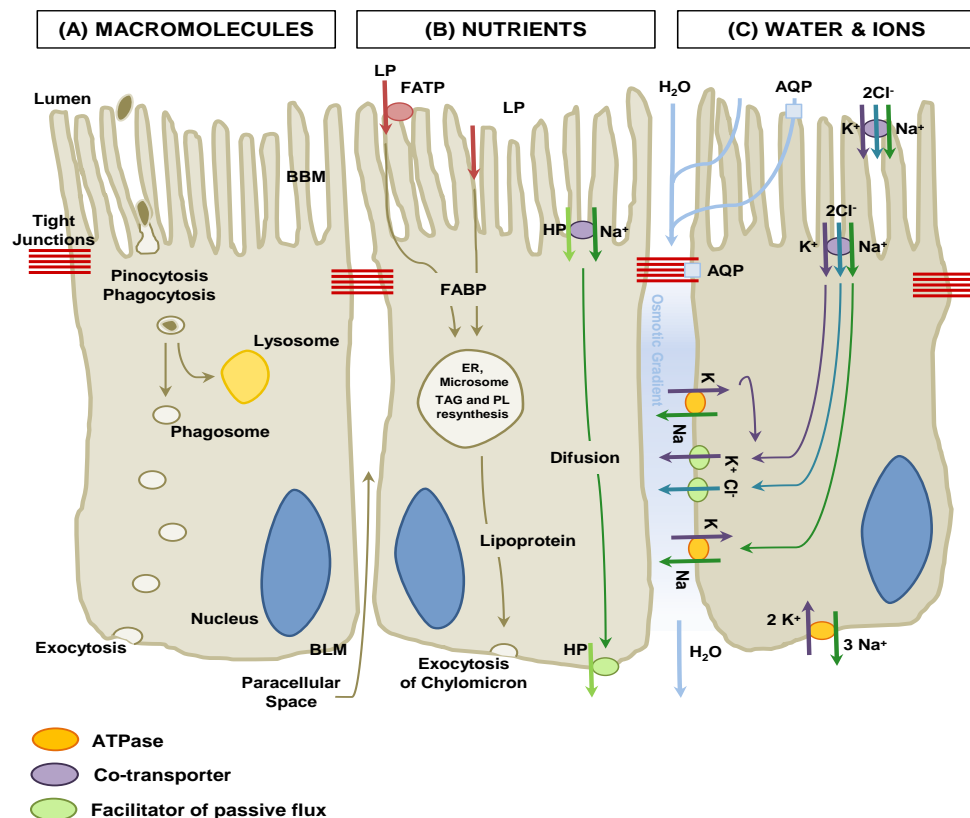


Figure 1.7. Schematic diagram showing the intestinal transepithelial transport occurring in fish intestines (adapted from Jutfelt, 2006). (A) Transepithelial transport of particles and macromolecules is initiated by phagocytotic or pinocytotic processes occurring at the brush border membrane (BBM): phagosomes are then transported either to digestive lysosomes or through the cell to the basolateral membrane (BLM) where exocytosis occurs. (B) Transepithelial transport of nutrients: lipophilic

1.4.2. Enteric barrier function

Adhesion to, and penetration through mucosal surfaces represents the primary portal of entry for many pathogens. Therefore, the intestine must establish a delicate balance between efficient absorption of nutrients and prevention of pathogen invasion and ingress of noxious components present in the diet or environment (Buddington *et al.*, 1997; Fuglem *et al.*, 2010). To meet these demands, the intestine possesses a selective and complex epithelial barrier. This barrier function works in conjunction with innate and adaptive immune responses, that together constitute the mucosal immune system (Cain & Swan, 2011).

1.4.2.1. *Extrinsic supra-epithelial barrier.* The glycocalyx covering the intestinal epithelium is predominantly composed of mucin glycoproteins released from epithelial mucous cells that are scattered along the epithelium (Shephard, 1994), although some components within the mucus may be produced elsewhere (Niklasson, 2013). Furthermore, the glycocalyx contains reactive oxygen species, hydrogen peroxidase, lysozyme, pro-inflammatory cytokines, complement factors and a broad range of secretory immunoglobulins and antimicrobial peptides (AMPs) (Roberts, 1989; Good, 2004; Urzúa, 2013). Therefore, this viscous layer is able to provide a physical and biochemical barrier which protects the underlying epithelial layer against mechanical and chemical damage, natural aggressors and other exogenous harmful agents (Buddington *et al.*, 1997; Sweetman *et al.*, 2010). It can act as a lubricant, aiding transport between the luminal

Figure 1.7. (continued from previous page) molecules (LP) cross the BBM by diffusion over the lipid bilayer and through fatty acid transport proteins (FATP). Triacylglycerol (TAG) and phospholipid (PL) resynthesis occurs in the endoplasmic reticulum (ER) before lipoprotein packaging and export of chylomicrons through exocytosis at the basolateral membrane takes place. Hydrophilic nutrients (HP), such as amino acids and glucose cross the BBM by secondary active transport (sodium co-transport is shown) and cross the BLM through the intervention of carrier proteins. (C) Na^+K^+ -ATPase activity at the BLM remove intracellular Na^+ . The NKCC co-transporter carries 2 Cl^- , Na^+ and K^+ across the BBM. Cl^- and K^+ exit through ion channels across the BLM. The osmotic gradient created in the paracellular space, with the highest osmolality, apically drives water diffusion transcellularly and through tight junctions. Aquaporins (AQP) may increase the BBM and / or BLM water permeability.

contents and the epithelial lining (Cain & Swan, 2011), as well as a diffusion medium that reduces the ability of pathogens to adhere and penetrate the underlying enterocyte cells (Verlhac & Kiron, 2004; Van der Marel *et al.*, 2014). Other components present in the mucus *e.g.* such as AMPs or complement factors, can opsonise pathogens to aid their uptake by macrophages, or, in the case of inflammatory cytokines and interferons, lead to the production of anti-viral proteins. These together, help to prevent the brush border membrane becoming colonised or invaded by infectious agents (Jutfet, 2006; Niklasson, 2013).

1.4.2.2. *Enteric epithelial barrier.* Intestinal enterocytes are a highly specialised cell type that not only function as a primary site of nutrient processing and absorption, but act as a very efficient physical barrier against invasion by a broad spectrum of foodborne pathogens or enteric resident microbiota, while allowing passage of nutrients to the systemic circulation (Mooseker, 1985; Torrecillas *et al.*, 2011). Their structure is thought to contribute to their function in regulating permeability. Adjacent enterocytes are joined together at the apical end of the lateral surface by several tight junctions (TJs; arrows in Figure 1.6) consisting mainly of protein complexes (*i.e.* claudins, occludins and the cytosolic proteins *zonula occludens* ZO-1, ZO-2 and ZO-3), which join the transmembrane proteins to the cytoskeletal actin of the enterocytes, forming a belt of anchoring adhesion that holds the epithelium together and regulates the permeability of the intestine to hydrophilic molecules and extraneous organisms (Jutfelt, 2006; Sundh, 2009). Alterations of the TJ protein formation and distribution through dephosphorylation of occludins, redistribution of ZO or alterations of actomyosin filaments, may affect the size and charge of the monolayer membrane pores handling the paracellular pathway and therefore their absorptive capability (Niklasson, 2013).

1.4.2.3. *Intrinsic sub-epithelial barrier.* The intestinal mucosa, particularly the gut associated lymphoid tissue (GALT), represents one of the first-line defences against invading microorganisms (Gomez *et al.*, 2013). Although recently, an antigen-sampling cell phenotype (*i.e.* cells with mammalian micro-fold dendritic cell morphology; or M-cell

analogues) was localised in the base regions of the mucosal folds (Fuglem *et al.*, 2010), there is no conclusive evidence that teleost fish possess specialised lymph nodes or Peyer's patches (Rombout *et al.*, 1993). Nonetheless, it has been suggested that the fish intestine is immuno-competent irrespective of the presence of such structures. Their enteric immune system contains no follicular lymphoid structures (Dalmo *et al.*, 1997; Press & Evensen, 1999), but rather a more diffusely distributed GALT consisting of a unique array of innate and adaptive cellular and humoral defence mechanisms that act together to protect the host by eliminating infected cells and attracting other immune cells (Nayak, 2010; Cerezuela *et al.*, 2013). Immune cells associated with the GALT include: populations of leucocytes and lymphocytes, plasma cells, macrophages, mast-cells, granulocytes and neutrophils (Zapata & Amemiya, 2000; Tort *et al.*, 2003; Bakke-McKellep *et al.*, 2007a; an updated review on the teleost fish GALT, including the description of all the immune cell types present has recently been published Rombout *et al.*, 2011).

Similar to other intestinal functions, there are regional differences in the distribution of those immune cells. For instance, in contrast to macrophages, which dominate in the epithelium of the posterior intestine, basophilic and eosinophilic granulocytes are mainly found in the connective tissue of the anterior segment (Rombout & Berg, 1989). Structural evidence suggests that cells in the posterior region of the intestine have higher phagocytic activity than those in the anterior region of the fish intestine. This also includes higher levels of antigen sampling by transferring antigen from the lumen to macrophages or neutrophils in the epithelium and *lamina propria* (Jutfelt, 2006), suggesting that this might be the primary site where immune responses are initiated and thus explains why the highest densities of intraepithelial antigen presenting cells, such as macrophages and neutrophils, are found in the distal intestine (Buddington *et al.*, 1997; Cain & Swan, 2011).

Cells involved in innate immunity can often recognise common molecular structures on pathogens and commensal bacteria through interactions with pattern recognition receptors on their cell surface (Gomez *et al.*, 2013). This cellular intervention requires no antigenic priming and could be either immediate or induced within a short time following an encounter

with foreign antigens (Cain & Swan, 2011). Upon activation, it mediates intracellular signalling cascades resulting in the production of pro-inflammatory cytokines and chemokines for recruitment of phagocytes such as macrophages, neutrophils and other granulocytes for clearance of the recognised pathogen (Sundh, 2009). Bacterial pathogens encountered by macrophages and neutrophils are phagocytosed and destroyed (Neumann *et al.* 2001). Degradation of phagocytosed pathogens can occur via respiratory burst activity, or phagocytes may produce proteins and peptides that have antimicrobial properties and act directly on pathogens (Neumann *et al.* 2001). Furthermore, enzymes and cellular proteins that are released from damaged host cells can prompt phagocyte influx and an inflammatory response (Magnadottir, 2010).

Adaptive immunity is critical to long-term protection from specific pathogens. Compared to the innate response, the adaptive response is much slower to develop, but can be directed at antigens specific to a pathogen and result in immune memory for that antigen (Verlhac & Kiron, 2004). Therefore, once a pathogen or other foreign substance is phagocytosed and digested, its cell surface antigenic epitopes are recognised by B or T lymphocytes, resulting in cytokine and other humoral factor release, which in turn stimulates additional T and B cells to the site of damage / infection. Thereafter, B cells will proliferate and begin to differentiate, resulting in the production of antibody-secreting plasma cells and memory B cells (Cain & Swan, 2011). Finally, activation of these cells can lead to the development of antigen-specific antibodies or immunoglobulins (Ig), which can eventually bind to conforming antigens and eliminate them from the system via neutralisation, agglutination, opsonisation and activation of the complement system (Gomez *et al.*, 2013). In fish, IgM is the principal antibody found in the serum and mucosa associated with intestinal lymphoid tissues, although other isotypes including IgD, IgT, IgZ and chimeric IgM-IgZ have been identified in various fish species (Hordvik *et al.*, 1999; Hordvik, 2002; Rombout *et al.*, 2011; Tadiso *et al.*, 2011).

Finally, the complement system serves as part of the humoral defences and represents a biochemical cascade that is involved both in innate and acquired immune system responses and is often the linking factor connecting both systems (Urzúa, 2013).

1.4.3. Osmoregulation and epithelial water transport

The intestinal epithelium of teleosts has an established role in osmoregulation, and its ability to effectively (re)absorb fluid is crucial to replenishing losses of water and electrolytes during routine physiological processes such as digestion and also to coping with dehydrating hyperosmotic environments (Buddington *et al.*, 1997; Marshall & Grosell, 2006; Whittamore, 2012).

In the intestine of marine fish, osmotic water absorption across the luminal epithelium may occur transcellularly and / or paracellularly between enterocytes through distinct routes: (1) driven by passive diffusion across the lipid bilayers; (2) co-transport of ions with nutrients, or by (3) diffusion through aquaporins (AQPs) within the membranes (Madsen *et al.*, 2011; a thorough and detailed review of osmoregulation and epithelial water transport from the intestine of marine teleost fish, has recently been published by Whittamore (2012); Figure 1.7 C). Regardless of the pathway used, water absorption is tightly linked to trans-epithelial monovalent ion transport, which creates a hyperosmotic gradient in the lateral interspace between enterocytes, causing water diffusion trans-cellularly and through the tight junctions (Usher *et al.*, 1991; Grosell, 2006, 2011). In addition, AQPs may serve as passive conduits for water movement in response to a transmembrane osmotic gradient, reducing the activation energy required for dissolution and diffusion of water molecules through co-transporters (Whittamore, 2012). Information on the identity, localisation and regulation of AQP in teleosts is still rather fragmentary. Currently, three AQP isoforms have been found in the intestinal tract of Atlantic salmon (*i.e.* Aqp1aa/ab, Aqp8ab and Aq3; Tipsmark & Madsen, 2012), and only Aqp1aa/ab have been localised in enterocytes and are thus suggested to be directly associated with water transport (Madsen *et al.*, 2011).

1.5. Diet mediated modulation and enteric integrity

Stimuli such as fasting (Baeverfjord & Kroghdahl, 1996; Kroghdahl & Bakke-McKellep, 2005; Ostaszewska *et al.*, 2006), stress (Hall & Bellwood, 1995; Olsen *et al.*, 2002, 2005), infection (Hemmer *et al.*, 1998; Ringø *et al.*, 2004; Ringø *et al.*, 2007; Del-Pozo *et al.*, 2010; Ronza *et al.*, 2011) and toxins (Crespo *et al.*, 1986; Kamunde *et al.*, 2001; Berntssen *et al.*, 2004; Glover *et al.*, 2007) have been shown to cause changes in the turnover of intestinal epithelial cells, which in turn can result in changes in proliferative activity, migration and apoptosis of structural and functional cells. A further factor that might impact the intestine as much as those mentioned above, is the resident microbiological flora and interrelated dietary modulation, which have also been found to stimulate epithelial proliferation and promote innate immune responses (*e.g.* Sanden *et al.*, 2005; Heikkinen *et al.*, 2006; Bakke-McKellep *et al.*, 2007b; Ringø *et al.*, 2007; Urán *et al.*, 2009a; Dimitroglou *et al.*, 2010; Nayak, 2010; Merrifield *et al.*, 2010; Abid *et al.*, 2013; Chikwati *et al.*, 2013b; Navarrete *et al.*, 2013).

1.5.1. Evaluation of the effects of nutritional modulation on fish intestinal health

Intestinal immune responses are multifaceted and involve a broad range of different effector molecules, receptors and cells (Verlhac & Kiron, 2004). Thus the assessment of immune modulation in relation to nutrition should be undertaken using a multi-pronged approach whereby an array of parameters that are indicative of the responses are evaluated, instead of measurement of only a single cellular function or tissue structural change (Trichet, 2010).

Fish health can be assessed using morphological, microbiological, haematological and / or immunological assays, as well as experimental disease challenges and vaccination. Various assays have been used to assess changes in physiological status or health of the intestine of fish that result from dietary modulation. Table 1.1 summarises some of the different methods that are currently used in nutritional research. Their sensitivity, ease of application, and rapidity are also mentioned. Depending on the potential target being examined to assess the effects of dietary modulation, different parameters could be chosen

as shown in Table 1.1. Ideally, the assessment of responses should cover a range of parameters ranging from whole fish response to events occurring at the tissue or cellular level (Kiron, 2012), selecting appropriate procedures and indices of health condition, which are objective, sensitive, precise, reproducible, rapid and cost-effective.

Table 1.1. Types of assessment employed in nutritional studies of fish, and their level of suitability (adapted from Verlhac & Kiron, 2004).

Parameters	Assay methodology	Sensitivity	Variability	Ease
Body condition factors	- Direct measurement of external body characteristics	Fair	Medium	Fair
Organosomic indices	- Direct measurement of internal organs	Medium	Medium	Fair
Microflora	- Bacterial culture and phenotypic identification	Medium	Wide	Fair
	- Bacterial culture and genotypic identification	High	Fair	Moderate
	- DGGE (denaturing gradient gel electrophoresis) and TGGE (temperature gradient gel electrophoresis) profiling gels	High	Fair	Complicate
	- Pyrosequencing	High	Fair	Complicate
Peripheral blood parameters	- Direct counting of diluted fresh samples	Fair	Medium	Fair
	- Staining of smears or cytocentrifuged cells	Medium	Medium	Fair
	- Flow cytometry	High	Medium	Moderate
	- Automatic analyser	High	Medium	Fair
Blood cells from mucosa associated tissues	- Percoll gradients and direct counting	Medium	Medium	Moderate
Lymphocyte proliferation	- Uptake of tritiated thymidine	High	Wide	Fair
	- Flow cytometry	High	Medium	Moderate
	- Tetrazolium	High	Medium	Moderate
Lymphocyte differentiation	- Radioimmuno-assay	Medium	Medium	Complicate
	- Mitogenesis	Fair	Wide	Fair
Chemotaxis	- Migration test in specific chambers and macroscopic observation	High	Medium	Complicate
Phagocytosis	- Staining and microscopy observation	High	Wide	Moderate
	- Flow cytometry	High	Medium	Moderate
	- Fluorescence	High	Medium	Complicate
Oxidative burst	- Flow cytometry	High	Medium	Moderate
	- Chemiluminescence with isoluminol, luminol or colorimetric assay	High	Medium	Complicate
Non specific cytotoxicity	- Chromium release assay	Fair	Wide	Moderate
	- Time resolved fluorescence	Fair	Wide	Moderate
	- Flow cytometry	Medium	Medium	Moderate
	- Lactate dehydrogenase assay	Medium	Wide	Moderate
Lysozyme	- Turbidimetry	Medium	Medium	Fair
	- Fluorimetry	Medium	Medium	Medium

Table 1.1. (continued from previous page)

Parameters	Assay methodology	Sensitivity	Variability	Ease
Complement	- Spectrophotometry	High	Wide	Fair
Specific antibody	- Passive haemolytic assay	High	Narrow	Moderate
	- ELISA (enzyme-linked immunosorbent assay)	High	Narrow	Moderate
	- Haemopoiesis	Medium	Medium	Moderate
	- IFAT (indirect fluorescent antibody techniques)	High	Narrow	Moderate
	- IHC (immunohistochemistry)	Medium	Medium	Moderate
Total immunoglobulin	- Spectrophotometry	Low	Medium	Moderate
	- Diffusion in gel techniques	Low	Medium	Moderate
Histomorphology	- Histochemical / IHC staining, microscopic observation and qualitative assessment	High	Medium	Moderate
	- Histochemical / IHC staining, microscopic observation and semi-quantitative scoring	High	Medium	Fair
	- Histochemical / IHC staining, microscopic observation and quantitative scoring	High	Narrow	Fair

Carefully designed infection or stress challenge experiments, where fish fed with different dietary treatments are later exposed to a pathogen or a stressful event (*i.e.* resulting in mortalities as an end point or post-exposure stress indication), are a means to study and to better understand integrated host-defence mechanisms, in terms of the animal's ability to resist disease or stress (Kiron, 2012). And, although regulated by the Animals Scientific Procedures (ASP, Act 1986) that animal experimentation should only be permitted when no other alternative research technique is available and that the expected benefits outweigh any possible adverse effects, the above mentioned approach is often employed in fish nutrition studies. Still, the reliability of such studies is very much dependent on reproducibility of experimental conditions and outcomes (Kiron, 2012).

Evaluation of fish health condition by observations and measurements of external characteristics and internal organs, which allow the calculation of generalised condition factors or organosomic indices is straightforward, however it is limited in terms of sensitivity and precision (Maita, 2007).

The fish intestinal bacterial community has traditionally been characterised by use of culture-dependent methods, followed by identification according to phenotypic and genotypic characteristics (Austin, 2006; Nayak, 2010). However, these methods have been

described as labour intensive, poorly reproducible and not suitable for the analysis of multiple samples. The use of genotyping fingerprint methods (*e.g.* DGGE, denaturing gradient gel electrophoresis; TGGE, temperature gradient gel electrophoresis) combined with culturing methods became extensively used in the past. A current rapid and more precise classification of large numbers of isolated bacteria has been reported in fish microbial studies by using random amplified polymorphic DNA (RAPD) and restriction fragment length polymorphism (RFLP) analyses (Urzúa, 2013).

Measurement of peripheral blood and plasma parameters is relatively easy to perform and can be carried out without killing the animal. Haematological characteristics such as haematocrit value (Hct), haemoglobin concentration (Hb) and red blood cell counts (RBC) have been examined to evaluate requirements for certain dietary micronutrients, and the quality of feed or feeding strategies (Maita, 2007). Complementary information gathered through other blood indices such as mean corpuscular volume (MCV), mean corpuscular haemoglobin (MCH) and mean corpuscular haemoglobin concentration (MCHC) may be also useful (Blaxhall & Daisley, 1973).

Blood- or serum-based assays constitute yet another battery of measurements that are frequently used to evaluate primarily innate immune responses. Humoral components commonly examined include complement activity, lysozyme activity, total immunoglobins, acute phase proteins and cytokine levels. In teleost fish, alternative complement activity is a fairly reliable indicator of humoral defence, though its measurement involves a tedious process (Verlhac & Kiron, 2004). Assessing the function of phagocytes is another measure of the animal's disease resistance. Phagocytic activity of cells harvested from the immune organs such as head kidney, spleen or intestine of fish subjected to different dietary treatments, is usually determined by ingestion of inert or antigenic particles. This can be measured either by microscopy or flow cytometry. While the former is a simple technique, the latter is preferred for its sensitivity. Phagocytic killing mechanisms can be assayed among others by measuring the oxygen radical production either spectro-photometrically or by flow cytometry (Verlhac & Kiron, 2004; Kiron, 2012), both techniques having very high

sensitivity. Lysozyme measurements by turbidimetry and fluorimetry on the other hand, tend to be less consistent or sensitive than the techniques mentioned above (Stolen *et al.*, 1990). Specific immune responses can be evaluated by measuring antibody production either by the relatively straightforward technique of passive haemolytic plaque assay or more quantitatively by determining antibody titres by employing techniques such as agglutination, precipitation or ELISA (enzyme-linked immunosorbent assay). Although the latter method measures a response fairly accurately, it has to be standardised thoroughly for the species and pathogen in question (Verlhac & Kiron, 2004). Lymphocyte proliferation is also a highly representative assay for acquired immune cell functions and can be employed to determine the overall responsiveness of T-cells (Kiron, 2012). In addition, as genomic and transcriptomic resources become more widely available and affordable, evaluation of inflammatory responses such as cell-specific cytokine profiles and mediators of inflammation, or even pathogen-recognising toll-like receptors (*i.e.* TLR) in relation to antigen presenting cells has become a reality (Kiron, 2012) through the use of quantitative PCR or real time PCR techniques. These techniques are fairly simple to undertake, however, they require specialised instruments and reagents which remain relatively costly. Nevertheless, these are extremely sensitive techniques and can prove extremely reliable.

Despite the increase in use of novel molecular techniques (*i.e.* assays at the level of DNA, RNA and proteins) to investigate the relationship between nutrients and gut health responses of teleost fish, conventional histology and immunohistochemistry remain the gold standards for monitoring tissue structural and functional alterations (Derde *et al.*, 2012), and in turn, for confirmation of the intestine's integrity. Histomorphometry, broadly defined as the measurement of the shape, area, number or form of a tissue and cells, is considered as an important tool that can help improve our understanding of dietary influences. It is particularly suitable for certain types of histological investigation since it offers objectivity and increased precision compared with direct visual appraisal, and makes statistical analysis easier (Anderson & Lowe, 1990). Quantitative analysis of intestinal architecture and the immunoreactivity of specific biomarkers, may provide valuable information for evaluating

dietary ingredients, that can either improve intestinal structure or ameliorate the effects of factors such as infectious diseases or anti-nutritional components that may otherwise ultimately cause physical disruption (Sweetman *et al.*, 2008, 2010). Besides being a relatively easy and rapid methodology to employ, it is also relatively cost-effective.

Despite the wide range of methodologies available for assessing the effects of dietary components on intestinal health, failure to standardise the experimental and assessment methodologies adopted between studies has limited the ability to compare trials and therefore draw robust conclusions (Maita, 2007).

1.5.1.1. *Enteritis model in Atlantic salmon.* As mentioned earlier, many of the assays currently employed to evaluate the effect that alternative feed ingredients may have on a fish's intestinal homeostasis require robust standardisation across studies. In order to achieve such standardisation, the availability of reproducible and predictable models is necessary.

Over the past few years, an effective intestinal inflammation model has been investigated across a number of dietary modulation studies. Specifically, these studies have involved the replacement of fish meal by soybean meal (SBM), which results in an inflammation of the distal intestine of Atlantic salmon, usually referred to as SBM-induced enteritis (Van den Ingh *et al.*, 1991; Krogdahl *et al.*, 2010). The severity of the response seems to be dependent on the amount and variety of soya employed (Urán, 2008; Knudsen, 2007). While animals showed normal growth and feed intake, they developed a severe inflammation in the second gut segment characterised by: shortening of the mucosal folds, infiltration of inflammatory cells in the *lamina propria*, widening of the central *stroma* within the mucosal folding, increase in the thickness of the connective tissue, a loss of supranuclear vacuolisation of the absorptive cells in the intestinal epithelium, and an increase in the number of goblet cells (Baeverfjord & Krogdahl, 1996; Romarhein *et al.*, 2013a). Moreover, during the inflammation process changes in a variety of immunological processes occur, including a marked increase of neutrophilic and eosinophilic granulocytes in the *lamina propria* (Bakke-McKellep *et al.*, 2000a; Reite & Evensen, 2006), a

degranulation of the eosinophils (Urán *et al.* 2009b) and an increased activity of T cell response based on the expression of clusters of differentiation-3 (Bakke-McKellep *et al.*, 2007a). Expression of transcripts for the pro-inflammatory cytokines interleukin 17A (IL-17A), IL-1 β , IL-10, interferon α 1 (IFN α 1) and IFN γ , as well as IL-17A receptor, T-cell receptor γ (TCR γ), cluster of differentiation 4 α (CD4 α), CD8 β , transforming growth factor β (TGF β), protease-activated receptor 2 (PAR2), myeloid differentiation primary response gene 88 (MyD88) and trypsin are also reported to be significantly up-regulated during early and / or late inflammation stages, while interferon- γ -inducible lysosomal thiol reductase (GILT) was down-regulated. Up-regulation of TCR γ from day seven suggests proliferation of intraepithelial $\gamma\delta$ T cells. IL-17A, up-regulated during early inflammation, indicates involvement of T helper 17 cells in the pathogenesis of the SBM-induced inflammatory response (Urán *et al.*, 2008; Lilleeng *et al.*, 2007; Marjara *et al.*, 2012; Sahlmann *et al.*, 2012; Romarheim *et al.*, 2013a).

Therefore SBM is claimed to be a good model for fish nutrition, specifically because it allows robust phenotypic and biochemical responses to be visualised, making this dietary model an attractive platform to assist in the development of analyses to identify the best, or the less harmful, ingredients to be used in the formulation of diets for aquaculture.

1.6. Projects' contextual background

Conventionally, the formulation of new aquafeed products is based on digestive efficiencies and animal growth responses (Galindo-Villegas & Hosokawa, 2004). However, a multidisciplinary approach for evaluating intestinal responses should provide much more detail concerning the benefits of new feed ingredients.

As described above, intestinal structure can respond rapidly and reversibly to changes in dietary composition. Consequently, diet-induced changes in intestinal structure can influence the uptake of nutrients, which in turn may affect the performance of the immune system. Knowledge of the structural and inter-related functional alterations that occur in cells or tissues, as part of adaptive or disease processes, can provide a clearer understanding of the mechanisms underlying various tissue changes and malignancies due

to dietary modulation. Thus, identification and characterisation of such changes are essential in the provision of definitive diagnoses of the health status of fish, and may assist the prediction of the course of disorders and provide insight into therapeutic dietetic interventions (Krenacs *et al.*, 2010; Shi *et al.*, 2012).

Image analysis of digitised histological sections provides a practical means for quantifiable assessment of structural and functional changes in tissue, being both objective and reproducible. Also molecular and genetic markers are becoming more readily available for teleost fish species, and these tools combined, could provide valuable information and insight into phenotypic and immunological adaptation of fish in response to new dietary ingredients and would thus support the development of new dietary formulations and feeding strategies for salmon aquaculture.

1.7. Project aims and outline

The primary aim of the project was to improve the understanding of salmonid intestinal function, structure and dynamics and thereby, to develop a model which would allow fish intestinal health to be assessed with respect to different feed components. The idea was to develop a method for measuring an array of different intestinal parameters that are indicative of the animal's intestinal response in a nutritional context. The ultimate aim of this project was to evaluate the usefulness of histological structural features and classical molecular markers of immune function, as tools to assess and monitor the effects of feed composition on fish health. In order to accomplish this, the thesis was divided into four discrete pieces of research outlined in Chapters 2 to 5 as described below:

CHAPTER 2. *Description and development of a semi-automated system to assess intestinal morphology of Atlantic salmon, based on advanced image analysis:* The overall aim of the work described in this chapter was to establish an efficient image processing and analysis pipeline, incorporating suitable algorithms to allow feature extraction and generation of morphometric data, for the purpose of evaluating the extent of morphological changes in the intestine of fish, which could be used in the development of a model to assess nutritional modification to the fish's diet.

CHAPTER 3. *Intestinal responses to dietary additives – Application of tools for rapid screening of novel dietary components*: Following the development of the semi-automated system to assess intestinal morphology of Atlantic salmon, the aim of this chapter was to examine the broader utility of a multivariate / multimodal approach for the screening of different dietary ingredients, and in turn to ascertain the level and reliability of the contribution that the developed image analysis system might make in such an assessment.

CHAPTER 4. *Histological evaluation of enteritis in Atlantic salmon: Quantitative image analysis vs semi-quantitative scores*: The goal of the work described in this chapter was to evaluate the consistency of and compare the level of agreement between this newly developed quantitative microscopic image analysis system with that of an established semi-quantitative histological grading system.

CHAPTER 5. *Quantitative immuno-staining analysis - Development of a biomarker panel for assessment of immune responses from intestinal tract of Atlantic salmon fed different diets*: The work described in this chapter aimed to evaluate the use of the newly developed system relative to the integration of biomarkers into the histological assessment. Specifically, it was intended to assess the image analysis application for the detection of potentially predictive immunohistochemical biomarkers, and the accurate quantification of small changes in the spatial distribution of proteins and their relative amounts in the tissue, through which it might be possible to describe the intestinal cellular responses at a molecular level.

CHAPTER 6. *Characterisation of mast cells / eosinophilic granule cells (MCs / EGCs) in the Atlantic salmon intestine*: while Chapters 3, 4 and 5 highlighted the presence of MCs / EGCs in the intestine of salmon, no attempt was made to determine their role in immune responses from the intestinal tract. The purpose of the work presented in the present chapter was to further characterise those cells and to try to elucidate their functional role in the intestinal immunity. Through an understanding of their distribution, composition and ultrastructure, the intention was to provide additional knowledge, so as to better characterise such cells and their functional properties.

Finally in CHAPTER 7, the results of the various studies were summarised and the significance of these discussed, together with suggestions for future work, and indicators of adoption of the developed techniques.

DESCRIPTION AND DEVELOPMENT OF A SEMI-AUTOMATED SYSTEM TO ASSESS INTESTINAL MORPHOLOGY OF ATLANTIC SALMON, BASED ON ADVANCED IMAGE ANALYSIS

2.1. Introduction

Knowledge of the structural and functional alterations that occur in cells or tissues as part of adaptive or disease processes, can provide a clearer understanding of the mechanisms underlying various tissue changes and pathologies. Thus, identification and characterisation of such changes are not only essential for understanding the day-to-day plasticity of tissues but are necessary for the provision of definitive diagnosis of pathological states, for prediction of the course of disease and for the guidance of therapeutic interventions (Baak, 1987; True, 1996; Gil *et al.*, 2002; Krenacs *et al.*, 2010; Shi *et al.*, 2012).

Despite the upsurge in use of new molecular techniques in pathology (*e.g.* molecular assays at the level of DNA, RNA and proteins), conventional histology remains the gold standard for monitoring tissue structural alterations, and in turn, for confirmation of the presence or absence of pathology and grading of pathological progression (Rahman & Itakura, 1996; Gurcan *et al.*, 2009; Rojo *et al.*, 2010; Derde *et al.*, 2012). The suitability of the use of histopathology alone has been increasingly questioned (Isse *et al.*, 2012), as it mainly relies on the visual interpretation of morphological evidence to classify pathologies and the use of descriptive, linguistic criteria to convey how conclusions are reached (Hamilton & Allen, 2005; Kriete & Boyce, 2005; Gunduz-Demir *et al.*, 2010). Some authors regard this approach as “insensitive”, “arbitrary” and “prone to subjective interpretation” (Wright *et al.*, 2003; Krenacs *et al.*, 2010; Kopec *et al.*, 2011). Traditional histopathology is also heavily dependent on the learned recognition skills and experience of the assessor, this being similarly difficult to assess in a reproducible manner (Jarvis, 1992; He *et al.*, 2012). The sometimes poor reliability and reproducibility of this approach may lead to

inaccurate diagnosis and in turn to inappropriate clinical decisions (e.g. on timing and type of therapy), with many possible clinical consequences (Sertel *et al.*, 2009a). There is therefore a need for alternative / supplemental methods that could provide a more practical, quantifiable means of assessing structural changes, and consequently allow the extraction of objective and accurate prognostic data.

It has long been recognised that the quantitative measurement of histological features can provide data, which can significantly improve the ability to make diagnostic decisions in pathology (Chaudhuri *et al.*, 1988; Anderson & Lowe, 1990; Gunduz-Demir *et al.*, 2010; Grunkin *et al.*, 2011; Kayser & Kayser, 2013). Morphometric quantification of structural elements has several advantages over conventional visual assessment. It allows description of the morphological changes in (semi-) continuous numerical terms, which are likely to be more reproducible than ordinal grading, since they are quantitative data. Furthermore, it assists the comparison process, as sets of numerical data are easier to manipulate and compare than a collection of images or descriptive notes. Moreover, statistical data can be more easily acquired from such quantitative measurements, making these methods particularly useful for hypothesis testing. Finally, such quantification of the data can also allow the detection of subtle changes not readily apparent to the unassisted observer (Baak *et al.*, 1977; Preston & Bartels, 1988; Wied *et al.*, 1989; True, 1996; Rahman & Itakura, 1996; Hamilton & Allen, 2005; Kriete & Boyce, 2005; Godlewski *et al.*, 2009; Mandarim-de-Lacerda *et al.*, 2010; Shamir *et al.*, 2010).

Histological sections still, however, pose a formidable challenge in quantitative analysis (Chubb *et al.*, 2006). Often they comprise a variety of overlapping cells and gross structures, such that their complex heterogeneous architecture makes the quantification process more difficult (Ong *et al.*, 1996; Ficsor *et al.* 2006; Potts *et al.*, 2010). Nonetheless, quantitative analyses of histological tissue sections are widely performed and continue to provide meaningful information (Preston & Bartels, 1988).

Currently, quantitative analysis of histological tissue sections can be performed manually by assessors or (semi-) automatically by computer-based systems. While manual

measurements are time-consuming, fastidious and error-prone (Mulrane *et al.*, 2008; Grunkin *et al.*, 2011; Kopec *et al.*, 2011; Derde *et al.*, 2012; Shi *et al.*, 2012), fully automated operations may provide measurements in a reliable and reproducible manner at a reasonable speed of execution (Wied *et al.*, 1989; Ong *et al.*, 1996; Benali *et al.*, 2003; He *et al.*, 2012; Webster *et al.*, 2012), although they may not be suitable for measurement of complex features. Semi-automated analysis, *i.e.* that possessing a greater or lesser degree of user input, can therefore provide a good compromise between speed of execution and accuracy.

Over the past decade, dramatic increases in computational power and improvement in image analysis algorithms have allowed the development of powerful computer-assisted analytical approaches to the capture and analysis of histological data (Loukas & Linney, 2004; Gurcan *et al.*, 2009; Mandarim-de-Lacerda *et al.*, 2010; Grunkin *et al.*, 2011; Derde *et al.*, 2012; Kayser & Kayser, 2013). Quantitative microscopy based on automated digital image analysis has come to be considered not just as a useful aid to clinicians, but as an essential tool for interpreting data, which has major diagnostic value (Leong & Leong, 2004; Loukas & Linney, 2004; Kuznetsov *et al.*, 2013). Several studies have demonstrated exceedingly effective automated analysis of histological sections for human pathology grading and diagnosis applications, including studies of sections relating to prostate (Doyle *et al.*, 2007; Naik *et al.*, 2007; Nielsen *et al.*, 2012), breast (Gil *et al.*, 2002; Roque & Andre, 2002; Weaver *et al.*, 2003; Petushi *et al.*, 2006; Naik *et al.*, 2008; Chekkoury *et al.*, 2012), cervix (Keenan *et al.*, 2000; Price *et al.*, 2003; Rahmadwati *et al.*, 2012), lung (Kayser *et al.*, 2002; Dagnon *et al.*, 2008; Wang & Yu, 2012), bladder (Wester *et al.*, 1999; Goddard *et al.*, 2002), larynx, gastric and colorectal tissues (Hamilton *et al.*, 1997; Esgiar *et al.*, 1998; Laitakari *et al.*, 2003; Ficsor *et al.*, 2006, 2008; Gunduz-Demir *et al.*, 2010; Kalkan *et al.*, 2012), lymphoma and neuroblastoma characterisation (Cambazoglu *et al.*, 2007; Kong *et al.*, 2007, 2009; Sertel *et al.*, 2009b; Schmitz *et al.*, 2012), melanoma (Ganster *et al.*, 2001; Orlov *et al.*, 2012), osteoporosis (Shi *et al.*, 2012) and brain (Benali *et al.*, 2003; Glotsos *et al.*, 2004; Sundstrøm *et al.*, 2013); *inter alia*. The extent and variety of such studies are

themselves an indication of the impact that computer-based systems have had in quantitative histological analysis (Jarvis, 1992; Preston & Bartels, 1988; Doi, 2007; Giger *et al.*, 2008; Gurcan *et al.*, 2009).

Even though current systems are technically complex and not easily operated by the average practising pathologist, automated quantification will increasingly be a part of standard practice in the future (Leong & Leong, 2003; Park *et al.*, 2012). Also, with the continuing rapid development of computer technologies and combined cost reductions, it is suggested that successful computer-based automated image analysis solutions will become commonplace and lie within the reach of individual pathologists, clinical researchers and other members of the wide-ranging histological community (McEachron *et al.*, 1989; Leong & Leong, 2004; Mulrane *et al.*, 2008; Krenacs *et al.*, 2010).

At a time when automated morphological classification of histological images is increasingly prevalent in routine practice for other disciplines, including human anatomic and clinical pathology, the use of this methodology is still largely absent from fish health and veterinary applications. A limited amount of research has been performed on the application of automated image analysis to fish histopathology. For example, studies on the description of the progression of amoebic gill disease have employed semi-automated digital image analysis to evaluate the mean number of branchial mucous and chloride cells (Adams & Nowak, 2003, 2004). Another study, which monitored stress in fish by examining the effects that two common environmental states would have on the morphology of skin from sea bass, *Dicentrarchus labrax*, employed an automated image analysis system to assess in particular the number and diameter of skin mucous cells (Vatsos *et al.*, 2010). In order to evaluate the intestinal lipid absorption and eventual liver hypertrophy in common carp larvae, *Cyprinus carpio*, a further study examined anterior intestine and liver histological sections using a semi-automated image analysis protocol (Fontagné *et al.*, 2000). A further study described the development of the axial musculature in first-feeding larvae of Atlantic cod, *Gadus morhua*, with muscle growth being assessed by determining the number of muscle fibres (*i.e.* hyperplasia) and the growth of existing fibres (*i.e.* hypertrophy), by use of

a semi-automated image analysis system (Galloway *et al.*, 1999). In quality trait studies of gilthead sea bream, *Sparus aurata*, morphometric measurements on the dorsal muscle were made from transverse sections using an interactive image analysis system (Valente *et al.*, 2011; Matos *et al.*, 2013). Overall, however, few studies employing automated image analysis as a tool for fish histopathology exist, particularly when contrasted to the extensive use in other organisms of commercial, medical or veterinary importance (Ahrens *et al.*, 1990; Veggetti *et al.*, 1993; Vaughan *et al.*, 1996; Anggraeni & Owens, 2000; Dolapchieva *et al.*, 2000; Chi & Liang, 2004; De Laat *et al.*, 2013).

Despite the paucity of studies employing automated image analysis on fish health-associated material, image analysis of histological sections is clearly appropriate to the requirements of fish pathologists, and the development of (semi-) automated quantitative tools would be an important advance, adding value to histomorphology-based disciplines. Therefore, the aim of the present study has been the development of a semi-automated system to assist pathologists with the histological evaluation of fish intestinal biopsies, while providing an alternative approach to the semi-quantitative scoring methods currently used for intestinal health assessment. Thus, the intention was to develop an efficient image processing and analysis pipeline, incorporating appropriate algorithms, to reliably quantify the extent of morphological and functional changes occurring in response to dietary and environmental modulation.

2.2. Material and methods

2.2.1. Histological tissue samples

Tissue samples, all taken from the anterior part of the distal intestine of Atlantic salmon and fixed in neutral buffered formalin (10 %, pH 7.2, room temperature ~20 °C), were obtained from Skretting ARC's histological archives so as to represent a range of pathological states. Subsequently, all cases were recoded for blind analysis, the samples dehydrated and embedded in paraffin (Tissue-Tek II Paraffin Wax, 54-57 °C, Sakura Finetek Europe B.V, Netherlands) and transverse sections of 5 µm thickness were cut

(Leica RM 2035, Leica Microsystems Ltd., UK). Sections were then dewaxed and stained with a combination of Harris' haematoxylin (bluish nuclear / acidic tissue stain), eosin-yellowish (red cytoplasmic / basic tissue stain) and Alcian blue (8 GX, pH 2.5, a turquoise stain particularly highlighting acid mucopolysaccharides of mucous cells) (Steedman, 1950; Lev & Spicer, 1964; see Appendix 1 for modified staining protocol).

The initial slide-review was undertaken using brightfield illumination. Each slide was evaluated by an expert pathologist and assigned to one of the following histological grades: (A) normal morphology, (B) mild to moderate inflammation and (C) severe enteritis (Figure 2.1). In order to develop the semi-automated image processing and analysis system, and to test its accuracy, this process ensured that the selected slides covered most of the anticipated tissue morphological variations among all three histological grades. Altogether, 105 specimens were selected from the histological archives and 25-30 single representative slides were designated for each histological grading.

2.2.2. Digital image acquisition

The selected slides were scanned using an automated slide-scanning system (MIRAX Desk, Carl Zeiss MicroImaging GmbH, Göttingen, Germany) equipped with a 20× apochromat objective and a SONY DFW-X710 camera. To reduce the differences among tissue samples, variations in illumination, reflectance and optical transmission over the microscopic field were normalised and whole-slide digital mosaics captured giving a full slide image equating to 47104 × 61440 pixels. Thereafter, by use of the MIRAX Viewer software (Version 1.12, 3DHISTECH, Budapest, Hungary) representative image fields were randomly selected and a distinct set of frames from different sizes (*i.e.* 1:1, 47275 × 26813 pixels; 1:2, 23637 × 13406 pixels; 1:4, 11818 × 6703 pixels) used to crop the selected fields at different software magnifications (*i.e.* 20×, 40×, 100× and 200×). Twenty-four bit digital images with a quality resolution setting of 0.23 microns per pixel, were extracted and saved as individual TIFF images (Figure 2.2).

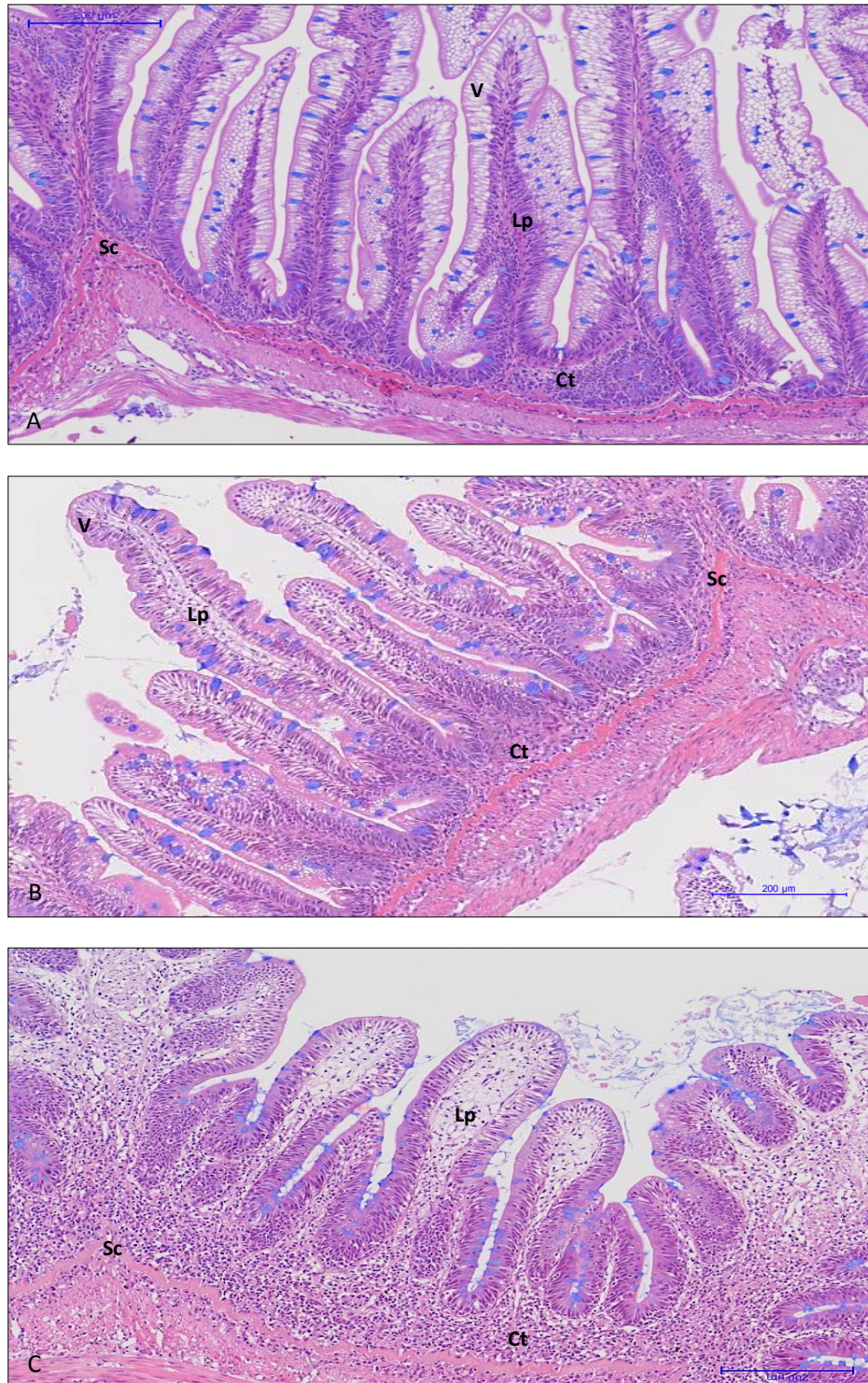


Figure 2.1. Images from Atlantic salmon distal intestine specimens showing the morphological tissue variations encountered across three different histological grades: (A) normal morphology, (B) mild to moderate inflammation and (C) severe enteritis. Typical signs of enteritis include the loss of vacuoles (V) in the absorptive enterocytes; the widening of *lamina propria* (Lp) in the mucosal folds; and an increase of the connective tissue (Ct) between the base of the mucosal folds and the *stratum compactum* (Sc). Intestinal transverse sections were stained with a combination of haematoxylin-eosin and Alcian blue 8 GX.

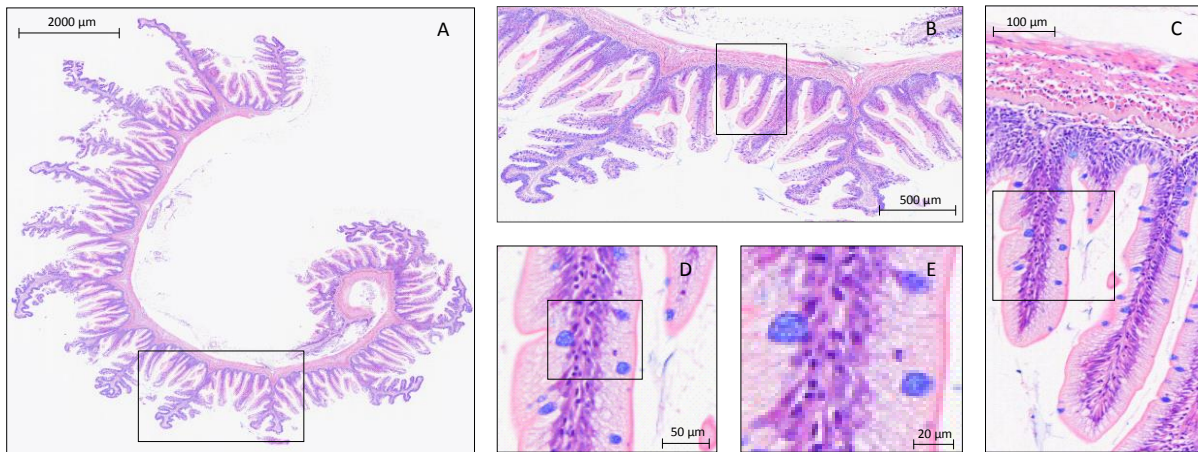


Figure 2.2. Digitised histological image of distal intestine tissue from Atlantic salmon, at successively higher magnification. (A) Original full scale image digitised at 20x. (B) A sample cropped image (4.85 MPixels) taken from the original image at 100x, approximately one tenth of the full scale image. (C) A portion of a cropped sample image visualised at 200x. (D-E) Digitised images visualised at 1200x and 2000x respectively, yielding incrementally more discriminatory information but giving smaller, less representative sampling windows. Intestinal sections were stained with a combination of haematoxylin-eosin and Alcian blue 8 GX.

2.2.3. Development tools – Image analysis hardware and software

The image processing and analysis algorithms described here were developed using Zeiss's proprietary macro programming language, deployed through commercially available image processing and analysis software (KS 300, Execution Environment, Version 3.0, Carl Zeiss MicroImaging GmbH, Göttingen, Germany). The custom system developed included algorithms for semi-automatic image segmentation and image identification, as well as for interactive analysis of images, feature extraction and data storage. Additionally, feedback in the form of guidance-notes for the operator, and visualisation of the generated images was made available at each step of the pipeline process (as shown in Technical Note A1).

Evaluation and deployment of the system was performed on a standard personal computer (Dell Latitude™ D630, Intel Pentium II 350 MHz processor, 128 MB RAM, 2 GB hard disk, under the environment of Microsoft™ Windows XP) operating the stand-alone KSRun software platform (Version 3.0, Carl Zeiss Vision GmbH, München-Hallbergmoos, Germany). In accordance with the MIRAX Viewer guidelines, the system was calibrated and measurements validated against a slide-graticule image captured at settings identical to

those used for capture of the experimental images. Measurements were also validated using a separate image analysis platform: ImageJ software (Version 1.45, US National Institutes of Health, Bethesda, Maryland, <http://rsb.info.nih.gov/ij/>).

2.2.4. Image processing and segmentation

The image segmentation workflow consisted of a succession of interactive and automated steps described in detail in Technical Note A1 and partly illustrated in the diagrams from Figures 2.3 and 3.1. These approaches were either global, in which they simultaneously segmented most morphological structures found in the entire image, or local, which targeted specific structures. Throughout the process, the operator was able to interactively correct erroneous automated object inclusion or deletion decisions.

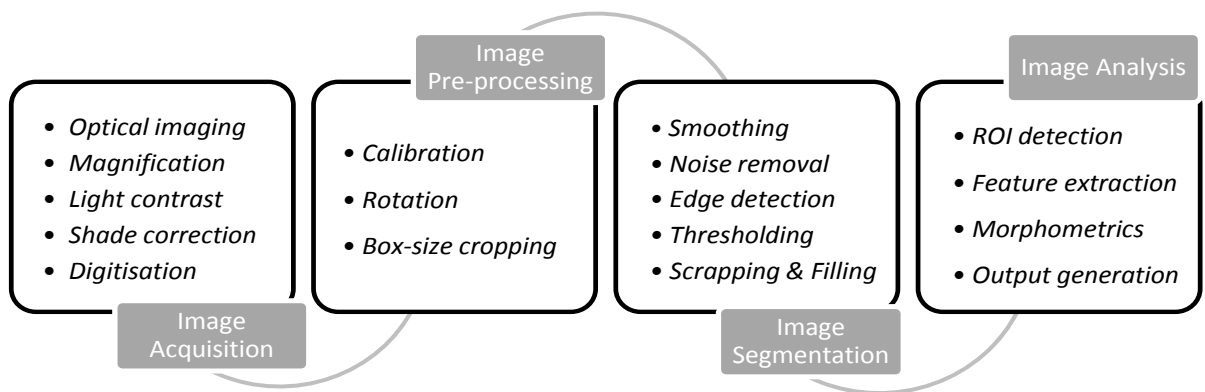


Figure 2.3. Flow diagram illustrating the sequence of image processing, for the proposed image analysis system. (ROI) Region of interest.

The following operations and parameter settings were employed in the segmentation of areas of interest within the image:

2.2.4.1. *Edge detection*. Prior to image processing, object boundaries were defined in accordance with an 8-pixel connectivity rule (*i.e.* the clustering method compared each pixel in the image with adjacent pixels in the 8-neighbouring pixel's positions and two image pixels were considered as connected when their vertices were horizontally, vertically or diagonally adjacent). This boundary rule allows optimal separation of "touching" adjacent objects, *e.g.* mucous cells.

2.2.4.2. *Noise removal.* Following correction of background lighting inhomogeneities, undesired artefacts were removed by a combination of use of morphological operators and direct manual tracing of contours.

2.2.4.3. *Colour thresholding.* Using a Hue, Lightness and Saturation (HLS) colour model which serves to best resolve observer-perceived colours, the colours associated with the object of interest (e.g. blue turquoise for mucous cells) were added to give a threshold range enabling capture of all objects with colours lying within the range.

2.2.4.4. *Morphological filtering.* Objects segmented by earlier operations were further filtered using morphological operators (i.e. objects smaller or larger than expected values for the type of object of interest were removed). The resulting binary (black and white) object markers / masks were employed to capture sub-images of the individual selected objects. Adjacent objects were separated using a combination of erosion and dilation steps and the use of a binary grain recognition algorithm.

2.2.4.5. *Intensity thresholding.* On the basis of pixel intensity characteristics i.e. lighter or darker areas within the image, the user interactively defined a greyscale range of pixel intensity values that encompassed objects of interest. Objects lying above this threshold were considered in further steps (e.g. tissue) with objects below this threshold being removed (e.g. background / intestinal lumen).

2.2.4.6. *Size scrapping and filling.* A sequence of filters was then applied, whereby small objects were removed by use of size-scrap operators and holes were filled using erosion and dilation operations and use of binary fills. Following the earlier operations the image was again filtered to remove specific size range objects. In addition, to reduce the noise and enhance the contrast of small cellular features, a Gaussian smoothing step (Gonzalez & Woods, 2002) was applied to the boundaries. Finally, a binary image incorporating the final regions of interest was created and stored.

2.2.4.7. *Intensity thresholding of inverted images.* Images were inverted using an inverse histogram equalisation operation, which provided a negative of the image (black =

white, white = black). Small objects in the thresholded binary image were then eliminated and small holes repaired by application of erosion and dilation operations. Ultimately, the resulting segmented object image was saved.

2.2.4.8. *Manual object delineation.* Specific regions were defined and selected by interactive freehand-drawing in the graphics plane of the displayed image.

2.2.5. Histological identification and post-processing overlays

The algorithms below were developed for the purpose of recognising specific histomorphological structures:

2.2.5.1. *Mucosal and submucosal tissues.* Intensity thresholding was employed to interactively segment the peritoneal edge of the *muscularis externa* and the internal intestinal lumen. Thereafter, using interactive drawing, the *stratum compactum* was defined, which allowed discrimination between different tissue areas (*i.e.* mucosal and submucosal tissues, respectively) – Figure 2.4.

2.2.5.2. *Mucous cells.* Subsequently, using an interactive HLS colour threshold, stained mucous cells were identified. Additionally, binary grain recognition was used to separate adjoining mucous cells, and the resulting objects were filtered by size-threshold-operators so as to ensure removal of artefacts (Figure 2.5 A-D).

2.2.5.3. *Tissue vacuolisation.* Thereafter, the source image was converted into a greyscale image and mucosal tissue vacuoles were recognised (Figure 2.5 A, F-H). Finally, once the tissue regions were defined, a boundary segmentation was performed and the luminal perimeter captured (Figure 2.4 D).

2.2.5.4. *Mask overlays.* Regions identified by thresholding ranges were then highlighted and object markers / masks were stored as binary images. Post-processing overlay masks deriving from the detected regions of interest were generated and stored as segmentation mask images (*i.e.* the original image, with identified objects highlighted by labels) – (Figures 1-7 from Technical Note A1).

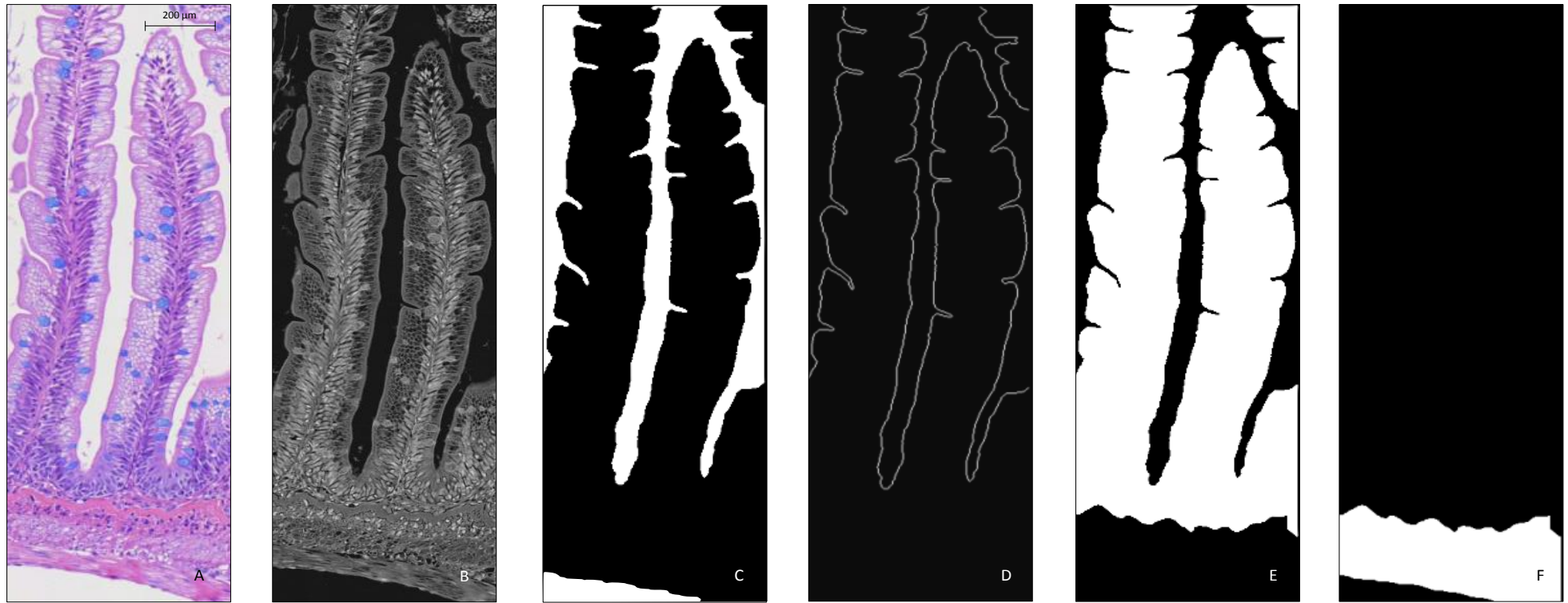


Figure 2.4. Images generated by the described image analysis algorithms, from which morphometric features were extracted and employed to quantify the phenotypic appearance of the specimen's distal intestine. (A) A portion of a digitised histological image, approximately one eighteenth of the full image used in the present study as described in Figure 2.3. (B) Greyscale sub-image extracted from the original's negative image, by use of an inverse histogram equalisation operation. (C) Binary image created during the image segmentation process, where the empty space was differentiated by inverting the original image to its negative and use of intensity differentiation, which in turn allows distinction of the peritoneal edge of the *muscularis externa* and the internal intestinal lumen. (D) Binary image of the perimeter line from the outside mucosal boundary, captured after appropriate segmentation of the luminal surface. (E, F) Binary images of mucosal and submucosal tissue areas, obtained by interactive drawing of the *stratum compactum* over Figure 2.4 A, which allowed discrimination between tissue areas.

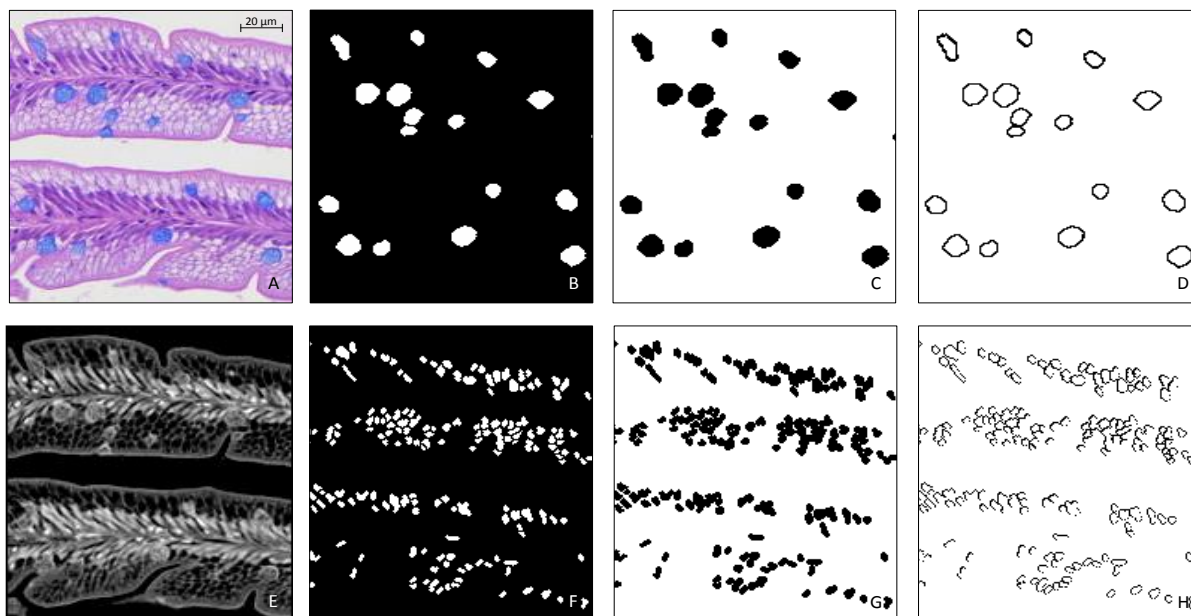


Figure 2.5. Images generated by the described image analysis algorithms, from which morphometric features were extracted and employed to quantify the phenotypic appearance of the specimen's distal intestine. (A) A portion of a digitised histological image, approximately 1:100 of the full image used in the present study as described in Figure 2.2. (B, C) Binary images obtained for the segmented and size-filtered mucous cells, after using an HLS colour model to threshold colours associated with them. (D) Object markers / masks for the objects captured as mucous cells, stored as a binary image. (E) Inverted greyscale sub-image created during the image segmentation process by use of an inverse histogram equalisation operation. (F, G) Binary images where the mucosal tissue vacuolisation was recognised by inverting the original image to its negative and through intensity differentiation, which in turn allows distinction of the peritoneal edge of the *muscularis externa* and the internal intestinal lumen. (H) Object markers / masks for mucosal tissue vacuolisation, stored as a binary image.

2.2.6. Feature extraction and output generation

The last stage of the developed system involved the extraction of image content descriptors (*i.e.* image features), which describe the image content quantitatively. Once a region of interest was detected using one of the algorithms described above, various automated arithmetic and geometric algorithms were employed to provide measurements of a number of morphometric parameters (see Table 2.2).

2.2.6.1. *Geometric features.* The area of a specific region was measured by direct counting of the number of pixels within the boundary of the filled region. The perimeter length was computed as the length of the region's outside contour estimated as a weighted

sum of the number of pixels around the region of interest (Figure 2.6). The lengths of the main (longest) and secondary (shortest) axes of an ellipse with the same geometric moment of inertia as the object of interest were measured in pixel numbers. Likewise, the maximal and minimum numbers of pixels for the Feret lengths of the object (*i.e.* caliper lengths of lines passing through the centre of gravity) were measured.

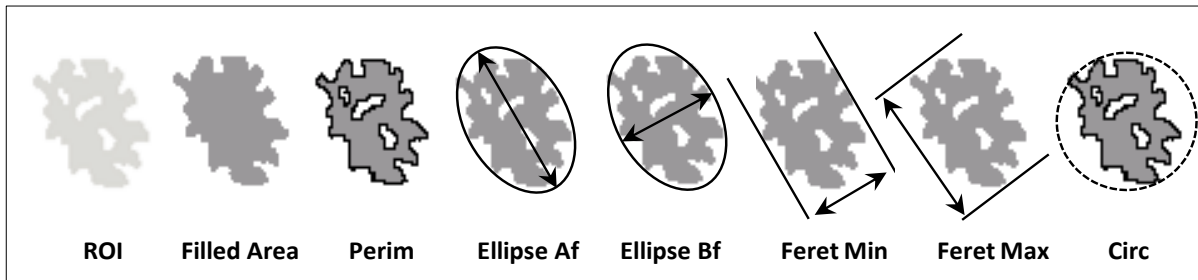


Figure 2.6. Geometric and shape feature measurements employed in the study. (ROI) Region of interest. (Filled Area) Number of pixels within the boundary of the filled region. (Perim) Length of the region's outside contour estimated as a weighted sum of the number of pixels around the region of interest. (Ellipse Af) The length of the main axis of an ellipse with the same geometric moment of inertia as the region of interest measured in pixels. (Ellipse Bf) The length of the secondary axis of an ellipse with the same geometric moment of inertia as the region of interest measured in pixels. (Feret Min) Number of pixels for the minimum Feret length of the region of interest. (Feret Max) Number of pixels for the maximal Feret length of the region of interest. (Circ) Circularity of the region of interest, estimated as the ratio of the perimeter length from the region of interest, over the perimeter of a circle with an equivalent area (Images adapted from KS300 electronic user notes).

2.2.6.2. *Shape features.* Circularity, representing the degree of roundness of the object (*i.e.* a value of 1 indicated a perfect circle) was estimated as the ratio of the perimeter of the object, over the perimeter of a circle with an equivalent area. Fractal dimensions were measured by use of the box-counting method (Russell *et al.*, 1980; Cross, 1994; Shang *et al.*, 2000). This method divides the binary image into successive grids of boxes, the boxes within each grid having a different size (λ) and counting the number of boxes intercepted by the perimeter line for each grid ($N(\lambda)$). Grids with large numbers of small boxes would give many intercepts while those with a small number of large boxes would show few intercepts (Figure 2.7). The fractal dimension of the perimeter would then be estimated from the slope of a regression line fitted to a plot of λ vs. $N(\lambda)$ on a log-log scale.

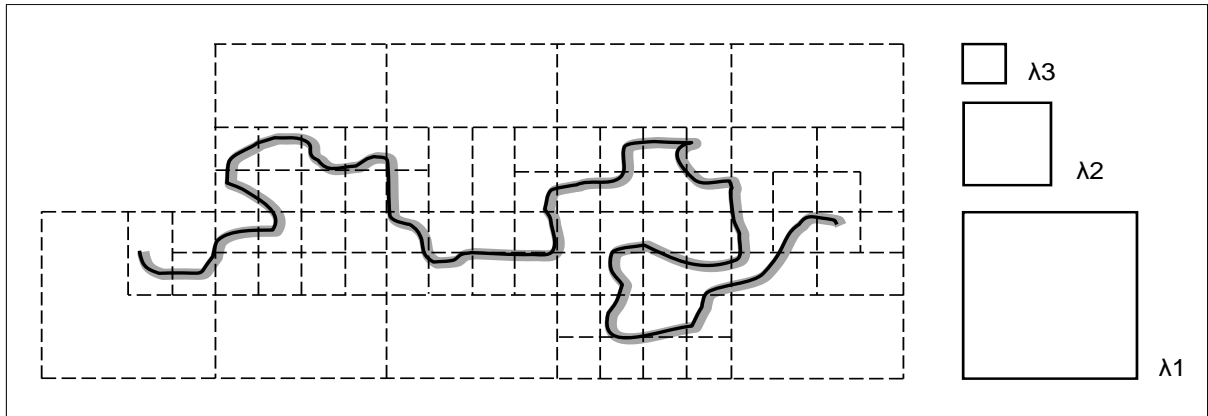


Figure 2.7. Schematic diagram of the box-counting method used to estimate fractal dimensions. The technique finds the number of boxes, required to cover the perimeter line, by superimposing a regular grid of boxes on to the image, and counting the number of occupied boxes. The procedure is then repeated using different box sizes (e.g. $\lambda_1 - \lambda_3$), up to the size of the image.

2.2.6.3. *Position and orientation features.* The absolute co-ordinates of the object centroid (x, y) were also recorded. This allows the user to relocate an object of interest in the original image.

2.2.6.4. *Output generation.* The obtained values were then transcribed from pixel values to SI base units using the image calibration file, and exported to a flat database file (Figure 8 from Technical Note A1). Quantitative variables were expressed as mean and standard deviations, unless otherwise specified.

2.2.7. System performance

The performance of the developed system was evaluated in terms of efficiency, accuracy and reproducibility. In order to do this, 25 additional test images from different study-cases were randomly selected.

2.2.7.1. *Efficiency.* First, the extent to which time effort was needed to accomplish the intended assessment tasks was evaluated. The total average computation times for feature extraction, feature calculation and output generation were determined for semi-automated processing as opposed to interactive and manual segmentation.

2.2.7.2. *Accuracy.* The accuracy of the algorithm denotes the degree to which the segmentation measurements agreed with the actual values of the region of interest. This

has been validated using two different approaches. First, a quantitative comparison between computational results and manual measurements gathered by experienced pathologists was conducted. Secondly, the same images were evaluated using an open source image analysis software, and results from the interactive and the semi-automated segmentations compared using ImageJ software (Version 1.46r, US National Institutes of Health, Bethesda, Maryland, USA, <http://rsb.info.nih.gov/ij/>).

2.2.7.3. Reproducibility. The system was then evaluated in terms of its precision. This was done by comparing the degree of agreement between measurements obtained for the same image, when the procedure was conducted by different users and at different time points.

2.2.7.4. Statistical analysis. The system's accuracy and reproducibility were evaluated by comparing the continuous variables derived from the developed image analysis algorithms, with that from the interactive segmentation accomplished by an open source image analysis software package, and through manual assessment done by an experienced histopathologist. Thereafter, Pearson's correlations were carried out on generated data and statistical significances were evaluated using Minitab (Version 16.1.0.0, Coventry, UK) statistical software package.

2.3. Results and discussion

In the present study, a novel semi-automated histological image analysis system was developed to evaluate the extent of morphological changes in the distal intestine of Atlantic salmon, due to dietary modulation.

Technical Note A1 provides a detailed description of the developed approach. In this approach, semi-automated image segmentation procedures were used to partition an image into interpretable regions or objects of interest, an essential process for most subsequent image analysis tasks, which included several algorithms for feature extraction and morphometric data generation. To achieve this goal, the overall procedure had to be standardised with respect to tissue staining, image acquisition, image pre-processing and image analysis. Moreover, the reliability of the system had to be validated.

2.3.1. Standardisation of staining

Several researchers have reasoned that standardisation of the staining method is crucial if an automated image analysis system is to be employed, since computer-assisted analysis appears to be more susceptible to variations in pixel colour than human visual recognition would be (Wittekind *et al.*, 1983; Wied *et al.*, 1989; Karlsson *et al.*, 1994; Mesker *et al.*, 1994; Johansson *et al.*, 2001). Thus, refinement and standardisation of staining procedures to improve the efficacy of the proposed system were an early concern.

In order to optimise the protocol, during the staining process (*i.e.* after each of staining steps) the colour development was visually checked under a microscope. Once the optimal staining times were established, all slides in series of batches were simultaneously stained for the same period of time. Also, extra care was taken to use freshly made staining solutions, or to use the same lot batch number if purchased from commercial sources.

The best staining contrast and minimal background were achieved with the protocol outlined in Appendix 1. Thereafter the staining variation between slide-batches was evaluated by comparing images from serial sections (*i.e.* prepared from the same tissue paraffin block). Colour coefficients of variation for these control slides, were roughly estimated between 11.5-15.0 %, 16.5-18.5 % and 19.0-23.0 % for the red, green and blue channels, respectively. This variation is very similar to that reported by Mosedale *et al.* (1996). This variability could, however, be considerably minimised by use of an automated staining machine as used in high-throughput human and animal health screening. Cost limitations in the current project did not, for the most part, permit implementation of such alternatives in this study.

Another matter of concern is that considerable changes in tissue volume may occur during the process of tissue fixation and dehydration, which may influence the morphometric results (Aherne & Dunnill, 1966; Deneff *et al.*, 1979; Gerdes *et al.*, 1982; Boonstra *et al.*, 1983). Some investigators have suggested that because this is a constant feature of fixed material and because all samples will have been treated the same way, there is no need for correction factors to be applied (Baur, 1973 *in* Baak *et al.*, 1977; Bouw,

1975 in Baak *et al.*, 1977). Nevertheless, in the present study stringent attempts were made to standardise all procedures (*i.e.* using the same fixative solutions / identical fixation periods for all the samples used; and follow optimised protocols for dehydration and histological tissue processing).

2.3.2. Image acquisition and pre-processing

The influence of routine acquisition and pre-processing capture methods on the ability of the system to efficiently segment regions of interest and extract image content descriptors was considered to be an extremely important factor in the outcome of overall analysis. Image acquisition was initially done by use of a high-resolution digital camera (Axiocam MRc5, Carl Zeiss, Cambridge, UK) attached to a light microscope (BX51, Olympus, Hamburg, Germany), although variations / inhomogeneities in the background intensity often occurred, leading in turn to inaccurate segmentation results. The decision was then made to use a whole-slide scanning system. This technology not only permitted capture of high resolution images with high fidelity in respect to the diagnostic material, but also proved to be highly robust in respect to variations in image illumination, contrast and brightness. Ultimately, other inherent advantages of using digital slides over glass slides in terms of the review process were also perceived (*e.g.* ability to view images simultaneously, portability and convenience of full slide scans, ease of image sharing and retrieval from image archives, possibility of provision of an audit trail, suitability of system for training, *etc.*; Leong & Leong, 2003, Rocha *et al.*, 2009, Bandyopadhyay, 2011, Pantanowitz *et al.*, 2011).

Another important area for consideration was the optimal image size and resolution to employ, as the quality and area coverage of the original image is a critical factor in the field of image analysis (Jeong *et al.*, 2010; Park *et al.*, 2012). Large, high resolution (pixel) images allow a greater proportion of the tissue to be sampled in a given window providing a better overview of overall tissue status. Small, high resolution images provide a more localised sample window and will hence increase variability between “replicate” samples. Lower resolution images will degrade the capability to resolve objects of interest accurately. Technical, financial and statistical requirements / constraints, however, mean that there needs

to be a compromise between high image quality and acceptable speed of image processing. Various studies have investigated the influence of resolution of digital histological images on subjective observer perception (Belien *et al.*, 1997; Vidmar *et al.*, 1999; Daniel *et al.*, 2000; Boellaard *et al.*, 2004). Despite this, there are no standardised thresholds defining minimal requirements in respect to the image quality needed to assure an assessment's accuracy.

In the present study, three different frame-sizes (*i.e.* 1:1, 47275 × 26813 pixels; 1:2, 23637 × 13406 pixels; 1:4, 11818 × 6703 pixels) at four distinct digital capture magnifications (*i.e.* 20×, 40×, 100× and 200×) were verified for development and deployment of the proposed segmentation methods. These specifications resulted in average file sizes of 12 MB to 2.22 GB (Table 2.1). While the use of higher resolution images coupled to larger frames provided the best tissue sample window and ability to resolve detail, practical constraints such as memory use and processor speed meant that systems ran too slowly to be of utility in an analytical / diagnostic context. Consequently, optimised parameters established within the described work (image size 11818 × 6703 pixels sampled at 100× magnification, resulting in an image file of 24 MB) were a compromise between processing time requirements, image quality, file size and computational hardware limitations.

Table 2.1. Image size and resulting image file size of 24-bit digital TIFF images, captured at different magnifications.

Magnification	Size (pixels)	File size (MB)
20×		
	(1:1)	47275 × 26813
	(1:2)	23637 × 13406
	(1:4)	11818 × 6703
40×		
	(1:1)	47275 × 26813
	(1:2)	23637 × 13406
	(1:4)	11818 × 6703
100×		
	(1:1)	47275 × 26813
	(1:2)	23637 × 13406
	(1:4)	11818 × 6703
200×		
	(1:1)	47275 × 26813
	(1:2)	23637 × 13406
	(1:4)	11818 × 6703

Footnotes: MB, megabytes.

2.3.3. Development, training and evaluation

In the context of automated image analysis, a computer-based pipeline for carrying out a procedure, *i.e.* image processing algorithm, may be used to process and analyse the captured digital slide image, making interpretation more straightforward and permitting a more objective quantitative assessment. Such algorithms may be incorporated into an image analysis software package enabling easier implementation by the end user. For the purposes of the work presented in this thesis, the Zeiss KS300 image analysis system (Version 3.0, Carl Zeiss MicroImaging GmbH, Göttingen, Germany), a widely recognised and employed image processing and analysis platform, was used for the majority of procedures. This system has the advantage of providing an extensive set of image processing and analysis tools in a uniform environment and a well-developed macro-writing and application environment as well as being associated with extensive pre-existing expertise at the Institute of Aquaculture allowing more rapid system development during the course of the project.

The system developed includes algorithms for semi-automatic image segmentation and image identification, as well as for interactive analysis of images, feature extraction and data storage. For the purpose of recognising specific structures, algorithms were developed to carry out five distinct segmentation of regions of interest: (i) mucosal and submucosal tissue regions, (ii) mucous cells, (iii) tissue vacuolisation, (iv) intestinal lumen and (v) luminal surface. Segmentation of these different histological components was carried out sequentially. Regions within the threshold ranges were highlighted, and the corresponding measurement values exported to an Excel flat sheet.

As part of the software workflow, marked-up images were provided across all steps within the pipeline. These, and the x, y coordinates of each detected object allowed assessment of the degree to which the segmentation algorithms correctly recognised and segmented the histological features in each image. During the training period, an experienced histopathologist visually evaluated such marked-up images as part of a quality

assurance step. This served as an opportunity to determine the accuracy of the algorithm and to judge the necessity for algorithm refinement.

Most algorithms demanded varying degrees of customisation that could have not been predicted, *a priori*. The testing and resetting of the algorithm parameters to converge on an optimal but flexible segmentation result was laborious and time-consuming. In all, it took just over eighteen months to develop a system showing optimal performance, illustrating the time required for development of such systems. In some respects this represents the time taken to encode the knowledge of the researcher in a computer-based system. The various algorithms were developed using a “training set” which comprised 6 images of distinct histological grades. Once the algorithms had been refined, the entire system was evaluated using the other 105 randomly selected images.

2.3.3.1. *Feature selection.* When deciding upon the morphometric extraction approach, the researchers tried to select a set of features that would best describe the different relevant intestinal morphological changes. For each image frame, the set of features summarised in Table 2.2 was extracted. The selection was based on the researchers’ personal experience from similar quantitative studies, or review of the relevant literature. Also algorithms were developed according to the researchers’ ideas about what additional features could be useful, this being based on experience from visual observation, identifying features that might express the properties used for visual discrimination between different histopathological gradings (e.g. fractal dimensions, circularity index, Feret and elliptical lengths).

A large number of image descriptors was used, varying from simple geometric features (e.g. perimeter, area, size and shape) to other descriptors based on density and texture content. Although not all features measured might be relevant to description of intestinal changes, the lack of additional time or computational overhead in their inclusion meant that the initial analytical steps included them all. The wide variety of initial descriptors were subsequently winnowed through use of multivariate statistical techniques, which reduced data dimensionality by ranking the features according to their discriminatory potential (as described in Chapters 3 and 4).

2.3.4. System performance

A priori the system required expert knowledge, provided by experienced pathologists, who were also involved in the design and validation processes. Once the system had been developed, an unassisted observer could very easily operate it. No high level knowledge of histology, pathology diagnosis, mathematics or computing is necessary, this having been encoded into the developed system. Nevertheless the semi-automated image analysis system described did require a degree of user learning and training. This learning curve was not steep, but did exist.

Table 2.2. List of measured morphological parameters and computed morphometric ratios used in the analysis.

Morphometric feature	Description
MTA	Mucosal tissue area
MCA	Mucous cell total area
MMCA	Mean mucous cell area
MCA / MTA	Ratio between the mucous cell area and the mucosal tissue area
MCN	Mucous cell number
MCN / MTA	Ratio between the mucous cell number and the mucosal tissue area
STA	Submucosal tissue area
MTA / STA	Ratio between the mucosal tissue area and the submucosal tissue area
MC Feret Min	Mucous cell minimum Feret length
MC Feret Max	Mucous cell maximum Feret length
MC Feret Ratio	Ratio of the mucous cell Feret lengths
MC Ellipse Af	Length of the main axis of an ellipse with the same geometric moment of inertia as the mucous cell
MC Ellipse Bf	Length of the secondary axis of an ellipse with the same geometric moment of inertia as the mucous cell
MC Ellipse Ratio	Ratio of the elliptical lengths Af and Bf for the mucous cell
MCirc	Mucous cell mean circularity index
P	Total perimeter length of the luminal surface
P / MTA	Ratio between total perimeter length of the luminal surface and mucosal tissue area
VC	Vacuolisation total area
VC / MTA	Ratio between the total vacuolisation area and the mucosal tissue area
MTA-Vac	MTA without the vacuolisation area
MCA / [MTA-Vac]	Ratio between mucous cell total area and the MTA without the vacuolisation area
MCN / [MTA-Vac]	Ratio between mucous cell number and the MTA without the vacuolisation area
FR	Fractal dimension of the perimeter line from the luminal surface

By optimising the implementation of the algorithms, acceptable processing speeds were achievable, even when using a relatively old personal computer. The average time for the whole digital slide image acquisition was approximately 4-12 min, depending on the amount of tissue to scan (with this step being capable of full automation, given an appropriate slide-loader). Image pre-processing and frame rotation / cropping was little more than 3 min per slide. The total average computation time from image upload to feature extraction, measurement and results data output for 12 continuous variables being roughly 20 to 25 min per frame, which greatly improved the efficiency of conducting such quantitative assessment as opposed to the possible alternative semi-quantitative approach.

2.3.4.1. *Efficiency.* The performance of the proposed system was evaluated by comparing the time effort required to accomplish the intended assessment tasks, with that required for manual assessment performed by an experienced histopathologist.

Of the objects of interest that were measured, parameters corresponding to mucous cells were selected for validation since these were the most easily established by manual assessment, by which means an assessor could establish a near “true value”.

Table 2.3 shows the average processing time for each segmentation method up to feature calculation and output generation. As expected, the longest mean time to view and morphometrically quantify an image was for the manual assessment (*i.e.* Count: 1'29" ± 24", Perimeter & Area: 4'16" ± 54"); also highly correlated to the number of or complexity of the regions of interest – Count: $r = 0.803$, $p < 0.001$; however not correlated to the size of the regions of interest – Area: $r = 0.296$, $p > 0.05$). Automated modes having the shortest mean times (Interactive mode: Count 0'23" ± 07", Perimeter&Area 4'16" ± 54"; Fully automated: Count 0'04" ± 00", Perimeter&Area 0'01" ± 00"). Furthermore, most images were segmented with little or no operator interaction, with processing times of the order of less than 4 seconds. More complicated images required some processing interaction and a total analysis time varying from 10 to 36 seconds, with most of this time devoted to inspection and comparison. Results suggest that the proposed assisted computer system can be a viable alternative to pathologist's scoring in a manner that is more practical and time-efficient.

Table 2.3. Total mean processing time required to accomplish the intended assessment tasks, by means of manual, interactive or automated threshold methods for mucous cell assessment.

Mucous cell assessment	Total average processing time
Count (N°)	
Manual	1'29" ± 24" (Min 0'54", Max 2'34")
Interactive	0'23" ± 07" (Min 0'10", Max 0'36")
Automated	0'04" ± 00" (Always 0'04")
Perimeter Length (µm) & Filled Area (µm ²)	
Manual	4'16" ± 54" (Min 2'41", Max 6'10")
Automated	0'01" ± 00" (Always 0'01")

Footnotes:

$n = 25$ Histological frames analysed for each feature measurement and threshold method employed.

The results obtained agree with previous studies (Sieren *et al.*, 2010; Galarraga *et al.*, 2012; Pajor *et al.*, 2012; Tapias *et al.*, 2013), which also observed that the automated process greatly reduces the time spent on appraisal, compared with the traditional manual process by effectively transferring the load of the assessment process to the computer.

2.3.4.2. *Accuracy.* To show the robustness of the proposed method, both manual and (semi-) automated analyses were performed on the same digital image. The quantitative evaluation was performed using Pearson correlations, and results acquired by both methodologies are illustrated in Table 2.4. Overall, measurements derived by use of interactive segmentation methods showed greater agreement with the ones obtained manually (Manual vs. interactive: $r_{\text{Count}} = 0.881$, $p_{\text{Count}} < 0.001$; Manual vs. automated: $r_{\text{Count}} = 0.803$, $p_{\text{Count}} < 0.001$; $r_{\text{Perimeter}} = 0.991$, $p_{\text{Perimeter}} < 0.001$; $r_{\text{Area}} = 1.000$, $p_{\text{Area}} < 0.001$). As expected, the disparity between the automatic and interactive methods was even smaller (Automated vs. interactive: $r_{\text{Count}} = 0.924$, $p_{\text{Count}} < 0.001$). We found the accuracy values of the interactive and automated approaches described here to be comparable to those of other widely accepted systems (Mango, 1994; Einstein *et al.*, 1997; Sims *et al.*, 2002; Naik *et al.*, 2008; Doyle *et al.*, 2007; Sieren *et al.*, 2010; Galarraga *et al.*, 2012; Nielsen *et al.*, 2012; Pajor *et al.*, 2012; Shi *et al.*, 2012; Tapias *et al.*, 2013).

Table 2.4. Correlations between measurements derived by using manual, interactive or automated threshold methods, for mucous cell assessment.

Comparison for mucous cells	Pearson correlation
Count (N°)	
Manual vs. interactive	$r = 0.881, p < 0.001$
Manual vs. automated	$r = 0.803, p < 0.001$
Automated vs. interactive	$r = 0.924, p < 0.001$
Perimeter Length (μm)	
Manual vs. automated	$r = 0.991, p < 0.001$
Filled Area (μm^2)	
Manual vs. automated	$r = 1.000, p < 0.001$

Footnotes:

$n = 25$ Histological frames analysed for each feature measurement and threshold method employed. Correlations were considered significant if $p < 0.05$.

Examples of processed images are presented in Figure 2.8, in order to show a direct and unbiased comparison between the manual counts of a histologist, and the counts obtained using the proposed image analysis system. Manually assessed cells are marked with yellow crosses or yellow contour delineations, and multi-coloured overlay masks identify the cells assessed by the automated system (*i.e.* without the operator interaction). The examples show how the proposed system's count for mucous cells is very similar to those of the histologist (Table 2.4). In fact, the results of the automated method are close to the mean values of the manual counts for each image, and fall within the standard deviation of the manual counting. This also holds true for mucous cell perimeter lengths and filled areas, this being irrespective of the segmentation threshold method used (*i.e.* automated or interactive) – Table 2.4 and Figure 2.8.

Insight into how well the automated assessment agrees with the pathologist's assessment was sought through comparisons of image outputs (Figure 2.8). Substantial agreement (*i.e.* lacking noteworthy or considerable errors) existed between the fully automated and the manual morphometric image segmentation. The level of agreement between human visual and computer-assisted mode was even more robust (images not shown). A noticeable source of error in the fully automated quantification (see arrow and star marks in Figure 2.8, as examples), was believed to be the lack of absolute "correction-

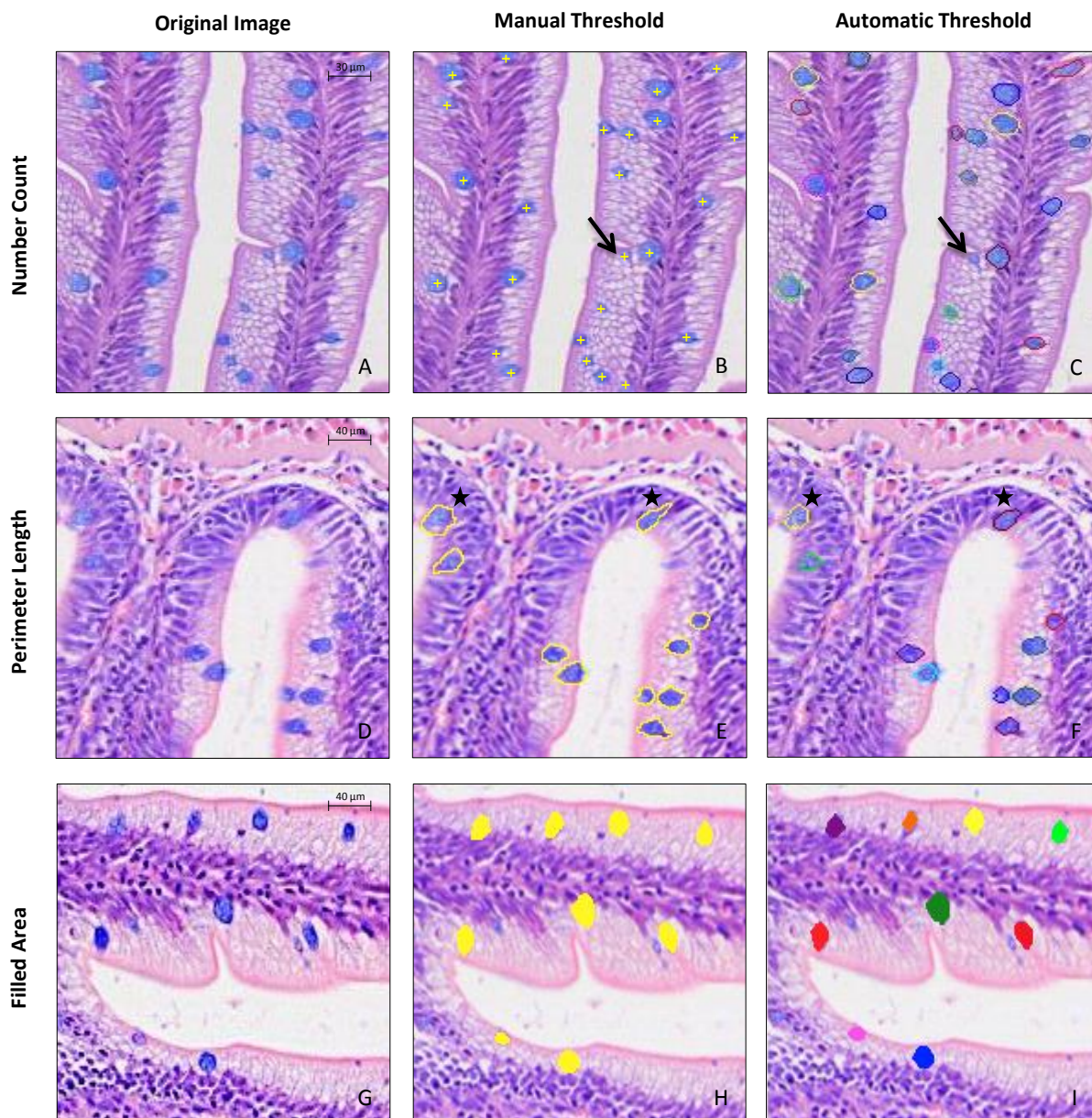


Figure 2.8. Images from Atlantic salmon distal intestine sections used in the comparison of results derived from the automatic algorithm system, against the manual measurements obtained by an expert histopathologist. (A, B, C) The first row shows the counting results for mucous cell number, while the second (D, E, F) and third rows (G, H, I) show the perimeter and filled area of cells, respectively. The assessed mucous cells are marked by yellow crosses (B, histopathologist's assessment) or by multi-colour overlays (C, automated system counts, without operator interaction). The arrows are pointing to a specific mucous cell, which was not picked up by the automated system because of the size thresholds that were implemented. The stars mark the same mucous cells being assessed with both methodologies therefore having slightly different perimeter delineations. Sections were stained with a combination of haematoxylin-eosin and Alcian blue 8 GX.

steps”, as opposed to the competence of the pathologist viewing the tissue irregularities or deficiencies in the staining protocol. Most automated systems fail to account for artefactual specimen variations (Webster *et al.*, 2012). Deviations in tissue orientation, handling, processing and staining among samples can be sources of segmentation inaccuracies. Such variations are routinely encountered and the algorithms need to be capable of being optimised to compensate for such inherent features.

By design, the developed system was not fully automated. Its interactive framework allows the operator, by manually gating histograms and thus visually checking the marked-up masks in the images created during the pseudo-segmentation process, to confirm that the field of the region of interest is acceptable for analysis and thus to accept it or reject it.

While it is true that longer processing times are required for this interactive “correction” (Table 2.3), we consider these interactive steps have great potential in providing increased accuracy, as corroborated by the correlation results shown in Table 2.4.

In order to evaluate the proposed software further, the same images were then evaluated using an open source image analysis system (here we used ImageJ software). The measurement results for representative measurements comprising the mucous cell total count, the luminal surface perimeter length and the mucosal tissue area, retrieved with the proposed image analysis system were plotted against those of ImageJ and shown in Figure 2.9. The comparison revealed a regression factor of 1.000 ($r = 1.000$, $p < 0.001$) for the counts, a factor of 0.974 ($r = 0.987$, $p < 0.001$) for the perimeter length, and 0.978 ($r = 0.987$, $p < 0.001$) for the filled area parameter, which suggested that the developed system is accurate and reliable.

2.3.4.3. Reproducibility. To determine the reproducibility of the system, an evaluation session was carried out separately and independently by two operators / observers (one trained histopathologist and one computer scientist). This was achieved by comparing the degree of agreement between measurements obtained for identical when the procedure was conducted by different operators and at two distinct time points. Although minor inter- and intra-operator variations were recorded, these did not influence the outcome. Analysis of

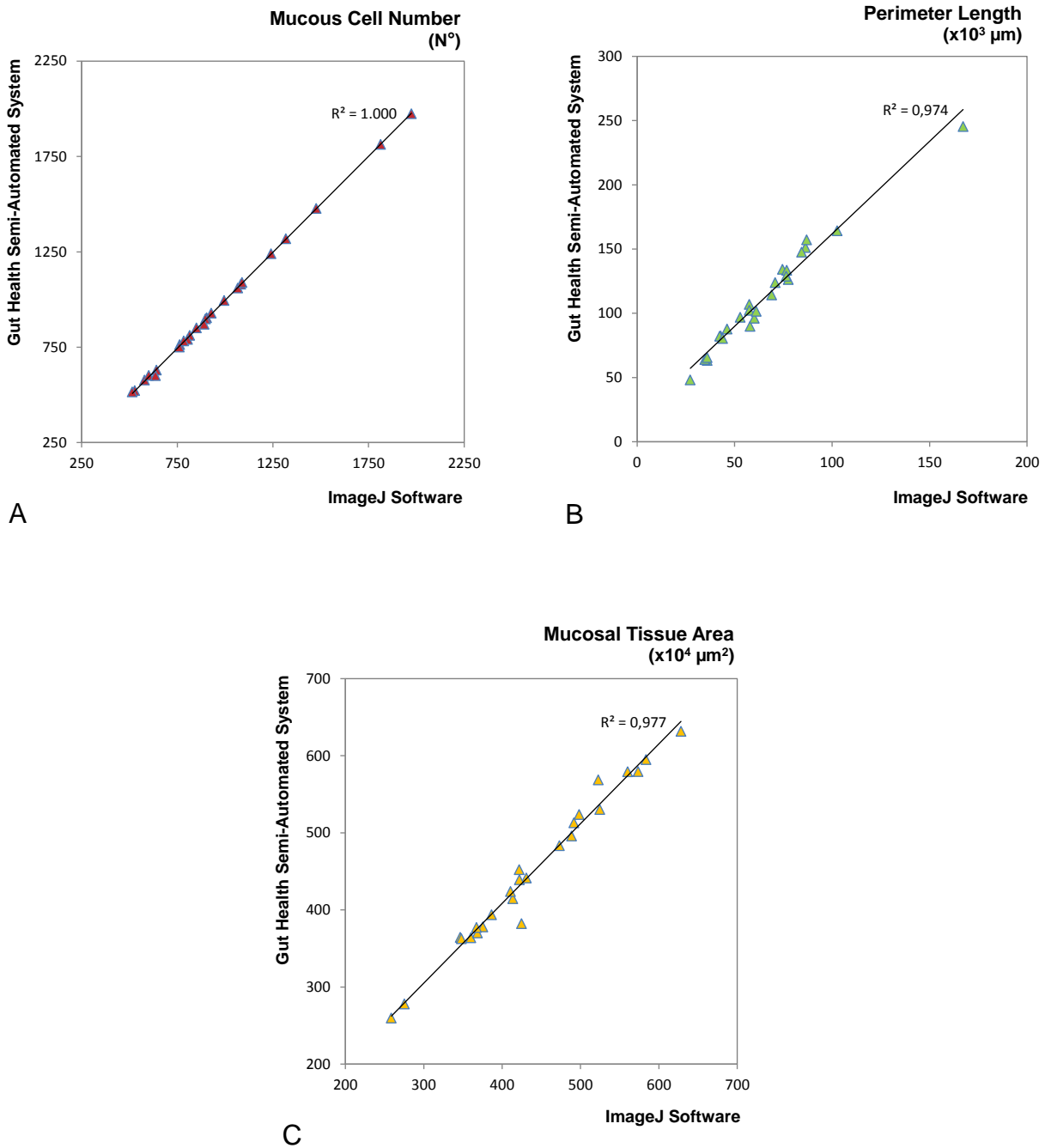


Figure 2.9. Scatter plots for the performance analysis results obtained by the proposed interactive image analysis system and an open source image analysis software (*i.e.* ImageJ). (A) Comparison of the total number of mucous cells. (B) Comparison of the total perimeter length of the luminal surface. (C) Comparison of the total mucosal tissue area. R^2 values, representing the square of the correlation coefficients.

the repeated measures, revealed intra-operator concordance correlations of $r_{\text{Count}} = 0.935$, $p_{\text{Count}} < 0.001$; $r_{\text{Perimeter}} = 0.732$, $p_{\text{Perimeter}} = 0.098$; $r_{\text{Area}} = 0.916$, $p_{\text{Area}} < 0.001$, while the inter-operator had a correlation coefficient of $r_{\text{Count}} = 0.956$, $p_{\text{Count}} < 0.001$; $r_{\text{Perimeter}} = 0.406$, $p_{\text{Perimeter}} = 0.244$; $r_{\text{Area}} = 0.834$, $p_{\text{Area}} < 0.001$. These values indicate high reproducibility for the developed system, as the correlation scores were overall greater than 0.7, with the exception of the inter-operator concordance for the perimeter length, which was somewhat lower (Table 2.5). This was unsurprising, since the pipeline for identification and further assessment of the perimeter length from the mucosal tissue luminal boundary, is far lengthier and involves various interactive processing steps, which were not undertaken by the second operator. For the count of mucous cells and total filled tissue area on the other hand, more straightforward and comprehensive selection processes are required (see Technical Note A1). Also for a true evaluation comparison to be performed, specific encoding rules or guidelines for operator-use should be agreed upon. Accordingly, extra time should have been allocated as to allow both appropriate discussion / understanding of the instructions to follow, as well as for the necessary training, which would likely have been reflected in the reproducibility scores obtained between intra- and inter-observers. It is worth mentioning that Operator A had considerably more training time than Operator B for the tasks considered, and therefore more experience using the software, which explains in some part, the inter-operator differences observed and also the mean time spent per slide (Table 2.5).

Nevertheless, it is recommended that the same operator should analyse all sections in a single batch. Choosing a single observer / operator, not only reduces variations but also allows the analysis to benefit from the operator's learned skills and experience gained in working with the system.

Further assessment of the reproducibility of the system should be undertaken in the future, to determine variation between groups of specimens, e.g. those having diverse body sizes or different maturation states within the same cohort. It is also imperative to estimate the consistency and variability that could be expected from the histological analysis within a

study group, and the sample size required to obtain meaningful results. Due to time constraints, such an analysis could not be undertaken for the present study.

Table 2.5. Reproducibility of the semi-automated image analysis system, accounting for intra- and inter-operator variation.

	Operator A			Operator B		
	Count (N°)	Perimeter Length (µm)	Filled Area (µm ²)	Count (N°)	Perimeter Length (µm)	Filled Area (µm ²)
Operator A	<i>Time average per slide: 11'53" ± 1'48" (Min 8'53", Max 18'22")</i>					
Count (N°)	$r^* = 0.935$ $p^\dagger < 0.001$	-	-	$r = 0.739$ $p = 0.015$	-	-
Perimeter Length (µm)	-	$r = 0.732$ $p = 0.098$	-	-	$r = 0.406$ $p = 0.244$	-
Filled Area (µm ²)	-	-	$r = 0.916$ $p < 0.001$	-	-	$r = 0.834$ $p < 0.001$
Operator B	<i>Time average per slide: 15'22" ± 1'36" (Min 12'19", Max 17'35")</i>					
Count (N°)	$r = 0.739$ $p = 0.015$	-	-	$r = 0.946$ $p < 0.001$	-	-
Perimeter Length (µm)	-	$r = 0.406$ $p = 0.244$	-	-	$r = 0.740$ $p = 0.082$	-
Filled Area (µm ²)	-	-	$r = 0.834$ $p < 0.001$	-	-	$r = 0.905$ $p < 0.001$

Footnotes:

* r , Pearson's correlation coefficient

† p , p -value or calculated probability is the estimated probability of rejecting the null hypothesis of the study question (*i.e.* that the two factors examined are unrelated), when that hypothesis is true.

$n = 10$ histological identical frames analysed twice per each operator. Correlations were considered significant if $p < 0.05$.

2.4. General conclusions

This chapter has described the development of a novel histological assessment system based upon advanced image analysis. Such a tool can provide a system for evaluation of the extent of morphological changes occurring in the distal intestine of Atlantic salmon following dietary modulation.

The analytical methodology can be conducted with minimal user-interaction, thus allowing rapid and objective assessment of 12 continuous variables per histological frame analysed. The processing time required for each histological frame was roughly 20-25 min, which greatly improved the efficiency of conducting such a quantitative assessment with respect to the time taken for a subjective semi-quantitative alternative approach.

The system was then evaluated in terms of its precision. Significant agreement between the fully automated and the manual morphometric image segmentation was achieved. The strength of this quantitative approach was enhanced by the employment of interactive procedures, which enabled the operator / observer to rectify preceding automated segmentation steps, and account for the specimen's variations.

The system also provided significant correlation to other well-established quantitative approaches. Results suggest that it can be a viable alternative to a pathologist's manual scoring, being more practical and time-efficient. This method could therefore reduce the workload of pathologists and serve to complement / supplement their observations.

The high reproducibility and lack of dependence on high user expertise makes it suitable for provision of large-scale data archives, providing a robust method to assess specific aspects of fish intestinal histology samples obtained under different experimental states and at different times.

Ultimately, it is envisaged that the development of such a tool will greatly assist in the evaluation of alternative dietary components for aquaculture feeds, leading in turn, to a more sustainable global industry and improved fish health and welfare.

USER GUIDELINES FOR OPERATION OF THE GUT HEALTH IMAGE PROCESSING AND ANALYSIS SEMI-AUTOMATED SYSTEM – PART I

A detailed, comprehensive protocol has been compiled to allow a better understanding of the image processing and analysis workflow. It provides step-by-step instructions in loading, initiating and operating the system, which is employed across the analyses presented in this thesis.

1. KS Run User Interface

The image processing, segmentation and analysis script developed is deployed using the stand-alone KS Run software platform (Version 3.0, Carl Zeiss Vision GmbH, München-Hallbergmoos, Germany). Instructions for installing the KSRun software and deploying the gut analysis script within it are provided in the KS Run user manual (KS Run User Interface Manual Guide B 40-613, Carl Zeiss Vision GmbH, München-Hallbergmoos, Germany). The following sections describe the user protocol for the gut image analysis script.

1.1. Image Processing and Analysis Workflow

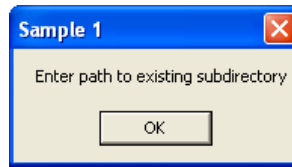
The image processing, segmentation and analysis pipeline consists of a succession of interactive and automated operational steps (⚙️). Feedback in the form of guideline-notes for the operator (ℹ️), and visualisation of the generated images (🖼️, Appendix 2 and Figures 3.4 and 3.5 from Chapter 3) was made available at each step of the pipeline process, as well as feature extraction and data generation (📄, Figure 8).

1.1.1. Start Up

⚙️A. All existing images, overlay masks and temporary databases from previous program runs are erased.

B. Maximal memory space is made available.

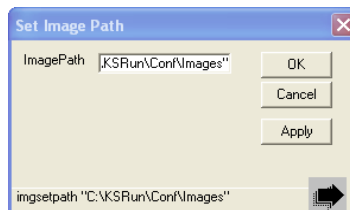
C. A 'Message Window' with written guidelines for the user appears.



1.1.2. Logistical Setup and Data Input

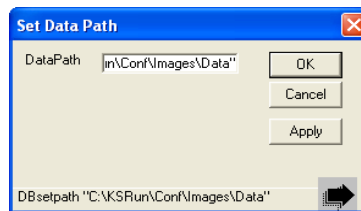
*D. An image upload-path is set according to the user.

i₁ "Enter the path to existing image sub-directory."
 e.g. C:\KSRUN\Conf\Images\Gut\Image_Folder\Data_Testing



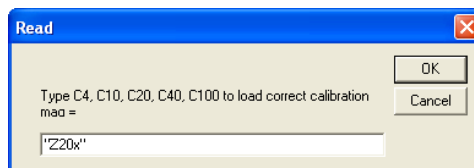
E. A database download-path is set according to the user.

i₂ "Enter the path to existing data base sub-directory."
 e.g. C:\KSRUN\Conf\Images\Gut\Image_Folder\Data_Testing



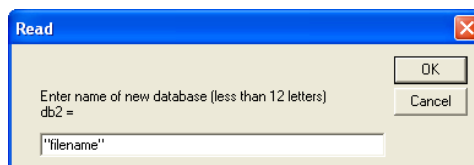
F. The appropriate calibration file is uploaded in accordance to the user's requirements.

i₃ "Type C4, C10, C20, C40, C100 or Z20x to load the correct calibration file."
 e.g. Z20x



G. A name is given to the new database file to allow sample identity to be recorded, and measurement columns are added to the database.

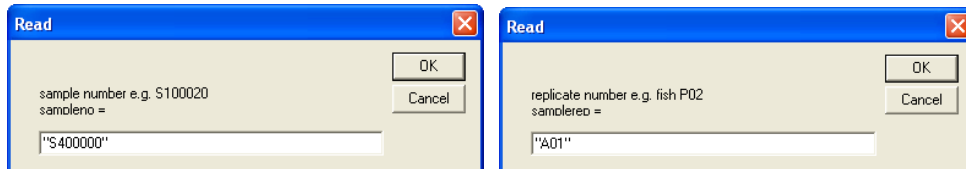
i₄ "Enter a name for the new database being generated."
 e.g. S400000_A01.xls



H. Object boundaries are defined in accordance to an 8-pixel connectivity rule.

I. An image is selected for analysis. The software expects a non-compressed TIFF image format.

①₅ "Enter the sample number." ①₆ "Enter the replicate number."
 e.g. S400000 e.g. A01

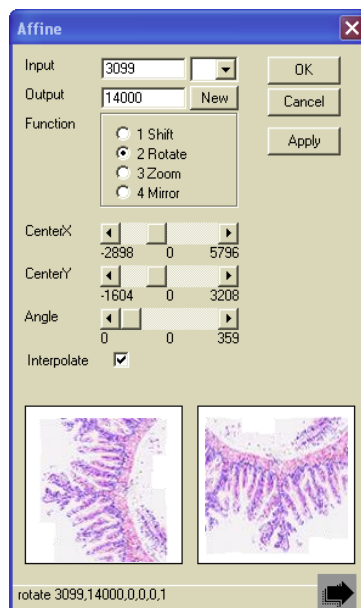


1.1.3. Image Pre-processing

⚙️ J. Rotation of the image is made possible to assist analysis.

①₇ "Left click in the middle of the right-hand side box to centre the image and hit 'Apply'. Use 'Rotate' and 'x / y sliders' to obtain a centred rotation and then hit 'Ok'."

🖼️ Image 1

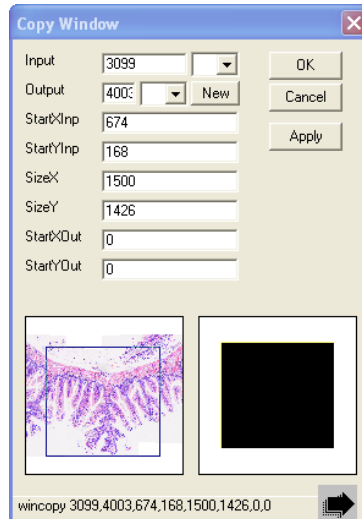


K. A microscope field is selected by the user and a fixed frame size (pixels) used to crop a-section from Image 1.

①₈ "Select a width and height for the cropping-window. Choose an area to copy, by clicking in the middle of the box and moving it. Be careful not to accidentally resize the box by clicking on an edge."

e.g. 1500 x 1426 pixels

🖼️ Image 1A
 e.g. S400000_A01.CRP.tif



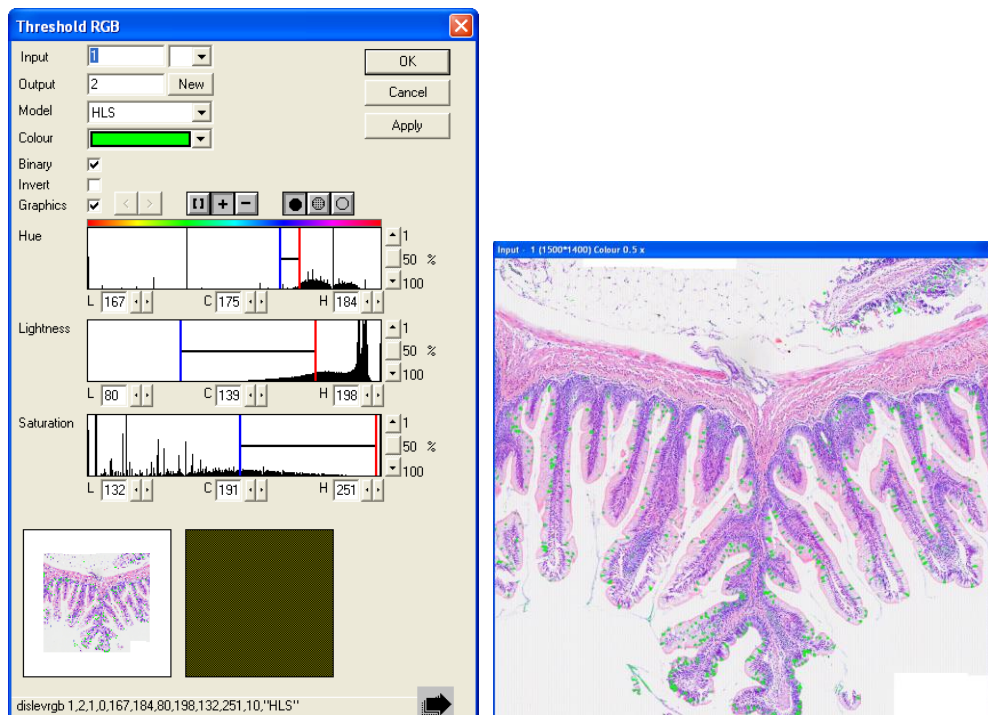
L. Details on the size of the cropped image are stored and the new image is placed into position 1 in the 'Gallery Window'.

1.1.4. Image Segmentation and Processing

M. Mucous cells present in the image are highlighted and segmented by an HLS colour thresholding operation.

9. *“Right click on the small left-hand image and choose ‘Big Display’’. Highlight the mucous cells using ‘square bracket’ depressed (as an initial starting point) and circling the area of interest. Then, successively add missing areas using ‘+’ depressed (or ‘<’ to undo the previous selection).”*

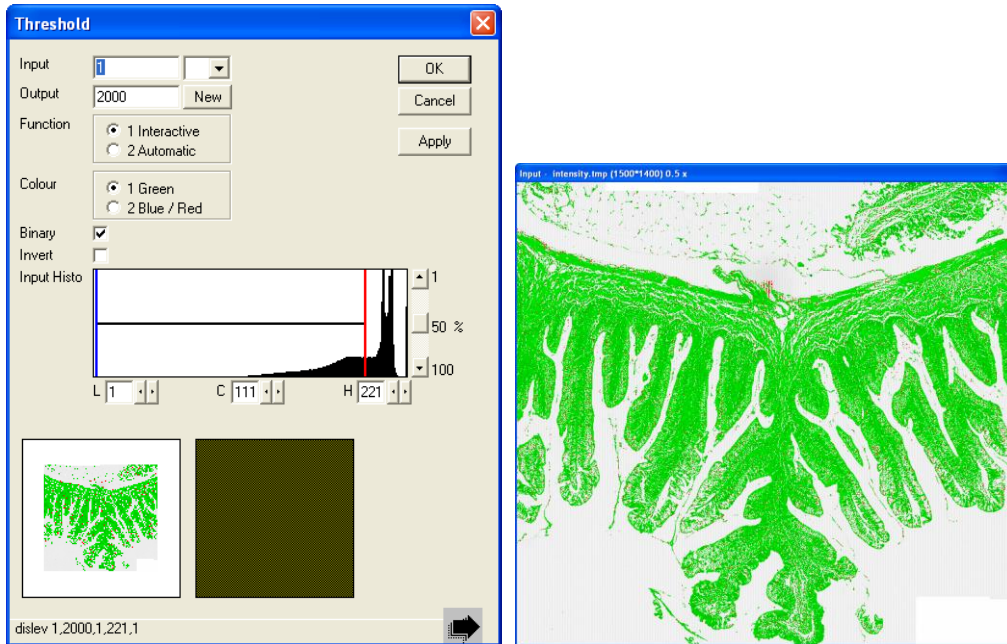
Image 2



N. Tissue is highlighted and segmented using an intensity threshold operation.

i₁₀ “Right click on small left-hand image and choose ‘Big Display’. Move the red (right-hand) boundary line in the data box to highlight tissue (i.e. exclude non-tissue / debris). Try to include full tissue edges (selected areas will appear in green) leaving the vacuoles surrounded. Though try not to encroach too much the luminal space.”

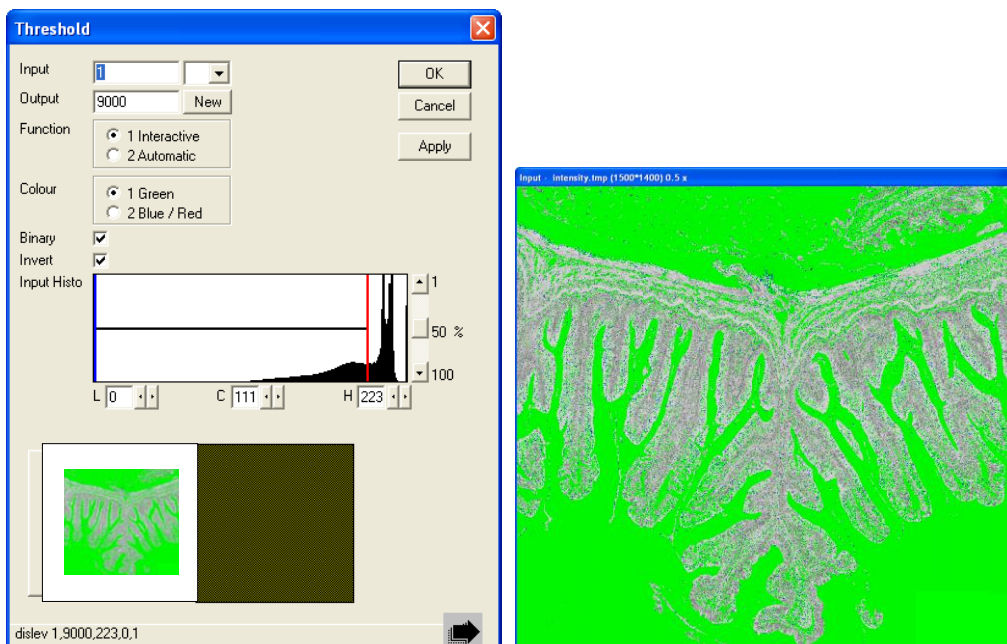
Image 3




O. Tissue vacuoles are highlighted and segmented by an inverse-intensity threshold.


i₁₁ “Right click on the small left-hand image and choose ‘Big Display’. Move the red (right-hand) boundary line in the data box, to highlight the vacuolisation. The luminal space will also be selected but it is fine (selected areas will appear in green)”.

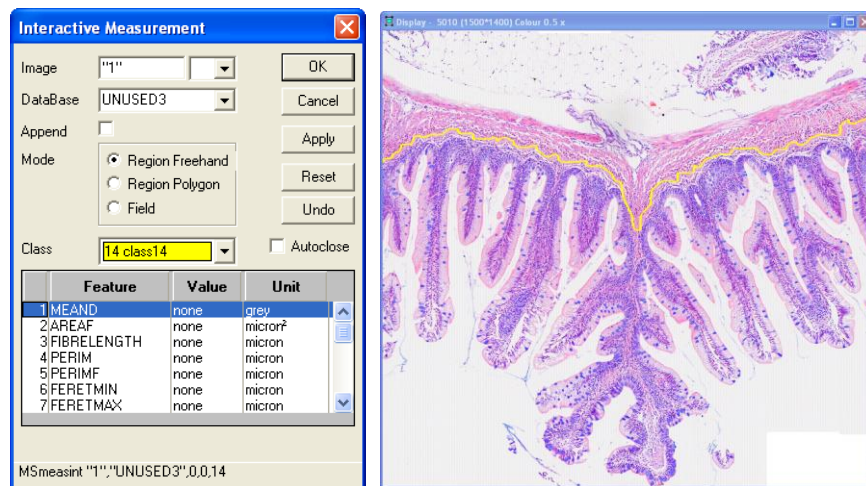
Image 4



P. The *stratum compactum* is delineated by interactive freehand-drawing in the graphics plane of the displayed image-scene.

 ¹² “Hit the ‘Reset’ button and untick the ‘Autoclose’ box, then outline the *stratum compactum* (i.e base of the mucosal tissue) only from edge to edge. Press and hold the left mouse button to draw continuously. Hit ‘OK’ when completed.”

 Image 5



Q. The box comprising mucosa and lumen are manually outlined (no drawing is required to outline the mucosal surface, which is defined by the previously detected tissue boundary).


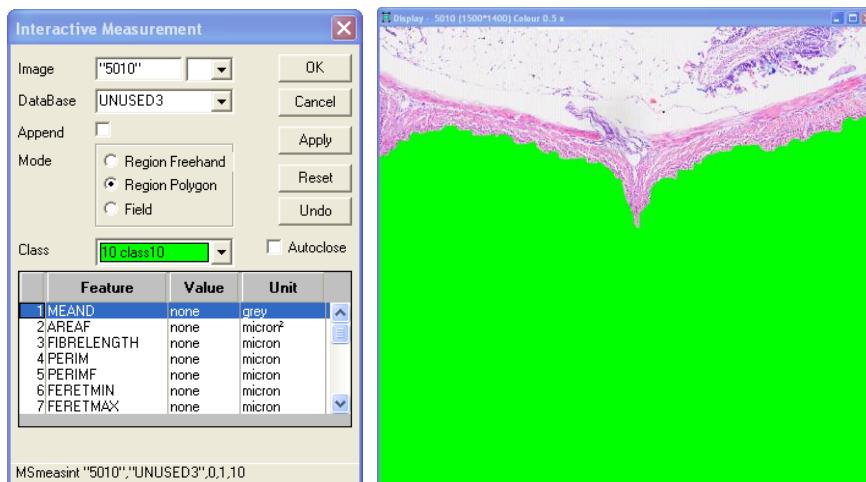
 ¹³ “Do not hit the ‘Reset’ button, but do untick the ‘Autoclose’ box. Follow the edge of the ‘Display Window’, starting at one end of the *stratum compactum* and following the window edge along the tissue and luminal space. Left click and release, to draw from point-to-point. Double click the left mouse button and check that no extra line is expected (check that by dragging the cursor across the screen). Hit ‘OK’ to finish. If you make a mistake hit ‘Undo’ and repeat the operation.”

 Image 6

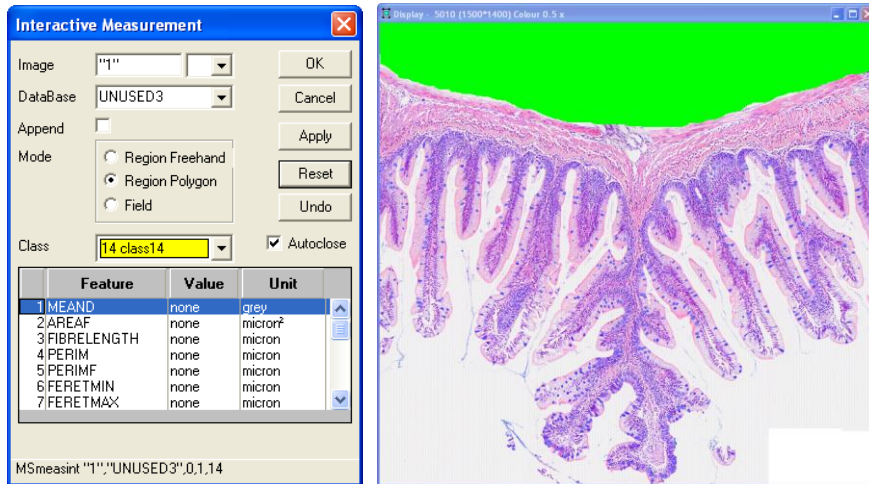


R. The *muscularis externa* is manually outlined.

①₁₄ “Hit the ‘Reset’ button before submucosal tissue is captured. Outline the peritoneal edge of the *muscularis externa* and any other space outside the intestinal wall. Follow the ‘Display Window’ edge if necessary.”

①₁₅ “Hit the ‘Reset’ button only if the captured area is inaccurate, then redo the outline of *muscularis externa*. Otherwise hit ‘OK’.”

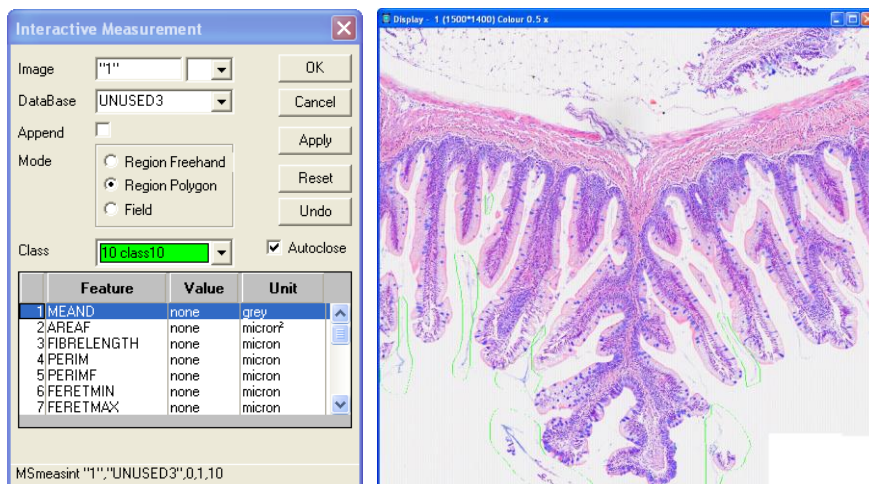
Image 7



S. Unwanted features such as artefacts created during histological processing or tissue debris extraneous to the analysis are removed by manual contour delineation.

①₁₆ “Hit the ‘Reset’ button, then draw round pieces of tissue or debris you don’t want measured (especially those touching useful tissue). Make sure you close the drawn boundary. If any large areas of lumen were filled earlier, draw around the luminal edge to help discard. Press and hold the left mouse button to draw continuously or to draw from point-to-point marking successive points with the left mouse button, releasing between points. To close the polygon hit the right mouse button.”

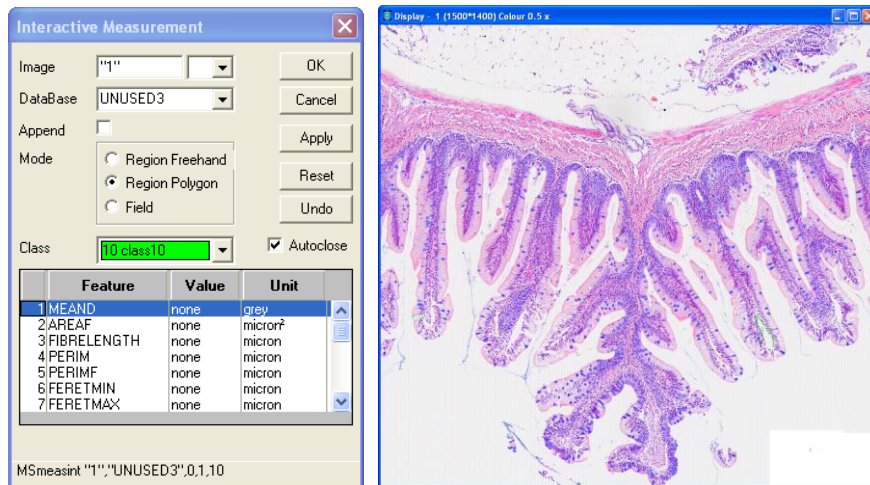
Image 8



①₁₇ “Hit the ‘Reset’ button then draw round pieces of lumen or vacuole you want measured as tissue. Press and hold the left mouse button to draw continuously or to draw from point-to-

point, mark successive points with the left mouse button, releasing between points. To close the polygon hit the right mouse button.”

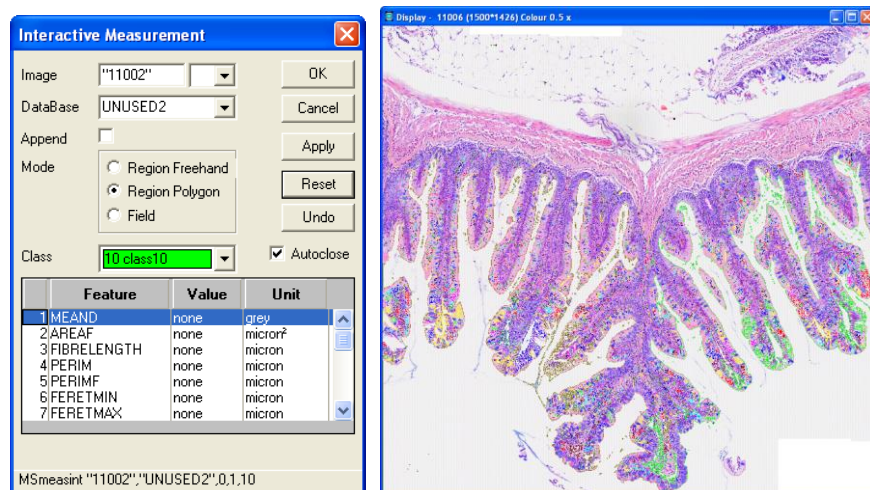
Image 9



T. Tissue vacuolisation areas are corrected by interactive freehand-drawing in the graphics plane of the displayed image-scene.

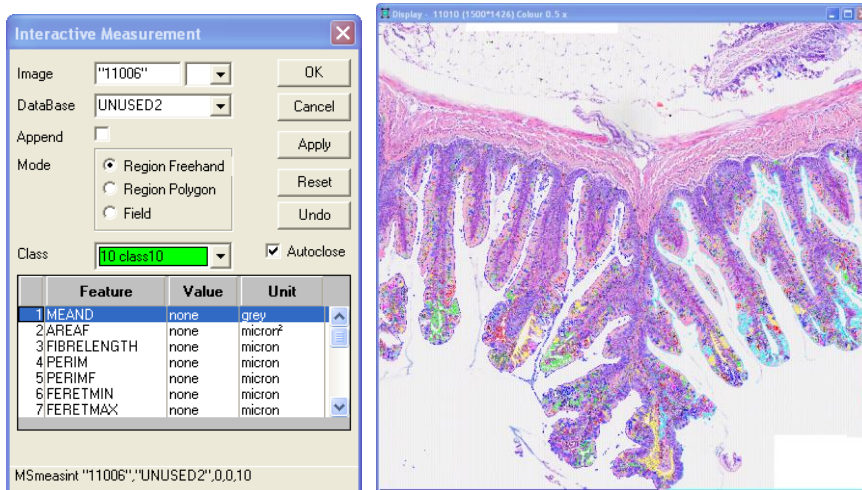
18 “Hit the ‘Reset’ button, then draw polygons around the regions within tissue that are not vacuolar, or part of the lumen (e.g. tissue rupture and other artefacts). Press and hold the left mouse button to draw continuously or to draw from point-to-point, mark successive points with the left mouse button, releasing between points. To close the polygon hit the right mouse button.”

Image 10



19 “Hit the ‘Reset’ button and untick the ‘Autoclose’ box. Draw continuous lines to close off / exclude areas of lumen continuous with vacuoles (these will share the same outline colour). Press and hold the left mouse button to draw continuously. Release the mouse button to finish the line.”

Image 11



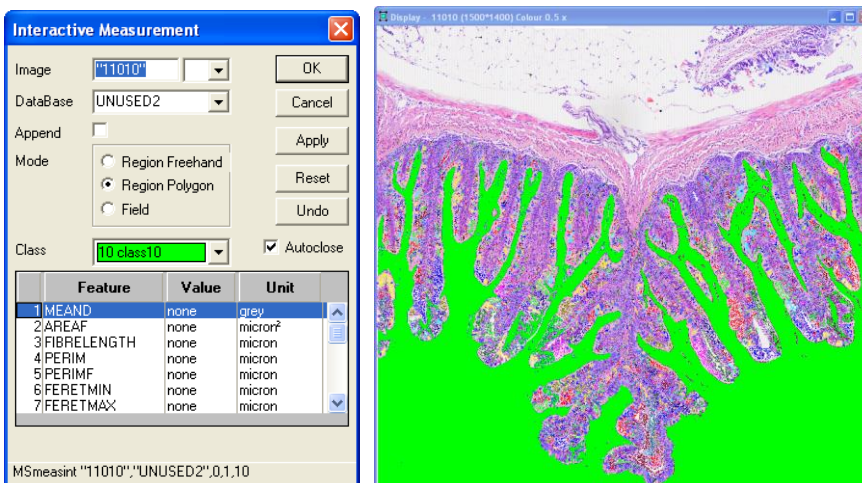
U. The luminal area is demarcated by interactive selection.

①₂₀ “Hit the ‘Reset’ button then draw small circles in each separate luminal area, marking them for removal. Press and hold the left mouse button to draw continuously or to draw from point-to-point, mark successive points with the left mouse button, releasing between points. To close the polygon hit the right mouse button.”

①₂₁ “Hit the ‘Reset’ button then draw continuous lines or polygons, to draw missing areas of lumen (i.e. add them to the lumen area). Press and hold the left mouse button to draw continuously. Release the mouse button to finish the line.”

①₂₂ “Hit the ‘Reset’ button then draw small circles in each missed luminal area, marking them for removal. Press and hold the left mouse button to draw continuously or to draw from point-to-point, mark successive points with the left mouse button, releasing between points. To close the polygon hit the right mouse button.”

Image 12



1.1.5. Histological Identification and Post-processing Overlays

✿V. Image frame box is created:

v1. Taking into account the image size details that were established in step ^WL, a frame border line 4 pixels thick, and 4 pixels smaller than the full image' size was generated.

 Image 13

^WW. Processing of the total tissue area is initiated:

w1. Image 3 is inverted to provide its negative image and a new binary image of the total tissue area is saved.

 Image 3A

w2. Smaller regions found in Image 3A, fitting into a specified size range (*i.e.* 500 to 1×10^{11} pixels) are eliminated by use of a 'Binscrap'⁴ operation.

 Image 3B

w3. Using a 'Binor'⁵ operation, vacuoles found in the tissue regions of interest are filled. Thus, objects not encountered in the region of interest (ROI) from Image 3B are eliminated from the original Image 3, and the resulting image saved.

 Image 3C

w4. To smooth the captured tissue edges and remove artefactual associations with tissue debris and other artefacts, the tissue from Image 3C is eroded by 5 pixels.

 Image 3D

w5. The remaining holes (*i.e.* 0 to 500 pixels) found in the tissue from Image 3D, are removed by use of size-scrap operators.

 Image 3E

w6. The region of interest remaining in Image 3E, is dilated to restore its original extent. Finally, a binary image comprising the final processed regions of interest is created and stored.

 Image 3F

⁴ **Scrap.** This function deletes or selects regions in a specified size range (*i.e.* on the basis of their total area in pixels) (KS 300 Imaging System Manual Guide B 40-613, Carl Zeiss Vision GmbH, München-Hallbergmoos, Germany).

⁵ **Binor.** This function undergoes a bitwise OR operation, which takes two bit patterns of equal length and performs the logical inclusive OR operation on each pair of corresponding bits. The result in each position is 1 if the first bit is 1 or the second bit is 1 or both bits are 1; otherwise, the result is 0. In this, we perform the addition of two bits, *i.e.* $0 + 1 = 1$, however $1 + 1 = 1$. For example: 0101 (Input 1) 0011 (Input 2) = 0111 (Output) (KS 300 Imaging System Manual Guide B 40-613, Carl Zeiss Vision GmbH, München-Hallbergmoos, Germany).

✚X. The *stratum compactum* is outlined:

x1. The contour line extracted from Image 5 is fattened and saved.

📄 Image 5A

x2. The thick line is then saved as an overlay into Image 1A.

📄 Image 5B

e.g. S400000_A01.STCOMP.tif (Figure 1)

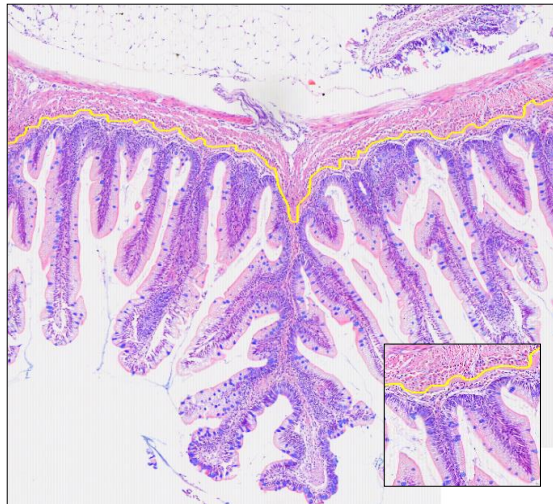


Figure 1. Output Image 5B showing the delineated *stratum compactum* as a yellow overlay.

✚Y. The mucosal tissue area is delineated:

y1. The lines captured in Image 6 are merged into Image 5A, and both lines fused by dilation operations.

📄 Image 6A

y2. The generated polygon is filled in green (*i.e.* Image 6B) and saved as an overlay mask into Image 1A.

📄 Image 6B

y3. The lines from the polygon saved in Image 6A are eroded back to their original thickness and a new binary image stored.

📄 Image 6C

Y4. Through a 'Binxor'⁶ operator comparing the regions captured in Images 3F and 14, a mucosal mask is then generated. In addition, correction of the border lines is achieved by deducting the objects found in Image 13.

 Image 6D

Y5. Polygons captured in Image 8 (e.g. tissue debris or other artefacts) are filled and their areas deducted from the tissue regions captured in Image 6E.

 Image 6F

Y7. Similarly, the polygons caught in Image 9 (e.g. lumen or vacuoles that should be considered as tissue) are filled and the regions of interest added to the tissue region from Image 6F.

 Image 6G


Y8. The mucosal tissue region is again amended by deduction of the vacuolisation area from Image (i.e. Image 17A).

 Image 6H_a

Y9. Finally the submucosa and *muscularis externa* regions are deducted from the mucosa (i.e. Image 7aaa).

 Image 6H_b

Y10. Thereafter, the mucosal tissue regions of interest are highlighted and overlay masks generated on top of Image 1A.

 ²⁴ "Right click on the small left-hand image and choose 'Big Display'. All tissue will be selected at the start (labelled in green), therefore use the left mouse button to deselect (labelled in red) the unwanted tissue. Use the right mouse button to increase and decrease the image size for better clarity. If unexpected red or green regions are apparent, zoom into the image to check their accuracy."

⁶ **Binxor**. This function carries out a bitwise XOR operation by electing two bit patterns of equal length and performs the logical exclusive OR operation on each pair of corresponding bits. The result in each position is 1 if only the first bit is 1 or only the second bit is 1, but will be 0 if both are 0 or both are 1. In this we perform the comparison of two bits, being 1 if the two bits are different, and 0 if they are the same. For example: 0101 (Input 1) 0011 (Input 2) = 0110 (Output) (KS 300 Imaging System Manual Guide B 40-614, Carl Zeiss Vision GmbH, München-Hallbergmoos, Germany).

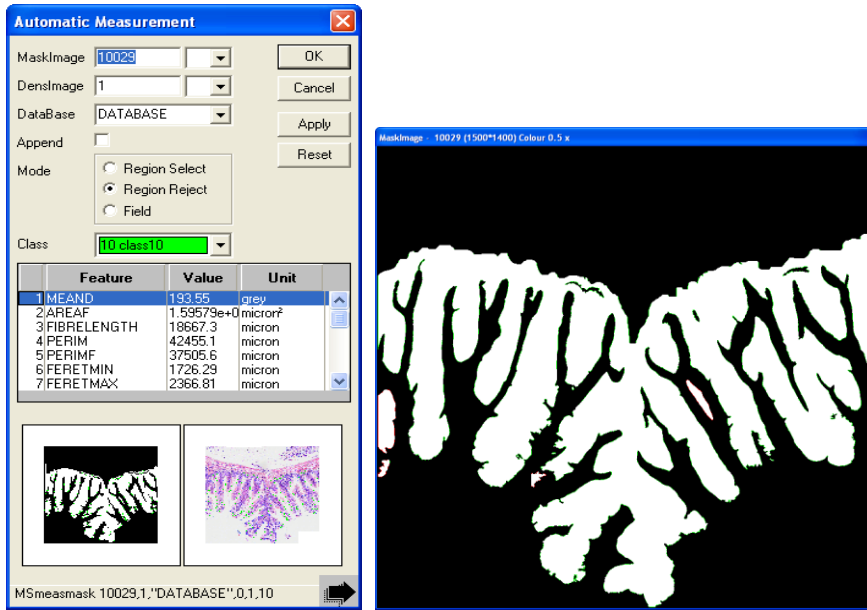


Image 6I
e.g. S400000_A01.TISSUE.tif (Figure 2)

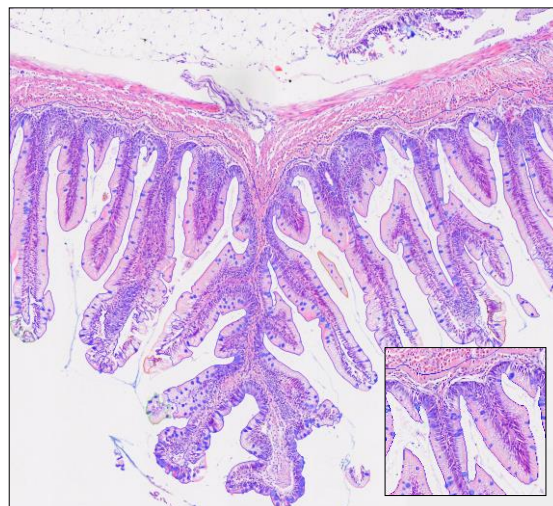


Figure 2. Output Image 6I, revealing the mucosal tissue delineated by a colour overlay.

z. The *muscularis externa* is outlined:

z1. The polygon captured in Image 7 is filled in green and saved as an overlay mask into Image 1A.

Image 7A

α. Processing of the submucosal tissue starts:

α1. The region corresponding to the filled polygon from Image 6B is subtracted from the tissue capture from Image 3F and the resulting area amended by subtraction of Image 13.

Image 14

a2. A submucosal tissue mask is generated by subtracting the regions demarked in Image 7 from Image 14.

25 “Right click on the small left-hand image and choose ‘Big Display’. All tissue will be selected at the start (labelled in green), therefore use the left mouse button to deselect (labelled in red) the unwanted tissue. Use the right mouse button to increase and decrease the image size for better clarity. If unexpected red or green regions are apparent, zoom into the image to check their accuracy.”

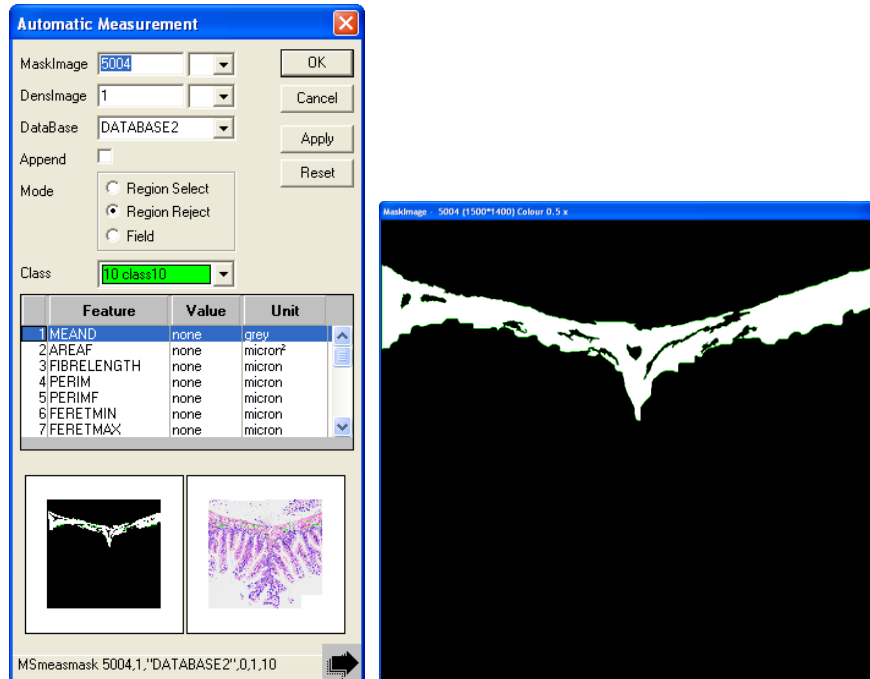


Image 14A

e.g. S40000_A01.SUBM.tif (Figure 3)

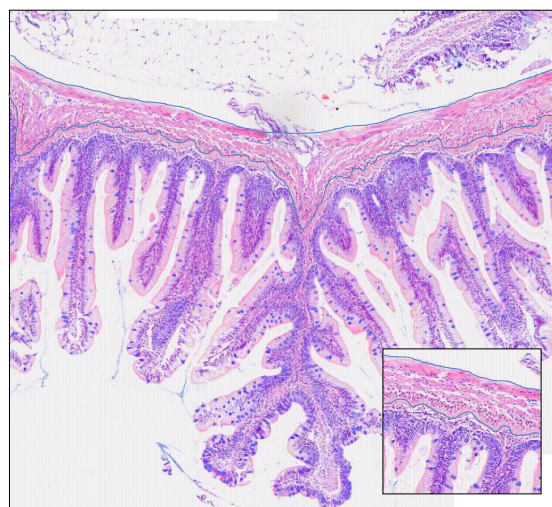


Figure 3. Output Image 14A, submucosal tissue delineated with a coloured overlay.

✳️β. Processing lumen region:

β1. Polygons captured in Image 8 (e.g. tissue debris or other artefacts) are filled and the marked regions added to the luminal region from Image 4.

 Image 4A

β2. Concurrently, polygons drawn in Image 9 (e.g. lumen or vacuoles that should be considered as tissue) are filled and subtracted from the luminal region of Image 4A.

 Image 4B

β3. The refractive luminal border from Image 15, which can be confused with mucous cell staining, is fattened, and subtracted from Image 4B.

 Image 4C

β4. The negative inverse of Image 7aa (i.e. submucosal and *muscularis externa* regions, Image 7aaa) are extracted from the region of interest captured in Image 4C.

 Image 4D

β5. Polygons marking regions within tissue that are not vacuolar (Image 10) are filled and the corresponding regions of interest, subtracted from the luminal region in Image 4D.

 Image 4E

β6. The lines from Image 11 are thickened and subtracted from the luminal area of Image 4E. Subsequently the image is revised and the outlines from Image 6A representing the *stratum compactum* and borderlines subtracted.


 Image 4F


β7. The user interactively marks contiguous areas of lumen in Image 4F, with small circles drawn in step ✳️U marking areas to be identified as lumen.

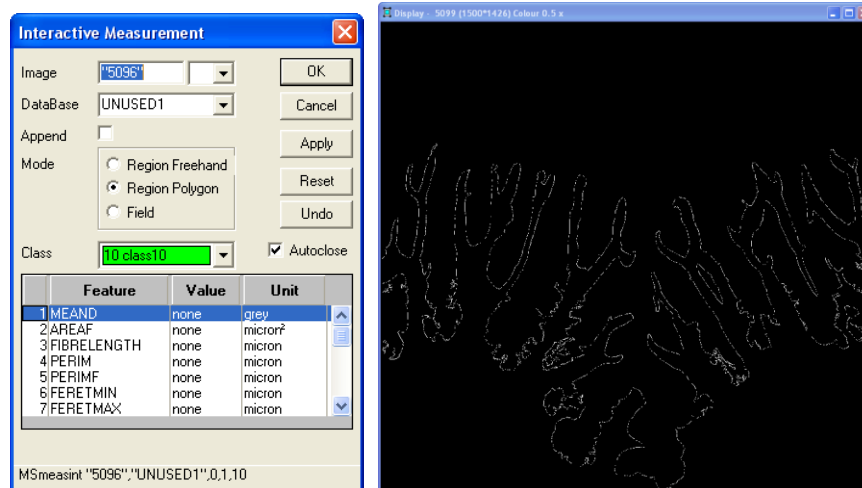
 Image 4G


β8. The luminal region (i.e. Image 4F) is segmented by an inverse intensity threshold, and objects (noise) fitting into a specified size range (i.e. 0-10 pixels) are removed by use of a 'Binscrap' operation. The resulting region of interest is inverted to its negative image and a new binary image saved.

 Image 4H

β9. Changes made over the following step (i.e. see guidelines ) are included to give an upgraded Image 4H and a new image of the luminal area created.

 *“Hit the ‘Reset’ button then draw polygons around the regions that are not part of the luminal surface. Press and hold the left mouse button to draw continuously or to draw from point-to-point mark successive point with the left mouse button, releasing between points. To close the polygon hit the right mouse button.”*



 Image 4I
e.g. S400000_A01.LUM.tif (Figure 4)

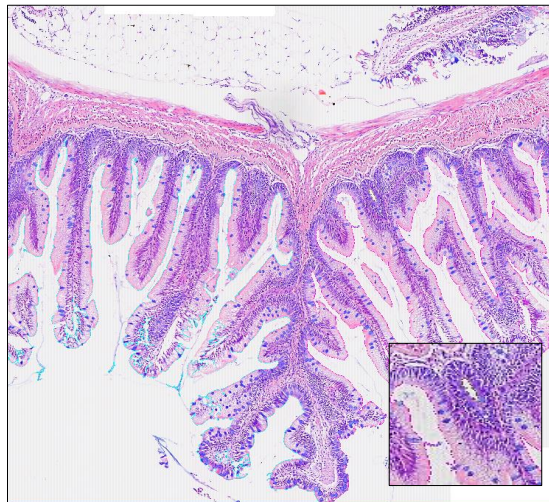



Figure 4. Output Image 4I, luminal regions being delineated by a colour overlay.

 γ. Extraction of the luminal perimeter:

γ1. The edge of the mucosal region captured in Image 6F is eroded twice. First, by removal of a 1x pixel layer, and thereafter by removal of a 3x pixels layer. The difference between

both giving the linear edge that will later be extracted from the luminal region (*i.e.* step β_3).

Image 15

2. A new perimeter line is generated by dilation of the luminal region from Image 4I and subtraction of the original non-dilated region from it. An overlay mask is saved into Image A1.

Image 15A

e.g. S40000_A01.PERIMETERS.tif (Figure 5)

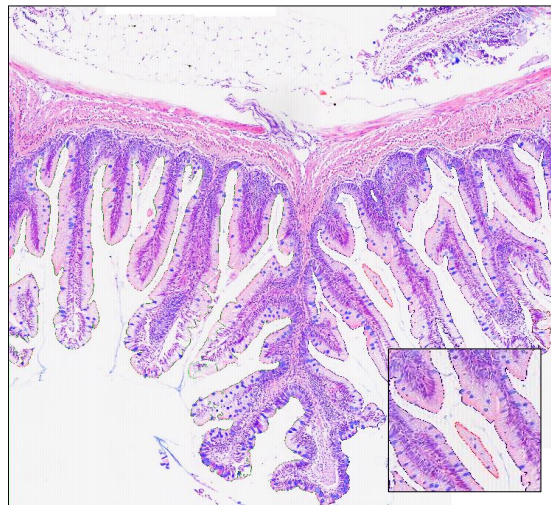


Figure 5. Output Image 15A, perimeter from the mucosal tissue being delineated with a coloured overlay.

Processing of the mucous cells initiated:

1. The refractive luminal border is removed from Image 2.

Image 2A

2. Small holes appearing in the middle of the objects in Image 2 were filled in, and small noise features (*i.e.* 0-3 pixels) around them, removed. The objects of interest are eroded and larger features extracted (*i.e.* 0-10 pixels).

Image 2B

ε3. Adjoining features are separated using a 'Grainsbin'⁷ operator, and the resultant objects dilated to their proper size.

Image 2C

ε4. The cells boundaries are made smoother, by successive erosion and dilation processes and a final mucous cell image saved.

Image 2D

ε5. The final mucosal tissue image (*i.e.* Image 6I) is taken and used to mask the recognised mucous cells within that tissue region (*i.e.* mucous cells can only occur in mucosal tissue). Mucous cell overlay mask is merged into Image A1.

Image 2E

e.g. S400000_A01.MASKEDCELLS.tif (Figure 6)

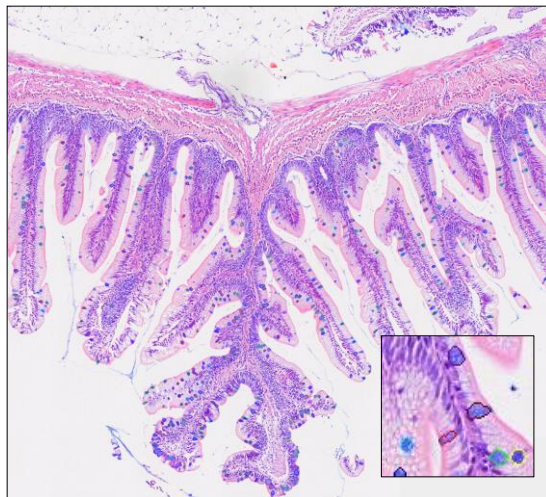


Figure 6. Output Image 2E revealing tissue mucous cells delineated by colour overlays.

ε. Extraction of vacuolar regions:

ε1. The luminal area within Image 12B is chosen and subtracted from the regions present in Image 4H. Regions of interest resulting from the subtraction are selected and small objects (*i.e.* 0 to 3 pixels) excluded.

Image 16A

⁷ **Grainsbin.** This function performs grain boundary reconstruction on binary images. According to the selected 'Mode', either the standard or euclidian method is used to generate a distance map from binary image Input. 'Smooth' specifies the strength of a procedure that is used to smooth the distance map. Large values result in a strong smoothing. If the value is set to 0 in a macro command line, no smoothing is performed (KS 300 Imaging System Manual Guide B 40-613, Carl Zeiss Vision GmbH, München-Hallbergmoos, Germany).

ε2. Vacuolar regions are highlighted, marking overlays generated and stored as a segmentation mask image when merged with Image 1A.

①₂₇ “Right click on the small left-hand image and choose ‘Big Display’. All tissue vacuoles will be selected at the start (labelled in green), therefore use the left mouse button to deselect (labelled in red) the unwanted vacuoles. Use the right mouse button to increase and decrease the image size for better clarity. If unexpected red or green regions are apparent, zoom into the image to check their accuracy.”

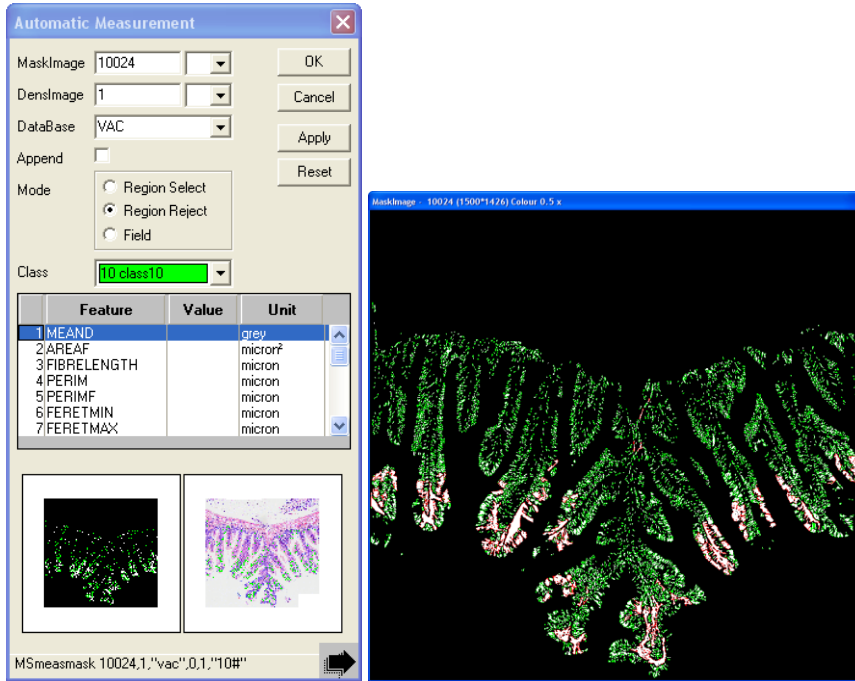


Image 16B
e.g. S400000_A01.VACUOLES.tif (Figure 7)

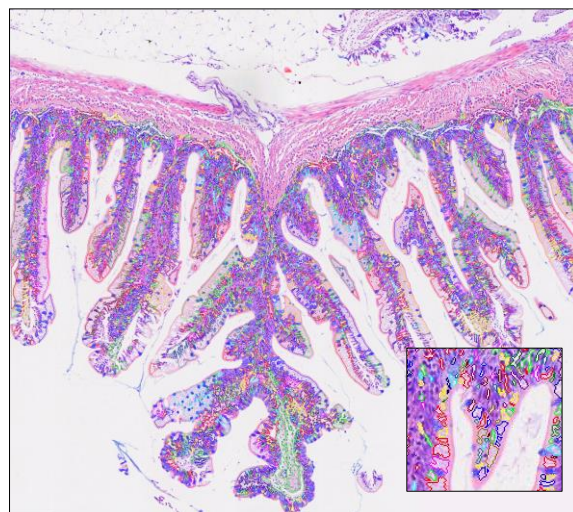


Figure 7. Output Image 16B, vacuolar regions being delineated by a colour overlay.

1.1.6. Feature Extraction and Data Generation

ζ. Mucous cells are identified (*i.e.* Image 2D) and measurements are taken.

- ✎ Mucous Cell Total Area (MCA, μm^2)
- ✎ Mean Mucous Cell Area (MMCA, μm^2)
- ✎ Mucous Cell Number (MCN, N°)
- ✎ Mucous Cell Minimum Feret Length (MC Feret Min, μm)
- ✎ Mucous Cell Maximum Feret Length (MC Feret Max, μm)
- ✎ Mucous Cell Feret Ratio (MC Feret Ratio)
- ✎ Mucous Cell Elliptical Length A (MC Ellipse Af, μm)
- ✎ Mucous Cell Elliptical Length B (MC Ellipse Bf, μm)
- ✎ Mucous Cell Ellipse Ratio (MC Ellipse Ratio)
- ✎ Mucous Cell Mean Circularity Index (MCirc)

η. Mucosal tissue is selected (*i.e.* Image 6I) and its total area calculated.

- ✎ Mucosal Tissue Area (MTA, μm^2)

θ. Submucosal tissue is elected (*i.e.* Image 14) and additional assessment undertaken.

- ✎ Submucosal Tissue Area (STA, μm^2)

ι. Tissue luminal surface (*i.e.* Image 15) extent and intricacy is estimated.

- ✎ Perimeter Length (P, μm)
- ✎ Perimeter Convolution (FR, fractal dimension values)

κ. Tissue vacuolisation is recognised (*i.e.* Image 16A) and further measurements undertaken.

- ✎ Total Tissue Vacuolisation Area (Vac, μm^2)

1.1.7. Analysis Conclusion

λ. Program terminates with audible warning once the analysis is finished.

- ⌚₂₈ "Measuring feature properties..."
- "Writing data to databases..."
- "Analysis finished."

	A	B	C	D	E	F	G	H	I	J	K	L	M
1	Treatment	Tank	Replicate	Indiv_Code	MCA_MTA	MCN_MTA	MTA_STA	FERET_Min	FERET_Max	FERET_Ratio	ELLIPSE_Af	ELLIPSE_Bf	
2	A	653	7	R110027x0D001	0.0233284	0.0001636	5.7781825	12.4157391	16.8810177	0.7447025	7.7720346	5.8348947	
3	A	653	7	R110027x0D002	0.0689930	0.0003935	5.4518557	13.0454464	18.8920040	0.7022222	8.7335815	5.9519248	
4	A	653	8	R110027x0E000	0.1036580	0.0004382	2.3143218	15.5550137	21.2390671	0.7447581	9.9019785	7.3278718	
5	A	653	8	R110027x0E001	0.1250168	0.0005293	3.0275407	15.4802103	21.2883034	0.7384234	9.9362612	7.2603154	
6	A	653	9	R110027x0F001	0.0572084	0.0003198	3.4192650	13.6005030	18.9078083	0.7309461	8.7632694	6.3344913	
7	A	653	9	R110027x0F003	0.2011189	0.0005524	3.8677554	18.5818253	25.8460121	0.7384496	12.1480207	8.7095995	
8	C	654	13	R110027x0G001	0.0966551	0.0004705	3.0729496	14.4555492	20.3098335	0.7248540	9.4111543	6.6755357	
9	C	654	13	R110027x0G002	0.1515709	0.0005832	2.5520418	15.2756777	22.5249348	0.7101780	10.4707613	6.9415827	
10	C	654	14	R110027x0H002	0.1217124	0.0004604	3.3311176	16.3076496	22.4321251	0.7350395	10.4474688	7.6676044	
11	C	654	14	R110027x0H004	0.0608436	0.0003536	4.3633943	13.2155342	18.5026054	0.7233794	8.5931673	6.2045488	
12	C	654	15	R110027x0I002	0.1174695	0.0005002	2.3033402	15.3561964	21.6018391	0.7261335	10.0991440	7.0871286	
13	C	654	15	R110027x0I003	0.0464272	0.0002532	6.4258184	13.1962986	18.3583202	0.7343094	8.5021992	6.1532927	
14	A	655	19	R110027x0J001	0.1075736	0.0005413	6.0379477	13.8450699	19.4866276	0.7223966	9.0629435	6.4787745	
15	A	655	19	R110027x0J002	0.1363479	0.0005821	3.0615244	15.5208588	21.1199780	0.7452034	9.8325930	7.2822657	
16	A	655	20	R110027x0K001	0.0392047	0.0002448	3.2565341	12.6830549	18.0744705	0.7138152	8.3922052	5.9334574	

Figure 8. Output Database, showing all the morphometric parameters that had been measured.

INTESTINAL RESPONSES TO DIETARY ADDITIVES – APPLICATION OF TOOLS FOR RAPID SCREENING OF NOVEL DIETARY COMPONENTS

3.1. Introduction

It is well established that feeding fish with diets that do not meet their nutritional requirements not only affects their growth and feed conversion, but also increases their susceptibility to disease and the appearance of signs of nutritional deficiency, resulting in altered behaviour and pathological changes (Hasan, 2001; Oliva-Teles, 2012). The general practice of intensive aquaculture can result in physiological responses which can negatively impact normal health and overall performance, with consequent economic losses for the fish farmer (Li & Gatlin, 2006; Welker *et al.*, 2011). Thus, the continued assessment of nutritional requirements for fish, leading to the formulation of balanced diets containing suitable dietary supplements, is an important area of current research. Such research is not only fundamental to gaining an understanding of the effects that these dietary supplements and essential nutrients have in terms of meeting nutritional basic requirements and enhancing fish growth, but can also contribute towards the maintenance of the overall health of the fish and improvement of the economic feasibility of commercial aquaculture production.

By convention, fish meal has been the main source of dietary protein in aquafeeds, especially for carnivorous fish species. However, in recent years increasing demand, high cost and inconsistent availability have promoted studies on its partial and complete substitution with alternative protein sources (Kaushik *et al.*, 1995; Olsen *et al.*, 2007; Sissener *et al.*, 2009a; Silva *et al.*, 2010). Amongst the potential fish meal substitutions, plant ingredients appear to be the most promising candidates (Tacon, 1995; Burel *et al.*, 2000; Kumar *et al.*, 2011a).

As a result of its comparatively high protein content and its relatively well-balanced amino acid profile, taken together with reasonable pricing and ready availability, soybean meal (SBM) appears to be one of the most cost-effective alternative protein sources for use in fish feeds. However, the amino acid composition differs significantly from that of fish meal, and feeding SBM can lead to essential amino acid deficiencies that in turn, compromise protein utilisation and restrict fish growth (Francis *et al.*, 2001; Hansen *et al.*, 2007). Alterations in blood chemistry and haematology suggest that SBM diets induce a physiological response, presumably related to the antigenic potential of the anti-nutritional factors (ANFs) present in most plant protein sources (Hemre *et al.*, 2005; Kumar *et al.*, 2010b). In salmonids, such ANFs are known to affect the intestinal integrity, which can lead to decreased nutrient digestibility and growth performance (Krogdahl *et al.*, 1994, 2003; Francis *et al.*, 2001).

In Atlantic salmon, enteritis induced by minimally-processed SBM is characterised by a shortening of the mucosal folds and microvilli, a decrease in the number of absorptive vacuoles in the intestinal epithelium, a widening of the central *stroma* within the mucosal folds, an increase in the connective tissue between the base of the mucosal folds and the *stratum compactum*, marked infiltration of inflammatory cells in the *lamina propria* or epithelium, and an increase in the number of mucous cells in the epithelium (Van den Ingh *et al.*, 1991, 1996; Baeverfjord & Krogdahl, 1996; Krogdahl *et al.*, 2000, Urán, 2008).

Although the occurrence of intestinal pathology in fish seems to vary with the degree of industrial treatment of the SBM, it remains unclear how soybean products cause this inflammatory response in salmonids. Immunological mechanisms are certainly involved in this pathogenesis, but the precise causes for the associated inflammatory response have, as yet, not been identified (Urán *et al.*, 2009a). Nevertheless, some authors suggest that alcohol-soluble components, such as phytosterols, oligosaccharides and / or soya-saponins, in synergy with one or more unidentified components play a key role in the onset of soybean-induced enteritis (Knudsen *et al.*, 2008; Iwashita *et al.*, 2009; Krogdahl *et al.*, 2010). Consequently, much research has focused on finding maximum levels of inclusion

that do not cause pathology in fish, or mixtures with other ingredients so as to keep the level of individual AFN low (Olsen *et al.*, 2007).

Biological and synthetic dietary compounds that support normal growth and enhance fish health are being promoted in aquaculture as a means of overcoming the immunosuppressive effects that fish may be subjected to when under intensive culture conditions (Gannam & Schrock, 2001; Galindo-Villegas & Hosokawa, 2004; Li & Gatlin, 2004). It is commonly accepted that such functional ingredients can alter the non-specific defence mechanisms by acting directly / indirectly through metabolic, neurological or endocrine pathways (Sealey & Gatlin, 2001; Bricknell & Dalmo, 2005; Meena *et al.*, 2012) enhancing the level of disease resistance against pathogens commonly associated with disease outbreaks in fish culture facilities.

The use of immunostimulants as dietary additives has sometimes been met with scepticism because the actions of these compounds are poorly understood and the results of feeding trials have been very inconsistent (Sakai, 1999; Meena *et al.*, 2012). Furthermore, the nature of certain commercial products is unclear and a convincing explanation for their mode of action, or documentation verifying their efficiency is often not publically available. Nevertheless, the use of immunostimulant dietary components has been shown to be an effective means of increasing the immuno-competency and disease resistance of fish (Hardie *et al.*, 1991; Raa *et al.*, 1992; Thompson *et al.*, 1993; Siwicki *et al.*, 1994; Verlhac *et al.*, 1996). A number of molecules such as beta-glucans, lactoferrin, levamisole, chitin (Sakai, 1999; Meena *et al.*, 2012; Vetvicka *et al.*, 2013) and exogenous nucleotides (Li & Gatlin, 2006) have been shown to exhibit immunodulatory effects. Beta-glucans in particular appear to be promising immunostimulatory compounds for use in aquaculture (Gannam & Schrock, 2001; Sealey & Gatlin, 2001; Gatlin, 2002).

Beta-glucans (β -glucans), consisting of glucose polymers, are structural components of the cell walls of bacteria and plants (Robertsen *et al.*, 1990; Trichet, 2010). As naturally occurring biomolecules, they are less likely to cause concerns about residues in food fish (Gannam & Schrock, 2001). The effect of β -glucans on the fish's growth performance and

immune response, and their potential to increase survival in disease states have been extensively investigated in numerous studies (Chen & Ainsworth, 1992; Raa, 1992; Matsuyama *et al.*, 1992; Jørgensen *et al.*, 1993; Siwicki, *et al.*, 1994; Dalmo *et al.*, 1996; Efthimiou, 1996; Jeney *et al.*, 1997; Santarem *et al.*, 1997; Whittington *et al.*, 2005; Gopalakannan & Arul, 2010; Refstie *et al.*, 2010; Siwicki *et al.*, 2010; Falco *et al.*, 2012; Miest *et al.*, 2012; Kühlwein *et al.*, 2013; Pionnier *et al.*, 2013).

Nucleotides are low molecular-weight compounds comprising a nitrogenous base, a five carbon sugar and a phosphate group, which are involved in many biological processes (Kenari *et al.*, 2013). As essential nutrients, cofactors in cell signaling and metabolism and precursors of DNA replication (Burrells *et al.*, 2001; Peng *et al.*, 2013), they are particularly important in cell repair and development since they are the core building blocks of nucleic acids (Trichet, 2010). To date, there have been few reports about the effects of exogenous nucleotides on digestion, absorption, metabolism and influences on various physiological responses especially in the expression of immune genes and modulation of immunoglobulin production (Leonardi *et al.*, 2003; Glencross & Rutherford, 2010; Tahmasebi-Kohyani *et al.*, 2011). Despite this, dietary nucleotide supplements have consistently shown beneficial influences when fed to various fish species (Li & Gatlin, 2006). Research related to nucleotide nutrition in fish, namely their effects on innate and adaptive immunity, stress responses and resistance to infectious diseases, has shown that they may improve growth performance, enhance intestinal morphology and function, aid liver function as well as modulating innate and adaptive immune responses (Burrells *et al.*, 2001; Sakai *et al.*, 2001; Low *et al.*, 2003; Malina *et al.*, 2005; Li & Gatlin, 2006; Li *et al.*, 2007; Jha *et al.*, 2007; Lin *et al.*, 2009; Tahmasebi-Kohyani *et al.*, 2012; Peng *et al.*, 2013).

The suitability of new aquafeed diets should be evaluated not only in terms of growth performance, but also in terms of impact on fish health, although these two parameters will inevitably tend to go hand in hand. Appropriate indices of fish health therefore need to be developed / refined to evaluate the efficacy of novel dietary components and to assist understanding of how dietary modulation regimes may influence fish health and improve

disease resistance (Maita, 2007). Various parameters have been used to assess changes in fish physiology and health due to dietary manipulation. These include assessment of growth performance, calculation of various body condition factors or haematological indices and measurement of various biochemical, immunological and histopathological parameters (Adams *et al.*, 1993). Each of these approaches has its own advantages and limitations depending on the purpose of the assessment. Moreover, because of the complex nature of the biological responses of vertebrates, it is unlikely that single parameters can accurately reflect an organism's response to dietary components. Therefore, evaluation of several individual factors together, should improve the accuracy of dietary assessment (*i.e.* the biological response to the diet) and help to identify suitable dietary components. The sensitivity, accuracy, ease of application, rapidity and cost-effectiveness of assessment methodologies are also important criteria for deciding which suite of indicators should be monitored (Maita, 2007).

The work reported in this chapter sought first, to produce a model feed trial capable of providing distinct / differentiable tissue and physiological states (*e.g.* inflammatory vs. non-inflammatory). Second, it sought to use classical growth assessment, immunological, haematological and physiological tools to examine and characterise the putative feed-derived states and third, it sought to deploy the newly developed image analysis tool (see Chapter 2) and to analyse data provided by it, in order to ascertain the level and reliability of the contribution that it might make in the assessment of the effects of different dietary components. The fourth objective of the presented work was to examine the wider utility of such a multivariate approach to the screening of novel dietary components.

3.2. Materials and methods

3.2.1. Experimental fish and fish husbandry

The feed trial described, was conducted at Skretting's Fish Trial Station (Lerang, Jørpeland, Norway). Post-smolt Atlantic salmon (*Salmo salar* L.) with an initial mean body weight of 79 ± 2 g and a mean fork-length of 19 ± 2 cm were randomly allocated into six

flow-through 100 L circular tanks. The tanks were maintained under a 24 h light photoperiod and supplied with fresh sand-filtered flow-through seawater at 11 ± 2 °C. Dissolved oxygen, ammonia, nitrate, nitrite and pH levels were monitored and maintained within recommended limits (Wedemeyer, 1996). Individual tanks were equipped with waste feed collectors and uneaten feed was collected twice per day. Fish behaviour and cumulative mortalities were recorded throughout the trial period.

3.2.2. Diets and feeding regime

Three experimental diets, comprising either a fish meal based control diet, a diet containing 25 % unrefined soybean meal concentrate or a fish meal diet supplemented with specific functional ingredients, were produced as 3 mm extruded pellets at Skretting's Feed Technology Plant (Stavanger, Norway). The diets were formulated to satisfy the nutritional requirements of salmonids (NCR, 1993) and contained similar amounts of available crude protein and gross fat. Information on the diet formulation and the commercial source of the various dietary components is shown in Table 3.1.

Fish were acclimated for a 3 week period, during which time they were maintained on a commercial fish meal based diet (Protec™, Skretting, Stavanger, Norway). Thereafter, throughout the 20-week experimental period, the fish were fed one of the three different experimental diets. The diets were randomly assigned to triplicate tanks prior to starting the trial. Fish were fed twice a day using automatic feeders. The amount of feed given was adjusted in accordance with biomass, thus aiming to overfeed by 20 %. Uneaten feed was collected, separated from faeces and quantified by weight after drying for 12-16 h at 90 °C.

3.2.3. Feed composition

The proximate chemical composition of the experimental diets was determined using Near Infrared Reflectance Spectroscopy (NIRS) technology. In essence, the sample was illuminated with near infrared light and the spectrum of light reflected by the chemical bonds between organic molecules recorded. That spectrum was automatically compared with standard spectra held in a central database. The principle of NIRS technology has been described by several authors (Corson *et al.*, 1999; González-Martín *et al.*, 2006; Berzaghi &

Riovanto, 2010; Cheli *et al.*, 2012). In this particular study, NIRS analysis was performed in triplicate ground feed samples of each diet, and results expressed as a percentage of dry weight (Table 3.1). Spectra were assessed using a FOSS analyser (NIRSystem 6500 device, Foss Analytical, Hillerød, Denmark), equipped with ISIScan™ (Version 1.26, Infrasofth International, Port Matilda, USA). The WinISI™ 2 software package (Version 1.04, Infrasofth International, Port Matilda, USA) was used for the chemometric analysis of data and for calibration of the routine analysis. In-house NIRS analyses, were first calibrated against official laboratory methods for crude protein content (Nordic Committee on Food Analysis – NMKL, Method no. 6, 4th edition, 2003; $n > 4000$, $r^2 = 0.99$), crude fat (NMKL no. 160, 1998; $n > 3700$, $r^2 = 0.99$), moisture content (NMKL no. 23, 1991; $n > 3000$, $r^2 = 0.99$), and ash (NMKL no. 23, 1991; $n > 2400$, $r^2 = 0.93$).

3.2.4. Sampling procedure

At the end of the experimental feeding period (*i.e.* after a 20-week feeding regime), the fish were starved 24 h prior to sampling. Six fish per experimental tank were randomly selected and euthanised with an overdose of anaesthetic (50 mg.L⁻¹, MS-222, Tricaine Methanesulphonate, Argent Chemical Laboratoires, Redmount, WA, USA). Blood was immediately obtained by caudal venepuncture using heparinised syringes and samples briefly kept on ice for haematological analysis. Following external assessment of fish appearance and general body condition, fish weights and fork-length measurements were taken. Intestinal sections from the distal intestinal region were then excised from the fish. Transverse intestinal rings of at least 1 cm in length were taken, cut open longitudinally and fixed in neutral buffered formalin (10 %, pH 7.2) at room temperature (16-20 °C) for at least 24 h before further histological processing. Subsequently, tissue was excised from the anterior kidney and placed in individual sterile tubes containing Leibowitz L-15 medium (L5520, Sigma-Aldrich, Ayrshire, UK) supplemented with 10 IU.mL⁻¹ heparin (H3149, Sigma-Aldrich, Dorset, UK). Kidney samples were kept on ice for the respiratory burst and phagocytosis activity assays described below.

Table 3.1. Formulation and proximate chemical composition of the feeds used in this experimental study.

	Diet A (Standard)	Diet B (SBM)	Diet C (Imm)
Feed ingredients (g.kg ⁻¹)			
Fish meal*	250.00	250.00	250.00
Soybean meal [†]	0.00	250.00	0.00
Soya protein concentrate [‡]	200.00	0.00	200.00
Wheat [§]	187.30	98.80	187.30
Wheat gluten	137.20	158.10	137.20
Pigment [¶]	00.50	00.50	00.50
Fish oil**	208.50	229.10	208.50
Minerals and vitamins ^{††}	16.50	13.50	16.50
Nucleotides, β-glucans and mix of natural additives ^{‡‡}	0.00	0.00	20.50
Chemical composition (% of dry weight)			
Crude protein	42.00	42.10	42.00
Crude fat	26.00	27.70	26.00
Ash	92.50	92.80	92.50
Moisture	7.50	7.20	7.50

Footnotes:

Standard, control; SBM, soybean meal; Imm, immunostimulants.

* Scandinavian Fish meal LT (Norsildmel, Fyllingsdalen, Norway).

† Defatted soybean meal (Denofa, Fredriskstad, Norway).

‡ IMCOSOY[®] (IMCOPA, Parana, Brasil).

§ Wheat (Stakorn, Oslo, Norway).

|| Wheat gluten (Skretting Norway, Stavanger, Norway).

¶ Carophyll Pink (DSM Nutritional Products, Basel, Switzerland).

** South American oil containing 30 % SFA of total fatty acids.

†† Mineral and vitamin premix to meet the National Research Council recommendations (NCR, 1993).

‡‡ Nucleotides, beta-glucans and a mix of natural additives supplied by Skretting Norway (Stavanger, Norway).

3.2.5. Growth performance and feed efficiencies

The specific growth rate (SGR), the feed conversion rate (FCR), the hepatosomatic index (HSI) and the condition factor (K), were determined for each treatment group according to the following formulae (Dimitroglou *et al.*, 2010): $SGR = [\ln (\text{Final Wt} / \text{Initial Wt})] \times d^{-1} \times 100$; $FCR = (\text{FI} / \text{Wt}) \times 100$; $K = \text{Wt} / \text{FL}^3 \times 100$; $HSI = (\text{LW} / \text{Wt}) \times 100$. Where Wt is the live weight gain (g), FI is the feed intake based on the dry matter quantification of the waste feed (g), d is the feeding days, FL is fish fork length (cm) and LW is liver weight (g). All values were expressed as means \pm standard deviation (SD).

3.2.6. Haematology and blood biochemistry

Immediately after sampling, haematological analysis and collection of plasma were performed according to standard haematological techniques (Hesser, 1960; Bain *et al.*,

2012). After centrifuging the whole blood samples in heparinised micro-haematocrit tubes on a Hawksley centrifuge (Haematospin 1300, Sussex, UK) for 4 min at $9300 \times g$, the haematocrit levels (Hct) were determined as a percentage of packed red cell volume in relation to the whole blood volume. For each fish, two blood smears were prepared and stained with RAPI-Diff[®] (Raymond A. Lamb Ltd, Sussex, UK), a Romanowsky-based staining kit, following the manufacturer's instructions. The slides were then examined blind with an Olympus BX-40 light microscope using a 100 \times objective. Two hundred white blood cells were counted for each slide and the cells classified either as lymphocytes, thrombocytes, granulocytes or monocytes. The total blood haemoglobin (Hb) was determined on whole blood samples using an automatic analyser (Hb 201+, HemoCue, Ängelholm, Sweden). The mean number of erythrocytes (RBC, red blood cells) and of leucocytes (WBC, white blood cells) were taken from whole blood samples diluted in phosphate buffered saline solution (WBC 1:100; RBC 1:1000; PBS, P4417, Sigma-Aldrich, Ayrshire, UK). Counts were carried out under a light microscope using a 40 \times objective, and an improved Neubauer haemocytometer counting chamber (0.0025 mm², 0.1 mm Tiefe Depth Profondeur, Marienfeld, Lauda-Königshofen, Germany). From these parameters the mean corpuscular volume (MCV), mean corpuscular haemoglobin (MCH) and mean corpuscular haemoglobin concentration (MCHC) were determined, using the following formulae (Bain *et al.*, 2012; Sissener *et al.*, 2009b): $MCV \text{ (fL)} = \text{Hct} / \text{RBC} (10^6 \cdot \mu\text{L}^{-1})$; $MCH \text{ (pg)} = [\text{Hb} \text{ (g.dL}^{-1}) \times 10] / \text{RBC} (10^6 \cdot \mu\text{L}^{-1})$; $MCHC \text{ (g.dL}^{-1}) = [\text{Hb} \text{ (g.dL}^{-1}) \times 10] / \text{Hct}$. The remaining blood samples were then centrifuged for 7 min at $3000 \times g$, and aliquots of plasma immediately stored at $-20 \text{ }^\circ\text{C}$.

Lysozyme activity from plasma was measured using a turbidimetric assay, following the protocol of Parry *et al.* (1965). Briefly, lyophilised *Micrococcus lysodeikticus* (M3770, Sigma-Aldrich, Steinheim, Germany) was added to a 0.004 M sodium phosphate buffer (SPB, pH 6.2) at a concentration of 0.2 mg.mL^{-1} bacteria, and the solution incubated at $25 \text{ }^\circ\text{C}$ for 30 min. Ten microlitres of plasma were added to four replicate wells of a multi-well microplate (611F96, Sterilin Limited, Newport, UK). Thereafter, 190 μL of the bacterial suspension was

added to all 4 wells and another 2 wells used as negative control wells, to which 200 μL of the bacterial suspension was added. After shaking the plate, the absorbance was recorded at 540 nm, 1 min after adding the buffer and then again after 5 min using a Synergy HT plate reader (BioTeck, Bedfordshire, UK). The rate of change of the absorbance was then calculated and a unit of lysozyme activity ($\text{U}\cdot\text{min}^{-1}\cdot\text{mL}^{-1}$) expressed as the amount of sample causing a decrease in absorbance of 0.001 min^{-1} .

The remaining plasma samples were analysed by means of a clinical chemistry analyser (Konelab-20, Thermo Fisher Scientific, Oslo, Norway), following the manufacturer's guidelines. The plasma total protein ($\text{g}\cdot\text{L}^{-1}$) was analysed according to the Biuret method standardised for use with the auto-analyser (Konelab™ method number TP0100; Konelab™ T-series Total Protein Plus, Ref 981826). Total albumin ($\text{g}\cdot\text{L}^{-1}$) was determined by means of Konelab™ method number BC0100 (Konelab™ Albumin-BCG, Ref 981358), and total creatine kinase ($\text{mg}\cdot\text{L}^{-1}$) reported as C-reactive protein quantified according to Konelab™ method number CKF060 (Konelab™ CRP Plus, Ref 981794).

All haematological values were expressed as means \pm standard deviation (SD).

3.2.7. Respiratory burst activity and phagocytic activity assays

Anterior kidney macrophages were isolated using the method described by Secombes (1990), with modifications. In brief, anterior kidneys placed in Leibowitz L-15 medium containing $10\text{ IU}\cdot\text{mL}^{-1}$ heparin, were aseptically disrupted by gently teasing the tissue through a $100\text{ }\mu\text{m}$ sterile mesh (352360, BD Falcon, BD Biosciences, Oxford, UK). The resulting cell suspension was adjusted to a concentration of $2 \times 10^7\text{ cells}\cdot\text{mL}^{-1}$, from which macrophage monolayers were prepared. For the respiratory burst assay, aliquots of the homogenised cell suspension were added to 12 replicate wells of a sterile flat-bottomed 96 multi-well microplate (3801-096, Iwaki Techno Glass Corp., Tokyo, Japan), and allowed to adhere for 2-3 h at $15\text{ }^\circ\text{C}$. Likewise, for the phagocytosis assay, aliquots of the cell suspension were placed into two large circles drawn on a microscope slide with an ImmEdge™ Pen (H-4000, Vector Labs, Peterborough, UK). The slides were then placed in a moist incubation chamber for 1-2 h at room temperature ($16\text{-}20\text{ }^\circ\text{C}$). Thereafter, the non-

adherent cells were removed by gently washing the microscope slides and multi-well microplates with Hank's balanced salt solution (HBSS, H6648, Sigma-Aldrich, Ayrshire, UK). Respiratory burst activity of head kidney macrophages was assessed by measuring the reduction of nitro blue tetrazolium (NBT) into blue formazan, by superoxide anion produced during this respiratory burst process. In accordance with the method described by Secombes (1990), the difference in absorbance between un-stimulated and stimulated cells was used to evaluate superoxide anion production. Macrophages in five replicate wells were stimulated by adding 100 μL of 1 $\text{mg}\cdot\text{mL}^{-1}$ NBT (N6876, Sigma-Aldrich, Ayrshire, UK) containing 1 $\mu\text{g}\cdot\text{mL}^{-1}$ phorbol-12-myristate 13-acetate (PMA, P8139, Sigma-Aldrich, Ayrshire, UK), while a further five replicate wells remained un-stimulated, by adding 100 μL of 1 $\text{mg}\cdot\text{mL}^{-1}$ NBT solution. The plate was incubated for 1 h at 15 °C before fixing the cells with methanol, air drying and dissolving the formazan by the addition of 120 μL 2M KOH and 140 μL dimethyl sulfoxide (DMSO, D2650 Sigma-Aldrich, Ayrshire, UK). Optical densities (OD) were measured at 630 nm. The two remaining replicate wells were used to determine the mean number of macrophages attached to the well, by adding 100 μL lysis buffer (0.1 M citric acid, C0706; 1 % Tween 20, P1379; 0.05 % crystal violet, C3886; Sigma-Aldrich, Ayrshire, UK) for 2 min, and counting the number of released nuclei using an improved Neubauer haemocytometer counting chamber. Values for the respiratory burst assay were expressed as mean NBT reduction (OD 630 nm) per 10^5 cells \pm standard deviation (SD).

The phagocytic assay was performed in accordance to Wang *et al.* (2006), with minor modifications. In brief, 100 μL of *Saccharomyces cerevisiae* yeast suspension (YSC2, Sigma-Aldrich, Ayrshire, UK; 5 $\text{mg}\cdot\text{mL}^{-1}$ in Leibovitz L-15 medium) was added to one of the microscope slide circles containing the resultant macrophage monolayer. To the second circle 100 μL of Leibovitz L-15 medium was added as control. The slides were incubated for 1 h, at room temperature (16-20 °C). To remove un-phagocytosed yeast, the macrophage monolayers were washed with HBSS, fixed with ethanol, air dried and stained with a Romanowsky-based staining kit (*i.e.* RAPI-Diff®). Finally, one hundred macrophage cells

were examined microscopically using a 100x objective lens. The number of macrophages containing phagocytosed yeast was recorded, as well as the number of phagocytosed yeast. From these counts, the phagocytic index (PI), phagocytic activity (PA) and phagocytic capacity (PC) was calculated as follow (Findlay & Munday, 2000): $PI = \text{Total number yeast cells engulfed} / \text{Number of macrophages phagocytosing}$; $PA = (\text{Total number of macrophages showing phagocytosis} / \text{Total number of macrophages counted}) \times 100$; $PC = (\text{Total number of macrophages containing a given number of yeast cells} / \text{Total number of macrophages containing any yeast cell}) \times 100$. The corresponding results were expressed as mean percentages \pm standard deviation (SD).

3.2.8. Histological staining and digital image acquisition

Formalin-fixed intestinal samples from 3 fish per treatment group were dehydrated and paraffin-embedded according to conventional histological procedures (Bancroft & Stevens, 1982) and three distinct paraffin blocks produced for each individual tissue sample (Tissue-TekII Paraffin Wax, 54-57 °C, Sakura Finetek Europe B.V, Netherlands). Transverse sections of 5 μm thickness were cut and mounted on glass slides. For each distinct paraffin block, one histological slide was prepared. After de-paraffinisation, sections were stained with Alcian blue (8 GX, pH 2.5) followed by standard Harris' haematoxylin and eosin-yellowish staining (Steedman, 1950; Lev & Spicer, 1964; see Appendix 1 for modified staining protocol).

Slides were then scanned using an automated slide-scanning system (MIRAX Desk, Carl Zeiss MicroImaging GmbH, Göttingen, Germany) and a digitised MRXS image of the complete section stored at a final magnification of 20x. MIRAX Viewer software (Version 1.12, 3DHISTECH, Budapest, Hungary) was used for visualisation and cropping of the images. For each into untiled TIFF files with sizes ranging from 13 to 14 MB.

3.2.9. Quantitative image analysis

Cropped images were randomised and evaluated blind. Algorithms for detection and feature extraction were developed using the KS300 software application module (Execution Environment, Version 3.0, Carl Zeiss MicroImaging GmbH, Göttingen, Germany).

Evaluation and implementation of the developed system was subsequently performed on a personal computer running KSRun software (Version 3.0, Carl Zeiss Vision GmbH, München, Germany). To give the true distance units, the micrometre scale used throughout the analysis was calibrated according to the MIRAX Viewer's guidelines, and thereafter validated against a slide-graticule. The image processing and analysis pipeline comprised a succession of interactive and automated steps. The operator was able to make decisions interactively so as to rectify preceding automated object inclusions or deletions (e.g. to eradicate artefacts created during histology processing or remove tissue debris extraneous to the analysis). Feedback in the form of guideline-notes for the operator, and visualisation of generated images was available at each step of the process.

The flow chart for the process pipeline is shown in Figure 2.3 and partly illustrated in Figures 2.4, 2.5, 3.1 and 3.2. For a more complete description please see Chapter 2. In brief, following a background correction and noise reduction from the source image, a binary image was created (Figure 3.2 B). The empty space (*i.e.* comprising no tissue or cells; within the area shown in Figure 3.2 B) was segmented by inverting the image to its negative and through intensity differentiation, which in turn allowed proper segmentation of the peritoneal edge of the *muscularis externa* and the internal intestinal lumen. Thereafter, the *stratum compactum* was defined by interactive drawing over the displayed tissue image so as to discriminate different tissue areas (*i.e.* mucosal and submucosal tissues; Figure 3.2 C-F respectively).

Using the original digitised images, an interactively defined HLS colour threshold (Hue, Lightness, Saturation: an alternative colour model to RGB providing a better match to perceived stain colours) was set for detection of Alcian blue staining and subsequent identification of objects such as mucous cells (Figure 3.2 G-H). Binary grain recognition was used to separate adjoining mucous cells, and the resulting objects filtered by size-threshold-operators to ensure removal of artefacts. The source image was then converted to a greyscale from which mucosal tissue vacuoles could then be visualised (Figure 3.2 I-J). Lastly, the luminal perimeter was captured (Figure 3.2 K-L) and the level of convolution

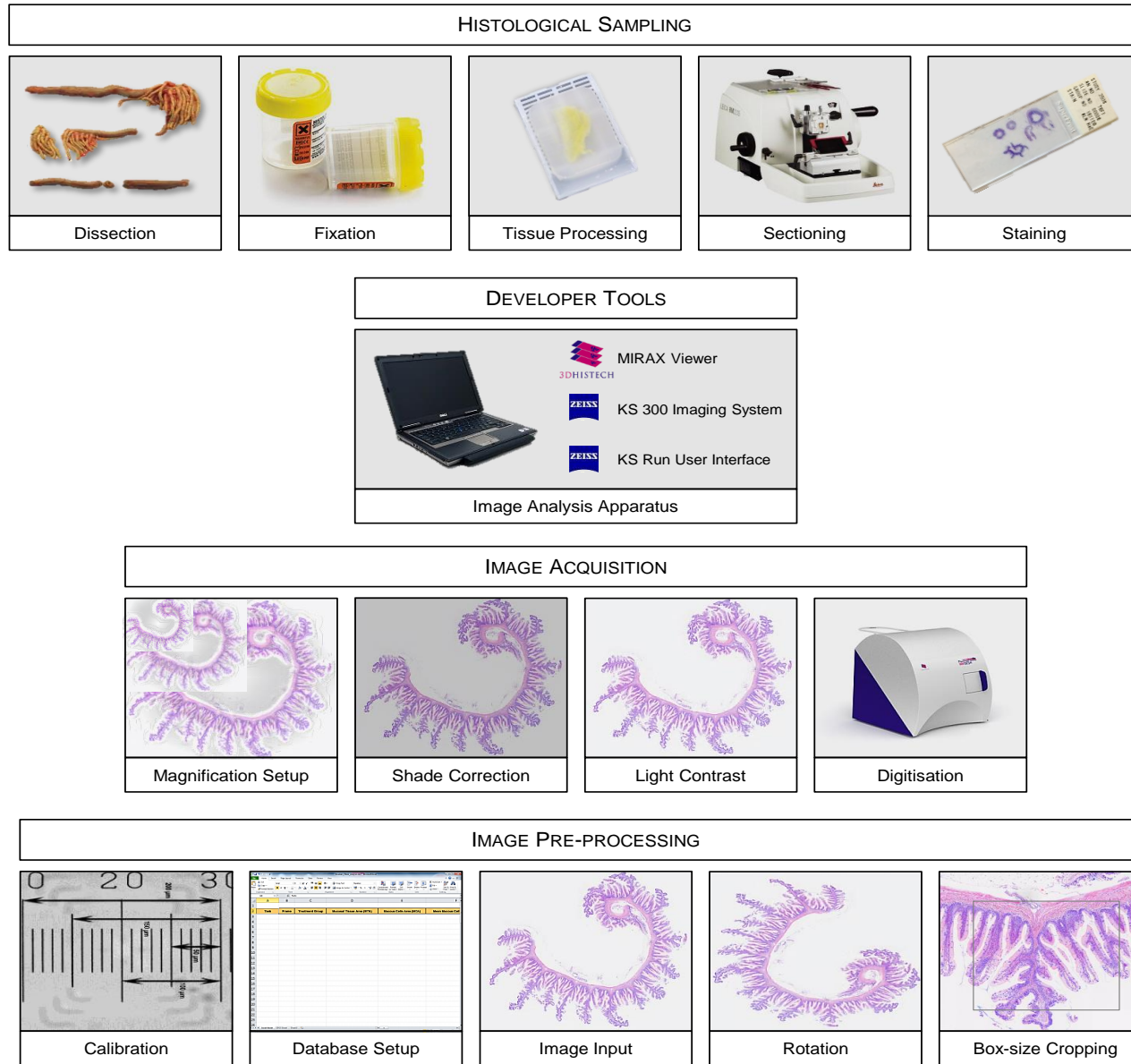


Figure 3.1. Flow chart illustrating the sequence of image processing algorithms (for a more complete description, please see Chapter 2).

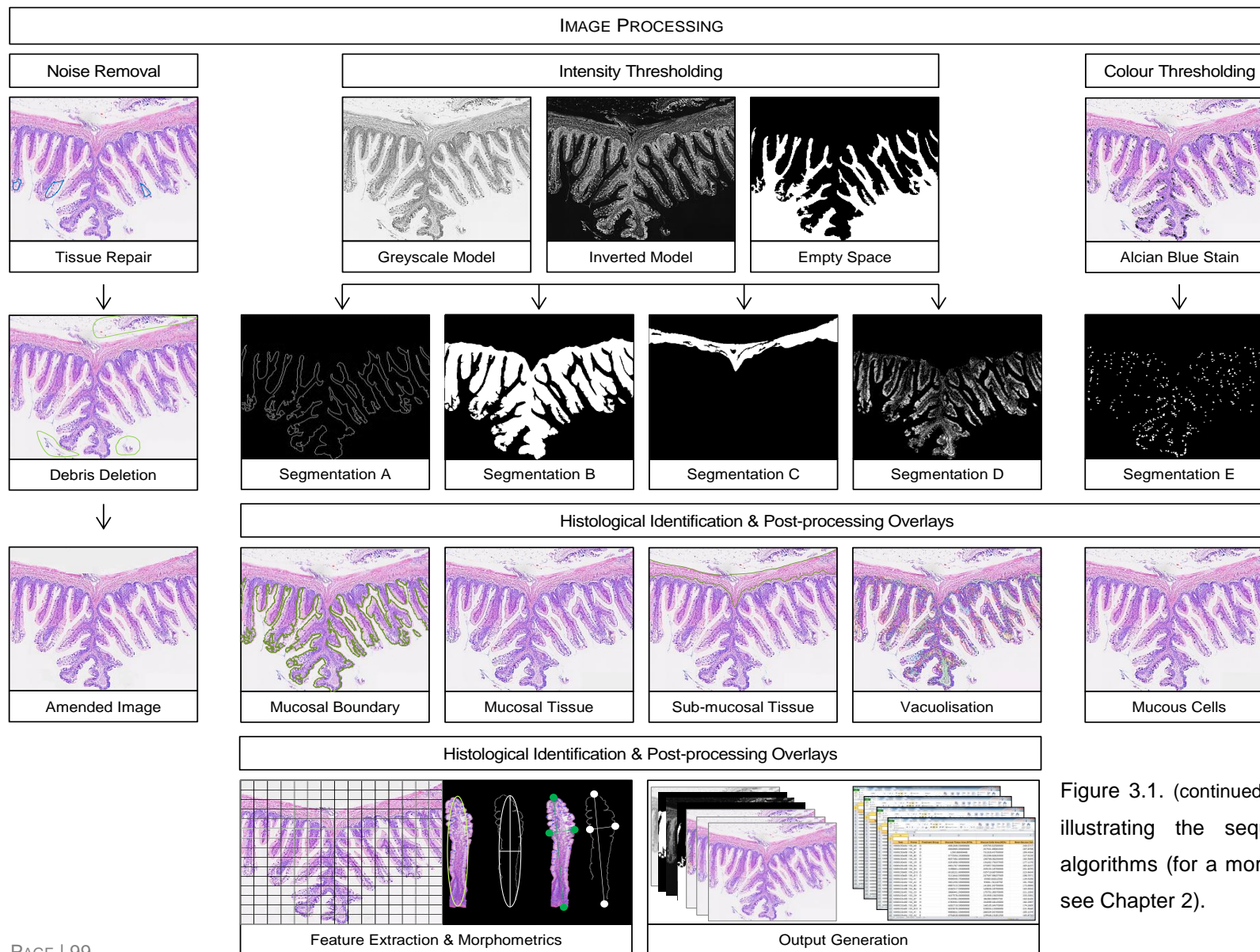


Figure 3.1. (continued from previous page) Flow chart illustrating the sequence of image processing algorithms (for a more complete description, please see Chapter 2).

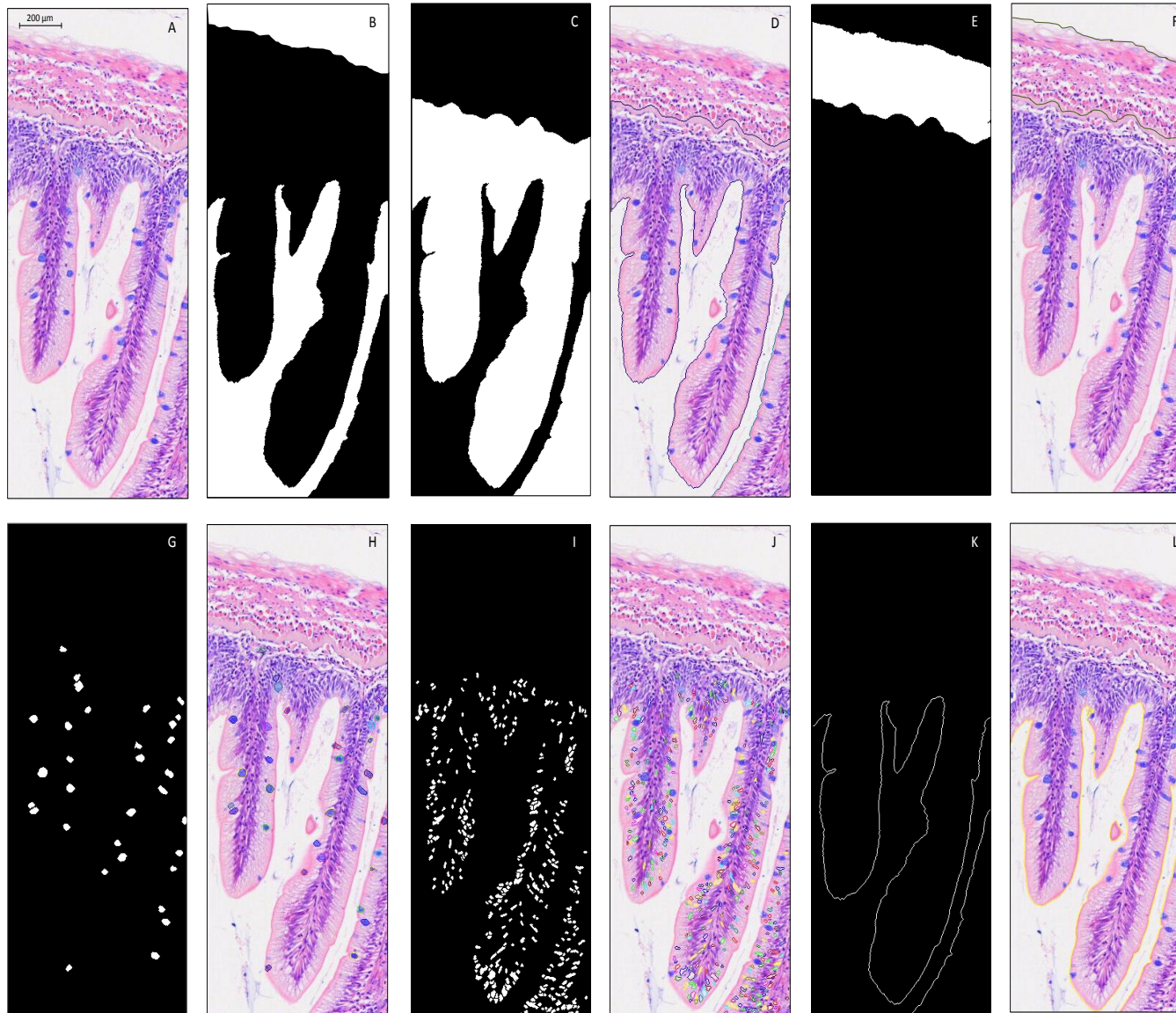


Figure 3.2. Image outputs generated by the described image analysis algorithms, from which morphometric features were extracted and employed to quantify aspects of the specimen's distal intestine. (A) A portion of a digitised histological image, approximately one sixteenth of the full image used in the present study. (B) Binary image created during the image segmentation process, where the empty space is differentiated by inverting the image to its negative and through intensity differentiation, which in turn allows proper distinction of the peritoneal edge of the *muscularis externa* and the internal intestinal lumen. (C, E, G, I, K) Bimodal images of mucosal tissue area, submucosal tissue area, mucous cells, vacuoles from mucosal tissue and the perimeter line from the outside mucosal boundary, respectively. (D, F, H, J, L) Regions within the established threshold ranges that were recognised were measured and had overlay masks reproduced. In sequence: mucosal tissue area, submucosal tissue area, mucous cells, vacuoles from mucosal tissue and the perimeter line from the outside mucosal boundary.

measured using the fractal box-counting method (Russell *et al.*, 1980; Cross, 1994; Shang *et al.*, 2000). For this, the number of boxes required to cover the perimeter line was determined by superimposing a regular grid of boxes over the image, and counting the number of occupied boxes. The procedure was then repeated using different box sizes, up to the size of the image. The number of occupied boxes increases with decreasing box size, as described by the following power law relationship $N(\lambda) = k \times \lambda^{-D}$ (Sreenivasan *et al.*, 1989; Wijesekera, 1996), where λ is the box size, N the number of boxes occupied by the perimeter line, k a constant, and D the fractal dimension. Thereafter, D can then be estimated from the slope of the linear trend of the log-to-log plot, of N versus λ . The endpoint of this process is an estimate of the perimeter convolution (Brooker, 2007). Segmentation of all these histological components was performed sequentially. Several image overlays were generated and stored as individual image outputs. Regions within the threshold ranges were highlighted and object masks produced (Figure 3.2). Various arithmetic and geometric automated algorithms were simultaneously employed for the resulting segmented objects and measurements for a number of morphometric parameters obtained (Table 2.2). Values for these were then transcribed and exported to a flat database file. Amongst those output variables, nine size parameters, two shape descriptors and one count variable were used to develop morphometric ratios (Table 2.2). Quantitative variables were expressed as mean and standard deviations unless otherwise specified.

3.2.10. Statistical analysis

Statistical analyses were conducted using SPSS (Version 19.0.01, IBM, Chicago, USA) and Minitab (Version 16.1.0.0, Coventry, UK) statistical software packages. Following tests for normality and homogeneity, analysis of variance (~ANOVA) and Tukey's *post-hoc* multiple comparison tests were employed to determine whether results from the growth performance and feed efficiencies were significantly different amongst experimental treatment groups. Group differences were regarded as significant when the probability of each significance test was less than 5 % ($p < 0.05$).

The results from the various morphological and immunological parameters were transformed where necessary to normalise the distribution, and the means compared by use of a hierarchical general linear model (GLM). When multiple groups were compared, the appropriate Holm-Bonferroni's significance values were used to compensate for the number of groups, so as to reduce the probability of detecting spurious differences. In order to establish which morphometric measurements gave the most information concerning the differences found in the morphology of the distal intestine from fish of different dietary groups, a principal component analysis (PCA) was performed. Varimax rotation and a Kaiser normalisation were employed to aid in obtaining optimal loadings of the parameters on the principal components and consequently better interpretation of components (Kaiser, 1974). In order to identify important trends in the morphological data set that would not be evident using univariate techniques, a discriminant function procedure was implemented. The program default criterion for F values (F_{Entry} : 3.84; F_{Remove} : 2.71) was used to determine the inclusion or removal of a variable from the analysis. Variables thus selected were subjected to a reverse stepwise discriminant method. Once the variable selection was complete, a discriminant model comprising a number of factors, each with its own coefficient and a constant was generated. A discriminant score was then calculated for each individual sample, and from this, subjects were automatically allocated to one of the treatment groups and the overall accuracy of the discriminant model tested.

3.3. Results

3.3.1. Fish behaviour and feed intake

Throughout the experimental trial fish mortalities had a singular mortality being recorded for fish fed the diet containing the SBM concentrate. No differences in the overall fish behaviour were observed, and the feeding response was very good irrespective of dietary treatment (Table 3.2).

Table 3.2. Growth response and feed efficiencies for Atlantic salmon fed the experimental diets.

	Diet A (Standard)		Diet B (SBM)		Diet C (Imm)		<i>p</i> -value
	Mean*	SD	Mean	SD	Mean	SD	
Weight gain (Wt, %)	233.17	27.30	215.41	3.18	224.47	13.82	0.79
Feed Intake (FI, g.d ⁻¹)	33.95	2.20	32.51	1.19	32.25	1.37	0.75
Specific Growth Rate (SGR, %·d ⁻¹)	1.10	0.08	1.04	0.01	1.08	0.05	0.79
Feed Conversion Rate (FCR) [†]	0.73 ^a	0.01	0.81 ^b	0.01	0.72 ^a	0.02	0.00
Condition Factor (K, %)	1.21	0.02	1.21	0.01	1.18	0.02	0.43
Hepatosomatic Index (HSI, %)	1.06	0.02	1.04	0.09	0.97	0.04	0.58

Footnotes:

Standard, control; SBM, soybean meal; Imm, immunostimulants.

* Data are expressed as mean and standard deviations (SD), $n = 3$ tanks per treatment group were assessed. Mean values within the same row, with different superscripts are significantly different (one-way ANOVA, $p < 0.05$).† The feed conversion rate could be expressed as kg dry feed kg⁻¹ wet weight gain.

3.3.2. Feed chemical composition

The proximate chemical composition (% of dry weight) of the formulated feeds used in this experimental study is shown in Table 3.1. No substantial differences were found among dietary groups in terms of crude protein, ash and moisture contents whereas slight fluctuations were seen for the crude fat content. The diets contained about 42 % crude protein and 26 to 27.7 % crude fat. Ash and moisture content were in the range of 92.5 to 92.8 % and 7.2 to 7.5 % respectively.

3.3.3. Growth performance and feed efficiencies

Feed efficiencies and growth performance of fish are presented in Table 3.3. Throughout the 20-week experimental trial, mean fish weight continuously increased. Although no significant growth differences were found between the different diets (Wt $F_{[1,3]} = 0.25$, $p > 0.05$; SGR $F_{[1,3]} = 0.24$, $p > 0.05$), there was a slight tendency towards a lower Wt and SGR as the diet's percentage of SBM increased. Similarly, fish fed on the diet containing plant protein displayed significantly lower FCR values ($F_{[1,3]} = 17.56$, $p < 0.05$) varying from 0.79 to 0.82 kg dry feed kg⁻¹ wet weight gain. In contrast, the HIS index remained unaffected by dietary treatment ($F_{[1,3]} = 0.59$, $p > 0.05$), values ranging from 0.97 to 1.06 %. The average daily feed intake exhibited very few changes amongst treatment

groups. While not statistically significantly different, the highest feed intake was recorded for fish from treatment group A, fed the fish meal based control diet ($33.95 \pm 2.20 \text{ g.d}^{-1}$; $F_{[1,3]} = 0.31$, $p > 0.05$). At the end of the feeding period, the body condition factor (overall 1.20 ± 0.02 %), was within the normal range and did not differ significantly between dietary treatments ($F_{[1,3]} = 0.97$, $p > 0.05$).

3.3.4. Haematology and blood biochemistry

The haematological profiles of Atlantic salmon fed the experimental diets are summarised in Table 3.3. Erythrocyte counts did not differ greatly among the three treatment groups ($F_{[2, 18]} = 0.01$, $p > 0.05$). The highest RBC count was observed for fish from group A, fed the fish meal based control diet ($14.99 \pm 1.31 \times 10^8 \text{ cells.mL}^{-1}$). Similarly, no significant differences were observed for haematocrit ($F_{[2, 18]} = 2.53$, $p > 0.05$) and haemoglobin ($F_{[2, 18]} = 0.78$, $p > 0.05$) values among dietary groups. The Hct values for fish fed the diet containing SBM were greater than for fish fed the other two diets, and the highest Hb values were attained for the same treatment group.

Soybean meal concentrate in the feed induced a significant effect on the total WBC count ($F_{[2, 18]} = 0.21$, $p < 0.05$). As the plant protein content in diets increased, an increase in the WBC count was observed. Nonetheless, differential leucocyte counts were not affected by the diets. Analysis of blood smears from the different treatment groups did not reveal any significant differences in the differential WBC counts (Figure 3.3; $p > 0.05$). The group indices with reference to monocytes and granulocytes were greater for treatment groups A and C fed on fish meal diets (Diet A, 3.50 ± 0.49 %, 11.11 ± 2.28 %; Diet B, 2.78 ± 0.35 %, 7.22 ± 1.11 %; Diet C, 3.44 ± 0.694 %, 8.278 ± 1.04 % respectively). The percentage of thrombocytes were higher for treatment group B fed the SBM diet (Diet A, 36.833 ± 2.631 %; Diet B, 40.22 ± 1.691 %, Diet C, 35.83 ± 2.24 %), while lymphocyte percentages were very similar between diets A and B (Diet A, 48.56 ± 3.50 %; Diet B, 49.78 ± 1.390 %, Diet C, 52.44 ± 2.53 %).

Table 3.3. Haematological profiles for Atlantic salmon fed the experimental diets.

	Diet A (Standard)		Diet B (SBM)		Diet C (Imm)		<i>p</i> -value
	Mean*	SD	Mean	SD	Mean	SD	
Erythrocyte Count (RBC, $\times 10^8$ cells.mL ⁻¹)	14.99	1.31	14.91	1.48	15.37	1.00	0.10
Leucocyte Count (WBC, $\times 10^7$ cells.mL ⁻¹)	13.41	13.43	14.56	8.11	14.38	9.63	0.81
Haematocrit (Hct, %)	42.39	0.78	43.80	1.37	40.27	0.75	0.16
Haemoglobin (Hb, g.dL ⁻¹)	9.40	0.19	9.88	0.21	9.22	0.24	0.50
Mean Corpuscular Volume (MCV, fL)	334.17	36.71	346.19	41.40	277.54	17.978	0.80
Mean Corpuscular Haemoglobin (MCH, pg)	867.94	115.44	712.51	46.43	726.08	99.72	0.65
MCH Concentration (MCHC, g.dL ⁻¹)	2.22	0.05	2.28	0.08	2.30	0.06	0.82
Lysozyme (Lys, U.min ⁻¹ .mL ⁻¹)	169.99	79.48	153.61	82.96	222.35	94.21	0.26
Total Protein (TP, g.L ⁻¹)	37.51	6.29	38.81	3.45	36.9	3.65	0.46
Albumin (Alb, g.L ⁻¹)	17.29	1.55	17.00	1.06	16.56	1.48	0.29
C-reactive Protein (CRP, mg.L ⁻¹)	16.36 ^a	9.23	10.62 ^b	6.35	8.96 ^b	4.43	0.01

Footnotes:

Standard, control; SBM, soybean meal; Imm, immunostimulants.

* Data are expressed as mean and standard deviation (SD), $n = 18$ individual fish per treatment group were assessed.^{a,b} Mean values within the same row with different superscripts are significantly different (hierarchical GLM: tank [treatment] fixed factor with 3 levels, $p < 0.05$).

Higher MCH values were observed for treatment groups fed the fish meal based diets, and these values, though not statistically different ($F_{[2, 18]} = 0.47$, $p > 0.05$), were lower for the group fed the diet containing SBM concentrate. In comparison greater MCV values were observed in diet group B, although similarly not statistically different from those in groups A and C ($F_{[2, 18]} = 0.23$, $p > 0.05$). Although statistically similar ($F_{[2, 18]} = 0.20$, $p > 0.05$), the highest MCHC were observed in the group fed functional ingredients as opposed to the group fed plant protein.

Total plasma protein (TP) concentration in fish fed the SBM diet although not statistically significant, was slightly higher when compared to fish fed the control fish meal diet or the immunostimulant diet ($F_{[2, 18]} = 0.78$, $p > 0.05$). No statistically significant differences were observed in lysozyme activity (Lys) in serum taken from fish fed the fish meal based diet, compared to that measured in fish fed an unrefined SBM diet ($F_{[2, 18]} = 1.70$, $p > 0.05$), although fish fed the immunostimulant diet had slightly higher values of activity. Likewise, the levels of plasma albumin (Alb) between all the experimental diets ($F_{[2, 18]} = 1.28$, $p > 0.05$) were fairly similar. C-reactive protein levels (CRP) were negligible in fish

fed both experimental diets, but were significantly higher in fish fed the control diet based on fish meal ($F_{[2, 18]} = 5.60, p < 0.05$; Table 3.3).

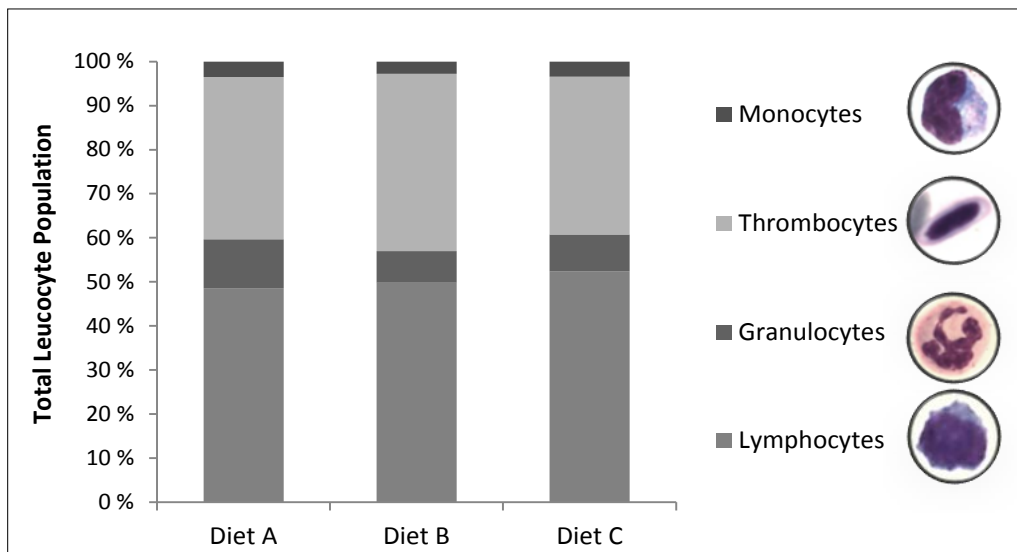


Figure 3.3. Effect of feeding the different experimental diets to Atlantic salmon on the mean differential leucocyte cell percentage. Columns represent cumulative mean percentage values, $n = 9$ individual fish per treatment group. Significant differences between treatment groups were not observed (hierarchical GLM: tank [treatment] fixed factor with 3 levels, $p > 0.05$). (Diet A) Standard fish meal based feed used as control diet. (Diet B) Soybean meal based feed. (Diet C) Standard feed with inclusion of immunostimulant ingredients. Cell photos courtesy of Christoforos Metochis.

3.3.5. Respiratory burst activity and phagocytic activity assays

Macrophage respiratory burst activity, as measured by NBT reduction was unaffected by the different dietary treatments ($F_{[2, 18]} = 0.97, p > 0.05$). Diets A and C gave intermediate levels of response, while the substitution by soya meal resulted in a trend for inhibition of respiratory burst (Diet A, 1.39 ± 1.12 ; Diet B, 1.02 ± 0.79 ; Diet C, 1.25 ± 0.98 abs per 10^5 cells; Figure 3.4).

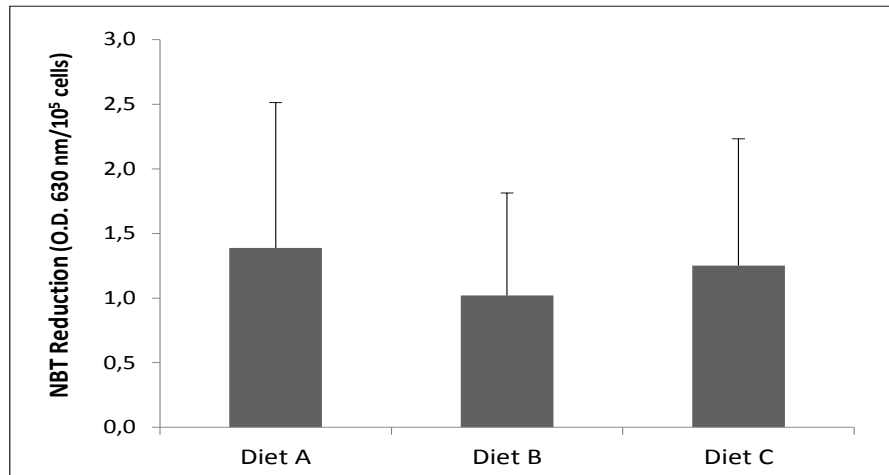


Figure 3.4. Respiratory burst activity of head kidney macrophages from Atlantic salmon stimulated with 1 mg.mL^{-1} NBT containing $1 \text{ }\mu\text{g.mL}^{-1}$ PMA, that were fed the different experimental diets. Columns represent mean values, and vertical bars indicate SD, $n = 18$ individual fish per treatment group. No significant differences between treatment groups were observed (hierarchical GLM: tank [treatment] fixed factor with 3 levels, $p > 0.05$). (Diet A) Standard fish meal based feed used as control diet. (Diet B) Soybean meal based feed. (Diet C) Standard feed with inclusion of immunostimulant ingredients.

Phagocytic activity of the isolated head kidney macrophages was assessed in terms of their ability to phagocytose *Saccharomyces cerevisiae* (Figure 3.5) and was characterised in terms of the previously described PI, PA and PC parameters.

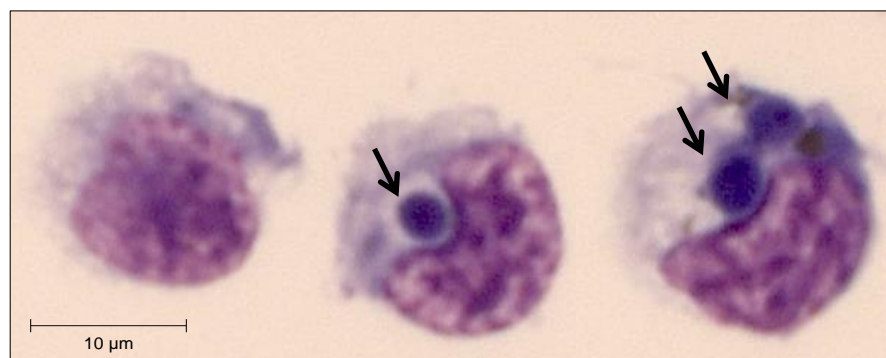


Figure 3.5. Light micrograph of Atlantic salmon head kidney macrophage cells (100 \times). Arrows showing yeast cells phagocytosed by macrophages.

As shown in Figure 3.6, there was an increase in the number of yeast cells engulfed per macrophage in fish fed diet B and C, however this was not significantly different from values for fish fed the control treatment diet ($F_{[2, 18]} = 0.66, p > 0.05$). Phagocytic activity values ranged from 80.95 % to 83.94 %. With regard to the phagocytic index, there were no major or significant differences between the different treatment groups (Figure 3.7). Fish from diet group A had a PI of 2.15 ± 0.37 , while values for diet B were 2.22 ± 0.48 and diet C were 2.28 ± 0.58 ($F_{[2,18]} = 0.27, p > 0.05$). For the macrophage cells isolated from fish fed diet A, 83.95 % had phagocytosed 1-3 yeast cells and 12.80 % had phagocytosed 4-6 yeast cells. Thus, for macrophages isolated from fish fed diets B and C, 82.15 % and 80.95 % had engulfed up to 3 yeast cells and 15.25 % and 16.46 % had engulfed up to 6 yeast cells respectively.

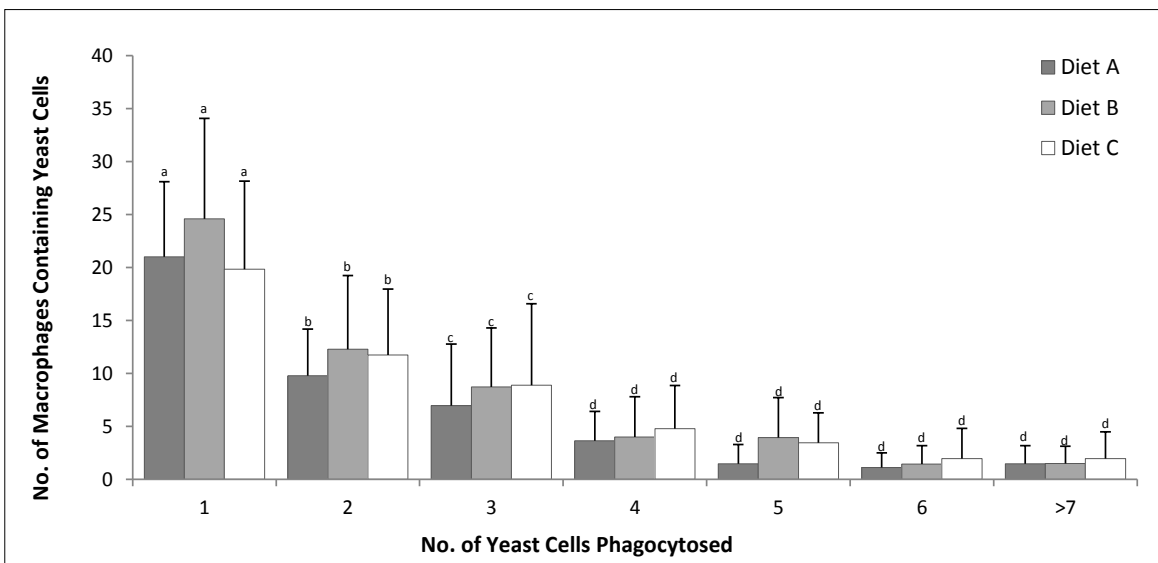


Figure 3.6. Phagocytic ability of macrophages from head kidneys of Atlantic salmon fed different experimental diets. Columns represent mean values, and vertical bars indicate SD, $n = 18$ individual fish per treatment group. Significant differences between the phagocytic capacity of different treatment groups are indicated by different superscripts (hierarchical GLM: tank [treatment] fixed factor with 3 levels, $p < 0.05$). (Diet A) Standard fish meal based feed used as control diet. (Diet B) Soybean meal based feed. (Diet C) Standard feed with inclusion of immunostimulant ingredients.

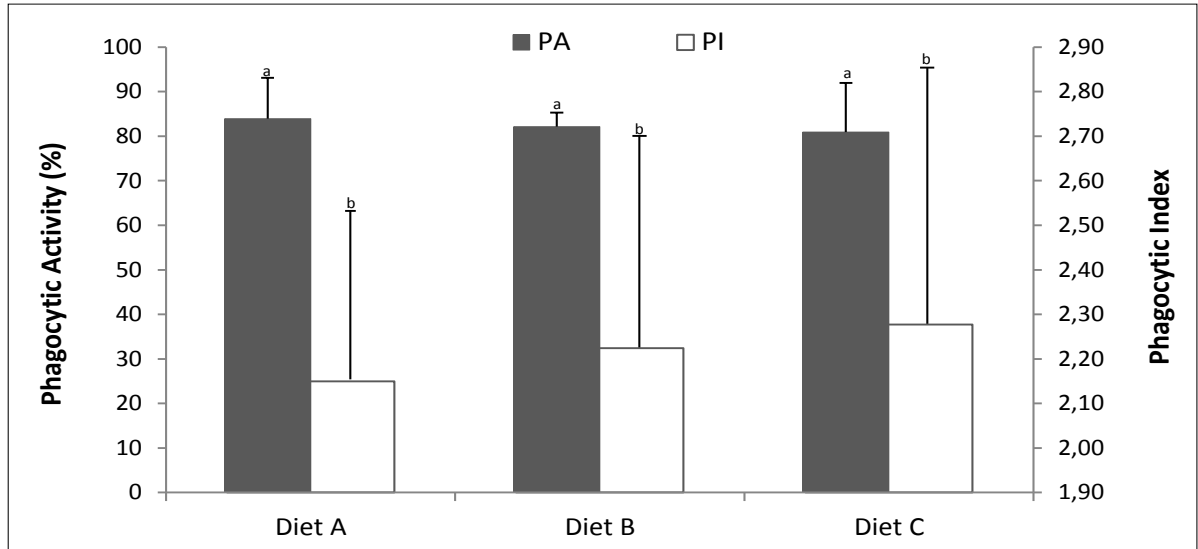


Figure 3.7. Phagocytic activity (%), (■ PA) and the phagocytic index (□ PI) of macrophages from head kidneys of Atlantic salmon fed different experimental diets. Columns represent mean values, and vertical bars indicate SD, $n = 18$ individual fish per treatment group. No significant differences between treatment groups were observed (hierarchical GLM: tank [treatment] fixed factor with 3 levels, $p < 0.05$). (Diet A) Standard fish meal based feed used as control diet. (Diet B) Soybean meal based feed. (Diet C) Standard feed with inclusion of immunostimulant ingredients.

3.3.6. Image analysis performance

The average time for the whole digital slide image acquisition was approximately 4-12 min. Image pre-processing and frame rotation / cropping was around 3 min per slide. The total average computation time from image upload until feature extraction, measurement and results data output for 12 continuous variables being roughly 20 to 25 min per frame, which greatly improved the efficiency of conducting such quantitative assessment as opposed to the semi-quantitative alternative approach. Consequently, the image analysis of 3 pathology cases with 27 individuals for each of which 2 frames were randomly analysed (representing 162 diagnostic frames in total) was performed over 10 days. The system described here required a degree of user learning / training to give consistent results.

Overall, the algorithm's performance and ability to detect objects of interest was very good (see Chapter 2 for a full discussion of performance). Mucous cells were correctly segmented, with their selection and separation being very precise on the whole. Similarly, the algorithm detecting the whole tissue surface and subsequently dividing it into mucosal

and submucosal layers also performed accurately. In contrast, the vacuolisation algorithm was less accurate, showing certain inaccuracy in its identification. Nevertheless, the interactive amendment-steps permitted the operator to easily correct errors in the automated selection. Additionally, the success of the interactive algorithm in excluding artefacts was very good. The overlay masks created by semi-automatic segmentation, recognising tissue areas, perimeter lines, mucous cells and vacuolisation visually agreed with the actual extent of these regions, as shown in output display-pictures in Figure 3.2. Very small discrepancies were observed, clearly illustrating the level of success of the image analysis system employed here.

Validation of measurements was performed by an experienced histopathologist, using ImageJ software (Version 1.45, US National Institutes of Health, Bethesda, Maryland, <http://rsb.info.nih.gov/ij/>). The results given by ImageJ's automatic and manual image segmentation closely mirrored the ones obtained with the developed macro. Correlation values being greater than 0.87 for most of the parameters measured (see Chapter 2 for full discussion of these results) suggesting that the proposed system is accurate and reliable.

3.3.7. Quantitative variables from image analysis

The 162 independent histological frame samples were evaluated using their measured morphometric and tissue cytometric parameters. The morphometric parameters used to provide an overview of the whole intestinal specimen condition are presented in Table 3.4.

With respect to the histological examination of the distal intestine (Figure 3.8), no differences in the structure of the epithelial mucosal layers were observed among sections from different treatment groups ($F_{[3, 36]} \text{ MTA / STA} = 1.51, p > 0.05$). Nor were there significant differences in the key morphometric parameters associated with the mucous cells. Mean mucous cell circularity indices and the mean elliptical and Feret length ratios were fairly similar among fish from different dietary groups ($F_{[3, 36]} \text{ MCirc} = 0.01$; $F_{[3, 36]} \text{ MC Ellipse Ratio} = 0.25$; $F_{[3, 36]} \text{ MC Feret Ratio} = 0.39$; $p > 0.05$).

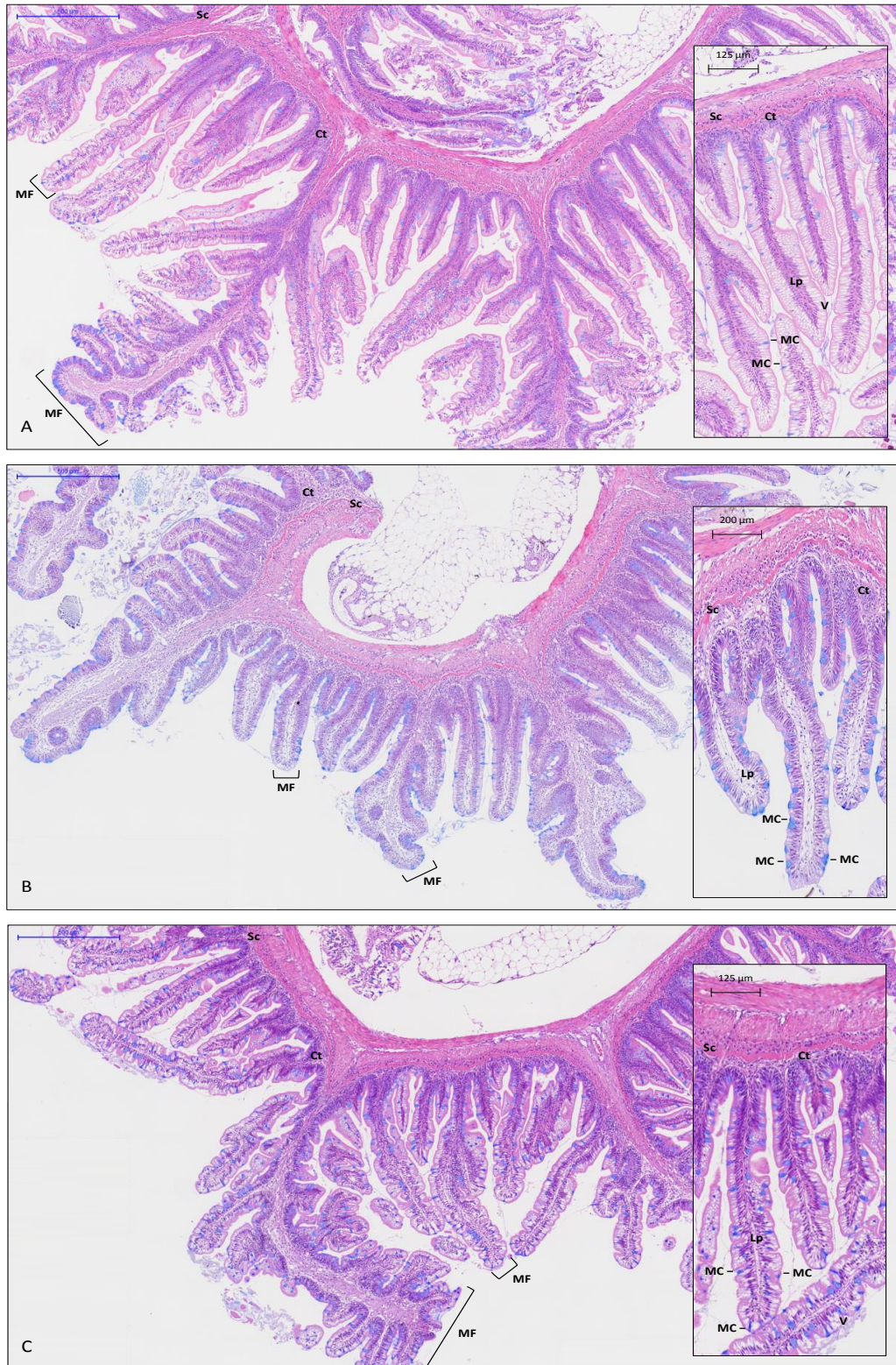


Figure 3.8. Representative images of morphological variations encountered across the distal intestine of Atlantic salmon fed different experimental diets: (A) fish meal based control diet, (B) diet containing 25 % defatted soybean meal and (C) diet with inclusion of immunostimulant ingredients. The morphology of fish meal fed fish is considered as being the normal status, whereas that of fish fed soybean meal reflects an inflammatory response characterised by the loss of vacuoles (V) in the absorptive enterocytes; the widening of *lamina propria* (Lp) in the mucosal folds (MF);

On the other hand, it should be emphasised that mean mucous cell area showed significant differences among treatment groups ($F_{[3, 36]} \text{ MMCA} = 7.05, p < 0.05$). Fish fed the fish meal based diet, exhibited significantly larger (μm^2) intestinal mucous cells, and subsequently the highest ratio between mucous cell total area and the mucosal tissue area ($F_{[3, 36]} \text{ MCA} / [\text{MTA-Vac}] = 10.17, p < 0.05$). No differences in the overall number of mucous cells were observed, however, for fish maintained under the various dietary treatment regimes ($F_{[3, 36]} \text{ MCN} / [\text{MTA-Vac}] = 4.39, p > 0.05$).

Table 3.4. Morphometric assessment of the distal intestine from Atlantic salmon fed the experimental diets.

Morphometric feature*	Diet A (Standard)		Diet B (SBM)		Diet C (Imm)		p-value
	Mean [†]	SD	Mean	SD	Mean	SD	
FR	1.28 ^a	0.048	1.23 ^b	0.05	1.27 ^a	0.05	0.04
MTA / STA	3.63	0.26	3.22	0.20	3.01	0.21	0.30
MMCA (μm^2)	236.81 ^a	9.55	206.78 ^b	5.10	204.33 ^b	6.26	0.03
MC Feret Ratio	0.74	0.004	0.74	0.01	0.73	0.04×10^{-1}	0.69
MC Ellipse Ratio	1.44	0.01	1.44	0.02	1.45	0.01	0.79
MCirc Index	0.85	0.01	0.85	0.01	0.85	0.01	0.99
P / MTA ($\mu\text{m} / \mu\text{m}^2$)	1.76×10^{-2a}	0.05×10^{-2}	1.41×10^{-2b}	0.05×10^{-2}	1.67×10^{-2a}	0.06×10^{-2}	0.04
VC / MTA	0.05	0.01	0.05	0.01	0.05	0.01	0.87
MCA / [MTA-Vac]	0.13 ^a	0.010	0.09 ^b	0.01	0.09 ^b	0.01	0.01
MCN / [MTA-Vac] ($\text{n}^0 / \mu\text{m}^2$)	0.51×10^{-3}	0.03×10^{-3}	0.45×10^{-3}	0.03×10^{-3}	0.43×10^{-3}	0.03×10^{-3}	0.07

Footnotes:

Standard, control; SBM, soybean meal; Imm, immunostimulants.

* Distal intestinal sections were assessed according to the morphometric features listed and described in Table 2.2. FR, fractal dimension of the perimeter line of the luminal surface, MTA / STA, ratio between the mucosal tissue area and the submucosal tissue area, MMCA, mean mucous cell area, MC Feret Ratio, ratio of the Feret lengths from mucous cells, MC Ellipse Ratio, ratio of the elliptical lengths from the mucous cells, MCirc, mucous cell mean circularity index, P / MTA, ratio between the total perimeter of the luminal surface and the mucosal tissue area, VC / MTA, ratio between total vacuolisation area and the mucosal tissue area, MCA, mucous cell total area, MTA-Vac, mucosal tissue area without the vacuolisation area, MCN, mucous cell number.

† Data are expressed as mean and standard deviation (SD), $n = 36$ histological frames per treatment group were assessed.

^{a,b} Mean values within the same row with different superscripts are significantly different (hierarchical GLM: tank [treatment] fixed factor with 3 levels, $p < 0.05$).

Figure 3.8. (continued from previous page) an increase of the connective tissue (Ct) between the base of the mucosal folds and the *stratum compactum* (Sc); and an increase in size of mucous cells (MC) in the epithelium. The morphological profile from fish fed the immunostimulant diet did not differ substantially from the fish meal fed fish. Intestinal transverse sections were stained with a combination of haematoxylin-eosin and Alcian blue 8 GX.

The control group exhibited higher vacuolisation per mucosal tissue area, however this was not significantly different from the other two dietary groups ($F_{[3, 36]} V / MTA = 0.14, p > 0.05$). In contrast to vacuolisation, the fish fed the diet containing plant protein revealed the lowest ratio between the perimeter length and the mucosal tissue area ($F_{[3, 36]} P / MTA = 6.12, p < 0.05$) and its fractal dimension ($F_{[3, 36]} FR = 5.96, p < 0.05$). Following univariate analyses, the values of each morphological parameter were multi-dimensionally analysed by including them all as variables in a multivariate model.

A principal component analysis (PCA) with orthogonal rotation was conducted. The Kaiser-Meyer-Olkin measure confirmed the sampling adequacy for the analysis, KMO = 0.63 (Hutcheson & Sofriniou, 1999 *in* Field, 2009), and Bartlett's test of sphericity $\chi^2 (36) = 752.08, p < 0.001$, indicated that correlations between replicates were sufficiently large for a PCA analysis (Bartlett, 1988). This approach allowed the full set of variables to be reduced to a smaller set of components (*i.e.* reduction of the dimensionality of the data). Table 3.5 gives a summary of the loading weightings and score coefficients assigned to each of the variables for the extracted components.

Four of the extracted components had Eigenvalues exceeding Kaiser's criterion of 1 (Field, 2009) and in combination they explained 89.28 % of the total variation in individual intestinal morphology. The two first components accounted for the 64.07 % of variation of this dataset, with 33.34 % of the variation explained by component 1 ($F_{[3, 36]} PC1 = 0.94; p = 0.392$; Diet A = Diet B = Diet C; $F_{[3, 36]} PC2 = 11.87, p < 0.001$, Diet A \neq Diet B, Diet A \neq Diet C, Diet B = Diet C; $F_{[3, 36]} PC3 = 2.36; p = 0.098$, Diet A = Diet B = Diet C).

The principal components obtained, are entities that can be visualised as a new classification axis (variable) along which the variables can be plotted, giving an idea of their relationship with the corresponding principal component (Figure 3.9). The first component PC1, which appeared to be related to mucous cell shape, was characterised by high loadings of the variables MC Feret Ratio and MCirc, against a high negative weighting for MC Ellipse Ratio. Two additional characters, MCA / [MTA-Vac] and MCN / [MTA-Vac], showed the highest positive relationship within the second component PC2, which related to

the mucous cell proportion within the tissue. Similarly, the P / MTA showed the highest positive, while FR the highest negative correlation within the third component PC3, which is related to luminal surface intricacy. The fourth component PC4, which is related to mucosal tissue area profile, showed a high positive weighting for MTA / STA and VC / MTA variables (Figure 3.9, Table 3.5).

Table 3.5. Factor loading weights and component score coefficients derived from principal component analysis, regarding morphometric features measured in the distal intestine of Atlantic salmon fed with the experimental diets.

Morphometric feature§	Principal components (PC)*							
	PC 1		PC 2		PC 3		PC4	
	LW†	SC‡	LW	SC	LW	SC	LW	SC
MC Ellipse Ratio	-0.967	-0.396	—	-0.070	—	0.061	—	-0.007
MC Feret Ratio	0.959	0.409	—	0.152	—	-0.053	—	0.079
MCirc Index	0.796	0.278	-0.456	-0.182	—	0.008	—	-0.040
MCA / [MTA-Vac]	—	0.048	0.954	0.506	—	-0.039	—	0.116
MCN / [MTA-Vac]	—	0.068	0.930	0.479	—	-0.081	—	-0.011
P / MTA	—	-0.067	—	-0.070	0.949	0.571	—	0.106
FR	—	0.038	—	0.067	-0.927	-0.536	—	-0.055
MTA / STA	—	0.111	—	0.150	—	0.000	0.848	0.634
VC / MTA	—	-0.058	—	-0.011	—	0.170	0.816	0.600
Eigen value	3.000		2.766		1.194		1.075	
Variance explained (%)	33.336		30.737		13.267		11.943	

Footnotes:

* Extraction method: principal component analysis using Varimax rotation with Kaiser normalisation for a total of 162 histological frames.

† LW, factor loading weights are only displayed for values ≤ -0.100 or ≥ 0.200 , some morphological features are excluded as they did not load onto any factor retained. Higher absolute values indicate that the morphometric variable is highly correlated to the respective principal component.

‡ SC, component score coefficients presented correspond to correlation coefficients.

§ Distal intestinal sections were assessed according to the morphometric features listed and described in Table 2.2.

MC Ellipse Ratio, ratio of the elliptical lengths from the mucous cells, MC Feret Ratio, ratio of the Feret lengths from mucous cells, MCirc, mucous cell mean circularity index, MCA, mucous cell total area, MTA-Vac, mucosal tissue area without the vacuolisation area, MMCA, mean mucous cell area, MCN, mucous cell number, P / MTA, ratio between the total perimeter of the luminal surface and the mucosal tissue area, FR, fractal dimension of the perimeter line of the luminal surface, MTA / STA, ratio between the mucosal tissue area and the submucosal tissue area, VC / MTA, ratio between total vacuolisation area and the mucosal tissue area.

According to the PCA analysis (Figure 3.10), two major clusters could be segregated and identified as (○) Diet A, comprising the group fed on the fish meal control diet, and (●) Diet B, the group fed the SBM concentrate. While less distinct (*i.e.* being very closely associated to the Diet A cluster), a third cluster corresponding to individuals from the Diet C group (◐) could also be distinguished.

Based upon this multivariate appraisal, one could suggest reducing the number of required classification features, with the most informative being MC Feret Ratio, MC Ellipse Ratio, MCA / [MTA-Vac], FR and MTA / STA for the evaluated histological states. A discriminant analysis undertaken on the data revealed two canonical functions. The first accounted for 76.8 % (canonical $R^2 = 0.25$) of the group variance, whereas the second function explained 23.2 % (canonical $R^2 = 0.09$). In combination these discriminant functions significantly differentiated the treatment groups, $\lambda = 0.68$, $\chi^2(6) = 38.97$, $p < 0.001$. After removal of the first function there was still highly significant discriminatory power, the second discriminant function still differentiating the treatment groups $\lambda = 0.91$, $\chi^2(2) = 9.76$, $p < 0.05$. Thus, the group differences could be explained in terms of two underlying dimensions in combination, explained by the following linear equations: [a] $D_1 \text{ score} = -6.80 + (0.51 \times \text{MTA} / \text{STA}) + (259.27 \times \text{P} / \text{MTA}) + (9.06 \times \text{MCA} / [\text{MTA-Vac}])$ and [b] $D_2 \text{ score} = 0.84 + (0.32 \times \text{MTA} /$

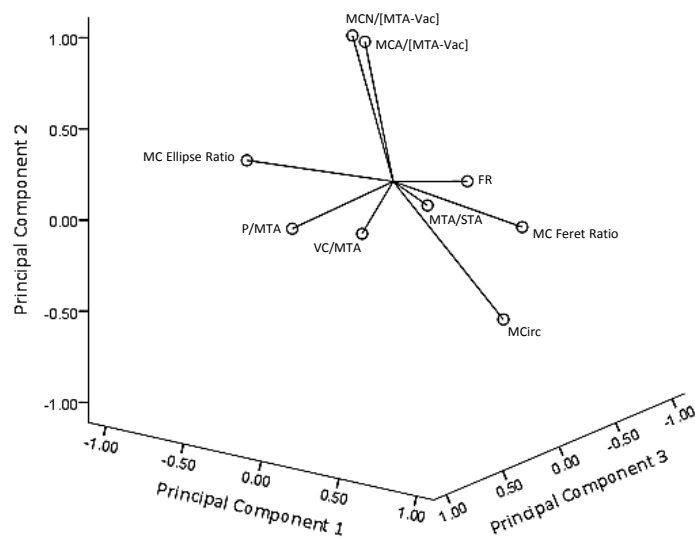


Figure 3.9. Component plot of the multivariate principal component analysis for the intestinal morphological features measured in Atlantic salmon fed different treatment diets. (PC) Principal component. (MCN) Mucous cell number. (MCA) Mucous cell total area. (MTA-Vac) Mucosal tissue area without the vacuolisation area. (MC Ellipse Ratio) Ratio of the elliptical lengths from the mucous cells. (FR) Fractal dimension of the perimeter line of the luminal surface. (MC Feret Ratio) Ratio of the Feret lengths from mucous cells. (P / MTA) Ratio between the total perimeter of the luminal surface and the mucosal tissue area. (MTA / STA) Ratio between the mucosal tissue area and the submucosal tissue area. (VC / MTA) Ratio between total vacuolisation area and the mucosal tissue area. (MCirc) Mucous cells mean circularity index.

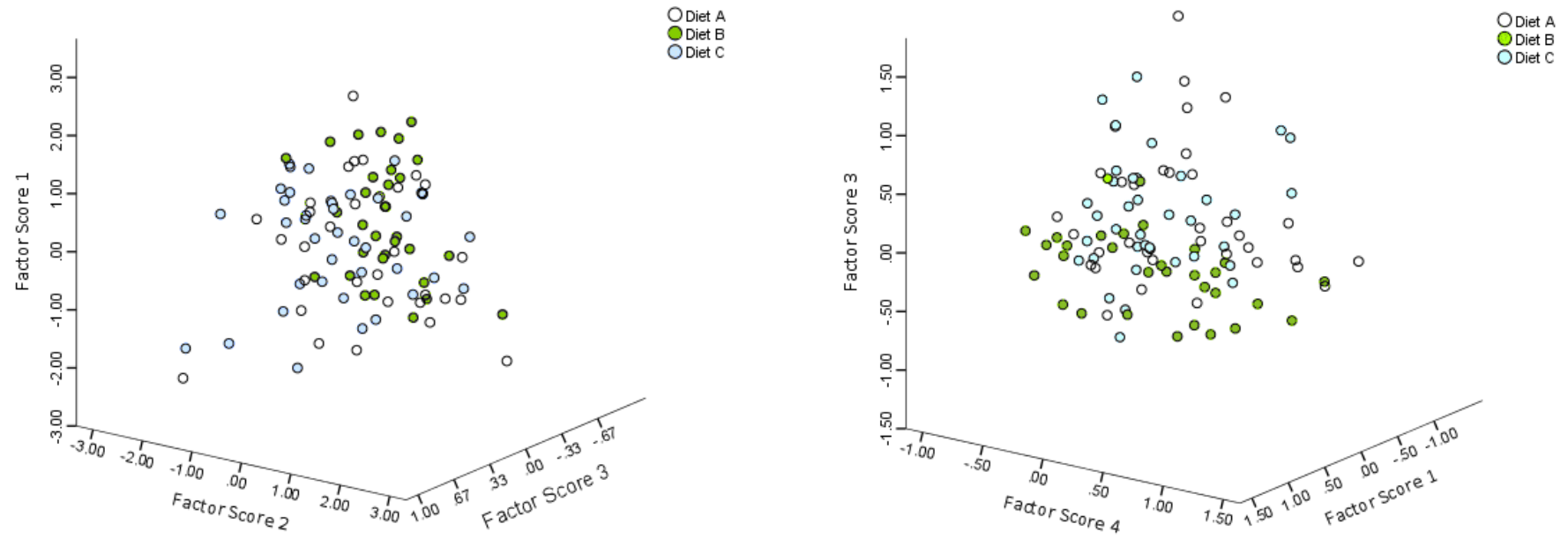


Figure 3.10. Factor plot of the multivariate principal component analysis for the intestinal morphology of Atlantic salmon fed different diets. (Diet A) Standard fish meal based feed used as control diet. (Diet B) Soybean meal based feed. (Diet C) Standard feed with inclusion of immunostimulant ingredients.

/ STA) + (-208.29 × P / MTA) + (14.37 × MCA / [MTA-Vac]). The correlations between the discriminant variables and standardised canonical discriminant functions, revealed that the primary variables in distinguishing between different dietary groups were P / MTA, MCA / [MTA-Vac], MTA / STA, FR and MCN / [MTA-Vac]. The P / MTA ($r_{D1} = 0.71$) and MCA / [MTA-Vac] ($r_{D1} = 0.50$), variables more highly associated with the first function, while FR ($r_{D2} = 0.60$) and MTA / STA ($r_{D2} = 0.50$) were more highly associated with the second function.

The discriminant function plot illustrated in Figure 3.11, clearly shows that the first function discriminated dietary group B from group A, and that the second function discriminated group C from groups A and B, but that this difference was not as sharp as for the first variable. The group centroids illustrated in the figure, are simply the mean variable scores for each treatment group ($D_1 = 0.73$ Diet A, -0.67 Diet B, -0.14 Diet C; $D_2 = 0.16$ Diet A, 0.30 Diet B, -0.43 Diet C).

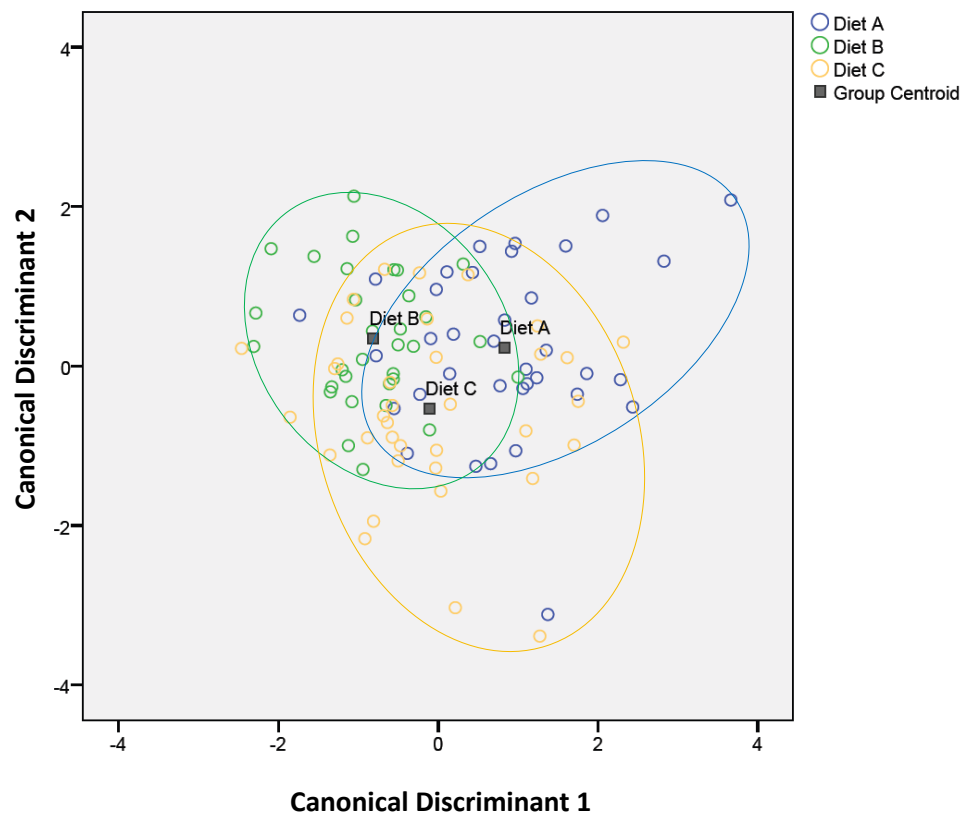


Figure 3.11. Scatterplot of the canonical scores and corresponding dietary group centroids, for a pair of discriminant functions, based on 9 morphometric features ($n = 36$ histological frames per treatment group). (Diet A) Standard fish meal based feed used as control diet. (Diet B) Soybean meal based feed. (Diet C) Standard feed with inclusion of immunostimulant ingredients.

A “leave-one-out” classification analysis (sensitivity analysis) was also employed in which the analysis was re-run once with each target individual sequentially excluded and then reassigned to a group based on the resulting discriminant function score. Such re-assignment classification resulted in 61.1 % of the individuals from group A being correctly assigned to their group. However, only around 42 to 59 % of individuals from groups B and C were assigned to the correct group. This gives an overall efficiency of 53.8 % for the discrimination of the dietary groups. Based on the overall analysis one could reduce the number of necessary classification features from ten to four, with P / MTA, MCA / [MTA-Vac], FR and MTA / STA being emphasised.

3.4. Discussion

3.4.1. Growth performance and nutrient intake

The chemical composition of the experimental diets was successfully matched (*i.e.* in terms of crude protein, lipid, ash and moisture contents), with optimal levels for salmonids being achieved (Helland *et al.*, 1991; Einen & Roem, 1997).

Overall, fish performance was good, with growth and feed efficiency being similar to results previously achieved for Atlantic salmon of comparable size and raised at similar temperatures (Austreng *et al.*, 1987). For the salmon fed the soybean meal diet, the Wt and SGR were lower than values reported for studies on the effect of dietary soybean meal on the growth rate for salmonids fed similar levels of SBM inclusion (Watanabe *et al.*, 1993; Oliva-Teles *et al.*, 1994; Refstie *et al.*, 1998; Carter & Hauler, 2000; Selden *et al.*, 2001; Romarheim *et al.*, 2006; Øverland *et al.*, 2009; Collins *et al.*, 2013). These minor differences were not due to differences in feed intake, as the feeding response was consistent irrespective of the dietary treatment. However, the use of unrefined soybean meal as an alternative protein source to fish meal in diets for salmonid has repeatedly been shown to induce morphological changes in the distal intestinal epithelium (Van den Ingh *et al.*, 1991; Baeverfjord & Kroghdahl, 1996; Buttle *et al.*, 2001; Urán *et al.*, 2008b; Sørensen *et al.*, 2011), along with reduced feed efficiency and weight gain (Olli *et al.*, 1994; Rumsey *et al.*, 1995;

Bureau *et al.*, 1998; Refstie *et al.*, 1998, 2001; Krogdahl *et al.*, 2003; Øverland *et al.*, 2009) the magnitude of which depends on the protein source, processing quality and level of replacement. It has also been suggested that such antigen-related inflammation of the distal intestinal, results in a distinct decrease in the brush border and mucosal enzyme activity levels, and thereby may contribute to reduced protein retention and growth in fish (Bakke-McKellep *et al.*, 2000b; Krogdahl *et al.*, 2003; Chikwati *et al.*, 2013a). Other studies have shown that the content of digestible energy in plant protein is lower than that of fish meal, and since utilisation of the feed energy can be predicted from the content of digestible energy, it is clear that substitution of fish meal with plant protein would reduce growth rates and impair feed conversion ratios (Sanz *et al.*, 1994; Aksnes & Opstvedt, 1998; Opstvedt *et al.*, 2003; Mundheim *et al.*, 2004; Sørensen *et al.*, 2011). The results of the present study are in accordance with other studies on replacement of fish meal by soybean protein concentrate, suggesting that the soybean protein could partially or totally substitute fish meal, without resulting in a substantive negative effect on feed intake and growth performance of the fish (Watanabe *et al.*, 1993; Kaushik *et al.*, 1995; De Francesco *et al.*, 2004; Kumar *et al.*, 2011b). It was, however, obvious from the results obtained with Diet C that supplementing fish feed with exogenous nucleotides and β -glucans did not exert the positive effect on growth and feed efficiency that was anticipated. This contradicts published studies involving other teleost species, in which enhanced growth performance and feed uptake has been associated with dietary nucleotide supplementation (Ramadan *et al.*, 1991; Burrells *et al.*, 2001; Li *et al.*, 2007; Lin *et al.*, 2009; Tahmasebi-Kohyani *et al.*, 2011; Abtahi *et al.*, 2013; Kenari *et al.*, 2013) and by administration of β -glucan (Cook *et al.*, 2003; Jaramillo & Gatlin, 2004; Misra *et al.*, 2006). Nevertheless, the growth-promoting effect of nucleotides and β -glucans has not always been observed (Efthimiou, 1996; Li *et al.*, 2004, 2005; Whittington *et al.*, 2005; Bagni *et al.*, 2005; Kumari & Sahoo, 2006; Welker *et al.*, 2011). Disparities in the results may be due to observations of different fish species, genetic backgrounds of strains, life stages, temperatures used, stocking densities and water quality

amongst other environmental variables, feeding duration, dosages or even the type of nucleotide and β -glucan supplemented (Li & Gatlin, 2006).

The results of the present study revealed that despite the fact that there were no significant differences in growth of fish between the different dietary treatments, the feed conversion rate remained lower with Diet B. It is difficult to pinpoint which factor(s) in the dietary formulation adversely affected the salmon, although according to earlier studies it is likely to have been phytosterols, oligosaccharides and / or soya-saponins in synergy with one or more unidentified components that follow the same solubility pattern within the soybean matrix (Knudsen *et al.*, 2008; Iwashita *et al.*, 2009; Krogdahl *et al.*, 2010). On the other hand, such factor(s) did not appear to be present, or were perhaps present at very low levels in the soya protein concentrate used in Diets A and C, since the feed conversion efficiency of fish fed the fish meal based and the immunostimulant diets was significantly greater. Furthermore, fish body condition and relative liver weights showed no significant differences between dietary treatments. The condition factor (K) and the hepatosomatic index (HSI) are commonly used as indirect evidence of the physiological and energy status of the fish in relation to its welfare (Bolger & Connolly, 1989). Values were similar across control and experimental groups, the reason for which may have been that fish were assimilating food efficiently, or, that the tested dietary levels did not affect the K and HSI values. This is in agreement with results obtained for similar dietary products fed to salmonids (Olli *et al.*, 1994, 1995; Refstie *et al.*, 1998), but in contrast to that found with some other fish meal replacement studies (Refstie *et al.*, 2001; Opstvedt *et al.*, 2003; Hemre *et al.*, 2005; Morris *et al.*, 2005) where HSI appeared to be affected by substitution of fish meal. Presumably the inclusion of soybean containing ANF in the present experimental diets was sufficiently low to still allow the detoxification system of the liver to cope efficiently without impairing liver function. Again, the inconsistencies observed between different studies may be due to inter-species variations, feeding duration, source of dietary components or even the level of substitution.

3.4.2. Haematology and blood biochemistry

Haematology and clinical chemistry analysis are an integral part of the methods elected for examining the health status of the fish, and have a role in feeding trials when evaluating the effects dietary components may have (Řehulka, 2002; Kopp *et al.*, 2011; Rawling *et al.*, 2012; Kiron, 2012).

In this study, red blood cell indices (*i.e.* RBC count, Hct and Hb) did not differ significantly among the different dietary groups. Consequently, MCV, MCH and MCHC values remained unchanged, and were within the normal range for healthy Atlantic salmon (Hardie *et al.*, 1990; Sandnes *et al.*, 1988; Fast *et al.*, 2002; Sissener *et al.*, 2009b), demonstrating that erythropoietic elements were not affected by the dietary components. Similarly, Burrells *et al.* (2001) reported no significant differences in RBC concentration for Atlantic salmon fed a basal fish meal diet containing a nucleotide supplement. Welker *et al.* (2011) and Jha *et al.* (2007) stated that nucleotide supplementation did not affect RBC, Hct or Hb levels in channel catfish (*Ictalurus punctatus*) and catla catla (*Cyprinus catla*), respectively. In the same vein, Del Rio-Zaragoza *et al.* (2011) established that Ht, RBC, MCV and MCH were unaffected by the dietary levels of β -glucans they fed to fish. Additionally, Kumar *et al.* (2010a) reported that SBM diets had no effect on RBC counts, Hct or Hb concentrations. Whereas in other studies (Hemre *et al.*, 2005; Kumar *et al.*, 2010b), significant increases in RBC counts, and consequently a reduction in MCV were observed in SBM-fed groups, possibly linked to an inflammatory reaction due to the presence of ANFs in soybeans that have an antigenic potential.

The fact that haematocrit levels were un-affected by the diets was anticipated, since it is very unusual to observe differences amongst fish, except in cases of explicit disease or extreme nutritional deprivation (Siwicki *et al.*, 1994; Rumsey *et al.*, 1995).

In the present study, leucocyte levels and the proportions of lymphocytes, granulocytes thrombocytes and monocytes were not significantly affected by the different dietary treatments. These values differed from values reported in the literature for WBC counts in healthy salmonids (Sandnes *et al.*, 1988). Fish fed either the SBM or the immunostimulant

diets, had slightly more leucocytes than that of the fish fed the fish meal control diet, although this was not significant. According to various authors (Rumsey *et al.*, 1995) an increase in the leucocyte count often indicates the beginning of an inflammatory response, onset of a hypersensitivity reaction, or a response to the immunogen.

The leucocyte counts might have been enhanced due to the ANFs present in the SBM (Sagstad *et al.*, 2007; Rumsey *et al.*, 1995). Likewise, the tendency towards elevated lymphocytes levels in the blood from fish fed nucleotides and β -glucans (Leonardi *et al.*, 2003; Tahmasebi-Kohyani *et al.*, 2011; Del Rio-Zaragoza *et al.*, 2011; Kenari *et al.*, 2013) may be interpreted as a response of the cellular immune system to such stimulation. Therefore, the haematological results reported here do not seem to support the findings of other authors. *i.e.* a stimulatory effect on the haematological parameters by dietary β -glucans and nucleotides and a negative effect by ANFs present in the SBM.

The activity of plasma lysozyme has been well documented for a variety of fish species (Fange *et al.*, 1976; Lie *et al.*, 1989; Engstad *et al.*, 1992). Recognised to be an opsonin, and capable of activating the complement system and phagocytes, lysozyme contributes to the innate immunity of animals through its bactericidal and anti-inflammatory properties (Magnadóttir, 2006). Although not reflecting the values reported for salmonids by other researchers (Hardie *et al.*, 1990; Thompson *et al.*, 1996; Fast *et al.*, 2002), the results from the current study show that the lysozyme activity was not statistically different between the dietary groups. However, higher lysozyme activity was observed in fish fed the immunostimulant diet (*i.e.* Diet C) when compared to the control fish meal diet and to the one containing SBM. Considering the numerous studies that earlier demonstrate the stimulating effect of glucans (Engstad *et al.*, 1992; Matsuyama *et al.*, 1992; Jørgensen *et al.*, 1993; De Baulny *et al.*, 1996; Thompson *et al.*, 1995; Paulsen *et al.*, 2001, Bagni *et al.*, 2005; Paredes *et al.*, 2013) and of dietary nucleotides (Sakai *et al.*, 2001, Jha *et al.*, 2007, Kenari *et al.*, 2013 and Peng *et al.*, 2013) on lysozyme activity, the apparent lack of significant difference for such dietary group and the control treatment group is surprising.

However, this may reflect the number of samples employed, rather than the lack of effect by the immunostimulant ingredients.

In future feeding trials different dosages and feeding periods should be considered in order to further dissect the findings of the present study.

The effect of unrefined dietary soybean proteins on the innate response of fish has been recognised in accordance with previous studies (Burrells *et al.*, 1999; Sitjà-Bobadilla *et al.*, 2005; Kokou *et al.*, 2012), in which serum lysozyme did not vary significantly. However, in other reports where SBM was fed to salmonids (Rumsey *et al.*, 1994; Krogdahl *et al.*, 2000) increased lysozyme activity was reported, which may be interpreted as a response to the inflammatory effects of plant proteins.

The concentration of total protein in blood is used as a basic index for health and nutritional status in fish (Kumar *et al.*, 2010b). Proteins such as albumin are important compounds in the serum and are essential for maintaining a healthy immune system (Kumar *et al.*, 2005). Significantly lower blood protein levels were normally observed in groups of fish with known nutritional deficiencies, increased catabolism in acute inflammation, impaired protein metabolism in the liver, or during disease (Ingram & Alexander, 1977; Bruno & Munro, 1986; Waagbø *et al.*, 1988; Řehulka, 2002; Kumar *et al.*, 2010b). In turn, increase in the serum protein and albumin levels are thought to be associated with a stronger innate response in fish (Jha *et al.*, 2007; Kenari *et al.*, 2013).

In the current study, biochemical parameters such as total protein and albumin content were not statistically different between treatment groups, but were within the normal range for protein concentrations found in the serum of salmonids (total protein: 3.3-80 g.L⁻¹; albumin: 18.3- 24.3 g.L⁻¹; Alexander, 1977; Sandnes *et al.*, 1988) indicating that fish were apparently healthy and coping with the tested ingredients.

C-reactive protein (CRP) is an acute phase protein, the levels of which may increase in response to acute infection or inflammatory stimulus. Upon cessation of the stimulus, CRP levels are known to decline very rapidly. This has made CRP useful as a clinical marker of the inflammatory process, and measurements of its concentration in serum could help

differentiate inflammatory from non-inflammatory conditions (Lund & Olafsen, 1998; Liu *et al.*, 2004). The CRP levels reported in the present study are the first report of CRP acute phase protein profiles for Atlantic salmon fed soybean meal diets. The interaction between β -glucan immunostimulants and this acute phase protein has, however, recently been described by Pionnier *et al.* (2013) in common carp, where oral administration significantly increased serum CRP levels up to 2-fold. Studies relating dietary nucleotides and CRP profiles have not yet been conducted, however.

In this experimental trial, 'normal' CRP levels in serum from fish fed the control diet ranged from 7.13-25.59 mg.L⁻¹. These levels are 7 and 11 times lower than the serum CRP concentration suggested for healthy Atlantic salmon (~50-300 μ g.mL⁻¹) or rainbow trout (83-105 μ g.mL⁻¹) (Lund & Olafsen, 1999; Liu *et al.*, 2004; Kodama *et al.*, 2004). For other fish species such as common carp (*Cyprinus carpio*), plaice (*Pleuronectes platessa*), snake headed murrel (*Channa punctatus*), dogfish (*Mustelus canis*) and lumpsucker (*Cyclopterus lumpus*), values were reported to range from 18 μ g.mL⁻¹, 55 μ g.mL⁻¹, 220 μ g.mL⁻¹, 400 μ g.mL⁻¹ to 2200 μ g.mL⁻¹ respectively (Fletcher *et al.*, 1977; Pepys *et al.*, 1982; Robey *et al.*, 1983; Mitra & Bhattacharya, 1992; Pionnier *et al.*, 2013). Contrary to what was expected, fish fed the control diet showed significantly higher CRP levels than those fed the SBM or the functional diet. The apparent contradiction between serum CRP concentrations might be explained by the fact that the levels of CRP could have reached an optimal / maximum circulating concentration and thereafter, by the sampling point, the levels could have decreased to regain homeostasis. Kodama *et al.* (2004) reported that exposure of rainbow trout to anti-ectoparasite chemicals such as formalin and metrifonate was found to cause a significant increase of CRP levels soon after exposure, but that levels in the treated fish decreased afterwards to levels lower than those observed in unexposed fish. Another more reasonable justification might be that different dietary stimulations led to different production patterns of acute phase proteins in these fish (e.g. a reduction instead of an increase), as some studies have previously suggested (Pionnier *et al.*, 2013; Liu *et al.*, 2004). For instance, a decrease was observed in serum CRP levels in channel catfish *I. punctatus*

during *Saprolegnia* sp. infection, meanwhile an increase in CRP values was induced by turpentine injection in the same fish species (Szalai *et al.*, 1994). It is clear that, although molecular studies of salmonid acute-phase proteins exist (Murai *et al.*, 1991; Jensen *et al.*, 1997; Lund & Olafsen, 1999), the kinetics of CRP production during inflammation still require clarification.

Screening haematological parameters for assessing fish health in relation to dietary changes has been found to be relatively non-specific (Blaxhall & Daisley, 1973; Sandnes *et al.*, 1988; Filho *et al.*, 1992; Sissener *et al.*, 2009a; Kopp *et al.*, 2011). Individual haematological variability is influenced by a number of exogenous and endogenous factors, which must be considered when interpreting the results. Biochemical indices and their fluctuation have been reported to be a result of variations in blood sampling and biochemical assays, fish size, age, season, genetic strain, sexual maturation, nutritional status, infectious disease, environment and stress (Sandnes *et al.*, 1988). Analyses of this kind should thus be rigorously standardised with respect to fish size, sampling procedures, analytical methods and designation, in order to make comparisons between different experimental studies possible (Sandnes *et al.*, 1988; Filho *et al.*, 1992). Nevertheless, for this particular study it must be concluded that the modulatory effect of the functional ingredients (*i.e.* β -glucans and nucleotides) did not substantially affect the blood profile of experimental fish.

3.4.3. Respiratory burst and phagocytic activity assays

Generation of reactive oxygen intermediates in a process called 'respiratory burst', is recognised as one of the most important early defence mechanisms in fish (Secombes, 1990; Sveinbjørnsson & Seljelid, 1994; Castro *et al.*, 2004; Lundén *et al.*, 2002; Chettri *et al.*, 2010). This metabolic event plays a crucial role in pathogen eradication, but has also been shown to be involved in tissue regeneration (Vera-Jimenez *et al.*, 2013). Consequently, it can be employed to monitor health status in fish and even the efficacy of distinct dietary ingredients. The respiratory burst activity of fish phagocytes can be modulated by dietary substances such as functional ingredients (Engstad *et al.*, 1992;

Siwicki *et al.*, 1994; Dalmo & Seljelid, 1995; Toranzo *et al.*, 1995; Novoa *et al.*, 1996, Santarem *et al.*, 1997; Castro *et al.*, 2004). It has been reported that an increase in the respiratory burst activity was achieved through dietary intake of β -glucans (Robertsen *et al.*, 1990; Jeney & Anderson, 1993; Sveinbjörnsson & Seljelid, 1994; Jørgensen & Robertsen, 1995; Yoshida *et al.*, 1995; Cook *et al.*, 2003), and also of nucleotides (Sakai *et al.*, 2001; Lin *et al.*, 2009; Peng *et al.*, 2013), although, in the present study, oxidative radical production by head kidney macrophages from fish fed the experimental diet containing nucleotides and β -glucans showed no positive stimulation. This could possibly be explained as an effect of long-term administration of those functional ingredients. Yoshida *et al.* (1995) for instance, demonstrate that the number of NBT-positive cells in African catfish (*Clarias gariepinu*) increased following oral administration of glucan over 30 days, but not over 45 days. Moreover, Li *et al.* (2004) stated that hybrid striped bass fed a nucleotide supplemented diet for 16 weeks failed to show any enhancement of innate immune responses, including blood neutrophil oxidative radical production and extracellular / intracellular superoxide anion production by head kidney cells, which was not consistent with the results after 8 weeks of feeding the same diet. These reports suggest that the feeding regime should be taken into consideration when evaluating functional dietary ingredients. At present, there is no definitive evidence that their efficacy is associated with administration duration (Sakai, 1999; Li & Gatlin, 2006) and comprehensive research is needed to clarify the possible effects of prolonged feeding of nucleotides and immunostimulants on this immune parameter. The suppression of the non-specific immune capacity by high concentrations of dietary soybean meal has previously been reported for rainbow trout (Burrells *et al.*, 1999). Long-term administration of soybean meal proteins may lead to a sensitivity reaction or a “burnout” status, and development of enteritis. Rumsey *et al.* (1994) warned against feeding high levels of soybean meal protein as a protein substitute, because its anti-nutritional components appeared to cause a gastrointestinal hypersensitivity reaction, impairing protein utilisation, resulting in slower growth and affecting the general health of the fish. Respiratory burst activity of macrophages from fish

fed the SBM diet, although not significantly different, appeared slightly inhibited. It should be noted that previous studies were carried out under different experimental conditions so the present results are not directly comparable.

Phagocytosis (*i.e.* engulfing and ingestion of bacteria or other foreign bodies by phagocytes) is also recognised as one of the main mediators of the host's innate immune defences against microorganisms, and the effect of the different dietary components on normal phagocytic activity of macrophage cells is a useful indicator for assessing the effect of dietary components on fish health (Bennani *et al.*, 1995).

Dietary β -glucans and nucleotides have proven protective in some teleost fish by enhancing phagocytic activities based on the number of bacteria engulfed and killed per cell (Chen & Ainsworth, 1992; Matsuyama *et al.*, 1992; Sakai *et al.*, 2001). Rumsey *et al.* (1995) also stated that phagocytic activity was higher in soya-fed fish, possibly indicating an inflammatory or hypersensitivity response. However, in the present study this seemed not to have been the case. There were no major or significant differences in the phagocytic activities (*i.e.* phagocytic index, activity and capacity) between the different dietary groups, indicating that the killing ability of the phagocytic cells was not greatly influenced by the composition of the diets. Nonetheless, when comparing results from these assays a range of different factors should be considered *e.g.* the temperature range, cell concentrations, variety of stimulating or inhibiting agents, different concentrations and exposure times, *etc.* (Kokou *et al.*, 2012).

3.4.4. Image analysis performance

Image analysis of digitised histological sections provides a practical means for quantifiable assessment of structural and functional changes in tissues, being both objective and reproducible. The image analysis work described in this chapter sought to examine the utility of the developed advanced image analysis tool in helping to characterise and quantify feed-associated features of the intestinal morphology / histology of Atlantic salmon. Histological analysis of the fish's digestive system is considered a good indicator of the health status of the animal (Krogdahl & Bakke-Mckellep, 2005; Rašković *et al.*, 2011).

The method employed in this work comprised a succession of interactive and automated image segmentation steps (as described in detail in Chapter 2 – Technical Note A1, and partly illustrated in Figure 3.1). The protocol allows the operator to interact during the workflow to amend preceding automated decisions, adding to the precision of the final outcome. Furthermore, the processing time required for each histological image frame was roughly ~25 min (*i.e.* accounting for 23 distinct parameters being assessed), which greatly improved the efficiency of conducting such an analysis with respect to a more subjective semi-quantitative scoring classification, which took around 15-18 min to assess semi-quantitatively only 4 parameters. Tests of the robustness of the proposed algorithms are detailed in Chapters 2 and 4.

Overall, the results indicate that this tool can be used to assist pathologists in quantifying feed-associated histological changes in intestinal samples. Besides being both rapid and practical, this approach has been shown to be very accurate, suitable for handling large data sets and able to deal with a broad set of morphometric features in a highly reproducible manner. Moreover, it is important to mention the utility of systems such as this, in helping train pathologists and others to identify particular aspects of change. Since the image analysis system will highlight particular differences, the user may then look at the original tissue sections themselves to see if differences are discernible.

3.4.5. Quantitative variables from image analysis

Accurate quantification of morphometric parameters associated with conventional histology could be a useful addition to haematological and growth data for evaluating the effect of different dietary components on the overall health status of fish (Rašković *et al.*, 2011). When deciding on morphometric parameters, it is necessary to select a set of features that best describe the relevant intestinal morphological changes (Figure 3.8). The selection made here was based on a review of relevant literature relating to morphological parameters characteristic of inflamed intestinal mucosae (Van den Ingh *et al.*, 1991, 1996; Refstie *et al.*, 2000; Buttle *et al.*, 2001), and also through appraisal of the parameters used in well-accepted

semi-quantitative scoring systems to assess the degree of enteritis in salmonids (Morris *et al.*, 2005; Urán, 2008; Penn *et al.*, 2011; Romarheim *et al.*, 2013b).

Based on widely available image analysis tools for histology, researchers have included other geometrical features (*i.e.* fractal dimensions, circularity index, Feret and elliptical lengths) that could perhaps correlate to, and better explain the visual disparities between different histopathological gradings. For the present study, a large set of morphometric parameters was selected with a view to incorporating a range of relevant features, which would provide the necessary information that expert histopathologists would ordinarily process during histological evaluation of intestinal sections. Some of the features selected were observed to be redundant or irrelevant for analysis of the states provided by the specific experiments undertaken but could nevertheless prove valuable in describing / characterising other intestinal states.

No significant individual morphological changes were observed in the distal intestine of fish fed any of the dietary treatments, except for those fed the SBM. As predicted, the inclusion levels of dietary unrefined soybean meal lead to an inflammatory response in the distal intestine. Morphological changes were consistent with previously described soy induced enteritis (Baeverfjord & Krogdahl, 1996; Bakke-McKellep *et al.*, 2007b; *inter alia*). Fish fed the SBM diet had a shortening of the mucosal folds, and a widening of the central *stroma* within the mucosal folds. An increase of the connective tissue between the base of the mucosal folds and the *stratum compactum* was also observed, explained here by parameters FR and P / MTA lower values. This was not surprising, since shorter and wider mucosal folds would appear stumpier, and accordingly the luminal surface appeared less intricate. Additionally, with an increase of the *lamina propria* and connective tissue, the total mucosal tissue area (MTA) was seen to increase and consequently the P / MTA ratio decreased. Even though there were no significant differences between dietary groups, subtle differences in vacuolisation of the absorptive enterocytes from the intestinal

epithelium were noted. Fish fed the SBM appeared to have slightly less enterocyte vacuolisation (VC / MTA), which agrees with the evidence provided by several authors (Bakke-McKellep *et al.*, 2000a; Nordrum *et al.*, 2000a; Krogdahl *et al.*, 2003; Krogdahl & Bakke-McKellep, 2005). More recently, Urán *et al.* (2009b) stated that in salmonids, higher inclusion levels of dietary SBM causes a marked endocytosis decrease, resulting in the absence of small vesicles that would customarily fuse into the enterocytes' supranuclear vacuoles.

Fish fed the fish meal base diet, appeared to have slightly larger mucous cells (MMCA). Although, tangential sectioning can sometimes lead to an inaccurate assessment of cell size, all tissues were cut in the same orientation and should therefore give equivalent sections. The results suggest that in fish fed with the SBM and the combination of dietary nucleotides and β -glucans, immunostimulant peptides and other inflammatory mediators might affect the rate of mucus release or pre-release storage volume, resulting in some mucous cells having smaller sectional areas. A further possibility could be the triggering of a more rapid cell turn-over, whereby immature replacement mucous cells might be smaller in size.

Overall, the morphological changes associated with the functional ingredients, are less extensive than those seen in fish fed the soybean meal diet, and appear largely undistinguishable from normal intestinal morphology. This is in contrast to the report by Peng *et al.* (2013), who observed that supplementation of nucleotides significantly increased the distal intestine's fold height, enterocyte height and microvillus height when compared to control diets. Similarly, Burrells *et al.* (2001) and Cheng *et al.* (2011) reported that dietary nucleotides significantly enhanced the lateral branching of the intestinal folds, which could lead to an increase in total intestinal surface area, and improved intestinal structure.

In this study, the use of FR and P / MTA as parameters to describe the development of intestinal pathology proved helpful and was able to distinguish between "normal" and enteritis-affected mucosa. However, it was not possible to distinguish between fish meal-fed

and immunostimulant-fed fish on the basis of these parameters alone. In accordance with earlier studies (Baeverfjord & Krogdahl, 1996; Urán *et al.*, 2008b), the thickness of the *stratum compactum*, the number and dispersion of eosinophilic granule cells, the height and appearance of the mucosal folds could be valuable markers to assess in future studies, to identify which fish suffered from nutrition-induced intestinal morphological changes.

As observed by Baeverfjord & Krogdahl (1996), the assessment of individual parameters is insufficient to describe numerically the variation in cell types and tissue structure. We, therefore, aimed to evaluate the capacity for synergy between a variety of distinct histological features to provide resolution of states. It was possible to reduce the number of required classification features based on a multivariate principal component analysis, from 10 to 5 parameters, with the most informative being MC Feret Ratio, MC Ellipse Ratio, MCA / [MTA-Vac], FR and MTA / STA. These appeared to be sufficient to reliably differentiate between histological states. On the other hand, a discriminant analysis determining features of importance revealed that P / MTA, MCA / [MTA-Vac], FR and MTA / STA were capable of discriminating between tissue patterns and could be extended to screening of nutritional dietary components. The overall accuracy of such a multivariate model in identifying histological grades of Diets A, B and C was 61.1 %, 42 % and 59 % respectively. To increase the overall efficiency of the system, use of larger sample numbers and further refinement of the algorithms are required, possibly with the inclusion of additional morphological features. Also, it is important to note that the most meaningful parameters identified in the present work might be best for examination of the histological grades described in this study, but not for others.

3.5. General conclusions

Feeding Atlantic salmon a high inclusion level of unrefined SBM (25 %) or a diet containing β -glucans and extraneous nucleotides as functional ingredients, caused no apparent differences in growth performance, body and liver condition, feed efficiency or haematological parameters (*i.e.* differential leucocyte counts, red blood cells, percentage and haemoglobin, haematological corpuscular volumes and concentrations, plasma

lysozyme, albumin and total protein level). However, dietary inclusion of soybean meal produced an inflammatory response in the distal intestine as previously described by other authors. No other individual diet-related haematological differences were detected, nor were there any differences in the functional immunological parameters measured (*i.e.* respiratory burst and phagocytosis assay for head kidney isolated macrophages). The model feed trial employed therefore successfully generated differentiable states, although these were not, for the most part, systemically differentiable through the majority of procedures used, being only detectable morphologically.

Quantitation of morphometric parameters associated with histological sections using the newly developed image analysis tool successfully allowed identification of major morphological changes occurring in the distal intestine as a result of feeding different dietary components. Image analysis has thus been shown to provide a powerful tool for describing the histomorphological structure of Atlantic salmon distal intestine. In turn, the semi-automated image analysis methods presented here are able to distinguish normal intestinal mucosa from those affected by enteritis with a fair amount of accuracy. While individual parameters were less discriminatory, use of multivariate techniques allowed better discrimination of states and is likely to prove the most productive approach in further studies. Furthermore, although the overall efficiency of the imaging system was somewhat limited by statistical power (*i.e.* the limited number of samples that were investigated), the most suitable classification features to be validated further were highlighted (*e.g.* P / MTA, MCA / [MTA-Vac], FR and MTA / STA). Nonetheless, the inclusion of additional morphometric features in future histological assessments might prove productive in better resolving differences between states.

HISTOLOGICAL EVALUATION OF ENTERITIS IN ATLANTIC SALMON: QUANTITATIVE IMAGE ANALYSIS VS SEMI-QUANTITATIVE SCORES

4.1. Introduction

Finding alternative sources of protein to replace fish meal in fish feeds is crucial to maintaining a sustainable global aquaculture industry (Tacon, 2008). Protein derived from plants provides an alternative source of protein to fish meal, however most plant protein sources contain a variety of anti-nutritional substances (ANFs) capable of affecting the intestinal integrity of fish, which in turn can lead to decreased nutrient digestibility and growth performance (Krogdahl *et al.*, 1994; Francis *et al.*, 2001; Waagbø *et al.*, 2013). Thus, it is important to consider the effects that new dietary ingredients can have on the fish's intestinal health, when evaluating new dietary ingredients for the aquaculture feed market.

Various parameters have been used to evaluate the effect of dietary modulation on the physiological health of teleosts, nevertheless, the gold standard for this has been histopathological examination of intestinal tissue. Histological evaluation of gut enteritis is normally carried out as a qualitative assessment, whereby typical changes in response to plant-derived protein are described and include: shortening of the mucosal folds, infiltration of inflammatory cells in the *lamina propria*, widening of the central *stroma* within the mucosal folding, increase in the thickness of the connective tissue and loss of supranuclear vacuolisation of the absorptive cells in the intestinal epithelium. Alternatively, semi-quantitative histopathology, a subjective multi-grade scoring system based on the parameters described above has also been used for assessment of dietary components (Morris *et al.*, 2005; Baeverfjord & Krogdahl, 1996; Knudsen *et al.*, 2008; Urán *et al.*, 2008b; Penn *et al.*, 2011; Laporte & Trushenski, 2012).

As a tool regularly used to evaluate intestinal morphology and histopathology, semi-quantitative assessment is a relatively rapid and easy to use method for examining the extent of histo-morphological changes within tissue sections. However, some authors consider this approach to be “arbitrary” and “open to subjective interpretation” (Wright *et al.*, 2003; Krenacs *et al.*, 2010; Kopec *et al.*, 2011). On the other hand, conventional visual assessment can be time-consuming, fastidious and prone to misinterpretation (Kopec *et al.*, 2011; Shi *et al.*, 2012).

Semi-quantitative assessment has proven useful for correlating dietary modulation with the degree of enteritis and / or intestinal morphological changes that occur as a result of feeding inappropriate dietary ingredients (Knudsen *et al.*, 2008; Urán *et al.*, 2009a; Marjara *et al.*, 2012; Penn *et al.*, 2011; Chikwati *et al.*, 2013a; Romarheim *et al.*, 2013a), however, it is prone to the subjective interpretation of observers and does limit the comparison between different studies. Also it can be difficult to assess subtle changes relating to the enteritis as a result of feeding novel dietary ingredients, and to analyse the scalar data obtained from the scoring system statistically (True, 1996; Hamilton & Allen, 2005, Turlin *et al.*, 2009).

Image analysis of digitised histological sections has the potential to provide a practical means for quantifiable assessment of structural changes in tissues, being both objective and reproducible with a reasonable speed of execution (He *et al.*, 2012; Webster *et al.*, 2012). A method to assess the intestinal morphology of Atlantic salmon, based on advanced image analysis was described in Chapters 2 and 3. This automated image analysis system has proven to be a valuable tool for measuring and characterising a range of features in intestinal tissue sections in a quantitative manner. Such an approach not only allows comparative analysis of samples to be carried out between different observers, but it has also been shown to be both accurate and suited for large-scale application.

It is necessary, however, to validate the semi-automated image analysis system to establish that it is measuring the parameters it is purported to be measuring, and to provide reassurance that it can reliably measure pre-determined features. Although the accuracy of the validation technique *per se* may influence the apparent accuracy of the assessment

technique, it has been recognised that the best way to confirm the validity of a new method is to compare the results obtained with those from a well-established method (Pilette *et al.*, 1998; Ricketts *et al.*, 1998). Thus, the aim of work reported in this chapter was to evaluate the reliability and agreement of our quantitative microscopic image analysis system with that of an established semi-quantitative histological grading system, by examining their ability to evaluate the severity of enteritis in Atlantic salmon intestine, using the same set of histological slides.

4.2. Materials and methods

4.2.1. Fish and rearing conditions

The original feeding trial upon which this study is based was carried out by researchers Knudsen D. and Koppe W.⁸ at Skretting's Fish Trial Station (Lerang, Jørpeland, Norway). Post-smolt Atlantic salmon (*Salmo salar* L.), with an initial mean body weight of 80 g ± 2, were randomly allocated into twelve flow-through 400 L circular tanks at a stocking density of seventy fish per treatment tank. The tanks were maintained under a 24 h light photoperiod and continuously supplied with seawater (15 L.min⁻¹ per tank) pumped from 90 m depth in the adjacent fjord. The inlet water had a salinity of ~34 mg.mL⁻¹ and an oxygen concentration of ~9 mg.mL⁻¹, and was held at a temperature between 8.5 °C and 8.7 °C. Individual tanks were equipped with waste feed collectors and uneaten feed was collected twice daily.

4.2.2. Diets and feeding regime

Four isoenergetic experimental diets comprising either a fish meal based control diet (Fish meal), a diet containing 25 % lupin kernel meal (Lupins), another diet based on 25 % lupin kernel meal with inclusion of 1.7 g.Kg⁻¹ soya saponin concentrate (Lupins+SSC) or a diet containing 25 % defatted soybean meal (SBM) were formulated. The diet formulations

⁸ The original feeding trial was designed for the purpose of a separate study, being partially described in the peer reviewed article: KNUDSEN, D., JUTFELT, F., SUNDH, H., SUNDELL, K., KOPPE, W. and FRØKIÆR, H., 2008. Dietary soya saponins increase gut permeability and play a key role in the onset of soyabean-induced enteritis in Atlantic salmon (*Salmo salar* L.). *British Journal of Nutrition*, **100**(1), pp. 120-129.

and background information on the different commercial sources of the various dietary components is shown in Table 4.1.

The feeds were produced at Skretting's Feed Technology Plant (Stavanger, Norway) as 3 mm pellets using a pre-conditioner (DDC; Wenger Manufacturing, Inc., Kansas City, MO, USA) coupled to a twin-screw extruder (TX57; Wenger Manufacturing, Inc.). The resulting extruded pellets were then left to dry for 25 min in a single belt dryer supplied with warm air (75 °C) and finally, under reduced pressure at 60 °C, the dried pellets were coated with fish oil.

Table 4.1. Formulation and proximate chemical composition of the feeds used in this experimental study.

	Diet A (Fish meal)	Diet B (Lupins)	Diet C (Lupins + SSC)	Diet D (SBM)
Feed ingredients (g.kg ⁻¹)				
Fish meal*	620.9	483.5	483.5	456.6
Lupin [†]	0.0	250.0	250.0	0.0
Soybean meal [‡]	0.0	0.0	0.0	250.00
Soya saponin concentrate [§]	0.0	0.0	1.7	0.0
Soya saponins	0.0	0.03	1.07	1.77
Wheat	80.0	80.0	78.3	80.0
Wheat starch	139.9	158.1	137.2	137.2
Minerals and vitamins [¶]	3.5	3.5	3.5	3.5
Pigment ^{**}	0.5	0.5	0.5	0.5
Fish oil ^{††}	155.2	182.5	182.5	209.4
Chemical composition (% of dry weight)				
Crude protein	454.0	455.0	444.0	467.0
Crude fat	228.0	291.0	283.0	264.0
Ash	91.0	80.0	77.0	84.0
Moisture content	916	969.0	956.0	945.0
N-free extract	133.0	134.0	142.0	118.0
Gross energy (MJ.kg ⁻¹) ^{‡‡}	22.1	24.5	24.1	23.5

Footnotes:

SSC, soya saponin concentrate; SBM, soybean meal.

* Scandinavian Fish meal LT (Norsildmel, Fyllingsdalen, Norway).

† Lupin kernel meal from sweet lupins (*Lupinus angustifolius*; Agracorp, West Perth, Western Australia).

‡ Defatted soybean meal (Denofa, Fredriskstad, Norway).

§ Soya saponin concentrate, 69 % purity (Organic Technologies, OH, USA).

|| Total level of soya saponins calculated based on the soya saponin analysis of dehulled lupins, defatted soybean meal and soya saponin concentrate (see Knudsen *et al.*, 2008 for detailed description).

¶ Mineral and vitamin premix to meet the National Research Council recommendations (NCR, 1993).

** Carophyll Pink (DSM Nutritional Products, Basel, Switzerland).

†† South American oil containing 30 % SFA of total fatty acids.

‡‡ Calculated by using physiological fuel values of 24, 39 and 17 KJ.g⁻¹ for protein, fat and carbohydrate, respectively, according to Jobling (1994).

Fish were acclimated for a 2 week period, during which time they were maintained on the fish meal based diet. Thereafter, the four different experimental diets were randomly assigned

to triplicate tanks and the salmon fed during a 53-day experimental period. The diets were fed twice a day using automatic feeders. The amount of feed given was adjusted in accordance with biomass, thus aiming to overfeed by 20 %. Uneaten feed was collected, separated from faeces and quantified by weight after drying for 12-16 h at 90 °C.

4.2.3. Feed composition

The chemical composition of the different experimental diets was determined using standard techniques for proximate analysis. Analysis was performed on triplicate feed samples of each diet. Crude protein content was determined by the Kjeldahl nitrogen analysis method, using a Kjeltex Auto Sampler System (Tecator AB, Hoganas, Sweden) in accordance with the Nordic Committee on Food Analysis – NMKL, method no. 6, 4th edition, 2003. To convert total nitrogen to total protein content as a percentage of dry weight, the factor 6.25 was implemented. Crude fat was measured by acid hydrolysis using a Soxtec 2050 extraction system (Foss Analytical, Hillerod, Denmark) following the NMKL, method no. 160, 1998. Moisture content was determined gravimetrically after thermal drying to constant weight in an oven at 102-105 °C for 16 to 18 h. Ash was measured by burning the samples at 550 °C for another 16 to 18 h. Gross energy was calculated according to Jobling (1994), using physiological fuel values of 24, 39 and 17 KJ.g⁻¹ for protein, fat and carbohydrate, respectively.

4.2.4. Sampling procedure

At the end of the experimental period, after having fed the experimental diets for 53-days, the fish were starved (*i.e.* 24 h prior to sampling) and five fish per experimental tank randomly selected and euthanised with an overdose of anaesthetic (50 mg.L⁻¹, MS-222, Tricaine Methanesulphonate, Argent Chemical Laboratories, Redmount, WA, USA). Intestinal sections from the distal region were then carefully excised from the fish. Rings of at least 2 cm in length were cut open longitudinally and fixed in phosphate-buffered formaldehyde (4 %, pH 7.2) at room temperature (16-20 °C), for at least 24 h before further histological processing.

4.2.5. Histological staining and evaluation

Similar to section 3.2.8, formalin-fixed intestinal samples were then dehydrated and embedded in paraffin, following conventional histological procedures (Bancroft & Stevens, 1982). Transverse sections of 3 µm thickness were cut (Leica RM 2035, Leica Microsystems Ltd., UK) and mounted on glass slides. For each fish sample, one histological slide was prepared. After de-waxing, sections were stained with a combination of haematoxylin-eosin and Alcian blue (8 GX, pH 2.5; Steedman, 1950; Lev & Spicer, 1964) – see Appendix 1 for modified staining protocol.

4.2.5.1. *Semi-quantitative scoring histological assessment.* The histological sections were randomised and evaluated blindly using light microscopy (Leica DM 5000B; Leica Microsystems GmbH, Wetzlar, Germany) according to the semi-quantitative method described by Knudsen *et al.* (2008), which assesses the degree of soybean meal induced enteritis in the distal intestine of Atlantic salmon in accordance with the following criteria: (1) the presence and size of supranuclear vacuoles; (2) the degree of widening of the *lamina propria* from simple mucosal folds; (3) the thickness of the connective tissue between the base of the mucosal folds and the *stratum compactum*; (4) the appearance and length of the mucosal folds. Each of these parameters was scored on a scale from 1 to 5, including half values between categories. A score of '1-2' represented normal morphology, a score of '3' was given to distinct morphological signs of inflammation, while a score of '5' was given to very severe symptoms of enteritis. Finally, an overall description score was calculated for each individual fish, as the mean score across the four parameters scored. A detailed description of the histomorphological appearance criteria for each parameter and for the different scoring values is given in Table 4.2.

4.2.5.2. *Quantitative image analysis histological assessment.* The same slides produced for the analysis described in the previous section, were then scanned using an automated slide-scanning system (MIRAX Desk, Carl Zeiss MicroImaging GmbH, Göttingen, Germany) and a digitised MRXS image of the complete section stored at a final magnification of 20x. MIRAX Viewer software (Version 1.12, 3DHISTECH, Budapest,

Hungary) was used for visualisation and cropping of the images. For each slide, two microscope fields were randomly selected and cropping performed at 60× magnification. A frame of 9.96 Mpixels was then used to crop the sections. Twenty-four bit digital images were extracted as individual TIFF images (1:4 magnification, 2048 × 2048 pixels tile size, 3570 × 2790 pixels image size) and saved at a file size of 72 MB with a quality setting of 0.23 microns per pixel. Thereafter, using IrfanView (Version 4.33, Wiener Neustadt, Austria) batch converter, all uncompressed bitmap tiled TIFF images were converted into untiled TIFF files with sizes ranging from 36.7 MB.

Table 4.2. Semi-quantitative scoring system according to Knudsen *et al.* (2008), using different parameters to assess the degree of histomorphological changes induced by soybean meal in the distal intestine of Atlantic salmon.

Score	Descriptive parameter
<i>Supranuclear vacuoles (Vac)</i>	
1	Large vacuoles occupy almost the entire apical part of the enterocytes
2	Medium-sized vacuoles occupy less than half of the enterocytes
3	Small vacuoles are present near the apical membrane in most enterocytes
4	Scattered small vacuoles are still present in some enterocytes
5	No supranuclear vacuoles seem to be present
<i>Lamina propria (LP)</i>	
1	<i>Lamina propria</i> is a very thin and delicate core of connective tissue
2	<i>Lamina propria</i> appears slightly more distinct in some of the folds
3	<i>Lamina propria</i> was markedly increased in most of the folds
4	<i>Lamina propria</i> is thick in many folds
5	<i>Lamina propria</i> is very thick in many folds
<i>Connective tissue (CT)</i>	
1	Almost no connective tissue between the base of the folds and the <i>stratum compactum</i>
2	Slightly increased amount of connective tissue beneath some of the mucosal folds
3	Clear increase of the connective tissue beneath most of the mucosal folds
4	Thick layer of connective tissue beneath many folds
5	Extremely thick layer of connective tissue beneath some folds
<i>Mucosal folds (MF)</i>	
1	Simple and complex folds appear long and thin
2	Simple folds have medium length, while the complex folds appear thicker
3	Simple folds have short to medium length, while the side branches on the complex folds are stubby
4	Simple folds are thick and short, while thick and stubby complex folds are prevalent
5	Both complex and simple folds appear very short and stubby

Cropped randomised images were then evaluated blindly. To automatically quantify the morphological features described in Table 4.3, several image processing algorithms that have been brought together in one image analysis application, named “Gut Image Processing &

Analysis (GUT-ImA)” were employed (see Chapter 2 and Appendixes A1-A2 for a detailed description of its development and deployment). Figure 4.1 illustrates the main components of the application, which were implemented in four three phases: 1) acquisition and pre-processing of the digital image, 2) processing and segmentation of the pre-processed image, 3) analysis of the processed image by identification of the regions of interest, feature extraction and measurement of the morphometric parameters. As described earlier, image processing and computer operations were performed on a personal computer (Dell Latitude™ D630, Intel Pentium II 350 MHz processor, 128 MB RAM, 2 GB hard disk, under the environment of Microsoft™ Windows XP) operating the stand-alone KSRun software platform (Version 3.0, Carl Zeiss Vision GmbH, München-Hallbergmoos, Germany), through which the original developed algorithms were implemented. Succinctly, after a background correction of the irregularities found in the source image, the corrected image was normalised (*i.e.* by expansion of its grey level histogram to the full range of available levels) and a binary image created. By inverting the image to a negative image (black to white and *vice versa*) and through intensity differentiation, proper segmentation of the peritoneal edge of the *muscularis externa* and the internal intestinal lumen was possible. Then, to discriminate between the mucosal and submucosal tissues, the *stratum compactum* was interactively identified by manually drawing a line over the displayed tissue image. Subsequently, through interactive selection, four individual simple-mucosal folds were randomly chosen and isolated from the remaining mucosal folds. The total and partial luminal perimeters were then captured, and the level of convolution measured using the fractal box-counting method (Russell *et al.*, 1980; Cross, 1994; Shang *et al.*, 2000; Brooker, 2007). Thereafter, by using the original digitised images, an interactively defined HLS colour threshold was set for detection of areas specifically stained by Alcian blue, and consequent identification of objects as mucous cells was conducted. Subsequently, to separate adjoining mucous cells, binary grain recognition operations were applied and to ensure removal of artefacts the resulting objects were filtered using size-threshold-operators (*i.e.* removal of objects smaller or much larger than the usual size range of mucous cells). The source image was then converted to a greyscale from which mucosal tissue vacuoles could be

visualised. Finally, the thresholded regions of interest were segmented and automatically processed by a sequence of mathematical algorithms, extracting several morphometric measurements (Table 4.3). Values for these were then transcribed and exported to a flat database file. Quantitative variables were expressed as mean and standard deviations (SD), unless otherwise specified.

Table 4.3. List of measured morphological parameters and computed morphometric ratios used in the quantitative image analysis approach.

Morphometric feature	Description
MTA	Mucosal tissue area
MCA	Mucous cell total area
MMCA	Mean mucous cell area
MCA / MTA	Ratio between the mucous cell area and the mucosal tissue area
MCN	Mucous cell number
MCN / MTA	Ratio between the mucous cell number and the mucosal tissue area
STA	Submucosal tissue area
MTA / STA	Ratio between the mucosal tissue area and the submucosal tissue area
MC Feret Min	Mucous cell minimum Feret length
MC Feret Max	Mucous cell maximum Feret length
MC Feret Ratio	Ratio of the mucous cell Feret lengths
MC Ellipse Af	Length of the main axis of an ellipse with the same geometric moment of inertia as the mucous cell
MC Ellipse Bf	Length of the secondary axis of an ellipse with the same geometric moment of inertia as the mucous cell
MC Ellipse Ratio	Ratio of the elliptical lengths Af and Bf for the mucous cell
P / MTA	Ratio between total perimeter length of the luminal surface and mucosal tissue area
VC / MTA	Ratio between the total vacuolisation area and the mucosal tissue area
MTA-Vac	MTA without the vacuolisation area
MCA / [MTA-Vac]	Ratio between mucous cell total area and the MTA without the vacuolisation area
MCN / [MTA-Vac]	Ratio between mucous cell number and the MTA without the vacuolisation area
FR	Fractal dimension of the perimeter line from the luminal surface
CT	Thickness of the connective tissue between the base of the mucosal folds and the <i>stratum compactum</i>
MF Area	Total mean area of four simple mucosal folds
MF Perimeter	Total mean perimeter length of four simple mucosal folds
MF Feret Min	Minimum Feret lengths mean of four simple mucosal folds
MF Feret Max	Maximum Feret lengths mean of four simple mucosal folds
MF Feret Ratio	Mean ratio of the Feret lengths of four simple mucosal folds
MF Ellipse Af	Mean length of the main axis of the ellipses with the same geometric moment of inertia as four of the simple mucosal folds
MF Ellipse Bf	Mean length of the secondary axis of the ellipses with the same geometric moment of inertia as the four of the simple mucosal folds
MF Ellipse Ratio	Mean ratio of the elliptical lengths Af and Bf for four simple mucosal folds

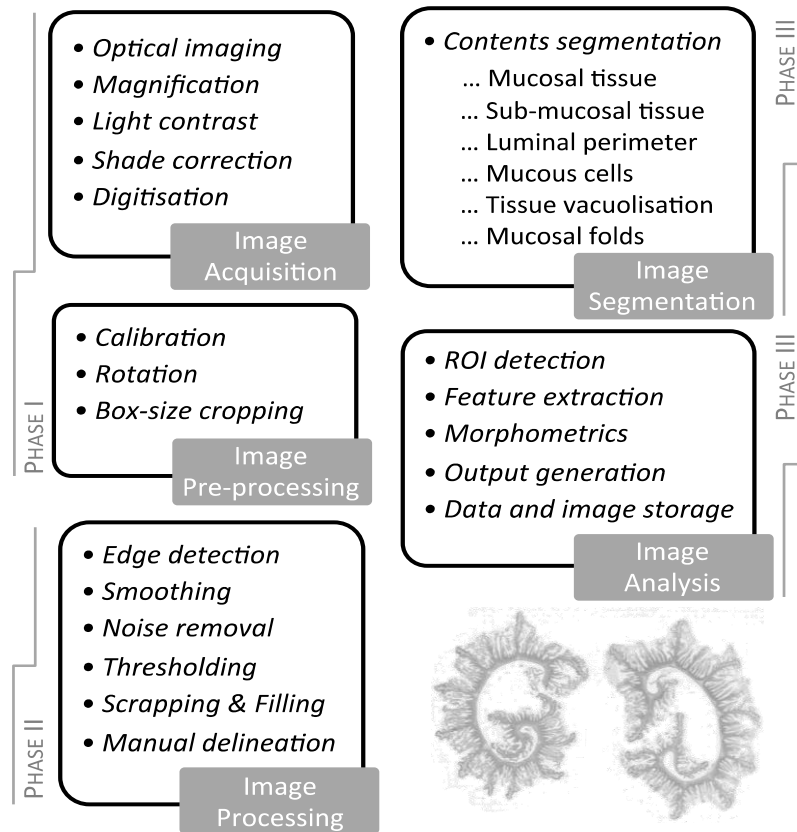


Figure 4.1. Chart of the main components involved in image analysis of the distal intestine morphometrics of Atlantic salmon. (Phase I) Acquisition and pre-processing of the digital image. (Phase II) Processing and segmentation of the pre-processed image. (Phase III) Analysis of the processed image by identification of the regions of interest, feature extraction and measurement of the morphometric parameters. (ROI) region of interest.

4.2.6. Statistical analysis

4.2.6.1. *Semi-quantitative histological data.* The histological scoring results were treated as non-parametric data. Kruskal-Wallis one-way ANOVAs were therefore applied to test for equality of treatment means. A Student-Newman-Keuls multiple comparisons test with mean ranks, was then used as a post-hoc test to compare all pairs of mean ranks. Group differences were regarded as significant when the probability of each significance test was less than 5 % ($p < 0.05$). These statistical analyses were performed using UNISTAT[®] Statistical package (Version 5.5, Unistat Ltd., London, UK).

4.2.6.2. *Quantitative image analysis histological data.* The various morphological parameters were transformed where necessary to normalise the distribution, and the means compared by use of a hierarchical general linear model (GLM). When multiple groups were compared by use of Tukey's HSD post-hoc tests, the appropriate Holm-Bonferroni's significance values (Holm, 1979) were used to compensate for the number of groups, so as to reduce the probability of detecting spurious differences.

To evaluate the relationship between the different morphometric variables, linear regression models were applied and Pearson's correlation coefficient values considered as significant, at intervals of 95 % confidence level (p -value < 0.05, two-tailed). In order to establish which morphometric measurements gave the most information concerning the differences found in the morphology of the distal intestine from fish of different dietary groups, a principal component analysis (PCA) was performed. To aid in obtaining optimal loadings of the parameters on the principal components and consequently better interpretation of components, a Varimax rotation and a Kaiser (1974) normalisation were employed. Moreover, so as to identify important trends in the morphological data set that would not be evident using univariate techniques, a discriminant function procedure was implemented. The program default criteria for F values (F_{Entry} : 3.84; F_{Remove} : 2.71) were used to determine the inclusion or removal of a variable from the analysis. Variables thus selected were subjected to a reverse stepwise discriminant method. Once the variable selection was complete, a discriminant model comprising a number of factors, each with its own coefficient and a constant was generated. A discriminant score was then calculated for each individual sample, and from this, subjects were automatically allocated to one of the treatment groups and the overall accuracy of the discriminant model tested.

These statistical analyses were conducted using SPSS (Version 19.0.01, IBM, Chicago, USA), Minitab (Version 16.1.0.0, Coventry, UK) and Unscrambler® (Version 10.3, CAMO, Oslo, Norway) statistical software packages.

4.2.6.3. *Comparison of the quantitative and semi-quantitative systems.* The performance of both systems was evaluated by comparison of the time / effort required to

accomplish the intended assessment tasks. In addition, to assess the differences between descriptive parameters from both classification systems, the resulting semi-quantitative scores and the mean continuous variables derived from the image analysis, were correlated using Spearman's rank correlation coefficients and statistical significances evaluated using Minitab (Version 16.1.0.0, Coventry, UK) statistical software package. Correlations were considered significant if a p -value < 0.05 (two-tailed).

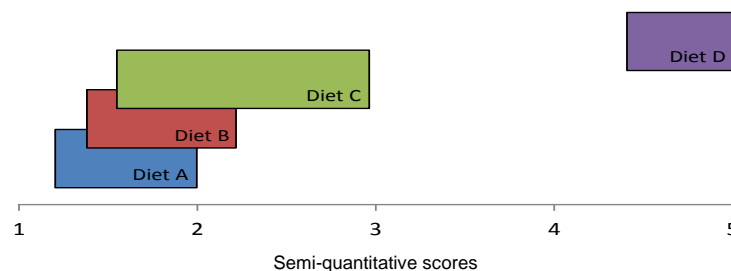
4.3. Results

4.3.1. Semi-quantitative histological assessment

Morphological changes in the distal intestine were evaluated for fifteen fish per experimental diet. Scoring results are given in Table 4.4.

Table 4.4. Semi-quantitative histological assessment of the intestinal sections and schematic overlapping-ranges of averaged summary scores, for fish fed the different experimental diets.

Descriptive parameter*	Diet A (Fish meal)		Diet B (Lupins)		Diet C (Lupins + SSC)		Diet D (SBM)	
	Mean [†]	SD	Mean	SD	Mean	SD	Mean	SD
Supranuclear vacuoles	1.8 ^a	1.1	1.3 ^a	0.4	2.3 ^{a,b}	1.1	4.6 ^c	0.5
Lamina propria	1.5 ^a	0.6	1.9 ^a	0.6	2.2 ^{a,b}	0.8	4.9 ^c	0.5
Connective tissue	1.6 ^a	0.5	2.2 ^{a,b}	0.7	2.2 ^{a,b}	1.0	4.7 ^c	0.5
Mucosal folds	1.5 ^a	0.4	1.7 ^a	0.4	2.5 ^b	0.7	4.8 ^c	0.4
Average score	1.6 ^a	0.4	1.8 ^{a,b}	0.4	2.3 ^{a,b}	0.7	4.7 ^c	0.3



Footnotes:

SSC, soya saponin concentrate; SBM, soybean meal.

* Distal intestinal sections were assessed according to the morphometric features listed and described in Table 4.2. A score of 1–2 represents “normal” morphology, a score of 3 was given to distinct morphological signs of inflammation, while a score of 5 represents severe symptoms of enteritis.

[†] Data are expressed as mean and standard deviation (SD), $n = 15$ histological sections per treatment group were assessed.

^{a,b} Mean values within the same row, with similar superscripts are not significantly different (multiple comparisons test with mean ranks, Student-Newman-Keuls, $\alpha = 0.05$).

Fish fed the fish meal based control diet displayed normal morphology (*i.e.* scoring between 1 and 2) while significant enteritis was observed in fish fed 25 % defatted soybean meal (*i.e.* scoring close to 5). No morphological changes could be seen in the distal intestine of fish fed 25 % lupin kernel meal alone (*i.e.* scoring between 1 and 2), however, the diet containing soya saponin concentrate in combination with lupin kernel meal had a significant effect (*i.e.* scoring close to 3) on all four histological parameters: the size of the absorptive vacuoles was reduced, thickness of the *lamina propria* had increased, the mucosal folds had become shorter and the amount of connective tissue between the base of the mucosal folds and the *stratum compactum* had increased. Representative digital microscopy images showing the morphological changes encountered across the distal intestine from fish fed the different experimental diets are shown in Figure 4.2.

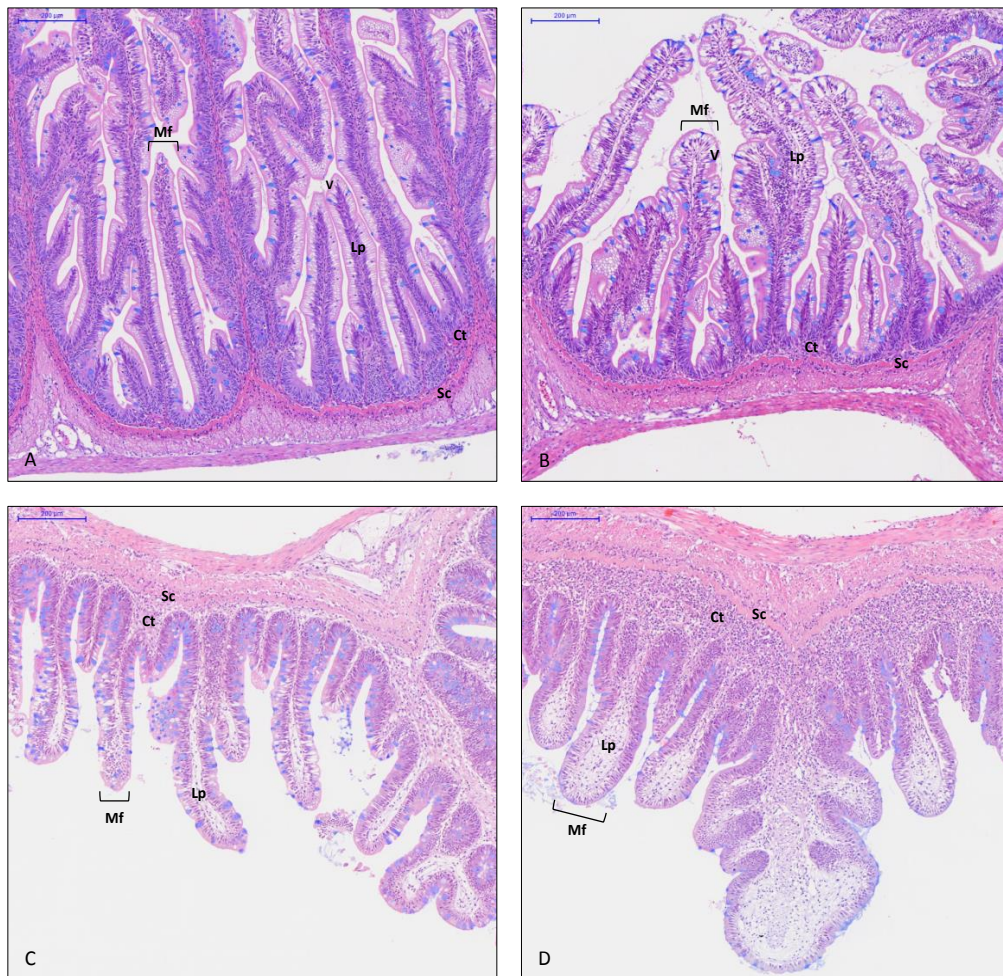


Figure 4.2. Images of morphological variations encountered across the distal intestine of Atlantic salmon fed different experimental diets: (A) fish meal based control diet, (B) diet containing 25 % lupin kernel meal, (C) 25 % lupin kernel meal

4.3.2. Quantitative histological assessment

The 120 independent histological frame samples taken from the exact same histological slides that were evaluated through the semi-quantitative approach were then re-evaluated using the proposed semi-automated quantification system. The measured morphometric and tissue cytometric parameters are shown in Table 4.5.

With respect to the quantitative histological examination of the distal intestine, no significant differences in the key morphometric parameters associated with the mucous cells were observed. Mucous cell individual mean area, elliptical and Feret length ratios were fairly similar among fish from different dietary groups ($F_{[4, 30]} \text{ MMCA} = 2.57$, $F_{[3, 36]} \text{ MC Ellipse Ratio} = 1.90$, $F_{[4, 30]} \text{ MC Feret Ratio} = 2.24$; $p > 0.05$). Nevertheless, it should be emphasised that mean mucous cell area showed a dose-response trend, where fish fed the fish meal based diet exhibited significantly larger (μm^2) intestinal mucous cells while fish fed diets containing higher inclusion of soya saponin (SS) displayed smaller cells. Consequently the highest ratios of mucous cell total area to mucosal tissue area ($F_{[4, 30]} \text{ MCA} / [\text{MTA-Vac}] = 6.18$, $p < 0.05$) were found in fish fed the control diet whereas fish fed the unrefined soybean meal (SBM) had the lowest ratios. Similarly, dose-responses in the overall number of mucous cells were observed for fish maintained under the various dietary treatment regimes ($F_{[4, 30]} \text{ MCN} / [\text{MTA-Vac}] = 7.40$, $p > 0.05$). It is noteworthy that for individuals fed the lupin kernel meal, the mucous cells were less spherical overall ($F_{[4, 30]} \text{ MCirc} = 4.85$, $p < 0.05$) than those of individuals fed the other treatment diets. Moreover, significant differences in the generalised structured of the epithelial mucosal layers were observed among sections from different treatment groups ($F_{[3, 36]} \text{ MTA} / \text{STA} = 6.77$, $p < 0.05$). Again a dose response to SS was observed, where the ratio between the total mucosal and submucosal tissue areas decreased as the inclusion levels of SS in the fed diets increased. Similarly, the fish fed

Figure 4.2 (continued from previous page) diet with inclusion of 1.7 g.kg^{-1} soya saponin concentrate, (D) diet containing 25 % defatted soybean meal. Typical signs of enteritis include the loss of vacuoles (V) in the absorptive enterocytes; the widening of the *lamina propria* (Lp) in the mucosal folds (MF); and an increase of the connective tissue (Ct) between the base of the mucosal folds and the *stratum compactum* (Sc). Intestinal sections were stained with a combination of haematoxylin-eosin and Alcian blue 8 GX.

Table 4.5. Quantitative image analysis histological assessment of the intestinal sections.

Morphometric feature*	Diet A (Fish meal)		Diet B (Lupins)		Diet C (Lupins + SSC)		Diet D (SBM)		p-value
	Mean [†]	SD	Mean	SD	Mean	SD	Mean	SD	
MMCA (μm^2)	207.291	4.932	205.634	5.521	201.472	4.511	191.655	4.946	0.128
MC Feret Ratio	0.688	0.003	0.681	0.003	0.689	0.002	0.701	0.003	0.161
MC Ellipse Ratio	1.539	0.009	1.569	0.013	1.529	0.008	1.501	0.012	0.206
MCirc	0.861 ^b	0.003	0.844 ^b	0.004	0.864 ^a	0.003	0.862 ^{ab}	0.004	0.033
MTA / STA	8.464 ^a	0.388	7.865 ^a	0.438	7.321 ^{ab}	0.343	4.859 ^b	0.232	0.014
P / MTA ($\mu\text{m} / \mu\text{m}^2$)	0.018 ^a	0.0004	0.017 ^a	0.0007	0.016 ^a	0.0004	0.009 ^b	0.0002	0.001
VC / MTA	0.159	0.005	0.143	0.007	0.140	0.004	0.098	0.004	0.081
MCA / [MTA-Vac]	0.062 ^a	0.004	0.060 ^a	0.004	0.053 ^{ab}	0.003	0.043 ^b	0.003	0.018
MCN / [MTA-Vac] ($n^0 / \mu\text{m}^2$)	0.293 $\times 10^{-3a}$	0.014 $\times 10^{-3}$	0.283 $\times 10^{-3a}$	0.016 $\times 10^{-3}$	0.255 $\times 10^{-3ab}$	0.012 $\times 10^{-3}$	0.218 $\times 10^{-3b}$	0.012 $\times 10^{-3}$	0.011
FR	1.270 ^b	0.007	1.260 ^b	0.010	1.237 ^b	0.007	1.137 ^a	0.007	0.001
CT (μm)	26.777 ^b	1.656	30.349 ^b	1.551	28.106 ^b	1.238	98.674 ^a	7.203	<0.001
MF Area (μm^2)	1.455 $\times 10^5$	6.217 $\times 10^3$	1.572 $\times 10^5$	6.951 $\times 10^3$	1.310 $\times 10^5$	4.441 $\times 10^3$	1.384 $\times 10^5$	5.605 $\times 10^3$	0.192
MF Perimeter (μm)	3.101 $\times 10^{3a}$	1.013 $\times 10^2$	3.139 $\times 10^{3a}$	0.940 $\times 10^2$	2.753 $\times 10^{3ab}$	0.731 $\times 10^2$	2.326 $\times 10^{3b}$	0.557 $\times 10^2$	0.006
MF Feret Ratio	0.224	0.010	0.235	0.011	0.229	0.009	0.264	0.010	0.113
MF Ellipse Ratio	6.469	0.312	6.122	0.263	6.058	0.220	5.277	0.260	0.114

Footnotes: SSC, soya saponin concentrate; SBM, soybean meal.

* Distal intestinal sections were assessed according to the morphometric features listed and described in Table 4.2. MMCA, mean mucous cell area, MC Feret Ratio, ratio of the Feret lengths from mucous cells, MC Ellipse Ratio, ratio of the elliptical lengths from the mucous cells, MCirc, mucous cell mean circularity index, MTA / STA, ratio between the mucosal tissue area and the submucosal tissue area, P / MTA, ratio between the total perimeter of the luminal surface and the mucosal tissue area, VC / MTA, ratio between total vacuolisation area and the mucosal tissue area, MCA, mucous cell total area, MTA-Vac, mucosal tissue area without the vacuolisation area, MCN, mucous cell number, FR, fractal dimension of the perimeter line of the luminal surface, CT, connective tissue thickness, MF Area, total area from mucosal folds, MF Perimeter, total perimeter length from mucosal folds, MF Feret Ratio, ratio of the Feret lengths from mucosal folds, MF Ellipse Ratio, ratio of the Feret lengths from mucosal folds.

[†] Data are expressed as mean and standard deviation (SD), $n = 30$ histological frames per treatment group were assessed.

^{a,b} Mean values within the same row with the same superscript are not significantly different (hierarchical GLM: tank [treatment] fixed factor with 3 levels, $p > 0.05$).

higher plant protein concentrations showed the lowest ratio between the perimeter length and the mucosal tissue area ($F_{[4, 30]} P / MTA = 19.06, p < 0.05$) and its related fractal dimension ($F_{[4, 30]} FR = 16.00, p < 0.05$). On the other hand, the thickness of the connective tissue was only significantly thicker for the SBM fed group ($F_{[4, 30]} CT = 50.24, p < 0.05$). No significant differences in the key morphometric parameters associated with the mucosal folds were observed. Mucosal fold mean area, elliptical and Feret length ratios were fairly similar across fish from different treatment groups ($F_{[4, 30]} MF Area = 2.01; F_{[4, 30]} MF Ellipse = 2.72, F_{[4, 30]} MF Feret Ratio = 2.75; p > 0.05$). However, for the MF perimeter length assessment, significant differences were observed. The mean perimeter length of the mucosal folds seemed to decrease as the inclusion levels of SS increased ($F_{[4, 30]} MF Perimeter = 9.23; p < 0.05$). To evaluate the relationship between the different morphometric variables, linear regression models were applied. Parameters showing Pearson's correlation values higher than 0.7 are reported, and the square of the correlation coefficient values as shown in Figure 4.3. MC Ellipse Ratio was negatively related to MC Feret Ratio and MCirc with Pearson's correlation coefficients of $r = -0.961$ and $r = -0.801$ respectively, which accounted for 93 % of the variance encountered in MC Feret Ratio ($F_{[119]} = 1460.345, p < 0.001$) and 62 % in MCirc ($F_{[119]} = 190.070, p < 0.001$). Moreover, the MC Feret Ratio was positively related to MCirc ($r = 0.718$) explaining 51 % of the variation between both variables. Conversely, as the MF Ellipse Ratio increased the MF Feret Ratio decreased, both being negatively related ($F_{[119]} = 813.227, r = -0.957, p < 0.001, 88 %$ variation). Also in Figure 4.4, P / MTA accounted for 90 % of the variation in FR ($F_{[119]} = 1032.493, r = -0.964, p < 0.001$), 52 % for CT ($F_{[119]} = 130.121, r = -0.774, p < 0.001$), and 30 % for MTA / STA ($F_{[119]} = 50.633, r = 0.626, p < 0.001$). While FR and CT variables were negatively related to the P / MTA variable, MTA / STA was positively correlated. Hence, MCN / [MTA-Vac] and MCA / [MTA-Vac] showed a very high correlation amongst ($F_{[119]} = 1542.672, r = 0.968, p < 0.001, 93 %$ variation), the luminal surface intricacy parameter was positively interrelated to the connective tissue length ($F_{[119]} = 132.708, r = 0.768, p < 0.001, 53 %$ variation). These correlations describe the indices of similarity between the different key-parameters (*i.e.* characterises the extent to which different

parameters would contribute comparable information or meaning for a particular set of features), allowing the researcher to decide upon which morphometric parameters to select based on their “discriminatory strength” and lack of “resemblance” to other analogous parameters.

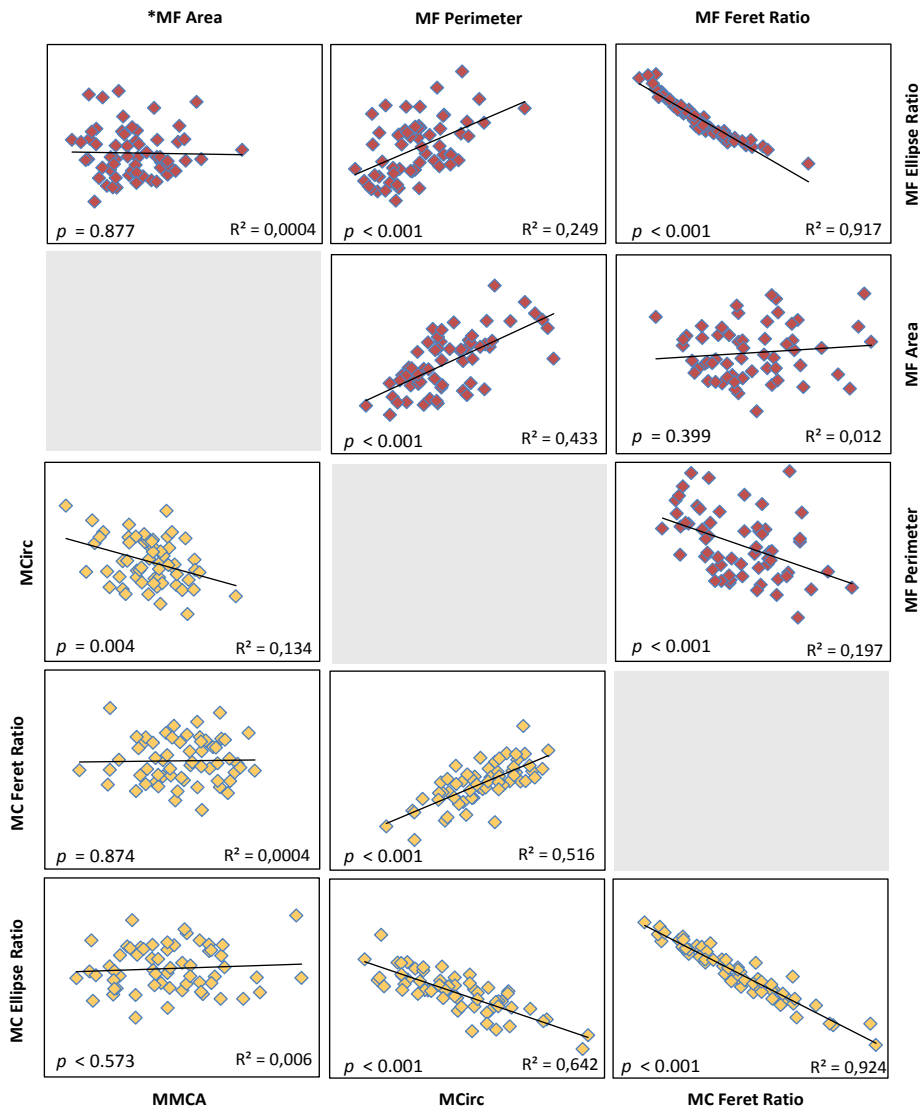


Figure 4.3. Correlations between the different morphological parameters detailed for the quantitative assessment analysis. R^2 values, representing the square of the correlation coefficients, p -values, the estimated probability of rejecting the null hypothesis of the study question (*i.e.* that the two factors examined are unrelated), when that hypothesis is true.

* $n = 60$ histological frames were quantitatively assessed and data expressed as means. Correlation coefficient values are not significantly different when $p > 0.05$. (MF Area) Total area from mucosal folds. (MF Perimeter) Total perimeter length from mucosal folds. (MF Feret Ratio) Ratio of the Feret lengths from mucosal folds. (MF Ellipse Ratio) Ratio of the Feret lengths from mucosal folds. (MCirc) Mucous cell mean circularity index. (MC Feret Ratio) Ratio of the Feret lengths from mucous cells. (MC Ellipse Ratio) Ratio of the elliptical lengths from the mucous cells. (MMCA) Mean mucous cell area.

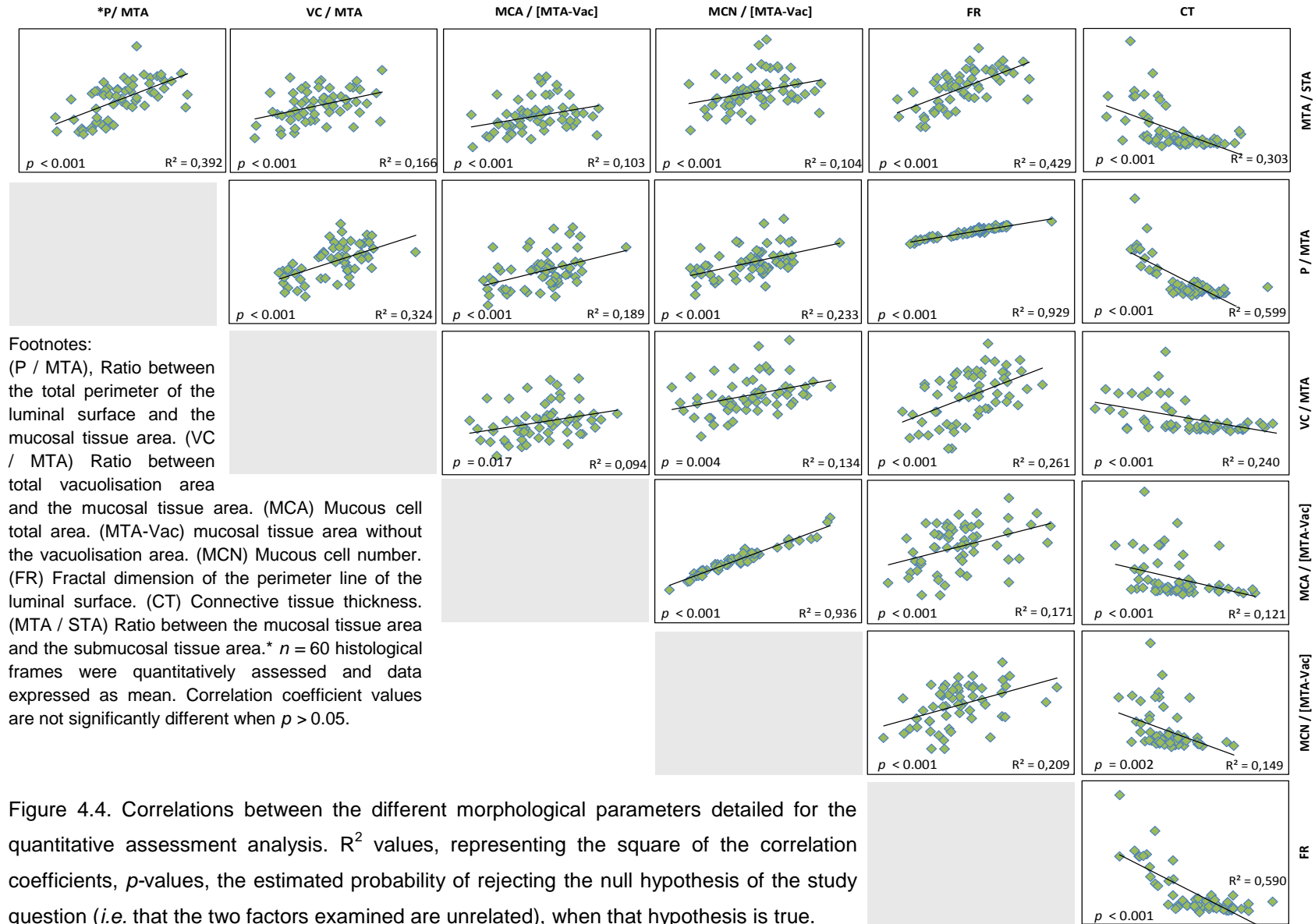


Figure 4.4. Correlations between the different morphological parameters detailed for the quantitative assessment analysis. R^2 values, representing the square of the correlation coefficients, p -values, the estimated probability of rejecting the null hypothesis of the study question (*i.e.* that the two factors examined are unrelated), when that hypothesis is true.

A principal component analysis (PCA) with orthogonal rotation was then conducted on the 60 individuals (*i.e.* 120 histological frame replicates). After removal of the MF Area variable (KMO = 0.383), the Kaiser-Meyer-Olkin measure confirmed the sampling adequacy for the analysis, KMO = 0.698 (Hutcheson & Sofriniou, 1999 *in* Field, 2009). Also the Bartlett's test of sphericity $\chi^2(55) = 1148.187$, $p < 0.001$, indicated that correlations between replicates were sufficiently large for a PCA analysis (Bartlett, 1988). This multivariate approach allowed the full set of variables to be reduced to a smaller set of components (*i.e.* reduction of the dimensionality of the data). Figure 4.5 gives a summary of the loading weightings and score coefficients assigned to each one of the variables / individuals for the extracted components.

Three of the extracted components had Eigenvalues above Kaiser's criterion of 1 (Field, 2009) and in combination they described 74 % of the total variation between individuals distal intestine morphology. The first component accounted for 44 % of such variation ($F_{[4, 30]} \text{ PC1} = 44.81$; $p < 0.001$; Diet A = Diet B, Diet A \neq Diet C \neq Diet D), while only 32 % of variation was explained by the other two components ($F_{[4, 30]} \text{ PC2} = 5.35$, $p = 0.002$, Diet A = Diet B, Diet A \neq Diet C \neq Diet D; $F_{[4, 30]} \text{ PC3} = 2.05$; $p = 0.111$, Diet A = Diet B = Diet C = Diet D).

The principal components obtained are entities that can be visualised using new classification axes (variables) along which the variables can be plotted, giving an idea of their correlation with the corresponding principal component loading (Figure 4.5). The first component PC1 which related to the structure of the epithelial mucosal layers and to the luminal surface intricacy, was characterised by high negative weighting of the variable P / MTA, against high positive loadings for FR and CT, whereas three additional characters MCirc, MCN / [MTA-Vac] and MCA / [MTA-Vac] showed the highest correlation within the second component PC2 which related to the mucous cell circularity and proportion within the tissue. Similarly, the MC Feret Ratio and VC / MTA showed the highest negatives within the third component PC3, which related to mucous cell shape and tissue vacuolisation (Figure 4.5).

According to the PCA analysis (Figure 4.6), two major clusters could be segregated and identified as Diet A (■) and B (●), comprising the fish group fed on the fish meal control diet

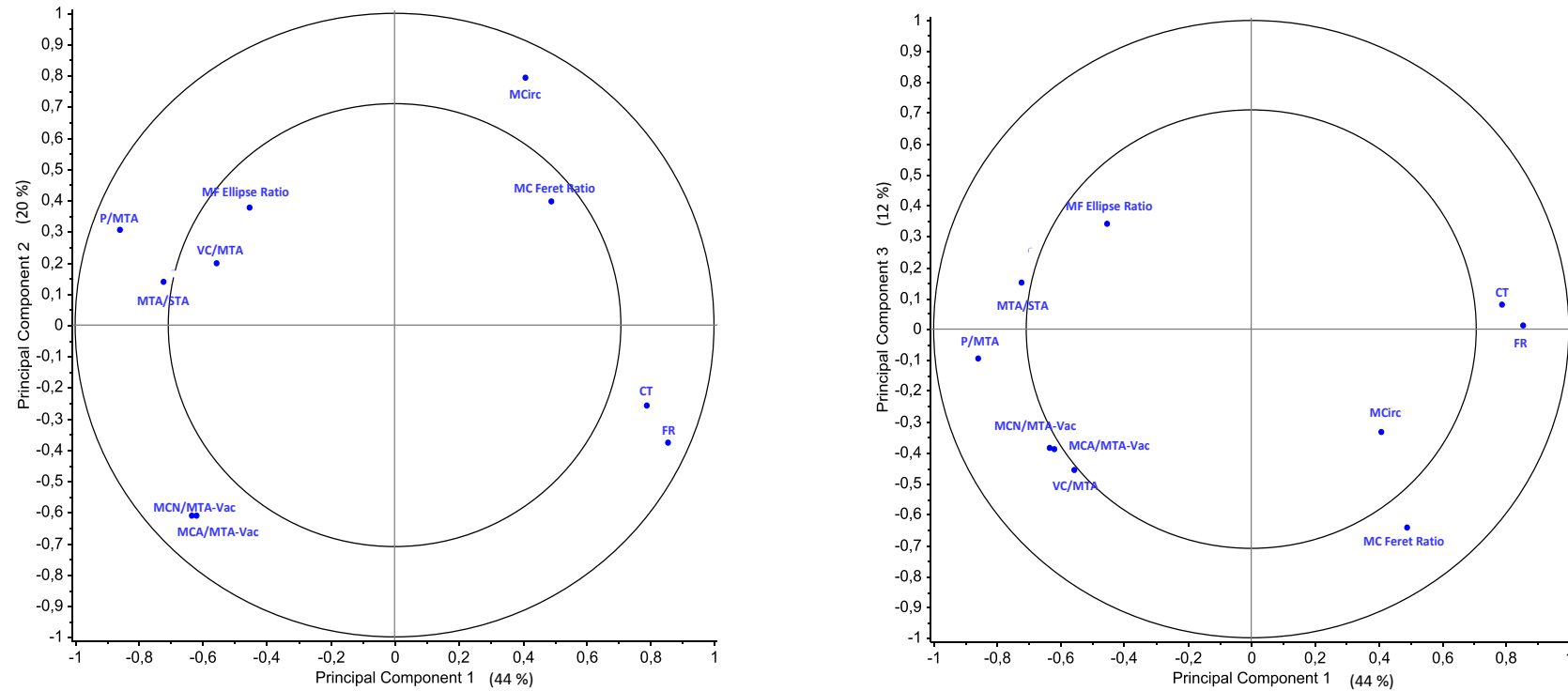


Figure 4.5. Component plot of the multivariate principal component analysis and corresponding loading weights, for the intestinal morphological features measured in Atlantic salmon fed different treatment diets. The 2-D plots contain two circumferences that indicate how much variance is taken into account by the model. The outer circle indicates 100%, while the inner ellipse indicates 50%. (MCirc) Mucous cell mean circularity index. (MC Feret Ratio) Ratio of the Feret lengths from mucous cells. (MF Ellipse Ratio) Ratio of the Feret lengths from mucosal folds. (P / MTA) Ratio between the total perimeter of the luminal surface and the mucosal tissue area. (VC / MTA) Ratio between total vacuolisation area and the mucosal tissue area. (MTA / STA) Ratio between the mucosal tissue area and the submucosal tissue area. (MCN) Mucous cell number. (MCA) Mucous cell total area. (MTA-Vac) Mucosal tissue area without the vacuolisation area. (FR) Fractal dimension of the perimeter line of the luminal surface. (CT) connective tissue thickness.

and the one fed on lupin kernel meal, and Diet D (♦), the group fed the unrefined SBM. While less distinct (*i.e.* being very closely associated to the Diet A cluster), a third cluster corresponding to individuals from the Diet C group (▲) and comprising fish fed the SSC, could also be marginally distinguished. Based upon this multivariate appraisal, one could suggest reducing the number of required classification features, with the most informative being P / MTA, FR, MCN / [MTA-Vac], MCirc, MC Feret Ratio for the evaluated histological states.

The PCA analysis was followed up by a reverse stepwise discriminant analysis, which revealed three canonical functions. The first accounted for 93.2 % (canonical $R^2 = 0.87$) of the group variance, whereas the second and third functions described 5.7 % (canonical $R^2 = 0.02$) and 1.1 % (canonical $R^2 = 0.07$) respectively. In combination these discriminant functions significantly differentiated the treatment groups, $\lambda = 0.087$, $\chi^2(21) = 276.671$, $p < 0.001$. After removal of the first function there was still highly significant discriminatory power, the combination of the second and third discriminant functions could still differentiate the treatment groups $\lambda = 0.662$, $\chi^2(12) = 46.873$, $p < 0.001$. Consequently, the observed differences among treatment groups could be explained in terms of two underlying dimensions in combination, explained by the following linear equations: [a] $D_1 \text{ score} = 11.711 + (3.843 \times \text{MCA} / \text{MTA}) + (-42.388 \times \text{MC Feret Ratio}) + (22.134 \times \text{MCirc}) + (191.694 \times \text{P} / \text{MTA}) + (16.542 \times \text{VC} / \text{MTA}) + (-5.199 \times \text{CT})$; [b] $D_2 \text{ score} = -29.474 + (19.376 \times \text{MCA} / \text{MTA}) + (-52.466 \times \text{MC Feret Ratio}) + (79.159 \times \text{MCirc}) + (-179.454 \times \text{P} / \text{MTA}) + (4.591 \times \text{VC} / \text{MTA}) + (-1.071 \times \text{CT})$ and [c] $D_3 \text{ score} = -41.513 + (17.116 \times \text{MCA} / \text{MTA}) + (-7.850 \times \text{MC Feret Ratio}) + (36.072 \times \text{MCirc}) + (144.448 \times \text{P} / \text{MTA}) + (12.986 \times \text{VC} / \text{MTA}) + (4.374 \times \text{CT})$. The correlations between the discriminant variables and the standardised canonical discriminant functions revealed that the primary variables in distinguishing between different dietary groups were CT, P / MTA, MCirc, MF Perimeter and VC / MTA. The CT ($r_{D1} = -0.697$) and P / MTA ($r_{D1} = 0.551$) variables being mostly loaded onto the first function, while MCirc ($r_{D2} = 0.619$) and MF Perimeter ($r_{D2} = -0.421$) were more highly loaded on the second function. For the third function VC / MTA ($r_{D3} = 0.553$) and CT ($r_{D3} = 0.503$) were the most highly loaded variables.

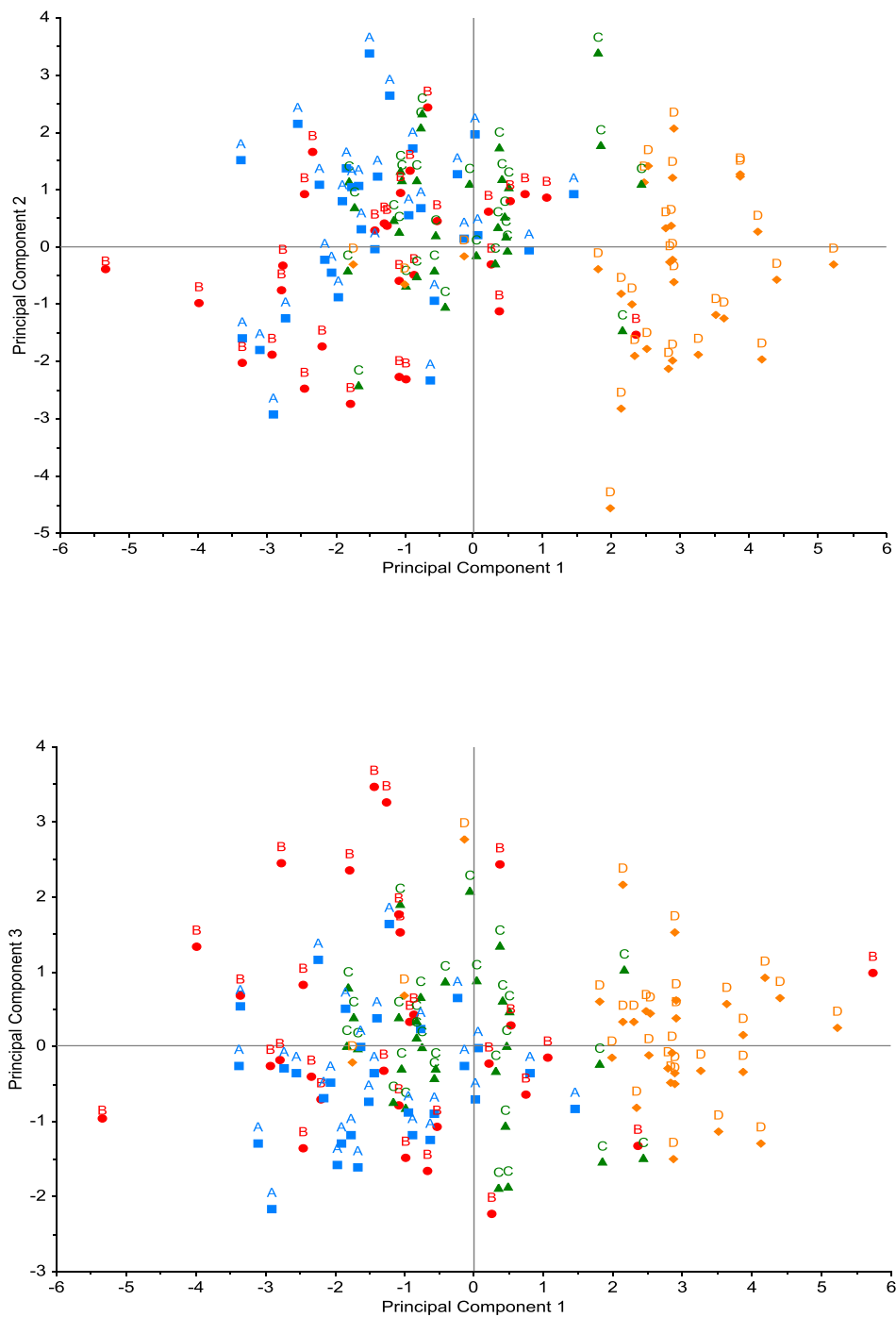


Figure 4.6. Factor plots of the multivariate principal components analysis for the intestinal morphology of Atlantic salmon fed different treatment diets: (A) fish meal based control diet, (B) diet containing 25 % lupin kernel meal, (C) 25 % lupin kernel meal diet with inclusion of 1.7 g.kg⁻¹ soya saponin concentrate, (D) diet containing 25 % defatted soybean meal.

The discriminant function plot illustrated in Figure 4.7, shows that the first function clearly discriminated dietary group D from groups A, B and C, and that the second function discriminated group D (○) from groups A (○) and C (○), but this difference was not as sharp as for the first variable. The group centroids illustrated in the figure, are simply the mean variable scores for each treatment group ($D_1 = 2.003$ Diet A, 1.285 Diet B, 1.034 Diet C, -4.322 Diet D; $D_2 = 0.271$ Diet A, -0.990 Diet B, 0.717 Diet C, 0.003 Diet D; $D_3 = 0.398$ Diet A, -0.132 Diet B, -0.332 Diet C, 0.066 Diet D).

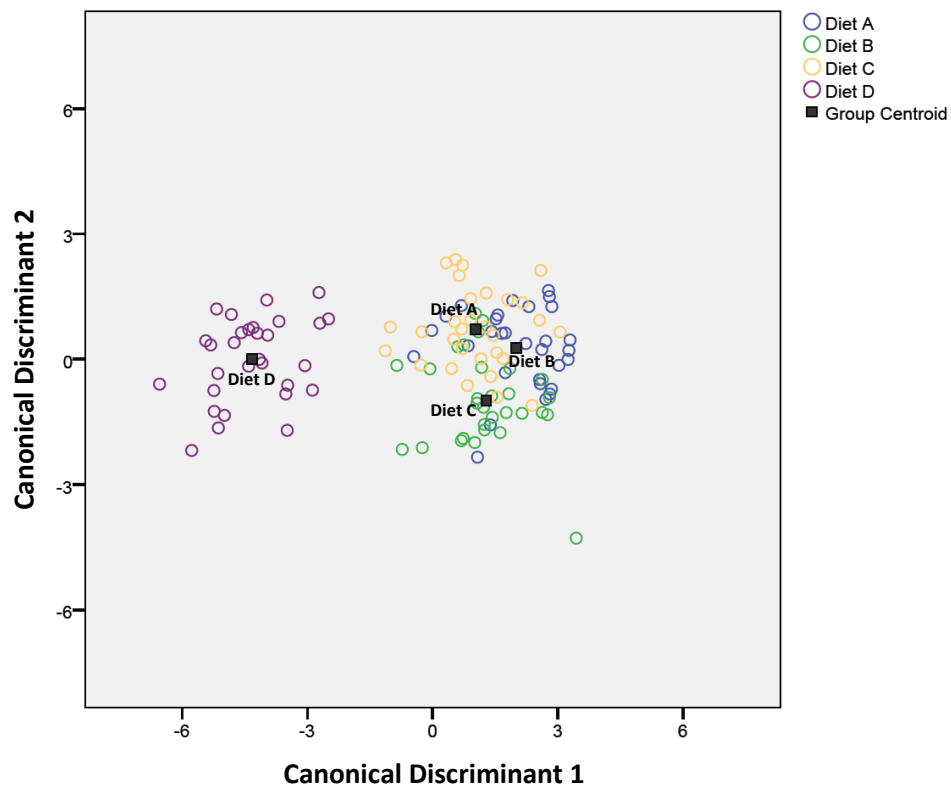


Figure 4.7. Scatterplot of the canonical scores and corresponding dietary group centroids, for a pair of discriminant functions, based on 9 morphometric features ($n = 30$ histological frames per treatment group). (A) Fish meal based control diet. (B) Diet containing 25 % lupin kernel meal. (C) 25 % lupin kernel meal diet with inclusion of 1.7 g.kg^{-1} soya saponin concentrate. (D) Diet containing 25 % defatted soybean meal.

A “leave-one-out” classification analysis (sensitivity analysis) was also employed, in which the analysis was re-run once with each target individual sequentially excluded and then reassigned to a group based on the resulting discriminant function score. Such re-

assignment classification resulted in all the individuals from group D being correctly assigned to their group. However, only around 67-70 % of individuals from groups A, B and C were assigned to the correct group. It is notable that among the individuals from these last groups, none were mis-assigned into group D. This gives an overall efficiency of 75.8 % for the discrimination of the dietary groups (Table 4.6).

Based on the overall analysis one could reduce the number of necessary classification features from ten to four, with CT, P / MTA, MCirc and VC / MTA being emphasised.

Table 4.6. Percentage of predicted classifications based on the discriminant function scores given to each individual fish fed the distinct experimental diets.

Original treatment group	Predicted treatment group				Total
	Diet A	Diet B	Diet C	Diet D	
Diet A (Fish meal)	66.7	6.7	26.6	0.0	100.0
Diet B (Lupins)	13.3	66.7	20.0	0.0	100.0
Diet C (Lupins + SSC)	16.7	13.3	70.0	0.0	100.0
Diet D (SBM)	0.0	0.0	0.0	100.0	100.0

Footnotes:

SSC, soya saponin concentrate; SBM, soybean meal.

4.3.3. Comparison of the quantitative and semi-quantitative systems

The semi-quantitative appraisal required expert knowledge, provided by an experienced pathologist who was used to routinely performing such scoring analysis. It takes some time and practice to ensure that the observer is differentiating changes in the same way each time. They would need to read the slides blind, even repeating some of the analyses to check that the same result would be obtained. The more frequently this was done, the more confident and accurate the observer would become with his appraisal. In the present study, the designated experienced histopathologist took on average 13-18 min to assess 4 different descriptive parameters per histological slide. Scoring one parameter at a time (*i.e.* going back and starting again on the same slide scoring the next parameter) and taking some breaks in between, the observer took approximately 4-5 days to score all 60 histological slides using the described semi-quantitative scoring system.

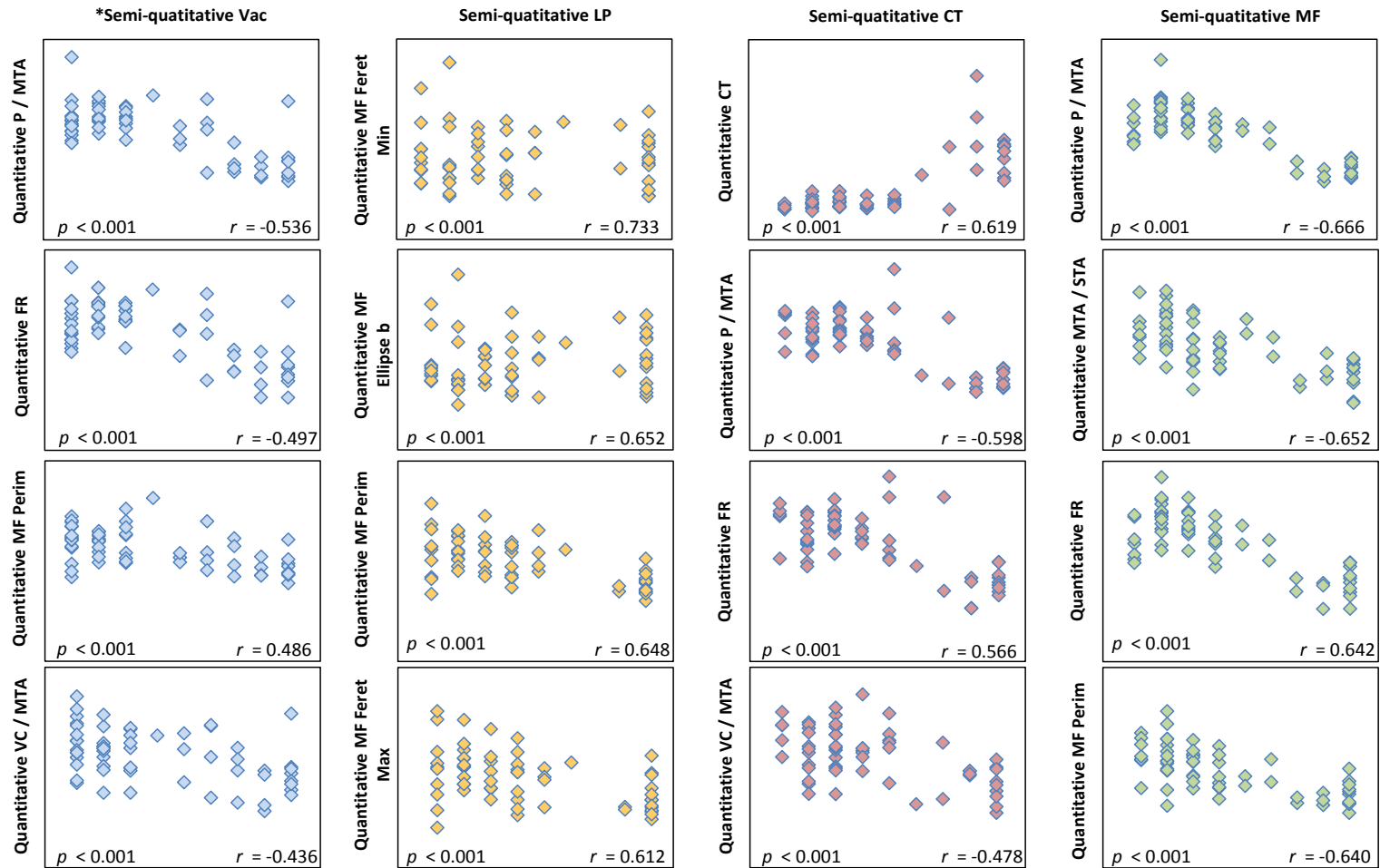
When using the proposed quantitative image analysis system the processing time required for each histological image frame was roughly 25 min per histological frame, accounting for 32 distinct parameters being assessed at a time. Consequently, the image analysis of all 60 histological slides (representing 120 diagnostic frames in total) was performed over approximately 7-8 days. No high level understanding of histology or pathology diagnosis was necessary for the observer to operate such image analysis system. The current assessment was readily performed by an unassisted observer, nevertheless, a degree of user learning and training was required.

The final aim of this study was to compare the descriptive parameters from both quantitative and semi-quantitative assessment systems (Figure 4.8). Such an evaluation revealed significant correlations between the MF parameter measured by the current scoring method of assessment and the P / MTA ($r = -0.666$, $p < 0.001$) measured by image analysis. Significant correlations were also observed for the MF and the MTA / STA ($r = -0.652$, $p < 0.001$), the FR ($r = 0.642$, $p < 0.001$) and the MF Perimeter ($r = -0.640$, $p < 0.001$).

Close correlations were further noted for the CT values measured using the two methods, and P / MTA and FR values ($r = 0.619$, -0.589 , 0.566 respectively; $p < 0.001$). With respect to the semi-quantitative parameter LP, there were stronger positive correlations with the quantitative MF Feret Min, MF Ellipse b and MF Perimeter measurements ($r = 0.733$, 0.652 , 0.648 ; $p < 0.001$). Despite weaker correlations, as demonstrated in Figure 4.8, the semi-quantitative Vac parameter correlated with the P / MTA ($r = -0.536$, $p < 0.001$), FR ($r = 0.497$, $p < 0.001$) and VC / MTA ($r = -0.436$, $p < 0.001$) quantitative descriptive variables. In summary then, overall correlation between semi-quantitative observer scores and quantitative image analysis measurements was good.

4.4. Discussion

Soybean meal is now a widely used feed ingredient for a number of fish and other animal species, and there is extensive knowledge of the potential anti-nutritive factors present in soybeans. Among these, proteinase inhibitors, saponins, lectins, oligosaccharides, phytic acid, fibres and phytoestrogens are considered to be the most important



Footnotes:
 (Vac) Supranuclear vacuoles. (LP) *Lamina propria*. (CT) Connective tissue. (MF) Mucosal folds. (P / MTA) Ratio between the total perimeter of the luminal surface and the mucosal tissue area. (MF Feret Min) Minimum Feret lengths mean of four simple mucosal folds. (FR) Fractal dimension of the perimeter line of the luminal surface. (MF Ellipse b) mean length of the secondary axis of the ellipses with the same geometric moment of inertia as the four of the simple mucosal folds. (MTA / STA) Ratio between the mucosal tissue area and the submucosal tissue area. (MF Perimeter) Total perimeter length from mucosal folds. (MF Ellipse Ratio. (VC / MTA) Ratio between total vacuolisation area and the mucosal tissue area. (MF Feret max) Maximum Feret lengths mean of four simple mucosal folds.* $n = 60$ histological frames were quantitatively assessed and data expressed as mean. Correlation coefficient values are not significantly different when $p > 0.05$.

Figure 4.8. Correlations between the different morphological parameters detailed for the quantitative image analysis and the semi-quantitative scoring assessments. r -values, representing the Spearman's rank rho correlation coefficients, p -values, the estimated probability of rejecting null hypothesis of the study question (*i.e.* that the two factors examined are unrelated), when that hypothesis is true.

(Van den Ingh *et al.*, 1996; Francis *et al.*, 2001). These are thought to be the cause of the major physiological effects seen with the inclusion of soybean meal in fish diets (e.g. impairment in digestion and absorption, with alterations in nutrient metabolism or inhibition of feed intake).

A large number of studies have established the link between oral delivery of SBM and the onset of a pathological condition in the distal intestine of salmonids (Van den Ingh *et al.*, 1991; Olli *et al.*, 1995; Refstie *et al.*, 2000; Buttle *et al.*, 2001; Bakke-McKellep *et al.*, 2007a; Lilleeng *et al.*, 2007; Chikwati *et al.*, 2012). Most of these studies have relied upon expert histological appraisal to explain the morphological changes encountered. Wageningen University for instance (Urán *et al.*, 2008a, also available at <http://edepot.wur.nl/121985>), has developed a semi-quantitative scoring system through which they have assessed the degree of SB-induced enteritis in Atlantic salmon. Amongst others (Morris *et al.*, 2005; Penn *et al.*, 2011) this is one of the most commonly used methodologies for evaluation of dietary modulation effects in fish. Inherent to such an approach is a dependence on assessment by experienced pathologists, as significant variability in the interpretation may occur through use of less experienced readers. The reliance on subjective interpretation by an expert observer has limited the degree to which results from individual studies could be compared with other studies (Berman *et al.*, 1998). The use of an accurate and objective quantitative analysis system would circumvent this problem by increasing the consistency of image interpretation, making it independent of the observer's histopathology skills.

The purpose of the current study was to determine the value of the quantitative image analysis system described in Chapters 2 and 3, for histomorphological assessment of soybean-induced enteritis in salmon biopsy specimens, and to systematically compare the results of semi-quantitative scoring with that of the quantitative image analysis. A semi-quantitative scoring system introduced previously in the thesis was employed to assess the degree of enteritis from the intestinal histological sections, for which four separate descriptive parameters were scored on a scale from 1 to 5, where an increasing score represented a more severe enteritis condition (Table 4.4).

As anticipated, the inclusion of soybean and lupin in the diets of Atlantic salmon in the current study induced classical signs of enteritis in the distal intestine, as previously described by other authors (Bureau *et al.*, 1998; Krogdahl *et al.*, 2003; Refstie *et al.*, 2001; Buttle *et al.*, 2001). The difference in response between experimental treatment groups seemed to be due to the amount of soya saponins (SS) consumed by fish, as the severity of the changes appeared to be dose-dependent, related to the level of SS inclusion (Tables 4.1 and 4.4). Fish fed the fish meal (SS = 0.00 g.Kg⁻¹) and the 25 % lupin kernel meal (SS = 0.03 g.Kg⁻¹) displayed “normal” intestinal morphology, whereas fish fed 25 % soybean meal (SS = 1.07 g.Kg⁻¹) developed severe enteritis. Interestingly, when soya saponins were added to 25 % lupin kernel meal distinct morphological changes were noted, however to a lower extent than that caused by the SBM inclusion (Figure 4.2), suggesting that the low levels of SS in the lupin kernel meal can still be tolerated by salmon, whereas the levels found in SBM are not. Knudsen *et al.* (2008) pointed out that maybe the activity of the saponins naturally present in the soybean meal, is greater when compared to their purified form. Additionally, it is possible that unidentified causative agent(s), which in synergy with the soya saponins might cause inflammation, are more abundant in SBM than in the lupin kernel meal.

The mucosal fold (MF) and the *lamina propria* (LP) appeared to be the most suitable parameters for perceiving differences in the morphology of the intestine of fish, since larger differences in these parameters could be distinguished between the different experimental dietary groups. The smaller variations observed in the scores for other descriptive parameters may indicate that these alterations occur at a later stage in enteritis development (Urán *et al.*, 2009a).

The same histological slides that were evaluated through the semi-quantitative approach were re-evaluated using the image analysis quantification system. The findings of the quantitative assessment for the histomorphological alterations in the distal intestine of fish fed the different experimental diets were consistent with those previous descriptions for

the semi-quantitative scoring (Table 4.5). Again, a dose-response with SS seemed to be supported.

Repair regeneration of the damaged tissue took place, with cells of the same type or with fibrous connective tissue. During this process, fish fed higher levels of SS appeared to have a widening of the central *stroma* within the mucosal folds and consequent shortening of the mucosal folds. An increase in MF Area, MF Feret Ratio and MF Ellipse Ratio, reflected the morphological changes observed. Shorter and wider mucosal folds were evident, and accordingly the intricacy of the luminal surface appeared less irregular (indicated by lower FR values and P / MTA ratio). Additionally, for fish fed greater dietary SS concentrations, there was an increase in the length of the connective tissue between the base of the mucosal folds and the *stratum compactum*. This, in combination with a widening of the *lamina propria*, resulted in an augmentation of the total mucosal tissue area (MTA) with respect to the total portion of sampled area, and consequently the P / MTA and MTA / STA ratios decreased.

Furthermore, although there were no significant differences between dietary groups, variations in vacuolisation of the absorptive enterocytes from the intestinal epithelium were noted. Fish fed the SBM clearly appeared to have less enterocyte vacuolisation (VC / MTA), while fish fed the fish meal based diet had more dispersed and intact supranuclear vacuoles. This could be indicative that particular components of the SS induce concurrent changes in the brush border membrane, blocking specific receptor sites in the distal intestine, which would disturb the process of endocytosis, leading to a reduction in the activity of the digestive enzymes present in the enterocytes and subsequent disappearance of the supranuclear vacuoles. This is in accordance with the evidence provided by other authors (*i.e.* Bakke-McKellep *et al.*, 2000a; Nordrum *et al.*, 2000a; Krogdahl *et al.*, 2003; Krogdahl & Bakke-McKellep, 2005) and more recently Urán *et al.* (2009b), who showed that in salmonids higher inclusion levels of dietary SBM caused a marked reduced endocytosis, resulting in the absence of small vesicles that would customarily fuse into the enterocytes' supranuclear vacuoles.

The number and size of mucous cells in the mucosal folds (*i.e.* MCN / [MTA-Vac] and MCA / [MTA-Vac]) decreased with increasing levels of SS inclusion. Mucous cells are known to be involved in the innate defence system through the production and secretion of mucins, which acts as a physical barrier to protect the underlying epithelium of the gastrointestinal tract against physical and chemical harm (Pajak & Danguy, 1993; Marchetti *et al.*, 2006). Therefore, if mucous cells consisting of a smaller sectional area are observed in fish fed higher levels of SS, the evidence suggests that these dietary components may have triggered mucous release (*i.e.* where cells that have expelled mucin appear smaller in size) or a rapid cell turn-over (*i.e.* immature replacement cells appearing smaller in size). Overall, these histomorphometric changes agree with the reports of Knudsen *et al.* (2008) and Chikwati *et al.* (2012), who suggested that a combination of soya saponins was capable of inducing lesions similar to those described for soy enteritis. Also, the increase in inflammation observed with increasing dietary SBM levels is in agreement with the studies of Krogdahl *et al.* (2003) and Urán *et al.* (2009b). Equally, it provides evidence that the features selected for the quantitative assessment agree with those previously described for changes encountered during soy-associated enteropathy. Taking the correlations (Figures 4.3 and 4.4) and interactions (Figures 4.5 and 4.6) among all those variables into account, MCirc, P / MTA, MTA / STA, MCN / [MTA-Vac], CT, MC Feret Ratio, VC / MTA and MF Perimeter proved to be the most useful morphometric parameters to describe the development of intestinal pathology and were able to distinguish between normal / benign tissue patterns and enteritis. Therefore, these particular parameters could be employed for screening nutritional dietary components, and by requiring a fairly reduced number of key-parameters this would considerably simplify the present script. This, in turn, could permit fuller automation of many analysis tasks, allowing more rapid assessment of larger sets of samples and freeing time for pathologists to undertake more complex interpretations or resolve differences turned up by the automated analysis.

In summary, the two histological techniques employed in this study, one of which is currently considered to be the gold standard for examining fish intestinal enteritis (*i.e.* the

semi-quantitative), showed clearly correlated outputs. Significant correlations were observed between the semi-quantitative and quantitative assessment parameters for intestinal inflammation seen in the cross-sectional comparison (Figure 4.7). The CT, P / MTA, FR, MTA / STA and MF Perimeter parameters used in the quantitative analysis gave strong correlations (*i.e.* $r > 0.490$, $p < 0.050$) with the MF, CT, LP and Vac descriptive parameters used in the semi-quantitative analysis. Furthermore, cross-sectional analysis demonstrated that the semi-quantitative method gave results on a scale 1-5, which correlated with the detailed continuous results from quantitative analysis. However, for each individual score a wide range of quantitative values was noted. For example, samples allocated a semi-quantitative score of one for LP demonstrated quantitative values ranging from 191.49 to 353.88 μm , and a semi-quantitative score of two accommodated quantitative values ranging between 193.94 and 282.89 μm . For the semi-quantitative score of one for CT, values ranged from 18.06 to 43.80 μm , for a score of two the corresponding values ranged between 21.65 to 44.18 μm , while for a semi-quantitative score of three quantitative values ranged from 23.18 up to 65.6 μm . These observations are indicative of a considerable degree of overlap between histological grading classes but also of subtler resolution of parameters. However, as shown by the figure displayed as part of Table 4.4, a fair degree of overlap was similarly observed in the semi-quantitative histological assessment with Diets A, B and C having a considerable degree of overlap between each other's scoring.

Overall, many biological traits exhibit considerable variability and for any histomorphometric measurement to be useful for determining whether a change has occurred, for example as a result of dietary modulation, it is important to establish how reproducible and reliable the results are (Alonzi *et al.*, 2010). Moreover, where minor but biologically relevant changes are sought, it is imperative that morphometric analysis is sufficiently sensitive to identify subtle, but biologically significant trends (Youssef *et al.*, 1998), and the current image analysis quantitative system, appeared proficient with respect

to all these essential requirements. The advantages over a semi-quantitative scoring system are:

- (1) *Robustness*: it produces objective, accurate, reliable and sensitive quantifications of intestinal enteritis (see Chapter 2), which correlate well with the gold standard semi-quantitative indices currently used.
- (2) *Reproducibility*: there seemed to be less inter-observer variability following the image analysis approach than with the semi-quantitative score (as suggested by the study presented in Chapter 2 from this thesis).
- (3) *Rapidity*: the examination of one histological frame is rapid (approximately 25 min for 32 assessed parameters), and faster than any other quantitative assessment method for the same number of parameters being evaluated.
- (4) *Simplicity*: operation of the system is relatively easy so that it can be performed by an unassisted operator. There is no need for a vast knowledge of pathology diagnostics or computer programming (although greater expertise will clearly assist downstream interpretation of results). A degree of user learning and training is nevertheless required. It is estimated that it takes approximately 2-5 h to establish user confidence according to previous experience.
- (5) *Exhaustiveness*: it can be employed for a large number of samples and it may be upgraded to provide analysis of the entire intestine section, instead of visualising just two randomised frames per each section.
- (6) *Quantitation*: the results generated by image analysis are continuous or semi-continuous variables rather than semi-quantitative scores / gradings. This allows more reliable comparisons between studies and facilitates statistical analysis.
- (7) *Adaptability*: the image analysis provides for some degree of operator intervention allowing the adjustment of morphometry thresholds as necessary. This permits an interactive reflection, which involves a dynamic process that formally incorporates corrective steps along the way.

However, some difficulties were encountered with this method:

- (a) *Sample size*: observations have shown that a sufficient surface / area extent of the sample is required for accurate performance of quantitative morphometric analysis. Also, the quality of biopsy tissue must be adequate (*i.e.* not too fragmented or degraded by pathology / fixation / processing procedures). A trained histopathologist using morphological features is able to ignore or compensate for those irregularities, while the current image analysis system cannot do this so easily.
- (b) *Costs*: image analysis is still expensive, although as laboratories become better equipped it will become common place and easily accessible. It is, however, arguable that commercial diagnostic histopathology services may also be costly and that over time, this cost could easily surpass the expenses of purchasing the necessary image analysis software and hardware.

4.5. General conclusions

This is, to the author's knowledge, the first broad-scale application of quantitative image analysis to the assessment of nutritionally-induced enteritis in fish, using such a large number of histomorphometric parameters and biopsy samples, as well as directly comparing the prognostic value of such a quantitative analysis against that of a semi-quantitative visual scoring system.

In summary, this study has shown that most quantitative indices performed equally well when compared to analogous semi-quantitative descriptive parameters of assessment for enteritis prognosis. The excellent reproducibility and accuracy performance levels indicate that the image analysis system is a useful and reliable morphometric method for the quantification of SB-induced enteritis in salmon. Other characteristics such as rapidity, simplicity and adaptability favour this method for image analysis, and are particularly useful where less experienced interpreters are performing the analysis. The quantitative assessment system using the proposed features outlined here, clearly identifies soy-associated enteropathy in experimental fish, and may thus be recommended for evaluation of related variations in salmon intestinal histomorphology.

USER GUIDELINES FOR OPERATION OF THE GUT HEALTH IMAGE PROCESSING AND ANALYSIS SEMI-AUTOMATED SYSTEM – PART II

A detailed protocol has been compiled to allow a better understanding of the image processing and analysis workflow. It provides step-by-step instructions for loading, initiating and operating the image analysis system, which is employed for work presented throughout the thesis.

1. KS Run User Interface

The image processing, segmentation and analysis script developed is deployed using the stand-alone KS Run software platform (Version 3.0, Carl Zeiss Vision GmbH, München-Hallbergmoos, Germany). Instructions for installing the KSRun software and deploying the gut analysis script within it are provided in the KS Run user manual (KS Run User Interface Manual Guide B 40-613, Carl Zeiss Vision GmbH, München-Hallbergmoos, Germany). The following sections describe the protocol for use of the gut image analysis script presented in Chapter 2.

1.1. Image Processing and Analysis Workflow

The image processing, segmentation and analysis pipeline comprises of a succession of interactive and automated operational steps (⚙️). Feedback in the form of guidance notes for the operator (ℹ️), and visualisation of the generated images (🖼️, Appendix 2 and Technical Note A1) was made available at each step of the pipeline process, as well as feature extraction and data generation (📄, Figure 8 from Technical Note A1).

1.1.1. Start Up

⚙️i. Operational steps ⚙️A to ⚙️C from Technical Note A1 (Chapter 2) are followed.

1.1.2. Logistical Setup and Data Input

ii. Operational steps D to I from Technical Note A1 (Chapter 2) are followed.

1.1.3. Image Pre-processing

iii. Operational steps J to L from Technical Note A1 (Chapter 2) are followed.

1.1.4. Image Segmentation and Processing

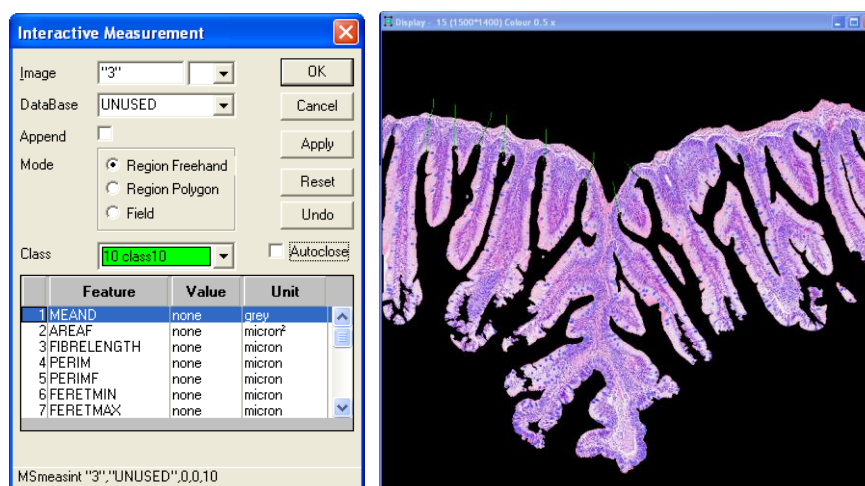
iv. Operational steps M to U from Technical Note A1 (Chapter 2) are followed.

v. Individual mucosal folds are interactively selected (based on a selection criterion that requires the plane of sectioning to pass through the centre of the mucosal fold), and individually separated from the remainder of the mucosal tissue (Image 6H_b from Appendix 2).

a *“Hit the ‘Reset’ button and untick the ‘Autoclose’ box, then draw point-to-point lines either side of each mucosal fold. If neighbouring mucosal folds merge with the mucosal fold of interest, draw lines to separate them. Keep the left mouse button depressed and release it to finish the line. Repeat this step as necessary.”*

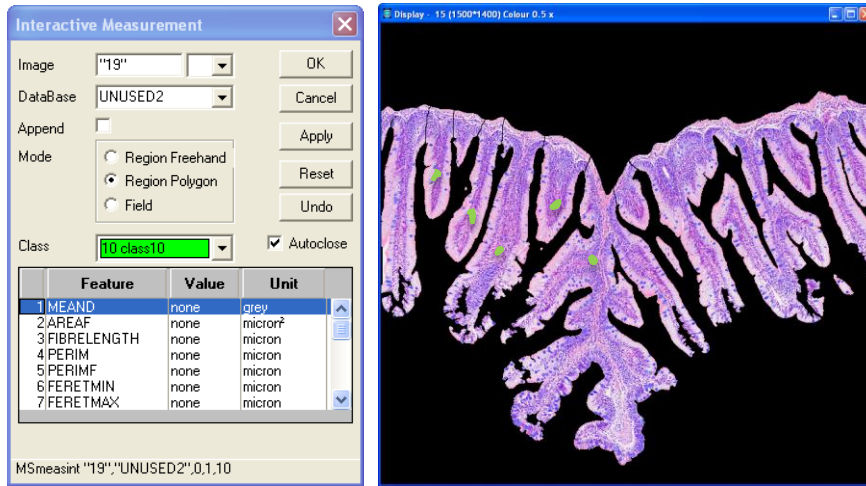
b *“Hit the ‘Reset’ button and untick the ‘Autoclose’ box, then draw point-to-point lines to link separated / broken mucosal fold fragments. Hit the right mouse button or double click to close the lines. Repeat this step as necessary.”*

Image A1



c *“Hit the ‘Reset’ button and then draw circles on each selected mucosal fold. Press and hold the left mouse button to draw continuously or to draw from point-to-point. Mark successive points with the left mouse button, releasing between points.”*

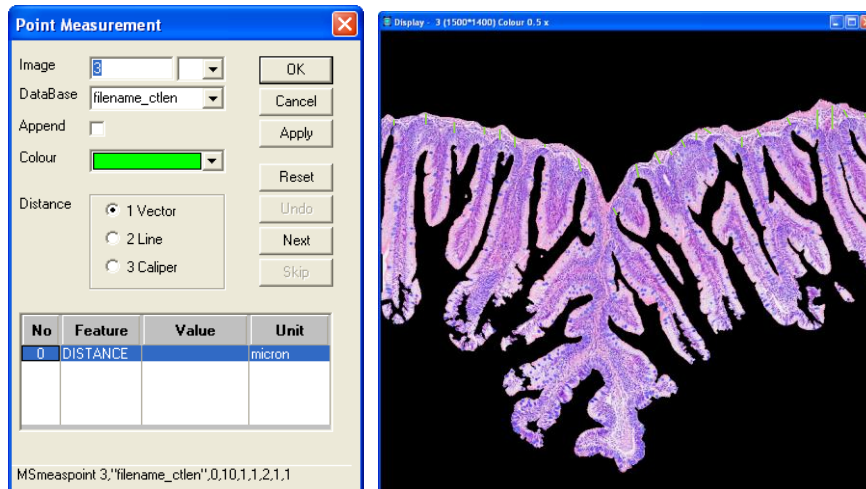
Image A1



vi. The thickness of the connective tissue layer is identified by interactive point-to-point manual demarcation of lines in the graphics plane of the displayed image.

①_d “Draw multiple point-to-point lines to measure the depth of the connective tissue at the ventral extension of the mucosal folds (i.e. between the base of the mucosal folds and the line of the stratum compactum). Repeat for at least 20 distinct areas.”

Image B



1.1.5. Histological Identification and Post-processing Overlays

vii. Operational steps V to E from Technical Note A1 (Chapter 2) are followed.

viii. Extraction of selected individual mucosal folds:

viii-1. The lines drawn in Image A (Appendix 2) are subtracted from it and saved as Image A1.

viii-2. Through a 'Binand'⁹ operation, filled objects drawn and merged into Image A1 coinciding with the regions of interest (ROI) from Image 6H_b are highlighted and masked into Image A2.

 Image A2

e.g. *S400000_A01.MFALL.tif* (Figure 1)

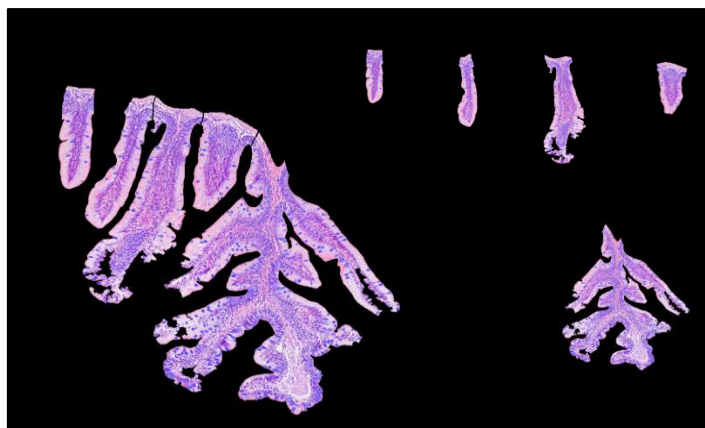


Figure 1. Output Image A2, showing the mucosal folds that were interactively selected.

viii-3. The edge of the mucosal region captured in Image 15 coinciding with the ROI masked in Image A2 were merged into Image A3.

 Image A3

e.g. *S400000_A01.MF_EDGE_ALL.tif* (Figure 2)



Figure 2. Output Image A3, luminal surface from the individual mucosal folds being delineated with a white coloured line.

⁹ **Binand**. This function carries out a bitwise AND operation by electing two bit patterns of equal length and performs the AND operation on each pair of corresponding bits. The result in each position is 1 if the first bit is 1 and the second bit is 1, otherwise, the result is 0. In this we perform the multiplication of two bits; $1 \times 0 = 0$ and $1 \times 1 = 1$. For example: 0101 (Input 1) 0011 (Input 2) = 0001 (Output) (KS 300 Imaging System Manual Guide B 40-614, Carl Zeiss Vision GmbH, München-Hallbergmoos, Germany).

1.1.6. Feature Extraction and Data Generation

ix. Operational steps ζ to K from Technical Note A1 (Chapter 2) are followed.

x. Mucosal folds are identified (*i.e.* Image C) and for each individual fold the following measurements are taken:

- ▣ Mucosal Fold Total Area (MF Area, μm^2)
- Mucosal Fold Perimeter Length (MF Perimeter, μm)
- Mucosal Fold Minimum Feret Length (MF Feret Min, μm)
- Mucosal Fold Maximum Feret Length (MF Feret Max, μm)
- Mucosal Fold Feret Ratio (MF Feret Ratio)
- Mucosal Fold Elliptical Length A (MF Ellipse Af, μm)
- Mucosal Fold Elliptical Length B (MF Ellipse Bf, μm)
- Mucosal Fold Ellipse Ratio (MF Ellipse Ratio)

1.1.7. Analysis Conclusion

xi. Program terminates with audible warning and textual descriptor once the analysis is finished.

- ⓘe *“Measuring feature properties...”*
- “Writing data to databases...”*
- “Analysis finished.”*

QUANTITATIVE IMMUNOSTAINING: DEVELOPMENT OF A BIOMARKER PANEL FOR ASSESSMENT OF IMMUNE RESPONSE IN THE INTESTINAL TRACT OF ATLANTIC SALMON PARR FED DIFFERENT DIETS

5.1. Introduction

'Immunohistochemistry' (IHC) is a term which refers to various antibody detection methods used to identify constituents (*i.e.* proteins or other molecules) of biological cells in tissue sections or whole mounts (Brandtzaeg, 1998). As its name suggests, it bridges three major disciplines: immunology, histology and chemistry (Ramos-Vara, 2011). The principle which underlies the techniques is that antibodies and antibody conjugates may be employed to identify explicit targets. The latter are linked to a marker, such as a fluorescent dye or colloidal gold that can be visualised histologically (Coons, 1971; Starczynski & Crocker, 2005).

In this context, the potential of immunostaining has been exploited not only to identify minute changes in the structural organisation of cells, which could not be determined by conventional analysis with haematoxylin and eosin (H&E) staining, but also to elucidate the functional events and the basic molecular mechanisms involved in, for instance, the development of pathological phenotypes (De Matos *et al.*, 2010; Pellicciari *et al.*, 2011).

Despite, in most instances, histomorphological assessment of H&E stained sections remaining the gold standard procedure practiced by most pathologists in performing diagnoses, the implementation of refined IHC techniques, has been shown to greatly improve the diagnostic and prognostic potential of their histological evaluations (Cregger *et al.*, 2006). The advantages of immunostaining include its wide availability, sensitivity, reliability, simplicity and relative low cost. Disadvantages include the influence of pre-analytical issues (including specimen handling, fixation, paraffin embedding, sectioning and

deparaffinisation), availability of good quality control samples for comparative analysis, and most importantly the difficulties of applying a subjective quantification system in the interpretation of the histological staining (Theodosiou *et al.*, 2007).

Since its inception in the early 30s (Marrack, 1934; Coons, 1971), the technical capabilities of this technique have improved immensely (Haines & West, 2005), especially due to a succession of advances in the methodology employed for immunostaining. From the introduction of non-fluorescent chromogens (Nakane & Pierce, 1966), through the discovery of antigen retrieval methods (Huang *et al.*, 1976), to the amplification of reaction detection methods (Hsu *et al.*, 1981), all have provided crucial improvements allowing immunolabelling methods to become accessible for a wider group of scientists and histopathologists. In addition, improvements in microscopy, particularly the development of confocal laser scanning microscopy (CLSM) have provided a step-change in the resolution achievable using light microscopy labelling techniques. Together these benefits have resulted in the use of immunolabelling in many research and diagnostic laboratories as a routine tool in the wider repertoire (Haines & West, 2005). A demonstration of this widespread adoption is provided by the exponential increase in the number of immunolabelling / immunostaining publications over recent decades, with this literature not only appearing in dedicated histochemical or cytochemical journals but being widely scattered across other journals dealing with cell and molecular biology, biotechnology, immunology, histopathology, neuroendocrinology, image analysis, forensics, physiology, nutrition, and toxicology amongst other topics (De Matos *et al.*, 2010; Brandtzaeg, 1998). The number and scope of publications referencing this technology reflects the key status that immunostaining currently holds as a highly flexible discipline having relevance both to basic and applied biological research.

Increasingly since the 1950s, IHC has been recognised as a discipline capable of relating biochemical changes to the altered histomorphological features characteristic of a specific disorder. As such, it has assisted histopathologists in determining the most appropriate measurable cellular, biochemical or molecular alterations, which might serve as

indices for health / physiology related assessments. Thus the overall aim of IHC analysis has been previously described in terms of the identification of reliable and unequivocal diagnostic / prognostic biomarkers that could enable recognition of the earliest signs of a pathological condition (Pellicciari *et al.*, 2011).

Unfortunately, this approach has proven to be constrained by both the limitations of intrinsic biomarkers and by the nature / preservation of the tissues being evaluated. The heterogeneity deriving from multiple protein homologues and the inter-individual variability in expression of the same gene, are particular limiting factors in the search of potential unique biomarkers displaying desirable properties for screening, diagnosis, and prognosis (Pellicciari *et al.*, 2011). Furthermore, very few individual biomarkers have been found to be sufficient for diagnosis without contribution from other markers or sources of evidence (Yaziji & Barry, 2006). Research focus has therefore shifted to a model that involves searching for and testing panels of multiple markers with the hope of improving performance and robustness.

Nevertheless, the rapid growth of molecular biology has expanded to the point at which the application of technically advanced genomics, metabolomics and proteomics have helped in the identification / generation of many candidate biomarkers, showing high sensitivity and specificity for the target they are expected to identify. Numerous studies have been published in recent decades, describing either the spatial distribution of specific IHC biomarkers and / or quantification of their expression in response to a range of perturbing factors in several organs / tissues from different teleost species. These factors include: dietary modulation (Himick & Peter, 1994; Berntssen *et al.*, 1999; Bakke-McKellep *et al.*, 2000b, 2007b; Picchiatti *et al.*, 2007; Ostaszewska *et al.*, 2010; Chikwati *et al.*, 2013a), toxicity (Eggens *et al.*, 1995; Ortego *et al.*, 1995; Goksøyr & Husøy, 1998; Kilemade *et al.*, 2002), infection or disease (Hemmer *et al.*, 1998; Bermúdez *et al.*, 2006; Silphaduang *et al.*, 2006; Dezfuli *et al.*, 2011a; Ronza *et al.*, 2011), vaccine administration (Sommerset *et al.*, 2005; Mosca *et al.*, 2012; Galeotti *et al.*, 2013), stress (Murray & Fletcher, 1976; Poltronieri *et al.*, 2009; Bernabò *et al.*, 2013), well-being (Sørensen *et al.*, 2012), sex differentiation

(Lorenzi & Grober, 2012), and physiology (Stefan & Falkmer, 1980; Byrd & Brunjes, 1995; Vieira-Lopes *et al.*, 2013).

The interpretation of many IHC stains is frequently qualitative and subjective, with quantification of the reaction having little or no importance. However, proper interpretation of most immunostains depends to some extent on an estimation of differential antigen content between positive and negative results. Numerous methods for visual scoring of IHC assays have been proposed to improve quantitation. These have been shown to have better reproducibility than visual estimates and often to be scientifically relevant. However these scoring systems still suffer from inter-observer discrepancies in reproducibility, and as a further improvement in quantitation, computer-assisted image analysis has proven superior to visual estimates in providing quantitative IHC (Seidal *et al.*, 2001).

A review of the literature confirms that to date, no quantitative assessments of teleost intestinal histo-immunoplasticity have been conducted. The intestinal epithelium of teleosts provides a dynamic interface that maintains structural and functional integrity in response to a range of stimuli such as dietary components or commensal microbiota, which have been shown to cause alterations in the proliferation, migration, differentiation and shedding of damaged or senescent epithelial cells by apoptosis (Chikwati *et al.*, 2013a). In this study, changes in the morphology of the intestinal epithelial cells occurring as a result of dietary modulation were studied and aspects of inflammatory infiltration were characterised using a panel of enzyme and IHC markers. Image analysis techniques were used to evaluate and systematically optimise a quantitative immunolabelling assessment protocol. In Chapters 2 and 4 the accuracy and reproducibility of the quantitative method, and the validity of the resulting protocol in comparison to use of conventional techniques were established. Here the application of a similar system is described for the detection of predictive protein biomarkers and for accurate quantification of small changes in the spatial distribution patterns of such proteins and their relative amounts in the tissue. The immunolabelling of mucosal fold tissues have been investigated for the distal intestinal region of salmon fed three different diets, a reference fish meal based control diet, another with inclusion of

immunostimulants and an experimental enteropathy-causing diet containing unrefined soybean meal.

5.2. Material and methods

5.2.1. Experimental fish and fish husbandry

The experimental trial was conducted at Skretting's Fish Trial Station (Lerang, Jørpeland, Norway). Post-smolt Atlantic salmon (*Salmo salar* L.) with an initial mean body weight of 79 ± 2 g and a mean fork-length of 19 ± 2 cm, were randomly allocated into six flow-through 100 L circular tanks. The tanks were maintained under a 24 h light photoperiod, and supplied with fresh sand-filtered flow-through seawater at 11 ± 2 °C. Dissolved oxygen, ammonia, nitrate, nitrite and pH levels were monitored and maintained within recommended limits (Wedemeyer, 1996). Individual tanks were equipped with automatic disc feeders and feed waste collectors.

5.2.2. Diets and feeding regime

The fish were acclimatised to the experimental conditions for 3 weeks, during which they received a reference fish meal based diet (Protec™, Skretting, Stavanger, Norway). Thereafter, three different experimental diets were randomly assigned to triplicate tanks and the salmon fed during a 20-week experimental period. The three experimental diets were produced as 3 mm extruded pellets at Skretting Feed Technology Plant (Stavanger, Norway). The experimental diets comprised either a fish meal based control diet, a diet containing 25 % unrefined soybean meal concentrate or a fish meal diet supplemented with functional ingredients. Formulations of the diets are presented in Table 3.1. from Chapter 3. All the diets were formulated to be approximately iso-nitrogenous and iso-energetic on a crude protein and gross energy basis, and to satisfy the nutritional requirements of salmonids (NCR, 1993). Fish were fed twice a day at 20 % biomass using automatic disc feeders. Uneaten feed was collected, separated from faeces and quantified by weight after drying for 12-16 h at 90 °C.

5.2.3. Sampling procedure

Following the twenty week feeding regime, 3 fish were randomly sampled from each designated replicate tank for each treatment group. All fish were starved 24 h prior to sampling, and euthanised with anaesthetic (50 mg.L⁻¹, MS-222, Tricaine Methanesulphonate, Argent Chemical Laboratoires, Redmount, WA, USA). The gastrointestinal tract was removed and freed of associated adipose tissue. Transverse rings of at least 1 cm in length were collected from the distal intestine region, cut open longitudinally and fixed in neutral buffered formalin (10 %, pH 7.2, 3800601, Leica Biosystems, Bucks, UK) at room temperature for at least 24 h before further histological processing.

5.2.4. Histology

For histological examination and IHC analyses, samples were processed according to standard histological methods (Bancroft & Stevens, 1982; Ramos-Vara, 2005, 2011). All tissue formalin-fixed samples were dehydrated and embedded in paraffin (Tissue-TekII Paraffin Wax, melting-point: 54-57 °C, Sakura Finetek Europe B.V, Netherlands). Three distinct paraffin blocks were produced for each individual tissue sample, and for each individual paraffin block, one histological slide was prepared. Transverse sections of 5 µm thickness were cut (Leica RM 2035, Leica Microsystems Ltd., UK), mounted on glass slides pre-coated with APES (3'aminopropyl triethoxysilane, A3648, Sigma-Aldrich, Ayrshire, UK) to improve section adherence and dried overnight at 37 °C.

5.2.5. Immunostaining assays – Immunolabelling of biomarkers

The immunostaining protocols given in Table 5.1 were developed following a series of troubleshooting and optimisation steps, including comparison of various demasking procedures and blocking solutions, use of different primary antibody concentrations and / or diverse chromogenic visualisation systems. The following procedures are those producing the most consistent results for the selected antigens in terms of compatibility with image analysis quantitation. In developing protocols, advice was sought from the Veterinary Diagnostics Service of the University of Glasgow. Mr. Iain MacMillan and Mrs. Lynn

Stevenson, histologists from this facility, provided practical assistance and specialist advice during optimisation of some of the protocols described.

All immunoreactivity steps were alternated with washings of the assigned rinsing buffer and all the incubation steps were carried out in a humidified chamber to avoid desiccation of the tissue, which could lead to non-specific binding and ultimately high background staining. Additionally, so as to evaluate the contribution of either non-specific antibody binding to endogenous Fc receptors (FcRs) or a combination of ionic and hydrophobic interactions giving background immunostaining, additional tissue sections were included and stained using an antibody directed to an irrelevant antigen (e.g. BrdU, monoclonal anti-bromodeoxyuridine antibody, B2531, Sigma-Aldrich, St. Louis, USA) in parallel with the slides being stained with the antibodies of interest, with the irrelevant antigen having the same isotype and concentration as the antibody of interest. Along with, or whenever an isotype control (*i.e.* using an antibody directed to the irrelevant antigen) was not possible, a negative antibody control was applied, simply by replacing the primary antibody with the antibody's diluent. Also, to ensure that the test antibodies were performing as expected, positive tissue controls known to contain the expressed antigens of interest (comprising sections of a canine skin tumour; from a feline brain and colonic carcinomas; from caprine tonsils and / or from a female rodent mammary gland to which the commercial antibodies are known to react and with well documented labelling profiles for proliferation, differentiation and shedding of damaged cells and kindly provided by Mrs. Finlayson and Mr. MacMillan from Moredun Research Institute and the Veterinary Diagnostics Services from the University of Glasgow, respectively), were also included in the staining process.

From each biopsy paraffin block a series of 7 serial sections were prepared and stained as follows (Sections 5.3.5.1 to 5.3.5.7). For one in every ten biopsies, an eighth section was prepared and stained as a negative control by omitting the primary antibody.

5.2.5.1. *Cell proliferation and regeneration (PCNA)*. Mounted tissue sections were deparaffinised in CitrocLEAR[®] (TCS Biosciences, Buckingham, UK) and rehydrated in a graded series of ethanol. Slides were then rinsed for 5 min in Tris-buffered saline Tween

solution (TBST, 150 mM NaCl, 50 mM Trizma base[®], 0.5 % Tween[®] 20, pH 7.5), and heat induced epitope retrieval performed using an Antigen Access Unit (MP-2002-CE, A. Menarini Diagnostics Ltd., Berkshire, UK) with sodium citrate buffer solution (10 mM Na₃C₆H₅O₇, pH 6.0) at 125 °C for 1 min and 40 sec. After rinsing of the slides with TBST, tissue endogenous peroxidase activity was inhibited by incubation in Peroxidase-Blocking-Solution (DAKO REAL™, S2023, DAKO, Glostrup, Denmark) for 5 min at room temperature. Slides were then incubated for 30 min at room temperature with a polyclonal rabbit antibody raised against proliferating cell nuclear antigen (FL-261, sc-7907, Santa Cruz Biotechnology, California, USA) diluted 1:1000 in Antibody-Diluent (DAKO REAL™, S2022, DAKO, Glostrup, Denmark). Subsequent to rinsing twice with TSBT for 5 min each, sections were incubated with a biotinylated labelled secondary antibody (EnVision™ System HRP labelled Polymer, K4003, DAKO, Glostrup, Denmark) for 30 min and the immunoreactivity visualised by use of the EnVision™ Peroxidase / DAB+ (K5007, DAKO, Glostrup, Denmark) for 10 min. Sections were rinsed twice with distilled water for 5 min each, counterstained for 26 sec with Gill's haematoxylin (RHS-345, CellPath Ltd., Newtown, UK), blued for 1 min with Scotts Tap Water Substitute (EGW-0200-23A, CellPath Ltd., Newtown, UK) and mounted with Pertex[®] mounting medium (00811, Histolab, Göteborg, Sweden), after dehydration through a series of graded ethanols and clearing of the tissue sections with CitrocLEAR[®].

5.2.5.2. *Programmed cell death or apoptosis (TUNEL)*. Apoptotic cells were detected using a combination of IHC and a terminal deoxynucleotide transferase-mediated deoxy-UTP nick-end labelling assay, using the ApopTag[®] Plus Peroxidase *In Situ* Apoptosis Detection Kit (S7101, Merck Millipore, Billerica, USA) and following the manufacturer's protocol. In brief, the sections were deparaffinised using xylene, hydrated through a graded series of alcohols and pre-treated with freshly made 20 µg.mL⁻¹ IHC Select[®] Proteinase K (21627, Merck Millipore, Billerica, USA) for 15 min at room temperature. Sections were then washed twice in phosphate buffered saline solution (PBS, 137 mM NaCl, 2.7 mM KCl, 10 mM Na₂HPO₄, 1.8 mM KH₂PO₄, pH 7.4) for 2 min each, and the endogenous peroxidase

activity quenched by using 3 % hydrogen peroxide (H1009, Sigma-Aldrich, Ayrshire, UK) in PBS for 5 min at room temperature. Slides were then rinsed twice with distilled water for 5 min each, and immediately dipped in ApopTag[®] Equilibration Buffer for 10-20 sec. The excess solution was tapped off and the sections incubated with ApopTag[®] Working Strength TdT Enzyme at 37 °C for 1 h. The slides were then transferred into a Coplin jar containing ApopTag[®] Working Strength Stop / Wash Buffer for 10 min, washed in 3 changes of PBS for 1 min each, and incubated for 30 min at room temperature with the ApopTag[®] Anti-digoxigenin Conjugate. Thereafter, the slides were washed with 4 changes of PBS for 2 min each, and the sections incubated for 5 min in ApopTag[®] Peroxidase Substrate at room temperature. The sections were washed three times in distilled water for 1 min each then counterstained with methyl green (H-3402, Vector Laboratories, Peterborough, UK) for 10 min and washed in distilled water. Finally, the slides were washed in 100 % N-butanol (B7906, Sigma-Aldrich, Ayrshire, UK), dehydrated through graded alcohols, cleared in xylene and mounted with Pertex[®] mounting media. The negative control excluded treatment with TdT-labeled-deoxynucleotides (*i.e.* disregarding incubation with ApopTag[®] Working Strength TdT Enzyme, but including proteinase K digestion control for nonspecific incorporation of nucleotides or for nonspecific binding of enzyme conjugate).

5.2.5.3. *Eosinophilic granule cells (Active Caspase-3)*. Paraffin-embedded sections were subjected to deparaffinisation using xylene and subsequent rehydration in decreasing concentrations of ethanol. Demasking of the tissue sections was performed by enzymatic antigen retrieval, using a Universal UNI-TRIEVE[®] solution (NB325, Innovex Biosciences, Richmond, USA) for 30 min at 65 °C in a water bath. Slides were rinsed twice in distilled water and, to inhibit endogenous peroxidase, the sections were then treated with EnVision[™] Dual Endogenous Enzyme Block (K4065, DAKO, Glostrup, Denmark) for 10 min at room temperature. Without washing, excess solution was blotted off and tissues were incubated overnight at 4 °C with a rabbit polyclonal antibody against caspase-3 (Anti-ACTIVE[®] Caspase-3 Ab, G7481, Promega, Madison, USA) diluted 1:250 in TBST solution. Thereafter the slides were rinsed twice with TBST for 5 min each, and sections incubated

with a biotinylated labelled secondary antibody (EnVision™ HRP Labelled Polymer, K4065, DAKO, Glostrup, Denmark) for 30 min. Slides were washed twice for 5 min each in TBST and the peroxidase activity revealed by incubating the tissue sections with in EnVision™ DAB (K4065, DAKO, Glostrup, Denmark) for 7 min. The reaction was stopped by immersing the slides in distilled water. Finally the sections were counter-stained with Harris's haematoxylin for 3 min (RALA361075, Reactifs RAL SA, VWR International Ltd, Leicestershire, UK) and blued in Scotts Tap Water Substitute by quick dips. Slides were rinsed in running tap water for 2 to 5 min, sections dehydrated through increasing concentrations of ethanol, cleared in xylene and mounted with Pertex®.

5.2.5.4. *T-cell-like cells (CD3ε)*. Embedded sections were deparaffinised using CitrocLEAR® and subsequently rehydrated in decreasing concentrations of ethanol. Sections were then rinsed for 5 min in TBST solution, and demasking of the sections was performed by hydrated autoclaving (Menarini ACESS Retrieval Unit, MP-2002-CE, Menarini Diagnostics Ltd., Berkshire, UK) at 125 °C for 1 min and 40 sec in sodium citrate buffer solution. Endogenous peroxidase activity was quenched with Peroxidase-Blocking-Solution (DAKO REAL™, S2023, DAKO, Glostrup, Denmark) for 5 min at room temperature, the sections rinsed with TBST and incubated for 30 min with the primary antibody 1:100 diluted in Antibody-Diluent (DAKO REAL™, S2022, DAKO, Glostrup, Denmark). The primary antibody comprised a polyclonal rabbit anti-human T-cell CD3 antibody, produced against a synthetic peptide from the cytoplasmic part of the ε-chain of the CD3 antigen (A0452, DAKO, Glostrup, Denmark). After rinsing the sections twice with TBST for 5 min, slides were incubated for 30 min with the peroxidase labelled polymer conjugated to rabbit immunoglobulins (EnVision™ System HRP Labelled Polymer, K4003, DAKO, Glostrup, Denmark), a secondary antibody. Sections were again rinsed twice in TBST and the peroxidase activity detected using the Peroxidase / DAB+ (K5007, DAKO, Glostrup, Denmark) provided with the EnVision™ Dual Link System-HRP (DAB+) Detection System kit from DAKO. The reaction was stopped after 10 min by rinsing the slides in distilled water. Finally the sections were counter-stained with Gill's haematoxylin for 26 sec, blued in Scotts

Tap Water Substitute for 1 min, dehydrated through a graded series of ethanols, cleared and mounted with Pertex[®] mounting medium.

5.2.5.5. *Mobilisation of stress related proteins for regenerative processes (HSP 70).*

For the IHC detection of heat shock protein 70, the slides were deparaffinised in xylene and rehydrated in decreasing concentrations of ethanol. Demasking of the HSP 70 epitopes was performed by hydrated autoclaving (Antigen Access Unit MP-2002-CE, A. Menarini Diagnostics Ltd., Berkshire, UK) with sodium citrate buffer solution at 121 °C for 15 min. Tissue sections were then incubated in 0.05 % phenyl hydrazine (P26252, Sigma-Aldrich, Ayrshire, UK) diluted in PBS for 40 min at 37 °C, to inactivate the endogenous peroxidase, and then treated for 20 min at room temperature, with 5 % bovine serum albumin (A9647, Sigma-Aldrich, Ayrshire, UK) and 0.5 % normal goat serum (G6767, Sigma-Aldrich, Ayrshire, UK) diluted in Tris-hydrochloride solution (Tris-HCl, 50 mM Trizma base[®], pH 7.6) to avoid non-specific binding. Excess solution was blotted off and tissues were incubated overnight at 4 °C, with the mouse monoclonal anti-Heat Shock Protein 70 antibody (H5147, Sigma-Aldrich, St. Louis, USA) diluted 1:1000 in Tris-HCl. Sections were rinsed twice with PBS for 5 min each, and antibody binding demonstrated using an EnVision™ Dual Link System-HRP (DAB+) (DAKO, Glostrup, Denmark) containing a secondary biotinylated antibody labelled according to the manufacturer's instructions. Slides were washed twice for 5 min each in PBS and then incubated with Diaminobenzidine (EnVision™ DAB, K4065, DAKO, Glostrup, Denmark). The reaction was stopped after 20 min by rinsing in tap water. Finally the sections were counter-stained with Harris's haematoxylin for 1 min, slides rinsed in running tap water for 2 to 5 min, sections dehydrated through increasing concentrations of ethanol, cleared in xylene and mounted with Pertex[®].

5.2.5.6. *Facilitation of nutrient uptake and ion transport (Na⁺K⁺-ATPase).* Paraffin-embedded sections were subjected to deparaffinisation using xylene and subsequently rehydrated in decreasing concentrations of ethanol. The slides were then rinsed in distilled water for 15 min, incubated overnight at 4 °C. with a monoclonal antibody against α 5-subunit of chicken Na⁺K⁺-ATPase (α 5, DSHB, Iowa, USA), diluted 1:200 with PBS containing

Table 5.1. Summary of immunostaining protocols used in this study.

Immunostaining assay	Antigen retrieval	Pre-treatment	Primary antibody	Secondary antibody	Detection system
PCNA	Sodium citrate buffer, pH 6; 1 min 40 sec; 125 °C; HIER.	REAL™ Peroxidase-Blocking solution (S2023, DAKO); 5 min; RT.	PCNA Polyclonal Rabbit FL-261 (sc-7907, Santa Cruz Biotechnology); 1:1000; 30 min; RT.	EnVision™ HRP Rabbit Polymer (K4003, DAKO); 20 min; RT.	REAL™ EnVision™ DAB+ (K5007, DAKO); 2 x 5 min; RT.
TUNEL	Proteinase K (21627, Merck Millipore); 20 µL.mL ⁻¹ ; 15 min; RT.	ApopTag® Working Strength TdT Enzyme (S7101, Merck Millipore); 1 h; 37 °C.	N.A.	ApopTag® Anti-Digoxigenin Conjugate (S7101, Merck Millipore); 30 min; RT.	ApopTag® Working Strength Peroxidase Substrate (S7101, Merck Millipore); 5 min; RT.
Active caspase-3	UNI-TRIEVE solution (NB325, Innovex); 30 min; 65 °C; water bath.	EnVision™ Dual Endogenous Enzyme Block (K4065, DAKO); 10 min; RT.	Anti-ACTIVE® Caspase-3 Polyclonal Rabbit (G748A, Promega); 1:250; overnight; 4 °C.	EnVision™ HRP Rabbit Polymer (K4065, DAKO); 30 min; RT.	EnVision™ DAB (K4065, DAKO); 7 min; RT.
CD3ε	Sodium citrate buffer, pH 6; 1 min 40 sec; 125 °C; HIER.	REAL™ Peroxidase-Blocking Solution (S2023, DAKO); 5 min; RT.	CD3 Polyclonal Rabbit Anti-human (A0452, DAKO); 1:100; 30 min; RT.	EnVision™ HRP Rabbit Polymer (K4003, DAKO); 20 min; RT.	REAL™ EnVision™ DAB+ (K5007, DAKO); 2 x 5 min; RT.
HSP 70	Sodium citrate buffer, pH 6; 2 min; 121 °C; HIER.	¹ 0.05 % Phenyl Hydrazine in PBS, pH 7.4; 40 min; 37 °C. ² 5 % BSA, 0.5 % NGS in Tris-HCl, pH 7.6; 20 min; RT.	HSP 70 Monoclonal Mouse Clone BRM-22 (H5147, Sigma); 1:1000; overnight; 4 °C.	EnVision™ HRP Rabbit Polymer (K4065, DAKO); 30 min; RT.	EnVision™ DAB (K4065, DAKO); 7 min; RT.
Na ⁺ K ⁺ -ATPase	N.A.	1 % BSA; 10 % NGS in PBS, pH 7.4; overnight (with primary antibody).	Na ⁺ K ⁺ -ATPase Monoclonal Anti-chicken α-Subunit (a5, DSHB); 1:200; overnight; 4 °C.	Peroxidase Conjugate of Goat Anti-mouse (A4416; Sigma); 1 h; RT.	Vector® DAB Peroxidase Substrate Kit (SK-4100; Vector Labs); 10 min; RT.

Footnotes: PCNA, proliferating cell nuclear antigen; HIER, heat induced epitope retrieval; DAKO, Glostrup, Denmark; RT, room temperature (16-20 °C); Santa Cruz Biotechnology Inc., California, USA; HRP, horseradish peroxidase; DAB, 3,3'-Diaminobenzidine; TUNEL, terminal deoxynucleotidyl transferase dUTP nick end labelling; Merck Millipore, Billerica, USA; N.A., non applicable; Active Caspase-3, protein member from the cysteine aspartic acid protease family; Innovex Biosciences, Richmond, USA; Promega, Madison, USA; CD3ε, T-cell surface glycoprotein cluster of differentiation epsilon chain; PBS, phosphate buffered saline solution, BSA, bovine serum albumin; NGS, normal goat serum; Tris-HCl, tris(hydroxymethyl)aminomethane hydrochloride; HSP 70, heat shock protein 70; Sigma, Sigma-Aldrich, St. Louis, USA; Na⁺K⁺-ATPase, sodium-potassium adenosine triphosphatase; DSHB, developmental studies hybridoma bank, Iowa, USA; IL, interleukin; TBS, tris(hydroxymethyl)aminomethane buffered saline solution; UK Vector Labs, Vector Laboratories Inc., Peterborough, UK.

10 % normal goat serum (G6767, Sigma-Aldrich, Ayrshire, UK) and 1 % bovine serum albumin (A9647, Sigma-Aldrich, Ayrshire, UK). Thereafter the sections were incubated with a peroxidase conjugated secondary antibody (A10551, Life Technologies Paisley, UK) diluted 1:100 in PBS for 1 h at room temperature, rinsed twice for 10 min each in PBS, and incubated for another 10 min with freshly prepared Vector[®] DAB Peroxidase Substrate (SK-4100, Vector Laboratories Inc., Peterborough, UK). Finally the sections were counter-stained with Harris's haematoxylin for 2 min, rinsed in running tap water for 2 to 5 min, dehydrated through increasing concentrations of ethanol, cleared in xylene and mounted with Pertex[®].

5.2.6. Digital image acquisition

Using an automated slide-scanning system (MIRAX Desk, Carl Zeiss MicroImaging GmbH, Göttingen, Germany) stained slides were scanned and a digitised MRXS image of the complete section was acquired at a final magnification of 20 \times . For visualisation and cropping of the images, MIRAX Viewer software (Version 1.12, 3DHISTECH, Budapest, Hungary) was used. For each slide, two microscope fields were randomly selected and cropping performed at 100 \times magnification. A frame of 4.85 Mpixels was used to crop the sections and twenty-four bit digital images were extracted as individual TIFF images (1:4 magnification, 2048 \times 2048 pixels tile size, 2960 \times 1640 pixels image size), and saved to give a file size of 24 MB with a quality setting of 0.23 microns per pixel. Subsequently, using IrfanView (Version 4.33, Wiener Neustadt, Austria) batch converter, all uncompressed bitmap tiled TIFF images were converted into untiled TIFF files with sizes ranging from 13 to 14 MB.

5.2.7. Quantitative image analysis of immunohistological labelling

Cropped images were randomised and evaluated blind. Image processing and computer operations were performed on a personal computer (Dell Latitude[™] D630, Intel Pentium II 350 MHz processor, 128 MB RAM, 2 GB hard disk, under the environment of Microsoft[™] Windows XP) operating the stand-alone KSRun software platform (Version 3.0, Carl Zeiss Vision GmbH, München-Hallbergmoos, Germany), through which the developed algorithms for detection and feature extraction were implemented. The flow chart for the process pipeline is shown in Figure 2.3 and partly illustrated in Figures 3.1 and 5.1. For a more complete

description please see Chapter 2 and Technical Notes A1 and B. In brief, following a background correction and noise reduction of the source image, a binary image was created (Figure 5.1 B). The empty space (*i.e.* comprising no tissue or cells; within the area shown in Figure 5.1 B) was segmented by inverting the image to its negative and through intensity differentiation, which in turn allowed proper segmentation of the peritoneal edge of the *muscularis externa* and the internal intestinal lumen. Thereafter, the *stratum compactum* was defined by interactive drawing over the displayed tissue image, so as to discriminate different tissue areas (*i.e.* mucosal and submucosal tissues; Figure 5.1 E-F respectively). Subsequently, for detection of the dark brown shades characteristic of the positive immunohistological reactions, an interactively defined HLS colour threshold (Hue, Lightness, Saturation: an alternative colour model to RGB providing a better match to perceived stain colours) was set. Simultaneously, the threshold operation defined the mean average intensity for the stained brown shades and divided selected thresholded pixels to white, and sub-threshold, background pixels to black (Figure 5.1 G-H). Thus, the resulting binary image represented the regions where the antigen protein expression had been detected. Thereafter the area fraction of positive staining in the tissue was estimated by the number of white pixels present in three distinct zones: (SUB) submucosal area, (SUP) above the *stratum compactum* and up to 15-30 cell thickness above the basal area of the intestinal mucosal folds, and (MUC) remaining mucosal area / apex of the intestinal folds (Figure 5.1 G-H).

Segmentation of all these histological components was performed sequentially. Regions within the threshold ranges were highlighted, image overlays generated and stored as individual image outputs. Finally, the thresholded regions of interest were automatically processed by a succession of mathematical algorithms, extracting the pre-selected measurements (Section 1.1.6 from Technical Note B). Values for these were then transcribed and exported to a flat

Figure 5.1. (following page) Image outputs generated by the described image analysis algorithms, from which morphometric features were extracted and employed to quantify and characterise specific immunohistochemical biomarkers in the specimen's distal gut. (A) A portion of a digitised histological image, approximately one sixteenth of the full image used in the present study. (B) Binary image created during the image segmentation process, where the empty space is differentiated by inverting

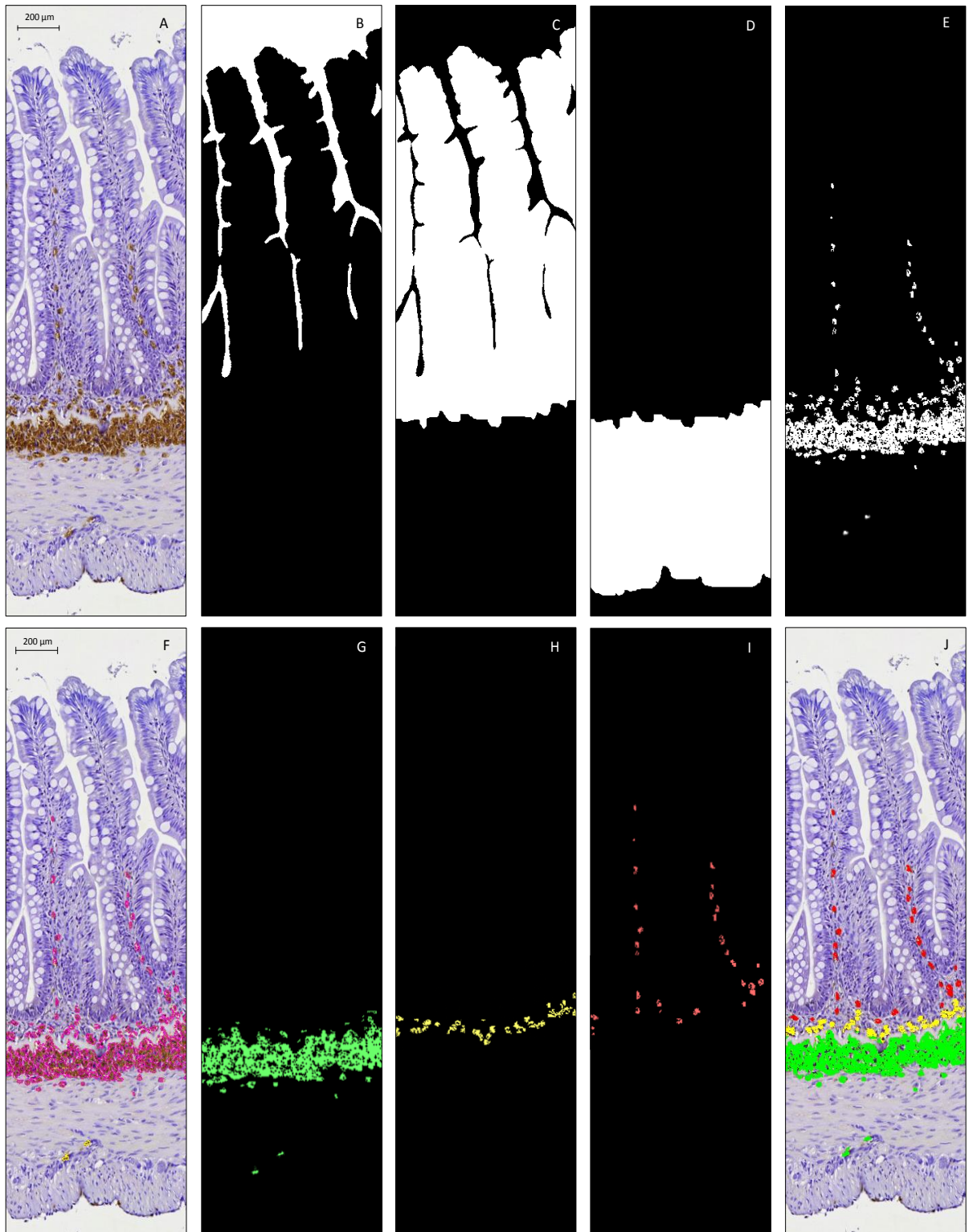


Figure 5.1. (continued from previous page) the image to its negative and through intensity differentiation, which in turn allows accurate recognition of the peritoneal edge of the *muscularis externa* and the internal intestinal lumen. (G, H, I) Regions within the established threshold ranges that were recognised, quantified and had overlay masks reproduced into Figures F and J. Correspondingly, the total immunohistochemically stained area for the entire tissue area (F, in pink), for the submucosal tissue (J, in green), for the zone above the *stratum compactum* (J, in yellow) and for the remaining mucosa (J, in red).

database file. Quantitative variables were expressed as mean and standard deviations (SD), unless otherwise specified.

5.2.8. Statistical analysis

Prior to statistical analysis, data were checked for normality and homogeneity of variance by using the Kolmogorov-Smirnov and Levene's test, respectively. All data satisfying both assumptions either with or without the need for transformation, were assessed by generalised linear mixed models (GLMM) with nested random factors, using the lme4 package (Bates & Maechler, 2010) provided by the statistical software R (Version 3.0.1, Bell Laboratories, Lucent Technologies, New Jersey, USA). An approximate F test on the least-square means was used to estimate the significance of difference for each treatment group in each comparison and Markov Chain Monte Carlo (MCMC) algorithms employed to give an estimation of probability for the random effect modelling. Thereafter, in order to determine if particular pairs of values were significantly different from each other Tukey's *post-hoc* multiple comparison tests were employed. Differences were considered statistically significant when p -value < 0.05.

5.3. Results

5.3.1. Intestinal histomorphology

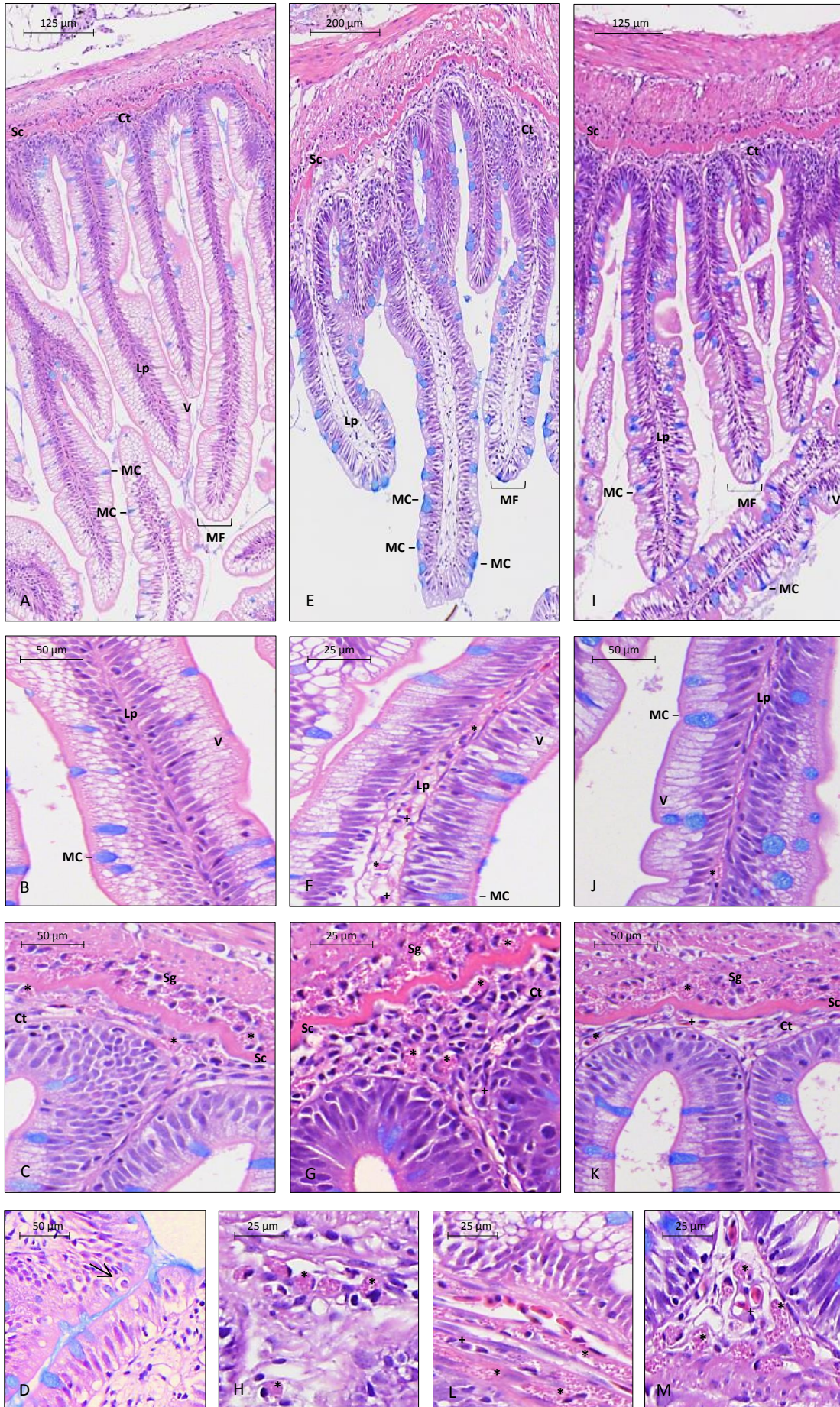
According to the normal histomorphological features previously described for salmonid intestines (Bullock, 1963; Løkka *et al.*, 2013), fish fed the fish meal and the immunostimulant diets exhibited normal histology of the distal intestine, characterised by tall mucosal folds; thin *lamina propria* and a submucosa with low to moderate numbers of intraepithelial leucocytes; presence of well-differentiated enterocytes with highly to moderate supranuclear vacuolisation and basally located nuclei (Figure 5.2. A-C, I-K). In contrast, inclusion of soybean meal in the diet induced histopathological changes in the distal intestine similar to those previously reported (Van den Ingh & Krogdahl, 1990; Baeverfjord & Krogdahl, 1996). The fish showed a progression of changes consistent with SBM-induced enteropathy, comprising a reduction of the normal supranuclear vacuolisation

of the absorptive cells in the intestinal epithelium; shortening of the height of the mucosal folds with an increased amount of connective tissue: and an increase of the *lamina propria* within the mucosal folds due to a prominent mixed leucocyte infiltration, including some eosinophilic granule cells (Figure 5.2 E-H).

5.3.2. Biomarker immunolabelling – visual observations of labelling pattern

5.3.2.1. *Cell proliferation and regeneration (PCNA)*. The antibody against proliferating cell nuclear antigen reacted against a population of dividing epithelial cells at the base of the mucosal folds, although a few immunoreactive nuclei-proliferating-enterocytes could also be seen scattered along the entire intestinal fold (Figure 5.3, arrows). The labelling profile observed for fish fed the immunostimulant diet did not differ substantially from the fish fed the fish meal control diet (Figure 5.3 G, I). The soybean meal feed seemed to have caused an increase in the PCNA-positive proliferative compartment at the base of the folds, since fish fed the SBM diet had longer stretches of PCNA reactive cells than those fed the other diets (Figure 5.3 J-K).

Figure 5.2. (following page) Representative images of morphological variations encountered across the distal intestine of Atlantic salmon fed different experimental diets: (A-C) fish meal based control diet, (E-G) diet containing 25 % defatted soybean meal and (I-K) diet with inclusion of immunostimulant ingredients. The morphology of fish meal fed fish is considered as being the normal standard, whereas fish fed soybean meal reflect an inflammatory response characterised by the loss of vacuoles (V) in the absorptive enterocytes; the widening of *lamina propria* (Lp) in the mucosal folds; an increase of the connective tissue (Ct) between the base of the mucosal folds and the *stratum compactum* (Sc); a relatively increased number of mucous cells (MC) in the epithelium; and an infiltration of inflammatory cells (e.g. asterisk, eosinophilic granule cells; cross, lymphocytes) in the *lamina propria* and submucosa. The morphological profile from fish fed the immunostimulant diet did not differ substantially from the fish meal fed fish. The first row of figures gives a general overview of differences in the simple mucosal folds in between the complex folds that are illustrated in Figure 3.8. The second and third rows detail areas along the simple mucosal folds (MF) and the basal fold area, respectively. Figure D illustrates an intracellular apoptotic body (arrow). Figures H, L and M from the fourth row, picture a mixed population of inflammatory cells distributed throughout the intestinal tissue. (Sg) *Stratum granulosum*. Sections were stained with a combination of haematoxylin-eosin and Alcian blue 8 GX.



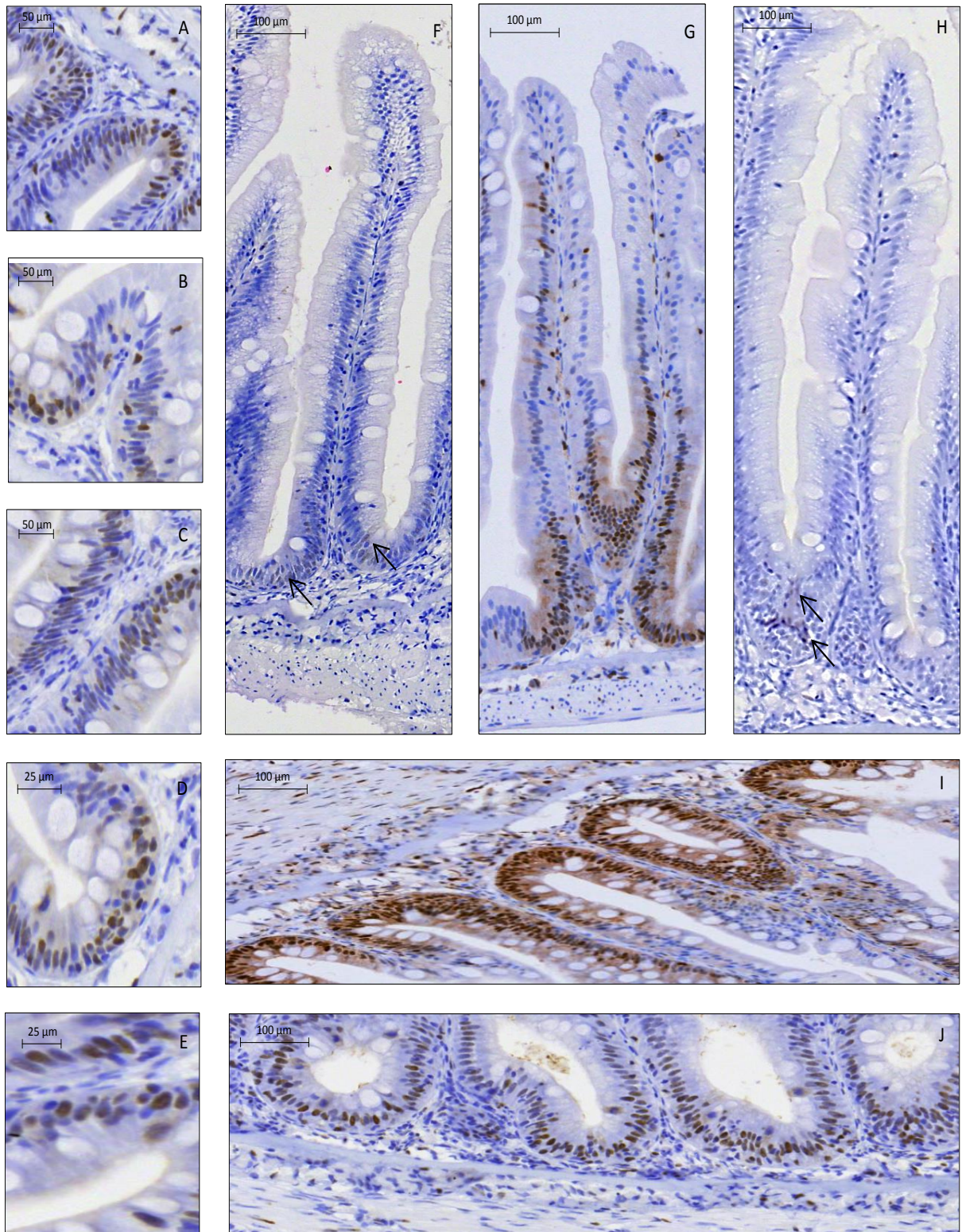


Figure 5.3. Immunohistochemical detection of proliferating cell nuclear antigen (PCNA) in distal intestinal tissue sections of Atlantic salmon fed either a (B, E, F) fish meal based control diet, a (A, C, G, I) diet containing 25 % defatted soybean meal or a (D, H, I) diet with inclusion of immunostimulant ingredients. The antibody directed against PCNA mainly reacted (brown colour) against a population of dividing epithelial cells at the base of the simple mucosal folds, although a few nuclei proliferating enterocytes could also be seen scattered along the entire intestinal fold (arrows). Sections were counterstained with Gill's haematoxylin.

5.3.2.2. *Programmed cell death or apoptosis (TUNEL)*. When intestinal sections from fish fed the different diets were compared, inclusion of immunostimulant ingredients had no apparent effect on the staining profile (Figure 5.4 A-C), with scarce apoptotic cells scattered mostly in the epithelium of the intestinal folds, although some were also seen along the *stratum compactum* (Figure 5.4). In contrast, a change of reactivity pattern was observed in response to SBM, in which fish showed widespread apoptosis (Figure 5.4 G-I, arrows).

5.3.2.3. *Eosinophilic granule cells (Active Caspase-3)*. Immunoreactive cells filled with strongly stained cytoplasmic granules, characteristic of eosinophilic granule cells (EGCs), were distributed along both sides of the *stratum compactum* (Sc) forming the continuous layer of the *stratum granuloseum* (Sg), Figure 5.5 D-E. Most cells were embedded in the external edge (Sc_{ext}) of the *stratum compactum*, whereas the internal edge (Sc_{int}) and the sub-epithelial layer of the *lamina propria* contained noticeably fewer cells (Figure 5.2; Figure 5.5 F and K). In the Sc and the *muscularis* layer, numerous EGCs were in close contact with blood capillaries (Figure 5.2 L). In both control and immunostimulant diets the Sg was rich in EGCs (Figure 5.5 A-C), but numbers seemed to be higher for fish fed the SBM diet. Besides being prominent in the subepithelial connective tissue along the Sc, the *lamina propria* and intestinal submucosa of SBM fed fish became infiltrated with immunostained cells (Figure 5.5 G-I).

Figure 5.4. (following page) Apoptosis labelled by a TUNEL assay in distal intestinal tissue sections of Atlantic salmon fed either a (A, B) fish meal based control diet, a (G-I) diet containing 25 % defatted soybean meal or a (C) diet with inclusion of immunostimulant ingredients. The majority of the TUNEL-positive apoptotic cells were dispersed at the uppermost

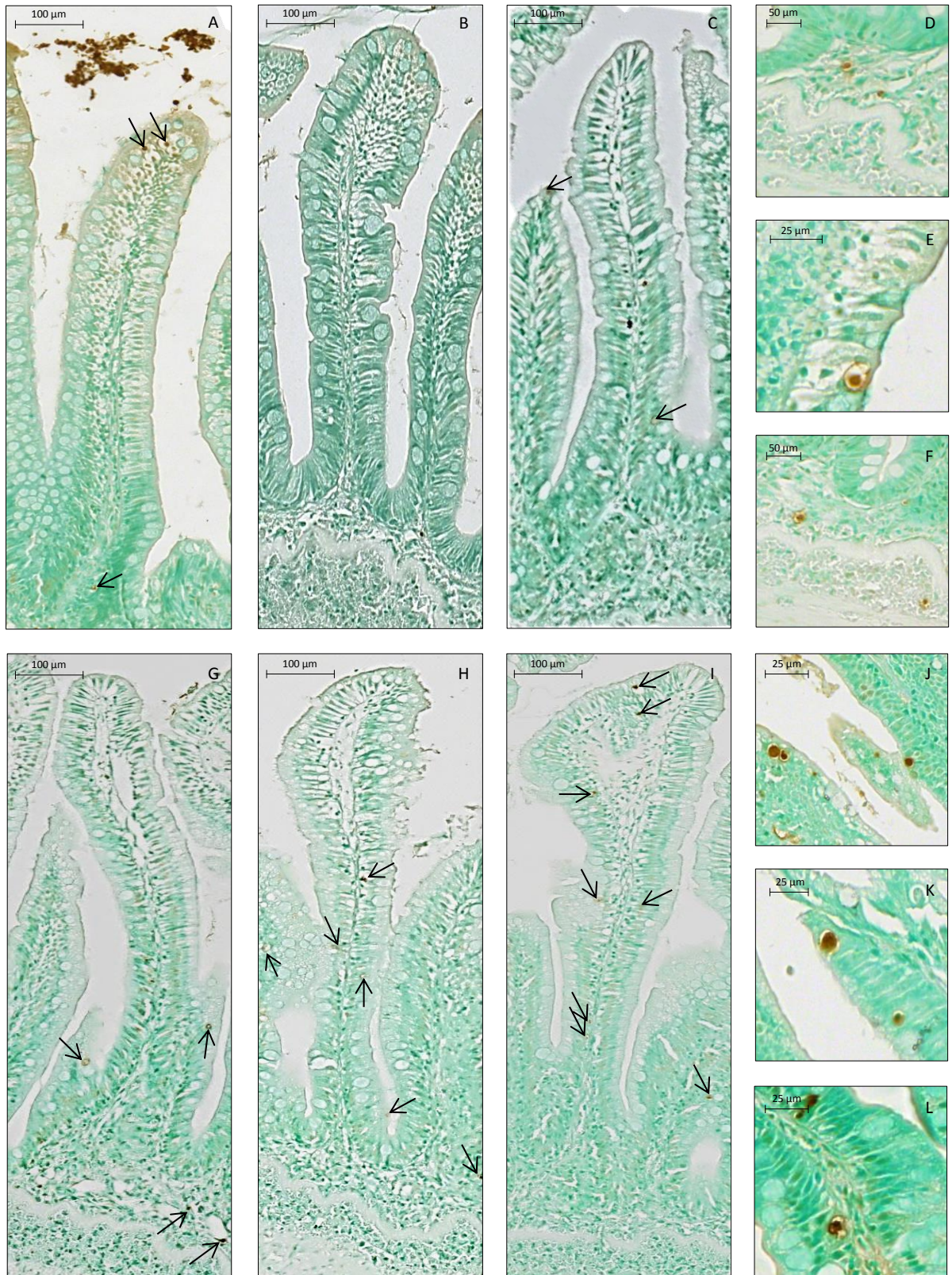


Figure 5.4. (continued from previous page) layer of the epithelium of the intestinal folds. (D-F, J-L) Several intracellular apoptotic bodies showing characteristic features of cell death, i.e. fragmented nucleus, rounding eosinophilic cytoplasm, chromatin condensation and marginalisation. Note the debris and detached tissue in the intestinal lumen from Figure A showing strong immunostaining reaction (brown colour) which is typical of apoptotic fragments. Intestinal sections were counterstained with methyl green.

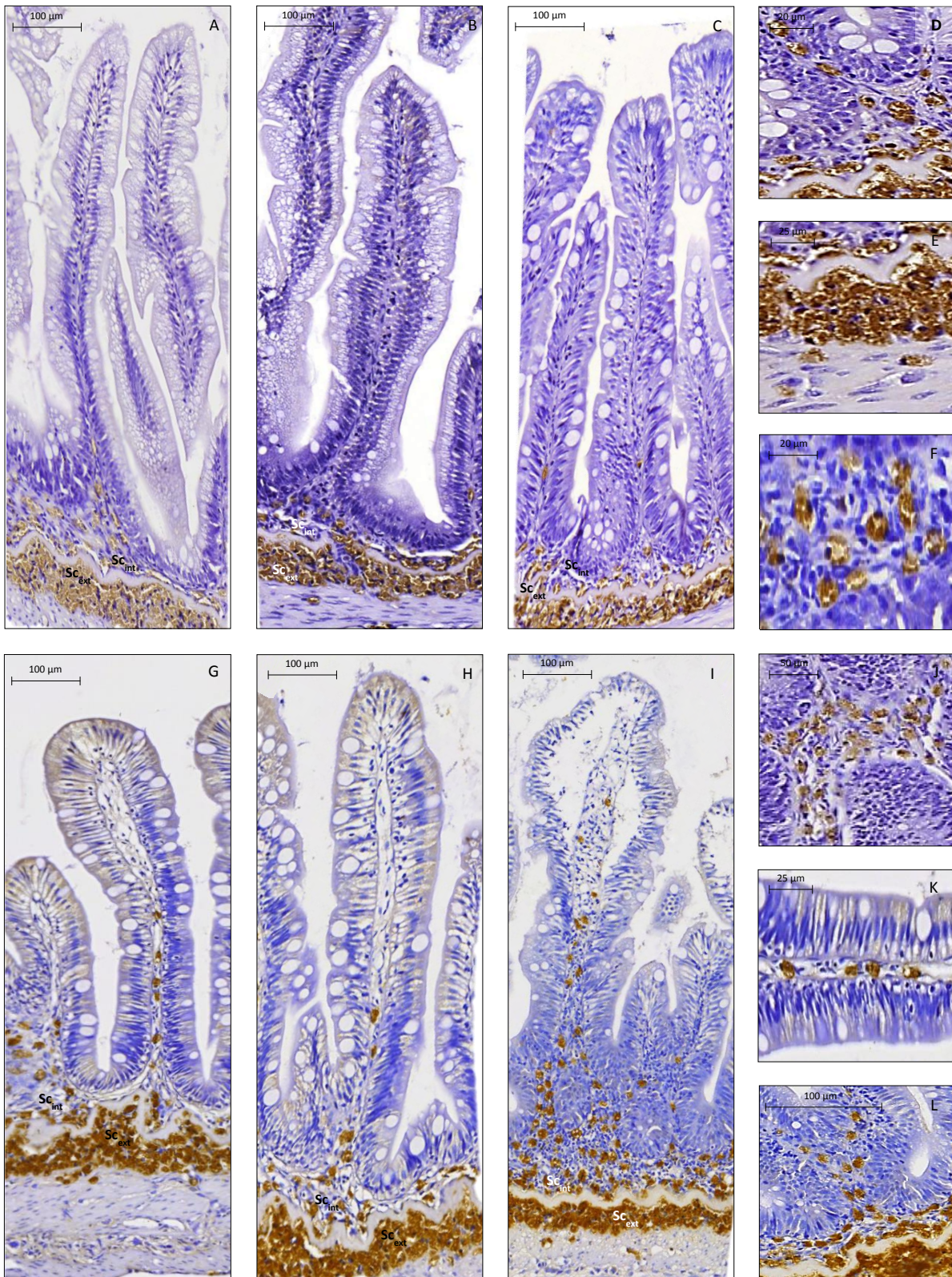


Figure 5.5. Immunostained eosinophilic granule cells (EGCs) in distal intestinal tissue sections of Atlantic salmon fed either a (A) fish meal based control diet, (B, C) a diet with inclusion of immunostimulant ingredients or (G-I) diet containing 25 % defatted soybean meal. A population of EGCs is observed distributed throughout the intestinal tissue with a relatively high number along the external edge of the *stratum compactum* (Sc_{ext}) forming a continuous layer, the *stratum*

5.3.2.4. *T-cell-like cells (CD3ε)*. Positive immunoreactive cells comprised a population of lymphocytes, exhibiting a pattern suggestive of cell membrane or cytoplasmic staining but no nuclear staining (Figure 5.6 A-F). Likewise, in the basal area of the mucosal folds and along the *stratum granulosum* where a population of granule cells featured, a weak diffuse reaction was commonly observed (Figure 5.6 H, J, K). The staining profile seen for fish fed the immunostimulant diet did not differ substantially from the fish fed the fish meal control diet (Figure 5.6 G-I), where the CD3ε antibody reacted against a cell population residing along the entire length of the mucosal folds in a basal intraepithelial position. Occasional reactive cells were found scattered along the *lamina propria* and submucosa. In fish fed the SBM, the positively reactive cells had a less regular position in the epithelium, occupying sites at different heights of the epithelium. Also a moderate increase in the number of anti-CD3ε reactive cells in the widened *lamina propria* and submucosa was also seen (Figure 5.6 J-L).

Figure 5.5. (continued from previous page) *granulosum* (Sg). Positive cells were rarer between the base of the epithelium and the *stratum compactum* (Sc), although some positive cells were found to be dispersed in the immediate vicinity of the mucosal folds. By contrast, in tissue sections from fish fed the soybean meal diet these cells seemed to have increased in number, and besides being prominent in the subepithelial connective tissue along the Sc, the *lamina propria* and intestinal submucosa showed highest infiltration with such immunostained cells. (E-D and J-L) Details of reactive EGCs (brown colour) dispersed in different areas of the intestinal folds and submucosa from fish fed with fish meal and SBM, respectively. (Sc_{int}) Internal edge of the Sc. Intestinal sections were counterstained with Harris's haematoxylin, and the immunoreactivity demonstrated by brown staining.

Figure 5.6. (following page) Immunoreactivity to the antibody directed against a CD3ε epitope. Immunoreactive cells exhibit a pattern suggestive of cell membrane or cytoplasmic staining. (A-F) Figure shows distal intestinal tissue sections of Atlantic salmon fed either a (G, H) fish meal based control diet, a (J-L) diet containing 25 % defatted soybean meal or (I) a diet with inclusion of immunostimulant ingredients.

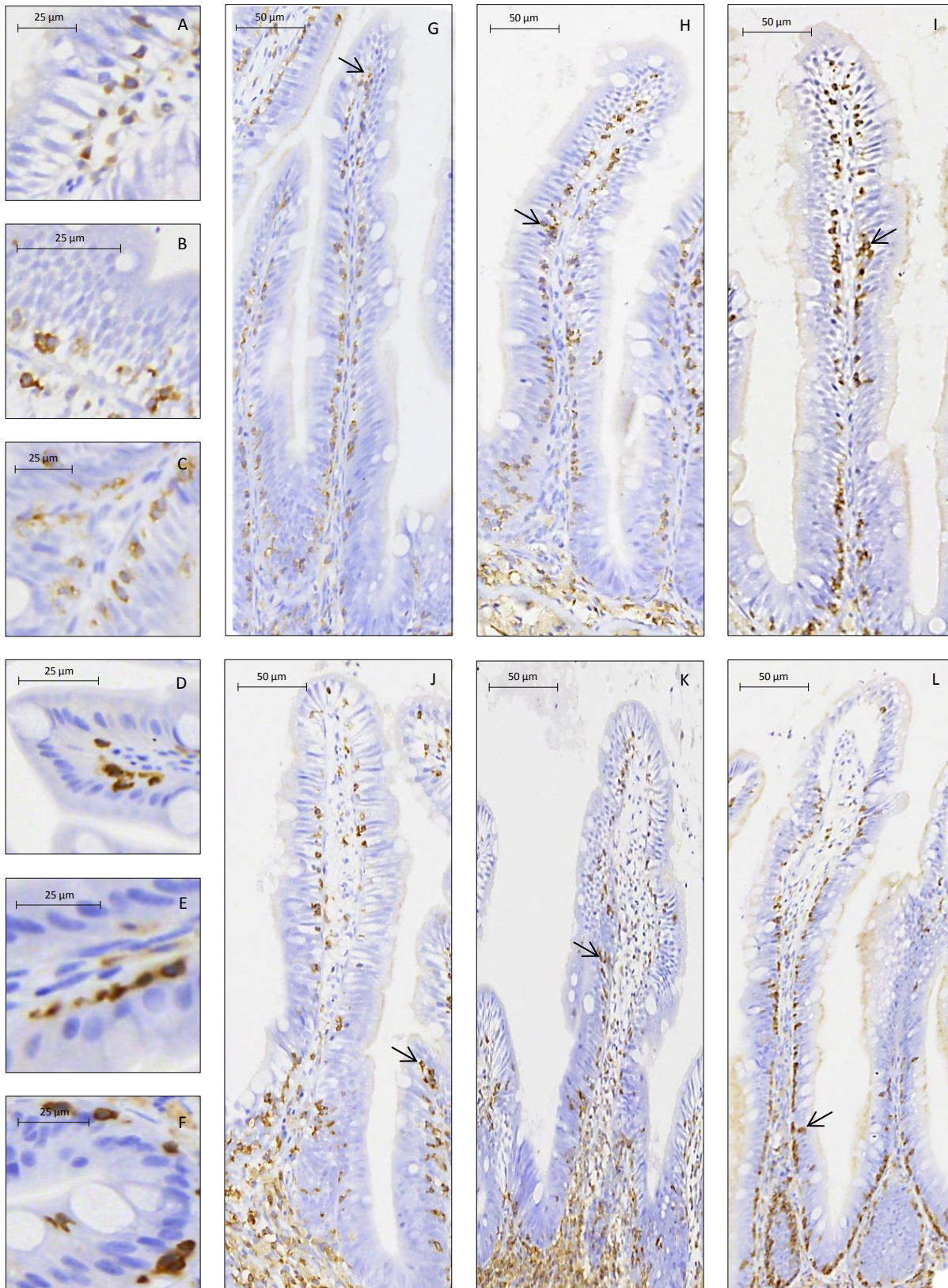


Figure 5.6. (continued from previous page) Positively stained cells (brown colour) appear to comprise a population of leucocytes which was located singularly or in small clusters (arrows) in the basal part of the intraepithelium along the mucosal folds although a few more were found scattered along the the *lamina propria* and submucosa, where a population of granule cells is also evident (yellowish granules). Intestinal sections were counterstained with Gill's haematoxylin.

5.3.2.5. Mobilisation of stress related proteins for regenerative processes (HSP 70).

Immunohistochemical localisation of heat shock protein did not always follow the expected labelling pattern. Although in appropriately expressing control tissue sections the elected epitope showed positive staining, the signal was generally weaker than anticipated (Figure 5.7, arrows indicate that immune-expression tended to be most pronounced in the region of highly differentiated tumour areas).

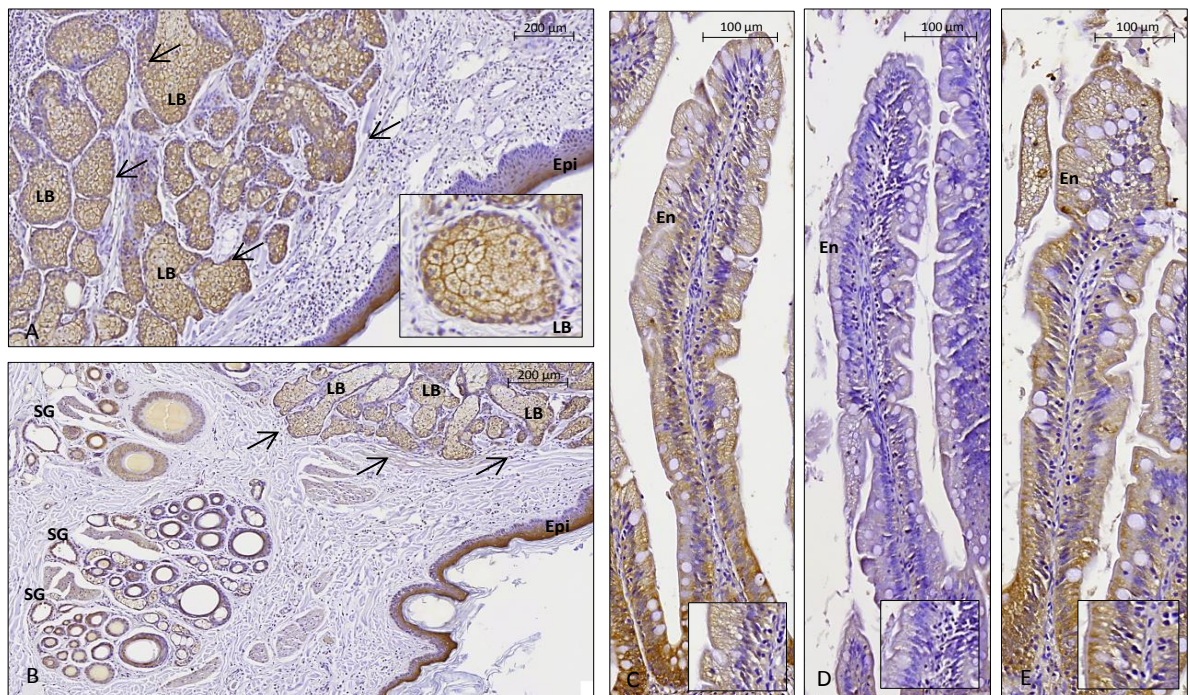


Figure 5.7. Immunohistochemical localisation of heat shock protein 70 (HSP 70) immunoreactive cells recognised by an antibody, which labels both the constitutive (HSP 73) and inducible (HSP 72) forms of HSP 70 in various tissues. (A, B) Canine cutaneous carcinoma tissues used as positive controls, showing strong expression in the cytoplasm and nuclei of integumental cancerigeous cells. Occasionally, immune-expression trended toward highly differentiated tumour areas (arrows) and the outmost layers of the epidermis (*i.e. stratum spinosum and granulosum* from the inside out). (C, D, E) Teleost intestinal sections where immunostaining was expected along a population of epithelial cells at the tip of the simple mucosal folds, however the immunoreactivity was once again not coherent or reproducible with respect to that previously obtained by other authors. (LB) Lobule of epithelial cells from the cutaneous tumour. (SG) Sweat glands. (Epi) Epidermis. (En) Intestinal enterocytes. Sections were counterstained with Gill's haematoxylin.

Additionally, the antibody occasionally showed inconsistent staining and inappropriate localisation of signal. Similarly, for Atlantic salmon intestinal sections where immunoreactivity was expected along a population of epithelial cells at the tip of the simple mucosal folds, the immunostaining signal was consistently minimal, being confined to less than 5 % of the mucosal folds and in some cases even being completely absent (Figure 5.7 D-E).

5.3.2.6. *Facilitation of nutrient uptake and ion transport (Na⁺K⁺-ATPase).* The distribution pattern of the Na⁺K⁺-ATPase staining for the control tissues from sea-water adapted Atlantic salmon, was clear in gill and kidney sections. In fish gills intense immunoreaction was confined to large spherical cells within the surface interlamellar regions of the filamental epithelium and the proximal end of the secondary lamellae (Figure 5.8 A, arrows), which correlated with the location of the so-called mitochondrial-rich ionocytes or chloride cells.

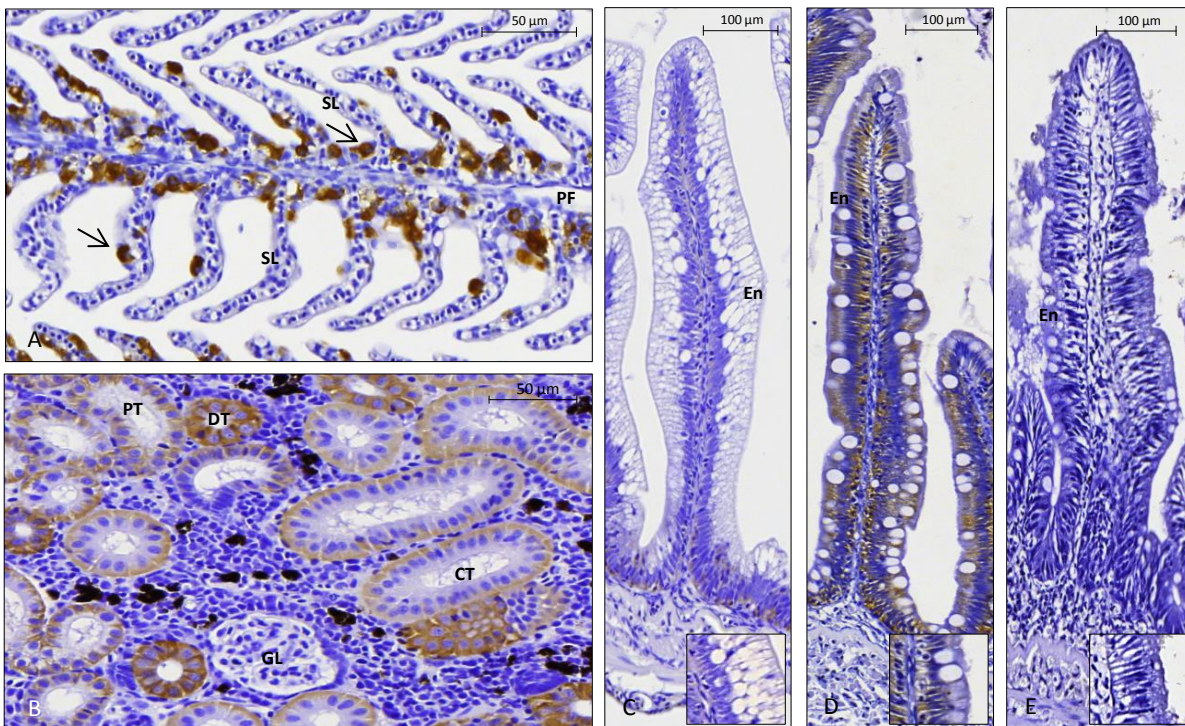


Figure 5.8. Immunohistochemical detection of Na⁺K⁺-ATPase immunoreactive cells (brown colour) recognised by an antibody against the conserved α -subunit region, in seawater-adapted Atlantic salmon gill, kidney and intestinal tissue sections. (A) In gills, intense immunoreaction was confined to mitochondrial-rich ionocytes or chloride cells (arrows). (B) In kidneys, the antibody stained the basolateral epithelium of proximal, distal convoluted and collecting tubules.

In kidney tissue, the antibody stained the basolateral epithelium of proximal and distal tubules, while no immunoreactivity was observed in the glomerulus (Figure 5.8 B), this being in accordance with previously published results. Although the immunoreaction for Na⁺K⁺-ATPase within the control gill and kidney tissues was considered effective, the staining obtained with intestinal sections incubated with the same antibody, using an identical staining protocol, did not show the same degree of specificity or consistency. Immunostaining was expected across the basolateral and apical surfaces of the columnar epithelial cells that line most of the luminal surface of the intestine, and this was not observed. Instead, non-specific staining was widely diffused throughout most of the mucosal fold tissue area.

5.3.3. Quantitative image analysis of immunohistological labelling

The results of quantification (*i.e.* immunoreactive indices and relative staining intensity) for the four successful immunological labelling assays are summarised in Figures 5.9 and 5.10.

5.3.3.1. *Cell proliferation and regeneration (PCNA)*. A substantial increase in the percentage of labelled proliferating cells from the distal intestine of fish fed the SBM diet was observed when compared to fish fed the other two experimental diets (Diet A, 0.468 ± 0.440 %; Diet B, 2.870 ± 4.890 %; Diet C, 0.551 ± 1.095 %; $p_{\text{MCMC Total}} = 0.174$; $p < 0.05$). The overall mean labelling index for the submucosal tissue (SUB) was 0.952 ± 1.543 %, for the base of the mucosal folds (SUP) was 2.181 ± 4.070 % and for the upper remaining area of the folds (MUC) was 1.397 ± 2.200 %. The positive immunoreactivity for the lower half of the folds and interfold valleys was greater than that for the remainder of the mucosal folds

Figure 5.8. (continued from previous page) However no immunoreactivity (brown colour) was observed for the glomerulus. Note the pyknotic debris and melanin granules (melanomacrophages) scattered throughout the tissue. (C-E) Intestinal sections incubated with the same antibody revealed no equivalent specific or consistent immunoreactive labelling. (PF) Primary filament / primary lamellae. (SL) Secondary lamellae. (PT) Proximal convoluted tubules. (DT) Distal tubule. (CTb) Collecting tubules. (GL) Glomerulus. (En) Intestinal enterocytes. Sections were counterstained with Harris's haematoxylin.

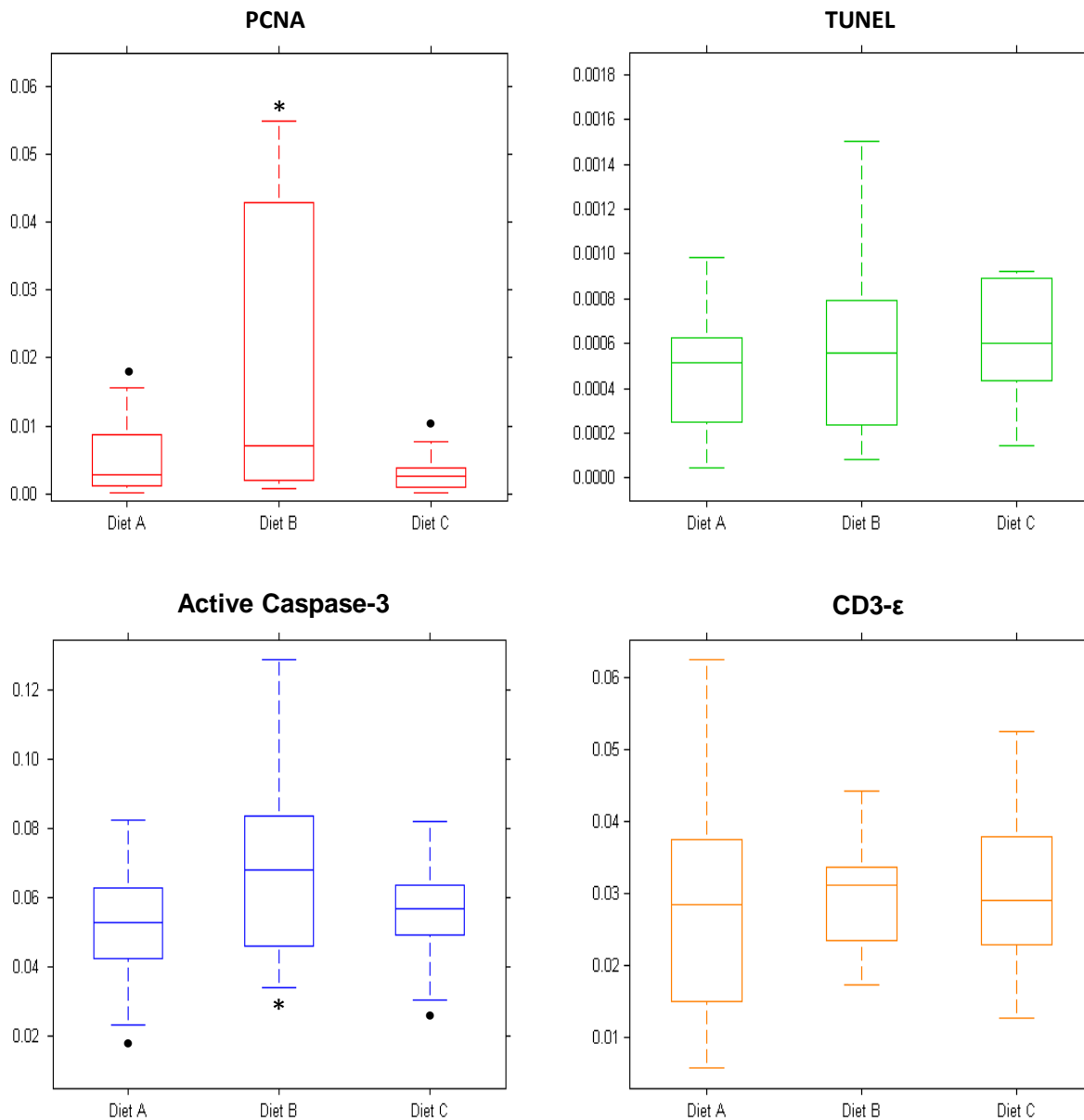
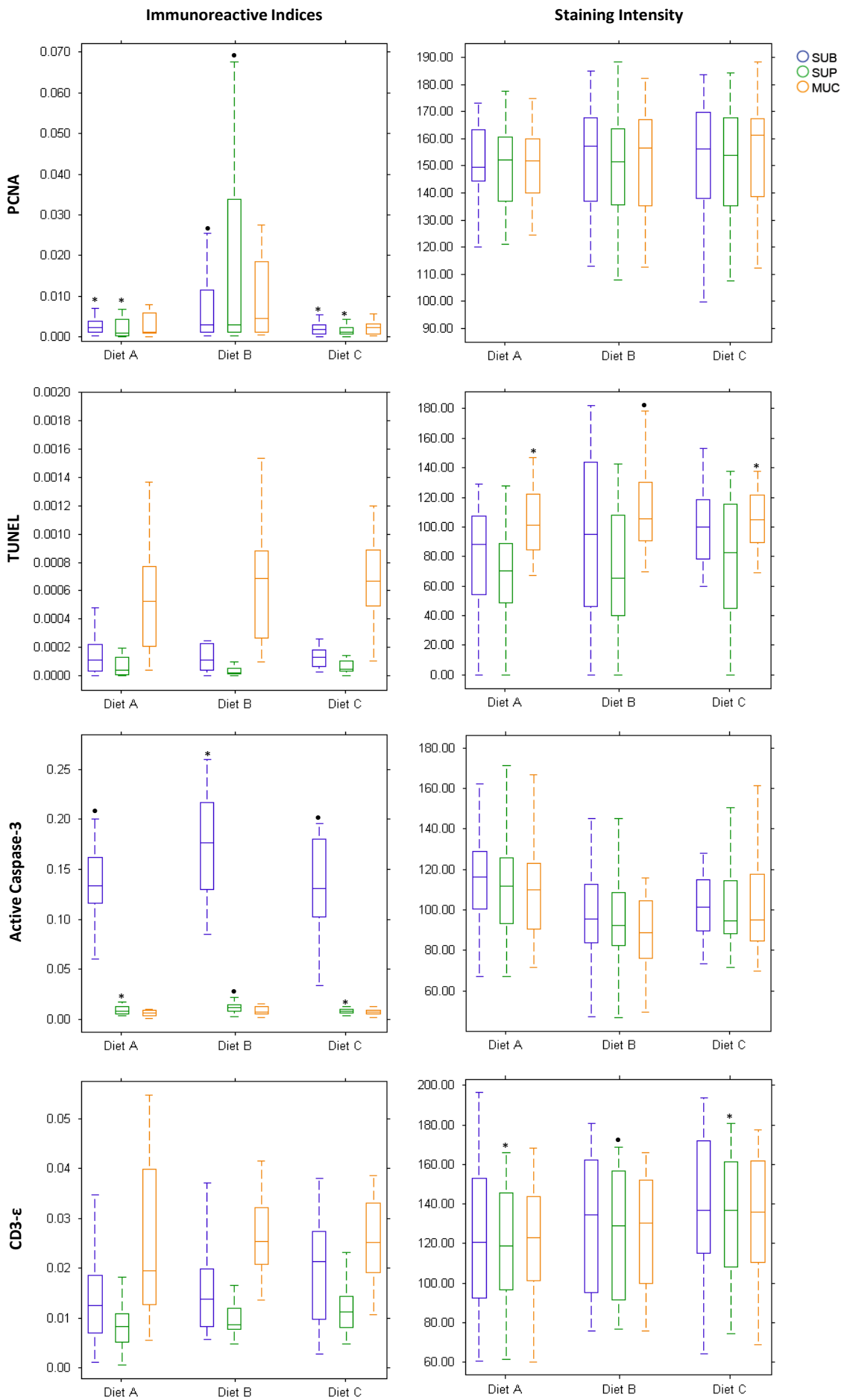


Figure 5.9. Immunoreactive indices (*i.e.* staining ratio per unit area) of the histolabelling with four distinct biomarkers, performed in distal intestinal histological sections from Atlantic salmon fed different experimental diets. (Diet A) Standard fish meal based feed used as control diet. (Diet B) Soybean meal based feed. (Diet C) Standard feed with inclusion of immunostimulant ingredients. (PCNA) Proliferating cell nuclear antigen. (TUNEL) Terminal deoxynucleotidyl transferase dUTP nick end labelling. (Active Caspase-3) Protein member from the cysteine aspartic acid protease family. (CD3 ϵ) T-cell surface glycoprotein cluster of differentiation epsilon chain. The middle line of the box plot indicates the median for each group, the box edges mark the distribution between the 25th and 75th percentiles, while the whiskers represent the maximum and the minimum values without being outliers. Different symbols indicate significant mean value differences at $p < 0.05$ ($n = 36$ histological frames per treatment group; Hierarchical GLMM: tank [treatment] fixed factor with 3 levels).

and submucosal tissue. In contrast, the overall labelling ratios for fish fed the fish meal diet and the immunostimulant diet, were substantially lower and did not appear to differ between the different segment zones (Diet A, $\text{SUB} 0.266 \pm 0.196 \%$, $\text{SUP} 0.265 \pm 0.332 \%$, $\text{MUC} 0.278 \pm 0.273 \%$; Diet C, $\text{SUB} 0.257 \pm 0.302 \%$, $\text{SUP} 0.317 \pm 0.764 \%$, $\text{MUC} 0.372 \pm 0.736 \%$; $p_{\text{MCMC SUB}} = 0.402$, $p_{\text{MCMC SUP}} = 0.133$, $p_{\text{MCMC MUC}} = 0.176$, $p > 0.05$). Furthermore, there was no apparent difference in the mean intensity values for the proliferative-staining at the base of the folds and upper half of the mucosal folds when compared with the submucosal tissue of other experimental diets ($p_{\text{MCMC } \rho\text{SUB}} = 0.368$, $p_{\text{MCMC } \rho\text{SUP}} = 0.813$, $p_{\text{MCMC } \rho\text{MUC}} = 0.347$, $p > 0.05$), with mean intensity values of 150.79 ± 22.04 pi (mean pixel intensity units).

5.3.3.2. *Programmed cell death or apoptosis (TUNEL)*. The results revealed no significant differences in the overall immunoreactive indices for intestinal apoptotic cells among the different experimental dietary groups (Diet A, $0.065 \pm 0.082 \%$; Diet B, $0.057 \pm 0.037 \%$; Diet C, $0.073 \pm 0.061 \%$; $p_{\text{MCMC Total}} = 0.399$; $p > 0.05$). Spatial distribution of apoptotic positive areas was not, however, similar among tissues, as a higher density of apoptotic bodies was observed in the upper half of the mucosal folds, especially for fish fed the SBM diet when compared to fish fed the control and immunostimulants diets (Diet A, $\text{SUB} 0.015 \pm$

Figure 5.10. (following page) Immunoreactive indices (*i.e.* staining ratio per unit area) and relative staining intensity (mean pixel values) of histolabelling with four distinct biomarkers, performed in distal intestinal histological sections from Atlantic salmon fed different experimental diets. Tissue area was partitioned into three distinct zones: (SUB) submucosal area, (SUP) above the *stratum compactum* up to 15-30 cell thickness above the basal area of the intestinal mucosal folds, and (MUC) remaining mucosal area / upper half of the intestinal folds. (Diet A) Standard fish meal based feed used as control diet. (Diet B) Soybean meal based feed. (Diet C) Standard feed with inclusion of immunostimulant ingredients. (PCNA) Proliferating cell nuclear antigen. (TUNEL) Terminal deoxynucleotidyl transferase dUTP nick end labelling. (Active Caspase-3) Protein member from the cysteine aspartic acid protease family. (CD3 ϵ) T-cell surface glycoprotein cluster of differentiation epsilon chain. The box plots are explained in the legend from Figure 5.10. Different symbols indicate significant mean value differences at $p < 0.05$, when different dietary treatment groups were compared ($n = 36$ histological frames per treatment group; Hierarchical GLMM: tank [treatment] fixed factor with 3 levels).



0.015 %, $\rho_{\text{SUB}} 0.034 \pm 0.117$ %, $\rho_{\text{MUC}} 0.057 \pm 0.040$ %; Diet B, $\rho_{\text{SUB}} 0.024 \pm 0.036$ %, $\rho_{\text{SUB}} 0.004 \pm 0.004$ %, $\rho_{\text{MUC}} 0.066 \pm 0.041$ %; Diet C, $\rho_{\text{SUB}} 0.048 \pm 0.120$ %, $\rho_{\text{SUB}} 0.007 \pm 0.007$ %, $\rho_{\text{MUC}} 0.079 \pm 0.062$ %; $p_{\text{MCMC SUB}} = 0.343$, $p > 0.05$; $p_{\text{MCMC SUP}} = 0.256$, $p > 0.05$; $p_{\text{MCMC MUC}} = 0.316$, $p < 0.05$). Moreover, no obvious differences in the mean intensity values for the apoptotic-staining at the base of the folds and submucosal tissue areas were noticed between the different dietary groups ($p_{\text{MCMC } \rho\text{SUB}} = 0.440$, $p_{\text{MCMC } \rho\text{SUP}} = 0.468$, $p > 0.05$), although a trend for more dense staining was perceived for the upper half of the mucosal folds, especially for fish fed the SBM diet ($p_{\text{MCMC } \rho\text{MUC}} = 0.220$, $p < 0.05$), whereas a lighter staining was apparent for the segmented area above the *stratum compactum* and across the base of the folds (Diet A, $\rho_{\text{SUB}} 83.39 \pm 35.47$ pi, $\rho_{\text{SUP}} 67.30 \pm 47.00$ pi, $\rho_{\text{MUC}} 103.33 \pm 22.67$ pi; Diet B, $\rho_{\text{SUB}} 93.7 \pm 52.10$ pi, $\rho_{\text{SUP}} 64.5 \pm 46.7$ pi, $\rho_{\text{MUC}} 109.32 \pm 28.90$ pi; Diet C, $\rho_{\text{SUB}} 100.17 \pm 25.19$ pi, $\rho_{\text{SUP}} 76.95 \pm 41.45$ pi, $\rho_{\text{MUC}} 104.30 \pm 20.98$ pi).

5.3.3.3. *Eosinophilic granule cells (Active Caspase-3)*. Immunoreactive indices were greater in fish fed the SBM diet, whereas the positive reaction for the intestinal sections from fish fed the other two diets was significantly lower, although not significantly dissimilar to one another (Diet A, 5.49 ± 2.15 %; Diet B, 6.91 ± 2.47 %; Diet C, 5.32 ± 2.19 %; $p_{\text{MCMC Total}} = 0.102$; $p < 0.05$). Besides having the more prevalent staining in the submucosal tissue areas of the intestine for all treatment groups, fish fed the SBM diet had the longest stretches of caspase-3 staining along the basal area of the mucosal folds, and alongside the internal edge of the *stratum compactum* (Diet A, $\rho_{\text{SUB}} 14.13 \pm 4.56$ %, $\rho_{\text{SUP}} 0.886 \pm 0.459$ %, $\rho_{\text{MUC}} 0.637 \pm 0.414$ %; Diet B, $\rho_{\text{SUB}} 17.07 \pm 5.03$ %, $\rho_{\text{SUP}} 1.228 \pm 0.703$ %, $\rho_{\text{MUC}} 0.890 \pm 0.590$ %; Diet C, $\rho_{\text{SUB}} 13.35 \pm 5.02$ %, $\rho_{\text{SUP}} 0.847 \pm 0.436$ %, $\rho_{\text{MUC}} 0.798 \pm 0.623$ %; $p_{\text{MCMC SUB}} = 0.104$, $p < 0.05$; $p_{\text{MCMC SUP}} = 0.112$, $p < 0.05$; $p_{\text{MCMC MUC}} = 0.239$, $p > 0.05$). While no noteworthy variations in the immunolabelling intensity were seen within tissue sections from distinct dietary groups nor across the three tissue segments ($p_{\text{MCMC } \rho\text{SUB}} = 0.193$, $p_{\text{MCMC } \rho\text{SUP}} = 0.158$, $p_{\text{MCMC } \rho\text{MUC}} = 0.211$, $p > 0.05$), staining for sections from fish fed SBM tended to be slightly less intense. Mean overall intensity values (*i.e.* for all experimental groups), were 105.35 ± 27.46 pi.

5.3.3.4. *T-cell-like cells (CD3ε)*. Whereas the overall staining indices were apparently higher for fish fed the diet containing immunostimulant ingredients (Diet A, 2.876 ± 1.627 %; Diet B, 3.023 ± 0.867 %; Diet C, 3.166 ± 1.085 %; $\rho_{\text{MCMC Total}} = 0.4180$; $p > 0.05$), this was shown not to be significantly different since there was substantial overlap from data obtained for all three tissue segments examined for the two other diets. (Diet A, $\text{SUB} 1.463 \pm 0.992$ %, $\text{SUP} 1.012 \pm 0.714$ %, $\text{MUC} 2.450 \pm 1.576$ %; Diet B, $\text{SUB} 1.598 \pm 0.993$ %, $\text{SUP} 0.991 \pm 0.370$ %, $\text{MUC} 2.599 \pm 0.696$ %; Diet C, $\text{SUB} 2.022 \pm 1.051$ %, $\text{SUP} 1.163 \pm 0.511$ %, $\text{MUC} 2.479 \pm 0.785$ %; $\rho_{\text{MCMC SUB}} = 0.175$, $\rho_{\text{MCMC SUP}} = 0.235$, $\rho_{\text{MCMC MUC}} = 0.247$, $p > 0.05$). There seemed to be no differences in the staining intensity of tissue samples observed, except for the area at the base of the mucosal folds and interfold valleys where fish fed the immunostimulant diet seemed to have a denser staining profile (Diet A, $\rho_{\text{SUB}} 125.18 \pm 38.05$ pi, $\rho_{\text{SUP}} 120.68 \pm 29.97$ pi, $\rho_{\text{MUC}} 121.38 \pm 29.39$ pi; Diet B, $\rho_{\text{SUB}} 132.25 \pm 35.16$ pi, $\rho_{\text{SUP}} 125.41 \pm 33.86$ pi, $\rho_{\text{MUC}} 125.46 \pm 32.02$ pi; Diet C, $\rho_{\text{SUB}} 137.44 \pm 41.21$ pi, $\rho_{\text{SUP}} 133.10 \pm 35.88$ pi, $\rho_{\text{MUC}} 133.11 \pm 35.01$ pi; $\rho_{\text{MCMC } \rho_{\text{SUB}}} = 0.612$; $p > 0.05$; $\rho_{\text{MCMC } \rho_{\text{SUP}}} = 0.146$, $p < 0.05$; $\rho_{\text{MCMC } \rho_{\text{MUC}}} = 0.356$, $p > 0.05$).

5.4. Discussion

The turnover of intestinal cells is a physiological mechanism which helps to ensure the structural and functional integrity of the intestine, this in turn playing an essential role in intestinal homeostasis and inflammation (Aherne *et al.*, 2013). Normal homeostasis of the intestinal epithelium is a dynamic process maintained by a balance between proliferation, migration, differentiation and apoptosis (Hong *et al.*, 1997). This process is regulated by numerous luminal nutrients, hormones, growth factors and / or cytokines, which may be influenced by several dietary elements.

While studies examining intestinal responses to dietary modulation in salmonid fish are common, information on the relationship between cellular differentiation, shedding and migration and how the dynamic equilibrium between these processes is influenced by diet is lacking. Thus, understanding how these cellular responses vary in the presence of different

dietary ingredients should help strengthen our understanding of the basic mechanisms involved in intestinal cell turnover and in turn help selection of optimal feed ingredients in the future. This study therefore attempts to provide a provisional quantitative assessment of selected functional changes occurring in the intestine during normal and pathological processes leading to teleost intestinal disorders, with particular emphasis on the characterisation of inflammation generated by an enteropathy-causing diet (*i.e.* unrefined soybean meal diet), through the investigation of quantifiable IHC biomarkers.

Soybean meal induced enteritis in Atlantic salmon, a widely documented inflammation of the hindgut, is considered to be a suitable model for diet-related mucosal disorders in teleosts. The condition, in which dietary soya saponins seem to affect the differentiation of distal intestinal epithelial cells and compromise overall intestinal integrity, seems analogous to several other pathophysiological intestinal responses. In this study, the morphological characteristics of the inflamed distal intestine of SBM fed fish were identical to those previously reported by other authors (Van den Ingh & Krogdahl, 1990; Baeverfjord & Krogdahl, 1996; Urán, 2008). By contrast the inclusion of immunostimulant in the diets used here, showed little difference from the control diet.

A number of different biomarkers have been used to visualize responses to various dietary ingredients (Sveinbjörnsson *et al.*, 1996; Sanden *et al.*, 2005; Bakke-McKellep *et al.*, 2007a, 2007b; Olsvik *et al.*, 2007; Ronza *et al.*, 2011; Romarheim *et al.*, 2011; Chikwati *et al.*, 2013a, 2013b; *inter alia*). In the present study five different features of tissue response were evaluated to assess the effects of the experimental diets used in the study: (1) cell proliferation and regeneration (PCNA); (2) programmed cell death or apoptosis (TUNEL); (3) eosinophilic granule cells (Active caspase-3) and t-cell like infiltration (CD3ε); (4) mobilisation of stress related protein regenerative processes (HSP 70) and (5) facilitation of nutrient uptake and ion transport (Na⁺K⁺-ATPase).

The selected markers were assessed and initially evaluated based on their assumed pattern of reactivity within positive control tissue sections that were known to express the epitopes of interest. Once a satisfactory staining protocol had been optimised (*i.e.* suitable

fixation, blocking, antigen retrieval and antibody incubation) for the positive tissue controls, in which a specific and strong reaction should be clearly seen indicating the presence and location of the antigen, the protocols were standardised for Atlantic salmon intestine. Despite some of the biomarkers sometimes giving inconclusive staining, most of the biomarkers assessed showed promising results.

5.4.1. Cell proliferation and regeneration (PCNA)

Proliferating cell nuclear antigen is a highly conserved auxiliary protein directly involved in DNA synthesis during all phases of the cell cycle, except the resting phase (Wolf & Dittrich, 1992; Ortego *et al.*, 1994), and is expressed during cell division and proliferation (Kilemade *et al.*, 2002). Cellular proliferation is a critical biological process (Hall *et al.*, 1994a), and plays an important role in compensatory cell renewal after loss of cells critically damaged by apoptosis, and hence is important for maintaining the integrity of fish tissue (Berntssen *et al.*, 2004).

Although teleost fish have less distinct compartmentalisation with regard to intestinal cell proliferation compared to higher vertebrates (Hemre *et al.*, 2004), under normal conditions of homeostasis, proliferating intestinal cells are more restricted to the basal part of intestinal folds (Ortego *et al.*, 1994; Berntssen *et al.*, 2004; Hemre *et al.*, 2004). The results from the present study corroborate this, and although proliferating cells were observed at all levels of the intestinal mucosal folds, labelled PCNA reactive cells were generally more abundant at the base and lower half of the mucosal folds.

The increased cell proliferation and resulting longer stretches of PCNA reactive cells seen in the distal intestine of SBM fed fish, are indicative of an increased rate of cell repair and / or cellular renewal. This may represent an attempt to compensate for an extensive loss of epithelial cells caused by the anti-nutritional factors present in the soya ingredients, which are known to induce enteritis in the fish (Bakke-McKellep *et al.*, 2007b; Romarheim *et al.*, 2011). Sanden *et al.* (2005) and Chikwati *et al.* (2013a) reported a similar response in cell proliferation in the distal intestine of salmon fed SBM. By contrast, the immunostimulant additives used in the fish feeds in the present study, did not seem to produce a similar level

of cell regeneration, as the labelling profile in these fish did not differ substantially from the fish fed the control diet.

5.4.2. Programmed cell death or apoptosis (TUNEL)

As mentioned earlier, intrinsic cell death has a crucial role in the normal development and homeostasis of multicellular organisms (Takle & Andersen, 2007). Under normal cellular kinetics, a balance between cell proliferation and regulated cell death maintains the tissue integrity of the intestine (Hall *et al.*, 1994a, 1994b; Berntssen *et al.*, 2004). Moreover, cell death is essential for many physiological events, including innate and adaptive immune defence mechanisms against extraneous agents. Conversely, it also plays an important role in the pathogenesis of a variety of diseases (Dos Santos *et al.*, 2008). Cell death can be considered as a normal process by which cell population dynamics are correctly maintained (Ferrando *et al.*, 2009). There are two types of cell death: necrosis and apoptosis. They correspond to cell death by extrinsic or intrinsic factors, respectively. Extrinsic factors include mechanical injury, the actions of infectious organisms, or toxic / anti-nutritional substances. Nevertheless, extrinsic factors could induce apoptosis indirectly, *i.e.* via the action of other intrinsic factors such as cytotoxic agents or hormones (Wyllie *et al.*, 1980; Bonga & Van der Meij, 1989). Necrosis is structurally characterised by swelling of cells and cellular compartments, followed by disruption. On the other hand, apoptotic cells show a characteristic sequence of cellular shrinkage, loss of cell-cell contacts, chromatin marginalisation and condensation, followed by eventual breakage of the cell into apoptotic bodies (Rojo & Gonzalez, 1998; Van Cruchten & Van den Broeck, 2002).

Staining of breaks in double or single stranded DNA by terminal transferase mediated dUTP nick end-labelling technique (TUNEL) can not by itself distinguish between DNA fragmentation occurring during apoptosis or necrotic cell death (Weber *et al.*, 2002). However, in the present study TUNEL-positive cells exhibited membrane blebbing and cell body shrinkage consistent with apoptotic cell morphology. Furthermore, the majority of the TUNEL-positive cells were non-contiguous, also consistent with apoptosis (Rojo & Gonzalez, 1998; Saraste & Pulkki, 2000).

The labelling pattern visualised by the TUNEL method, both in respect to the appearance of the cells and their distribution, corroborates previous IHC findings indicative of apoptosis (Bakke-McKellep *et al.*, 2007b; Ostaszewska *et al.*, 2010). The staining was not localised to any particular region of the intestine, but a general staining of epithelial cells scattered along the mucosal folds and across the *stratum granulosum* was observed. The relatively increased number of apoptotic cells in SBM fed fish appeared to be a response to the unidentified anti-nutritional factors in the diet, which induced enteritis. This increase in TUNEL-positive cells may be an indication of cellular recovery via an apoptotic pathway (Bakke-McKellep *et al.*, 2007b). This could partially explain the shortening of the mucosal folds characteristic of the pathological condition in question.

Despite an increasing trend in the number of individual apoptotic cells in the intestine of SBM fed salmon, the lack of a significant increase in the total area of reactivity when compared to the other dietary groups, is most likely due to the sample sizes and the fact that the total stained area was assessed instead of counting individual cells. Denser staining was seen among cells found in the upper half of the mucosal folds. This is not entirely surprising, considering that the intestinal cell turn-over is mediated by the formation of new cells in the crypts of the intestinal folds, which migrate towards the tips of the intestinal folds where they are lost after regulated cell death (Hall *et al.*, 1994b; Berntssen *et al.*, 1999). Also, during the apoptotic process, all cellular constituents including fragmented DNA are packaged into vesicles (*i.e.* more condensed structures consequently resulting in a higher staining intensity) forming apoptotic bodies, in order to be absorbed and recycled by neighbouring tissue and cells (Weber *et al.*, 2002).

5.4.3. Eosinophilic granule cells (Active Caspase-3)

Eosinophilic granule cells (EGCs) are specialised mononuclear cells, which are considered to have a role in inflammation and the host defense of teleosts, and can be found in a variety of tissues, including the gastrointestinal tract, skin and gills (Ezeasor & Stokoe, 1980; Ellis, 1985; Sveinbjørnsson *et al.*, 1996; Murray *et al.*, 2007).

The general morphology, staining characteristics and tissue distribution together with discussion of some of the proposed functions of these cells are thoroughly reviewed in the following Chapter 6 of this thesis and therefore will not be discussed in detail in the present chapter. The question of the exact physiological function of EGCs and the content of their prominent granules remains somewhat controversial, however, cytochemical characteristics and their tissue distribution have led to the suggestion that these cells are analogous to mammalian mast cells (Powell *et al.*, 1993a; Sire & Vernier, 1995; Matsuyama & Iida, 1999; Dezfuli *et al.*, 2008). Studies have shown that an increase in the number of these cells is often associated with chronically-inflamed tissues, whereas acute tissue damage causes eosinophilic granule cell degranulation and release of mediators of inflammation (Reite & Evensen, 2006; Manera *et al.*, 2011; Lauriano *et al.*, 2012). Therefore, EGCs may be linked with immune-hypersensitive responses that occur in the intestine, due to dietary modulation and hence the quantitative appraisal of their distribution in intestinal tissue would provide valuable information.

In the present study, the antibody against caspase-3 reacted explicitly with cells resembling EGCs both in their distribution and their morphology (see Chapter 6 for additional information relating to this finding). These cells had a granular cytoplasm and were usually localised in the connective tissue adjacent to the *stratum compactum*. Furthermore, for adjacent serial tissue sections, the cytoplasmic granules in those cells stained red with H&E, blue / bluish violet with MGG stain, and red with phloxine-tartrazine stain, which according to Sveinbjørnsson *et al.* (1996) and Reite (1997) confirms that the cells labelled with the caspase-3 antibody were indeed EGCs.

The anti-ACTIVE[®] Caspase-3 polyclonal (G7481, Promega, Madison, USA) used here, is commercially endorsed for its ability to specifically recognize the cleaved active form of caspase-3, a key component in mediating the execution phase of apoptosis. However, the role of caspase-3 in regulating EGC degranulation remains unknown, although Wyllie *et al.* (1980) suggested that degranulating EGCs are not undergoing apoptosis or necrosis, since no evidence of changes in the nuclear envelope or the chromatin distribution within the

nucleus is evident. Thus, although the epitopes that might be cross-reacting / recognised by this antibody can not be currently confirmed, data presented in Chapter 6 may help support the hypothesis that prominent degranulating subcellular features from the cytoplasmic granules of these cells demonstrate the presence and accumulation of elements positive to caspase-3.

In the present study, feeding SBM to fish resulted in a significant increase in the inflammatory cells identified as EGCs (with the anti-caspase 3 antibody), along the basal area of the mucosal folds and the internal edge of the *stratum compactum*. Such dynamic behaviour of EGC-labelled intestinal cells in the inflamed distal intestine of SBM fed Atlantic salmon, is in accordance with that previously described (Bakke-McKellep *et al.*, 2000b; Knudsen, 2007) and it is speculated that they play an important role in immune surveillance. However, given that specific markers of the activation state of these cells in salmonids are lacking, further studies are needed to determine whether the described dynamics are a result of / or of themselves induce the perceived changes observed in intestinal mucosal immunity.

In contrast to the findings of Picchiatti *et al.* (2007), who showed that feeding probiotics increased the number of these cells in the intestine of Atlantic salmon, the immunostimulants included in one of the experimental diets used in the present study, did not seem to influence the mobilisation of EGCs. Nevertheless, it is important to remember that in this specific study we were looking at constitutive rather than responsive mobilisation. Therefore, the ideal approach to evaluate the responsiveness of these cells would have been via *in vivo* infectious challenge tests. In these differentially fed animals might have been challenged and / or stimulated under unfavourable environmental conditions, or confronted with virulent / infectious pathogens. For these reason, the prospect of including such testing models in future studies (especially in the initial screening phase), is very appealing.

5.4.4. T-cell-like cells (CD3ε)

Intestine-associated lymphocytes have been described in fish, but their involvement and functional relevance in immune responses still remains to be defined (Bernard *et al.*, 2006; Rombout *et al.*, 2011).

The polyclonal against human Cd3ε, part of the T-cell receptor (TCR) complex, used in this experiment, has been shown to cross-react with T cells in teleosts (Liu *et al.*, 2008). Immunohistochemistry using this antibody indicates the presence of putative T-cells in the epithelial lining, *lamina propria* and submucosa of the intestine and suggests that these cells make up a large proportion of the inflammatory cell infiltrate observed in salmon fed SBM, as earlier described by Bakke-McKellep *et al.* (2007a), Lilleeng *et al.* (2009) and Ronza *et al.* (2011). However, contrary to what was expected, the overall staining indices in the present study did not significantly increase with supplementation of SBM or immunostimulants in the diet. This may be partly due to the fact that different immune mechanisms occur at different time points along an immune response profile and that perhaps the T-cells were sensitised towards the soya antigens earlier on, and were down-regulated at the time of the sampling. It may be, however, that simply because of the sample sizes being analysed, such changes might not have been resolvable. Nevertheless, it is still uncertain whether this reaction is involved in the induction of inflammatory processes or as a defence against possibly epithelial injury. The underlying regulatory mechanisms remain unknown, and again the lack of specific antibodies for T-cell precursors in fish, constrains further understanding of pathogenesis through the use of immunomarkers in IHC (Bakke-McKellep *et al.*, 2000b, 2007a; Lilleeng *et al.*, 2009; Romarheim *et al.*, 2013a). Thus, further studies are again required to detail the T-cell involvement in the soybean-induced enteropathy.

5.4.5. Mobilisation of stress-related proteins for regenerative processes (HSP 70)

Heat shock proteins (HSPs) are a group of highly conserved intracellular proteins, classified into several families on the basis of their approximate molecular weight (Mosca *et al.*, 2012). In teleosts there are constitutive members (*e.g.* HSC 70), which are required in

various aspects of metabolism to maintain cellular homeostasis, and inducible forms (e.g. HSP 70), which are expressed at detectable levels in response to acute stressors (Poltronieri *et al.*, 2009; Iwama *et al.*, 1998). HSPs are considered to comprise a regulative component of the immune system response, being involved in protecting against excessive inflammatory events by optimising antigen processing and / or inducing the release of cytokines (Asea *et al.*, 2000; Mosca *et al.*, 2012). They are induced by a wide spectrum of physical, chemical and biological stimuli, including hyperthermia, osmotic stress, heavy metal exposure, chemical shock, oxidative stress caused both by anoxia and hypoxia, fever or inflammation amongst others (Sandnes *et al.*, 1995; Iwama *et al.*, 1998; Gornati *et al.*, 2004; Maradonna & Carnevali 2007; Fujikawa *et al.*, 2012). Within this context, the assessment of HSP expression an indicator of stress and animal health status appears very promising (Iwama *et al.*, 2004; Antonopoulou *et al.*, 2013).

Some authors have also suggested that induction of heat shock protein 70 (HSP 70, 68-73 kDa) during inflammation could reflect an attempt to regulate the apoptotic pathway and mediate cellular recovery (Bakke-McKellep *et al.*, 2007b; Poltronieri *et al.*, 2009; Mosca *et al.*, 2012). For this reason, a change of reaction pattern as part of an inflammatory response, in which the SBM diet was expected to cause an increase in the HSP 70 reactivity over the epithelial cells at the tips of the mucosal folds, was anticipated. However, the pattern of reactivity seen with the anti HSP 70 was less obvious, and in some cases of enteropathy even absent. It might thus be speculated that HSP 70 related protein-products may be short-lived and that maybe affected cells disappear rapidly. In fact, most inducible HSPs do not contain introns, therefore within a few minutes of exposure to stressors their mRNA may be translated into protein (Mayer *et al.*, 2000). This may be an explanation as to why the IHC expression documented in the current study was so unpredictable, unreliable and inconsistent. Also there are fewer instances where the cellular localisation of HSP70 by IHC has been described in the literature (Burkhardt-Holm *et al.*, 1998; Kagawa *et al.*, 1999; Santos *et al.*, 2008; Poltronieri *et al.*, 2009), thus, further work is needed to better define

and understand the functional significance of HSP 70 in the immune response of fish, particularly with respect to factors involved in the innate and adaptive immune system.

5.4.6. Facilitation of nutrient uptake and ion transport (Na⁺K⁺-ATPase)

Absorption of nutrients depends on the activity of a range of enzymes, in particular those located in the brush border section of the intestine as Na⁺K⁺-ATPase (Tibaldi *et al.*, 2006; Tresguerres *et al.*, 2010; Zhao *et al.*, 2012). Therefore their expression is essential in driving a number of transepithelial transport processes important for nutrient uptake (Wilson & Castro, 2011). This would suggest that measuring the activities of such intestinal enzymes may represent a sensitive tool to study the influence different dietary ingredients have on nutrient uptake and to ascertain their individual nutritional status. Since much of the intestinal nutrient transport across the intestinal enterocytes is facilitated by membrane anchored Na⁺ co-transporters, Na⁺K⁺-ATPase expression may be utilised to evaluate those interrelated kinetic activities (Gal-Garber *et al.*, 2003).

Previous studies on the expression of intestinal Na⁺K⁺-ATPase, have ascertained that the fish's nutritional status could alter the expression and the affinity of the Na⁺ transporter, and that a decrease in epithelial Na⁺K⁺-ATPase activity was often associated with intestinal inflammation (Musch *et al.*, 2002). Anti-nutritional factors found in plant ingredients such as SBM are known to affect certain physiological processes of the gastrointestinal tract and disrupt particular intestinal regulatory mechanisms (Krogdahl *et al.*, 2010). This diminishes the carrier-mediated nutrient transport in enterocytes, thus leading to a marked reduction in the activities of the intestine's epithelium enzymes (Krogdahl *et al.*, 2003; Bureau *et al.*, 1998; Bakke-McKellep *et al.*, 2000a; Nordrum *et al.*, 2000a).

Our findings do not fully agree with these studies. The IHC detection of Na⁺K⁺-ATPase was performed using an antibody raised against a synthetic peptide corresponding to a highly conserved sequence of the Na⁺K⁺-ATPase α -subunit, which has been widely used for the detection of Na⁺K⁺-ATPase in gill mitochondria-rich cells in various teleost species with high specificity (Uchida *et al.*, 1996; Witters *et al.*, 1996; Teranishi & Kaneko, 2010) and has proven successful for staining chloride cells in gills of fish used for the present study

(Nilantha Jayasuriya, *personal communication*). Despite the findings of earlier work in the current study the specificity and reproducibility of the reaction pattern was not consistent throughout the evaluation process. Although the immunoreaction for Na⁺K⁺-ATPase within the control gill and kidney tissues was considered effective, the staining obtained with intestinal sections incubated with the same antibody, using an identical staining protocol, did not show the same degree of specificity or consistency. The so-called positive-control tissues (*i.e.* sections from fish gills and kidney), should, however, have been fixed and processed in a manner identical to the rest of the intestinal tissue (same fixative, fixation time, *etc.*), however, this was not the case which may explain the discrepancy.

5.4.7. Technical pitfalls potentially affecting the immunolabelling

Although a relatively simple technique, positive staining depends on many factors (De Matos *et al.*, 2010). One crucial factor is that the antigenicity of the protein recognised by the antibody is preserved and accessible in the tissue sections. The end result of immunostaining is therefore reliant on the fixation and handling processes that the tissue sample undergoes. Moreover, it should not be presumed that one standard procedure can maintain the structural integrity of different histological tissues, retain all types of antigens, and still preserve their antigenicity equally (Brandtzaeg, 1998). Therefore, the appropriate processing method must be adjusted according to the application and the target antigen being used. As the IHC assay is a multi-step procedure, optimisation of the various steps is required to maximize the resulting signal. This has proven relatively time-consuming and requires technical experience.

The basic principle of any immunolabelling technique is that a specific antibody will bind with its specific antigen to give an exclusive antibody-antigen complex. However, antibody specificity to the respective antigen is not always exact. For example in the present work, commercial antibodies developed against mammalian forms of the antigens were employed on the basis of their cross-reactivity with similar constitutive isoforms in salmonids. These were initially appraised based on their assumed pattern of reactivity within sections of positive tissue controls. The reliability and accuracy of the results was continuously

checked, until satisfactory staining was obtained for the elected intestinal tissue samples. Unfortunately that was not the case for antibodies tested against HSP 70 and Na⁺K⁺-ATPase, and further optimisation is still necessary to ensure that the selected antibodies react with the appropriate antigens. It is interesting to note that these antibodies were both monoclonal, and that all the other antibodies evaluated were polyclonal. There are various factors to consider when selecting a primary antibody, as there are advantages and disadvantages of using a monoclonal or polyclonal antibody. Commonly researchers opt for monoclonal antibodies because batches produced are identical and allow a certain level of standardisation of the staining procedure. Furthermore, they are less likely to have background staining and / or cross-react (Ramos-Vara *et al.*, 2008; Boenisch, 2009). Polyclonal antibodies recognise multiple isoforms (epitopes) on the same antigen, they have higher affinity and wider reactivity, being more tolerant to minor differences in the antigen (e.g. polymorphism, heterogeneity of glycosylation or slight denaturation) (Mighell *et al.*, 1998; Nelson *et al.*, 2000; De Matos *et al.*, 2010) and therefore are the preferred choice when species-specific antibodies are not available.

As mentioned earlier, interpretation of IHC results requires familiarity with the expected pattern of immunoreactivity based on the location of the antigen (*i.e.* nuclear, membrane or cytoplasmic staining). In order to acquire information about the localisation of antigens, a comparison of individual IHC staining patterns was therefore performed using a series of serial sections. The generation of serial sections for this purpose was considered extremely "laborious" since at least 8 distinct sections were needed for all the antibodies being evaluated, and challenging, since small structural details are often not present in two adjacent sequential sections. For this reason among others (e.g. saving time and reagents; reduction of variability; the possibility of assessing the spatial relationship of targets and determination of whether such targets are present in different cells, in the same cell or even in the same cellular compartment (Van der Loos, 2008; Christensen & Winther, 2009), multiple-staining techniques were also attempted, where two or more antigens would be detected in the same tissue specimen by use of chromogenic substrates with different

colours. However, there was a problem when certain targets were found to co-localise (because imbalanced colour-mixing made it difficult to evaluate the staining quantitatively), and also because some of the primary antibodies used were of the same immunoglobulin isotype subclass making it difficult to use different secondary antibodies. Double-staining proved to be challenging, and although unsatisfactory results were obtained, it is worth persisting in optimising this methodology since this could greatly enhance the information obtained from each slide and reduce the need, and time, to perform single staining of sequential slides.

5.4.8. Quantification of immunohistolabelling

As the need to quantify immunostaining increases, computer-assisted quantitative analysis methods for IHC detection have been increasingly pursued (Mesker *et al.*, 1994; Seidal *et al.*, 2001; Dunstan *et al.*, 2011). The study employed in Chapter 2 to compare image analysis with manual methods for quantifying the degree of pathology present in intestinal tissues demonstrated that, even when performed by different observers, the image analysis was better than manual quantification. It is less time-consuming than other traditional approaches evaluated and has proven reliable and efficient, especially in terms of quantification of more than one specific marker. In addition, the imaging techniques employed allowed important analytical measurements of the total proportion of area stained and the intensity of the staining, to be performed with greater objectivity and with statistical confidence being assigned to measurements. Through partition of the tissue into different zones, one could ensure an accurate description of the pattern of antigen distribution, which may be useful in providing an understanding of evolving immunological and morphological responses.

Although within the described work, immuno-labelling distribution patterns measured between the various treatment groups were not largely found to show significant differences, the trends in the collected image analysis data nevertheless reflected those observed by visual observation. It is therefore suggested that by increasing the number of replicate samples per dietary treatment group analysed, or by further optimising protocols to

increase consistency, e.g. by using automated processing as occurs in human medicine, differences would be more easily resolved. Thus a key suggestion for consideration in future work would be an increase in sample size and consistency of labelling.

Several investigators have argued that standardisation of IHC methods is necessary if computerised methods are to be adopted (Karlsson *et al.*, 1994; Mesker *et al.*, 1994), in order to achieve a quantifiable / coherent result with an image analysis system. Therefore the areas in assay procedure that lead to significant variability (*i.e.* fixation, sectioning, antigen retrieval, protocols reagents, tissue controls) were targeted as areas for improvement, as previously described in Chapter 3. To minimise variations in the staining intensity of the chromogen produced by differences in incubation time and amounts of reagent, all tissue sections were stained in a single batch on the same day by the same person, followed by the analysis of these sections by a single operator. This helped to provide optimal reproducibility. Another approach, which may have served to further reduce variability, was the use of an automated staining method as demonstrated for use with PCNA and CD3 labelling, when compared to the other labelling performed manually (as shown in Figure 5.11). The accuracy of the system should also be reviewed. It should account not only for the measurement of the biomarker in a particular section, but also the ability to repeat the result with the same tissue sample, on a day to day basis, in the same and in different laboratories, and the ability to obtain the same measurement for different specimens and cases, again reproducibly (Taylor & Levenson, 2006). In this context, accuracy (and reproducibility) can be determined only if rigorous quantifiable reference standards are available and are used to calibrate the system. Perhaps for this purpose, the use of tissue microarrays (TMAs) may be important. TMAs are constructed from circular cores extracted from blocks of formalin-fixed paraffin-embedded tissue and arrayed in an empty paraffin block, resulting in up to 1000 cores from individual biopsies residing in a single block. As a large number of sections can then be cut from the resulting TMA block, these sections may be processed alongside the core specimen (Figure 5.11) as quantifiable

reference-standards that could be used to calibrate the systems and allow comparison between different slides with different staining intensities (Saxena & Badve, 2009).

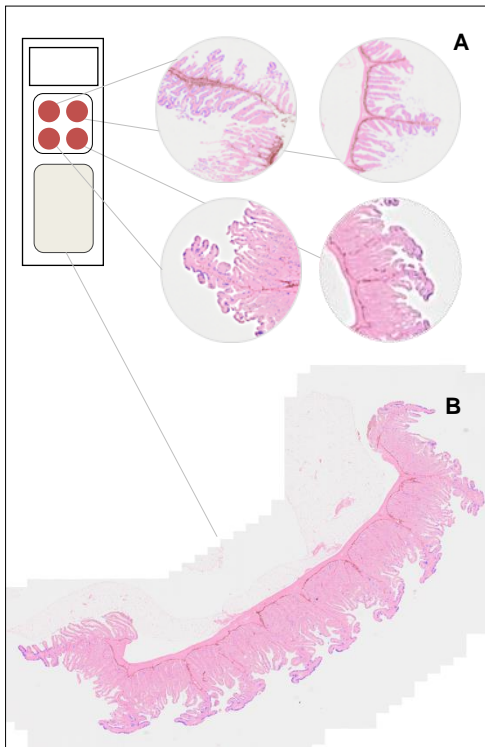


Figure 5.11. Schematic description of a TMA slide. (A) Cylindrical cores obtained from 4 distinct formalin fixed, paraffin embedded tissue blocks. These cores could be used when performing an immunohistochemical staining, with cores used to ensure that the staining procedure actually worked, and as a means to standardise the variability in staining intensity of the chromogen. (B) The key sample to be analysed.

5.4.9. Perspectives

In this chapter a rational and methodical approach was taken in order to select an appropriate biomarker panel for use in this study. Covering most of the general diagnostic categories of interest, the selection was based on the morphologic and structural features described earlier with regard to a given histopathology context. Promising markers have been identified to predict prognosis and likelihood of response for such diets, and which might therefore be employed in order to better design dietary treatment regimes in the future. Following the successful results obtained for this initial panel, one could always add additional differential diagnosis biomarkers to widen the analysis. Several authors have reported that the immunocytochemical assays correlate well with transcriptional gene expression studies (Olsvik *et al.*, 2007; Lilleeng *et al.*, 2009; Skugor *et al.*, 2011; Kortner *et al.*, 2011; Marjara *et al.*, 2012; Tacchi *et al.*, 2011; Sahlmann *et al.*, 2012; *inter alia*) and

together, these techniques may help indicate how diet-related enteropathies are triggered, and thus aid in selecting potential biomarkers for future IHC analysis.

5.5. General conclusions

This chapter described a digital computer-assisted quantification method for a biomarker panel intended for assessment of the immune response to dietary modulation, using IHC staining techniques for cell proliferation and regeneration (PCNA); programmed cell death or apoptosis (TUNEL); EGCs and t-cell like infiltrates (active caspase-3 and CD3 respectively); mobilisation of stress-related protein regenerative processes (HSP 70) and facilitation of nutrient uptake and ion transport (Na^+K^+ -ATPase). Through the description of the intestinal cellular responses at a molecular level, such IHC expression profiling further characterised the inflammatory reaction generated by the enteropathic diet. Also, a number of potential diagnostic parameters were described for fish intestinal health (e.g. the relative levels of antigenicity and the spatial distribution of antigens in tissues). Moreover, the proposed system holds potential for improving the accuracy and reproducibility of quantitative analysis of IHC reactions, as well as being a practical tool for inter-laboratory studies.

The introduction of new dietary components and the confirmation of prognosis through these predictive markers, along with the use of new image analysis screening tools, may enable pathologists to help tailor specific diets by maximising functional ingredient efficacy and minimising adverse effects and inclusion of antinutritional factors. Finally, it is necessary to point out the need for stringent validation of these algorithms by use of larger cohorts of samples and possibly the use of TMA sections for standardisation of staining.

USER GUIDELINES FOR OPERATION OF THE GUT HEALTH IMAGE PROCESSING AND ANALYSIS SEMI-AUTOMATED SYSTEM

A detailed, comprehensive protocol has been compiled to allow a better understanding of the image processing and analysis workflow. It provides step-by-step instructions in loading, initiating and operating the system, which is mentioned across this thesis.

'Technical Note B' is an amendment to the previous user guidelines note (see Technical Note A1 Chapter 2). In this section, description of the procedures established for the quantification and characterisation of specific immunohistochemical biomarkers (*i.e.* measure of the amount, intensity and spatial distribution of immunostaining), by means of digital image analysis algorithms, are presented.

1. KS Run User Interface

The image processing, segmentation and analysis script developed is deployed using the stand-alone KS Run software platform (Version 3.0, Carl Zeiss Vision GmbH, München-Hallbergmoos, Germany). Instructions for installing the KSRun software and deploying the gut analysis script within it are provided in the KS Run user manual (KS Run User Interface Manual Guide B 40-613, Carl Zeiss Vision GmbH, München-Hallbergmoos, Germany). The following sections describe the user continued-protocol for the gut image analysis script presented in Chapter 2.

1.1. Image Processing and Analysis Workflow

The image processing, segmentation and analysis pipeline comprises of a succession of interactive and automated operational steps (⚙️). Feedback in the form of guideline-notes for the operator (ℹ️), and visualisation of the generated images (🖼️, Appendix 2 and Technical Note A1) was made available at each step of the pipeline process, as well as feature extraction and data generation (📄, Figure 8 from Technical Note A1).

1.1.1. Start Up

a. Operational steps A to C from Technical Note A1 (Chapter 2) are followed.

1.1.2. Logistical Setup and Data Input

b. Operational steps D to I from Technical Note A1 (Chapter 2) are followed.

1.1.3. Image Pre-processing

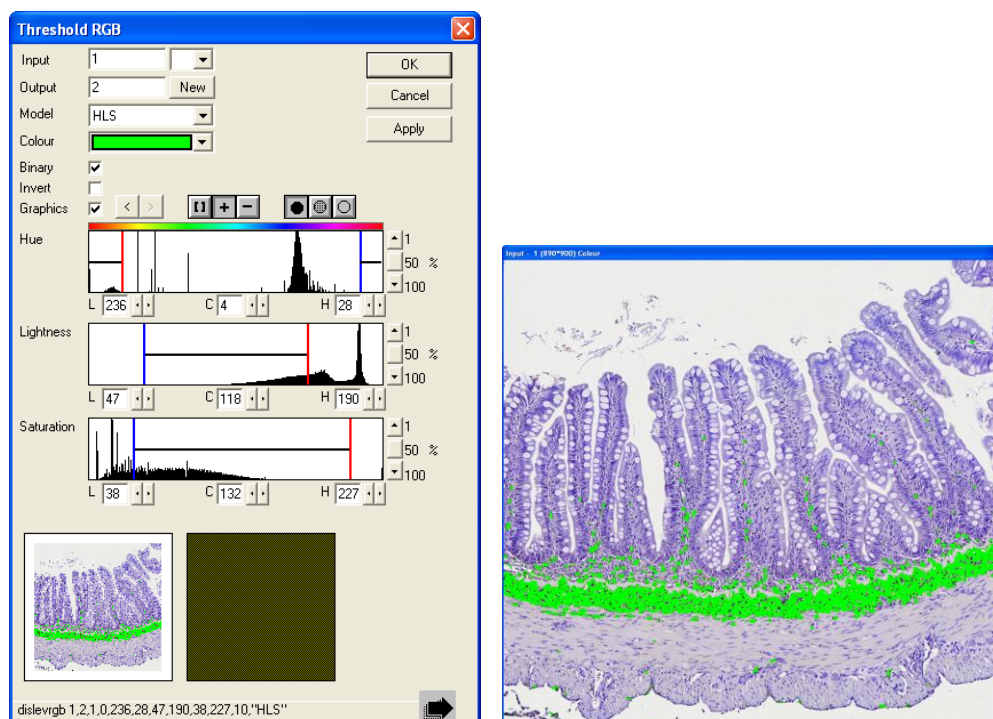
c. Operational steps J to L from Technical Note A1 (Chapter 2) are followed.

1.1.4. Image Segmentation and Processing

d. Immunohistochemical positive stained cells present in the image are highlighted and segmented by an HLS colour thresholding operation.

i “Right click on the small left-hand image and choose ‘Big Display’. Highlight the immunohistochemical positive cells using ‘square bracket’ depressed (as an initial starting point) and circling the area of interest. Then, successively add missing areas using ‘+’ depressed (or ‘<’ to undo the previous selection).”

Image I



e. Operational steps N to U from Technical Note A1 (Chapter 2) are followed.

1.1.5. Histological Identification and Post-processing Overlays

f. Operational steps V to Y from Technical Note A1 (Chapter 2) are followed.

g. Processing of the immunohistochemical positive stained areas:

g1. The final total tissue image (i.e. Image 3F) is taken and used to mask the recognised positive stained area (i.e. protein expression can only occur in the mucosal and submucosal tissues). The regions of interest are highlighted and an overlay mask corresponding to the total immunostained area is merged into Image A, and Image I-2 generated.

ii *“Right click on the small left-hand image and choose ‘Big Display’. All immunohistochemical positive areas will be selected at the start (labelled in green), therefore use the left mouse button to deselect (labelled in red) the unwanted areas. Use the right mouse button to increase and decrease the image size for better clarity. If unexpected red or green regions are apparent, zoom into the image to check their accuracy.”*

Image I-1.

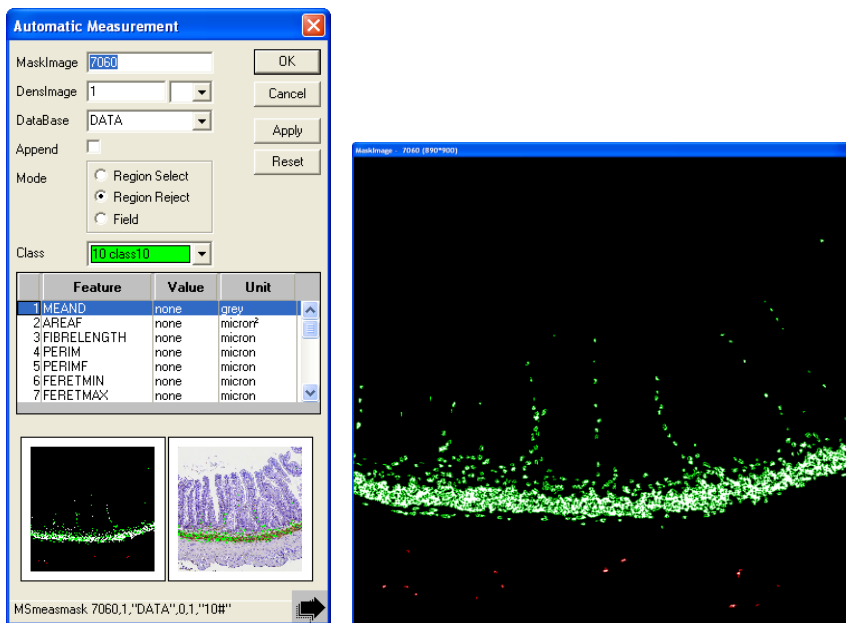


Image I-2

e.g. R110027_P01.TotalEGC.tif (Figure 1)

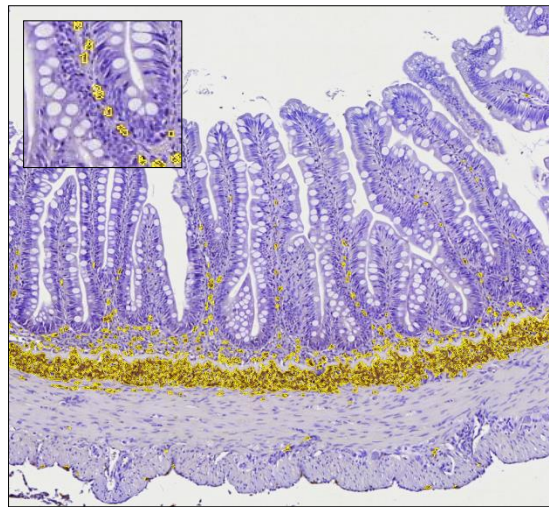
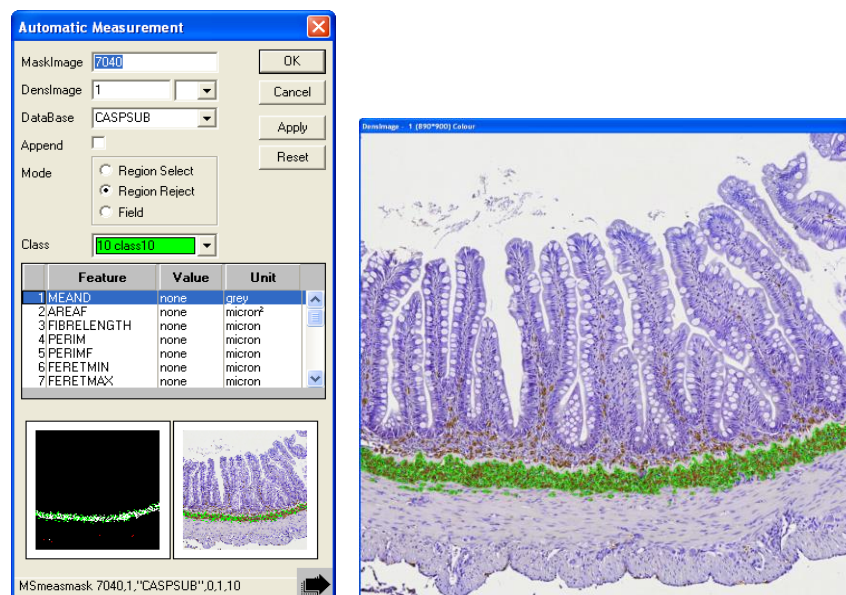


Figure 1. Output Image I-1, total immunohistochemical positive stained area being demarked with a yellow coloured overlay.

g2. The final submucosal tissue image (*i.e.* Image 14A) is then taken and used to mask the recognised immunohistochemical positive areas within that tissue region. Overlay masks are generated and merged with Image 1A, into Image V as green labelled areas of interest.

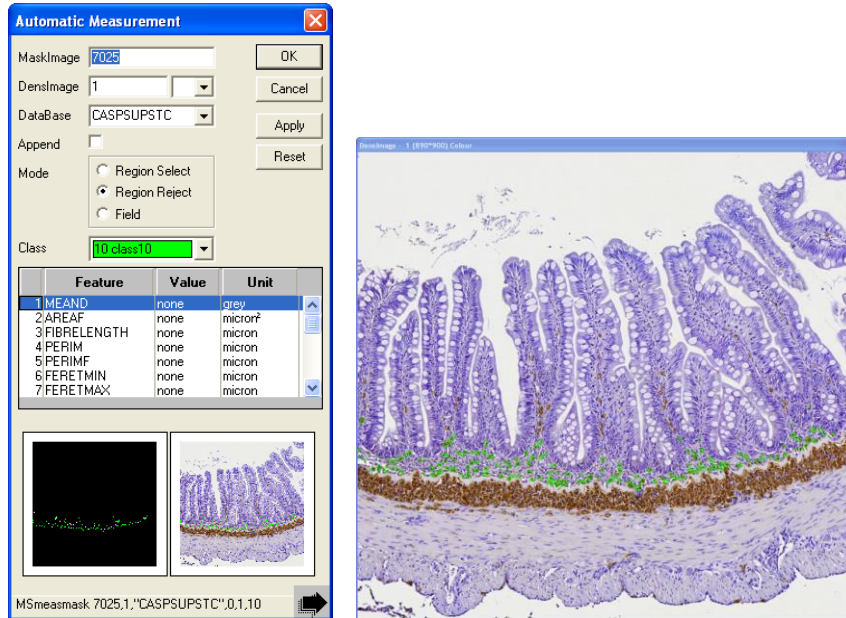
Image II



g3. The *stratum compactum* line from Image 5 is thickened and the corresponding region of interest in Image I-1 highlighted. Subtracted from this, is the area equivalent to the submucosal area (*i.e.* Image 14A), resulting in the identification of immunohistochemical

positive areas immediately above the *stratum compactum*. For the areas of interest recognised, overlay masks are generated and merged into Image V as yellow labels.

Image III



g4. The remaining immunohistochemical positive areas (*i.e.* corresponding to the protein expression in cells infiltrating the intestinal mucosal folds) are highlighted and corresponding red overlay masks created on top of Image V.

Image IV

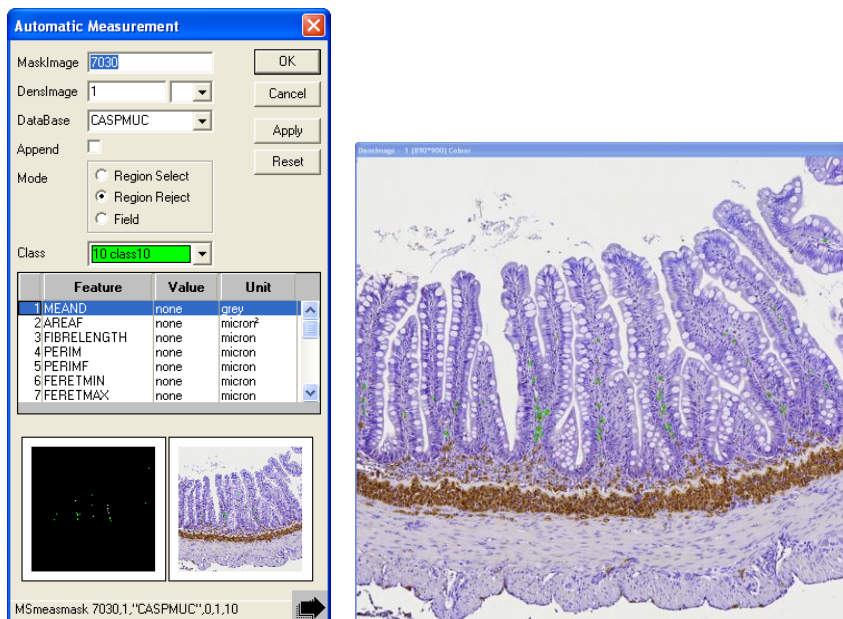


Image V

e.g. R110027_P01.ZonedEGC.tif (Figure 2)

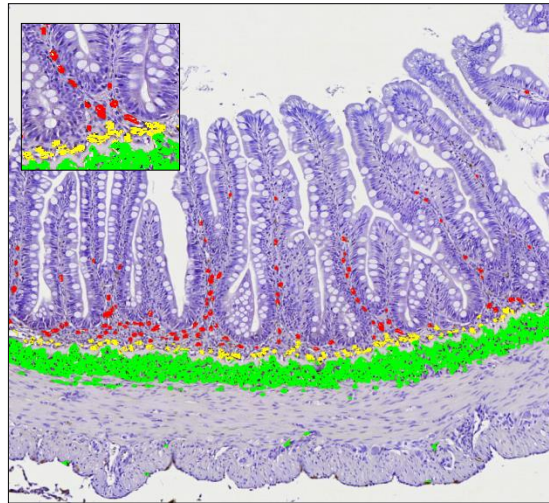


Figure 2. Output Image V, immunohistochemical positive stained areas being demarked with a yellow coloured overlay for cells located above the *stratum compactum*, in red for cells infiltrated along the mucosal folds and in green for submucosal cells.

1.1.6. Feature Extraction and Data Generation

⚙️h. Immunohistochemical (IHC) positive stained areas are identified (*i.e.* Images I-1, II-IV)

and for each dispersion level the following measurements are taken:

- 📏 Total IHC Stained Area (e.g. EGC Area, μm^2)
Average Staining Intensity for Total IHC Stained Area (e.g. EGC Intensity, mean pixel value)
- 📏 Total IHC Stained Area for the submucosa tissue (e.g. EGC Sub, μm^2)
Average Staining Intensity for IHC in submucosa (e.g. EGC Sub Intensity, mean pixel value)
- 📏 IHC Stained Area for zone above the *stratum compactum* (e.g. EGC Sup, μm^2)
Average Staining Intensity for IHC in zone above the *stratum compactum* (e.g. EGC Sup Intensity, mean pixel value)
- 📏 IHC Stained Area for remainder mucosa (e.g. EGC Muc, μm^2)
Average Staining Intensity for remainder mucosa (e.g. EGC Muc Intensity, mean pixel value)

i. Operational steps ⚙️η to ⚙️θ from Technical Note A1 (Chapter 2) are followed.

1.1.7. Analysis Conclusion

⚙️j. Program terminates with audible warning once the analysis is finished.

- 🔔iii “Measuring feature properties...”
“Writing data to databases...”
“Analysis finished.”

CHARACTERISATION OF MAST CELLS / EOSINOPHILIC GRANULE CELLS IN THE ATLANTIC SALMON INTESTINE

6.1. Introduction

The posterior intestine plays an important immunogenic role in teleost fish. Antigens present in the intestinal lumen that cross the gut epithelium are transported to the gut associated lymphoid tissue (GALT), which is known to be involved in intestinal mucosal immune responses (Gomez *et al.*, 2013; Urzúa, 2013).

In teleosts the level of the GALT organisation is lower than in mammals, and although it has a more diffusely organised immune system, it still comprises many lymphoid cells, macrophages, neutrophilic and eosinophilic granulocytes (Tort *et al.*, 2003). Generally, these granulocytes are considered to be important initiators and effectors of the innate immune response and to play a crucial role in regulating adaptive immune responses in the intestinal mucosa (Silphaduang & Noga, 2001; Mulero *et al.*, 2008), and are involved in many pathologic processes such as defence against infectious agents, chronic stress or food hypersensitivity (Dezfuli *et al.*, 2002; Penissi *et al.*, 2003; Rocha & Chiarini-Garcia, 2007; Urán *et al.*, 2008; Sundh, 2009). However, data evidence for their function in fish remains sparse.

In the intestine of fish, these granule cells appear morphologically as large ovoid cells possessing a large eccentric nucleus and showing characteristic large, membrane-bounded granules in the cytoplasm such that these cells strongly resemble mammalian mast cells (Ezeasor & Stokoe, 1980; Burka & Powell, 1993; Rombout *et al.*, 2011). These cells are widely distributed in the subepithelial *lamina propria*, and distributed on both sides of the *stratum compactum*. On the luminal side these cells are found as either single cells or clustered in small clumps, whereas on the muscle side they form a continuous layer, the *stratum granulorum* (Dorin *et al.*, 1993; Sveinbjörnsson *et al.*, 1996; Manera & Borreca, 2012).

There remains considerable controversy with respect to the staining properties of their cytoplasmic granules, which are frequently described as either basophilic, staining blue (*i.e.* without showing metachromasia) after application of some of the blue cationic dyes (*e.g.* Bolton, 1933; Smith, 1975; Rocha & Chiarini-Garcia, 2007) or eosinophilic, staining red with eosin (*e.g.* Gulland, 1898; Ezeasor & Stokoe, 1980). Studies have suggested that this feature is often fish species dependent and that these cells have both acidophilic and basophilic components in their granules (Reite, 1996, 1997; Leknes, 2007). It has also been suggested that some staining properties might be an artefact of fixation of tissues in aqueous fixatives, and that the use of alcohol based fixatives can, in some cases, retain basophilic and metachromatic properties of the granules (Schmale *et al.*, 2004). Therefore, it is sensible not to over-emphasise their staining characteristics (Vallejo & Ellis, 1989), and hence following the classification of Reite & Evensen (2006) we have chosen to use the term mast cell / eosinophilic granule cell (MCs / EGCs) throughout the present chapter, to describe such cells.

The granules of fish MCs / EGCs, have an arginine-rich core and are known to contain a number of components common to mammalian mast cell granules, including alkaline, acid phosphatases, leucine aminopeptidase, arylsulphatase, 5-nucleotides, tryptase, and a range of antimicrobial peptides including lysozyme, piscidin and pleurocidin (Ellis, 1985; Ezeasor & Stokoe, 1980; Powell *et al.*, 1992; Sire & Vernier, 1995; Sveinbjørnsson *et al.*, 1996; Dezfuli *et al.*, 2000; Silphaduang & Noga, 2001; Dobson *et al.*, 2008; Mulero *et al.*, 2008). Whether they also contain characteristic metachromatic sulphate glycosaminoglycans, including heparin and hyaluronic acid, remains unclear (Vallejo & Ellis, 1989; Holland & Rowley, 1998). From reviews of the literature on this subject (*i.a.* Reite & Evensen, 2006; Mulero *et al.*, 2008; Crivellato & Ribatti, 2010) it is evident that the precise granule content of fish MCs / EGCs and their ensuing physiological function, still remain poorly understood. It is, however generally accepted that these cells may be involved in defence mechanisms, and a role in inflammation is suggested (Powell *et al.*, 1993a; Sveinbjørnsson *et al.*, 1996; Matsuyama & Iida, 1999; Paulsen *et al.*, 2001; Dezfuli & Giari, 2008). These cells are often

located around blood vessels associated with host-environment interfaces such as skin, gills and intestine (Roberts *et al.*, 1971; Powell *et al.*, 1990). Release of their contents by cell degranulation occurs in response to acute tissue damage, or when tissues are exposed to pathological challenges after inoculation with pathogens or certain substances (e.g. *Aeromonas salmonicida* and *Vibrio anguillarum* toxins, compound 48/80, formalin-killed *A. salmonicida*, substance-p, capsaicin; Ellis, 1985; Vallejo & Ellis, 1989; Lamas *et al.*, 1994; Powell *et al.*, 1993a, 1993b; Reite & Evensen, 1994; Holland & Rowley, 1998); their number increases in regions of active inflammatory response, especially those associated with bacterial and parasitic infections (Reimschuessel *et al.*, 1987; Sharp *et al.*, 1989; Buchmann *et al.*, 1999; Dezfuli *et al.*, 2003a; Schmale *et al.*, 2004; Murray *et al.*, 2007; Dezfuli *et al.*, 2012). In addition to this, vasodilation, migration and accumulation of neutrophils and macrophage activation have repeatedly been observed at sites where MC / EGC degranulation has occurred (Reite, 1997; Reite & Evensen, 1994; Matsuyama & Iida, 2001), suggesting that fish MCs / EGCs are able to contain or generate a variety of mediators that induce chemical leucocyte-attraction and / or neutrophil chemotaxis, as observed for mammal counterparts (Reite & Evensen, 2006; Dezfuli & Giari, 2008; Crivellato & Ribatti, 2010).

Overall, the general morphology, tissue distribution and staining characteristics together with some of the suggested functions have led researchers to postulate that fish MCs / EGCs are analogous to mammalian mast cells (Ellis, 1985; Powell *et al.*, 1993b; Sire & Vernier, 1995; Reite, 2005; Dezfuli & Giari, 2008; Mulero *et al.*, 2007; Lauriano *et al.*, 2012). However, despite bearing structural and functional similarities, some of their cytochemical characteristics do not support exact homology. For example, with respect to the two biogenic amines present on the granules of mammalian MCs, namely serotonin and histamine, all the studies performed to date have shown that fish MCs / EGCs contain the former but lack the latter (Lamas *et al.*, 1991; Matsuyama & Iida, 1999; Dezfuli *et al.*, 2000; Mulero *et al.*, 2007; Rombout *et al.*, 2011). Thus the physiological function and the content of the granules from fish MCs / EGCs is still a matter of debate, as well as their homology to mammalian mast cells.

Chapters 3, 4 and 5 highlighted the presence of MCs / EGCs in the intestine of salmon but made no attempt to determine their role in immunity. The purpose of the work presented in the present chapter was to further characterise intestinal MCs / EGCs and to try to elucidate their functional role in the intestinal immune responses. Through an understanding of their distribution, composition and ultrastructure, the intention was therefore to provide additional knowledge, so as to better characterise these cells and their functional properties.

6.2. Material and methods

6.2.1. Histochemical and ultrastructural features of intestinal MCs / EGCs

6.2.1.1. Histology tissue samples

Samples from the anterior part of the distal intestine of Atlantic salmon, fixed in phosphate-buffered formaldehyde (4 %, pH 7.2), were selected from the histology archives of Skretting ARC, which represented a range of different pathological states including soybean meal induced enteritis; damage of the mucosal epithelium of the gut by infection with an acanthocephalan and samples from fish infected with the infectious salmon anaemia virus (ISAV), a member of the Orthomyxoviridae. In addition, clinical samples from a trematode infection of Atlantic salmon, were kindly provided by Prof. Randolph Richards (Diagnostic Services, Institute of Aquaculture, University of Stirling, UK).

Samples for histological examination were processed according to standard histological methods (Bancroft & Stevens, 1982; Ramos-Vara, 2005, 2011). All formaldehyde-fixed samples were dehydrated and embedded in paraffin (Tissue-TekII Paraffin Wax, melting-point: 54-57°C, Sakura Finetek Europe B.V, Netherlands). Transverse serial sections of 5 µm thickness were cut (Leica RM 2035, Leica Microsystems Ltd., UK) and mounted onto SuperFrost Plus® microscope slides (Menzel-Gläser, Braunschweig, Germany).

After deparaffinisation in xylene and rehydration through graded ethanol, some of the serial sections were histochemically stained (Section 6.2.1.2), while others were subjected to immunohistochemistry (IHC) methods (Section 6.2.1.3).

6.2.1.2. Histochemical staining

Serial sections were stained with either [1] Haematoxylin-Eosin (H&E), [2] Haematoxylin-Erythrosin-Safran (HES) [3] Thionin, [4] Azur A, [5] May-Grünwald-Giemsa (MGG), [6] Toluidine Blue, [7] Periodic-Acid-Schiff-Haematoxylin (PAS-H), [8] Periodic-Acid-Schiff-Alcian-Blue (PAS-AB), [9] Haematoxylin-Eosin-Alcian blue (H&E-AB) and [10] Astra blue, according to standard staining procedures specified in Table 7.1 (see Appendix 1 for further detail of staining protocols). After staining, the sections were briefly rinsed in distilled water, dehydrated through 70% ethanol and absolute ethanol into xylene, to be mounted using a synthetic resinous mountant.

Table 6.1. Histochemical methods employed in the evaluation of intestinal mast cells / eosinophilic granule cells from Atlantic salmon.

Histochemical method
[1] Haematoxylin-Eosin, <i>in</i> Bancroft & Stevens (1982)
[2] Haematoxylin-Erythrosin-Safran, <i>in</i> Gurr (1957)
[3] Thionin, Cook (1961)
[4] Azur A, Hughesdon (1949)
[5] May-Grünwald-Giemsa, May & May (1902), Giemsa (1902)
[6] Toluidine Blue, Schubert & Hammerman (1956)
[7] Periodic-Acid-Schiff-Haematoxylin, <i>in</i> Leblond & Clermont (1952)
[8] Periodic-Acid-Schiff-Alcian-Blue, Mowry & Winkler (1956)
[9] Haematoxylin-Eosin-Alcian blue, <i>in</i> Lillie (1965)
[10] Astra blue, Blaies & Williams (1981)

6.2.1.3. Immunohistochemical labelling

After being dewaxed and rehydrated, the serial sections were subjected to a series of different affinity-isolated antibodies raised against [a] Tryptase, [b] c-Kit, [c] Myeloperoxidase, [d] Lysozyme, [e] Substance-p, [f] Met-enkephalin, [g] Chymase, [h] Serotonin, [i] Pre-caspase 3, [j] Caspase 7, [k] Active caspase-3 using a range of IHC protocols. A summary of the respective immunostaining protocols is presented in Table 7.2. Most of the protocols described of here are the result of a series of troubleshooting and amelioration steps including comparison of various demasking procedures and blocking solutions, use of different primary antibody concentrations and / or diverse chromogenic visualisation systems. The procedures presented are those producing the most consistent

Table 6.2. Summary of immunohistochemical staining protocols employed in the evaluation of intestinal mast cells / eosinophilic granule cells from Atlantic salmon.

IHC assay	Antigen retrieval	Pre-treatment	Primary antibody	Secondary antibody	Detection system
[a] Tryptase	Sodium citrate buffer, pH 6; 1 min 40 sec; 125 °C; HIER.	REAL™ Peroxidase-Blocking Solution (S2023, DAKO); 5 min; RT.	Mast Cell Tryptase Monoclonal Mouse Anti-human Clone AA1 (M7052, DAKO); 1:200; 30 min; RT.	EnVision™ HRP Mouse Polymer (K4001, DAKO); 20 min; RT.	REAL™ EnVision™ DAB+ (K5007, DAKO); 2 x 5 min; RT.
[b] C-Kit	Sodium citrate buffer, pH 6; 1 min 40 sec; 125 °C; HIER.	REAL™ Peroxidase-Blocking Solution (S2023, DAKO); 5 min; RT.	CD117, c-kit Polyclonal Rabbit Anti-human (A4502, DAKO); 1:800; 30 min; RT.	EnVision™ HRP Rabbit Polymer (K4003, DAKO); 20 min; RT.	REAL™ EnVision™ DAB+ (K5007, DAKO); 2 x 5 min; RT.
[c] Myeloperoxidase	Proteinase K Ready-to-Use (S3020, Dako); 5 min; RT.	REAL™ Peroxidase-Blocking Solution (S2023, DAKO); 5 min; RT.	Myeloperoxidase Polyclonal Rabbit Anti-human (A0398, DAKO); 1:2000; 30 min; RT.	EnVision™ HRP Rabbit Polymer (K4003, DAKO); 20 min; RT.	REAL™ EnVision™ DAB+ (K5007, DAKO); 2 x 5 min; RT.
[d] Lysozyme	Proteinase K Ready-to-Use (S3020, Dako); 10 min; RT.	REAL™ Peroxidase-Blocking Solution (S2023, DAKO); 5 min; RT.	Lysozyme Polyclonal Rabbit Anti-human Clone EC 3.2.1.17 (A0099, DAKO); 1:1000; 30 min; RT.	EnVision™ HRP Rabbit Polymer (K4003, DAKO); 20 min; RT.	REAL™ EnVision™ DAB+ (K5007, DAKO); 2 x 5 min; RT.
[e] Substance-p	N.A.	¹ 0.6 % Hydrogen Peroxide in 1:500 Methanol; 15 min; RT. ² 0.1 % NGS in Tris-HCl, pH 7.6; 30 min; RT.	Substance-p Polyclonal Rabbit (IHC7451, Peninsula Lab); 1:800; 2 h; RT.	EnVision™ HRP Rabbit Polymer (K4002, DAKO); 30 min; RT.	0.04 % DAB in Tris-HCl, pH 7.6 and 0.005 % Hydrogen Peroxidase; 4 min; RT.
[f] Met-enkephalin	N.A.	¹ 0.6 % Hydrogen Peroxide in 1:500 Methanol; 15 min; RT. ² 0.1 % NGS in Tris-HCl, pH 7.6; 30 min; RT.	Met-enkephalin Polyclonal Rabbit (IHC8602, Peninsula Lab); 1:150; 2 h; RT.	EnVision™ HRP Rabbit Polymer (K4002, DAKO); 30 min; RT.	0.04 % DAB in Tris-HCl, pH 7.6 and 0.005 % Hydrogen Peroxidase; 4 min; RT.

Table 6.2. (continued from previous page)

IHC assay	Antigen retrieval	Pre-treatment	Primary antibody	Secondary antibody	Detection system
[g] Chymase	UNI-TRIEVE solution (NB325, Innovex); 30 min; 65 °C; water bath.	EnVision™ Dual Endogenous Enzyme Block (K4065, DAKO); 10 min; RT.	Mast Cell Chymase Monoclonal Mouse Clone CC1 (ab2377, abcam); 1:200; overnight; 4 °C.	EnVision™ HRP Mouse Polymer (K4065, DAKO); 30 min; RT.	EnVision™ DAB (K4065, DAKO); 7 min; RT.
[h] Serotonin	UNI-TRIEVE solution (NB325, Innovex); 30 min; 65 °C; water bath.	EnVision™ Dual Endogenous Enzyme Block (K4065, DAKO); 10 min; RT.	Serotonin Polyclonal Rabbit (ab938, Merck Millipore); 1:1000; overnight; 4 °C.	EnVision™ HRP Rabbit Polymer (K4065, DAKO); 30 min; RT.	EnVision™ DAB (K4065, DAKO); 7 min; RT.
[i] Pre-caspase 3	UNI-TRIEVE solution (NB325, Innovex); 30 min; 65 °C; water bath.	EnVision™ Dual Endogenous Enzyme Block (K4065, DAKO); 10 min; RT.	Pro Caspase 3 Monoclonal Rabbit Clone E61 (ab32150, abcam); 1:10; overnight; 4 °C.	EnVision™ HRP Rabbit Polymer (K4065, DAKO); 30 min; RT.	EnVision™ DAB (K4065, DAKO); 7 min; RT.
[j] Caspase 7	UNI-TRIEVE solution (NB325, Innovex); 30 min; 65 °C; water bath.	EnVision™ Dual Endogenous Enzyme Block (K4065, DAKO); 10 min; RT.	Caspase 7 Monoclonal Mouse Clone 7-1-11 (ab110923, abcam); 10 µg.mL ⁻¹ ; overnight; 4 °C.	EnVision™ HRP Mouse Polymer (K4065, DAKO); 30 min; RT.	EnVision™ DAB (K4065, DAKO); 7 min; RT.
[k] Active caspase-3	UNI-TRIEVE solution (NB325, Innovex); 30 min; 65 °C; water bath.	EnVision™ Dual Endogenous Enzyme Block (K4065, DAKO); 10 min; RT.	Anti-ACTIVE® Caspase-3 Polyclonal Rabbit (G748A, Promega); 1:250; overnight; 4 °C.	EnVision™ HRP Rabbit Polymer (K4065, DAKO); 30 min; RT.	EnVision™ DAB (K4065, DAKO); 7 min; RT.

Footnotes: IHC, immunohistochemical; Trypsin, most abundant secretory granule-derived serine proteinase contained in mammalian mast cells; HIER, heat induced epitope retrieval; DAKO, Glostrup, Denmark; RT, room temperature (16-20 °C); HRP, horseradish peroxidase; DAB, 3,3'-Diaminobenzidine; c-Kit, transmembrane tyrosine protein kinase receptor kit or CD117 is a protein encoded by the KIT gene, and commonly expressed by mammalian mast cells; CD117, cluster of differentiation 117; Substance-p, neuropeptide that functions as a neurotransmitter and as a neuromodulator that was found in some teleost fish's cytoplasmic granulated cells (Dezfuli *et al.*, 2000); N.A., non applicable; NGS, normal goat serum; Tris-HCl, tris(hydroxymethyl)aminomethane hydrochloride; Peninsula Lab, Belmont, USA; Met-enkephalin, sometimes referred to as opioid growth factor it is a naturally occurring, endogenous opioid peptide that is a major mediator secreted by mammalian mast cells; Chymase, family of serine proteases found primarily in mammalian mast cells; Innovex Biosciences, Richmond, USA; abcam, Cambridge, UK; Serotonin, 5-hydroxytryptamine is a monoamine neurotransmitter found in mammalian mast cells; Merck Millipore, Billerica, USA; Myeloperoxidase, peroxidase enzyme most abundantly expressed in mammalian neutrophil granulocytes; Lysozyme, enzyme capable of damaging the bacterial cell walls that was demonstrated in mammalian eosinophils, neutrophils, histiocytes, in epithelioid cells, mast cells, and some lining cells of lymph node sinuses; Pre-caspase 3, Caspase 7, Active Caspase-3, protein members from the cysteine aspartic acid protease family related to the apoptosis process; Promega, Madison, USA.

staining results for the selected antigens, at least for mammalian positive control tissues. The outcome of this work was only possible due to collaboration with the Veterinary Diagnostic Services at University of Glasgow. Their technical staff are highly skilled in a wide variety of specialist techniques including histochemistry and immunohistochemistry, and their support and advice greatly helped in the development and optimisation of the methodologies outlined here. The serial sections for the tryptase, c-kit, myeloperoxidase and lysozyme immunostaining were processed in accordance with the protocol outlined in Section 5.2.5.4. For the first two antibodies, demasking of the antigens was performed by heat-induced epitope retrieval in a hydrated autoclave. For the next two antibodies, enzymatic antigen retrieval using Proteinase K Ready-to-Use (S3020, DAKO, Glostrup, Denmark) was performed for 5 and 10 min incubated at room temperature. The specificity of reactions was tested by incubating serial sections of the same sample with normal mouse or rabbit serum (10410 and PLN5001 respectively, Life Technologies Ltd., Paisley, UK) instead of the primary antibody although at the same dilution as these. Sections of human colonic carcinoma and tonsils (kindly provided by Mr. MacMillan from the Veterinary Diagnostics Services, University of Glasgow) were used as positive controls for the target antigens mentioned above.

Sections employed for the substance-p and met-enkephalin immunostaining, were kindly processed by Ms. Samantha Squerzanti (Department of Life Sciences and Biotechnologies, University of Ferrara, Ferrara, Italy). Briefly, following the protocol published by Dezfuli *et al.* (2003a), endogenous peroxidase activity and non-specific staining was blocked by treating the sections with 0.6 % hydrogen peroxide in methanol for 15 min, and in 0.1 % goat normal serum for other 30 min. After 2 h incubation with the respective primary antibodies (shown in Table 7.2.), the sections were incubated for another 30 min with EnVision™ HRP Rabbit Polymer (K4002, DAKO) and rinsed with Tris-hydrochloride (Tris-HCl, 50 mM Trizma base®, pH 7.6) for 5 min.

The peroxidase reaction was developed using a solution of 3-3'diaminobenzidine tetrachloride (0.04 % w/v in Tris-HCl) and 0.005 % hydrogen peroxidase. Thereafter, the

sections were counterstained with Mayer's haematoxylin (MHS1, Sigma-Aldrich, St. Louis, USA) and mounted with a synthetic resinous mountant. To confirm the specificity of the reaction, intestinal tissue sections of *Salmo trutta*, naturally infected with *Cyathocephalus truncates* were used as positive control (Dezfuli *et al.* 2000). Similarly, negative controls were prepared by substituting the primary antibody with normal rabbit serum (R9133, Sigma-Aldrich, Ayrshire, UK) at the same dilution.

The remaining serial sections were subjected to an indirect immunohistochemical method (described in Section 5.2.5.3) using the chymase, serotonin, pre-caspase 3, caspase 7 and active caspase-3 affinity isolated antibodies listed in Table 7.2. Nonspecific staining of the primary antibodies was evaluated by substitution of the former with non-immune rabbit or mouse serum respectively (PLN5001 and 10410, Life Technologies Ltd., Paisley, UK) in serial sections used as negative control, for the rabbit and mouse primary antibodies, respectively. Sections of human tonsils, sections from a canine small skin tumour and cytopins for feline isolated lymphocytes (kindly provided by Mr. MacMillan from the Veterinary Diagnostics Services from the University of Glasgow) were used as surrogates for the known target antigens and served as positive controls for all the above mentioned staining.

6.2.1.4. Light microscopy examination

Observations for both histochemical and immunohistochemical slides were made using a light microscope (Leica DM 5000B, Leica Microsystems GmbH, Wetzlar, Germany), with a dark field phase contrast and equipped with a high resolution digital camera (DFC320, Leica Microsystems Imaging Solutions Ltd., Cambridge, UK) for image capturing.

6.2.1.5. Immunofluorescent Antibody Test (IFAT)

Due to the unexpected immunohistochemical staining pattern observed in tissue sections when subjected to the IHC protocol described in Section 5.2.5.3 using a rabbit polyclonal antibody against caspase-3 (Anti-ACTIVE[®] Caspase-3 Ab, G7481, Promega, Madison, USA), IFAT was undertaken to confirm the immunostaining reaction obtained in IHC.

Paraffin-embedded serial sections from the tissue samples mentioned in Section 6.2.1.1, were deparaffinised and rehydrated as described above. Subsequently, the sections were treated in accordance with the protocol outlined in Section 5.2.5.3, until the rinsing stage just before incubation with the secondary antibody. The slides were then incubated at room temperature for 2 h in the dark, with a goat anti-rabbit IgG antibody, conjugated with fluorescein isothiocyanate (FITC; F0382, Sigma-Aldrich, St. Louis, USA) 1:100 diluted in phosphate buffered saline solution (PBS, 137 mM NaCl, 2.7 mM KCl, 10 mM Na₂HPO₄, 1.8 mM KH₂PO₄, pH 7.4). Slides were washed twice for 20 min each in PBS, and incubated at room temperature for 30 min in the dark, with 20 µg mL⁻¹ of the nuclear counter-stain (Propidium iodide, P4170, Sigma-Aldrich, St. Louis, USA) diluted in PBS. The slides were cover-slipped and then sealed with a transparent nail varnish (Avon Products Inc., London, UK) and kept in the dark at 4 °C until visualised.

Control samples for determining the level of auto-fluorescence / non-specific binding of labelled secondary to tissue sections being used, were prepared in parallel to the test slides by replacing the primary antibody with PBS.

6.2.1.6. Confocal laser scanning microscopy (CLSM)

Tissue sections were visualised using a Leica TCS SP2 AOBS confocal laser scanning microscope coupled to an inverted DM TRE2 microscope (CLSM; Leica Microsystems, Milton Keynes, UK). Through the use of two sequential excitation laser lines (*i.e.* at 488 nm for the FITC dye, and at 535 nm for the Propidium iodide dye) and three photomultiplier channels (blue 411-483 nm, green 498-587 nm and red 600-698 nm), each respective fluorescent dye was excited and serial 1 µm depth-images captured at a 63× magnification (CSLM's Leica Confocal Software, Version 6.21, Leica Microsystems, Milton Keynes, UK). Eight bit serial digital images with a frame size of 1024 × 1024 pixels were taken, and 25 to 30 serial depth-images were automatically stacked and then saved as a single 3D stereo anaglyph TIFF image or colour coded multiple channel images.

6.2.1.7. Transmission electron microscopy (TEM)

Samples for electron microscopy, were obtained from the feeding trial described in Chapter 3 (*i.e.* intestinal samples from post-smolt Atlantic salmon either feed a fish meal based control diet - showing normal morphology, or a diet containing 25 % unrefined soybean meal concentrate – therefore with severe enteritis).

Following the twenty week feeding regime, 15 fish from each designated treatment group were euthanised using an overdose of anaesthetic (50 mg.L⁻¹, MS-222, Tricaine Methanesulphonate, Argent Chemical Laboratoires, Redmount, WA, USA), and 1 cm long transverse portions excised from the distal intestine region. These were cut open longitudinally, and were fixed in 2.5 % glutaraldehyde in 0.1 M sodium cacodylate buffer (see Appendix 1 for recipes), at 4 °C for 24-27 h. The fixed tissues were then washed overnight in the same buffer containing 0.1 M sucrose (S7903, Sigma-Aldrich, Ayrshire, UK), trimmed into 2 mm³ cubes, and post-fixed at 4 °C for 3 h in 1 % osmium tetroxide (O5500, Sigma-Aldrich, Ayrshire, UK) in 0.1 M sodium cacodylate buffer (pH 7.3). Samples were then dehydrated in a graded series of increasing acetones (in 60 %, 90 % and twice in 100 %, for 30 min each), infiltrated with agar low viscosity resin (AGR1078, Electron Technology Ltd., Essex, UK) 50 % (v/v) in acetone for 45 min, and finally for another 60 min each in two successive changes of 100 % resin. Infiltrated tissues were then polymerised (60 °C for 24 h) to give blocks for sectioning.

Ultra-thin sections (70 nm) cut on a Reichert Ultracut-E ultramicrotome (Leica, Leica Microsystems Ltd., UK) were supported on 200 µm mesh Formvar-coated nickel grids (G2002, Electron Technology Ltd., Essex, UK) and left to dry overnight, prior to immunogold labelling (Section 6.2.1.8). Semi-thin sections (2 µm) were also placed into SuperFrost Plus[®] microscope slides for use as immunostained control samples to be examined under light microscopy. These were stained in accordance to the IHC protocol described above (Section 5.2.5.3), to confirm that the structures stained by IHC were present in the ultra-thin sections prepared for immunogold labelling.

The grids comprising the labelled ultra-thin sections were visualised with a Tecnai G2 Spirit Bio Twin™ transmission electron microscope (Tecnai, Eindhoven, Netherlands), operated at 120 kV. Micrograph photos were captured and saved as TIFF images.

6.2.1.8. Immunogold labelling (IGL)

In virtue of the fact that immunolocalisation of the antigen reacting against the rabbit polyclonal antibody for caspase-3 (Anti-ACTIVE® Caspase-3 Ab, G7481, Promega, Madison, USA) was sought, indirect immunolabelling with colloidal gold particles for the same primary antibody was pursued. All incubations were carried out in individual 51 mm Petri dishes, containing water-soaked filter paper with a piece of ParafilmM™ (Pechiney Plastic Packaging Company, Chicago, USA) placed on top. The grids comprising the ultra-thin sections, were allowed to float section-side-down on distilled water drops placed on the ParafilmM™ for 10 min at room temperature. Thereafter, endogenous peroxidase activity was blocked by floating the grids section-side-down in drops of EnVision™ Dual Endogenous Enzyme Block (K4065, DAKO, Glostrup, Denmark), for 1 h at room temperature. They were then placed section-side-up, on a piece of blotting paper for a few seconds, and immediately transferred to drops of a rabbit polyclonal antibody against caspase-3 (Anti-ACTIVE® Caspase-3 Ab, G7481, Promega, Madison, USA) diluted 1:250 / 1:500 / 1:1000 in Tris-buffered saline Tween solution (TBST, 150 mM NaCl, 50 mM Trizma base®, 0.5 % Tween® 20, pH 7.5), and incubated overnight at 4 °C. Subsequently, the tissue sections were washed extensively by floating the grids on TBST contained within a 24 well plate with occasional agitation for 20 min. The grids were then transferred to fresh TBST and washed for another 20 min. Subsequently the grids were incubated overnight at 4 °C, section-side-down in drops of 1:16 and 1:32 FluoroNanogold™ goat anti-rabbit IgG (Nanoprobes Inc., Yaphank, USA) covalently conjugated with uniform 1.4 nm diameter nanogold particles. Thereafter, the tissue sections were washed as previously described, twice for 40 min each in 24 multi-well plate (3527, Corning, New York, USA) with TBST. Then the gold probe was enhanced (*i.e.* by increasing the size of the 1.4 nm gold particle to *circa* 30 – 40 nm) by placing the grids section-side-down on drops of GoldEnhance™

(Nanoprobes Inc., Yaphank, USA) for 12 min. The reaction was stopped by carefully dipping the grids into distilled water for *circa* 2 min.

The specificity of reactions was confirmed by incubating serial sections of the same samples with normal rabbit serum (H 110, TCS Biosciences Ltd, Buckingham, UK) instead of the primary antibody but using the same dilutions as used for the primary antibody. Finally the sections were counter-stained using 4 % uranyl acetate for 4 min, and Reynold's lead citrate for another 7 min, washing between these with a graded series of decreasing ethanol up to distilled water (see Appendix 1 for the staining protocol).

6.2.2. Isolation and characterisation of intestinal MCs / EGCs

6.2.2.1. Tissue sample collection

Healthy adult Atlantic salmon, weighting 150-200 g were maintained for 2-3 days, in the Aquatic Research Facility, Institute of Aquaculture (University of Stirling, UK). Fish were kept in a 100 L rectangular tank with artificial sea salt water (32 mg.L^{-1} , Tropic Marin Salt[®], Tropic Marine Centre, Bristol, UK) supplied with aeration stones, and maintained at temperatures of $12 \pm 2 \text{ }^\circ\text{C}$ under a 12 h light: 12 h dark photoperiod.

For sampling, individuals were euthanised with an anaesthetic overdose (10 % benzocaine, E1501, Sigma-Aldrich, Ayrshire, UK). All procedures were conducted in accordance with the UK Home Office regulations (Animals Scientific Procedures, Act 1986). Blood was immediately withdrawn by caudal venepuncture, and transverse intestinal sections from the distal intestinal region aseptically excised from the fish. The associated adipose tissue was trimmed off, sections cut open longitudinally and kept for no longer than 5 min in ice-cold trypsin neutraliser buffered saline solution (TN, 10 mM Tris-HCl, 137 mM NaCl, pH 7.5).

6.2.2.2. Isolation of MCs / EGCs

Tissue fragments of $\sim 2 \text{ g}$ were then rinsed twice with ice-cold TN and transferred into 25 mL of TN buffer containing 0.37 mg.mL^{-1} of ethylenediaminetetraacetic acid (EDTA, EDS, Sigma-Aldrich, Ayrshire, UK) and 0.145 mg.mL^{-1} diethiothreitol (DTT, D5545, Sigma-Aldrich, Ayrshire, UK). After incubation at $20 \text{ }^\circ\text{C}$ in a shaking water bath set at 150

cycles.min⁻¹ for 1 h, the tissue fragments were thoroughly rinsed with 20 mL TN buffer and incubated for another 2 h, in 25 mL TN buffer containing 0.15 mg.mL⁻¹ collagenase type II and 0.1 mg.mL⁻¹ deoxyribonuclease (C2674 and D5025 respectively, Sigma-Aldrich, Ayrshire, UK). The tissue fragments were then aseptically teased through a 100 µm sterile mesh (352360, BD Falcon, BD Biosciences, Oxford, UK), the cell suspension collected and centrifuged at 400 × g, for 14 min at 4 °C. Thereafter the supernatant was discarded and the cells re-suspended in ice-cold TN buffer containing a protease inhibitor cocktail (TNPI; 04693116001, Complete Protease Inhibitor Tablets, Roche Diagnostics, UK). After a second pass through the same mesh, the cell suspension was again centrifuged at 600 × g, for 7 min at 4 °C, and the cells rinsed two additional times with ice-cold TNPI buffer. The resulting cell pellet was re-suspended to give a concentration of approximately 2 × 10⁷ cells.mL⁻¹, and the MCs / EGCs isolated as described by Bayne (1986), Dorin *et al.* (1993) and McMillan & Secombes (1997). In brief, 2 mL of the adjusted cell suspension was carefully layered on top of cold Percoll gradient comprising densities of 1.060, 1.070, 1.085, 1.108 and 1.118 g.mL⁻¹ (Percoll[®], P1644, Sigma-Aldrich, Ayrshire, UK; see the product information sheet on how to prepare the continuous density gradient using a 1.5 M NaCl solution) and centrifuged at 450 × g, for 45 min at 4 °C. The continuous density gradients were monitored by means of coloured density marker beads (17-0459-01, Pharmacia Biotech, Uppsala, Sweden).

The cell homogenates from the different gradients were collected and transferred into separate tubes with ice-cold TNPI buffer. Thereafter, the cell suspension was centrifuged at 600 × g, for 7 min at 4 °C, the supernatant discarded and the cells re-suspended in ice-cold TNPI buffer. This procedure was repeated twice, by the end of which the cell pellet was re-suspended and adjusted to give a concentration of 2 × 10⁶ cells.mL⁻¹ with cold TNBI buffer.

The cell population located in each density fraction was confirmed by microscopic examination of cytopins stained either with haematoxylin and eosin (H&E, see Appendix 1 for the staining protocol), or by the IHC protocol described in Section 5.2.5.3. For this

purpose, aliquots of 100 μ L from each sample were diluted in 1:1 foetal bovine serum (FB1000, Biosera Ltd., East Sussex, UK), and spun onto cytoslides using a cyto centrifuge (Shandon Cytospin[®] 3, Thermo Fisher Scientific Inc., UK) at 1000 \times *g*, for 4 min. The slides were then fixed for 7 min with 100 % ethanol, allowed to dry and kept at 4 °C until used. Meanwhile, the cell suspensions prepared earlier were aliquoted into smaller volumes and the insoluble fraction of the cells isolated (*i.e.* membrane covered granules) as described by Lindstedt & Kovanen (2001), with some modifications. The cell suspensions were subjected to mild sonication in a water bath (Bench-top ultrasonic 1210, Geneve, Switzerland) for 30 s at 4 °C, and the samples then centrifuged at 150 \times *g*, for 10 min at 4 °C. Cell pellets were re-suspended in ice-cold TNPI buffer, and sonication / centrifugation steps repeated twice. Supernatants containing the soluble remnant were collected each time, whereas the insoluble remnants were re-suspended. Finally, both soluble and insoluble fractions were transferred to separate cryogenic vials, to which equal volumes of sodium dodecyl sulphate (SDS) sample buffer (0.5 M Tris-HCl, 20 % glycerol, 4 % SDS, 2 mM DTT, 0.02 % bromophenol blue, pH 6.8) were added before storing at -70 °C, until analysed using polyacrylamide gel electrophoresis under denaturing conditions (Section 6.2.2.3).

6.2.2.3. Electrophoresis and western blot

Western blot was performed to determine the molecular weight of the antigen that the rabbit polyclonal antibody against caspase-3 (Anti-ACTIVE[®] Caspase-3 Ab, G7481, Promega, Madison, USA) recognises in Atlantic salmon intestinal MCs / EGCs obtained by the isolation procedure described in Section 6.2.2.2.

After denaturing for 2 min in a boiling water bath, both soluble and insoluble remnants samples were centrifuged at 16000 \times *g*, for 5 min and each loaded onto an electrophoresis well of a 12 % polyacrylamide gel (Pro-Pure Next Gel[™], M257, AMRESCO, Solon, USA) with 0.015 % 1,2-bis(dimethylamino)ethane (TEMED, T9281, Sigma-Aldrich, Ayrshire, UK) and 0.07 % ammonium persulphate (A3678, Sigma-Aldrich, Ayrshire, UK). Precision Plus Protein[™] Kaleidoscope[™] prestained standards (161-0375, Bio-Rad Labs Ltd., Hertfordshire,

UK) were also loaded into one of the electrophoresis wells, so as to allow the estimation of the subsequent molecular weight of the unknown proteins being identified. The running buffer used was Next Gel™ Running (M259, AMRESCO, Solon, USA). Electrophoresis was carried out at 100 V for 15 min and at 175 V for 1 h (Mini Protean® II Electrophoresis system, Bio-Rad Labs Ltd., Hertfordshire, UK).

Subsequent to the SDS-PAGE (Sodium Dodecyl Sulphate – Polyacrylamide Gel Electrophoresis), proteins in the gel slabs were transferred to a nitrocellulose membrane (GE™ Healthcare Amersham Hybond™ Membranes, 45-000-839 Thermo Fisher Scientific Inc., UK). After equilibrating the membrane and the gel for 20 min in a transblot buffer (161-0734, Bio-Rad Labs Ltd., Hertfordshire, UK), they were transferred into a wet blotting apparatus (SE250 Mighty Small II Mini-vertical Gel Electrophoresis Unit, Hoefer Inc., Holliston, USA) before applying 60V for 60 min. The membrane was then incubated for 60 min at room temperature, with 1 % bovine serum albumin (A9647, Sigma-Aldrich, Ayrshire, UK) in TBST.

Thereafter, the membrane was washed three times, for 5 min each, with TBST and left to incubate overnight with a rabbit polyclonal antibody against caspase-3 (Anti-ACTIVE® Caspase-3 Ab, G7481, Promega, Madison, USA), diluted 1:250 in TBST. After this incubation, the membrane was washed again three times, for 5 min each, before incubating for 1 h at room temperature, with a peroxidase conjugated anti-rabbit IgG secondary antibody (Goat Anti-Rabbit IgG-HRP, G21234, Life Technologies Paisley, UK), 1:100 diluted in PBS. The membrane was washed twice with TBST for 5 min each, and finally the peroxidase activity was developed with a KLP-kit chromogen / substrate solution (4CN Membrane Peroxidase Substrate System (2-C) KPL Kit, 507304, Wembley, UK). The reaction was stopped after 10 min with distilled water.

6.3. Results

6.3.1. Anatomical distribution of MCs / EGCs

In the distal intestine of Atlantic salmon, granule cells resembling MCs / EGCs, were observed in the *stratum granulosum externum* (Sg_{ext}), where they were organised in three or four rows distributed along both sides of a compact layer of collagen, the *stratum compactum* (Figure 6.1 A). Some of the cells were also found to be scattered in the *lamina propria* and in connective tissue strands of the mucosal folds (Figure 6.1 B). However, the *internal stratum granulosum* (Sg_{int}) and the subepithelial layers of the *propria* contained noticeably fewer cells. These granulated cells were easily recognised by their morphology, which has previously been described by Smith (1975), Ezeasor & Stokoe (1980), Bergeron & Woodward (1983) and are termed mast cells / eosinophilic granule cells (MCs / EGCs) throughout the present chapter.

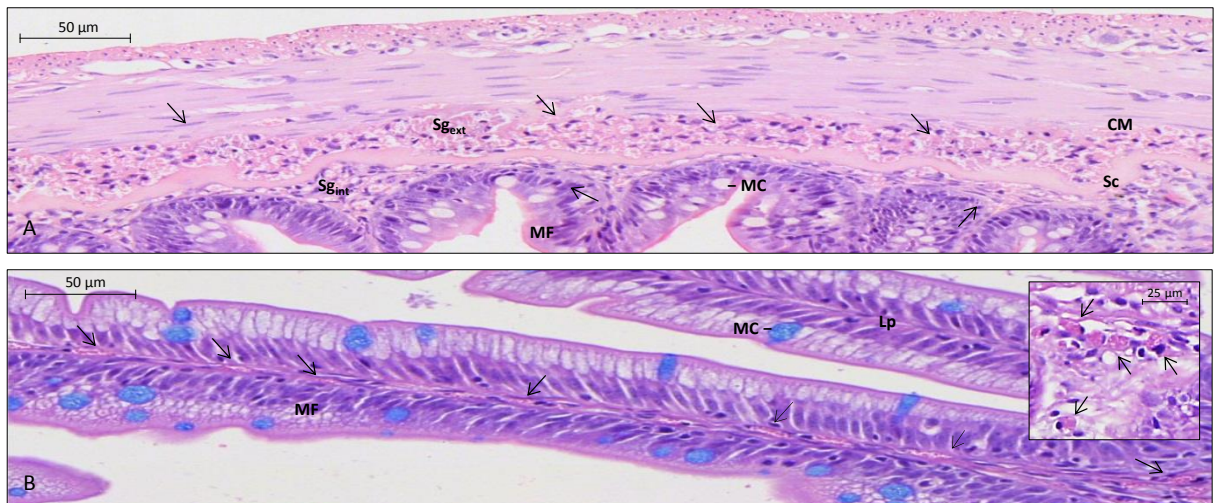


Figure 6.1. Granule cells resembling mammalian MCs / EGCs (arrows), found in the distal intestine of Atlantic salmon (A) between the circular muscle layer (CM) and the *stratum compactum* (Sc), forming a layer of a few rows of granulocytes in the *Stratum granulosum* (Sg), but also (B) scattered in the *lamina propria* and in connective tissue strands of the mucosal folds (MF). Mucous cell (MC). Transverse intestinal sections were stained with either (A) haematoxylin and eosin or a (B) combination of haematoxylin-eosin and Alcian blue.

6.3.2. Histochemical contents

Light microscopy showed the identified MCs / EGCs to be around 8-15 μm in length and 5-8 μm wide. They display a range of morphologies, but when unconstrained by surrounding tissues they were oval, and had a spherical nucleus, sometimes indented (Figure 6.1 B, Figure 6.2 E). When in areas compressed by other tissues, the cells appeared ruptured and the granules dispersed (Figure 6.2 A-D). In some cells nucleus was not observed (probably because of the section's thickness), but they were nevertheless packed with highly refractile round-granules (Figure 6.2 B-C). Such membrane bounded cytoplasmic granules stained bright red or pink with haematoxylin-eosin (H&E; Figure 6.3 A), haematoxylin-erythrosin-safran (HES; Figure 6.3 B) or a combination of haematoxylin-eosin and Alcian blue (H&E-AB; Figure 6.4 E), whereas they stained blue or bluish violet with May-Grünwald-Giemsa (MGG; Figure 6.4 A).

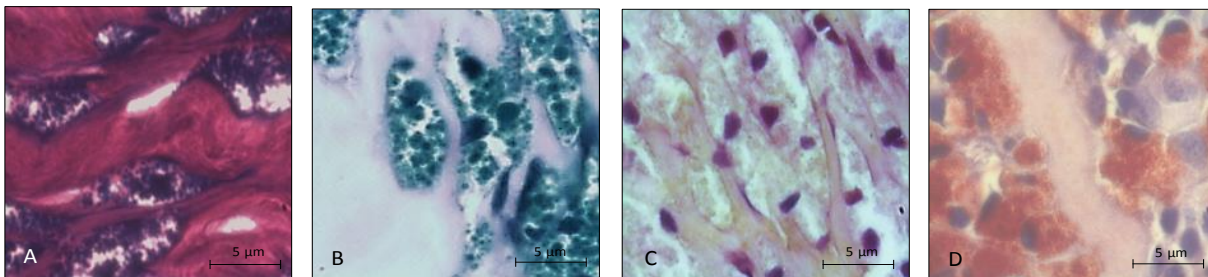


Figure 6.2. The granules of MCs / EGCs in the distal intestine of Atlantic salmon stained with different dyes and chromogens. (A) a Romanowsky Rapidiff® stain kit, (B) thionin, (C) anti-Caspase 3 antibody with an EnVision™ DAB chromogen and (D) anti-Active Caspase-3® with Vector®Nova Red™ chromogen.

The MC / EGC granules displayed no affinity for toluidine blue, staining very pale blue instead of the expected red-purple metachromatic colour seen in mammalian mast cells and attributed to the heparin content precursor staining (Figure 6.4 B). Likewise, numerous cells treated with thionin or Azur A (Figure 6.3 C and D respectively), displayed a strongly blue coloured precipitation instead of purple or deep violet. While they seemed not to stain with Astra blue (Figure 6.4. F), they proved faintly positive with the combined periodic acid Schiff

(PAS-Alcian Blue and PAS-Haematoxylin; Figure 6.4 B and C respectively), while epithelial mucous cells stained intensively purplish-pink and blue showing the validity of these methods.

In addition to the histological examination described above, the MCs / EGCs were also investigated using a number of antibodies known to recognise components of mammalian mast cells in immunohistochemistry. Figures 6.5 and 6.6 show transverse sections cut through the distal intestine of Atlantic salmon in parallel with mammalian positive control tissues staining for the selected antigens. The majority of the anti-mammalian mast cell antibodies did not show affinity for components of salmon intestinal MCs / EGCs, although they showed a positive reaction with mammalian control tissues employed alongside (*i.e.* Figure 6.5 A, C, E, G, I, K). No reaction was obtained with anti-tryptase (Figure 6.5 B), anti-myeloperoxidase (Figure 6.5 F), anti-lysozyme (figure 6.5 H) and anti-chymase (Figure 6.5 L) antibodies against fish MCs / EGCs. On the other hand, whilst incubation of the same intestinal region with an anti-c-Kit antibody from a CD117 transmembrane tyrosine protein kinase receptor kit gave a negative reaction with fish MCs / EGCs (Figure 6.5 D), fish rodlet cells were occasionally positively stained with this antibody.

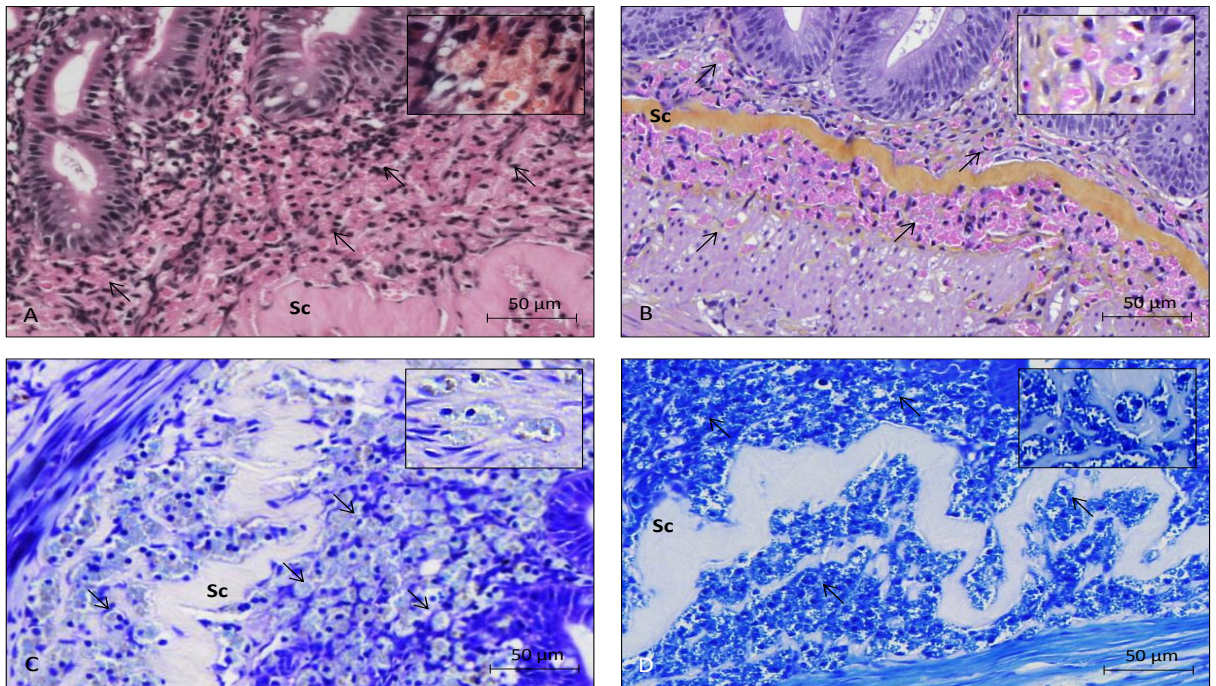


Figure 6.3. Photomicrographs of normal distal intestine of Atlantic salmon, showing (arrows) MCs / EGCs lying along the *stratum granulosum* adjacent to the *stratum compactum* (Sc). Transverse sections were stained with (A) haematoxylin and eosin, (B) haematoxylin-erythrosin-safran, (C) thionin and (D) Azur A.

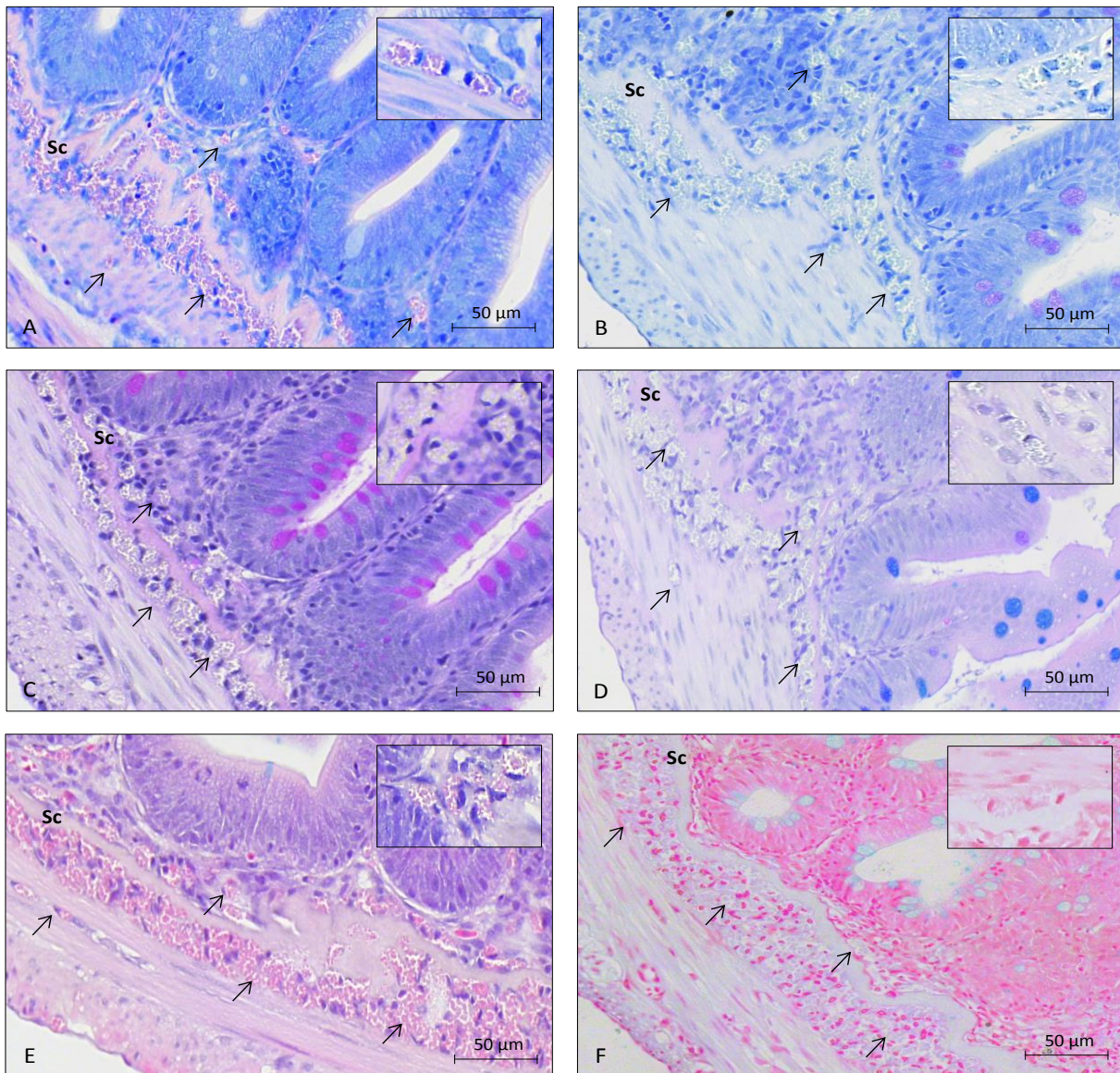


Figure 6.4. Photomicrographs of normal distal intestine of Atlantic salmon, showing (arrows) MCs / EGCs lying along the *stratum granulosum* adjacent to the *stratum compactum* (Sc). Transverse sections were stained with (A) May-Grünwald-Giemsa, (B) toluidine blue, (C) periodic acid Schiff and haematoxylin, (D) periodic acid Schiff and Alcian blue, (E) haematoxylin-eosin-Alcian blue and (F) Astra blue.

Immunohistochemical staining of salmon intestinal tissue sections with the antibody met-enkephalin gave a positive reaction with MC / EGC granules in cells located along the *stratum compactum* (Figure 6.5 J; Note that the concentration of antibody for this IHC should probably be optimised since there seems to be over-staining in some regions), whereas with the substance-p antibody the cytoplasmic granules appeared negative, while

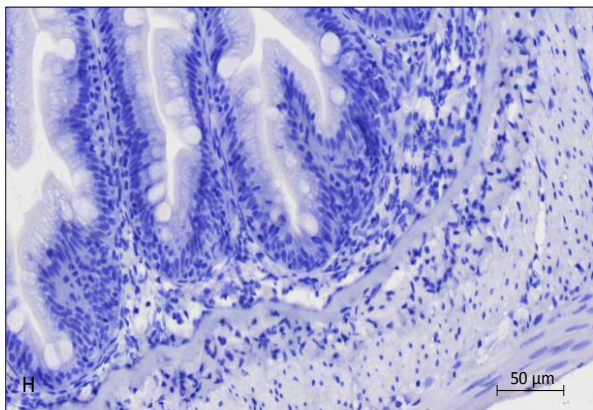
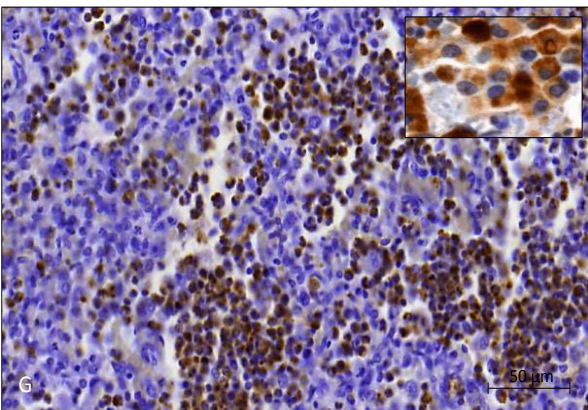
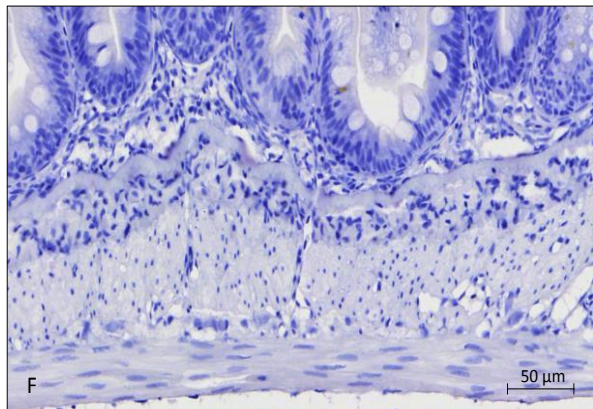
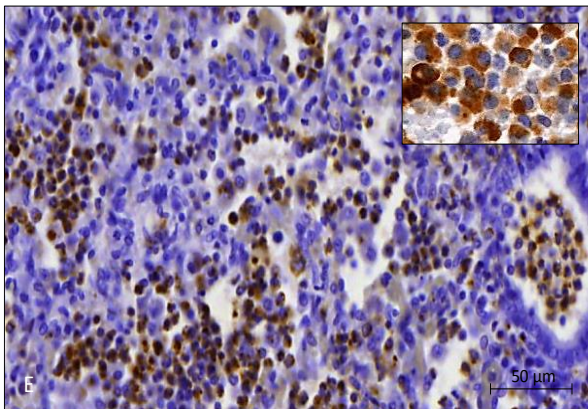
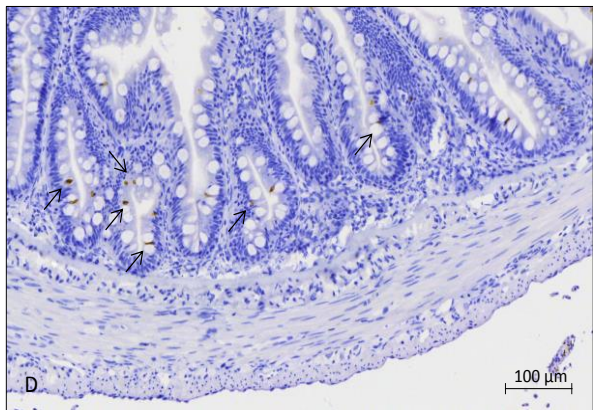
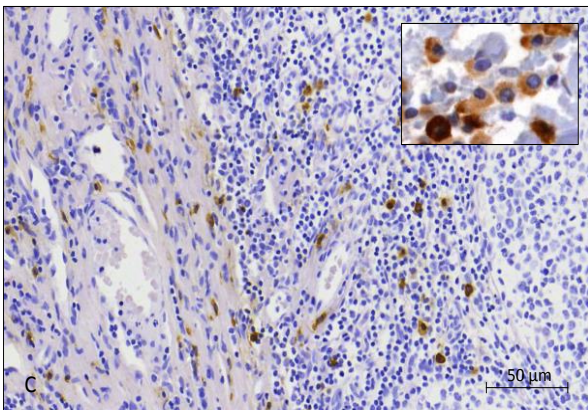
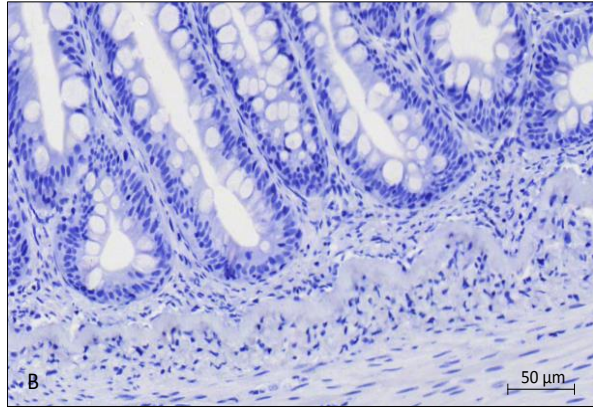
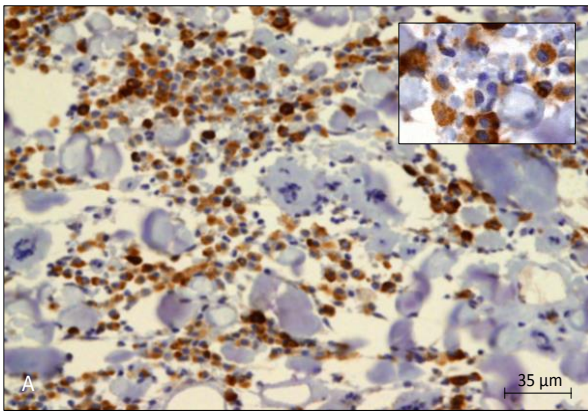
the cytoplasm of a few MCs / EGCs seemed positive (Figure 6.5 I) – Dr. Bahram Dezfuli *pers. communication*.

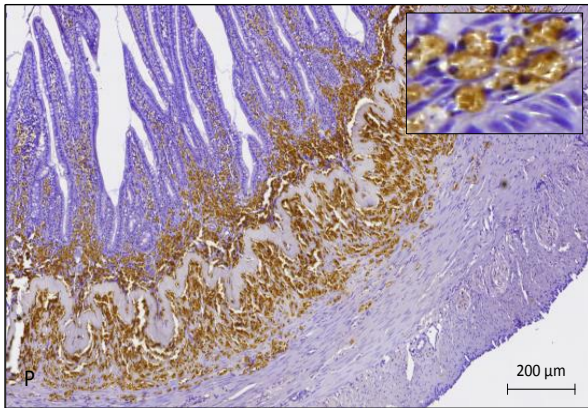
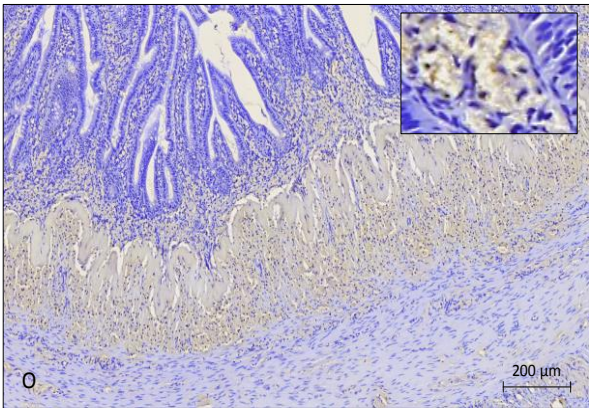
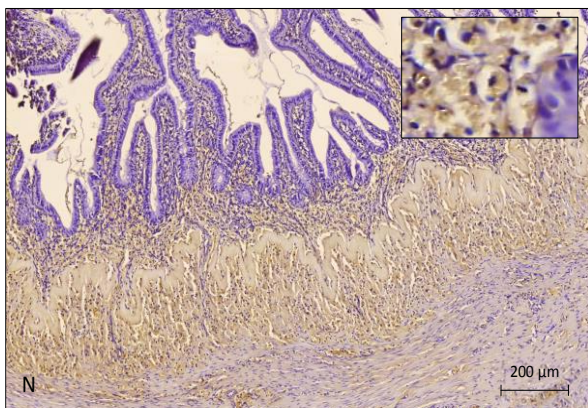
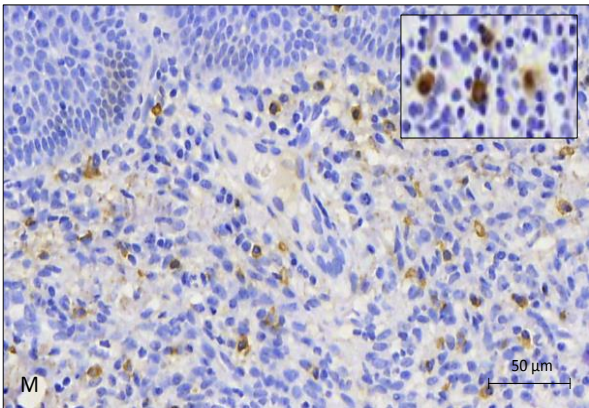
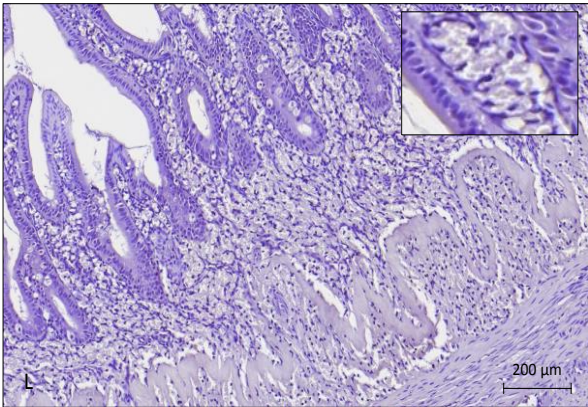
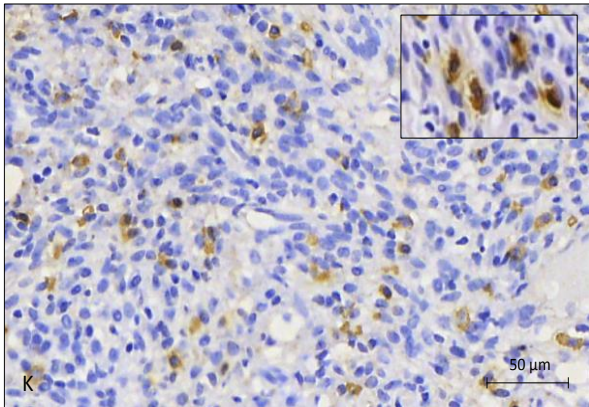
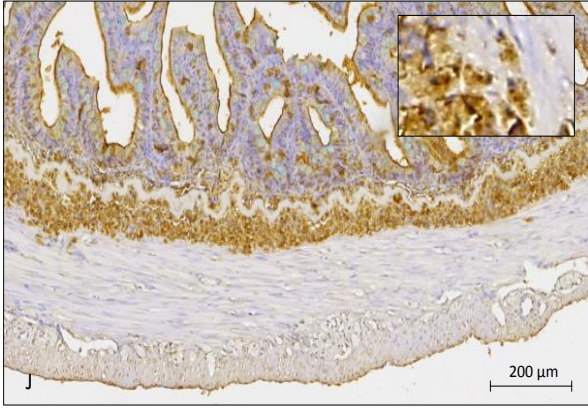
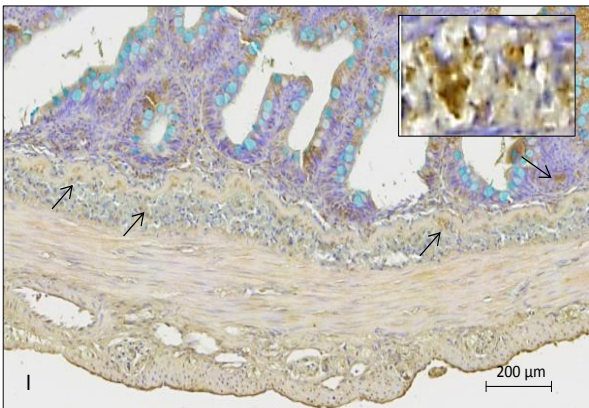
As shown in Figure 6.6 A-D, the antibody against human caspase-3 reacted specifically with Atlantic salmon MCs / EGCs cytoplasmic granules. These cells also stained positively with anti-serotonin (Figure 6.5 N) and anti-caspase 7 (Figure 6.5 P), although very faintly positive granules were only occasionally observed with an anti-pre-caspase 3 antibody (Figure 6.5 O).

6.3.3. Ultrastructure morphology and cytochemistry

At an ultrastructural level, it could be seen that the granule cells closely resemble those previously described by Ezeasor & Stokoe (1980). The majority of the intestinal MCs / EGCs were arranged in a definite layer along both sides of the *stratum compactum*. Observed individually or in groups, these cells were invariably ensheathed in fibroblast-like connective tissue cells (Figure 6.7 A and C). MCs / EGCs were shown to be variable in shape and contained numerous round granules ranging from 0.4-1.2 μm in size (Figure 6.7 A). With surrounding perigranular halos (Figure 6.7 B-D), these granules were of

Figure 6.5. (following two pages) Photomicrographs showing IHC labelling of MCs / EGCs (brown colour) using different antibodies, either in distal intestinal tissue sections of Atlantic salmon or in mammalian positive control tissue sections known to express the antigens of interest. (A) Cytospin for feline isolated lymphocytes where MCs were positively stained for tryptase. (B) Teleost intestinal tissue section showing absence of tryptase immunoreactivity in MCs / EGCs. (C) Human colonic carcinoma tissue section with positive immunoreactive MCs to the anti-c-Kit antibody. (D) Distal intestine tissue section from a salmonid, showing MCs / EGCs negatively stained for the CD117 transmembrane tyrosine protein kinase receptor kit, whilst (arrows) rodlet cells were occasionally immunoreactive. (E and G) Human tonsil tissue sections demonstrating a positive reaction for myeloperoxidase and lysozyme in MCs respectively. (F and H) Serial tissue sections from a salmonid distal intestine sample displaying no immunoreactivity of MCs / EGCs for anti-myeloperoxidase and anti-lysozyme antibodies, respectively. (I) Teleost MC / EGC cytoplasmic granules showing negative labelling for substance-p antibody, while (arrows) the cytoplasm of a few cells are positive. (J) Salmon intestinal MC / EGC granules showing positive staining with met-enkephalin. (K) Chymase and (M) serotonin IHC of MCs from tissue sections of a canine skin tumour. (L) Fish intestinal section showing no MC / EGC immunoreactivity for chymase. (N) Salmonid intestinal MCs / EGCs displaying immunostaining for (O) serotonin, (P) pre-caspase-3 and (Q) caspase-7.





variable electron densities and frequently compressed the nucleus to one side of the cell (Figure 6.7 B and D). Based on their ultrastructure, these granule cells were easily recognised and comparable to those observed in serial (Figure 6.6 E-F) or adjacent (Figure 6.8) semi-thin sections, stained in parallel using IHC and an immunofluorescence antibody method with an antibody directed against a peptide from the p17 fragment of human caspase-3 and where, the ultrastructural granular matrix was consistently found to be positively stained for caspase 3. Likewise, caspase-3 immunogold-reactivity was found within the electron-dense core of the cytoplasmic granules (Figure 6.9), in a concentration-dependent manner.

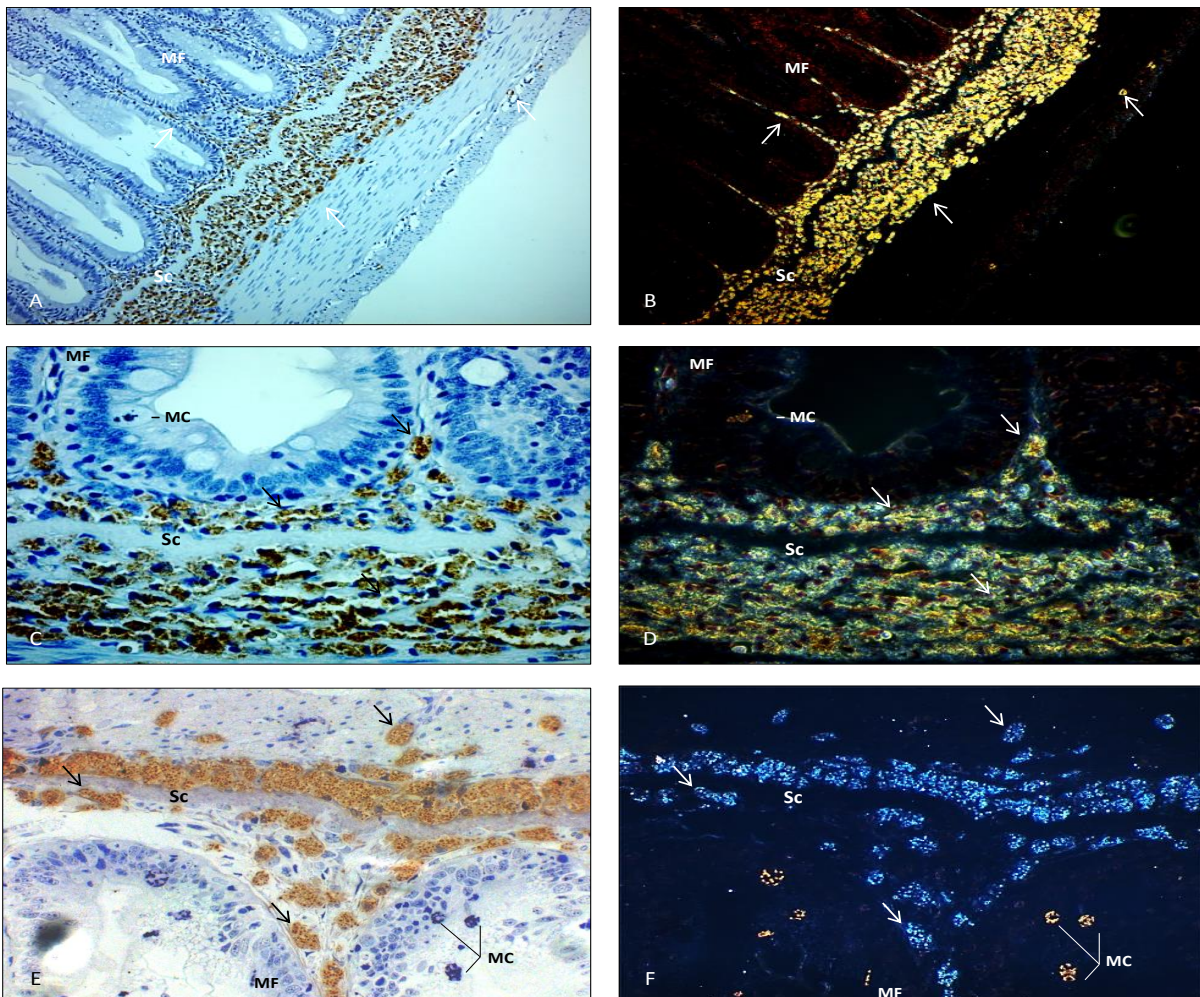


Figure 6.6. Atlantic salmon distal intestine MCs / EGCs (arrows), staining positively for an antibody directed against a peptide from the p17 fragment of human caspase-3. Photomicrographs comprising sections (A-D) 7 μ m and (E-F) 2 μ m thick observed either under light microscopy with (A, C, E) the sub-stage condenser removed or with (B, D, F) a dark field phase contrast showing more clearly the refractive granules. (Sc) *Stratum compactum*. (MF) Mucosal fold. (MC) Mucous cell. (Lp) *Lamina propria*.

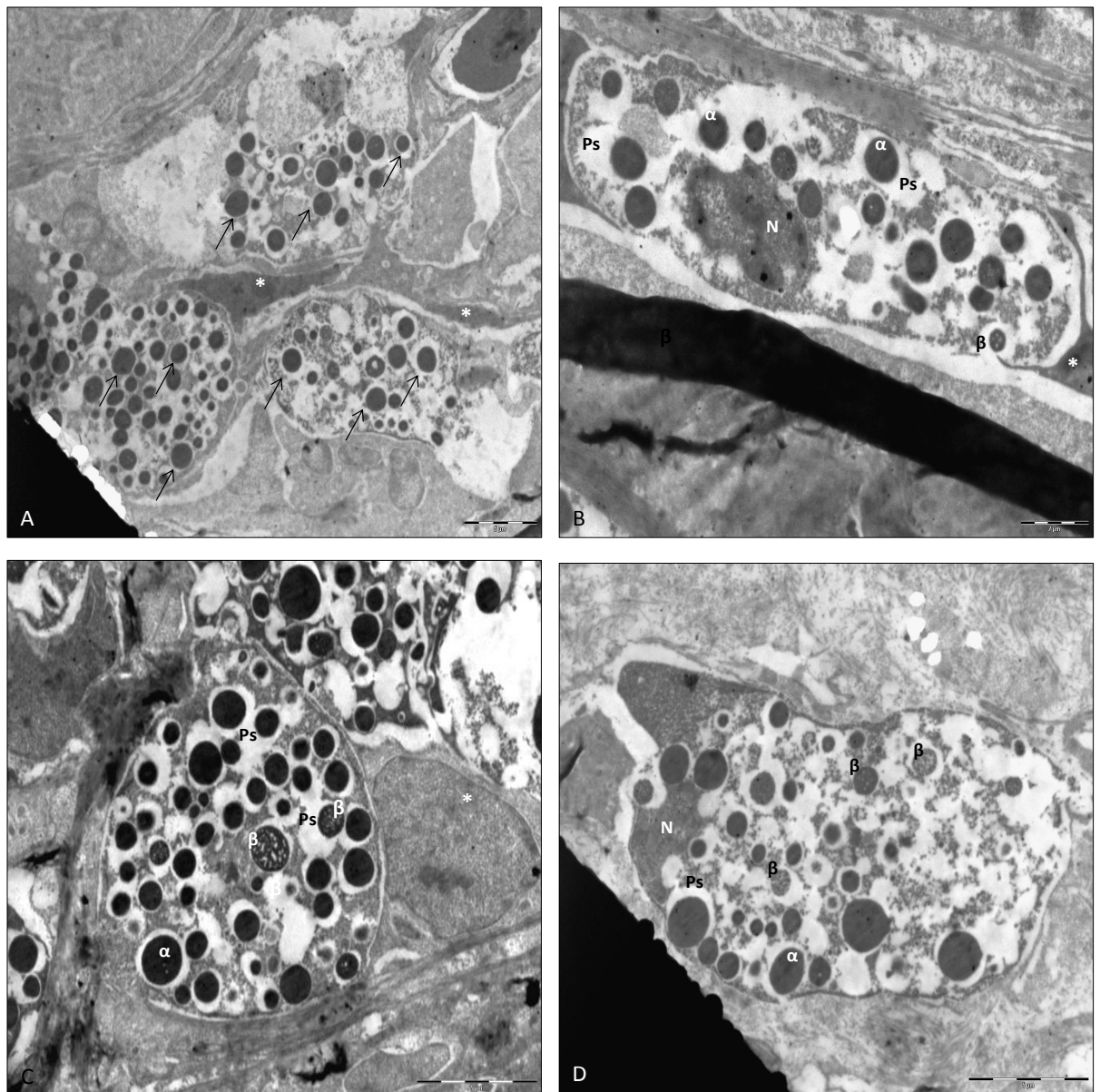


Figure 6.7. Electron micrograph of MCs / EGCs from the distal intestine of Atlantic salmon (Bar = 5 μ m). The cytoplasm of these cells contains several (α) highly dense homogenous core granules, and (β) low electron density cores or with those having pronounced vacuolisation, that were surrounded by a filamentous matrix. (N) Nucleus. (Ps) Perigranular halo or space. (arrows) Granules. (asterisk) Surrounding cells.

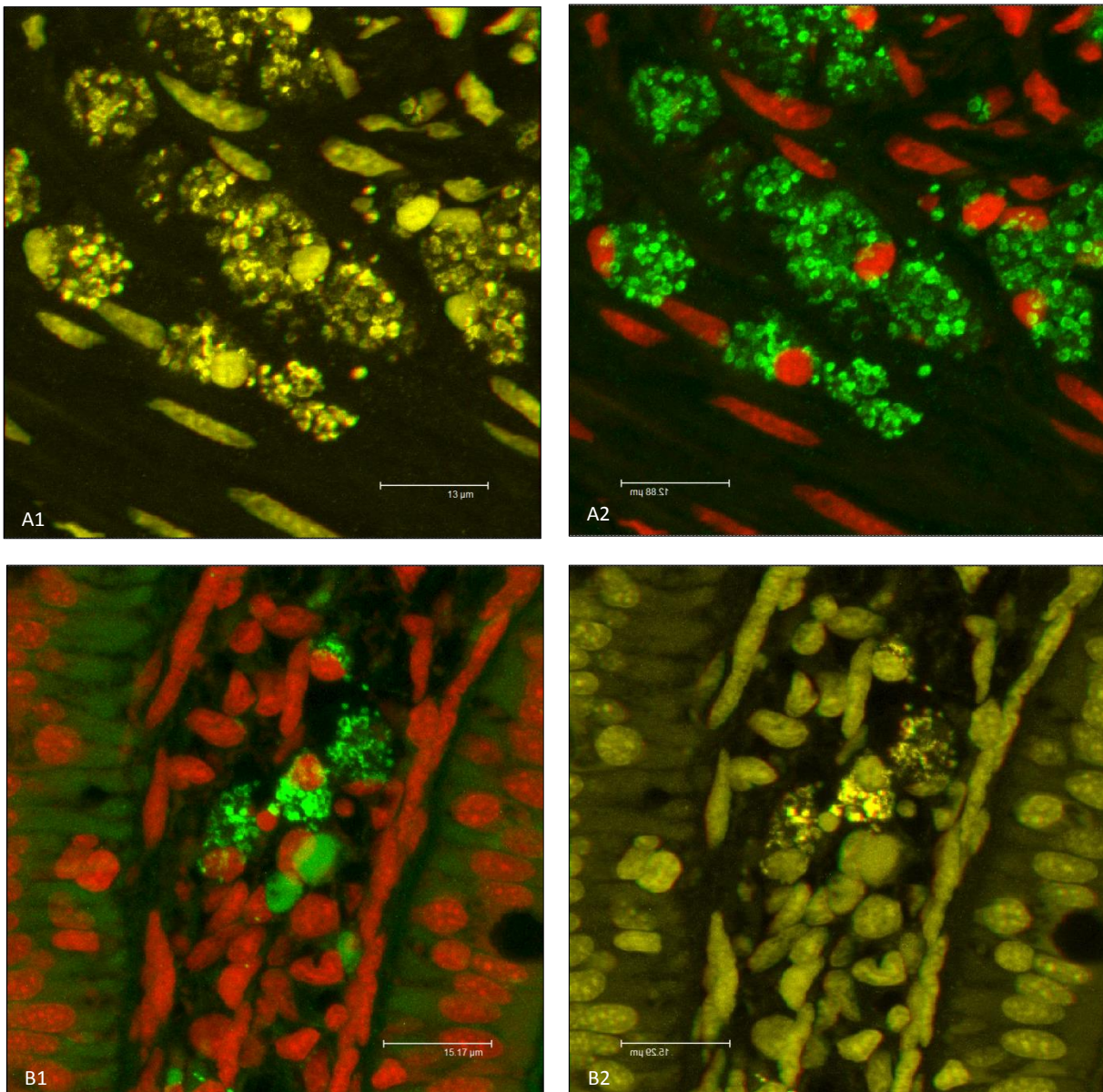


Figure 6.8. Confocal micrographs showing the immunolocalisation of MC / EGC granules from the distal intestine of Atlantic salmon, incubated with a caspase-3 FITC-conjugated antibody and counterstained with a red nuclear stain. (A1 and B2). 3D anaglyph images equivalent to the lateral adjacent 2D coloured micrographs, corresponding to a double fluorescent staining. (A2 and B1) Cytoplasmic granules labelled in green by FITC dye, and the nucleus in red by Propidium iodide dye.



Please make use of the glasses included at the end of this thesis, to visualise the 3D anaglyph image-micrographs presented in Figure 6.8 A1 and B2.

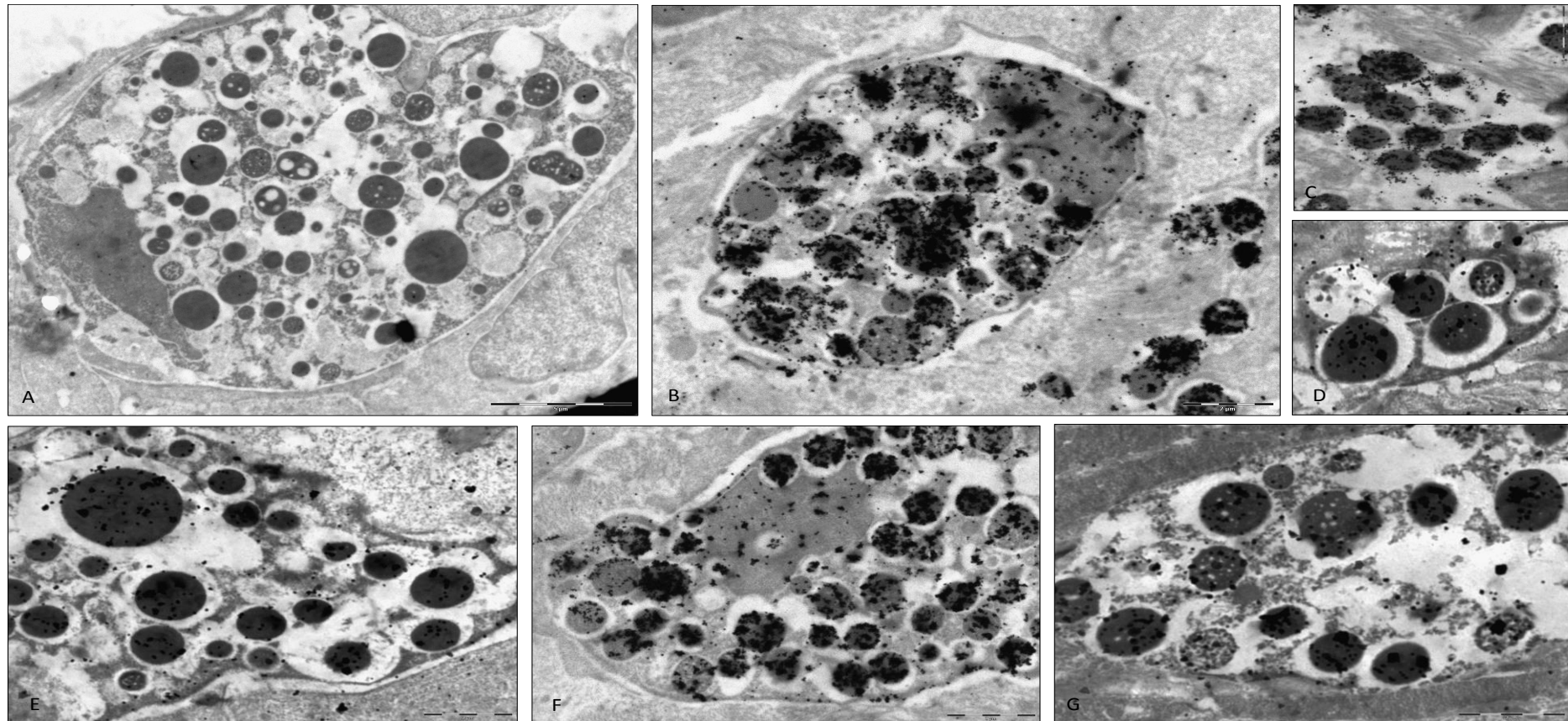


Figure 6.9. Ultrastructural immunogold labelling of Atlantic salmon intestinal MC / EGC granules, using a gold-covalently-conjugated antibody directed against a peptide from the p17 fragment of human caspase-3 (Bar = 2 μ m). (A) Ultra-thin control tissue section incubated with rabbit normal serum instead of the primary antibody, shows absence of gold particle deposits. (B-G) Ultra-thin tissue sections incubated with different concentrations (B-C, 1:250; D-E and G, 1:10000; F, 1:500) of the conjugated caspase-3 antibody. Note the coarse deposits of colloidal gold particles in the granular matrix areas.

6.3.3.1. Isolation of intestinal granulocytes and immunoblotting characterisation

Cell fractions recovered from the intestinal cell suspensions and subjected to a Percoll[®] differential density gradient comprised erythrocytes, lymphocytes, macrophages and granulocytes. The 1.060 g.mL⁻¹ fraction (Figure 6.10 A) was composed mainly of cellular and epithelial debris, several lymphocytes and some macrophages, whereas fraction 1.070 g.mL⁻¹ comprised granulocytes and several lymphocytes (Figure 6.10 B). While fractions 1.085 g.mL⁻¹ and 1.108 g.mL⁻¹ were composed almost exclusively of granulocytes (Figure 6.10 C and D, respectively), the 1.118 g.mL⁻¹ fraction contained erythrocytes and rare lymphocytes (Figure 6.10 E). It is worth noting that the vast majority (~60-75 %) of the granulocytes were immunohistochemically positive for the anti-caspase 3 antibody.

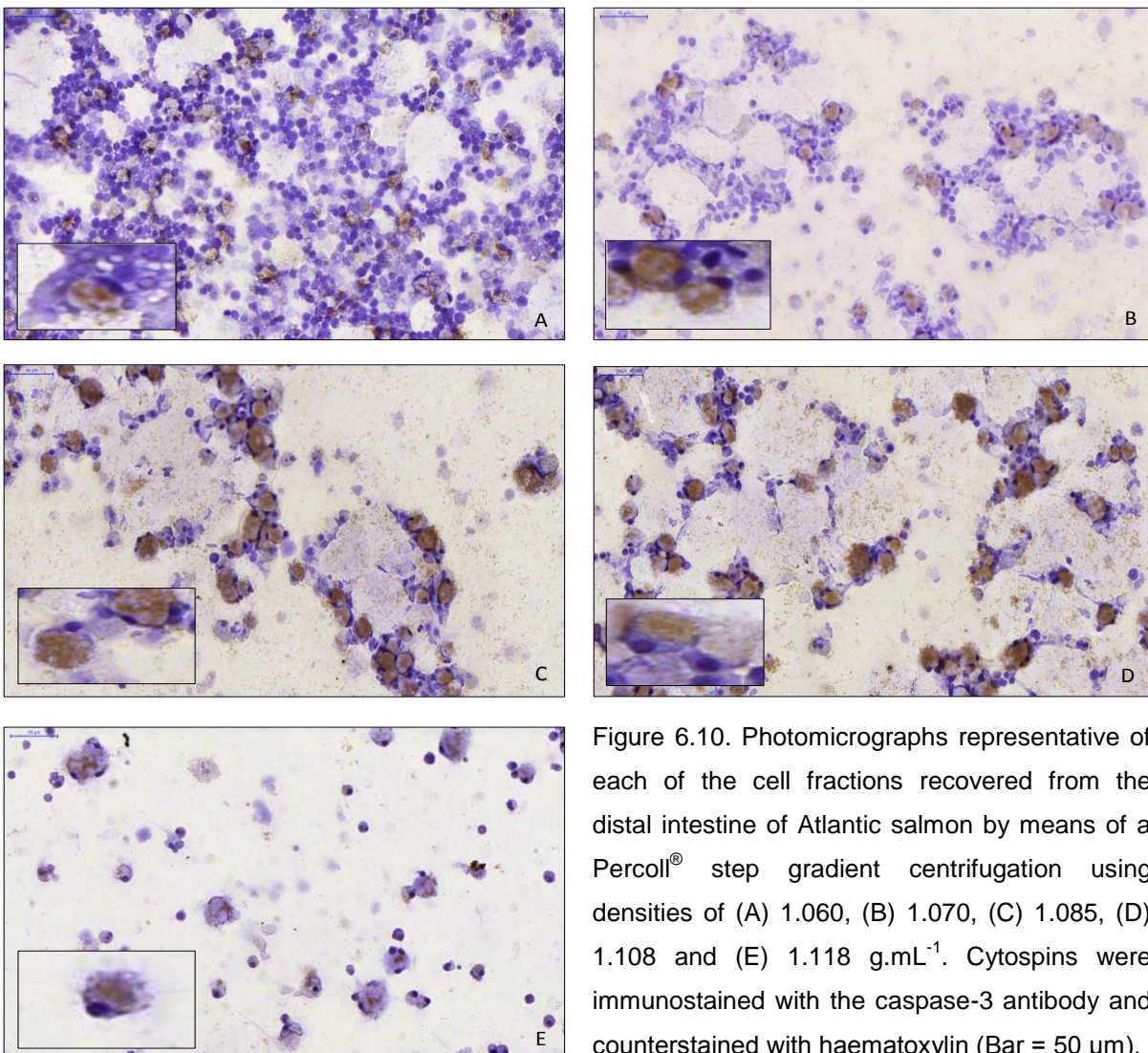


Figure 6.10. Photomicrographs representative of each of the cell fractions recovered from the distal intestine of Atlantic salmon by means of a Percoll[®] step gradient centrifugation using densities of (A) 1.060, (B) 1.070, (C) 1.085, (D) 1.108 and (E) 1.118 g.mL⁻¹. Cytospins were immunostained with the caspase-3 antibody and counterstained with haematoxylin (Bar = 50 µm).

The gradients between densities 1.070 g.mL^{-1} and 1.108 g.mL^{-1} enabled recovery of a cell population almost exclusively composed of granule cells resembling those described in Sections 6.2.1.2 and 6.2.1.3, and were therefore the ones used for the gel electrophoresis and immunoblotting. Regardless of the incubation time with the caspase-3 antibody or the blocking agent employed, the protein profile for these MCs / EGCs could not be demonstrated (*i.e.* no distinct bands were formed within the lanes, but rather a continuous smear was noticeable in the stained gels), this being particularly evident for the insoluble remnant fraction, although for the soluble remnants a similar situation occurred.

6.4. Discussion

One of the principal aims of the work presented in the current chapter was to examine the cytochemistry and ultrastructure of salmon intestinal MCs / EGCs, as a basis for understanding their potential function and in order to allow their potential characterisation / quantification through the use of the image analysis system described in Chapters 1 to 5 presented in this thesis. The latter system was developed to assist pathologists with the histological evaluation of fish intestinal biopsies, while providing an alternative approach to the semi-quantitative scoring methods currently used for intestinal fish health assessment. In this respect, the quantification / description of the presence and spatial distribution of cells considered to be key mediators of inflammatory responses initiated through food hypersensitivity or any of a wide range of other physiological and pathological immune states, that are of particular interest.

The classification system mentioned throughout this thesis has been based on advanced image analysis techniques that need to be able to discriminate very particular features of the tissue / cell structure in order to recognise histomorphological and histochemical changes. Aspects of colour, size, shape or texture, are the features most easily detected and measured. Thus for the imaging software to be able to identify MCs / EGCs, or similar cell types, staining / labelling techniques need to be able to highlight these cells with respect to surrounding tissue.

Based on the morphological descriptions gathered for these types of cells from the literature, discrimination based on regional distribution, texture or size thresholds appeared feasible. However, for this to be possible, image segmentation using pixel colour was a principal requirement. Thus, selection of an adequate discriminatory colouring-profile was a priority.

From a review of the literature it was evident that there is considerable controversy with respect to the staining properties of fish MC / EGC cytoplasmic granules. Besides variations between different fish species, the nature of the fixative solution employed is also reported to have an effect on the staining-profile outcome (Blackstock & Pickering, 1980; Reite, 1997; Jordanova *et al.*, 2007; Schmale *et al.*, 2004). Nevertheless, the review of teleost MC / EGC staining properties by Reite & Evensen (2006) provides relevant information on how to specifically stain such granulocyte cells using techniques that appear suitable for morphometric analysis using an image analysis system. It should be noted, however, that staining techniques do not always prove to be ideal for image analysis (Bianchi & Mugnai, 1990), as the human capacity to resolve subtle differences vastly exceeds that of computer software.

While it is possible to filter original images to enhance the object of interest, such operations tend to alter the image information and can be highly subjective in application. Hence the best approach is to start with an original digital image in which the object of interest is already substantially differentiated from the surrounding tissue. With this in mind, a panel of ten different histochemical stains (listed in Table 6.1) commonly employed for MCs / EGCs were screened, with the aim of finding the one most suitable for imaging identification (*i.e.* a staining technique of high reproducibility and uniformity in terms of colour and intensity of staining; providing strong contrast with the surrounding background; having relatively low time / cost overheads and being simple to perform).

Morphologically, the cells identified as MCs / EGCs in the present study were identical to those described by other authors for similar salmonid tissues (Bolton, 1933; Smith, 1975; Ezeasor & Stokoe, 1980; Bergeron & Woodward, 1983; Sire & Vernier, 1995). In common

with these studies cells were scattered in the *lamina propria* and in the connective tissue strands of the mucosal folds and were distributed on both sides of the *stratum compactum*. These cells appeared round or ovoid-shaped with a large marginally-placed nucleus, in tissue fixed for light microscopy, and were filled with highly refractile cytoplasmic granules. In electron micrographs they revealed to be more elongated and showed a large eccentric nucleus often indented to one side of the cell, with several electron dense membrane-bound granules contained within.

Histochemically, the cytoplasmic granules stained bright red or pink with H&E, and HES which demonstrates acidophilic components within the granules, whereas the blue or bluish violet staining obtained with MGG revealed basophilic components. These staining properties were as previously reported, and in part might be associated with the use of buffered formalin as a fixative solution, which may have removed a considerable portion of the basophilic components from the granules (Roberts *et al.*, 1971; Blackstock & Pickering, 1980; Reite, 1997; Walls *et al.*, 1990; Ostrander, 2000; Rocha & Chiari-Garcia, 2007). This may explain why the term “eosinophilic granule cell” is not entirely accepted by some authors as a reference to this cell type and therefore perhaps the term “mast cell”, would be more appropriate.

The MC / EGC nucleus stained strongly blue, with toluidine blue indicating the presence of nuclei acid (Bergeron & Woodward, 1983), however the cytoplasmic granules were metachromatic-negative. The metachromatic properties of the granules are believed to be due to the heparin and acid sulphated mucopolysaccharide content (Schubert & Hamerman, 1956) at least in mammalian MCs. Consequently one might conclude from the present study that these substances are not a key component of the granule cells of salmonids. This said, other studies have shown metachromatic staining of cells resembling granule cells for Atlantic salmon and rainbow trout tissues (Reite, 1997; Reite & Evensen, 1994; Mulero *et al.*, 2007). Other studies have demonstrated that this feature is often an artefact of fixation of tissues in aqueous fixatives such as formalin, as used in the present study, and that the use of alcohol based fixatives can in some cases allow retention of the

basophilic and metachromatic properties of the granules (Schmale *et al.*, 2004; Reite, 1998; Sigh & Buchmann, 2000). Thus the extent of metachromatic disparity probably depends as much on the intrinsic properties of the fixative being used as upon the level of the associated proteins in the granule.

Similarly, the MCs / EGCs gave a negative response to the methachromatic procedure for the thionin and Azur A reactions, but seemed fairly positive for neutral polysaccharides. Again, because previous studies showed metachromatic staining of the granules in tissues of rainbow trout, brown trout and Atlantic salmon fixed in ethanol and stained with thionin (Reite 1994, 1997; Sigh & Buchmann, 2000), this strengthens the view that different fixatives may help to retain the metachromatic properties of the granules.

For example, Wingren & Enerbäck (1983) have stated that aldehyde fixation can adversely affect the staining of mammalian mucosal mast cell granules, by combining with cationic protein groups such as primary amino groups of lysine and guanidinium groups of arginine and form cross-links between polypeptide chains that consequently increase the basophilia of MC granules. Such an increase has also been described by Spicer (1963) as a blocking of cationic protein groups, which would otherwise have repelled the dye molecules from anionic glycosaminoglycan sites.

Moreover, whilst the cytoplasmic granules of these cells were not stained with the Astra blue dye, and a slight positive staining was obtained with the combined PAS procedure, this may be indicative of the presence of sulphated and neutral glycosaminoglycans in the granule contents. In contrast, previous studies (Weinreb & Bilstad, 1955; Smith, 1975) have shown no PAS staining of MC / EGCs. The PAS histochemistry selectively stains carbohydrates, by the formation of an aldehyde which reacts to the Schiff reagent to form a magenta colour, and indicates the presence of glycol groups or their amino equivalents (Bancroft & Stevens, 1982). Therefore, if the precursor substance is diffusible or present in very low concentrations, no colour will be obtained.

In summary, salmonid MCs / EGCs have shown strong affinity for dyes such as erythrosine, eosin and methylene blue without background staining, and can therefore be

selectively stained using either H&E, HES or the MGG histological stains for morphometric appraisal using image analysis. It is worth noting that no variation in the staining of individual granules was observed, which may suggest that the membrane around the granules is impervious to most of these stains.

The HES stain proved to be just as effective as the other two stains, but with the added benefit of discriminating the *stratum compactum* in orange-yellow, which was a feature intentionally identified by the image analysis system to allow the morphometric distinction and formal division of the mucosal and submucosal tissue areas. Also, by combination with the AB dye, similarly to what has been shown with the H&E-AB staining profile, mucous cells could provide an additional measurement using the same digital image. Thus, of the ten staining profiles evaluated, HES+AB was selected as the best stain to evaluate intestinal histological sections through use of the morphometric image analysis system.

While histochemical stains carry advantages in terms of speed of staining, often they may be very general in their staining properties and may not reveal extensive information concerning the functional properties of the MCs / EGCs. An alternative approach is the use of IHC which, while often slower, more costly and more difficult to perform, can give highly specific and functionally informative labelling, which is useful both for image analysis and for the histopathologist. In this chapter, a number of IHC targets were examined (listed in Table 6.2).

The immunocytochemical study showed that salmonid MCs / EGCs were tryptase, c-kit, myeloperoxidase, lysozyme, chymase negative, whereas the granules seemed met-enkephalin and serotonin positive. The cytoplasm of some MCs / EGCs appearing positive for substance-p.

As regards serotonin, a biogenic amine present in the granules of mammalian mast cells, most of the studies performed with teleost species so far have shown that fish MCs / EGCs contain it (Reite, 1969; Nilsson & Holmgren, 1992; Khan & Deschaux, 1997; Mulero *et al.*, 2007; Dezfuli *et al.*, 2008, 2012). Serotonin (5-Hydroxytryptamine, 5-HT) is one of the most extensively studied neurotransmitters of the mammalian central nervous system, and

it was shown that 5-HT is involved in interactions between the central nervous and immune systems. Serotonin may mediate interactions of these two systems by T cell and natural killer cell activation, delayed-type hypersensitivity responses, production of chemotactic factors, and natural immunity delivered by macrophages (Mösener *et al.*, 1998; Mekori & Metcalfe, 2000; *inter alia*). While serotonin is one of the major mediators secreted by mammalian MCs, little is known about its role in the immune system of fish. By analogy with mammals, it is possible that 5-HT may influence the functioning of immunocompetent cells. In fact, metabolism of brain serotonin in fish has been found to be associated with stressful conditions and hypothesised to influence the functioning of other physiological systems, notably the immune system (Khan & Deschaux, 1997). Other studies using fish parasite infection systems, have documented the presence of serotonin in fish MCs / EGCs, and suggested that it exerts a variety of effects that may favourably affect the survival of the infected cells (Dezfuli *et al.*, 2000, 2003b, 2005), however, it is mentioned again that further information on the relationship between serotonin and the fish immune system, is required (Dezfuli *et al.*, 2011b).

The negative results obtained in the present study showing the absence of chymase immunoreactivity in MCs / EGCs, substantiates previous findings that this protease is not present in teleosts (Chiu & Lagunoff, 1972). However, recent reports have indicated the presence of granzyme-like serine proteases in teleost cytotoxic cells' granule exocytosis (Praveen *et al.*, 2006; Wernersson *et al.*, 2006) and it is well established that secretion of mammalian MCs' cell-specific serine protease chymase regulates the intestinal barrier function during disease and homeostasis (Groschwitz *et al.*, 2009).

The failure to demonstrate tryptase, c-kit, myeloperoxidase and lysozyme histochemically in salmon MCs / EGCs disagrees with the previous reports by Ishizeki *et al.* (1994), Sveinbjörnsson *et al.* (1996) and Dobson (2008). However, the numerous negative results in the immunohistochemistry, cannot be regarded as conclusive, and whether or not these differences are truly indicative of salmonid MC / EGC granule composition, cannot be ascertained without more thorough study. Systematic studies on the nature of the protein

components of teleostean MC / EGC granules are lacking, and there are only very few mentioned in the literature (Reite, 1998), and variation in the fish species being evaluated and the antibody sources could also be the basis for such differences observed and further studies are required.

It is worth mentioning that although an anti-c-Kit antibody gave a negative reaction with MCs / EGCs, fish rodlet cells were occasionally positively stained with this antibody. Previous immunohistochemical investigations of the latter cells in sunfish scale epidermis cultures have proven that the rodlet cell cortex was enriched with phosphotyrosine, whose activity has been implicated in some aspects of muscle contraction, and is suggested to be involved in triggering the rodlet cells to discharge (DePasquale, 2012).

With regard to met-enkephalin, in mammals this neuropeptide generates proliferative and / or antiproliferative responses of mucosal lymphocytes and intestinal epithelial cells and affects cytokine production and immunoglobulin synthesis by immune cells (Sirinek & O'dorisio, 1991; Genton & Kudsk, 2003). However, although its function is well known in mammals, the same function has not yet been established in fish (Dezfuli *et al.*, 2011b). Nonetheless, immunohistochemical staining studies referring to alterations in the neuroendocrine system of fish alimentary canal due to the presence of parasites, demonstrated the presence and accumulation MCs / EGCs positive for met-enkephalin antisera, in close proximity to the infected areas (Dezfuli *et al.*, 2000, 2002, 2005, 2008). These observations make it reasonable to presume that by increasing the amount of the met-enkephalin-like substance released by MCs / EGCs degranulation, the inflammation caused by the parasites would be modulated through a possible array of immunoregulatory functions involving potential granulocyte effector activities or merely through enhancement of lymphocyte natural killer activity as happens with their mammalian MCs counterparts (Payan *et al.*, 1983).

Immunohistochemical screening using an antibody raised against substance-p revealed a positive reaction for some of the MCs / EGCs cytoplasm. Substance-p is a neuropeptide secreted by inflammatory cells and has pro-inflammatory effects in immune and epithelial

cells (e.g. Payan, 1989; O'Connor *et al.*, 2004). Previous studies performed by Dezfuli *et al.* (2008), where immunohistochemical tests were applied on sections of brown trout intestinal tissue of healthy and parasitised infected fish, revealed a significantly higher number of positive endocrine cells in the epithelium of infected individuals, as well as the occurrence of substance-p-like material in cytoplasmic granules of MCs / EGCs. In rainbow trout, it was reported that Substance-p stimulates MC / EGC degranulation (Powell *et al.*, 1991, 1993b). Thus, it is not unreasonable to expect that it would have a similar effect on such activity in Atlantic salmon.

Moreover, a commercial antibody directed against a peptide from the p17 fragment of human caspase-3, was found to react strongly to intestinal MCs / EGCs. While initially intended for use as a marker of apoptosis (see Chapter 5), this strong positive reaction from the majority of MCs / EGCs was not expected, and therefore was later analysed by immunofluorescent and immunogold techniques, in order to confirm the immuno-localisation of the antigen reacting with this antibody. Both laser scanning confocal IFAT and electron TEM visualisation of IGL revealed that the antibody in question reacted strongly with features from the cytoplasmic granules of the MCs / EGCs. Thus the protein or peptide being labelled is limited to the granular matrix, and hypothetically could be relevant to the functional properties of these cells.

For over a century fish histologists and immunologists have attempted to determine the origin and functions of these cells, however from the review of the literature it is evident that fish MCs / EGCs still are a conundrum in this context, particularly regarding their functional properties, which are very unclear. Some consider these granulocyte cells to be a component of the teleost's innate immune system and to be involved in active inflammatory responses, especially those associated with infectious agents, chronic stress or food hypersensitivity reactions (Dezfuli *et al.*, 2002; Penissi *et al.*, 2003; Rocha *et al.*, 2007; Urán *et al.*, 2008; Sundh, 2009). Thus, having found a sensitive marker for these enigmatic cells, it may be possible to try and further elucidate their functional role in intestinal immunity.

Anti-ACTIVE[®] Caspase-3 antibody (G7481, Promega, Madison, USA) is an affinity-purified polyclonal antibody intended to detect the active form of caspase-3 that occur in apoptotic cells, thus making the antibody useful as an *in situ* marker for apoptosis. According to the manufacturer, this antibody was generated using an antigenic peptide that has an identical amino acid sequence in human, mouse, rat and hamster proteins, and therefore from the start it was anticipated that it could possibly cross-react with other species.

The same antibody has been reported to successfully detect apoptotic cells in intestinal tissue from Atlantic salmon (Bakke-McKellep *et al.*, 2007b) and from rainbow trout (Ronza *et al.* 2011), this being a key reason why this antibody was selected for screening in the identification of apoptotic cells for the current project. Surprisingly, in the present study this antibody cross-reacted with a very specific fish antigen located in the cytoplasmic granules of intestinal MCs / EGCs from Atlantic salmon. For this reason a western blot was conducted in order to help identify the molecular weight of the protein this antibody was labelling in fish. Unfortunately no protein profile was obtained, even after 5 distinct trials and because of the associated cost and time restrictions the intended analysis could not be completed.

The failure of the western membrane blotting might have been related to: (1) purification and concentration of the active enzyme from the cell extract may have been minimal; (2) during cell isolation, the protease inhibitor cocktail employed was not sufficient to avoid degradation of the material; (3) sonication step may have been excessive, causing protein degradation, which resulted in the smear band observed for the gels; or because (4) as the antibody's manufacturers stated that this product was not recommended for western blot (although no further information relating to this could be obtained from the manufacturer when requested).

Clearly, better optimisation of the isolation process needs to be performed. Besides testing higher concentrations of the broader protease inhibitor, it might be worth trying some kind of purification and quantitation procedure (e.g. affinity chromatography column kits for

caspase-3 using an appropriate protease inhibitor). Evaluation of different sonication procedures with frequent microscopic checks of samples, to ensure that the granular membranes are ruptured, might also be helpful. Another suggestion would be to use a positive control sample known to express caspase-3 during the electrophoresis and blotting procedures, e.g. using a cell line undergoing cell-death / apoptosis that should label with the antibody being tested. According to Herath (2010) salmonid alphavirus-1 virus infected Chinook salmon embryo cells at 5-6 days might be a good option in this context.

It is worth noting that, according to the manufacturer's published article (Promega Notes 75, available online from the authors Riss *et al.*, unknown year), the polyclonal in question may also detect the large subunit of recombinant active caspase-7. These authors state that while performing a western blot, although reactivity was much lower than with active caspase-3, caspase-7 also gave a signal. Such cross-reactivity is not surprising as caspase-3 and caspase-7 are in the same caspase sub-family and have similarities in their amino acid sequences. This being the reason it was decided to test a caspase-7 antibody in serial tissue sections where it was previously shown to be reactive to the caspase-3 antibody, and following IHC intestinal MCs / EGCs were shown to be also positive for caspase-7.

With respect to the isolation of MCs / EGCs and subsequent identification of the protein profile through electrophoresis and antigen blotting, the intention was to subsequently excise bands of interest from the SDS-Page gel, and use them for liquid chromatography-tandem mass spectrometry (LC MS/MS), in order to identify proteins from caspase-3 positive granules by shotgun proteome analysis. Knowing their composition, it would then be easier to make tentative hypotheses concerning their functional properties. For this purpose, contact was established with Dr. Neil Inglis of Moredun Research Institute's Proteomic Facility Services, and protocols for sample preparation were discussed. However, with the restrictions on time left to complete the current study and failure of initial isolation attempts, this research avenue was forced to be put on hold pending a later collaborative project.

Nevertheless, the anti-caspase 3 antibody has shown to have clear applications in the identification and histochemical characterisation of salmon MCs / EGCs, either alone or in combination with other biomarkers. Caspases are a family of cysteine proteases expressed as inactive zymogens in virtually all animal cells¹³. These enzymes play a central role in most cell death pathways leading to apoptosis, but growing evidence now implicates caspases in non-apoptotic functions (Schwerk & Schulze-Osthoff, 2003; Launay *et al.*, 2005). Several of these enzymes play a role in the mammalian innate immune response by processing some of the cytokines involved in the inflammatory response. Moreover, they are necessary for terminal differentiation of specific cell types. These enzymes also play a role in T and B lymphocyte proliferation and, in some circumstances, appear to be required for cell dispersion. These pleiotropic functions implicate caspases in the “control of life and death”, however the fine regulation of their dual function remains poorly understood (Ishizaki *et al.*, 1998; Wilhelm *et al.*, 1998; Sordet *et al.*, 2002; Miura *et al.*, 2004; Rohn *et al.*, 2004; Launay *et al.*, 2005; Kuranaga & Miura, 2007; Rosado *et al.*, 2006; Siegel, 2006; Lamkanfi *et al.*, 2006).

Characteristic morphological features of apoptotic cells include cell shrinkage, condensation of chromatin, fragmentation of DNA, and formation of apoptotic bodies (Gerbautlet *et al.*, 2006). In this respect it seems clear that the MCs / EGCs being stained by the caspase-3 and -7 antibodies were not likely to be undergoing cell death in either normal or inflamed tissue states, or at least not all of them at the same time. Thus the observation of caspase activity and the identification of caspase substrates in the absence of cell death

¹³ **Cysteine proteases**, are synthesised as inactive proenzymes (pre-caspases) and can be classified into two main groups according to the length of their N-terminal pro-domain. Pre-caspases with a short domain (*i.e.* pre-caspase 3, 6 and 7) occur in the cells as dimers that require proteolysis at internal aspartate residues to generate two large and two small subunits. Active enzymes result from heterodimerisation of these subunits, thus include two active sites. These caspases are the main effectors of apoptotic cell death. Other pre-caspases such as pre-caspase 8, 9 and 10 are characterised by their long pro-domain, and exist in living cells as monomers and require dimerisation or oligomerisation for activation that can occur in the absence of any proteolytic cleavage. These are normally the initiators of a caspase cascade although the main functions of some do not relate to apoptosis (Sordet *et al.*, 2002; Launay *et al.*, 2005; Lamkanfi *et al.*, 2006).

have sparked a strong interest in confirming if what is being labelled is in fact the peptide caspase-3, and not an instance of cross-reactivity.

Teleosts' MCs / EGCs are known to have the capability to immediately respond to appropriate stimuli by degranulating, a process characterised by the extrusion of the cytoplasmic granule contents into the extracellular space by a process of exocytosis. Consequently, they have the capacity to release a variety of mediators, which may have a profound influence on surrounding tissues and could result in a wide array of cellular responses, including induction of immune and inflammatory responses. For instance, migration and accumulation of neutrophils and macrophage activation have repeatedly been observed at sites where MC / EGC degranulation has occurred (Reite, 1997; Reite & Evensen, 1994; Matsuyama & Iida, 2001), suggesting that fish MCs / EGCs could possibly contain or generate a variety of mediators, caspase-3 and / or caspase-7 included perhaps, that could induce cellular dispersion, differentiation or proliferation as observed for mammalian MCs (Thornberry *et al.*, 1992; Sordet *et al.*, 2002; Rohn *et al.*, 2004; Lamkanfi *et al.*, 2006; Reite & Evensen, 2006; Dezfuli & Giari, 2008; Crivellato & Ribatti, 2010).

6.5. General conclusions

This study has examined aspects of the general morphology, histochemistry and tissue distribution of intestinal MCs / EGCs in salmon, as well as discussing proposed functions of these cells, in a bid to further characterise them and try to elucidate their functional role in the intestinal immune response. However, the histochemical properties of these cells still can not be said to have been established without question. Their physiological function and the content of their granules still remain somewhat obscure, although a role as immunodulatory cells reacting to various exogeneous signals through a finely regulated process, comparable to that causing the degranulation of mammalian MCs, has been suggested.

The histochemical staining properties described here for salmonid MCs / EGCs, seem to resemble those of mammalian mucosal mast cells, with both acidophilic and basophilic components in their granules. They also similarly contain neuromodulator /

neurotransmitter-peptides such as serotonin, met-enkephalin and substance-p. Furthermore, distinguishable bio-chromogenic markers have been identified, which seem to be of potential use in helping to generate a discriminatory profile for such cells, that could later be assessed by image analysis systems. Specifically, haematoxylin-erythrosin-safran (HES) and May-Grünwald-Giemsa (MGG) histochemical staining, and the immunolabelling with anti-serotonin, met-enkephalin, substance-p and caspases-3 / -7 antibodies show promise for further studies.

The original hope that this study of specific components of mast cell granules would lead towards the critical function or functions of these cells has not been wholly realised. Instead, however, an extreme degree of variability was uncovered that provides an entirely new set of questions about their function in fish. In particular, the results presented here demonstrate the reactivity of caspase-3 and -7 with the cytoplasmic granules of MCs / EGCs, in the absence of apoptosis and cell death. Albeit speculatively, it is suggested that this is indicative of a novel non-apoptotic function for this enzyme, supporting a possible involvement in cellular development, activation, proliferation, differentiation or dispersion indirectly or directly involved in the intestinal immune response, as happens in their mammalian counterparts. This prompts an interest in further examining and evaluating the possible roles of caspases in the Atlantic salmon intestinal MCs / EGCs as regulators of signalling molecules in cells that might control critical biological cellular responses beyond apoptosis. To achieve this, an attempt to begin identifying the protein profile for the granules, through combined electrophoresis and antigen blotting and subsequent use of liquid chromatography-tandem mass spectrometry was made but had to be curtailed for lack of available time.

Despite the above comments, from the observations described in this chapter it was clear that salmonid MCs / EGCs share some of the staining affinities, immunohistochemical and ultrastructural similarities with mucosal mammalian MCs, and this could therefore be used to argue in favour of their analogy with mammalian mast cells. Nevertheless, their

exact function remains debatable and further research on the granule composition needs to be conducted to enable them to be considered as homologous to mammalian MCs.

GENERAL SYNTHESIS

7.1. Introduction

The contribution of aquaculture to world food-production has increased tremendously over recent decades, and the rapid growth in this sector has highlighted the need to ensure that development is based on sustainable and responsive practices, this including activities associated with aquafeed development (FAO, 2012). The aquaculture feed industry currently aims to optimise the quality of their products and to include ingredients that both meet the physiological requirements of the animals, as well as having specific health benefits, minimal environmental impact and being economically viable (Kiron, 2012). Thus, over the past few years there has been a great deal of research focusing on improving growth efficiency and resistance to disease in fish through manipulation of dietary formulations (Cerezuela *et al.*, 2013).

The evidence for successful nutritional modulation, the mechanisms by which it occurs and the underlying biological reasons for the difficulties associated with demonstrating the effectiveness of such an approach have been reviewed extensively in a number of recent articles (Fuentes *et al.*, 2013; Lewis *et al.*, 2013; Martinez-Rubio *et al.*, 2013; Navarrete *et al.*, 2013; Wu *et al.*, 2013). Numerous studies have shown that whole diets, individual nutrients and feed components can all influence the functional tissue ultrastructure and immune response of a number of different organs (Trichet, 2010). Other studies have provided some guidance as to how best to assess specific physiological functional and morphological changes in tissues, and what confounding factors and methodological aspects to consider when assessing changes through dietary manipulation (e.g. Stolen *et al.*, 1990; Maita, 2007; Verlhac & Kiron, 2004; Rašković *et al.*, 2011). However, it is generally accepted that the complexity involved in the physiological processes of digestion

and immunity has made assessment of the effects of nutritional modulation extremely challenging (Blazer, 1992; Albers *et al.*, 2013). Consequently, no single method or biomarker can be employed to predict the effect of a dietary intervention on the overall physiological and anatomical state of the host, including their immune response. Therefore, an integrative approach is needed to help standardise the methodologies that are currently being employed to do this, as well as introducing new, more accurate techniques to assess changes at the level of the tissues, cells and gene expression. This should assist in providing a better understanding of the mechanisms involved in changes in fish physiology related to dietary manipulation. To this end, the overall aim of the present study was to provide guidance on suitable methods for the assessment and interpretation of the effects of dietary modulation in Atlantic salmon.

7.2. General study aim

In the past, the teleost gastrointestinal tract has principally been considered in terms of its role in mediating nutrient uptake, but more recently there has been increased interest in its physical structure and its role as an immunological barrier, and more importantly its pivotal role in maintaining and regulating the entire host's metabolism and physiological homeostasis (Salinas *et al.*, 2011). This is not surprising considering that it provides a dynamic interface for nutrient digestion and absorption, as well as comprising the first barrier against exogenous pathogens which can colonise or enter the host cells and tissues. In addition, it constantly renews itself through the activity of intestinal stem cells and is therefore a tissue undergoing constant restructuring (Choct, 2009). In view of this, the gastrointestinal tract represents a highly intricate system, the functions of which include the maintenance of macro- and micro-structural integrity, balancing of the intestinal microflora and controlling the intestinal immune system. The signaling pathways, effector molecules and regulatory mechanisms involved are not yet fully understood, and knowledge on the functional outcome of these is somewhat fragmented, except for a few economically important fish species (Pott & Hornef, 2012). Thus, if one wishes to advocate a method that ensures that alternate feed ingredients, when added to fish diets do meet the requirements

of the animal, and / or demonstrate clear attributes linked to a specific nutrient or additive, an improvement is needed in the understanding of the physiological dynamics which maintain intestinal homeostasis in salmonids, and to use this information to characterise how changes in these dynamics affect the intestine's physiological function and structure. To develop a method for assessing this, an array of parameters that are indicative of the animal's intestinal response to a nutritional context need to be measured. The main focus of his thesis, therefore, was to evaluate the usefulness of histological features and specific molecular markers of immune function, as tools to assess and monitor the effects of feed composition on fish health.

7.3. Research approach

For the past fifty years, the role of dietary nutrients in determining / modulating the immune functions of fish has been investigated and a vast amount of information has been acquired (Lim & Webster, 2001; Halver & Hardy, 2002; Nakagawa *et al.*, 2007). A wide variety of parameters can be used to assess different aspects of the host's physiology and immune system (Stolen *et al.*, 1990, 1992, 1994, 1995; Ostrander, 2000; Maita, 2007). Nevertheless, monitoring the histological structure of the gastrointestinal system remains the principal method of choice for assessing the effects of nutritional modulation and this is still considered to be a good indicator of the physiological status of the fish (Rašković *et al.*, 2011). Various methods of histological analysis have been used to do this, with semi-quantitative scoring systems most frequently applied, although morphometric procedures, stereology and histochemical methods have also been employed.

Traditional histological assessment, based on the use of semi-quantitative scoring systems, are considered to be less accurate than quantitative approaches, relatively insensitive and subjective (*e.g.* Pilette *et al.*, 1998; Kopec *et al.*, 2011; Hall *et al.*, 2013). Digital imaging analysis on the other hand, appears to provide a more accurate analysis because histological sections are quantified on a continuous scale and the inter-observer variability is noticeably reduced (Mandarim-de-Lacerda *et al.*, 2010; Shamir *et al.*, 2010). The result also appears to correlate well with pathologists' semi-quantitative evaluations (Hall *et*

al., 2013; Campos *et al.*, 2014). Thus, there is a current trend for the use of digital image analysis as an alternative or supplementary method of assessment.

Thus an assessment model was developed based on interactive image analysis for histological sections of the intestine within this project. The intention of this work was to reliably quantify the extent of morphological and functional changes occurring in response to dietary and / or environmental modulation. In order to accomplish this goal four interrelated study phases (presented in Chapters 2-6) were implemented. The outcomes of the experiments outlined at the start of the project, provided the basis for the subsequent phases that followed. Thus, the work presented in later chapters included adjustments and improvements as appropriate, based on the finding of earlier chapters.

7.4. Summary of study outcomes

At the outset of this work, a dietary model was used whereby different levels of enteropathy were specifically induced, with the purpose of providing a range of extreme histopathological and immunological states that could be used for developing and assessing the performance of new tools and assessment methodologies. Chapter 2 focused on the development of a novel semi-automated image analysis system, providing a template for the future development of tools to assist pathologists with the histological evaluation of fish intestinal biopsies. The intention was to deploy an efficient image processing and analysis pipeline, incorporating appropriate algorithms for feature extraction and morphometric data generation, for the purpose of evaluating the extent of morphological changes in the intestine of fish, which could be attributed to the nutritional model employed.

A key aspect of the work described, was the need to develop a highly consistent methodology with respect to tissue staining and image acquisition. In order to achieve this, a standardised protocol for staining and image pre-processing was defined, that eliminated or minimised as many sources of variation as possible. In developing the image analysis system, a set of features that best describe the different intestinal morphological changes observed were selected, based on the personal experience of the researcher, input from fish pathologists or similar quantitative studies reported in the literature. Subsequently, a

programming environment was selected, an outline produced of what the envisaged tool needed to be capable of measuring, and appropriate scripts written to accomplish those tasks. Once the scripts were written, the accuracy and usability of the system was assessed *i.e.* the degree to which the individual measurements agreed with the actual values of the region of interest, the time and effort required to use the system, and the level of reproducibility between different observers and the same observer at two distinct time points. First, a quantitative comparison between computational results and manual measurements gathered by experienced pathologists was conducted. Second, the same images were evaluated using open source image analysis software, and results from the interactive and the semi-automated segmentations compared. The outcome of this initial work demonstrated that the image analysis method developed could be conducted with minimal user-interaction, thus allowing rapid and objective assessment of salmon intestinal histology. This greatly improved the efficiency of conducting quantitative assessment as opposed to the subjective alternative approach employed during the normal evaluation procedure. Moreover, a significant degree of agreement was achieved between the measurements obtained from the semi-automated imaging system and the manual morphometric image segmentation. Also, the strength of this quantitative approach was enhanced by the employment of interactive procedures, which enable the operator to rectify preceding automated segmentation steps, and account for a given specimen's variations. Furthermore, the system provided significant correlation to other well-established quantitative approaches, suggesting that it can be a viable complement / alternative to the pathologist's manual scoring, being both more practical and time-efficient, and although minor inter- and intra-operator variations were recorded, these did not influence the analytical outcomes. Such high reproducibility and lack of dependence on the user's expertise make this approach suitable for delivering large-scale data sets, providing a robust method to assess the histology of fish intestinal tissue sections, obtained under different experimental states and different time intervals.

In Chapter 3, following development of the new system, and because evaluation of several individual parameters together should improve the accuracy of dietary assessment, the newly developed image analysis tool was then used in conjunction with a range of other techniques (*i.e.* classical growth assessment, immunological, haematological and physiological tools). The work reported in this chapter was aimed at examining the broader utility of a multivariate / multimodal approach to the screening of different dietary ingredients, and to ascertain the reliability and contribution that such an image analysis system might make in dietary assessment. This was an attempt to establish its usefulness in screening a wider range of specific dietary components, and characterising putative feed-derived histological states. In order to achieve this, a larger set of samples was assessed (these having different properties to those used earlier for the training of the software and to define the appropriate parameters incorporated into the imaging system). Through the use of multivariate statistical techniques, the extensive variety of morphometric descriptors initially used in the analysis was narrowed down to a few that best described the histological status portrayed. This fine-tuning would, in turn, improve the time required to perform subsequent analyses and improve the efficacy of this morphometric approach.

The model feed trial employed in Chapter 3, successfully generated differentiable histological / immunological states and although these were not, for the most part, systemically differentiable through the majority of procedures performed they were detectable morphologically. The newly developed image analysis tool could effectively and accurately identify and describe the major morphological changes that occurred in the distal intestine, reflecting the different components fed to the fish. Furthermore, the use of multivariate techniques, which reduced the dimensionality of the data by ranking the features according to their discriminatory potential (described both in Chapters 3 and 4) allowed better discrimination of states and is likely to prove the most productive approach for further discriminatory studies.

While as a stand-alone method of assessment, the proposed image analysis system was demonstrated to be useful, it was considered imperative to validate the system's

performance against that of more well-accepted and established methodologies. This was important not only to establish that the developed system is successfully measuring the parameters it is purported to be measuring, but also to provide reassurance that it could reliably measure aspects of the histology that are relevant to histopathological analyses. Thus, the aim of the work presented in Chapter 4, was to evaluate the consistency and level of agreement of the newly developed quantitative microscopic image analysis system with that of an established semi-quantitative histological grading system. This was achieved by examining the capacity for both methodologies to analyse and assess the same set of histological slides.

The outcomes of the work described in this chapter indicated that, despite variations in scoring between the two independent methods, most quantitative image analysis indices performed at least as well when compared to analogous semi-quantitative descriptive parameters of assessment. These data indicated that either image analysis or traditional semi-quantitative scoring can generate accurate data. From this work it was therefore apparent that it is safe to employ either method depending on the complexity and the practicality of the task at hand. However, characteristics such as rapidity, simplicity and adaptability favour the image analysis method, and it can prove particularly useful where less experienced interpreters perform the analysis.

In Chapter 5, the utility of the newly developed system in relation to integration of additional modes of assessment was scrutinised. In addition to generalised histomorphological features, protein markers that might correlate to the functional status of the fish were assessed for their usefulness and consistency in providing knowledge as to the state of the fish. Thus, the work covered in Chapter 5 aimed to describe the application of image analysis to the detection of potentially predictive biomarkers and the accurate quantification of small changes in the spatial distribution of proteins and their relative amounts in the tissue. Therefore, this chapter aimed to generate an optimised immunohistochemical staining and image analysis protocol, through which a description of intestinal cellular responses at a molecular level could be undertaken.

Various cytological biomarkers for proliferation, migration, differentiation and shedding of damaged or senescent cells by apoptosis, were tested in an attempt to characterise the morphological changes of the intestinal epithelial cells and of the inflammatory infiltrate due to the dietary ingredients being evaluated. Subsequently, the dispersion and area fraction of positive staining in the tissue, were appraised for three distinct zones: (1) submucosal area, (2) above the *stratum compactum* and up to the basal area of the intestinal mucosal folds, and (3) remaining mucosal area / apex of the intestinal folds.

In brief, the work described in this chapter, led to the development of a digital computer-assisted quantification method targeting a selected panel of specific immunohistochemical markers intended for assessment of the immune response to dietary modulation. Expression profiling of the final selected biomarkers (*i.e.* PCNA, TUNEL, active caspase-3 and CD3 ϵ) was shown to be able to assist in further characterising the tissue responses generated, and the proposed system was demonstrated to provide considerable potential for improving the sensitivity, accuracy and reproducibility of quantitative analysis of tissue responses to dietary or environmental modulation.

Chapter 6 emerged as an additional study resulting from the histochemical labelling results generated by work reported in the previous chapter. In brief, while searching for appropriate cytological biomarkers to describe the morphological changes occurring in the intestinal mucosal tissues due to the dietary ingredients being evaluated, histolabelling protocols for intestinal mast cells / eosinophilic granule cells (MCs / EGCs) were sought.

Teleostean MCs / EGCS are considered to be key mediators of inflammatory responses initiated through food hypersensitivity and are involved in many pathologic processes such as the ones related in the defence against infectious agents or towards chronic stress. In this respect, the quantification / description of the presence and spatial distribution of such cells is considered to be of particular interest. However, the physiological function of MCs / EGCs and the content of their prominent granules still remain somewhat controversial. Therefore in an attempt to further understand their role in intestinal immune responses, this chapter examined their anatomical distribution in the

tissue and their histochemical affinity to different staining procedures and immunolabelling techniques, and finally provided a description of their ultrastructural features. First, screening of different functional histological staining protocols was performed, and second, the identification of putative functional antibodies reacting positively to antigens contained in the cytoplasmic granules of these cells was sought, and light and electron transmission microscopy employed for visualisation and ultrastructural investigation.

In terms of staining properties, the examined MCs / EGCs seemed to resemble mammalian mucosal mast cells, with both acidophilic and basophilic components in their granules, and containing compatible neuromodulator / neurotransmitter-peptides such as serotonin, met-enkephalin and substance-p, which, in a way, may strengthen the premise that fish MCs / EGCs could be considered homologous to mammalian MCs, in terms of their role in inflammatory mechanisms and immuno-modulatory responses.

Additionally, for these particular granular cells, appropriately discriminatory colouring-profiles were achieved, and these were apparently efficacious for the evaluation of intestinal histological sections, through use of the morphometric image analysis tools developed in this thesis. Staining gave low background and relatively high reproducibility and uniformity in terms of colour and intensity of staining. Nevertheless, from the present study their function remains to be elucidated and further research on the granules' composition, particularly using shotgun proteomics techniques, should be performed.

7.5. Future considerations

While the current study has employed a range of multivariate techniques to analyse and interpret the data, as more data accumulates and new methodologies are incorporated, the use of artificial neural network classifiers and other machine learning systems¹¹ might be envisaged as a way to categorise samples e.g. good, medium and poor health (or) high, medium and low enteropathy based on the features screened. As part of this approach it

¹¹ **Machine learning**, is a branch of artificial intelligence research that employs a variety of statistical, probabilistic and optimisation technique that allows computers to learn from past examples and to then use that prior training to classify new data, identify new patterns or predict novel trends (Mitchell, 1997).

will be important to combine as many modes of assessment as possible, including aspects of haematology, growth, digestibility, histological and molecular parameters, for better discrimination of individual variability and the performance of different diets being evaluated. Moreover, an important factor in determining the resolution of different states is the sample size employed for analysis (Bartlett, 1998). While sample sizes in the current study have been relatively low, size of future sample sets may be improved through increasing system automation, and by focusing the assessment on a restricted number of highly discriminative parameters by use of techniques reducing the dimensionality of the data¹². This in turn, is likely to enable the proposed system and related techniques / analyses to detect even more subtle responses as a result of dietary change.

Additionally, with the growing interest in assessment applications for fish, it is pertinent to review the present findings with regards to other fish species and, in terms of an intra-species approach, it will be pertinent to consider the life-stage (e.g. maturation, smoltification) as well as other environmental factors (e.g. temperature, salinity).

In regard to the intestinal MC / EGC characterisation, so as to allow identification of the protein profile through use of mass spectrometry techniques, optimisation of the isolation protocol is a critical consideration. This would then make it easier to hypothesise upon the granules' composition and consequently speculate upon the functional properties of salmonid MCs / EGCs.

7.6. Adoption of the developed technology

As observed in other health-related disciplines, widespread adoption of digital histology has been hindered not only by the cost and technical issues, but also largely by the mind-

¹² **Dimensionality reduction**, is the process of transduction of a high-dimensional dataset into a lower-dimensional space while retaining as much of the information content of the data as possible. As a pre-processing step for supervised classification algorithms, dimensionality reduction achieves several important goals. It reduces the storage requirements and algorithm complexity by reducing the input space of the data. It can improve performance of learning algorithms by rejecting spurious or noisy features prior to training and testing. Dimensionality reduction can also protect against over-fitting by reducing the number of parameters learned by the classifier (Parrish & Gupta, 2012). Linear dimensional methods such as principal components analysis (PCA), factor analysis (FA), principal factor analysis (PFA), projection pursuit (PP), and independent component analysis (ICA) have been extensively used (Fodor, 2002).

set of traditional pathologists (Pantanowitz *et al.*, 2012). The cumbersome user interface, dependence on a mouse and keyboard, rather than the easy to use slide stage without a slide-holder which allows rapid scanning of slides, has biased existing pathologists towards continued use of traditional microscopy rather than examining digital slides (Hassell *et al.*, 2011). Nevertheless, computer-aided diagnosis of digital images offers something more than traditional microscopy can (Weinstein *et al.*, 2009). This technology is becoming increasingly important as anatomical histology requires more quantitative image analysis (Pantanowitz, 2010) and with this emerging imaging tool, digital histology will undoubtedly allow pathologists to make more accurate and consistent diagnoses in the near future.

Most of the new techniques developed in the current study are now being employed and expanded upon by the sponsor of this project. Aquatic Animal Health R&D manager Dr. Charles McGurk, working at Skretting Aquaculture Research Centre (ARC) makes the following comments with respect to the use of image analysis by Skretting: “At the ARC we invested in such an approach, and we are now pioneering its use in fish health and nutrition research, and it is enabling us to generate masses of data with relatively little user input. This refinement has revealed previously undetectable differences in gut structures. For example, using such customised image analysis software to extract quantitative data from tissue sections, a newly developed diet (*i.e.* Optiline HT, Skretting, Norway) was shown to reduce subclinical changes in gut morphology in fish reared in water temperatures above the optimum. And the potential of this approach is not limited to studying intestines!”

The level of enquiry from other fish health professionals whilst presenting the current work at international meetings and conferences, further suggests that many researchers are keen to investigate and possibly adopt this type of technology. Thus the prospects for wider adoption of image analysis techniques in aquaculture health screening are high, and the technology has great potential to provide a more subtle and sophisticated understanding of the effects of diet on fish health.

7.7. Concluding remarks

Through standardisation of the sampling and preparation methodologies, staining protocols and digital capture thresholds and techniques, an image analysis system has been developed that can help pathologists and others screen new dietary components in terms of effects on intestinal morphology, histochemistry and immunohistochemistry, and thereby, interpreted function. This assessment system has proven to be an efficient, accurate and objective method, the data outputs of which do not differ significantly when the analysis is performed by different observers with varying levels of expertise in histopathological assessment. Furthermore, by employing multivariate statistical / classification techniques on data derived from multimodal analyses, the synergy to be gained through simultaneously assessing a wide range of discrete features (instead of evaluating each discriminatory feature individually) has been successfully examined and the tissue features best able to describe the functional and histopathological alterations observed, identified.

Despite the apparent usefulness of this system for discriminating between histopathological / immunological states, it is nevertheless clear that in order to fully understand and exploit the knowledge gained from these tools and techniques and to rationally develop such system further, it is critical to maintain a close relationship and continuous involvement of immunologists, feed specialists and histopathologists who are able to provide a contextual interpretation, not just observe and measure differences.

It is ultimately envisaged that the further development of the tools and techniques described in this thesis will greatly assist in the evaluation of alternative dietary components for aquaculture feeds, leading, in turn, to a more sustainable global industry, and improved fish health and welfare.

BIBLIOGRAPHIC REFERENCES

- ABAURREA, M., NUÑEZ, M. and OSTOS, M., 1993. Ultrastructural study of the Distal part of the intestine of *Oncorhynchus mykiss*. Absorption of dietary protein. *Micron*, **24**(5), pp. 445-450.
- ABAURREA-EQUISOAIN, M. and OSTOS-GARRIDO, M., 1996. Enterocytes in the anterior intestine of *Oncorhynchus mykiss*: Cytological characteristics related to osmoregulation. *Aquaculture*, **139**(1), pp. 109-116.
- ABID, A., DAVIES, S., WAINES, P., EMERY, M., CASTEX, M., GIOACCHINI, G., CARNEVALI, O., BICKERDIKE, R., ROMERO, J. and MERRIFIELD, D., 2013. Dietary synbiotic application modulates Atlantic salmon (*Salmo salar*) intestinal microbial communities and intestinal immunity. *Fish & Shellfish Immunology*, **35**(6), pp. 1948-1956.
- ABTAHI, B., YOUSEFI, M. and KENARI, A.A., 2013. Influence of dietary nucleotides supplementation on growth, body composition and fatty acid profile of Beluga sturgeon juveniles (*Huso huso*). *Aquaculture Research*, **44**(2), pp. 254-260.
- ADAMS, M.B. and NOWAK, B.F., 2003. Amoebic gill disease: sequential pathology in cultured Atlantic salmon, *Salmo salar* L. *Journal of Fish Diseases*, **26**(10), pp. 601-614.
- ADAMS, M.B. and NOWAK, B.F., 2004. Sequential pathology after initial freshwater bath treatment for amoebic gill disease in cultured Atlantic salmon, *Salmo salar* L. *Journal of Fish Diseases*, **27**(3), pp. 163-173.
- ADAMS, S. M., A. M. BROWN, and R. W. GOEDE. 1993. A quantitative health assessment index for rapid evaluation of fish condition in the field. *Transactions of the American Fisheries Society*, **122**: pp. 63-73.
- AHERNE, C.M., COLLINS, C.B. and ELTZSCHIG, H.K., 2013. Netrin-1 guides inflammatory cell migration to control mucosal immune responses during intestinal inflammation. *Tissue Barriers*, **1**: e24957.
- AHERNE, W. and DUNNILL, M.S., 1966. Quantitative aspects of placental structure. *Journal of Pathology and Bacteriology*, **91**(1), pp. 123-139.
- AHRENS, P., SCHLEICHER, A., ZILLES, K. and WERNER, L., 1990. Image analysis of Nissl-stained neuronal perikarya in the primary visual cortex of the rat: Automatic detection and segmentation of neuronal profiles with nuclei and nucleoli. *Journal of Microscopy*, **157**(3), pp. 349-365.
- AKSNES, A. and OPSTVEDT, J., 1998. Content of digestible energy in fish feed ingredients determined by the ingredient-substitution method. *Aquaculture*, **161**(1-4), pp. 45-53.
- ALBERS, R., BOURDET-SICARD, R., BRAUN, D., CALDER, P.C., HERZ, U., LAMBERT, C., LENOIR-WIJNKOOP, I., MEHEUST, A., OUWEHAND, A. and PHOTHIRATH, P., 2013. Monitoring immune modulation by nutrition in the general population: identifying and substantiating effects on human health. *British Journal of Nutrition*, **110**(S2), pp. S1-S30.
- ALEXANDER, J., 1977. Protein concentration in the serum of the Atlantic salmon (*Salmo salar*) in North-west England and Northern Ireland. *Journal of Fish Biology*, **11**(6), pp. 673-679.

- ALONZI, R., TAYLOR, N.J., STIRLING, J.J., D'ARCY, J.A., COLLINS, D.J., SAUNDERS, M.I., HOSKIN, P.J. and PADHANI, A.R., 2010. Reproducibility and correlation between quantitative and semiquantitative dynamic and intrinsic susceptibility-weighted MRI parameters in the benign and malignant human prostate. *Journal of Magnetic Resonance Imaging*, **32**(1), pp. 155-164.
- ANDERSON, J.M. and LOWE, J., 1990. "Histometry and image analysis" in Bancroft, D. and Stevens, A. (Eds.). *Theory and practice of histological techniques*, Churchill Livingstone Publisher, Edinburgh, UK, pp. 597-618.
- ANGGRAENI, M.S. and OWENS, L., 2000. The haemocytic origin of lymphoid organ spheroid cells in the penaeid prawn *Penaeus monodon*. *Diseases of Aquatic Organisms*, **40**(2), pp. 85-92.
- ANTONOPOULOU, E., KENTEPOZIDOU, E., FEIDANTISIS, K., ROUFIDOU, C., DESPOTI, S. and CHATZIFOTIS, S., 2013. Starvation and re-feeding affect Hsp expression, MAPK activation and antioxidant enzymes activity of European Sea Bass (*Dicentrarchus labrax*). *Comparative Biochemistry and Physiology Part A: Molecular & Integrative Physiology*, **165**(1), pp. 79-88.
- ASEA, A., KRAEFT, S., KURT-JONES, E.A., STEVENSON, M.A., CHEN, L.B., FINBERG, R.W., KOO, G.C. and CALDERWOOD, S.K., 2000. HSP70 stimulates cytokine production through a CD14-dependant pathway, demonstrating its dual role as a chaperone and cytokine. *Nature Medicine*, **6**(4), pp. 435-442.
- AUSTIN, B., 2006. The bacterial microflora of fish, revised. *The Scientific World Journal*, **6**, pp. 931-945.
- AUSTRENG, E., STOREBAKKEN, T. and ÅSGÅRD, T., 1987. Growth rate estimates for cultured Atlantic salmon and rainbow trout. *Aquaculture*, **60**(2), pp. 157-160.
- AWAD, E., AUSTIN, D. and LYNDON, A.R., 2013. Effect of dietary supplement of black cumin seed oil (*Nigella sativa*) and Nettle extract (Quercetin) on enhancement of immunity in rainbow trout, *Oncorhynchus mykiss* (Walbaum). *Aquaculture*, **388-391**, pp. 193-197.
- BAAK, J., 1987. The principles and advances of quantitative pathology. *Analytical and Quantitative Cytology and Histology*, **9**(2), pp. 89-95.
- BAAK, J.P.A., OORT, J., BOUW, G.M. and STOLTE, L.A.M., 1977. Quantitative morphology: methods and materials: I. Stereology and morphometry. *European Journal of Obstetrics & Gynaecology and Reproductive Biology*, **7**(1), pp. 43-52.
- BAEVERFJORD, G. and KROGDAHL, Å., 1996. Development and regression of soybean meal induced enteritis in Atlantic salmon, *Salmo salar* L., distal intestine: a comparison with the intestines of fasted fish. *Journal of Fish Diseases*, **19**(5), pp. 375-387.
- BAGNI, M., ROMANO, N., FINOIA, M.G., ABELLI, L., SCAPIGLIATI, G., TISCAR, P.G., SARTI, M. and MARINO, G., 2005. Short- and long-term effects of a dietary yeast β -glucan (Macrogard) and alginic acid (Ergosan) preparation on immune response in sea bass (*Dicentrarchus labrax*). *Fish & Shellfish Immunology*, **18**(4), pp. 311-325.
- BAIN, B.J., BATES, I., LAFFAN, M.A., LEWIS, and S.M., 2012. Dacie and Lewis practical haematology. Churchill Livingstone, London, pp. 668.

- BAKKE, A. M., GLOVER, C. and KROGDAHL Å., 2011. "Feeding, digestion and absorption of nutrients" in Grosell, M., Farrell, A.P., Brauner, C.J. (Eds.). *The multifunctional gut of fish*, Wiley-Backwell, San Diego, USA, pp. 57-111.
- BAKKE-McKELLEP, A., NORDRUM, S., KROGDAHL, Å. and BUDDINGTON, R., 2000a. Absorption of glucose, amino acids, and dipeptides by the intestines of Atlantic salmon (*Salmo salar* L.). *Fish Physiology and Biochemistry*, **22**(1), pp. 33-44.
- BAKKE-McKELLEP, A., PRESS, C.M., BAEVERFJORD, G., KROGDAHL, Å. and LANDSVERK, T., 2000b. Changes in immune and enzyme histochemical phenotypes of cells in the intestinal mucosa of Atlantic salmon, *Salmo salar* L., with soybean meal-induced enteritis. *Journal of Fish Diseases*, **23**(2), pp. 115-127.
- BAKKE-McKELLEP, A.M., FRØYSTAD, M.K., LILLEENG, E., DAPRA, F., REFSTIE, S., KROGDAHL, Å. and LANDSVERK, T., 2007a. Response to soy: T-cell-like reactivity in the intestine of Atlantic salmon, *Salmo salar* L. *Journal of Fish Diseases*, **30**(1), pp. 13-25.
- BAKKE-McKELLEP, A.M., PENN, M.H., SALAS, P.M., REFSTIE, S., SPERSTAD, S., LANDSVERK, T., RINGO, E. and KROGDAHL, A., 2007b. Effects of dietary soyabean meal, inulin and oxytetracycline on intestinal microbiota and epithelial cell stress, apoptosis and proliferation in the teleost Atlantic salmon (*Salmo salar* L.). *British Journal of Nutrition*, **97**(4), pp. 699-713.
- BANCROFT, J.D. and STEVENS, A. 1982. *Theory and Practice of Histological Techniques*. 2nd Edition, Churchill-Livingstone, New York, USA, pp. 436.
- BANDYOPADHYAY, S.K., 2011. Digital Pathology: An Electronic environment for performing pathologic analyses from image. *International Journal of Computer Science & Engineering Technology*, **1**(3), pp. 127-130.
- BARKER, G., 2000. Novel methods to reduce disease in aquaculture. *Fish Veterinary Journal*, **5**, pp. 66-71.
- BARTLETT, P.L., 1998. The sample complexity of pattern classification with neural networks: the size of the weights is more important than the size of the network. *Information Theory, IEEE Transactions on*, **44**(2), pp. 525-536.
- BATES, D. and MAECHLER, M., 2010. lme4: linear mixed-effects models using Eigen and R syntax. *R package version 0.999375-34*. Available at: <http://CRAN.R-project.org/package=lme4>.
- BAYNE, C.J., 1986. Pronephric leucocytes of *Cyprinus carpio*: Isolation, separation and characterization. *Veterinary Immunology and Immunopathology*, **12**(1-4), pp. 141-151.
- BELIEN, J., BAAK, J., VANDIEST, P. and VANGINKEL, A., 1997. Counting mitoses by image processing in Feulgen stained breast cancer sections: The influence of resolution. *Cytometry*, **28**(2), pp. 125-140.
- BENALI, A., LEEFKEN, I., EYSEL, U.T. and WEILER, E., 2003. A computerized image analysis system for quantitative analysis of cells in histological brain sections. *Journal of Neuroscience Methods*, **125**(1-2), pp. 33-43.
- BENNANI, N., SCHMID-ALLIANA, A. and LAFABRIE, M., 1995. Evaluation of phagocytic activity in a teleost fish, *Dicentrarchus labrax*. *Fish & Shellfish Immunology*, **5**(3), pp. 237-246.

- BERGERON, T. and WOODWARD, B., 1983. Ultrastructure of the granule cells in the small intestine of the rainbow trout (*Salmo gairdneri*) before and after *stratum granulosum* formation. *Canadian Journal of Zoology*, **61**(1), pp. 133-138.
- BERMAN, D., KANG, X., VAN TRAIN, K., LEWIN, H., COHEN, I., AREEDA, J., FRIEDMAN, J., GERMANO, G., SHAW, L. and HACHAMOVITCH, R., 1998. Comparative prognostic value of automatic quantitative analysis versus semiquantitative visual analysis of exercise myocardial perfusion single-photon emission computed tomography. *Journal of the American College of Cardiology*, **32**(7), pp. 1987-1995.
- BERMÚDEZ, R., VIGLIANO, F., MARCACCINI, A., SITJÀ-BOBADILLA, A., QUIROGA, M.I. and NIETO, J.M., 2006. Response of Ig-positive cells to *Enteromyxum scophthalmi* (Myxozoa) experimental infection in turbot, *Scophthalmus maximus* (L.): A histopathological and immunohistochemical study. *Fish & Shellfish Immunology*, **21**(5), pp. 501-512.
- BERNABÒ, I., BONACCI, A., COSCARELLI, F., TRIPEPI, M. and BRUNELLI, E., 2013. Effects of salinity stress on *Bufo balearicus* and *Bufo bufo* tadpoles: Tolerance, morphological gill alterations and Na⁺/K⁺-ATPase localization. *Aquatic Toxicology*, **132–133**(0), pp. 119-133.
- BERNARD, D., SIX, A., RIGOTTIER-GOIS, L., MESSIAEN, S., CHILMONCZYK, S., QUILLET, E., BOUDINOT, P. and BENMANSOUR, A., 2006. Phenotypic and functional similarity of gut intraepithelial and systemic T cells in a teleost fish. *The Journal of Immunology*, **176**(7), pp. 3942-3949.
- BERNTSSEN, M.H., HYLLAND, K., BONGA, W.S.E. and MAAGE, A., 1999. Toxic levels of dietary copper in Atlantic salmon (*Salmo salar* L.) parr. *Aquatic Toxicology*, **46**(2), pp. 87-99.
- BERNTSSEN, M.H.G., HYLLAND, K., JULSHAMN, K., LUNDEBYE, A.K. and WAAGBØ, R., 2004. Maximum limits of organic and inorganic mercury in fish feed. *Aquaculture Nutrition*, **10**(2), pp. 83-97.
- BERZAGHI, P. and RIOVANTO, R., 2010. Near infrared spectroscopy in animal science production: principles and applications. *Italian Journal of Animal Science*, **8**(3s), pp. 39-62.
- BIANCHI, S. and MUGNAI, L., 1990. Mast cell fixation and staining in image analysis. *European Journal of Basic and Applied Histochemistry*, **35**(2), pp. 161-174.
- BLACKSTOCK, N. and PICKERING, A., 1980. Acidophilic granular cells in the epidermis of the brown trout, *Salmo trutta* L. *Cell and Tissue Research*, **210**(3), pp. 359-369.
- BLAIES, D.M. and WILLIAMS, J.F., 1981. A simplified method for staining mast cells with astra blue. *Biotechnic & Histochemistry*, **56**(2), pp. 91-94.
- BLAXHALL, P.C. and DAISLEY, K.W., 1973. Routine haematological methods for use with fish blood. *Journal of Fish Biology*, **5**(6), pp. 771-781.
- BLAZER, V.S., 1992. Nutrition and disease resistance in fish. *Annual Review of Fish Diseases*, **2**, pp. 309-323.
- BOELLAARD, R., KRAK, N.C., HOEKSTRA, O.S. and LAMMERTSMA, A.A., 2004. Effects of noise, image resolution, and ROI definition on the accuracy of standard uptake values: A simulation study. *Journal of Nuclear Medicine*, **45**(9), pp. 1519-1527.

- BOENISCH, T., 2009. "Antibodies" in Kumar, G.L. and Rudbeck, L. (Eds.) *Educational guide: Immunohistochemical (IHC) staining methods*. Dako North America, California, pp. 1-10.
- BOLGER, T. and CONNOLLY, P., 1989. The selection of suitable indices for the measurement and analysis of fish condition. *Journal of Fish Biology*, **34**(2), pp. 171-182.
- BOLTON, L.L., 1933. Basophile (mast) cells in the alimentary canal of salmonoid fishes. *Journal of Morphology*, **54**(3), pp. 549-591.
- BONGA, W.S.E. and VAN DER MEIJ, C. J. M., 1989. Degeneration and death, by apoptosis and necrosis, of the pavement and chloride cells in the gills of the teleost *Oreochromis mossambicus*, *Cell and Tissue Research*, **225**(1), pp. 235-243.
- BOONSTRA, H., OOSTERHUIS, J., OOSTERHUIS, A. and FLEUREN, G., 1983. Cervical tissue shrinkage by formaldehyde fixation, paraffin wax embedding, section cutting and mounting. *Virchows Archiv A-Pathological Anatomy and Histopathology*, **402**(2), pp. 195-201.
- BRANDTZAEG, P., 1998. The increasing power of immunohistochemistry and immunocytochemistry. *Journal of Immunological Methods*, **216**(1), pp. 49-67.
- BRICKNELL, I. and DALMO, R.A., 2005. The use of immunostimulants in fish larval aquaculture. *Fish & Shellfish Immunology*, **19**(5), pp. 457-472.
- BROOKER, A.J., 2007. Aspects of the biology and behaviour of *Lernaecera branchialis* (Linnaeus, 1767) Copepoda: Pennellidae. PhD Dissertation Thesis, University of Stirling, Stirling, UK, pp. 224.
- BRUNO, D. and MUNRO, A., 1986. Haematological assessment of rainbow trout, *Salmo gairdneri* Richardson, and Atlantic salmon, *Salmo salar* L., infected with *Renibacterium salmoninarum*. *Journal of Fish Diseases*, **9**(3), pp. 195-204.
- BRUNO, D.W. and POPPE, T.T., 1996. A colour Atlas of Salmonid Diseases. Academic Press, London, UK, pp. 194.
- BUDDINGTON, R.K. and DIAMOND, J.M., 1987. Pyloric ceca of fish: a "new" absorptive organ. *American Journal of Physiology-Gastrointestinal and Liver Physiology*, **252**(1), pp. G65-G76.
- BUDDINGTON, R.K. and KUZ'MINA, V., 2000. "Digestive system" in Ostrand, G.K. (Eds.). *The laboratory fish*, Academic Press, London, UK, pp. 379-384.
- BUDDINGTON, R.K., KROGDAHL, A. and BAKKE-McKELLEP, A.M., 1997. The intestines of carnivorous fish: structure and functions and the relations with diet. *Acta Physiologica Scandinavica Supplementum*, **638**, pp. 67-80.
- BUI, H.T.D., KHOSRAVI, S., FOURNIER, V., HERAULT, M. and LEE, K., 2014. Growth performance, feed utilization, innate immunity, digestibility and disease resistance of juvenile red seabream (*Pagrus major*) fed diets supplemented with protein hydrolysates. *Aquaculture*, **418-419**(0), pp. 11-16.
- BULLOCK, W.L., 1963. Intestinal histology of some salmonid fishes with particular reference to the histopathology of acanthocephalan infections. *Journal of Morphology*, **112**(1), pp. 23-44.
- BUREAU, D.P., HARRIS, A.M. and CHO, C.Y., 1998. The effects of purified alcohol extracts from soy products on feed intake and growth of chinook salmon (*Oncorhynchus tshawytscha*) and rainbow trout (*Oncorhynchus mykiss*). *Aquaculture*, **161**, pp. 27-43.

- BUREL, C., BOUJARD, T., KAUSHIK, S.J., BOEUF, G., VAN DER GEYTEN, S., MOL, K.A., KÜHN, E.R., QUINSAC, A., KROUTI, M. and RIBAILLIER, D., 2000. Potential of plant-protein sources as fish meal substitutes in diets for turbot (*Psetta maxima*): growth, nutrient utilisation and thyroid status. *Aquaculture*, **188**(3), pp. 363-382.
- BURKA, J. and POWELL, L.H., 1993. Eosinophilic granule cells of Salmonids: A potential target for anti-inflammatory therapy? Available at: <http://vetmed.tamu.edu/common/docs/public/aavpt/symposia/Burka58-63.pdf>.
- BURKHARDT-HOLM, P., SCHMIDT, H. and MEIER, W., 1998. Heat shock protein (hsp70) in brown trout epidermis after sudden temperature rise. *Comparative Biochemistry and Physiology Part A: Molecular & Integrative Physiology*, **120**(1), pp. 35-41.
- BURNSTOCK, G., 1959. The morphology of the gut of the brown trout (*Salmo trutta*). *Quarterly Journal of Microscopical Science*, **3**(50), pp. 183-198.
- BURRELLS, C., WILLIAMS, P., SOUTHGATE, P. and CRAMPTON, V., 1999. Immunological, physiological and pathological responses of rainbow trout (*Oncorhynchus mykiss*) to increasing dietary concentrations of soybean proteins. *Veterinary Immunology and Immunopathology*, **72**(3), pp. 277-288.
- BURRELLS, C., WILLIAMS, P.D., SOUTHGATE, P.J. and WADSWORTH, S.L., 2001. Dietary nucleotides: a novel supplement in fish feeds: 2. Effects on vaccination, salt water transfer, growth rates and physiology of Atlantic salmon (*Salmo salar* L.). *Aquaculture*, **199**(1-2), pp. 171-184.
- BUTTLE, L., BURRELLS, A., GOOD, J., WILLIAMS, P., SOUTHGATE, P. and BURRELLS, C., 2001. The binding of soybean agglutinin (SBA) to the intestinal epithelium of Atlantic salmon, *Salmo salar* and Rainbow trout, *Oncorhynchus mykiss*, fed high levels of soybean meal. *Veterinary Immunology and Immunopathology*, **80**(3), pp. 237-244.
- BYRD, C.A. and BRUNJES, P.C., 1995. Organization of the olfactory system in the adult zebrafish: histological, immunohistochemical, and quantitative analysis. *Journal of Comparative Neurology*, **358**(2), pp. 247-259.
- CAIN, K. and SWAN, C., 2011. "Barrier function and immunology" in Grosell, M., Farrell, A.P., Brauner, C.J. (Eds.). *The multifunctional gut of fish*, Wiley-Blackwell, San Diego, USA, pp. 112-135.
- CAMBAZOGLU, B.B., SERTEL, O. and KONG, J. 2007. Efficient processing of pathological images using the grid. *Proceedings of the Fifth International Workshop on Challenges of Large Applications in Distributed Environments*, Monterey Bay, 25 June, pp. 35-41.
- CAMPOS, C., PAIVA, D., PERAZZO, H., MOREIRA, P., ARECO, L., TERRA, C., PEREZ, R. and FIGUEIREDO, F., 2014. An inexpensive and worldwide available digital image analysis technique for histological fibrosis quantification in chronic hepatitis C. *Journal of Viral Hepatitis*, **21**(3), pp. 216-222.
- CARTER, C.G. and HAULER, R.C., 2000. Fish meal replacement by plant meals in extruded feeds for Atlantic salmon, *Salmo salar* L. *Aquaculture*, **185**(3-4), pp. 299-311.

- CASTRO, R., ZARRA, I. and LAMAS, J., 2004. Water-soluble seaweed extracts modulate the respiratory burst activity of turbot phagocytes. *Aquaculture*, **229**(1), pp. 67-78.
- CEREZUELA, R., FUMANAL, M., TAPIA-PANIAGUA, S.T., MESEGUER, J., MORIÑIGO, M.Á. and ESTEBAN, M.Á., 2013. Changes in intestinal morphology and microbiota caused by dietary administration of inulin and *Bacillus subtilis* in gilthead sea bream (*Sparus aurata* L.) specimens. *Fish & Shellfish Immunology*, **34**(5), pp.1063-1070.
- CHANG, Y., LIU, C., WU, C., CHIANG, C., LIAN, J. and HSIEH, S., 2012. Dietary administration of zingerone to enhance growth, non-specific immune response, and resistance to *Vibrio alginolyticus* in Pacific white shrimp (*Litopenaeus vannamei*) juveniles. *Fish & Shellfish Immunology*, **32**(2), pp. 284-290.
- CHAUDHURI, B., RODENACKER, K. and BURGER, G., 1988. Characterization and featuring of histological section images. *Pattern Recognition Letters*, **7**(4), pp. 245-252.
- CHEKKOURY, A., KHURD, P., NI, J., BAHLMANN, C., KAMEN, A., PATEL, A., GRADY, L., SINGH, M., GROHER, M., NAVAB, N., KRUPINSKI, E., JOHNSON, J., GRAHAM, A. and WEINSTEIN, R., 2012. Automated malignancy detection in breast histopathological images. *Medical Imaging 2012: Computer-Aided Diagnosis*, **8315**, pp. 1-13.
- CHELI, F., BATTAGLIA, D., PINOTTI, L. and BALDI, A., 2012. State of the Art in Feedstuff Analysis: A technique-oriented perspective. *Journal of Agricultural and Food Chemistry*, **60**(38), pp. 9529-9542.
- CHEN, D. and AINSWORTH, A., 1992. Glucan administration potentiates immune defence mechanisms of channel catfish, *Ictalurus punctatus* Rafinesque. *Journal of Fish Diseases*, **15**(4), pp. 295-304.
- CHENG, Z., BUENTELLO, A. and GATLIN, D.M., 2011. Dietary nucleotides influence immune responses and intestinal morphology of red drum *Sciaenops ocellatus*. *Fish & Shellfish Immunology*, **30**(1), pp. 143-147.
- CHETTRI, J.K., HOLTEN-ANDERSEN, L. and BUCHMANN, K., 2010. Factors influencing *in vitro* respiratory burst assays with head kidney leucocytes from rainbow trout, *Oncorhynchus mykiss* (Walbaum). *Journal of Fish Diseases*, **33**(7), pp. 593-602.
- CHI, F.L. and LIANG, Q., 2004. The quantification of endolymphatic hydrops in an experimental animal model with guinea pigs. *Orl-Journal for Oto-Rhino-Laryngology and its Related Specialties*, **66**(2), pp. 56-61.
- CHIKWATI, E.M., GU, J., PENN, M.H., BAKKE, A.M. and KROGDAHL, Å., 2013a. Intestinal epithelial cell proliferation and migration in Atlantic salmon, *Salmo salar* L.: effects of temperature and inflammation. *Cell and Tissue Research*, **353**, pp. 123-137.
- CHIKWATI, E.M., SAHLMANN, C., HOLM, H., PENN, M.H., KROGDAHL, Å. and BAKKE, A.M., 2013b. Alterations in digestive enzyme activities during the development of diet-induced enteritis in Atlantic salmon, *Salmo salar* L. *Aquaculture*, **402–403**(0), pp. 28-37.
- CHIKWATI, E.M., VENOLD, F.F., PENN, M.H., ROHLOFF, J., REFSTIE, S., GUTTVIK, A., HILLESTAD, M., KROGDAHL, Å., VAN DEN INGH, T. and KROGDAHL, Å., 2012. Interaction of

- soyasaponins with plant ingredients in diets for Atlantic salmon, *Salmo salar* L. *British Journal of Nutrition*, **107**(11), pp. 1570.
- CHIU, H. and LAGUNOFF, D., 1972. Histochemical comparison of vertebrate mast cells. *The Histochemical Journal*, **4**(2), pp. 135-144.
- CHOCT, M., 2009. Managing gut health through nutrition. *British Poultry Science*, **50**(1), pp. 9-15.
- CHRISTENSEN, N.K. and WINTHER, L., 2009. "Multi-staining immunohistochemistry" in Kumar, G.L. and Rudbeck, L. (Eds.) *Educational guide: Immunohistochemical (IHC) staining methods*. Dako North America, California, pp. 103-108.
- CHUBB, C., INAGAKI, Y., SHEU, P., CUMMINGS, B., WASSERMAN, A., HEAD, E. and COTMAN, C., 2006. BioVision: An application for the automated image analysis of histological sections. *Neurobiology of Aging*, **27**(10), pp. 1462-1476.
- COLLIE, N.L. and FERRARIS, R.P., 1995. Nutrient fluxes and regulation in fish intestine. *Biochemistry and Molecular Biology of Fishes*, **4**, pp. 221-239.
- COLLINS, S.A., ØVERLAND, M., SKREDE, A. and DREW, M.D., 2013. Effect of plant protein sources on growth rate in salmonids: Meta-analysis of dietary inclusion of soybean, pea and canola / rapeseed meals and protein concentrates. *Aquaculture*, (**400–401**), 85-100.
- COOK, H.C., 1961. A modified thionin technique for mast cells in tissue sections. *The Journal of Medical Laboratory Technology*, **18**, pp. 188-189.
- COOK, M.T., HAYBALL, P.J., HUTCHINSON, W., NOWAK, B.F. and HAYBALL, J.D., 2003. Administration of a commercial immunostimulant preparation, EcoActiva™ as a feed supplement enhances macrophage respiratory burst and the growth rate of snapper (*Pagrus auratus*, Sparidae (Bloch and Schneider) in winter. *Fish & Shellfish Immunology*, **14**(4), pp. 333-345.
- COONS, A.H., 1971. Introduction: the development of immunohistochemistry. *Annals of the New York Academy of Sciences*, **177**(1), pp. 5-9.
- CORSON, D., WAGHORN, G., ULYATT, M. and LEE, J., 1999. NIRS: Forage analysis and livestock feeding, *Proceedings of the Conference - New Zealand Grassland Association*, pp. 127-132.
- CREGGER, M., BERGER, A.J. and RIMM, D.L., 2006. Immunohistochemistry and quantitative analysis of protein expression. *Archives of Pathology & Laboratory Medicine*, **130**(7), pp. 1026-1030.
- CRESPO, S., NONNOTTE, G., COLIN, D., LERAY, C., NONNOTTE, L. and AUBREE, A., 1986. Morphological and functional alterations induced in trout intestine by dietary cadmium and lead. *Journal of Fish Biology*, **28**(1), pp. 69-80.
- CRIVELLATO, E. and RIBATTI, D., 2010. The mast cell: an evolutionary perspective. *Biological Reviews*, **85**(2), pp. 347-360.
- CROSS, S.S., 1994. The application of fractal geometric analysis to microscopic images. *Micron*, **25**(1), pp. 101-113.

- DAGNON, K., HEUDES, D., BERNAUDIN, J. and CALLARD, P., 2008. Computerized morphometric analysis of microvasculature in non-small cell lung carcinoma. *Microvascular Research*, **75**(1), pp. 112-118.
- DALMO, R. and SELJELID, R., 1995. The immunomodulatory effect of Lps, laminaran and sulfated laminaran [Beta(1,3)-D-Glucan] on Atlantic Salmon, *Salmo salar* L, Macrophages In-Vitro. *Journal of Fish Diseases*, **18**(2), pp. 175-185.
- DALMO, R., BOGWALD, J., INGEBRIGTSEN, K. and SELJELID, R., 1996. The immunomodulatory effect of laminaran [β (1, 3)-D-glucan] on Atlantic salmon, *Salmo salar* L., anterior kidney leucocytes after intraperitoneal, peroral and peranal administration. *Journal of Fish Diseases*, **19**(6), pp. 449-457.
- DALMO, R., INGEBRIGTSEN, K. and BØGWALD, J., 1997. Non-specific defence mechanisms in fish, with particular reference to the reticuloendothelial system (RES). *Journal of Fish Diseases*, **20**(4), pp. 241-273.
- DANIEL, D., SCHLESNER, J., WEHRSTEDT, K., HUFNAGL, P. and DIETEL, M., 2000. Influence of image resolution on image quality in telepathology. *Electronic Journal of Pathology and Histology*, **6**(3), pp. 1-21.
- DE BAULNY, M., QUENTEL, C., FOURNIER, V., LAMOUR, F. and LEGOUVELLO, R., 1996. Effect of long term oral administration of Beta-glucan as an immunostimulant or an adjuvant on some non-specific parameters of the immune response of turbot *Scophthalmus maximus*. *Diseases of Aquatic Organisms*, **2**, pp.139-147.
- DE FRANCESCO, M., PARISI, G., MÉDALE, F., LUPI, P., KAUSHIK, S.J. and POLI, B.M., 2004. Effect of long-term feeding with a plant protein mixture based diet on growth and body/fillet quality traits of large rainbow trout (*Oncorhynchus mykiss*). *Aquaculture*, **236**(1), pp. 413-429.
- DE LAAT, M.A., PATTERSON-KANE, J.C., POLLITT, C.C., SILLENCE, M.N. and MCGOWAN, C.M., 2013. Histological and morphometric lesions in the pre-clinical, developmental phase of insulin-induced laminitis in Standardbred horses. *The Veterinary Journal*, **195**(3), pp. 305-312.
- DE MATOS, L.L., TRUFELLI, D.C., DE MATOS, MARIA GRACIELA LUONGO and DA SILVA PINHAL, MARIA APARECIDA, 2010. Immunohistochemistry as an important tool in biomarkers detection and clinical practice. *Biomarker Insights*, **5**, pp. 9-20.
- DEL RIO-ZARAGOZA, O., FAJER-ÁVILA, E. and ALMAZÁN-RUEDA, P., 2011. Influence of β -glucan on innate immunity and resistance of *Lutjanus guttatus* to an experimental infection of *Dactylogyrid monogeneans*. *Parasite Immunology*, **33**(9), pp. 483-494.
- DEL-POZO, J., CRUMLISH, M., TURNBULL, J. and FERGUSON, H., 2010. Histopathology and Ultrastructure of Segmented Filamentous Bacteria-Associated Rainbow Trout Gastroenteritis. *Veterinary Pathology Online*, **47**(2), pp. 220-230.
- DENEFF, J.F., CORDIER, A.C., MESQUITA, M. and HAUMONT, S., 1979. Influence of Fixation procedure, embedding medium and section thickness on morphometric data in thyroid-gland. *Histochemistry*, **63**(2), pp. 163-171.

- DENSTADLI, V., VEGUSDAL, A., KROGDAHL, Å., BAKKE-McKELLEP, A., BERGE, G., HOLM, H., HILLESTAD, M. and RUYTER, B., 2004. Lipid absorption in different segments of the gastrointestinal tract of Atlantic salmon (*Salmo salar* L.). *Aquaculture*, **240**(1), pp. 385-398.
- DEPASQUALE, J.A., 2012. Tyrosine phosphatase inhibitor triggers rodlet cell discharge in sunfish scale epidermis cultures. *Acta Zoologica*, **0**: pp. 1-10.
- DERDE, M., ANTANAS, L., DE RAEDT, L. and GUIZA GRANDAS, F., 2012. An interactive learning approach to histology image segmentation. *Proceedings of the 24th Benelux Conference on Artificial Intelligence Pages*, Maastricht, 25-26 October, **24**, pp. 1-8.
- DEZFULI, B. and GIARI, L., 2008. Mast cells in the gills and intestines of naturally infected fish: evidence of migration and degranulation. *Journal of Fish Diseases*, **31**(11), pp. 845-852.
- DEZFULI, B., ARRIGHI, S., DOMENEGHINI, C. and BOSI, G., 2000. Immunohistochemical detection of neuromodulators in the intestine of *Salmo trutta* L. naturally infected with *Cyathocephalus truncatus* Pallas (Cestoda). *Journal of Fish Diseases*, **23**(4), pp. 265-273.
- DEZFULI, B., CASTALDELLI, G., BO, T., LORENZONI, M. and GIARI, L., 2011b. Intestinal immune response of *Silurus glanis* and *Barbus barbus* naturally infected with *Pomphorhynchus laevis* (Acanthocephala). *Parasite Immunology*, **33**(2), pp. 116-123.
- DEZFULI, B., GIARI, L., SIMONI, E., BOSI, G. and MANERA, M., 2002. Histopathology, immunohistochemistry and ultrastructure of the intestine of *Leuciscus cephalus* (L.) naturally infected with *Pomphorhynchus laevis* (Acanthocephala). *Journal of Fish Diseases*, **25**(1), pp. 7-14.
- DEZFULI, B.S., GIARI, L., ARRIGHI, S., DOMENEGHINI, C. and BOSI, G., 2003b. Influence of enteric helminths on the distribution of intestinal endocrine cells belonging to the diffuse endocrine system in brown trout, *Salmo trutta* L. *Journal of Fish Diseases*, **26**: pp. 155-166.
- DEZFULI, B.S., GIARI, L., KONECNY, R., JAEGER, P. and MANERA, M., 2003a. Immunohistochemistry, ultrastructure and pathology of gills of *Abramis brama* from Lake Mondsee, Austria, infected with *Ergasilus sieboldi* (Copepoda). *Diseases of Aquatic Organisms*, **53**(3), pp. 257-262.
- DEZFULI, B.S., GIARI, L., LUI, A., LORENZONI, M. and NOGA, E.J., 2011a. Mast cell responses to *Ergasilus* (Copepoda), a gill ectoparasite of sea bream. *Fish & Shellfish Immunology*, **30**(4), pp. 1087-1094.
- DEZFULI, B.S., GIARI, L., SIMONI, E., SHINN, A., MANERA, M. and BOSI, G., 2005. Histopathology, ultrastructure and immunohistochemistry of *Coregonus lavaretus* hearts naturally infected with *Ichthyocotylurus erraticus* (Trematoda). *Diseases of Aquatic Organisms*, **66**(3), pp. 245-254.
- DEZFULI, B.S., GIOVINAZZO, G., LUI, A. and GIARI, L., 2008. Inflammatory response to *Dentitruncus truttae* (Acanthocephala) in the intestine of brown trout. *Fish & Shellfish Immunology*, **24**(6), pp. 726-733.
- DEZFULI, B.S., LUI, A., GIARI, L., CASTALDELLI, G., SHINN, A. and LORENZONI, M., 2012. Innate immune defence mechanisms of tench, *Tinca tinca* (L.), naturally infected with the tapeworm *Monobothrium wagneri*. *Parasite Immunology*, **34**(11), pp. 511-519.

- DIMITROGLOU, A., MERRIFIELD, D.L., SPRING, P., SWEETMAN, J., MOATE, R. and DAVIES, S.J., 2010. Effects of mannan oligosaccharide (MOS) supplementation on growth performance, feed utilisation, intestinal histology and gut microbiota of gilthead sea bream (*Sparus aurata*). *Aquaculture*, **300**(1–4), pp. 182-188.
- DOBSON, J.T., SEIBERT, J., TEH, E.M., DA'AS, S., FRASER, R.B., PAW, B.H., LIN, T. and BERMAN, J.N., 2008. Carboxypeptidase A5 identifies a novel mast cell lineage in the zebrafish providing new insight into mast cell fate determination. *Blood*, **112**(7), pp. 2969-2972.
- DOI, K., 2007. Computer-aided diagnosis in medical imaging: Historical review, current status and future potential. *Computerized Medical Imaging and Graphics*, **31**(4–5), pp. 198-211.
- DOLAPCHIEVA, S., EGGERS, R. and KÜHNEL, W., 2000. Automatic image analysis of the postnatal growth of axons and myelin sheaths in the tibial and peroneal nerves of the rabbit. *Annals of Anatomy - Anatomischer Anzeiger*, **182**(2), pp. 133-142.
- DOMENEGHINI, C., DI GIANCAMILLO, A., ARRIGHI, S. and BOSI, G., 2006. Gut-trophic feed additives and their effects upon the gut structure and intestinal metabolism. State of the art in the pig, and perspectives towards humans, *Histology and Histopathology*, **21** (3), pp. 273-283.
- DONG, X., GENG, X., TAN, B., YANG, Q., CHI, S., LIU, H. and LIU, X., 2013. Effects of dietary immunostimulant combination on the growth performance, non-specific immunity and disease resistance of cobia, *Rachycentron canadum* (Linnaeus). *Aquaculture Research*, [Epub ahead of print].
- DORIN, D., SIRE, M. and VERNIER, J., 1993. Endocytosis and intracellular degradation of heterologous protein by eosinophilic granulocytes isolated from rainbow trout (*Oncorhynchus mykiss*) posterior intestine. *Biology of the Cell*, **79**(3), pp. 219-224.
- DOS SANTOS, N., SILVA, M. and VALE, A.D., 2008. Fish and apoptosis: studies in disease and pharmaceutical design. *Current Pharmaceutical Design*, **14**(2), pp. 170-183.
- DOYLE, S., HWANG, M., SHAH, K., MADABHUSHI, A., FELDMAN, M. and TOMASZEWSKI, J., 2007. Automated grading of prostate cancer using architectural and textural image features. *4th IEEE International Symposium on Biomedical Imaging: Macro to Nano*, Volumes 1-3, New Jersey, 12-15 April, pp. 1284-1287.
- DUNSTAN, R.W., WHARTON, K.A., QUIGLEY, C. and LOWE, A., 2011. The Use of Immunohistochemistry for Biomarker Assessment - Can It Compete with Other Technologies? *Toxicologic pathology*, **39**(6), pp. 988-1002.
- EFTHIMIOU, S., 1996. Dietary intake of β -1,3/1,6 glucans in juvenile dentex (*Dentex dentex*), Sparidae: effects on growth performance, mortalities and non-specific defense mechanisms. *Journal of Applied Ichthyology*, **12**(1), pp. 1-7.
- EGGENS, M., BERGMAN, A., VETHAAK, D., VAN DER WEIDEN, M., CELANDER, M. and BOON, J.P., 1995. Cytochrome P4501A indices as biomarkers of contaminant exposure: results of a field study with plaice (*Pleuronectes platessa*) and flounder (*Platichthys flesus*) from the southern North Sea. *Aquatic Toxicology*, **32**(2), pp. 211-225.
- EINEN, O. and ROEM, A.J., 1997. Dietary protein/energy ratios for Atlantic salmon in relation to fish size: growth, feed utilization and slaughter quality. *Aquaculture Nutrition*, **3**(2), pp. 115-126.

- EINSTEIN, A.J., GIL, J., WALLENSTEIN, S., BODIAN, C.A., SANCHEZ, M., BURSTEIN, D.E., WU, H. and LIU, Z., 1997. Reproducibility and accuracy of interactive segmentation procedures for image analysis in cytology. *Journal of Microscopy*, **188**(2), pp. 136-148.
- ELLIS, A., 1985. Eosinophilic granular cells (EGC) and histamine responses to *Aeromonas salmonicida* toxins in rainbow trout. *Developmental & Comparative Immunology*, **9**(2), pp. 251-260.
- ENGSTAD, R.E., ROBERTSEN, B. and FRIVOLD, E., 1992. Yeast glucan induces increase in lysozyme and complement-mediated haemolytic activity in Atlantic salmon blood. *Fish & Shellfish Immunology*, **2**(4), pp. 287-297.
- ESGIAR, A.N., NAGUIB, R.N., BENNETT, M.K. and MURRAY, A., 1998. Automated feature extraction and identification of colon carcinoma. *Analytical and Quantitative Cytology and Histology*, **20**(4), pp. 297-301.
- EZEASOR, D. and STOKOE, W., 1980. A cytochemical, light and electron microscopic study of the eosinophilic granule cells in the gut of the rainbow trout, *Salmo gairdneri* Richardson. *Journal of Fish Biology*, **17**(6), pp. 619-634.
- EZEASOR, D. and STOKOE, W., 1981. Light and electron microscopic studies on the absorptive cells of the intestine, caeca and rectum of the adult rainbow trout, *Salmo gairdneri*, Rich. *Journal of Fish Biology*, **18**(5), pp. 527-544.
- FALCO, A., FROST, P., MIEST, J., PIONNIER, N., IRNAZAROW, I. and HOOLE, D., 2012. Reduced inflammatory response to *Aeromonas salmonicida* infection in common carp (*Cyprinus carpio* L.) fed with β -glucan supplements. *Fish & Shellfish Immunology*, **32**(6), pp. 1051-1057.
- FANGE, R., LUNDBLAD, G. and LIND, J., 1976. Lysozyme and Chitinase in Blood and Lymphomyeloid Tissues of Marine Fish. *Marine Biology*, **36**(3), pp. 277-282.
- FANNING, A.S., MITIC, L.L. and ANDERSON, J.M., 1999. Transmembrane proteins in the tight junction barrier. *Journal of the American Society of Nephrology*, **10**(6), pp. 1337-1345.
- FAO, 2012. The state of world fisheries and aquaculture. FAO Fisheries and Aquaculture Department, Rome, Italy, pp. 209.
- FAST, M.D., ROSS, N.W., MUSTAFA, A., SIMS, D.E., JOHNSON, S.C., CONBOY, G.A., SPEARE, D.J., JOHNSON, G. and BURKA, J.F., 2002. Susceptibility of rainbow trout *Oncorhynchus mykiss*, Atlantic salmon *Salmo salar* and coho salmon *Oncorhynchus kisutch* to experimental infection with sea lice *Lepeophtheirus salmonis*. *Diseases of Aquatic Organisms*, **52**(1), pp. 57-68.
- FERRANDO, S., FERRANDO, T., GIROSI, L., MAUCERI, A., FASULO, S. and TAGLIAFIERRO, G., 2009. Apoptosis, cell proliferation and serotonin immunoreactivity in gut of *Liza aurata* from natural heavy metal polluted environments: preliminary observations. *European Journal of Histochemistry*, **49**(4), pp. 331-340.
- FERRARIS, R.P. and AHEARN, G.A., 1984. Sugar and amino acid transport in fish intestine. *Comparative Biochemistry and Physiology Part A: Physiology*, **77**(3), pp. 397-413.

- FICSOR, L., VARGA, V., BERCZI, L., MIHELLER, P., TAGSCHERER, A., WU, M.L., TULASSAY, Z. and MOLNAR, B., 2006. Automated virtual microscopy of gastric biopsies. *Cytometry Part B - Clinical Cytometry*, **70B**(6), pp. 423-431.
- FICSOR, L., VARGA, V.S., TAGSCHERER, A., TULASSAY, Z. and MOLNAR, B., 2008. Automated classification of inflammation in colon histological sections based on digital microscopy and advanced image analysis. *Cytometry Part A*, **73A**(3), pp. 230-237.
- FIELD, A., 2009. Discovering statistics using SPSS: (and sex and drugs and rock 'n' roll). SAGE Publications Ltd., London, UK, pp. 822.
- FILHO, D.W., EBLE, G.J., KASSNER, G., CAPRARIO, F.X., DAFRÉ, A.L. and OHIRA, M., 1992. Comparative hematology in marine fish. *Comparative Biochemistry and Physiology Part A: Physiology*, **102**(2), pp. 311-321.
- FINDLAY, V. and MUNDAY, B., 2000. The immunomodulatory effects of levamisole on the nonspecific immune system of Atlantic salmon, *Salmo salar* L., *Journal of Fish Diseases*, **23**, pp. 369-378.
- FLETCHER, T.C., WHITE, A. and BALDO, B.A., 1977. C-reactive protein-like precipitin and lysozyme in the lump sucker *Cyclopterus lumpus* L. during the breeding season. *Comparative Biochemistry and Physiology Part B: Comparative Biochemistry*, **57**(4), pp. 353-357.
- FODOR, I.K., 2002. *A survey of dimension reduction techniques*. Lawrence Livermore National Laboratory technical report (UCRL-ID-148494), U. S. Department of Energy by the University of California, pp. 26.
- FONTAGNÉ, S., BURTAIRE, L., CORRAZE, G. and BERGOT, P., 2000. Effects of dietary medium-chain triacylglycerols (tricaprylin and tricaproin) and phospholipid supply on survival, growth and lipid metabolism in common carp (*Cyprinus carpio* L.) larvae. *Aquaculture*, **190**(3-4), pp. 289-303.
- FRANCIS, G., MAKKAR, H. and BECKER, K., 2001. Anti-nutritional factors present in plant-derived alternate fish feed ingredients and their effects in fish. *Aquaculture*, **199**(3-4), pp. 197-227.
- FUENTES, E.N., SAFIAN, D., EINARSDOTTIR, I.E., VALDÉS, J.A., ELORZA, A.A., MOLINA, A. and BJÖRNSSON, B.T., 2013. Nutritional status modulates plasma leptin, AMPK and TOR activation, and mitochondrial biogenesis: Implications for cell metabolism and growth in skeletal muscle of the fine flounder. *General and Comparative Endocrinology*, **186**, pp. 172-180.
- FUGLEM, B., JIRILLO, E., BJERKÅS, I., KIYONO, H., NOCHI, T., YUKI, Y., RAIDA, M., FISCHER, U. and KOPPANG, E.O., 2010. Antigen-sampling cells in the salmonid intestinal epithelium. *Developmental & Comparative Immunology*, **34**(7), pp. 768-774.
- FUJIKAWA, C., NAGASHIMA, M., MAWATARI, K. and KATO, S., 2012. HSP70 Gene Expression in the Zebrafish Retina After Optic Nerve Injury: A Comparative Study Under Heat Shock Stresses. *Retinal Degenerative Diseases*. Springer, pp. 663-668.
- GALARRAGA, M., CAMPION, J., MUNOZ-BARRUTIA, A., BOQUE, N., MORENO, H., ALFREDO MARTINEZ, J., MILAGRO, F. and ORTIZ-DE-SOLORZANO, C., 2012. Adiposoft: automated software for the analysis of white adipose tissue cellularity in histological sections. *Journal of Lipid Research*, **53**(12), pp. 2791-2796.

- GALEOTTI, M., 1998. Some aspects of the application of immunostimulants and a critical review of methods for their evaluation. *Journal of Applied Ichthyology*, **14**(3–4), pp. 189-199.
- GALEOTTI, M., ROMANO, N., VOLPATTI, D., BULFON, C., BRUNETTI, A., TISCAR, P.G., MOSCA, F., BERTONI, F., MARCHETTI, M.G. and ABELLI, L., 2013. Innovative vaccination protocol against vibriosis in *Dicentrarchus labrax* (L.) juveniles: Improvement of immune parameters and protection to challenge. *Vaccine*, **31**(8), pp. 1224-1230.
- GAL-GARBER, O., MABJEESH, S., SKLAN, D. and UNI, Z., 2003. Nutrient transport in the small intestine: Na⁺, K⁺-ATPase expression and activity in the small intestine of the chicken as influenced by dietary sodium. *Poultry Science*, **82**(7), pp. 1127-1133.
- GALINDO-VILLEGAS, J. and HOSOKAWA, H., 2004. Immunostimulants: Towards temporary prevention of diseases in marine fish. *Simposium Internationale de Nutricion Acuicola*, Sonora, 16-19 November, pp. 279-319.
- GALLOWAY, T.F., KJORSVIK, E. and KRYVI, H., 1999. Muscle growth and development in Atlantic cod larvae (*Gadus morhua* L.) related to different somatic growth rates. *Journal of Experimental Biology*, **202**(15), pp. 2111-2120.
- GANNAM, A.L. and SCHROCK, R.M., 1999. Immunostimulants in fish diets. *Journal of Applied Aquaculture*, **9**(4), pp. 53-89.
- GANNAM, A.L. and SCHROCK, R.M., 2001. "Immunostimulants in fish diets" in Lim, C., Webster, C.D. (Eds.). *Nutrition and fish health*, The Haworth Press Inc., Binghamton, USA, pp. 235-266.
- GANSTER, H., PINZ, A., ROHRER, R., WILDLING, E., BINDER, M. and KITTLER, H., 2001. Automated melanoma recognition. *IEEE Transactions on Medical Imaging*, **20**(3), pp. 233-239.
- GATLIN, D.M., 2002. "Nutrition and fish health" in Halver, J.E., Hardy, R.W. (Eds.), *Fish nutrition*, Academic Press, San Diego, USA, pp. 671-702.
- GENTON, L. and KUDSK, K.A., 2003. Interactions between the enteric nervous system and the immune system: role of neuropeptides and nutrition. *The American Journal of Surgery*, **186**(3), pp. 253-258.
- GEORGOPOULOU, U., DABROWSKI, K., SIRE, M. and VERNIER, J., 1988. Absorption of intact proteins by the intestinal epithelium of trout, *Salmo gairdneri*. *Cell and Tissue Research*, **251**(1), pp. 145-152.
- GERBAULET, A., HARTMANN, K. and MEKORI, Y.A., 2006. "Mast cell apoptosis" in Krishnaswamy, G., Chi, D.S. (Eds.), *Mast cells: methods and protocols*. Humana Press, New Jersey, USA, pp. 407-423.
- GERDES, A., KRISEMAN, J. and BISHOP, S., 1982. Morphometric study of cardiac muscle: the problem of tissue shrinkage. *Laboratory Investigation; a Journal of Technical Methods and Pathology*, **46**(3), pp. 271-274.
- GIEMSA, G., 1902. Färbemethoden für malariaparasiten. *Zentralbl Bakteriol*, **31**:429-430.
- GIGER, M.L., CHAN, H. and BOONE, J., 2008. Anniversary Paper: History and status of CAD and quantitative image analysis: The role of Medical Physics and AAPM. *Medical Physics*, **35**(12), pp. 5799-5820.

- GIL, J., WU, H.S. and WANG, B.Y., 2002. Image analysis and morphometry in the diagnosis of breast cancer. *Microscopy Research and Technique*, **59**(2), pp. 109-118.
- GLENCROSS, B. and RUTHERFORD, N., 2010. Dietary strategies to improve the growth and feed utilization of barramundi, *Lates calcarifer* under high water temperature conditions. *Aquaculture Nutrition*, **16**(4), pp. 343-350.
- GLOTSOS, D., SPYRIDONOS, P., PETALAS, P., CAVOURAS, D., RAVAZOULA, P., DADIOTI, P.A., LEKKA, I. and NIKIFORIDIS, G., 2004. Computer-based malignancy grading of astrocytomas employing a support vector machine classifier, the WHO grading system and the regular hematoxylin-eosin diagnostic staining procedure. *Analytical and Quantitative Cytology and Histology*, **26**(2), pp. 77-83.
- GLOVER, C.N., PETRI, D., TOLLEFSEN, K., JØRUM, N., HANDY, R.D. and BERNTSEN, M.H., 2007. Assessing the sensitivity of Atlantic salmon (*Salmo salar*) to dietary endosulfan exposure using tissue biochemistry and histology. *Aquatic Toxicology*, **84**(3), pp. 346-355.
- GODDARD, J.C., SUTTON, C.D., FURNESS, P.N., KOCKELBERGH, R.C. and O'BYRNE, K.J., 2002. A computer image analysis system for microvessel density measurement in solid tumours. *Angiogenesis*, **5**(1-2), pp. 15-20.
- GODLEWSKI, M.M., TUROWSKA, A., JEDYNAK, P., PUG, D.M. and NEVALAINEN, H., 2009. "Quantitative analysis of fluorescent image: from descriptive to computational microscopy" in Goldys, E.M. (Ed.). *Fluorescence applications in biotechnology and life science*, Wiley-Blackwell, New Jersey, USA, pp. 99-116.
- GOKSØYR, A. and HUSØY, A., 1998. Immunochemical approaches to studies of CYP1A localization and induction by xenobiotics in fish. *Fish Ecotoxicology*. Springer, pp. 165-202.
- GOMEZ, D., SUNYER, J.O. and SALINAS, I., 2013. The mucosal immune system of fish: The evolution of tolerating commensals while fighting pathogens. *Fish & Shellfish Immunology*, **35**(6), pp. 1729-1739.
- GONZALEZ, R.C. and WOODS, R.E., 2002. Digital image processing, Prentice-Hall, Inc., New Jersey, USA, pp. 302.
- GONZÁLEZ-MARTÍN, I., ÁLVAREZ-GARCÍA, N. and HERNÁNDEZ-ANDALUZ, J., 2006. Instantaneous determination of crude proteins, fat and fibre in animal feeds using near infrared reflectance spectroscopy technology and a remote reflectance fibre-optic probe. *Animal Feed Science and Technology*, **128**(1), pp. 165-171.
- GOOD, J., 2004. Replacement of dietary fish oil with vegetable oils: effects on fish health. PhD Dissertation Thesis, University of Stirling, Stirling, UK, pp. 381.
- GOPALAKANNAN, A. and ARUL, V., 2010. Enhancement of the innate immune system and disease-resistant activity in *Cyprinus carpio* by oral administration of β -glucan and whole cell yeast. *Aquaculture Research*, **41**(6), pp. 884-892.
- GORNATI, R., PAPIS, E., RIMOLDI, S., TEROVA, G., SAROGLIA, M. and BERNARDINI, G., 2004. Rearing density influences the expression of stress-related genes in sea bass (*Dicentrarchus labrax*, L.). *Gene*, **341**, pp. 111-118.

- GOVIND, P. and MADHURI, S., 2012. Immunostimulant effect of medicinal plants on fish, *International Research Journal of Pharmacy*, **3**(3), pp. 112-114.
- GROSCWITZ, K.R., AHRENS, R., OSTERFELD, H., GURISH, M.F., HAN, X., ÅBRINK, M., FINKELMAN, F.D., PEJLER, G. and HOGAN, S.P., 2009. Mast cells regulate homeostatic intestinal epithelial migration and barrier function by a chymase/Mcpt4-dependent mechanism. *Proceedings of the National Academy of Sciences*, **106**(52), pp. 22381-22386.
- GROSELL, M., 2006. Intestinal anion exchange in marine fish osmoregulation. *Journal of Experimental Biology*, **209**(15), pp. 2813-2827.
- GROSELL, M., 2011. "The role of the gastrointestinal tract in salt and water balance" in Grosell, M., Farrell, A.P., Brauner, C.J. (Eds.). *The multifunctional gut of fish*, Wiley-Blackwell, San Diego, USA, pp. 135-164.
- GRUNKIN, M., RAUNDAHL, J. and FOGED, N.T., 2011. "Signal transduction immunohistochemistry: Methods and protocols in Molecular Biology" in Kalyuzhny, A.E. (Ed.). *Methods in molecular biology*, Volume 717, Springer-Verlag, New York, USA, pp. 143-154.
- GUILLAUME, J. and CHOUBERT, G. (2001) "Digestive physiology and nutrient digestibility in fishes" in Guillaume, J., Kaushik, P., Bergot, P., Metailler, R. (Eds.). *Nutrition and feeding of fish and crustaceans*, Springer-Praxis Publishing, Chichester, USA, pp. 27-56.
- GULLAND, G.L., 1898. The minute structure of the digestive tract of the salmon and the changes which occur in fresh water. *Anatomischer Anzeiger*, **14**, pp. 441-455.
- GUNDUZ-DEMIR, C., KANDEMIR, M., TOSUN, A. B. and SOKMENSUER, C., 2010. Automatic segmentation of colon glands using object-graphs. *Medical Image Analysis*, **14**(1), pp. 1-12.
- GURCAN, M. N., BOUCHERON, L. E., CAN, A., MADABHUSHI, A., RAJPOOT, N. M. and YENER, B., 2009. Histopathological image analysis: A review. *Biomedical Engineering, IEEE Reviews*, **2**, pp. 147-171.
- GURR, G.T., 1957. Biological staining methods. Cornell University, USA, pp. 87.
- HAINES, D.M. and WEST, K.H., 2005. Immunohistochemistry: Forging the links between immunology and pathology. *Veterinary Immunology and Immunopathology*, **108**(1), pp. 151-156.
- HALL, A.P., DAVIES, W., STAMP, K., CLAMP, I. and BIGLEY, A., 2013. Comparison of computerized image analysis with traditional semiquantitative scoring of Perls' Prussian Blue stained hepatic iron deposition. *Toxicologic Pathology*, **41**(7), pp. 992-1000.
- HALL, K. and BELLWOOD, D.R., 1995. Histological effects of cyanide, stress and starvation on the intestinal mucosa of *Pomacentrus coelestis*, a marine aquarium fish species. *Journal of Fish Biology*, **47**(3), pp. 438-454.
- HALL, P., COATES, P., GOODLAD, R. and HART, I., 1994a. Proliferating cell nuclear antigen expression in non-cycling cells may be induced by growth factors *in vivo*. *British Journal of Cancer*, **70**(2), pp. 244.
- HALL, P.A., COATES, P.J., ANSARI, B. and HOPWOOD, D., 1994b. Regulation of cell number in the mammalian gastrointestinal tract: the importance of apoptosis. *Journal of Cell Science*, **107**(12), pp. 3569-3577.
- HALVER, J.E. and HARDY, R.W., 2002. *Fish Nutrition*, Academic Press, San Diego, USA, pp.824.

- HAMILTON, P. W. and ALLEN, D. C., 2005. "Quantitative methods in tissue pathology" in Crocker, J. and Burnett, D. (Eds.). *The science of laboratory diagnosis*, 2nd Edition, John Wiley & Sons Ltd., West Sussex, UK, pp. 69-81.
- HAMILTON, P.W., BARTELS, P.H., THOMPSON, D., ANDERSON, N.H., MONTIRONI, R. and SLOAN, J.M., 1997. Automated location of dysplastic fields in colorectal histology using image texture analysis. *The Journal of Pathology*, **182**(1), pp. 68-75.
- HANSEN, A., ROSENLUND, G., KARLSEN, Ø., KOPPE, W. and HEMRE, G., 2007. Total replacement of fish meal with plant proteins in diets for Atlantic cod (*Gadus morhua*, L.) I – Effects on growth and protein retention. *Aquaculture*, **272**(1), pp. 599-611.
- HARDER, W., 1975. The digestive tract. Anatomy of fishes. Part1: Text. Stuttgart: E. Dvhweizerbart'sche Verlagsbuchhand-lung. pp. 128-186.
- HARDIE, L., FLETCHER, T. and SECOMBES, C., 1990. The effect of vitamin E on the immune response of the Atlantic salmon (*Salmo salar*, L.). *Aquaculture*, **87**(1), pp. 1-13.
- HARDIE, L., FLETCHER, T. and SECOMBES, C., 1991. The effect of dietary vitamin C on the immune response of the Atlantic salmon (*Salmo salar* L.). *Aquaculture*, **95**(3), pp. 201-214.
- HART, S., WRATHMELL, A.B., HARRIS, J.E. and GRAYSON, T.H., 1988. Gut immunology in fish: A review. *Developmental & Comparative Immunology*, **12**(3), pp. 453-480.
- HASAN, M.R. 2001. "Nutrition and feeding for sustainable aquaculture development in the third millennium" in Subasinghe, R.P., Bueno, P., Phillips, M.J., Hough, C., McGladdery, S.E., Arthur, J.R. (Eds.) *Aquaculture in the third millennium. Technical. Proceedings of the Conference on Aquaculture in the Third Millennium*, Bangkok, 20-25 February, pp. 193-219.
- HASSELL, L.A., FUNG, K. and CHASER, B., 2011. Digital slides and ACGME resident competencies in anatomic pathology: An altered paradigm for acquisition and assessment. *Journal of Pathology Informatics*, **2**, pp. 27.
- HAYAT, M., 1986. *Basic techniques for transmission electron microscopy*. Academic Press, California, USA, pp. 411.
- HE, L., LONG, L. R., ANTANI, S. and THOMA, G. R., 2012. Histology image analysis for carcinoma detection and grading. *Computer Methods and Programs in Biomedicine*, **107**(3), pp. 538-556.
- HEIKKINEN, J., VIELMA, J., KEMILÄINEN, O., TIIROLA, M., ESKELINEN, P., KIURU, T., NAVIA-PALDANIUS, D. and VON WRIGHT, A., 2006. Effects of soybean meal based diet on growth performance, gut histopathology and intestinal microbiota of juvenile rainbow trout (*Oncorhynchus mykiss*). *Aquaculture*, **261**(1), pp. 259-268.
- HELLAND, S., STOREBAKKEN, T. and GRISDALE-HELLAND, B., 1991. "Atlantic salmon, *Salmo salar*" in Wilson, R.P. (Ed.). *Handbook of nutrient requirements of finfish*, CRC Press Inc., Boca Raton, USA, pp.13-22.
- HEMMER, N., STEINHAGEN, D., DROMMER, W. and KOERTING, W., 1998. Changes of intestinal epithelial structure and cell turnover in carp *Cyprinus carpio* infected with *Goussia carpelli* (Protozoa: Apicomplexa). *Diseases of Aquatic Organisms*, **34**(1), pp. 39-44.

- HEMRE, G., DENG, D., WILSON, R.P. and BERNTSSEN, M.H.G., 2004. Vitamin A metabolism and early biological responses in juvenile sunshine bass (*Morone chrysops*×*M. saxatilis*) fed graded levels of vitamin A. *Aquaculture*, **235**(1–4), pp. 645-658.
- HEMRE, G., SANDEN, M., BAKKE-McKELLEP, A., SAGSTAD, A. and KROGDAHL, Å., 2005. Growth, feed utilization and health of Atlantic salmon *Salmo salar* L. fed genetically modified compared to non-modified commercial hybrid soybeans. *Aquaculture Nutrition*, **11**(3), pp. 157-167.
- HERATH, T. K., 2010. Cellular and molecular pathogenesis of salmonid alphavirus 1 in Atlantic salmon, *Salmo salar* L. PhD Dissertation Thesis, University of Stirling, Stirling, UK, pp. 263.
- HESSER, E. F., 1960. Methods for routine fish hematology. *The Progressive Fish-Culturist*, **22**(4), pp. 164-171.
- HIBIYA, T., YOKOTE, M., OGURI, M., SATO, H., TAKASHIMA, F. and AIDA, K., 1982. An atlas of fish histology: Normal and pathological features, Gustav Fischer Verlag., New York, USA, pp.147.
- HIMICK, B.A. and PETER, R.E., 1994. CCK/gastrin-like immunoreactivity in brain and gut, and CCK suppression of feeding in goldfish. *American Journal of Physiology-Regulatory, Integrative and Comparative Physiology*, **267**(3), pp. R841-R851.
- HOLLAND, J.W. and ROWLEY, A.F., 1998. Studies on the eosinophilic granule cells in the gills of the rainbow trout, *Oncorhynchus mykiss*. *Comparative Biochemistry and Physiology Part C: Pharmacology, Toxicology and Endocrinology*, **120**(2), pp. 321-328.
- HOLM, S., 1979. A simple sequentially rejective multiple test procedure. *Scandinavian Journal of Statistics*, **6**, pp. 65-70.
- HOLMGREN, S. and OLSSON, C., 2009. "The neuronal and endocrine regulation of gut function" in Bernier, N.J., Van der Kraak, G., Farrell, A.P., Brauner, C.J. (Eds.). *Fish neuroendocrinology*, Academic Press, Amsterdam, Netherland, pp. 467-512.
- HONG, M.Y., CHANG, W.L., CHAPKIN, R.S. and LUPTON, J.R., 1997. Relationship among colonocyte proliferation, differentiation, and apoptosis as a function of diet and carcinogen. *Nutrition and Cancer*, **28**(1), pp. 20-29.
- HORDVIK, I., 2002. Identification of a novel immunoglobulin δ transcript and comparative analysis of the genes encoding IgD in Atlantic salmon and Atlantic halibut. *Molecular Immunology*, **39**(1), pp. 85-91.
- HORDVIK, I., THEVARAJAN, J., SAMDAL, I., BASTANI, N. and KROSSOY, B., 1999. Molecular cloning and phylogenetic analysis of the Atlantic salmon immunoglobulin D gene. *Scandinavian Journal of Immunology*, **50**(2), pp. 202-210.
- HSU, S., RAINE, L. and FANGER, H., 1981. The use of antiavidin antibody and avidin-biotin-peroxidase complex in immunoperoxidase technics. *American Journal of Clinical Pathology*, **75**(6), pp. 816-821.
- HUANG, S., MINASSIAN, H. and MORE, J., 1976. Application of immunofluorescent staining on paraffin sections improved by trypsin digestion. *Laboratory Investigation; a Journal of Technical Methods and Pathology*, **35**(4), pp. 383-390.

- HUGHESDON, P., 1949. Two uses of uranyl nitrate. *Journal of the Royal Microscopical Society*, **69**(1), pp. 1-8.
- INGRAM, G.A. and ALEXANDER, J.B., 1977. Serum protein changes in brown trout (*Salmo trutta* L.) after single injections of soluble and cellular antigens. *Journal of Fish Biology*, **11**(3), pp. 283-291.
- ISHIZAKI, Y., JACOBSON, M.D. and RAFF, M.C., 1998. A role for caspases in lens fiber differentiation. *The Journal of Cell Biology*, **140**(1), pp. 153-158.
- ISHIZEKI, K., NAWA, T., TACHIBANA, T., SAKAKURA, Y. and IIDA, S., 1984 Hemopoietic sites and development of eosinophil granulocytes in the loach, *Misgurnus anguillicaudatus*. *Cell Tissue Research*, **235**, pp. 419-426.
- ISSE, K., LESNIAK, A., GRAMA, K., ROYSAM, B., MINERVINI, M. I. and DEMETRIS, A. J., 2012. Digital transplantation pathology: Combining whole slide imaging, multiplex staining and automated image analysis. *American Journal of Transplantation*, **12**(1), pp. 27-37.
- IWAMA, G.K., AFONSO, L.O., TODGHAM, A., ACKERMAN, P. and NAKANO, K., 2004. Are hsp suitable for indicating stressed states in fish? *Journal of Experimental Biology*, **207**(1), pp. 15-19.
- IWAMA, G.K., THOMAS, P.T., FORSYTH, R.B. and VIJAYAN, M.M., 1998. Heat shock protein expression in fish. *Reviews in Fish Biology and Fisheries*, **8**(1), pp. 35-56.
- IWASHITA, Y., SUZUKI, N., MATSUNARI, H., SUGITA, T. and YAMAMOTO, T., 2009. Influence of soya saponin, soya lectin, and cholytaurine supplemented to a casein-based semipurified diet on intestinal morphology and biliary bile status in fingerling rainbow trout *Oncorhynchus mykiss*. *Fisheries Science*, **75**(5), pp. 1307-1315.
- JARAMILLO, F. and GATLIN, D., 2004. Comparison of purified and practical diets supplemented with or without β -Glucan and selenium on resistance of hybrid striped bass *Morone chrysops*♀ \times *M. saxatilis*♂ to *Streptococcus iniae* Infection. *Journal of the World Aquaculture Society*, **35**(2), pp. 245-252.
- JARVIS, L., 1992. The microcomputer and image-analysis in diagnostic pathology. *Microscopy Research and Technique*, **21**(4), pp. 292-299.
- JENEY, G. and ANDERSON, D.P., 1993. Glucan injection or bath exposure given alone or in combination with a bacterin enhance the non-specific defence mechanisms in rainbow trout (*Oncorhynchus mykiss*). *Aquaculture*, **116**(4), pp. 315-329.
- JENEY, G., GALEOTTI, M., VOLPATTI, D., JENEY, Z. and ANDERSON, D.P., 1997. Prevention of stress in rainbow trout (*Oncorhynchus mykiss*) fed diets containing different doses of glucan. *Aquaculture*, **154**(1), pp. 1-15.
- JENSEN, L.E., HINEY, M.P., SHIELDS, D.C., UHLAR, C.M., LINDSAY, A.J. and WHITEHEAD, A.S., 1997. Acute phase proteins in salmonids: evolutionary analyses and acute phase response. *The Journal of Immunology*, **158**(1), pp. 384-392.
- JEONG, W., SCHNEIDER, J., TURNEY, S.G., FAULKNER-JONES, B.E., MEYER, D., WESTERMANN, R., REID, R., LICHTMAN, J. and PFISTER, H., 2010. Interactive histology of

- large-scale biomedical image stacks. *Visualization and Computer Graphics, IEEE Transactions on*, **16**(6), pp. 1386-1395.
- JHA, A.K., PAL, A., SAHU, N., KUMAR, S. and MUKHERJEE, S., 2007. Haemato-immunological responses to dietary yeast RNA, ω -3 fatty acid and β -carotene in *Catla catla* juveniles. *Fish & Shellfish Immunology*, **23**(5), pp. 917-927.
- JOBLING, M., 1994. "*Fish bioenergetics*", Chapman & Hall, London, UK, pp. 328.
- JOHANSSON, A.C., VISSE, E., WIDEGREN, B., SJOGREN, H.O. and SIESJO, P., 2001. Computerized image analysis as a tool to quantify infiltrating leukocytes: A comparison between high-and low-magnification images. *Journal of Histochemistry & Cytochemistry*, **49**(9), pp. 1073-1079.
- JORDANOVA, M., MITEVA, N. and ROCHA, E., 2007. A quantitative study of the hepatic eosinophilic granule cells and rodlet cells during the breeding cycle of Ohrid trout, *Salmo letnica* Kar. (Teloestei, Salmonidae). *Fish & Shellfish Immunology*, **23**(2), pp. 473-478.
- JØRGENSEN J.B., SHARP G.J.E., SECOMBES C.J. and ROBERTSEN B., 1993. Effect of a yeast-cellwall glucan on the bactericidal activity of rainbow trout macrophages. *Fish and Shellfish Immunology*, **3**, pp. 315-343.
- JØRGENSEN, J.B. and ROBERTSEN, B., 1995. Yeast β -glucan stimulates respiratory burst activity of Atlantic salmon (*Salmo salar* L.) macrophages. *Developmental & Comparative Immunology*, **19**(1), pp. 43-57.
- JUTFELT, F., 2006. The intestinal epithelium of salmonids: Transepithelial transport, barrier function and bacterial interactions. PhD Dissertation Thesis, University of Gothenburgh, Sweden, pp. 66.
- KAGAWA, N., RYO, K. and MUGIYA, Y., 1999. Enhanced expression of stress protein 70 in the brains of goldfish, *Carassius auratus*, reared with bluegills, *Lepomis macrochirus*. *Fish Physiology and Biochemistry*, **21**(2), pp. 103-110.
- KAISER, H.F., 1974. An index of factorial simplicity. *Psychometrika*, **39**(1), pp. 31-36.
- KALKAN, H., NAP, M., DUIN, R.P.W. and LOOG, M., 2012. Automated classification of local patches in colon histopathology, *21st International Conference on Pattern Recognition*, Tsukuba, 11-15 November, pp. 61-64.
- KAMUNDE, C.N., GROSELL, M., LOTT, J.N. and WOOD, C.M., 2001. Copper metabolism and gut morphology in rainbow trout (*Oncorhynchus mykiss*) during chronic sublethal dietary copper exposure. *Canadian Journal of Fisheries and Aquatic Sciences*, **58**(2), pp. 293-305.
- KARLSSON, M.G., DAVIDSSON, A. and HELLQUIST, H.B., 1994. Quantitative computerized image-analysis of immunostained lymphocytes. *Pathology Research and Practice*, **190**(8), pp. 799-807.
- KAUSHIK, S., CRAVEDI, J., LALLES, J., SUMPTER, J., FAUCONNEAU, B. and LAROCHE, M., 1995. Partial or total replacement of fish meal by soybean protein on growth, protein utilization, potential estrogenic or antigenic effects, cholesterolemia and flesh quality in rainbow trout, *Oncorhynchus mykiss*. *Aquaculture*, **133**(3), pp. 257-274.
- KAYSER, G. and KAYSER, K., 2013. Quantitative pathology in virtual microscopy: History, applications, perspectives. *Acta Histochemica*, **115**(6), pp. 527-532.

- KAYSER, G., RIEDE, U., WENER, M., HUFNAGL, P. and KAYSER, K., 2002. Towards an automated morphological classification of histological images of common lung carcinomas. *Electronic Journal of Pathology and Histology*, **8**(2), pp. 22-30.
- KEENAN, S.J., DIAMOND, J., GLENN MCCLUGGAGE, W., BHARUCHA, H., THOMPSON, D., BARTELS, P.H. and HAMILTON, P.W., 2000. An automated machine vision system for the histological grading of cervical intraepithelial neoplasia (CIN). *The Journal of Pathology*, **192**(3), pp. 351-362.
- KENARI, A.A., MAHMOUDI, N., SOLTANI, M. and ABEDIANKENARI, S., 2013. Dietary nucleotide supplements influence the growth, haemato-immunological parameters and stress responses in endangered Caspian brown trout (*Salmo trutta caspius* Kessler, 1877). *Aquaculture Nutrition*, **19**(1), pp. 54-63.
- KHAN, N. and DESCHAUX, P., 1997. Role of serotonin in fish immunomodulation. *Journal of Experimental Biology*, **200**(13), pp. 1833-1838.
- KILEMADE, M., LYONS-ALCANTARA, M., ROSE, T., FITZGERALD, R. and MOTHERSILL, C., 2002. Rainbow trout primary epidermal cell proliferation as an indicator of aquatic toxicity: an *in vitro/in vivo* exposure comparison. *Aquatic Toxicology*, **60**(1), pp. 43-59.
- KIRON, V., 2012. Fish immune system and its nutritional modulation for preventive health care. *Animal Feed Science and Technology*, **173**(1–2), pp. 111-133.
- KNUDSEN, D. L., 2007. Soybean-induced enteritis in Atlantic salmon. PhD Dissertation Thesis, Technical University of Denmark, Denmark, pp. 118.
- KNUDSEN, D., JUTFELT, F., SUNDH, H., SUNDELL, K., KOPPE, W. and FRØKIÆR, H., 2008. Dietary soya saponins increase gut permeability and play a key role in the onset of soyabean-induced enteritis in Atlantic salmon (*Salmo salar* L.). *British Journal of Nutrition*, **100**(01), pp. 120-129.
- KODAMA, H., MATSUOKA, Y., TANAKA, Y., LIU, Y., IWASAKI, T. and WATARAI, S., 2004. Changes of C-reactive protein levels in rainbow trout (*Oncorhynchus mykiss*) sera after exposure to anti-ectoparasitic chemicals used in aquaculture. *Fish & Shellfish Immunology*, **16**(5), pp. 589-597.
- KOKOU, F., RIGOS, G., HENRY, M., KENTOURI, M. and ALEXIS, M., 2012. Growth performance, feed utilization and non-specific immune response of gilthead sea bream (*Sparus aurata* L.) fed graded levels of a bioprocessed soybean meal. *Aquaculture*, **364–365**(0), pp. 74-81.
- KONG, J., SERTEL, O., SHIMADA, H., BOYER, K.L., SALTZ, J.H. and GURCAN, M.N., 2009. Computer-aided evaluation of neuroblastoma on whole-slide histology images: Classifying grade of neuroblastic differentiation. *Pattern Recognition*, **42**(6), pp. 1080-1092.
- KONG, J., SHIMADA, H., BOYER, K., SALTZ, J. and GURCAN, M., 2007. Image analysis for automated assessment of grade of neuroblastic differentiation. *4th IEEE International Symposium on Biomedical Imaging: Macro to Nano*, Volumes 1-3, Ohio, 12-15 April, pp. 61-64.
- KOPEC, C. D., BOWERS, A. C., PAI, S. and BRODY, C. D., 2011. Semi-automated atlas-based analysis of brain histological sections. *Journal of Neuroscience Methods*, **196**(1), pp. 12-19.
- KOPP, R., MAREŠ, J., LANG, Š., BRABEC, T. and ZIKOVÁ, A., 2011. Assessment of ranges

- plasma indices in rainbow trout (*Oncorhynchus mykiss*) reared under conditions of intensive aquaculture. *Acta Universitatis Agriculturae et Silviculturae Mendelianae Brunensis*, **59**, pp. 24.
- KORTNER, T.M., VALEN, E.C., KORTNER, H., MARJARA, I.S., KROGDAHL, Å. and BAKKE, A.M., 2011. Candidate reference genes for quantitative real-time PCR (qPCR) assays during development of a diet-related enteropathy in Atlantic salmon (*Salmo salar* L.) and the potential pitfalls of uncritical use of normalization software tools. *Aquaculture*, **318**(3), pp. 355-363.
- KRENACS, T., ZSAKOVICS, I., MICSIK, T., FONYAD, L., VARGA, S.V., FICSOR, L. and MOLNAR, B., 2010. "Digital microscopy - the upcoming revolution in histopathology teaching, diagnostics, research and quality assurance" in MENDEZ-VILAS, A. and DIAZ, J. (Eds.). *Microscopy: Science, technology, applications and education*, Volume 2, Formatex Research Center, Badajoz, Spain, pp. 965-977.
- KRIETE, A. and BOYCE, K., 2005. Automated tissue analysis - a bioinformatics perspective. *Methods of Information in Medicine*, **44**(1), pp. 32-37.
- KROGDAHL, Å. and BAKKE-McKELLEP, A., 2005. Fasting and refeeding cause rapid changes in intestinal tissue mass and digestive enzyme capacities of Atlantic salmon (*Salmo salar* L.). *Comparative Biochemistry and Physiology Part A: Molecular & Integrative Physiology*, **141**(4), pp. 450-460.
- KROGDAHL, Å., BAKKE-McKELLEP, A. and BAEVERFJORD, G., 2003. Effects of graded levels of standard soybean meal on intestinal structure, mucosal enzyme activities, and pancreatic response in Atlantic salmon (*Salmo salar* L.). *Aquaculture Nutrition*, **9**(6), pp. 361-371.
- KROGDAHL, Å., LEA, T.B. and OLLI, J.J., 1994. Soybean proteinase inhibitors affect intestinal trypsin activities and amino acid digestibilities in rainbow trout (*Oncorhynchus mykiss*). *Comparative Biochemistry and Physiology Part A: Physiology*, **107**(1), pp. 215-219.
- KROGDAHL, Å., PENN, M., THORSEN, J., REFSTIE, S. and BAKKE, A.M., 2010. Important anti-nutrients in plant feedstuffs for aquaculture: an update on recent findings regarding responses in salmonids. *Aquaculture Research*, **41**(3), pp. 333-344.
- KROGDAHL, BAKKE-McKELLEP, RØED and BAEVERFJORD, 2000. Feeding Atlantic salmon *Salmo salar* L. soybean products: effects on disease resistance (furunculosis), and lysozyme and IgM levels in the intestinal mucosa. *Aquaculture Nutrition*, **6**(2), pp. 77-84.
- KÜHLWEIN, H., MERRIFIELD, D., RAWLING, M., FOEY, A. and DAVIES, S., 2013. Effects of dietary β -(1, 3)(1, 6)-D-glucan supplementation on growth performance, intestinal morphology and haemato-immunological profile of mirror carp (*Cyprinus carpio* L.). *Journal of Animal Physiology and Animal Nutrition*, [Epub ahead of print].
- KUMAR, S., SAHU, N., PAL, A., CHOUDHURY, D., YENGGOKPAM, S. and MUKHERJEE, S., 2005. Effect of dietary carbohydrate on haematology, respiratory burst activity and histological changes in *L. rohita* juveniles. *Fish & Shellfish Immunology*, **19**(4), pp. 331-344.
- KUMAR, V., MAKKAR, H. and BECKER, K., 2010a. Dietary inclusion of detoxified *Jatropha curcas* kernel meal: effects on growth performance and metabolic efficiency in common carp, *Cyprinus carpio* L. *Fish Physiology and Biochemistry*, **36**(4), pp. 1159-1170.

- KUMAR, V., MAKKAR, H. and BECKER, K., 2011a. Detoxified *Jatropha curcas* kernel meal as a dietary protein source: growth performance, nutrient utilization and digestive enzymes in common carp (*Cyprinus carpio* L.) fingerlings. *Aquaculture Nutrition*, **17**(3), pp. 313-326.
- KUMAR, V., MAKKAR, H. and BECKER, K., 2011b. Nutritional, physiological and haematological responses in rainbow trout (*Oncorhynchus mykiss*) juveniles fed detoxified *Jatropha curcas* kernel meal. *Aquaculture Nutrition*, **17**(4), pp. 451-467.
- KUMAR, V., MAKKAR, H.P., AMSELGRUBER, W. and BECKER, K., 2010b. Physiological, haematological and histopathological responses in common carp (*Cyprinus carpio*, L.) fingerlings fed with differently detoxified *Jatropha curcas* kernel meal. *Food and Chemical Toxicology*, **48**(8), pp. 2063-2072.
- KUMARI, J. and SAHOO, P., 2006. Dietary β -1, 3 glucan potentiates innate immunity and disease resistance of Asian catfish, *Clarias batrachus* (L.). *Journal of Fish Diseases*, **29**(2), pp. 95-101.
- KURANAGA, E. and MIURA, M., 2007. Nonapoptotic functions of caspases: caspases as regulatory molecules for immunity and cell-fate determination. *Trends in Cell Biology*, **17**(3), pp. 135-144.
- KUZNETSOV, V., LEE, H.K., MAURER-STROH, S., MOLNAR, M.J., PONGOR, S., EISENHABER, B. and EISENHABER, F., 2013. How bioinformatics influences health informatics: usage of biomolecular sequences, expression profiles and automated microscopic image analyses for clinical needs and public health. *Health Information Science and Systems*, **1**(2), pp. 1-18.
- LAITAKARI, J., HARRISON, D. and STENBACK, F., 2003. Automated image analysis of proliferating cells in carcinoma of the larynx. *Acta Oto-Laryngologica*, **123**(6), pp. 759-766.
- LAMAS, J., BRUNO, D.W., SANTOS, Y., ANADÓN, R. and ELLIS, A.E., 1991. Eosinophilic granular cell response to intraperitoneal injection with *Vibrio anguillarum* and its extracellular products in rainbow trout, *Oncorhynchus mykiss*. *Fish & Shellfish Immunology*, **1**(3), pp. 187-194.
- LAMAS, J., SANTOS, Y., BRUNO, D., TORANZO, A. and ANADON, R., 1994. Non-specific cellular responses of rainbow trout to *Vibrio anguillarum* and its extracellular products (ECPs). *Journal of Fish Biology*, **45**(5), pp. 839-854.
- LAMKANFI, M., FESTJENS, N., DECLERCQ, W., BERGHE, T.V. and VANDENABEELE, P., 2006. Caspases in cell survival, proliferation and differentiation. *Cell Death & Differentiation*, **14**(1), pp. 44-55.
- LANDOLT, M.L., 1989. The relationship between diet and the immune response of fish. *Aquaculture*, **79**(1-4), pp. 193-206.
- LAPORTE, J. and TRUSHENSKI, J., 2012. Production performance, stress tolerance and intestinal integrity of sunshine bass fed increasing levels of soybean meal. *Journal of Animal Physiology and Animal Nutrition*, **96**(3), pp. 513-526.
- LAUNAY, S., HERMINE, O., FONTENAY, M., KROEMER, G., SOLARY, E. and GARRIDO, C., 2005. Vital functions for lethal caspases. *Oncogene*, **24**(33), pp. 5137-5148.
- LAURIANO, E.R., CALÒ, M., SILVESTRI, G., ZACCONE, D., PERGOLIZZI, S. and LO CASCIO, P., 2012. Mast cells in the intestine and gills of the sea bream, *Sparus aurata*, exposed to a polychlorinated biphenyl, PCB 126. *Acta Histochemica*, **114**(2), pp. 166-171.

- LEBLOND, C. and CLERMONT, Y., 1952. Definition of the stages of the cycle of the seminiferous epithelium in the rat. *Annals of the New York Academy of Sciences*, **55**(4), pp. 548-573.
- LEKNES, I.L., 2007. Eosinophilic granule cells and endocytic cells in intestinal wall of pearl gouramy (Anabantidae: Teleostei). *Fish & Shellfish Immunology*, **23**(4), pp. 897-900.
- LEONARDI, M., SANDINO, A. and KLEMPAU, A., 2003. Effect of a nucleotide-enriched diet on the immune system, plasma cortisol levels and resistance to infectious pancreatic necrosis (IPN) in juvenile rainbow trout (*Oncorhynchus mykiss*). *Bulletin of the European Association of Fish Pathologists*, **23**(2), pp. 52-59.
- LEONG, F.J.W. and LEONG, A.S.Y., 2003. Digital imaging applications in anatomic pathology. *Advances in Anatomic Pathology*, **10**(2), pp. 88-95.
- LEONG, F.J.W.M. and LEONG, A.S.Y., 2004. Digital imaging in pathology: theoretical and practical considerations, and applications. *Pathology*, **36**(3), pp. 234-241.
- LEV, R. and SPICER, S.S. 1964. Specific staining of sulphated groups with alcian blue at low pH. *Journal of Histochemistry and Cytochemistry*, **12**: pp. 309.
- LEWIS, M.J., HAMID, N.K.A., ALHAZZAA, R., HERMON, K., DONALD, J.A., SINCLAIR, A.J. and TURCHINI, G.M., 2013. Targeted dietary micronutrient fortification modulates n-3 LC-PUFA pathway activity in rainbow trout (*Oncorhynchus mykiss*). *Aquaculture*, **412-413**, pp. 215-222.
- LI, P. and GATLIN, D.M., 2004. Dietary brewers yeast and the prebiotic Grobiotic™AE influence growth performance, immune responses and resistance of hybrid striped bass (*Morone chrysops* × *M. saxatilis*) to *Streptococcus iniae* infection. *Aquaculture*, **231**(1–4), pp. 445-456.
- LI, P. and GATLIN, D.M., 2006. Nucleotide nutrition in fish: Current knowledge and future applications. *Aquaculture*, **251**(2–4), pp. 141-152.
- LI, P., BURR, G.S., GOFF, J., WHITEMAN, K.W., DAVIS, K.B., VEGA, R.R., NEILL, W.H. and GATLIN, D.M., 2005. A preliminary study on the effects of dietary supplementation of brewers yeast and nucleotides, singularly or in combination, on juvenile red drum (*Sciaenops ocellatus*). *Aquaculture Research*, **36**(11), pp. 1120-1127.
- LI, P., GATLIN, D.M. and NEILL, W.H., 2007. Dietary supplementation of a purified nucleotide mixture transiently enhanced growth and feed utilization of juvenile red drum, *Sciaenops ocellatus*. *Journal of the World Aquaculture Society*, **38**(2), pp. 281-286.
- LI, P., LEWIS, D.H. and GATLIN, D.M., 2004. Dietary oligonucleotides from yeast RNA influence immune responses and resistance of hybrid striped bass (*Morone chrysops* × *Morone saxatilis*) to *Streptococcus iniae* infection. *Fish & Shellfish Immunology*, **16**(5), pp. 561-569.
- LIE, Ø., EVENSEN, Ø., SØRENSEN, A. and FRØYSADAL, E., 1989. Study on lysozyme activity in some fish species. *Diseases of Aquatic Organisms*, **6**, pp. 1-5.
- LILLEENG, E., FROYSTAD, M.K., OSTBY, G.C., VALEN, E.C. and KROGDAHL, A., 2007. Effects of diets containing soybean meal on trypsin mRNA expression and activity in Atlantic salmon (*Salmo salar* L). *Comparative Biochemistry and Physiology Part A: Molecular & Integrative Physiology*, **147**(1), pp. 25-36.
- LILLEENG, E., PENN, M.H., HAUGLAND, Ø., XU, C., BAKKE, A.M., KROGDAHL, Å., LANDSVERK, T. and FRØYSTAD-SAUGEN, M.K., 2009. Decreased expression of TGF-β, GILT and T-cell

- markers in the early stages of soybean enteropathy in Atlantic salmon (*Salmo salar* L.). *Fish & Shellfish Immunology*, **27**(1), pp. 65-72.
- LILLIE, R. and FULMER, H., 1965. *Histological technique and practical histochemistry*, McGraw-Hill, New York, USA, pp. 942.
- LIM, C. and WEBSTER, C.D., 2001. *Nutrition and fish health*. Taylor & Francis, New York, USA, pp. 365.
- LIN, Y., WANG, H. and SHIAU, S., 2009. Dietary nucleotide supplementation enhances growth and immune responses of grouper, *Epinephelus malabaricus*. *Aquaculture Nutrition*, **15**(2), pp. 117-122.
- LINDSTEDT, K.A. and KOVANEN, P.T., 2001. Isolation of Mast Cell Granules. *Current Protocols in Cell Biology*, **29**:3, pp. 16.1–3.16.13.
- LIU, Y., IWASAKI, T., WATARAI, S. and KODAMA, H., 2004. Effect of turpentine oil on C-reactive protein (CRP) production in rainbow trout (*Oncorhynchus mykiss*). *Fish & Shellfish Immunology*, **17**(3), pp. 203-210.
- LIU, Y., MOORE, L., OLAF KOPPANG, E. and HORDVIK, I., 2008. Characterization of the CD3 ζ , CD3 $\gamma\delta$ and CD3 ϵ subunits of the T cell receptor complex in Atlantic salmon. *Developmental & Comparative Immunology*, **32**(1), pp. 26-35.
- LØKKA, G., AUSTBØ, L., FALK, K., BJERKÅS, I. and KOPPANG, E.O., 2013. Intestinal morphology of the wild Atlantic salmon (*Salmo salar*). *Journal of Morphology*, **274**(8), pp. 859-876.
- LORENZI, V. and GROBER, M.S., 2012. Immunohistochemical localization of serotonin in the brain during natural sex change in the hermaphroditic goby *Lythrypnus dalli*. *General and Comparative Endocrinology*, **175**(3), pp. 527-536.
- LOUKAS, C.G. and LINNEY, A., 2004. A survey on histological image analysis-based assessment of three major biological factors influencing radiotherapy: proliferation, hypoxia and vasculature. *Computer Methods and Programs in Biomedicine*, **74**(3), pp. 183-199.
- LOVELL, T., 1998. *Nutrition and feeding in fish*. Kluwer Academic Publishers, Massachusetts, USA, pp.271.
- LOW, C., WADSWORTH, S., BURRELLS, C. and SECOMBES, C., 2003. Expression of immune genes in turbot (*Scophthalmus maximus*) fed a nucleotide-supplemented diet. *Aquaculture*, **221**(1), pp. 23-40.
- LUND, V. and OLAFSEN, J.A., 1998. A comparative study of pentraxin-like proteins in different fish species. *Developmental & Comparative Immunology*, **22**(2), pp. 185-194.
- LUND, V. and OLAFSEN, J.A., 1999. Changes in serum concentration of a serum amyloid P-like pentraxin in Atlantic salmon, *Salmo salar* L., during infection and inflammation. *Developmental & Comparative Immunology*, **23**(1), pp. 61-70.
- LUNDÉN, T., LILIUS, E. and BYLUND, G., 2002. Respiratory burst activity of rainbow trout (*Oncorhynchus mykiss*) phagocytes is modulated by antimicrobial drugs. *Aquaculture*, **207**(3–4), pp. 203-212.

- MADSEN, S.S., OLESEN, J.H., BEDAL, K., ENGELUND, M.B., VELASCO-SANTAMARÍA, Y.M. and TIPSMARK, C.K., 2011. Functional characterization of water transport and cellular localization of three aquaporin paralogs in the salmonid intestine. *Frontiers in Physiology*, **2**(56), pp.1-14.
- MAGNADÓTTIR, B., 2006. Innate immunity of fish (overview). *Fish & Shellfish Immunology*, **20**(2), pp. 137-151.
- MAGNADOTTIR, B., 2010. Immunological control of fish diseases. *Marine Biotechnology*, **12**(4), pp. 361-379.
- MAITA, M., 2007. "Fish health assessment" in Nakagawa, H., Sato, M. and Gatlin, D. (Eds.). *Dietary supplements for the health and quality of cultured fish*, Cromwell Press, Trowbridge, UK, pp.10-34.
- MALINA, A., TASSAKKA, A. and SAKAI, M., 2005. Current research on the immunostimulatory effects of CpG oligodeoxynucleotides in fish. *Aquaculture*, **246**(1-4), pp. 25-36.
- MANDARIM-DE-LACERDA, C.A., FERNANDES-SANTOS, C. and AGUILA, M.B. 2010. "Image analysis and qualitative morphology" in Hamilton, T.D. and Darby, I.A. (Eds.). *Methods in molecular biology*, Volume 611, Humana Press, New York, USA, pp. 211-225.
- MANERA, M. and BORRECA, C., 2012. Assessment of mast cells degranulation in rainbow trout (*Oncorhynchus mykiss* Walbaum) by means of gray level and texture analysis (Gray Level Correlation Matrices). *Research in Veterinary Science*, **93**(2), pp. 886-891.
- MANGO, L.J., 1994. Computer-assisted cervical cancer screening using neural networks. *Cancer Letters*, **77**(2-3), pp. 155-162.
- MARADONNA, F. and CARNEVALI, O., 2007. Vitellogenin, zona radiata protein, cathepsin D and heat shock protein 70 as biomarkers of exposure to xenobiotics. *Biomarkers*, **12**(3), pp. 240-255.
- MARCHETTI, L., CAPACCHIETTI, M., SABBITI, M.G., ACCILI, D., MATERAZZI, G. and MENGHI, G., 2006. Histology and carbohydrate histochemistry of the alimentary canal in the rainbow trout *Oncorhynchus mykiss*. *Journal of Fish Biology*, **68**(6), pp. 1808-1821.
- MARJARA, I.S., CHIKWATI, E.M., VALEN, E.C., KROGDAHL, Å. and BAKKE, A.M., 2012. Transcriptional regulation of IL-17A and other inflammatory markers during the development of soybean meal-induced enteropathy in the distal intestine of Atlantic salmon (*Salmo salar* L.). *Cytokine*, **60**(1), pp. 186-196.
- MARRACK, J., 1934. Nature of antibodies. *Nature*, **133**, pp. 292-293.
- MARSHALL, W. and GROSELL, M., 2006. Ion transport, osmoregulation, and acid-base balance. *The Physiology of Fishes*, **3**, pp. 177-230.
- MARTINEZ-RUBIO, L., MORAIS, S., EVENSEN, Ø., WADSWORTH, S., VECINO, J.G., RUOHONEN, K., BELL, J.G. and TOCHER, D.R., 2013. Effect of functional feeds on fatty acid and eicosanoid metabolism in liver and head kidney of Atlantic salmon (*Salmo salar* L.) with experimentally induced Heart and Skeletal Muscle Inflammation. *Fish & Shellfish Immunology*, **34**(6), pp. 1433-1545.
- MATOS, E., SILVA, T.S., WULFF, T., VALENTE, L.M.P., SOUSA, V., SAMPAIO, E., GONÇALVES, A., SILVA, J.M.G., DINIS, M.T., RODRIGUES, P.M. and DIAS, J., 2013. Influence of

- supplemental maslinic acid (olive-derived triterpene) on the post-mortem muscle properties and quality traits of gilthead seabream. *Aquaculture*, **396-399**(1), pp. 146-156.
- MATSUYAMA, H., MANGINDAAN, R.E. and YANO, T., 1992. Protective effect of schizophyllan and scleroglucan against *Streptococcus* sp. infection in yellowtail (*Seriola quinqueradiata*). *Aquaculture*, **101**(3), pp. 197-203.
- MATSUYAMA, T. and IIDA, T., 1999. Degranulation of eosinophilic granular cells with possible involvement in neutrophil migration to site of inflammation in tilapia. *Developmental & Comparative Immunology*, **23**(6), pp. 451-457.
- MATSUYAMA, T. and IIDA, T., 2001. Influence of tilapia mast cell lysate on vascular permeability. *Fish & Shellfish Immunology*, **11**(7), pp. 549-556.
- MAY, R. and MAY, G.L., 1902. Grünwald stain. *Zentralbl Für Innere Med*, **23**, pp. 265.
- MAYER, M.P., SCHRÖDER, H., RÜDIGER, S., PAAL, K., LAUFEN, T. and BUKAU, B., 2000. Multistep mechanism of substrate binding determines chaperone activity of Hsp70. *Nature Structural & Molecular Biology*, **7**(7), pp. 586-593.
- McEACHRON, D.L., HESS, S., KNECHT, L.B. and TRUE, L.D., 1989. Image-processing for the rest of us - the potential utility of inexpensive computerized image-analysis in clinical pathology and radiology. *Computerized Medical Imaging and Graphics*, **13**(1), pp. 3-30.
- McLEAN, E. and DONALDSON, E.M., 1990. Absorption of bioactive proteins by the gastrointestinal tract of fish: a review. *Journal of Aquatic Animal Health*, **2**(1), pp. 1-11.
- McLEAN, E., RØNSHOLDT, B. and STEN, C., 1999. Gastrointestinal delivery of peptide and protein drugs to aquacultured teleosts. *Aquaculture*, **177**(1), pp. 231-247.
- McMILLAN, D.N. and SECOMBES, C.J., 1997. Isolation of rainbow trout (*Oncorhynchus mykiss*) intestinal intraepithelial lymphocytes (IEL) and measurement of their cytotoxic activity. *Fish & Shellfish Immunology*, **7**(8), pp. 527-541.
- MEENA, D., DAS, P., KUMAR, S., MANDAL, S., PRUSTY, A., SINGH, S., AKHTAR, M., BEHERA, B., KUMAR, K. and PAL, A., 2012. Beta-glucan: an ideal immunostimulant in aquaculture (a review). *Fish Physiology and Biochemistry*, **39** (3), pp. 1-27.
- MEKORI, Y.A. and METCALFE, D.D., 2000. Mast cells in innate immunity. *Immunological Reviews*, **173**(1), pp. 131-140.
- MERRIFIELD, D.L., HARPER, G.M., DIMITROGLOU, A., RINGØ, E. and DAVIES, S.J., 2010. Possible influence of probiotic adhesion to intestinal mucosa on the activity and morphology of rainbow trout (*Oncorhynchus mykiss*) enterocytes. *Aquaculture Research*, **41**(8), pp. 1268-1272.
- MESKER, W.E., OUD, P.S., KNEPFLE, C.F., SCHIPPER, N.W. and TANKE, H.J., 1994. Detection of immunocytochemically stained rare events using image analysis. *Cytometry*, **17**(3), pp. 209-215.
- MIEST, J.J., FALCO, A., PIONNIER, N.P.M., FROST, P., IRNAZAROW, I., WILLIAMS, G.T. and HOOLE, D., 2012. The influence of dietary β -glucan, PAMP exposure and *Aeromonas salmonicida* on apoptosis modulation in common carp (*Cyprinus carpio*). *Fish & Shellfish Immunology*, **33**(4), pp. 846-856.
- MIGHELL, A., HUME, W. and ROBINSON, P., 1998. An overview of the complexities and subtleties of immunohistochemistry. *Oral Diseases*, **4**(3), pp. 217-223.

- MISRA, C.K., DAS, B.K., MUKHERJEE, S.C. and PATTNAIK, P., 2006. Effect of long term administration of dietary β -glucan on immunity, growth and survival of *Labeo rohita* fingerlings. *Aquaculture*, **255**(1), pp. 82-94.
- MITCHELL, T.M., 1997. *Machine learning*, McGraw Hill, New York, USA, pp. 417.
- MITRA, S. and BHATTACHARYA, S., 1992. Purification of C-reactive protein from *Channa punctatus* (Bloch). *Indian Journal of Biochemistry and Biophysics*, **29**, pp. 508-511.
- MIURA, M., CHEN, X., ALLEN, M.R., BI, Y., GRONTHOS, S., SEO, B., LAKHANI, S., FLAVELL, R.A., FENG, X. and ROBEY, P.G., 2004. A crucial role of caspase-3 in osteogenic differentiation of bone marrow stromal stem cells. *Journal of Clinical Investigation*, **114**(12), pp. 1704-1713.
- MONTAGNE, L., PLUSKE, J. and HAMPSON, D., 2003. A review of interactions between dietary fibre and the intestinal mucosa, and their consequences on digestive health in young non-ruminant animals. *Animal Feed Science and Technology*, **108**(1), pp. 95-117.
- MOOSEKER, M. S., 1985. Organization, chemistry, and assembly of the cytoskeletal apparatus of the intestinal brush border. *Annual Review of Cell Biology*, **1** (209–241), pp. 209-241.
- MORRIS, P. C., GALLIMORE, P., HANDLEY, J., HIDE, G., HAUGHTON, P. and BLACK, A., 2005. Full-fat soya for rainbow trout (*Oncorhynchus mykiss*) in freshwater: Effects on performance, composition and flesh fatty acid profile in absence of hind-gut enteritis. *Aquaculture*, **248**, 147-161.
- MOSCA, F., ROMANO, N., MALATESTA, D., CECCARELLI, G., BRUNETTI, A., BULFON, C., VOLPATTI, D., ABELLI, L., GALEOTTI, M. and FALCONI, A., 2012. Heat shock protein 70 kDa (HSP70) increase in sea bass (*Dicentrarchus labrax* L., 1758) thymus after vaccination against *Listonella anguillarum*. *Fish Physiology and Biochemistry*, **39**(3), pp. 1-12.
- MOSEDALE, D.E., METCALFE, J.C. and GRAINGER, D.J., 1996. Optimization of immunofluorescence methods by quantitative image analysis. *Journal of Histochemistry & Cytochemistry*, **44**(9), pp. 1043-1050.
- MÖSSNER, R. and LESCH, K., 1998. Role of serotonin in the immune system and in neuroimmune interactions. *Brain, Behavior, and Immunity*, **12**(4), pp. 249-271.
- MOWRY, R. and WINKLER, C.H., 1956. The coloration of acidic carbohydrates of bacteria and fungi in tissue sections with special reference to capsules of *Cryptococcus neoformans*, pneumococci, and staphylococci. *American Journal of Pathology*, **32**, pp. 628-629.
- MULERO, I., NOGA, E.J., MESEGUER, J., GARCÍA-AYALA, A. and MULERO, V., 2008. The antimicrobial peptides piscidins are stored in the granules of professional phagocytic granulocytes of fish and are delivered to the bacteria-containing phagosome upon phagocytosis. *Developmental & Comparative Immunology*, **32**(12), pp. 1531-1538.
- MULERO, I., SEPULCRE, M.P., MESEGUER, J., GARCÍA-AYALA, A. and MULERO, V., 2007. Histamine is stored in mast cells of most evolutionarily advanced fish and regulates the fish inflammatory response. *Proceedings of the National Academy of Sciences*, **104**(49), pp. 19434-19439.

- MULRANE, L., REXHEPAJ, E., PENNEY, S., CALLANAN, J.J. and GALLAGHER, W.M., 2008. Automated image analysis in histopathology: a valuable tool in medical diagnostics. *Expert Review of Molecular Diagnostics*, **8**(6), pp. 707-725.
- MUNDHEIM, H., AKSNES, A. and HOPE, B., 2004. Growth, feed efficiency and digestibility in salmon (*Salmo salar* L.) fed different dietary proportions of vegetable protein sources in combination with two fish meal qualities. *Aquaculture*, **237**(1–4), pp. 315-331.
- MURAI, T., KODAMA, H., NAIKI, M., MIKAMI, T. and IZAWA, H., 1991. Isolation and characterization of rainbow trout C-reactive protein. *Developmental & Comparative Immunology*, **14**(1), pp. 49-58.
- MURRAY, C.K. and FLETCHER, T.C., 1976. The immunohistochemical localization of lysozyme in plaice (*Pleuronectes platessa* L.) tissues. *Journal of Fish Biology*, **9**(4), pp. 329-334.
- MURRAY, H.M., LEGGIADRO, C.T. and DOUGLAS, S.E., 2007. Immunocytochemical localization of pleurocidin to the cytoplasmic granules of eosinophilic granular cells from the winter flounder gill. *Journal of Fish Biology*, **70**, pp. 336-345.
- MUSCH, M.W., CLARKE, L.L., MAMAH, D., GAWENIS, L.R., ZHANG, Z., ELLSWORTH, W., SHALOWITZ, D., MITTAL, N., EFTHIMIOU, P. and ALNADJIM, Z., 2002. T cell activation causes diarrhoea by increasing intestinal permeability and inhibiting epithelial Na⁺/K⁺-ATPase. *Journal of Clinical Investigation*, **110**(11), pp. 1739-1747.
- NAIK, S., DOYLE, S., AGNER, S., MADABHUSHI, A., FELDMAN, M. and TOMASZEWSKI, J., 2008. Automated gland and nuclei segmentation for grading of prostate and breast cancer histopathology. *IEEE International Symposium on Biomedical Imaging: from Nano to Macro*, New Jersey, 14-17 May, pp. 284-287.
- NAIK, S., MADABHUSHI, A., TOMASZEWSKI, J. and FELDMAN, M.D., 2007. A quantitative exploration of efficacy of gland morphology in prostate cancer grading. *IEEE 33rd Annual Northeast Bioengineering Conference*, New Jersey, 10-11 March, pp. 58-59.
- NAKAGAWA, H., SATO, M. and GATLIN, D., 2007. *Dietary supplements for the health and quality of cultured fish*, Cromwell Press, Trowbridge, UK, pp. 244.
- NAKANE, P.K. and PIERCE, G.B., 1966. Enzyme-labeled antibodies: preparation and application for the localization of antigens. *Journal of Histochemistry & Cytochemistry*, **14**(12), pp. 929-931.
- NAVARRETE, P., FUENTES, P., LA FUENTE, L., BARROS, L., MAGNE, F., OPAZO, R., IBACACHE, C., ESPEJO, R. and ROMERO, J., 2013. Short-term effects of dietary soybean meal and lactic acid bacteria on the intestinal morphology and microbiota of Atlantic salmon (*Salmo salar*). *Aquaculture Nutrition*, **19**(5), pp. 827-836.
- NAYAK, S.K., 2010. Probiotics and immunity: A fish perspective. *Fish & Shellfish Immunology*, **29**(1), pp. 2-14.
- NELSON, P.N., REYNOLDS, G.M., WALDRON, E.E., WARD, E., GIANNOPOULOS, K. and MURRAY, P.G., 2000. Demystified ...: Monoclonal antibodies. *Molecular Pathology*, **53**(3), pp. 111-117.

- NEUMANN, N.F., STAFFORD, J.L., BARREDA, D., AINSWORTH, A.J. and BELOSEVIC, M., 2001. Antimicrobial mechanisms of fish phagocytes and their role in host defense. *Developmental & Comparative Immunology*, **25**(8), pp. 807-825.
- NIELSEN, B., ALBREGTSEN, F. and DANIELSEN, H.E., 2012. Automatic segmentation of cell nuclei in Feulgen-stained histological sections of prostate cancer and quantitative evaluation of segmentation results. *Cytometry Part A*, **81A**(7), pp. 588-601.
- NIKLASSON, L., 2013. Intestinal mucosal immunology of salmonids: Response to stress and infection and crosstalk with the physical barrier. PhD Dissertation Thesis, University of Gothenburgh, Sweden, pp. 79.
- NILSSON, S. and HOLMGREN, S., 1992. "Cardiovascular control by purines, 5-hydroxytryptamine, and neuropeptides" in Hoar, W.S., Randall, D.J., Farrell, A.P. (Eds.) *Fish physiology*. Academic Press, London, UK, pp. 301-341.
- NORDRUM, S., BAKKE-McKELLEP, A.M., KROGDAHL, Å. and BUDDINGTON, R.K., 2000a. Effects of soybean meal and salinity on intestinal transport of nutrients in Atlantic salmon (*Salmo salar* L.) and rainbow trout (*Oncorhynchus mykiss*). *Comparative Biochemistry and Physiology Part B: Biochemistry and Molecular Biology*, **125**(3), pp. 317-335.
- NORDRUM, S., KROGDAHL, Å., RØSJØ, C., OLLI, J.J. and HOLM, H., 2000b. Effects of methionine, cysteine and medium chain triglycerides on nutrient digestibility, absorption of amino acids along the intestinal tract and nutrient retention in Atlantic salmon (*Salmo salar* L.) under pair-feeding regime. *Aquaculture*, **186**(3-4), pp. 341-360.
- NOVOA, B., FIGUERAS, A., ASHTON, I. and SECOMBES, C.J., 1996. *In vitro* studies on the regulation of rainbow trout (*Oncorhynchus mykiss*) macrophage respiratory burst activity. *Developmental & Comparative Immunology*, **20**(3), pp. 207-216.
- NRC (National Research Council), 1993. *Nutrient Requirements of Fish*. National Academy Press, Washington D.C., USA. pp. 114.
- O'CONNOR, T.M., O'CONNELL, J., O'BRIEN, D.I., GOODE, T., BREDIN, C.P. and SHANAHAN, F., 2004. The role of substance P in inflammatory disease. *Journal of Cellular Physiology*, **201**(2), pp. 167-180.
- OLIVA-TELES, A., 2012. Nutrition and health of aquaculture fish. *Journal of Fish Diseases*, **35**(2), pp. 83-108.
- OLIVA-TELES, A., GOUVEIA, A.J., GOMES, E. and REMA, P., 1994. The effect of different processing treatments on soybean meal utilization by rainbow trout, *Oncorhynchus mykiss*. *Aquaculture*, **124**(1-4), pp. 343-349.
- OLLI, J.J., KROGDAHL, Å. and VÅBENO, A., 1995. Dehulled solvent-extracted soybean meal as a protein source in diets for Atlantic salmon, *Salmo salar* L. *Aquaculture Research*, **26**, pp. 167-174.
- OLLI, J.J., KROGDAHL, Å., VAN, D.I. and BRATTÅS, L.E., 1994. Nutritive value of four soybean products in diets for Atlantic Salmon (*Salmo salar*, L.). *Acta Agriculturae Scandinavica, Section A - Animal Science*, **44**(1), pp. 50-60.

- OLSEN, R., MYKLEBUST, R., KRYVI, H., MAYHEW, T. and RINGØ, E., 2001. Damaging effect of dietary inulin on intestinal enterocytes in Arctic charr (*Salvelinus alpinus* L.). *Aquaculture Research*, **32**(11), pp. 931-934.
- OLSEN, R.E., HANSEN, A., ROSENLUND, G., HEMRE, G., MAYHEW, T.M., KNUDSEN, D.L., TUFAN EROLDÖĞAN, O., MYKLEBUST, R. and KARLSEN, Ø., 2007. Total replacement of fish meal with plant proteins in diets for Atlantic cod (*Gadus morhua*, L.) II – Health aspects. *Aquaculture*, **272**(1), pp. 612-624.
- OLSEN, R.E., SUNDELL, K., HANSEN, T., HEMRE, G., MYKLEBUST, R., MAYHEW, T.M. and RINGØ, E., 2002. Acute stress alters the intestinal lining of Atlantic salmon, *Salmo salar* L.: An electron microscopical study. *Fish Physiology and Biochemistry*, **26**(3), pp. 211-221.
- OLSEN, R.E., SUNDELL, K., MAYHEW, T.M., MYKLEBUST, R. and RINGØ, E., 2005. Acute stress alters intestinal function of rainbow trout, *Oncorhynchus mykiss* (Walbaum). *Aquaculture*, **250**(1), pp. 480-495.
- OLSVIK, P., TORSTENSEN, B. and BERNTSEN, M., 2007. Effects of complete replacement of fish oil with plant oil on gastrointestinal cell death, proliferation and transcription of eight genes' encoding proteins responding to cellular stress in Atlantic salmon *Salmo salar* L. *Journal of Fish Biology*, **71**(2), pp. 550-568.
- ONG, S.H., JIN, X.C., JAYASOORIAH and SINNIAH, R., 1996. Image analysis of tissue sections. *Computers in Biology and Medicine*, **26**(3), pp. 269-279.
- OPSTVEDT, J., AKSNES, A., HOPE, B. and PIKE, I.H., 2003. Efficiency of feed utilization in Atlantic salmon (*Salmo salar* L.) fed diets with increasing substitution of fish meal with vegetable proteins. *Aquaculture*, **221**(1-4), pp. 365-379.
- ORLOV, N.V., WEERARATNA, A.T., HEWITT, S.M., COLETTA, C.E., DELANEY, J.D., MARK ECKLEY, D., SHAMIR, L. and GOLDBERG, I.G., 2012. Automatic detection of melanoma progression by histological analysis of secondary sites. *Cytometry Part A*, **81A**(5), pp. 364-373.
- ORTEGO, L., HAWKINS, W., WALKER, W., KROL, R. and BENSON, W., 1994. Detection of proliferating cell nuclear antigen in tissues of three small fish species. *Biotechnic & Histochemistry*, **69**(6), pp. 317-323.
- ORTEGO, L.S., HAWKINS, W.E., WALKER, W.W., KROL, R.M. and BENSON, W.H., 1995. Immunohistochemical detection of proliferating cell nuclear antigen (PCNA) in tissues of aquatic animals utilized in toxicity bioassays. *Marine Environmental Research*, **39**(1), pp. 271-273.
- OSTASZEWSKA, T., DABROWSKI, K., KAMASZEWSKI, M., GROCHOWSKI, P., VERRI, T., RZEPKOWSKA, M. and WOLNICKI, J., 2010. The effect of plant protein-based diet supplemented with dipeptide or free amino acids on digestive tract morphology and PepT1 and PepT2 expressions in common carp (*Cyprinus carpio* L.). *Comparative Biochemistry and Physiology Part A: Molecular & Integrative Physiology*, **157**(2), pp. 158-169.
- OSTASZEWSKA, T., KORWIN-KOSSAKOWSKI, M. and WOLNICKI, J., 2006. Morphological changes of digestive structures in starved tench *Tinca tinca* (L.) juveniles. *Aquaculture International*, **14**(1-2), pp. 113-126.
- OSTRANDER, G.K., 2000. *The Laboratory Fish*. Academia Press, London, UK, pp. 645.

- ØVERLAND, M., SØRENSEN, M., STOREBAKKEN, T., PENN, M., KROGDAHL, Å. and SKREDE, A., 2009. Pea protein concentrate substituting fish meal or soybean meal in diets for Atlantic salmon (*Salmo salar*) – Effect on growth performance, nutrient digestibility, carcass composition, gut health, and physical feed quality. *Aquaculture*, **288**(3–4), pp. 305-311.
- PAJAK, B. and DANGUY, A., 1993. Characterization of sugar moieties and oligosaccharide sequences in the distal intestinal epithelium of the rainbow trout by means of lectin histochemistry. *Journal of Fish Biology*, **43**(5), pp. 709-722.
- PAJOR, G., ALPAR, D., KAJTAR, B., MELEGH, B., SOMOGYI, L., KNEIF, M., BOLLMANN, D., PAJOR, L. and SULE, N., 2012. Automated signal pattern evaluation of a bladder cancer specific multiprobe-fish assay applying a user-trainable workstation. *Microscopy Research and Technique*, **75**(6), pp. 814-820.
- PANTANOWITZ, L., 2010. Digital images and the future of digital pathology. *Journal of Pathology Informatics*, **1**, pp. 15.
- PANTANOWITZ, L., SZYMAS, J., YAGI, Y. and WILBUR, D., 2012. Whole slide imaging for educational purposes. *Journal of Pathology Informatics*, **3**, pp.46
- PANTANOWITZ, L., VALENSTEIN, P.N., EVANS, A.J., KAPLAN, K.J., PFEIFER, J.D., WILBUR, D.C., COLLINS, L.C., COLGAN, T.J., 2011. Review of the current state of whole slide imaging in pathology. *Journal of Pathology Informatics*, **2**(36), pp. 1-10.
- PAREDES, M., GONZALEZ, K., FIGUEROA, J. and MONTIEL-EULEFI, E., 2013. Immunomodulatory effect of prolactin on Atlantic salmon (*Salmo salar*) macrophage function. *Fish Physiology and Biochemistry*, **39**(5), pp.1215-21.
- PARK, S., PANTANOWITZ, L. and PARWANI, A.V., 2012. Digital imaging in pathology. *Clinics in Laboratory Medicine*, **32**(4), pp. 558-584.
- PARRISH, N. and GUPTA, M.R., 2012. Dimensionality reduction by local discriminant Gaussians. *Proceedings of the 29th International Conference on Machine Learning*, Edinburgh, Scotland, UK, pp. 7.
- PARRY, R.M., CHANDAN, R.C. and SHAHANI, K.M., 1965. A rapid sensitive assay of Muramidase. *Proceedings of the Society for Experimental Biology and Medicine*, **119**(2), pp. 384-386.
- PAULSEN, S.M., ENGSTAD, R.E. and ROBERTSEN, B., 2001. Enhanced lysozyme production in Atlantic salmon (*Salmo salar* L.) macrophages treated with yeast β -glucan and bacterial lipopolysaccharide. *Fish & Shellfish Immunology*, **11**(1), pp. 23-37.
- PAYAN, D.G., 1989. Neuropeptides and inflammation: the role of substance P. *Annual Review of Medicine*, **40**(1), pp. 341-352.
- PAYAN, D.G., BREWSTER, D. and GOETZL, E., 1983. Specific stimulation of human T lymphocytes by substance P. *The Journal of Immunology*, **131**(4), pp. 1613-1615.
- PELLICCIARI, C. and MALATESTA, M., 2011. Identifying pathological biomarkers: histochemistry still ranks high in the omics era. *European journal of histochemistry: European Journal of Histochemistry*, **55**(e42), pp.235-238.
- PENG, M., XU, W., AI, Q., MAI, K., LIUFU, Z. and ZHANG, K., 2013. Effects of nucleotide supplementation on growth, immune responses and intestinal morphology in juvenile turbot fed

- diets with graded levels of soybean meal (*Scophthalmus maximus* L.). *Aquaculture*, **392–395**(0), pp. 51-58.
- PENISSI, A., RUDOLPH, M. and PIEZZI, R., 2003. Role of mast cells in gastrointestinal mucosal defense. *Biocell*, **27**(2), pp. 163-172.
- PENN, M.H., BENDIKSEN, E.Å., CAMPBELL, P. and KROGDAHL, Å., 2011. High level of dietary pea protein concentrate induces enteropathy in Atlantic salmon (*Salmo salar* L.). *Aquaculture*, **310**(3–4), pp. 267-273.
- PEPYS, M.B., DE BEER, F.C., MILSTEIN, C.P., MARCH, J.F., FEINSTEIN, A. and BUTRESS, N., 1982. C-reactive protein and serum amyloid P component in the plaice (*Pleuronectes platessa* L.), a marine teleost, are homologous with their human counterparts. *Biochemistry Biophysics Acta*, **704**, pp. 123-133.
- PETUSHI, S., GARCIA, F., HABER, M., KATSINIS, C. and TOZEREN, A., 2006. Large-scale computations on histology images reveal grade-differentiating parameters for breast cancer. *BMC Medical Imaging*, **6**(1), pp. 14.
- PICCHIETTI, S., MAZZINI, M., TADDEI, A.R., RENNA, R., FAUSTO, A.M., MULERO, V., CARNEVALI, O., CRESCI, A. and ABELLI, L., 2007. Effects of administration of probiotic strains on GALT of larval gilthead seabream: immunohistochemical and ultrastructural studies. *Fish & Shellfish Immunology*, **22**(1), pp. 57-67.
- PILETTE, C., ROUSSELET, M.C., BEDOSSA, P., CHAPPARD, D., OBERTI, F., RIFFLET, H., MAÏGA, M.Y., GALLOIS, Y. and CALÈS, P., 1998. Histopathological evaluation of liver fibrosis: Quantitative image analysis vs semi-quantitative scores: Comparison with serum markers. *Journal of Hepatology*, **28**(3), pp. 439-446.
- PIONNIER, N., FALCO, A., MIEST, J., FROST, P., IRNAZAROW, I., SHRIVE, A. and HOOLE, D., 2013. Dietary β -glucan stimulate complement and C-reactive protein acute phase responses in common carp (*Cyprinus carpio*) during an *Aeromonas salmonicida* infection. *Fish & Shellfish Immunology*, **34**, pp. 819-831.
- POLTRONIERI, C., NEGRATO, E., BERTOTTO, D., MAJOLINI, D., SIMONTACCHI, C. and RADAELLI, G., 2009. Immunohistochemical localization of constitutive and inducible Heat Shock Protein 70 in carp (*Cyprinus carpio*) and trout (*Oncorhynchus mykiss*) exposed to transport stress. *European Journal of Histochemistry*, **52**(3), pp. 191-198.
- POTT, J. and HORNEF, M., 2012. Innate immune signalling at the intestinal epithelium in homeostasis and disease. *EMBO Reports*, **13**(8), pp. 684-698.
- POTTS, S.J., YOUNG, G.D. and VOELKER, F.A., 2010. The role and impact of quantitative discovery pathology. *Drug Discovery Today*, **15**(21–22), pp. 943-950.
- POWELL, M., WRIGHT, G. and BURKA, J., 1990. Eosinophilic granule cells in the gills of rainbow trout, *Oncorhynchus mykiss*: evidence of migration? *Journal of Fish Biology*, **37**(3), pp. 495-497.
- POWELL, M.D., BRIAND, H.A., WRIGHT, G.M. and BURKA, J.F., 1992. Ultrastructural localisation of acid phosphatase in intestinal eosinophilic granule cells (EGC) of rainbow trout (*Oncorhynchus mykiss*) following degranulation with capsaicin. *Histology and Histopathology*, **7**(2), pp. 301-305.

- POWELL, M.D., BRIAND, H.A., WRIGHT, G.M. and BURKA, J.F., 1993a. Rainbow trout (*Oncorhynchus mykiss*, Walbaum) intestinal eosinophilic granule cell (EGC) response to *Aeromonas salmonicida* and *Vibrio anguillarum* extracellular products. *Fish & Shellfish Immunology*, **3**(4), pp. 279-289.
- POWELL, M.D., WRIGHT, G.M. and BURKA, J.F., 1991. Degranulation of eosinophilic granule cells induced by capsaicin and substance P in the intestine of the rainbow trout (*Oncorhynchus mykiss* Walbaum). *Cell and Tissue Research*, **266**(3), pp. 469-474.
- POWELL, M.D., WRIGHT, G.M. and BURKA, J.F., 1993b. Morphological and distributional changes in the eosinophilic granule cell (EGC) population of the rainbow trout (*Oncorhynchus mykiss* Walbaum) intestine following systemic administration of capsaicin and substance P. *Journal of Experimental Zoology*, **266**(1), pp. 19-30.
- PRAVEEN, K., LEARY III, J.H., EVANS, D.L. and JASO-FRIEDMANN, L., 2006. Nonspecific cytotoxic cells of teleosts are armed with multiple granzymes and other components of the granule exocytosis pathway. *Molecular Immunology*, **43**(8), pp. 1152-1162.
- PRESS, C.M. and EVENSEN, Ø., 1999. The morphology of the immune system in teleost fishes. *Fish & Shellfish Immunology*, **9**(4), pp. 309-318.
- PRESTON, K. and BARTELS, P.H., 1988. "Automated image processing for cells and tissue" in Newhouse, V.L. (Ed.). *Progress in medical imaging*, Springer-Verlag, New York, USA, pp. 1-121.
- PRICE, G.J., MCCLUGGAGE, W.G., MORRISON, M.L., McCLEAN, G., VENKATRAMAN, L., DIAMOND, J., BHARUCHA, H., MONTIRONI, R., BARTELS, P.H., THOMPSON, D. and HAMILTON, P.W., 2003. Computerized diagnostic decision support system for the classification of preinvasive cervical squamous lesions. *Human Pathology*, **34**(11), pp. 1193-1203.
- RAA, J., ROERSTAD, G., ENGSTAD, R. and ROBERTSEN, B., 1992. The use of immunostimulants to increase resistance of aquatic organisms to microbial infections. *Diseases in Asian Aquaculture*, **1**, pp. 39-50.
- RAHMADWATI, R., NAGHDY, G., ROS, M. and TODD, C., 2012. Computer aided decision support system for cervical cancer classification. *Applications of Digital Image Processing Xxxv*, **8499**, pp. 849919.
- RAHMAN, S. and ITAKURA, H., 1996. Morphometry in histopathology - an image analysis workstation for the pathology laboratory. *Analytical and Quantitative Cytology and Histology*, **18**(6), pp. 471-480.
- RAMADAN, A., ATEF, M. and AFIFI, N., 1991. Effect of the biogenic performance enhancer (Ascogen "S") on growth rate of tilapia fish. *Acta Veterinaria Scandinavica*, **87**, S304-S306.
- RAMOS-VARA, J., 2005. Technical aspects of immunohistochemistry. *Veterinary Pathology Online*, **42**(4), pp. 405-426.
- RAMOS-VARA, J., 2011. "Principles and methods of immunology" in Gautier, J. (Ed.) *Drug safety evaluation: Methods and protocols. Methods in Molecular Biology*, **691**, pp. 83-96.
- RAMOS-VARA, J.A., KIUPEL, M., BASZLER, T., BLIVEN, L., BRODERSEN, B., CHELACK, B., WEST, K., CZUB, S., DEL PIERO, F. and DIAL, S., 2008. Suggested guidelines for

- immunohistochemical techniques in veterinary diagnostic laboratories. *Journal of Veterinary Diagnostic Investigation*, **20**(4), pp. 393-413.
- RAŠKOVIĆ, B.S., STANKOVIĆ, M.B., MARKOVIĆ, Z.Z. and POLEKSIĆ, V.D., 2011. Histological methods in the assessment of different feed effects on liver and intestine of fish. *Journal of Agricultural Sciences, Belgrade*, **56**(1), pp. 87-100.
- RAWLING, M., MERRIFIELD, D., SNELGROVE, D., KÜHLWEIN, H., ADAMS, A. and DAVIES, S., 2012. Haemato-immunological and growth response of mirror carp (*Cyprinus carpio*) fed a tropical earthworm meal in experimental diets. *Fish & Shellfish Immunology*, **32**(6), pp. 1002-1007.
- REFSTIE, S., KORSØEN, Ø.J., STOREBAKKEN, T., BAEVERFJORD, G., LEIN, I. and ROEM, A.J., 2000. Differing nutritional responses to dietary soybean meal in rainbow trout (*Oncorhynchus mykiss*) and Atlantic salmon (*Salmo salar*). *Aquaculture*, **190**(1), pp. 49-63.
- REFSTIE, S., STOREBAKKEN, T. and ROEM, A.J., 1998. Feed consumption and conversion in Atlantic salmon (*Salmo salar*) fed diets with fish meal, extracted soybean meal or soybean meal with reduced content of oligosaccharides, trypsin inhibitors, lectins and soya antigens. *Aquaculture*, **162**(3-4), pp. 301-312.
- REFSTIE, S., STOREBAKKEN, T., BAEVERFJORD, G. and ROEM, A., 2001. Long-term protein and lipid growth of Atlantic salmon (*Salmo salar*) fed diets with partial replacement of fish meal by soy protein products at medium or high lipid level. *Aquaculture*, **193**(1-2), pp. 91-106.
- ŘEHULKA, J., 2002. *Aeromonas* causes severe skin lesions in rainbow trout (*Oncorhynchus mykiss*): Clinical pathology, haematology, and biochemistry. *Acta Veterinaria Brno*, **71**(3), pp. 351-360.
- REIMSCHUESSEL, R., BENNETT, R., MAY, E. and LIPSKY, M., 1987. Eosinophilic granular cell response to a microsporidian infection in a sergeant major fish, *Abudefduf saxatilis* (L.). *Journal of Fish Diseases*, **10**(4), pp. 319-322.
- REITE, O. and EVENSEN, Ø., 1994. Mast cells in the swimbladder of Atlantic salmon *Salmo salar*: Histochemistry and responses to compound 48/80 and formalin-inactivated *Aeromonas salmonicida*. *Diseases of Aquatic Organisms*, **20**(2), pp. 95-100.
- REITE, O.B. and EVENSEN, Ø., 2006. Inflammatory cells of teleostean fish: a review focusing on mast cells/eosinophilic granule cells and rodlet cells. *Fish & Shellfish Immunology*, **20**(2), pp. 192-208.
- REITE, O.B., 1969. The evolution of vascular smooth muscle responses to histamine and 5-hydroxytryptamine. *Acta Physiologica Scandinavica*, **75**(1-2), pp. 221-239.
- REITE, O.B., 1996. The mast cell nature of granule cells in the digestive tract of the pike, *Esox lucius*: similarity to mammalian mucosal mast cells and globule leucocytes. *Fish & Shellfish Immunology*, **6**(5), pp. 363-369.
- REITE, O.B., 1997. Mast cells/eosinophilic granule cells of salmonids: staining properties and responses to noxious agents. *Fish & Shellfish Immunology*, **7**(8), pp. 567-584.
- REITE, O.B., 1998. Mast cells/eosinophilic granule cells of teleostean fish: a review focusing on staining properties and functional responses. *Fish & Shellfish Immunology*, **8**(7), pp. 489-513.

- REITE, O.B., 2005. The rodlet cells of teleostean fish: their potential role in host defence in relation to the role of mast cells/eosinophilic granule cells. *Fish & Shellfish Immunology*, **19**(3), pp. 253-267.
- RICKETTS, D., WATSON, T., LIEPINS, P. and KIDD, E., 1998. A comparison of two histological validating techniques for occlusal caries. *Journal of Dentistry*, **26**(2), pp. 89-96.
- RINGØ, E., JUTFELT, F., KANAPATHIPPILLAI, P., BAKKEN, Y., SUNDELL, K., GLETTE, J., MAYHEW, T.M., MYKLEBUST, R. and OLSEN, R.E., 2004. Damaging effect of the fish pathogen *Aeromonas salmonicida* ssp. *salmonicida* on intestinal enterocytes of Atlantic salmon (*Salmo salar* L.). *Cell and Tissue Research*, **318**(2), pp. 305-311.
- RINGØ, E., OLSEN, R.E., VECINO, J.L.G., WADSWORTH, S. and SONG, S.K., 2012. Use of immunostimulants and nucleotides in aquaculture: a review. *Journal of Marine Science: Research & Development*, **1**(104), pp.1-22.
- RINGØ, E., SALINAS, I., OLSEN, R., NYHAUG, A., MYKLEBUST, R. and MAYHEW, T., 2007. Histological changes in intestine of Atlantic salmon (*Salmo salar* L.) following *in vitro* exposure to pathogenic and probiotic bacterial strains. *Cell and Tissue Research*, **328**(1), pp. 109-116.
- RISS, T., MORAVEX, R. and O'BRIEN, M., (year unknown). Anti-ACTIVE[®] Caspase-3 pAB for the detection of apoptosis. *High Throughput Systems – Promega Notes 75*. Available at: <http://www.promega.com/~media/files/resources/promega%20notes/75>.
- ROBERTS, R.J., 1989. *Fish Pathology*. Bailliere Tindall, London, UK, pp. 467.
- ROBERTS, R.J., YOUNG, H. and MILNE, J.A., 1971. Studies on the skin of plaice (*Pleuronectes platessa* L.). *Journal of Fish Biology*, **4**(1), pp. 87-98.
- ROBERTSEN, B., RØRSTAD, G., ENGSTAD, R. and RAA, J., 1990. Enhancement of non-specific disease resistance in Atlantic salmon, *Salmo salar* L., by a glucan from *Saccharomyces cerevisiae* cell walls. *Journal of Fish Diseases*, **13**(5), pp. 391-400.
- ROBEY, F.A., TANAKA, T. and LIU, T.Y., 1983. Isolation and characterization of two major serum proteins from the dogfish, *Mustelus canis*, C-reactive protein and amyloid P component. *Journal of Biological Chemistry*, **258**, pp. 3889-3894.
- ROCHA, J.S. and CHIARINI-GARCIA, H., 2007. Mast cell heterogeneity between two different species of *Hoplias* sp. (Characiformes: Erythrinidae): Response to fixatives, anatomical distribution, histochemical contents and ultrastructural features. *Fish & Shellfish Immunology*, **22**(3), pp. 218-229.
- ROCHA, R., VASSALLO, J., SOARES, F., MILLER, K. and GOBBI, H., 2009. Digital slides: Present status of a tool for consultation, teaching, and quality control in pathology. *Pathology Research and Practice*, **205**(11), pp. 735-741.
- ROHN, T.T., CUSACK, S.M., KESSINGER, S.R. and OXFORD, J.T., 2004. Caspase activation independent of cell death is required for proper cell dispersal and correct morphology in PC12 cells. *Experimental Cell Research*, **295**(1), pp. 215-225.
- ROJO, M. and GONZALEZ, M., 1998. In situ detection of apoptotic cells by TUNEL in the gill epithelium of the developing brown trout (*Salmo trutta*). *Journal of Anatomy*, **193**(3), pp. 391-398.

- ROJO, M.G., BUENO, G. and SLODKOWSKA, J., 2010. Review of imaging solutions for integrated quantitative immunohistochemistry in the pathology daily practice. *Folia Histochemica et Cytobiologica*, **47**(3), pp. 349-348.
- ROMARHEIM, O.H., HETLAND, D.L., SKREDE, A., ØVERLAND, M., MYDLAND, L.T. and LANDSVERK, T., 2013a. Prevention of soya-induced enteritis in Atlantic salmon (*Salmo salar*) by bacteria grown on natural gas is dose dependent and related to epithelial MHC II reactivity and CD8 α intraepithelial lymphocytes. *British Journal of Nutrition*, **109**, pp. 1062-1070.
- ROMARHEIM, O.H., LANDSVERK, T., MYDLAND, L.T., SKREDE, A. and ØVERLAND, M., 2013b. Cell wall fractions from *Methylococcus capsulatus* prevent soybean meal-induced enteritis in Atlantic salmon (*Salmo salar*). *Aquaculture*, **402-403**, pp. 13-18.
- ROMARHEIM, O.H., ØVERLAND, M., MYDLAND, L.T., SKREDE, A. and LANDSVERK, T., 2011. Bacteria grown on natural gas prevent soybean meal-induced enteritis in Atlantic salmon. *The Journal of nutrition*, **141**(1), pp. 124-130.
- ROMARHEIM, O.H., SKREDE, A., GAO, Y., KROGDAHL, Å., DENSTADLI, V., LILLEENG, E. and STOREBAKKEN, T., 2006. Comparison of white flakes and toasted soybean meal partly replacing fish meal as protein source in extruded feed for rainbow trout (*Oncorhynchus mykiss*). *Aquaculture*, **256**(1-4), pp. 354-364.
- ROMBOUT, J. and BERG, A., 1989. Immunological importance of the second gut segment of carp. I. Uptake and processing of antigens by epithelial cells and macrophages. *Journal of Fish Biology*, **35**(1), pp. 13-22.
- ROMBOUT, J.H., TAVERNE-THIELE, A.J. and VILLENA, M.I., 1993. The gut-associated lymphoid tissue (GALT) of carp (*Cyprinus carpio* L.): An immunocytochemical analysis. *Developmental & Comparative Immunology*, **17**(1), pp. 55-66.
- ROMBOUT, J.H.W.M., ABELLI, L., PICCHIETTI, S., SCAPIGLIATI, G. and KIRON, V., 2011. Teleost intestinal immunology. *Fish & Shellfish Immunology*, **31**(5), pp. 616-626.
- RONZA, P., BERMÚDEZ, R., LOSADA, A.P., ROBLES, A. and QUIROGA, M.I., 2011. Mucosal CD3⁺ cell proliferation and gut epithelial apoptosis: implications in rainbow trout gastroenteritis (RTGE). *Journal of Fish Diseases*, **34**(6), pp. 433-443.
- ROQUE, A.C. and ANDRE, T.C.S.S., 2002. Mammography and computerized decision systems - A review. *Techniques in Bioinformatics and Medical Informatics*, **980**, pp. 83-94.
- ROSADO, J.A., LOPEZ, J.J., GOMEZ-ARTETA, E., REDONDO, P.C., SALIDO, G.M. and PARIENTE, J.A., 2006. Early caspase-3 activation independent of apoptosis is required for cellular function. *Journal of Cellular Physiology*, **209**(1), pp. 142-152.
- RUMSEY, G., ENDRES, J., BOWSER, P., EARNEST-KOONS, K., ANDERSON, D. and SIWICKI, A., 1995. "Soy protein in diets of rainbow trout: effects on growth, protein absorption, gastrointestinal histology, and nonspecific serologic and immune response" in LIM, C.E., Sessa, D.J. (Eds.) *Nutrition and utilization technology in aquaculture*, AOCS Press, Champaign, USA, pp. 166-188.

- RUMSEY, G.L., SIWICKI, A.K., ANDERSON, D.P. and BOWSER, P.R., 1994. Effect of soybean protein on serological response, non-specific defense mechanisms, growth, and protein utilization in rainbow trout. *Veterinary Immunology and Immunopathology*, **41**(3–4), pp. 323-339.
- RUSSELL, D.A., HANSON, J.D. and OTT, E., 1980. Dimension of strange attractors. *Physical Review Letters*, **45**(14), pp. 1175-1178.
- RUST, M., 2002. "Nutritional physiology" in Halver, J., Hardy, R. (Eds.) *Fish nutrition*, Academic Press, London, UK, pp. 368-446.
- SAGSTAD, A., SANDEN, M., HAUGLAND, Ø., HANSEN, A., OLSVIK, P. and HEMRE, G., 2007. Evaluation of stress and immune response biomarkers in Atlantic salmon, *Salmo salar* L., fed different levels of genetically modified maize (Bt maize), compared with its near-isogenic parental line and a commercial suprex maize. *Journal of Fish Diseases*, **30**(4), pp. 201-212.
- SAHLMANN, C., SUTHERLAND, B.J., KORTNER, T.M., KOOP, B.F., KROGDAHL, Å. and BAKKE, A.M., 2012. Early response of gene expression in the distal intestine of Atlantic salmon (*Salmo salar* L.) during the development of soybean meal induced enteritis. *Fish & Shellfish Immunology*, **34**(2), pp. 599-609.
- SAHOO, P., 2007. Role of immunostimulants in disease resistance of fish. *CAB reviews: Perspectives in Agriculture, Veterinary Science, Nutritional and Natural Resources*, **2**(45), pp. 18.
- SAKAI, M., 1999. Current research status of fish immunostimulants. *Aquaculture*, **172**(1), pp. 63-92.
- SAKAI, M., TANIGUCHI, K., MAMOTO, K., OGAWA, H. and TABATA, M., 2001. Immunostimulant effects of nucleotide isolated from yeast RNA on carp, *Cyprinus carpio* L. *Journal of Fish Diseases*, **24**(8), pp. 433-438.
- SALINAS, I., ZHANG, Y. and SUNYER, J.O., 2011. Mucosal immunoglobulins and B cells of teleost fish. *Developmental & Comparative Immunology*, **35**(12), pp. 1346-1365.
- SANDEN, M. and OLSVIK, P.A., 2009. Intestinal cellular localization of PCNA protein and CYP1A mRNA in Atlantic salmon *Salmo salar* L. exposed to a model toxicant. *BMC Physiology*, **9**(3), pp. 1-11.
- SANDEN, M., BERNTSSEN, M., KROGDAHL, Å., HEMRE, G. and BAKKE-MCKELLEP, A., 2005. An examination of the intestinal tract of Atlantic salmon, *Salmo salar* L., parr fed different varieties of soy and maize. *Journal of Fish Diseases*, **28**(6), pp. 317-330.
- SANDNES, K., LIE, Ø. and WAAGBØ, R., 1988. Normal ranges of some blood chemistry parameters in adult farmed Atlantic salmon, *Salmo salar*. *Journal of Fish Biology*, **32**(1), pp. 129-136.
- SANTAREM, M., NOVOA, B. and FIGUERAS, A., 1997. Effects of β -glucans on the non-specific immune responses of turbot (*Scophthalmus maximus*, L.). *Fish & Shellfish Immunology*, **7**(6), pp. 429-437.
- SANTOS, H., THOMÉ, R., ARANTES, F., SATO, Y., BAZZOLI, N. and RIZZO, E., 2008. Ovarian follicular atresia is mediated by heterophagy, autophagy, and apoptosis in *Prochilodus argenteus* and *Leporinus taeniatus* (Teleostei: Characiformes). *Theriogenology*, **70**(9), pp. 1449-1460.

- SANZ, A., MORALES, A.E., DELAHIGUERA, M. and CARDENETE, G., 1994. Sunflower meal compared with soybean-meal as partial substitutes for fish-meal in rainbow-trout (*Oncorhynchus mykiss*) diets – protein and energy-utilization. *Aquaculture*, **128**(3–4), pp. 287-300.
- SARASTE, A. and PULKKI, K., 2000. Morphologic and biochemical hallmarks of apoptosis. *Cardiovascular Research*, **45**(3), pp. 528-537.
- SAXENA, R. and BADVE, S., 2009. “Tissue microarray – Construction and quality assurance” in Kumar, G.L. and Rudbeck, L. (Eds.) *Educational guide: Immunohistochemical (IHC) staining methods*. Dako North America, California, pp. 43-50.
- SCHEP, L., TUCKER, I., YOUNG, G. and BUTT, A., 1997. Regional permeability differences between the proximal and distal portions of the isolated salmonid posterior intestine. *Journal of Comparative Physiology B*, **167**(5), pp. 370-377.
- SCHMALE, M.C., VICHA, D. and CACAL, S.M., 2004. Degranulation of eosinophilic granule cells in neurofibromas and gastrointestinal tract in the bicolor damselfish. *Fish & Shellfish Immunology*, **17**(1), pp. 53-63.
- SCHMITZ, A., SCHÄFER, T., SCHÄFER, H., DÖRING, C., ACKERMANN, J., DICHTER, N., HARTMANN, S., HANSMANN, M. and KOCH, I., 2012. Automated image analysis of Hodgkin lymphoma. Seminar on “Structure Discovery in Biology: Motifs, Networks & Phylogenies”, Dagstuhl, 14 September, pp. 1-12.
- SCHUBERT, M. and HAMERMAN, D., 1956. Metachromasia; chemical theory and histochemical use. *Journal of Histochemistry & Cytochemistry*, **4**(2), pp. 159-189.
- SCHWERK, C. and SCHULZE-OSTHOFF, K., 2003. Non-apoptotic functions of caspases in cellular proliferation and differentiation. *Biochemical Pharmacology*, **66**(8), pp. 1453-1458.
- SEALEY, W. and GATLIN, D., 2001. “Overview of nutritional strategies affecting the health of marine fish” in Lim, C. and Webster, C.D. (Eds.), *Nutrition and fish health*, Haworth Press, Binghamton, USA, pp. 103-118.
- SEALEY, W.M. and GATLIN, D.M., 1999. Overview of nutritional strategies affecting health of marine fish. *Journal of Applied Aquaculture*, **9**(2), pp. 11-26.
- SECOMBES, C.J., 1990. “Isolation of salmonid macrophages and analysis of their killing activity” in Stolen, J. S., Fletcher, T.C., Anderson, D.P., Roberston, B.S., Van Muiswinkel, W.B. (Eds.). *Techniques in fish immunology – FITC1*, SOS Publications, New Jersey, USA, pp. 137-154.
- SEIDAL, T., BALATON, A.J. and BATTIFORA, H., 2001. Interpretation and quantification of immunostains. *The American Journal of Surgical Pathology*, **25**(9), pp. 1204-1207.
- SELDEN, G.L., BROWN, P.B., OSTROWSKI, A.C., FLORES, R.A. and JOHNSON, L.A., 2001. Evaluation of soybean meal-red blood cell coextruded feed ingredient in diets fed to rainbow trout *Oncorhynchus mykiss*. *Journal of the World Aquaculture Society*, **32**(4), pp. 409-415.
- SERTEL, O., KONG, J., CATALYUREK, U. V., LOZANSKI, G., SALTZ, J. H. and GURCAN, M. N., 2009a. Histopathological image analysis using model-based intermediate representations and color texture: Follicular lymphoma grading. *Journal of Signal Processing Systems for Signal Image and Video Technology*, **55**(1–3), pp. 169-183.

- SERTEL, O., KONG, J., SHIMADA, H., CATALYUREK, U.V., SALTZ, J.H. and GURCAN, M.N., 2009b. Computer-aided prognosis of neuroblastoma on whole-slide images: Classification of stromal development. *Pattern Recognition*, **42**(6), pp. 1093-1103.
- SHAMIR, L., DELANEY, J.D., ORLOV, N., ECKLEY, D.M. and GOLDBERG, I.G., 2010. Pattern recognition software and techniques for biological image analysis. *Plos Computational Biology*, **6**(11), pp. e1000974.
- SHANG, C.J., DALY, C., MCGRATH, J. and BARKER, J., 2000. Analysis and classification of tissue section images using directional fractal dimension features. *International Conference on Image Processing*, Volume 1, Vancouver, 10-13 September, pp. 164-167.
- SHARP, G., PIKE, A. and SECOMBES, C., 1989. The immune response of wild rainbow trout, *Salmo gairdneri* Richardson, to naturally acquired plerocercoid infections of *Diphyllbothrium dendriticum* (Nitzsch, 1824) and *D. ditremum* (Creplin, 1825). *Journal of Fish Biology*, **35**(6), pp. 781-794.
- SHEEHAN, D.C. and HRAPCHAK, B.B. 1980. Theory and practice of histotechnology. 2nd Edition, Mosby Company, St. Louis, USA, pp. 481.
- SHEPHARD, K.L., 1994. Functions for fish mucus. *Reviews in Fish Biology and Fisheries*, **4**(4), pp. 401-429.
- SHI, L., LIU, S., WANG, D., WONG, H., HUANG, W., WANG, WANG, Y., GRIFFITH, J., LEONG, P. and AHUJA, A. T., 2012. Computerized quantification of bone tissue and marrow in stained microscopic images. *Cytometry Part A*, **81A**(10), pp. 916-921.
- SIEGEL, R.M., 2006. Caspases at the crossroads of immune-cell life and death. *Nature Reviews Immunology*, **6**(4), pp. 308-317.
- SIEREN, J.C., WEYDERT, J., BELL, A., DE YOUNG, B., SMITH, A.R., THIESSE, J., NAMATI, E. and MCLENNAN, G., 2010. An automated segmentation approach for highlighting the histological complexity of human lung cancer. *Annals of Biomedical Engineering*, **38**(12), pp. 3581-3591.
- SIGH, J. and BUCHMANN, K., 2000. Associations between epidermal thionin-positive cells and skin parasitic infections in brown trout *Salmo trutta*. *Diseases of Aquatic Organisms*, **41**, pp. 135-139.
- SILPHADUANG, U. and NOGA, E.J., 2001. Antimicrobials: peptide antibiotics in mast cells of fish. *Nature*, **414**(6861), pp. 268-269.
- SILPHADUANG, U., COLORNI, A. and NOGA, E., 2006. Evidence for widespread distribution of piscidin antimicrobial peptides in teleost fish. *Diseases of Aquatic Organisms*, **72**(3), pp. 241.
- SILVA, J.M.G., ESPE, M., CONCEIÇÃO, L.E.C., DIAS, J., COSTAS, B. and VALENTE, L.M.P., 2010. Feed intake and growth performance of Senegalese sole (*Solea senegalensis* Kaup, 1858) fed diets with partial replacement of fish meal with plant proteins. *Aquaculture Research*, **41**(9), pp. e20-e30.
- SIMS, A., BENNETT, M. and MURRAY, A., 2002. Comparison of semi-automated image analysis and manual methods for tissue quantification in pancreatic carcinoma. *Physics in Medicine and Biology*, **47**(8), pp. 1255.

- SIRE, M. and VERNIER, J., 1995. Partial characterization of eosinophilic granule cells (EGCs) and identification of mast cells of the intestinal lamina propria in rainbow trout (*Oncorhynchus mykiss*). Biochemical and cytochemical study. *Biology of the Cell*, **85**(1), pp. 35-41.
- SIRE, M., LUTTON, C. and VERNIER, J., 1981. New views on intestinal absorption of lipids in teleostean fishes: an ultrastructural and biochemical study in the rainbow trout. *Journal of Lipid Research*, **22**(1), pp. 81-94.
- SIRE, M.F. and VERNIER, J.M., 1992. Intestinal absorption of proteins in teleost fish. *Comparative Biochemistry and Physiology* **103A**, 771-781.
- SIRINEK, L. and O'DORISIO, M., 1991. Modulation of immune function by intestinal neuropeptides. *Acta Oncologica*, **30**(4), pp. 509-517.
- SISSENER, N., SANDEN, M., BAKKE, A.M., KROGDAHL, Å. and HEMRE, G., 2009a. A long term trial with Atlantic salmon (*Salmo salar*, L.) fed genetically modified soy; focusing general health and performance before, during and after the parr-smolt transformation. *Aquaculture*, **294**(1), pp. 108-117.
- SISSENER, N.H., BAKKE, A.M., GU, J., PENN, M.H., EIE, E., KROGDAHL, A., SANDEN, M. and HEMRE, G.I., 2009b. An assessment of organ and intestinal histomorphology and cellular stress response in Atlantic salmon (*Salmo salar* L.) fed genetically modified Roundup Ready (R) soy. *Aquaculture*, **298**(1-2), pp. 101-110.
- SITJÀ-BOBADILLA, A., PEÑA-LLOPIS, S., GÓMEZ-REQUENI, P., MÉDALE, F., KAUSHIK, S. and PÉREZ-SÁNCHEZ, J., 2005. Effect of fish meal replacement by plant protein sources on non-specific defence mechanisms and oxidative stress in gilthead sea bream (*Sparus aurata*). *Aquaculture*, **249**(1-4), pp. 387-400.
- SIWICKI, A., ANDERSON, D. and RUMSEY, G., 1994. Dietary intake of immunostimulants by rainbow trout affects non-specific immunity and protection against furunculosis. *Veterinary Immunology and Immunopathology*, **41**(1-2), pp. 125.
- SIWICKI, A.K., ZAKĘŚ, Z., TERECH-MAJEWSKA, E., KAZUŃ, K., LEPA, A. and GŁĄBSKI, E., 2010. Dietary Macrogard reduces *Aeromonas hydrophila* mortality in tench (*Tinca tinca*) through the activation of cellular and humoral defence mechanisms. *Reviews in Fish Biology and Fisheries*, **20**(3), pp. 435-439.
- SKUGOR, S., GRISDALE-HELLAND, B., REFSTIE, S., AFANASYEV, S., VIELMA, J. and KRASNOV, A., 2011. Gene expression responses to restricted feeding and extracted soybean meal in Atlantic salmon (*Salmo salar* L.). *Aquaculture Nutrition*, **17**(5), pp. 505-517.
- SMITH, H., 1975. Eosinophilic granular cells of salmonids. MSc Thesis, University of Stirling, Stirling, UK, pp. 36.
- SOMMERSET, I., SKERN, R., BIERING, E., BLEIE, H., FIKSDAL, I.U., GROVE, S. and NERLAND, A.H., 2005. Protection against Atlantic halibut nodavirus in turbot is induced by recombinant capsid protein vaccination but not following DNA vaccination. *Fish & Shellfish Immunology*, **18**(1), pp. 13-29.

- SORDET, O., RÉBÉ, C., PLENCHETTE, S., ZERMATI, Y., HERMINE, O., VAINCHENKER, W., GARRIDO, C., SOLARY, E. and DUBREZ-DALLOZ, L., 2002. Specific involvement of caspases in the differentiation of monocytes into macrophages. *Blood*, **100**(13), pp. 4446-4453.
- SØRENSEN, C., NILSSON, G.E., SUMMERS, C.H. and ØVERLI, Ø., 2012. Social stress reduces forebrain cell proliferation in rainbow trout (*Oncorhynchus mykiss*). *Behavioural Brain Research*, **227**(2), pp. 311-318.
- SØRENSEN, M., PENN, M., EL-MOWAFI, A., STOREBAKKEN, T., CHUNFANG, C., ØVERLAND, M. and KROGDAHL, Å., 2011. Effect of stachyose, raffinose and soya-saponins supplementation on nutrient digestibility, digestive enzymes, gut morphology and growth performance in Atlantic salmon (*Salmo salar*, L). *Aquaculture*, **314**(1), pp. 145-152.
- SPICER, S., 1963. Histochemical properties of mucopolysaccharide and basic protein in mast cells. *Annals of the New York Academy of Sciences*, **103**(1), pp. 322-333.
- SREENIVASAN, K.R., PRASAD, R.R., MENEVEAU, C. and RAMSHANKAR, R., 1989. The Fractal geometry of interfaces and the multifractal distribution of dissipation in fully turbulent flows. *Pure and Applied Geophysics*, **131**(1-2), pp. 43-60.
- STARCZYNSKI, J. and CROCKER, J., 2005. "Immunohistochemistry" in Crocker, J. and Burnett, D. (Eds.). *The science of laboratory diagnosis*, 2nd Edition, John Wiley & Sons Ltd., West Sussex, UK, pp. 35-44.
- STEEDMAN, H.F., 1950. Alcian blue 8GS; a new stain for mucin. *Quarterly Journal of Microscopic Science*, **91**, pp. 477-479.
- STEFAN, Y. and FALKMER, S., 1980. Identification of four endocrine cell types in the pancreas of *Cottus scorpius* (Teleostei) by immunofluorescence and electron microscopy. *General and Comparative Endocrinology*, **42**(2), pp. 171-178.
- STOLEN, J.S., FLETCHER, T., ANDERSON, R., KAATTARI, S. and ROWLEY, S., 1992. *Techniques in fish immunology; 2*. SOS Publications, Fair Haven, USA, pp. 196.
- STOLEN, J.S., FLETCHER, T., ANDERSON, R., ROBERSON, B. and VAN MUISWINKEL, W., 1990. *Techniques in fish immunology; 1*. SOS Publications, Fair Haven, USA, pp. 197.
- STOLEN, J.S., FLETCHER, T., ANDERSON, R., ROWLEY, S., ZELIKOFF, J. KAATTARI, S. and SMITH, S., 1994. *Techniques in fish immunology; 3*. SOS Publications, Fair Haven, USA, pp. 190.
- STOLEN, J.S., FLETCHER, T., SMITH, S., ZELIKOFF, J., ANDERSON, R., SODERHALL, K., KAATTARI, S. and., WEEKS-PERKINS, A., 1995. *Techniques in fish immunology; 4*. SOS Publications, Fair Haven, USA, pp. 190.
- SUNDH, H., 2009. Chronic stress and intestinal barrier function: Implications for infection and inflammation in intensive salmon aquaculture. PhD Dissertation Thesis, University of Gothenburgh, Sweden, pp. 75.
- SUNDSTRØM, T., DAPHU, I., WENDELBO, I., HODNELAND, E., LUNDERVOLD, A., IMMERVOLL, H., SKAFTNESMO, K.O., BABIC, M., JENDELOVA, P., SYKOVA, E., LUND-JOHANSEN, M., BJERKVIG, R. and THORSEN, F., 2013. Automated tracking of nanoparticle-labeled melanoma

- cells improves the predictive power of a brain metastasis model. *Cancer Research*, **78**(8), pp. 2445-2456.
- SVEINBJØRNSSON, B. and SELJELID, R., 1994. Aminated β -1,3-d-polyglucose activates salmon pronephros macrophages *in vitro*. *Veterinary Immunology and Immunopathology*, **41**(1–2), pp. 113-123.
- SVEINBJØRNSSON, B., OLSEN, R. and PAULSEN, S., 1996. Immunocytochemical localization of lysozyme in intestinal eosinophilic granule cells (EGCs) of Atlantic salmon, *Salmo salar* L. *Journal of Fish Diseases*, **19**(5), pp. 349-355.
- SWEETMAN, J., DIMITROGLOU, A., DAVIES, S. and TORRECILLAS, S., 2008. Nutrient Uptake – Gut morphology a key to efficient nutrition. *International Aquafeed*, **1-2**, pp. 26-30.
- SWEETMAN, J.W., TORRECILLAS, S., DIMITROGLOU, A., RIDER, S., DAVIES, S.J. and IZQUIERDO, M.S., 2010. Enhancing the natural defences and barrier protection of aquaculture species. *Aquaculture Research*, **41**(3), pp. 345-355.
- SZALAI, A.J., BLY, J. and CLEM, L., 1994. Changes in serum concentrations of channel catfish (*Ictalurus punctatus* Rafinesque) phosphorylcholine-reactive protein (PRP) in response to inflammatory agents, low temperature-shock and infection by the fungus *Saprolegnia* sp. *Fish & Shellfish Immunology*, **4**(5), pp. 323-336.
- TACCHI, L., BICKERDIKE, R., DOUGLAS, A., SECOMBES, C.J. and MARTIN, S.A., 2011. Transcriptomic responses to functional feeds in Atlantic salmon (*Salmo salar*). *Fish & Shellfish Immunology*, **31**(5), pp. 704-715.
- TACON, A.G. and METIAN, M., 2008. Global overview on the use of fish meal and fish oil in industrially compounded aquafeeds: Trends and future prospects. *Aquaculture*, **285**(1), pp. 146-158.
- TACON, A.G., 1995. Feed ingredients for carnivorous fish species: alternatives to fishmeal and other fishery resources. *Sustainable Fish Farming*, pp. 89-114.
- TADISO, T.M., LIE, K.K. and HORDVIK, I., 2011. Molecular cloning of IgT from Atlantic salmon, and analysis of the relative expression of τ , μ and δ in different tissues. *Veterinary Immunology and Immunopathology*, **139**(1), pp. 17-26.
- TAHMASEBI-KOHYANI, A., KEYVANSHOKOOH, S., NEMATOLLAHI, A., MAHMOUDI, N. and PASHA-ZANOOSI, H., 2011. Dietary administration of nucleotides to enhance growth, humoral immune responses, and disease resistance of the rainbow trout (*Oncorhynchus mykiss*) fingerlings. *Fish & Shellfish Immunology*, **30**(1), pp. 189-193.
- TAHMASEBI-KOHYANI, A., KEYVANSHOKOOH, S., NEMATOLLAHI, A., MAHMOUDI, N. and PASHA-ZANOOSI, H., 2012. Effects of dietary nucleotides supplementation on rainbow trout (*Oncorhynchus mykiss*) performance and acute stress response. *Fish Physiology and Biochemistry*, **38**(2), pp. 431-440.
- TAKLE, H. and ANDERSEN, Ø., 2007. Caspases and apoptosis in fish. *Journal of Fish Biology*, **71**(sc), pp. 326-349.

- TAPIAS, V., GREENAMYRE, J.T. and WATKINS, S.C., 2013. Automated imaging system for fast quantitation of neurons, cell morphology and neurite morphometry *in vivo* and *in vitro*. *Neurobiology of Disease*, **54**(0), pp. 158-168.
- TAYLOR, C. and LEVENSON, R., 2006. Quantification of immunohistochemistry – issues concerning methods, utility and semiquantitative assessment II. *Histopathology*, **49**(4), pp. 411-424.
- TERANISHI, K. and KANEKO, T., 2010. Spatial, cellular, and intracellular localization of Na⁺/K⁺-ATPase in the sterically disposed renal tubules of Japanese eel. *Journal of Histochemistry & Cytochemistry*, **58**(8), pp. 707-719.
- THEODOSIOU, Z., KASAMPALIDIS, I.N., LIVANOS, G., ZERVAKIS, M., PITAS, I. and LYROUDIA, K., 2007. Automated analysis of FISH and immunohistochemistry images: A review. *Cytometry Part A*, **71A**(7), pp. 439-450.
- THOMPSON, I., WHITE, A., FLETCHER, T., HOULIHAN, D. and SECOMBES, C., 1993. The effect of stress on the immune response of Atlantic salmon (*Salmo salar*, L.) fed diets containing different amounts of vitamin C. *Aquaculture*, **114**(1), pp. 1-18.
- THOMPSON, K.D, CACHOS, A. and INGLIS, V., 1995. Immunomodulating effects of glucans and oxytetracycline in rainbow trout, *Oncorhynchus mykiss*, on serum lysozyme and protection. *Diseases in Asian Aquaculture*, **11**, pp. 433-439.
- THOMPSON, K.D., TATNER, M.F. and HENDERSON, R.J., 1996. Effects of dietary (n-3) and (n-6) polyunsaturated fatty acid ratio on the immune response of Atlantic salmon, *Salmo salar* L. *Aquaculture Nutrition*, **2**(1), pp. 21-31.
- THORNBERRY, N.A., BULL, H.G., CALAYCAY, J.R., CHAPMAN, K.T., HOWARD, A.D., KOSTURA, M.J., MILLER, D.K., MOLINEAUX, S.M., WEIDNER, J.R. and AUNINS, J., 1992. A novel heterodimeric cysteine protease is required for interleukin-1 β processing in monocytes. *Nature*, **356**(6372), pp. 768-774.
- TIBALDI, E., HAKIM, Y., UNI, Z., TULLI, F., DE FRANCESCO, M., LUZZANA, U. and HARPAZ, S., 2006. Effects of the partial substitution of dietary fish meal by differently processed soybean meals on growth performance, nutrient digestibility and activity of intestinal brush border enzymes in the European sea bass (*Dicentrarchus labrax*). *Aquaculture*, **261**(1), pp. 182-193.
- TIPSMARK, C.K. and MADSEN, S., 2012. Tricellulin, occludin and claudin-3 expression in salmon intestine and kidney during salinity adaptation. *Comparative Biochemistry and Physiology Part A: Molecular & Integrative Physiology*, **162**(4), pp. 378-385.
- TORANZO, A., DEVESA, S., ROMALDE, J., LAMAS, J., RIAZA, A., LEIRO, J. and BARJA, J., 1995. Efficacy of intraperitoneal and immersion vaccination against *Enterococcus* sp. infection in turbot. *Aquaculture*, **134**(1), pp. 17-27.
- TORRECILLAS, S., MAKOL, A., BENÍTEZ-SANTANA, T., CABALLERO, M.J., MONTERO, D., SWEETMAN, J. and IZQUIERDO, M., 2011. Reduced gut bacterial translocation in European sea bass (*Dicentrarchus labrax*) fed mannan oligosaccharides (MOS). *Fish & Shellfish Immunology*, **30**(2), pp. 674-681.
- TORT, L., BALASCH, J. and MACKENZIE, S., 2003. Fish immune system. A crossroads between innate and adaptive responses. *Inmunología*, **22**(3), pp. 277-286.

- TRESGUERRES, M., LEVIN, L.R., BUCK, J. and GROSELL, M., 2010. Modulation of NaCl absorption by $[\text{HCO}_3^-]$ in the marine teleost intestine is mediated by soluble adenylyl cyclase. *American Journal of Physiology-Regulatory, Integrative and Comparative Physiology*, **299**(1), pp. R62-R71.
- TRICHET, V.V., 2010. Nutrition and immunity: an update. *Aquaculture Research*, **41**(3), pp. 356-372.
- TRUE, L., 1996. Morphometric applications in anatomic pathology. *Human Pathology*, **27**(5), pp. 450-467.
- TURLIN, B., RAMM, G.A., PURDIE, D.M., LAINÉ, F., PERRIN, M., DEUGNIER, Y. and MACDONALD, G.A., 2009. Assessment of hepatic steatosis: comparison of quantitative and semiquantitative methods in 108 liver biopsies. *Liver International*, **29**(4), pp. 530-535.
- UCHIDA, K., KANEKO, T., YAMAUCHI, K. and HIRANO, T., 1996. Morphometrical analysis chloride cell activity in the gill filaments and lamellae and changes in Na^+ , K^+ -ATPase activity during seawater adaptation in chum salmon fry. *Journal of Experimental Zoology*, **276**(3), pp. 193-200.
- UNKNOWN a, 1998. KS Run User Interface (User Guide B 40-613), Carl Zeiss Vision GmbH, München-Hallbergmoos, Germany, pp. 1-39.
- UNKNOWN b, 1999. KS 300 Imaging System (User Guide B 40-614), Carl Zeiss Vision GmbH, München-Hallbergmoos, Germany, pp. 1-855.
- URÁN, P., SCHRAMA, J., JAAFARI, S., BAARDSEN, G., ROMBOUT, J., KOPPE, W. and VERRETH, J., 2009a. Variation in commercial sources of soybean meal influences the severity of enteritis in Atlantic salmon (*Salmo salar* L.). *Aquaculture Nutrition*, **15**(5), pp. 492-499.
- URÁN, P.A., 2008. Etiology of soybean-induced enteritis in fish. PhD Dissertation Thesis, Wageningen University, The Netherlands, pp. 175.
- URÁN, P.A., AYDIN, R., SCHRAMA, J.W., VERRETH, J.A.J. and ROMBOUT, J.H.W.M., 2008a. Soybean meal-induced uptake block in Atlantic salmon *Salmo salar* distal enterocytes. *Journal of Fish Biology*, **73**(10), pp. 2571-2579.
- URÁN, P.A., SCHRAMA, J.W., ROMBOUT, J.H.W.M., OBACH, A., JENSEN, L., KOPPE, W. and VERRETH, J.A.J., 2008b. Soybean meal-induced enteritis in Atlantic salmon (*Salmo salar* L.) at different temperatures. *Aquaculture Nutrition*, **14**(4), pp. 324-330.
- URÁN, P.A., SCHRAMA, J.W., ROMBOUT, J.H.W.M., TAVERNE-THIELE, J.J., OBACH, A., KOPPE, W. and VERRETH, J.A.J., 2009b. Time-related changes of the intestinal morphology of Atlantic salmon, *Salmo salar* L., at two different soybean meal inclusion levels. *Journal of Fish Diseases*, **32**(9), pp. 733-744.
- URZÚA, F., 2013. Intestinal microbiota and transcriptomic responses in Atlantic salmon (*Salmo salar*) fed soybean meal and microbial ingredients. PhD Dissertation Thesis, Norwegian University of Life Sciences, Ås, Norway, pp. 210.
- USHER, M., TALBOTT, C. and EDDY, F., 1991. Intestinal water transport in juvenile Atlantic salmon (*Salmo salar* L.) during smolting and following transfer to seawater. *Comparative Biochemistry and Physiology Part A: Physiology*, **100**(4), pp. 813-818.
- VALENTE, L.M.P., CORNET, J., DONNAY-MORENO, C., GOUYGOU, J.P., BERGÉ, J.P., BACELAR, M., ESCÓRCIO, C., ROCHA, E., MALHÃO, F. and CARDINAL, M., 2011. Quality

- differences of gilthead sea bream from distinct production systems in Southern Europe: Intensive, integrated, semi-intensive or extensive systems. *Food Control*, **22**(5), pp. 708-717.
- VALLEJO, A. N. and ELLIS, A. E., 1989. Ultrastructural study of the response of eosinophil granule cells to *Aeromonas salmonicida* extracellular products and histamine liberators in rainbow trout *Salmo gairdneri* Richardson. *Developmental and Comparative Immunology*, **13**, pp. 133–148.
- VAN CRUCHTEN, S. and VAN DEN BROECK, W., 2002. Morphological and biochemical aspects of apoptosis, oncosis and necrosis. *Anatomia, Histologia, Embryologia*, **31**(4), pp. 214-223.
- VAN DEN INGH, T., OLLI, J. and KROGDAHL, Å., 1996. Alcohol-soluble components in soybeans cause morphological changes in the distal intestine of Atlantic salmon, *Salmo salar* L. *Journal of Fish Diseases*, **19**(1), pp. 47-53.
- VAN DEN INGH, T.S. and KROGDAHL, A., 1990. Negative effects of anti-nutritional factors from soybeans in Salmonidae. *Tijdschrift Voor Diergeneeskunde*, **115**(20), pp. 935-938.
- VAN DEN INGH, T.S.G.A.M., KROGDAHL, Å., OLLI, J.J., HENDRIKS, H.G.C.J.M. and KONINKX, J.G.J.F., 1991. Effects of soybean-containing diets on the proximal and distal intestine in Atlantic salmon (*Salmo salar*): a morphological study. *Aquaculture*, **94**(4), pp. 297-305.
- VAN DER LOOS, C. M., 2008. Multiple immunoenzyme staining: methods and visualizations for the observation with spectral imaging. *Journal of Histochemistry & Cytochemistry*, **56**(4), pp. 313-328.
- VAN DER MAREL, M., PRÖPSTING, M., BATTERMANN, F., JUNG-SCHROERS, V., HÜBNER, A., ROMBOUT, J. and STEINHAGEN, D., 2014. Differences between intestinal segments and soybean meal-induced changes in intestinal mucus composition of common carp *Cyprinus carpio* L. *Aquaculture Nutrition*, **20**(1), pp.12-24.
- VATSOS, I.N., KOTZAMANIS, Y., HENRY, M., ANGELIDIS, P. and ALEXIS, M.N., 2010. Monitoring stress in fish by applying image analysis to their skin mucous cells. *European Journal of Histochemistry*, **54**(2), pp. 107-111.
- VAUGHAN, L., FITZPATRICK, E., BOLAND, M.P. and ROCHE, J.F., 1996. A histological study of corpora lutea from superovulated beef heifers. *Animal Reproduction Science*, **43**(1), pp. 1-14.
- VEGGETTI, A., MASCARELLO, F., SCAPOLO, P., ROWLERSON, A. and CARNEVALI, M.C., 1993. Muscle growth and myosin isoform transitions during development of a small teleost fish, *Poecilia reticulata* (Peters) (*Atheriniformes, Poeciliidae*): a histochemical, immunohistochemical, ultrastructural and morphometric study. *Anatomy and Embryology*, **187**(4), pp. 353-361.
- VERA-JIMENEZ, N.I., PIETRETTI, D., WIEGERTJES, G.F. and NIELSEN, M.E., 2013. Comparative study of β -glucan induced respiratory burst measured by nitroblue tetrazolium assay and real-time luminol-enhanced chemiluminescence assay in common carp (*Cyprinus carpio* L.). *Fish & Shellfish Immunology*, **34**(5), pp. 1216-1222.
- VERLHAC, V. and KIRON, V., 2004. Nutrition and immune modulation in aquatic animals. *Aqua Feeds: Formulation & Beyond*, **1**, pp. 5-9.
- VERLHAC, V., GABAUDAN, J., OBACH, A., SCHÜEP, W. and HOLE, R., 1996. Influence of dietary glucan and vitamin C on non-specific and specific immune responses of rainbow trout (*Oncorhynchus mykiss*). *Aquaculture*, **143**(2), pp. 123-133.

- VERNIER, J. and MELLINGER, J., 1990. Intestine ultrastructure in relation to lipid and protein absorption in teleost fish. *Comparative Physiology*, **5**, pp. 166-175.
- VETVICKA, V., VANNUCCI, L. and SIMA, P., 2013. The effects of β -glucan on fish immunity. *North American Journal of Medical Sciences*, **5**(10), pp. 580-588.
- VIDMAR, D.A., CRUESS, D., HSIEH, P., DOLECEK, Q., PAK, H., GWYNN, M., MAGGIO, K., MONTEMORANO, A., POWERS, J., RICHARDS, D., SPERLING, L., WONG, H. and YEAGER, J., 1999. The effect of decreasing digital image resolution on teledermatology diagnosis. *Telemedicine Journal*, **5**(4), pp. 375-383.
- VIEIRA-LOPES, D.A., PINHEIRO, N.L., SALES, A., VENTURA, A., ARAÚJO, F.G., GOMES, I.D. and NASCIMENTO, A.A., 2013. Immunohistochemical study of the digestive tract of *Oligosarcus hepsetus*. *World Journal of Gastroenterology*, **19**(12), pp. 1919-1929.
- WAAGBØ, R., 1994. The impact of nutritional factors on the immune system in Atlantic salmon, *Salmo salar* L.: a review. *Aquaculture Research*, **25**(2), pp. 175-197.
- WAAGBØ, R., BERNTSSEN, M., DANIELSEN, T., HELBERG, H., KLEPPA, A., BERG LEA, T., ROSENLUND, G., TVENNING, L., SUSORT, S. and VIKESÅ, V., 2013. Feeding Atlantic salmon diets with plant ingredients during the seawater phase – a full-scale net production of marine protein with focus on biological performance, welfare, product quality and safety. *Aquaculture Nutrition*, **19**(4), pp. 598-618.
- WAAGBØ, R., SANDNES, K., ESPELID, S. and LIE, Ø., 1988. Haematological and biochemical analyses of Atlantic salmon, *Salmo salar* L., suffering from coldwater vibriosis ('Hitra disease'). *Journal of Fish Diseases*, **11**(5), pp. 417-423.
- WALLS, A., ROBERTS, J., GODFREY, R., CHURCH, M. and HOLGATE, S., 1990. Histochemical heterogeneity of human mast cells: disease-related differences in mast cell subsets recovered by bronchoalveolar lavage. *International Archives of allergy and Immunology*, **92**(3), pp. 233-241.
- WANG, C.W. and YU, C.P., 2012. Automated morphological classification of lung cancer subtypes using H&E tissue images. *Machine Vision and Applications*, **24**, pp. 1383-1392.
- WANG, W., WANG, Y., HU, W., LI, A., CAI, T., ZHU, Z. and WANG, J., 2006. Effects of the "all-fish" growth hormone transgene expression on non-specific immune functions of common carp, *Cyprinus carpio* L. *Aquaculture*, **259**(1-4), pp. 81-87.
- WATANABE, T., PONGMANEERAT, J., SATO, S. and TAKEUCHI, T., 1993. Replacement of fish meal by alternative protein sources in rainbow trout diets. *Bulletin of the Japanese Society of Scientific Fisheries*, **59**(9), pp.1573-1579.
- WEAVER, D.L., KRAG, D.N., MANNA, E.A., ASHIKAGA, T., HARLOW, S.P. and BAUER, K.D., 2003. Comparison of pathologist-detected and automated computer-assisted image analysis detected sentinel lymph node micrometastases in breast cancer. *Modern Pathology*, **16**(11), pp. 1159-1163.
- WEBER, L.P., KIPARISSIS, Y., HWANG, G.S., NIIMI, A.J., JANZ, D.M. and METCALFE, C.D., 2002. Increased cellular apoptosis after chronic aqueous exposure to nonylphenol and quercetin in

- adult medaka (*Oryzias latipes*). *Comparative Biochemistry and Physiology Part C: Toxicology & Pharmacology*, **131**(1), pp. 51-59.
- WEBSTER, J.D., MICHALOWSKI, A.M., DWYER, J.E., CORPS, K.N., WEI, B., JUOPPERI, T., HOOVER, S.B. and SIMPSON, R.M., 2012. Investigation into diagnostic agreement using automated computer-assisted histopathology pattern recognition image analysis. *Journal of Pathology Informatics*, **3**, pp. 18-18.
- WEDEMEYER, G. A., 1996. Physiology of fish in intensive culture systems. Chapman & Hall, New York, pp. 326.
- WEINREB, E. L. and BILSTAD, N. M., 1955. Histology of the digestive tract and adjacent structures of a rainbow trout, *Salmo gairdneri irideus*. *Copeia*, **3**, 194-204.
- WEINSTEIN, R.S., GRAHAM, A.R., RICHTER, L.C., BARKER, G.P., KRUPINSKI, E.A., LOPEZ, A.M., ERPS, K.A., BHATTACHARYYA, A.K., YAGI, Y. and GILBERTSON, J.R., 2009. Overview of telepathology, virtual microscopy, and whole slide imaging: prospects for the future. *Human Pathology*, **40**(8), pp. 1057-1069.
- WELKER, T.L., LIM, C., YILDIRIM-AKSOY, M. and KLESIUS, P.H., 2011. Effects of dietary supplementation of a purified nucleotide mixture on immune function and disease and stress resistance in channel catfish, *Ictalurus punctatus*. *Aquaculture Research*, **42**(12), pp. 1878-1889.
- WERNERSSON, S., REIMER, J.M., POORAFSHAR, M., KARLSON, U., WERMENSTAM, N., BENGTÉN, E., WILSON, M., PILSTRÖM, L. and HELLMAN, L., 2006. Granzyme-like sequences in bony fish shed light on the emergence of hematopoietic serine proteases during vertebrate evolution. *Developmental & Comparative Immunology*, **30**(10), pp. 901-918.
- WESTER, K., RANEFALL, P., BENGTSSON, E., BUSCH, C. and MALMSTROM, P.U., 1999. Automatic quantification of microvessel density in urinary bladder carcinoma. *British Journal of Cancer*, **81**(8), pp. 1363-1370.
- WHITTAMORE, J.M., 2012. Osmoregulation and epithelial water transport: lessons from the intestine of marine teleost fish. *Journal of Comparative Physiology B*, **182**(1), pp. 1-39.
- WHITTINGTON, R., LIM, C. and KLESIUS, P.H., 2005. Effect of dietary β -glucan levels on the growth response and efficacy of *Streptococcus iniae* vaccine in Nile tilapia, *Oreochromis niloticus*. *Aquaculture*, **248**(1), pp. 217-225.
- WIED, G.L., BARTELS, P.H., BIBBO, M. and DYTCH, H.E., 1989. Image-Analysis in Quantitative Cyto-Pathology and Histopathology. *Human Pathology*, **20**(6), pp. 549-571.
- WIJESEKERA, H.W., 1996. Fractal dimension as an indicator for turbulent mixing in the thermocline. *Journal of Geophysical Research-Oceans*, **101**(C7), pp. 16,703-16,709.
- WILHELM, S., WAGNER, H. and HÄCKER, G., 1998. Activation of caspase-3-like enzymes in non-apoptotic T cells. *European Journal of Immunology*, **28**(3), pp. 891-900.
- WILSON, J.M. and CASTRO, L.F.C., 2011. "Morphological diversity of the gastrointestinal tract in fishes" in Grosell, M., Farrell, A.P., Brauner, C.J. (Eds.). *The multifunctional gut of fish*, Wiley-Blackwell, San Diego, USA, pp. 2-55.

- WINGREN, U. and ENERBÄCK, L., 1983. Mucosal mast cells of the rat intestine: a re-evaluation of fixation and staining properties, with special reference to protein blocking and solubility of the granular glycosaminoglycan. *The Histochemical Journal*, **15**(6), pp. 571-582.
- WITTEKIND, D., REINHARDT, E., KRETSCHMER, V. and ZIPFEL, E., 1983. Influence of staining on fast automated cell segmentation, feature-extraction and cell image-analysis. *Analytical and Quantitative Cytology and Histology*, **5**(1), pp. 55-60.
- WITTERS, H., BERCKMANS, P. and VANGENECHTEN, C., 1996. Immunolocalization of Na⁺, K⁺-ATPase in the gill epithelium of rainbow trout, *Oncorhynchus mykiss*. *Cell and Tissue Research*, **283**(3), pp. 461-468.
- WOLF, H. and DITTRICH, K., 1992. Detection of proliferating cell nuclear antigen in diagnostic histopathology. *Journal of Histochemistry & Cytochemistry*, **40**(9), pp. 1269-1273.
- WRIGHT, M., THURSZ, M., PULLEN, R., THOMAS, H. and GOLDIN, R., 2003. Quantitative versus morphological assessment of liver fibrosis: Semi-quantitative scores are more robust than digital image fibrosis area estimation. *Liver International*, **23**(1), pp. 28-34.
- WU, P., JIANG, J., LIU, Y., HU, K., JIANG, W., LI, S., FENG, L. and ZHOU, X., 2013. Dietary choline modulates immune responses, and gene expressions of TOR and eIF4E-binding protein2 in immune organs of juvenile Jian carp (*Cyprinus carpio* var. Jian). *Fish & Shellfish Immunology*, **186**, pp. 172-180.
- WYLLIE, A.H., KERR, J.F. and CURRIE, A.R., 1980. Cell death: the significance of apoptosis. *International Review Cytology*, **68**: pp. 251-306.
- YAMAMOTO, T., 1966. An electron microscope study of the columnar epithelial cell in the intestine of fresh water teleosts: Goldfish (*Carassius auratus*) and rainbow trout (*Salmo irideus*). *Zeitschrift für Zellforschung und mikroskopische Anatomie*, **72**(1), pp. 66-87.
- YASUTAKE, W.I. and WALES, J.H., 1983. Microscopic Anatomy of Salmonids: An Atlas. Resource Publication ISO, Washington DC, USA, pp. 189.
- YAZIJI, H. and BARRY, T., 2006. Diagnostic immunohistochemistry: what can go wrong? *Advances in Anatomic Pathology*, **13**(5), pp. 238-246.
- YOSHIDA, T., KRUGER, R. and INGLIS, V., 1995. Augmentation of non-specific protection in African catfish, *Clarias gariepinus* (Burchell), by the long-term oral administration of immunostimulants. *Journal of Fish Diseases*, **18**(2), pp. 195-198.
- YOUSSEF, P.P., SMEETS, T.J., BRESNIHAN, B., CUNNANE, G., FITZGERALD, O., BREEDVELD, F. and TAK, P.P., 1998. Microscopic measurement of cellular infiltration in the rheumatoid arthritis synovial membrane: a comparison of semiquantitative and quantitative analysis. *Rheumatology*, **37**(9), pp. 1003-1007.
- ZAPATA, A. and AMEMIYA, C., 2000. Phylogeny of lower vertebrates and their immunological structures. *Origin and Evolution of the Vertebrate Immune System*. Springer, pp. 67-107.
- ZHAO, J., LIU, Y., JIANG, J., WU, P., CHEN, G., JIANG, W., LI, S., TANG, L., KUANG, S., FENG, L. and ZHOU, X., 2012. Effects of dietary isoleucine on growth, the digestion and absorption capacity and gene expression in hepatopancreas and intestine of juvenile Jian carp (*Cyprinus carpio* var. Jian). *Aquaculture*, **368-369**(0), pp. 117-128.

ZHOU, Q., BUENTELLO, J.A. and GATLIN, D.M., 2010. Effects of dietary prebiotics on growth performance, immune response and intestinal morphology of red drum (*Sciaenops ocellatus*). *Aquaculture*, **309**(1), pp. 253-257.

STOCK SOLUTIONS AND BUFFERS

This section provides recipes for the buffers and solutions that were employed for the protocols described in the previous chapters. When preparing solutions, deionized or distilled water and reagents of the highest available grade were employed. Sterilisation by filtration through a 0.22 µm filter or by autoclaving (120 °C for 20 min) was applied to most of the solutions stored at room temperature (16-20 °C) and was essential for the cell culture applications. Where storage conditions were not specified, solutions were stored for up to 6 months at room temperature.

1 % ACID ALCOHOL

REAGENTS

Hydrogen chloride (HCl)	1.0 g
Methylated spirit	100.0 mL

PROCEDURE

1. Measure the methylated spirits into a Winchester bottle and carefully add the hydrochloric acid.

NOTE

The solution should be prepared fresh.

ALCIAN BLUE, PH 2.5

REAGENTS

3 % Glacial acetic acid (C ₂ H ₄ O ₂)	100.0 mL
Alcian blue 8GX (C ₅₆ H ₆₈ Cl ₄ CuN ₁₆ S ₄)	1.0 g

PROCEDURE

1. Weigh out the dry reagent and place in a 250 mL conical flask.
2. Add the liquid reagent and stir it very well.
3. Adjust the pH to 2.5, using acetic acid.
4. Filter the solution and add a crystal of thymol as preservative.

NOTE

The solution will be stable for 2 to 6 months at room temperature.

1 % ASTRA BLUE SOLUTION

REAGENTS

0.7 M Hydrochloride acid (HCl)	100.0 mL
Astra blue (C ₄₇ H ₅₂ CuN ₁₄ O ₆ S ₃)	1.0 g

PROCEDURE

1. Dissolve the dry reagent with the hydrochloric acid solution, in a 150 mL conical flask.
2. Filter the solution.

NOTE

The solution will be stable for 6 to 9 months years at room temperature.

0.1 % AZURE A

REAGENTS

Azure A (C ₁₄ H ₁₄ ClN ₃ S)	0.1 g
Distilled water	70.0 mL
Ethanol (C ₂ H ₆ O)	30.0 mL

PROCEDURE

1. Dissolve the dry reagent with the distilled water, in a 150 mL conical flask.
2. Add the ethanol and stir it very well.
3. Filter the solution.

NOTE

The solution will be stable for 2 years at room temperature.

EOSIN-ASTRA SOLUTION

REAGENTS

1 % Phloxine B (C ₂₀ H ₂ Br ₄ Cl ₄ Na ₂ O ₅)	30.0 mL
1 % Yellowish eosin solution	200.0 mL
95 % Ethanol (C ₂ H ₆ O)	1560.0 mL
Acetic acid (CH ₃ COOH)	6.0 mL

PROCEDURE

1. Mix the liquid reagents by stirring in a 2 L conical flask. Filter the solution.

NOTE

The solution will be stable for 6 to 9 months years at room temperature.

1 % ERYTHROSINE

REAGENTS

Distilled water	100.0 mL
Erythrosine B ($C_{20}H_{14}Na_2O_5$)	1.0 g

PROCEDURE

1. Dissolve the dry reagent with the distilled water, in a 150 mL conical flask.
2. Filter the solution.
3. Add a few drops of chloroform as preservative.

NOTE

The solution will be stable for 3 months at room temperature.

GIEMSA WORKING SOLUTION

REAGENTS

Giemsa solution (328840, Sigma-Aldrich, Ayrshire, UK)	25.0 mL
Sorenson's phosphate buffer solution	190.0 mL

PROCEDURE

1. Mix the liquid reagents by stirring in a 250 mL conical flask.

NOTE

The solution should be prepared fresh.

1.0 M GLACIAL ACETIC ACID

REAGENTS

Distilled water	200.0 mL
98 % Glacial acetic acid ($C_2H_4O_2$)	12.2 mL

PROCEDURE

1. Weigh out the dry reagent and place in a 250 mL conical flask.
2. Add the liquid reagent and stir it very well.

NOTE

The solution should be prepared fresh.

3 % GLACIAL ACETIC ACID

REAGENTS

99.5 % Acetic acid (CH_3COOH)	3.0 mL
Distilled water	100.0 mL

PROCEDURE

1. Mix both reagents in a 250 mL conical flask.
2. Adjust the pH to 2.5, using acetic acid.

NOTE

The solution will be stable for 1 year at room temperature.

MAYER'S HAEMATOXYLIN

REAGENTS

Chloral hydrate (C ₂ H ₃ Cl ₃ O ₂)	50.0 g
Citric acid (C ₆ H ₈ O ₇)	1.0 g
Distilled water	1000.0 mL
Haematoxylin (C ₁₆ H ₁₄ O ₆)	2.0 g
Potassium alum (2KAl(SO ₄))	50.0 g
Sodium iodate (NaIO ₃)	0.2 g

PROCEDURE

1. Weigh out the Haematoxylin, Potassium alum and Sodium iodate and place in a 2 L beaker.
2. Add the liquid reagent and stir the solution overnight.
3. Add the rest of the dry reagents and heat the solution until boiling. Keep at boiling point for another 5 min.
4. Allow the solution to cool and then filter it.

NOTE

The solution will be stable for 6 months at room temperature.

MAY-GRÜNWARD WORKING SOLUTION

REAGENTS

May-Grünwald solution (32856, Sigma-Aldrich, Ayrshire, UK)	25.0 mL
Sorenson's phosphate buffer solution	190.0 mL

PROCEDURE

1. Mix the liquid reagents by stirring in a 250 mL conical flask.

NOTE

The solution should be prepared fresh.

4 % PARAFORMALDEHYDE

REAGENTS

Paraformaldehyde ($\text{HO}(\text{CH}_2\text{O})_n\text{H}$)	4.9 g
Phosphate buffered saline solution	100.0 mL

PROCEDURE

1. Place the weighed dry reagent into a conical flask and add to it 90 mL of PBS.
2. Cover the flask with ParafilmM™ and transfer it into a fume hood.
3. Place the flask on top of a hotplate set to medium, with moderate stirring.
4. Allow the solution to warm up (when it will turn from being cloudy to clear it will be ready).
5. Keep the stirring while allowing the solution to cool down.
6. When cooled, make up the volume to 100mL and store it at 4 °C.

NOTE

Inspect regularly to avoid over-heating and consequent spilling.
The solution should be prepared fresh.

0.5 % PERIODIC ACID

REAGENTS

Distilled water	100.0 mL
Periodic acid (H_5IO_6)	0.5 g

PROCEDURE

1. Dissolve the weighed dry reagent with 90 mL distilled water, in a 100 mL conical flask.

NOTE

The solution will be stable for 1 year at 4 °C.

PHOSPHATE BUFFERED SALINE (PBS), PH 7.4

REAGENTS

Distilled water	1000.0 mL
Potassium chloride (KCl)	0.2 g
Potassium phosphate monobasic (Na_2HPO_4)	2.4 dg
Sodium chloride (NaCl)	8.0 g
Sodium phosphate dibasic (Na_2HPO_4)	14.4 dg

PROCEDURE

1. Dissolve the dry reagents in 800 mL of distilled water using a 2 L volumetric beaker.
2. Adjust pH to 7.4 with hydrochloric acid solution.
3. Add the distilled water to prefill the volume of 1 L.

NOTE

The solution will be stable for 3 months at room temperature or for longer at 4 °C.

REYNOLD'S LEAD CITRATE

REAGENTS

1 M Sodium hydroxide (NaOH)	8.0 mL
Distilled water	50.0 mL
Lead nitrate (PbNO_3^{2-})	13.3 dg
Sodium citrate ($\text{Na}_3\text{C}_6\text{H}_5\text{O}_7 \cdot 2\text{H}_2\text{O}$)	17.6 dg

PROCEDURE

1. Dissolve the weighed dry reagents in 15 mL of distilled water, and mix it very well.
2. Allow the solution to stand for 30 min, then add 8 mL 1M sodium hydroxide and mix.
3. Make up to 50 mL with distilled water.

NOTE

The solution will be stable for 1 month at 4 °C (discard the solution if an apparent precipitate develops). The solution should be centrifuged prior to use.

2 % SAFFRON

REAGENTS

Distilled water	100.0 mL
Saffron	2.9 g
Formalin (CH_2O)	1.0 mL
5 % Tannic acid ($\text{C}_{76}\text{H}_{52}\text{O}_{46}$)	1.0 mL

PROCEDURE

1. Dissolve the weighed dry reagent with distilled water, in a 150 mL conical flask.
2. Stir it very well and heat it for one hour in boiling water.
3. Filter the solution and add the formalin and the tannic acid.

NOTE

The solution will be stable for only a few weeks at room temperature.

SCHIFF'S REAGENT

REAGENTS

Basic fuchsin ($\text{C}_{20}\text{H}_{19}\text{N}_3 \cdot \text{HCl}$)	10.0 g
Distilled water	1000.0 mL

Hydrochloric acid (HCl)	10.0 mL
Sodium metabisulphite ($\text{Na}_2\text{S}_2\text{O}_5$)	18.0 g

PROCEDURE

1. Dissolve the weighed dry reagents with distilled water, in a 1 L dark flask.
2. Stir it very well (overnight or for at least 2 h until the solution turns clear).

NOTE

The solution will be stable for 6 months year at 4 °C.

To test the Schiff's reagent pour 10 mL of 37 % formalin into a watch glass. To this add a few drops of the Schiff's reagent to be tested. A good Schiff reagent will rapidly turn a red-purple color. A deteriorating Schiff's reagent will give a delayed reaction and the color produced will be a deep blue-purple.

SCOTT'S TAP WATER SUBSTITUTE

REAGENTS

Distilled water	1000.0 mL
Magnesium sulphate (MgSO_4)	20.0 g
Sodium bicarbonate (NaHCO_3)	3.5 g

PROCEDURE

1. Mix both reagents in a 2 L volumetric beaker.
2. Add the distilled water and dissolve the dry reagents by heating.
3. Add crystals of thymol as preservative.

NOTE

The solution will be stable for 3 months at room temperature.

1.0 M SODIUM ACETATE SOLUTION

REAGENTS

Distilled water	200.0 mL
Sodium acetate (CH_3COONa)	16.4 g

PROCEDURE

1. Weigh out the dry reagent and place in a 250 mL conical flask.
2. Add the liquid reagent and stir it very well.

NOTE

The solution should be prepared fresh.

SODIUM CACODYLATE BUFFER, PH 7.3

REAGENTS

Distilled water	240.0 mL
Sodium cacodylate ((CH ₃) ₂ AsO ₂ Na . 3H ₂ O)	10.7 g

PROCEDURE

1. Dissolve the weighed dry reagent with 240 mL distilled water, in a 1 L volumetric beaker.
2. Adjust the pH to 7.3 (using a 1 M hydrochloric acid) and final volume to 250 mL.

NOTE

The solution will be stable for 6 to 9 months at 4 °C.

1 % SODIUM CHLORIDE SOLUTION, PH 2.3

REAGENTS

Distilled water	50.0 mL
Sodium chloride (NaCl)	0.5 g

PROCEDURE

1. Dissolve the weighed dry reagent with 40 mL distilled water, in a 100 mL conical flask.
2. Adjust the pH to 2.3 (using a 1 M hydrochloric acid solution) and final volume to 50 mL.

NOTE

The solution should be prepared fresh.

SODIUM CITRATE BUFFER, PH 6.0

REAGENTS

Distilled water	1000.0 mL
Sodium citrate dihydrate (C ₆ H ₅ Na ₃ O ₇ . 2H ₂ O)	29.4 dg

PROCEDURE

1. Mix both reagents in a 2 L volumetric beaker.
2. Adjust pH to 6.0 with 1 M sodium hydroxide solution.

NOTE

The solution will be stable for 3 months at room temperature or for longer at 4 °C.

SODIUM DODECYL SULPHATE SAMPLE BUFFER, PH 6.8

REAGENTS

0.5 M Tris-hydrochloride (Tris-HCl, pH 6.8)	2.5 mL
10 % Sodium dodecyl sulphate buffer (SDS buffer)	4.0 mL

Bromophenol blue (C ₁₉ H ₁₀ Br ₄ O ₅ S)	2.0 mg
Distilled water	10.0 mL
Dithiothreitol (DTT)	0.31 mg
Glycerol (OCH ₂ CH(OH)CH ₂ OH)	2.0 mL

PROCEDURE

1. Mix all the reagents in a 15 mL Falcon™ tube, and stir it well.
2. Adjust the pH to 6.8 by adding 1 M hydrochloric acid solution, and the final volume to 10 mL.

NOTE

The solution can be aliquoted into small 1.2 mL eppendorf tubes and stored at -20 °C.

SORENSEN'S PHOSPHATE BUFFER, PH 7.2

REAGENTS

0.2 M Sodium phosphate dibasic solution (Na ₂ HPO ₄)	72.0 mL
0.2 M Sodium phosphate monobasic solution (H ₂ NaO ₄ P)	28.0 mL
Distilled water	100.0 mL

PROCEDURE

1. Mix the liquid reagents by stirring in a 250 mL conical flask.

NOTE

The solution should be prepared fresh.

TEM FIXATIVE

REAGENTS

25 % Glutaraldehyde (OHC(CH ₂) ₃ CHO)	10.0 mL
Distilled water	45.0 mL
Sodium cacodylate buffer	45.0 mL

PROCEDURE

1. Dilute the sodium cacodylate buffer with distilled water, transfer the solution to a 250 mL conical flask, and stir it very well.
2. Add the glutaraldehyde and continue the stirring.
3. Dispense 2-3 mL aliquots in glass vials and store in the freezer.

NOTE

The solution will be stable for 6 to 9 months at room temperature 4 °C.

THIONIN DYE SOLUTION, PH 4.3

REAGENTS

0.5 % Thionin stock solution	18.0 mL
Acetic acid solution	21.0 mL
Glacial acetic acid (C ₂ H ₄ O ₂)	12.2 mL
Sodium acetate solution	9.0 mL

PROCEDURE

1. Mix the liquid reagents by stirring in a 100 mL conical flask.

NOTE

The solution should be prepared fresh.

0.5 % THIONIN STOCK SOLUTION

REAGENTS

Distilled water	1000.0 mL
Thionin (C ₁₂ H ₉ N ₃ S · C ₂ H ₄ O ₂)	5.0 g

PROCEDURE

1. Weigh out the dry reagent and place in a 1 L conical flask.
2. Add the liquid reagent and stir it very well.
3. Filter the solution.

NOTE

The solution will be stable for 2 to 6 months at room temperature.

TOLUIDINE BLUE STOCK SOLUTION

REAGENTS

70 % Ethanol (C ₂ H ₆ O)	100.0 mL
Toluidine blue O (C ₁₅ H ₁₆ ClN ₃ S)	1.0 g

PROCEDURE

1. Weigh out the dry reagent and place in a 200 mL conical flask.
2. Add the liquid reagent and stir it very well.
3. Filter the solution.

NOTE

The solution will be stable for 2 to 6 months at room temperature.

TOLUIDINE BLUE WORKING SOLUTION, PH 2.4

REAGENTS

1 % Sodium chloride solution (NaCl)	45.0 mL
Toluidine blue stock solution	5.0 mL

PROCEDURE

1. Dissolve the weighed dry reagent with 40 mL distilled water, in a 100 mL conical flask.
2. Adjust the pH to 2.4 (using a 1 M hydrochloric acid solution) and final volume to 50 mL.
3. Filter the solution.

NOTE

The solution should be prepared fresh.

TRIS-BUFFERED SALINE (TBS), PH 7.5

REAGENTS

Distilled water	1000.0 mL
Sodium chloride (NaCl)	87.6 dg
Trizma base [®] (C ₄ H ₁₁ NO ₃)	60.7 dg

PROCEDURE

1. Dissolve the weighed dry reagents with distilled water, in a 2 L volumetric beaker.
2. Adjust the pH to 7.5 with 1 M hydrochloric solution.
3. Make the volume up to 1 L.

NOTE

The solution will be stable for 3 months at room temperature.

TRIS-BUFFERED SALINE TWEEN (TBST), PH 7.5

REAGENTS

Tris Buffered Saline (TBS)	1000.0 mL
Tween [®] 20 (C ₅₈ H ₁₁₄ O ₂₆)	5.0 mL

PROCEDURE

1. Add Tween[®] 20 to the TBS solution and mix very well.

NOTE

The solution will be stable for 6 months at 4 °C.

TRIS-ETHYLENEDIAMINETETRACETIC ACID (TRIS-EDTA), PH 9.0

REAGENTS

Distilled water	1000.0 mL
EDTA (C ₁₀ H ₁₆ N ₂ O ₈)	3.7 dg
Trizma base [®] (C ₄ H ₁₁ NO ₃)	12.1 dg

PROCEDURE

1. Dissolve the weighed dry reagents with 800 mL distilled water, in a 2 L volumetric beaker.
2. Check the pH of the solution and if necessary adjust it.

NOTE

The solution will be stable for 3 months at 4 °C.

TRIS-HYDROCHLORIDE (TRIS-HCL), PH 7.6

REAGENTS

Distilled water	1000.0 mL
Trizma base [®] (C ₄ H ₁₁ NO ₃)	60.7 dg

PROCEDURE

1. Dissolve the weighed dry reagents with 800 mL distilled water, in a 2 L volumetric beaker.
2. Add around 30 mL of 1 M hydrochloric acid solution.
3. Adjust the pH to 7.6 and final volume to 1 L.

NOTE

The solution will be stable for 1 year at 4 °C.

TRYPSIN NEUTRALISER BUFFERED SALINE (TN), PH 7.5

REAGENTS

Distilled water	2000.0 mL
Sodium chloride (NaCl)	160.1 dg
Trizma base [®] (C ₄ H ₁₁ NO ₃)	24.3 dg

PROCEDURE

1. Dissolve the weighed dry reagents with 800 mL distilled water, in a 2 L volumetric beaker.
2. Adjust the pH to 7.6 by adding 1 M hydrochloric acid solution, and adjusting the final volume to 2 L.

NOTE

The solution should be prepared fresh and autoclaved.

4 % URANYL ACETATE

REAGENTS

50 % Ethanol (C ₂ H ₆ O)	5.0 mL
Uranyl acetate (UO ₂ (OCOCH ₃) ₂ · 2H ₂ O)	2.0 dg

PROCEDURE

1. Dissolve the weighed dry reagent with 5 mL distilled water, in an amber bottle.
2. Place the bottle of uranyl acetate solution in a sonicator, under a fume hood, and sonicate for 1 h.
3. When sonication is completed, wrap some ParafilmM™ around the cover and store in the dark.

NOTE

The solution will be stable for 1 month at 4 °C.

1 % YELLOWISH EOSIN

REAGENTS

Distilled water	100.0 mL
Eosin (C ₂₀ H ₆ Br ₄ Na ₂ O ₅)	1.0 g

PROCEDURE

1. Weigh out the eosin and place in a 250 mL conical flask.
2. Add the liquid reagent and stir it very well.
3. Filter the solution.

NOTE

The solution will be stable for 2 to 4 months at room temperature.

1 % ZINC SULPHATE SOLUTION

REAGENTS

Zinc sulphate (ZnSO ₄ · 7H ₂ O)	0.1 g
Distilled water	100.0 mL

PROCEDURE

1. Dissolve the dry reagent with the distilled water, in a 150 mL conical flask.

NOTE

The solution should be prepared fresh.

HISTOCHEMICAL STAINING PROTOCOLS

This section provides a detailed description of the protocols mentioned in the previous chapters. Different protocols using either different dye stains, exposure timings / concentrations, stain solution's pH, rinsing steps, etc., were tried initially. The procedures being presented here are the ones that produced consistent results for the histological stain. The described procedures are for formalin fixed paraffin-embedded histological sections.

ALCIAN BLUE & HAEMATOXYLIN-EOSIN

PRINCIPAL

Alcian blue is a group of polyvalent basic dyes that are water soluble. The blue color is due to the presence of copper in the molecule. The 3 % acetic acid solution (pH 2.5) Alcian blue stains both sulphated and carboxylated acid mucopolysaccharides and sulphated and carboxylated sialomucins (glycoproteins). It is believed to form salt linkages with the acid groups of acid mucopolysaccharides.

PROCEDURE

1. Deparaffinise the sections in xylene and hydrate them through graded alcohols up to distilled water.
2. Place in acetic acid and thereafter without rinsing, drain the excess diluent on a paper towel.
3. Stain in Alcian blue pH 2.5 solution.
4. Wash in running tap water until excess stain stops leaching from tissue. Rinse with distilled water.
5. Counterstain in Mayer's haematoxylin and 1 % yellowish eosin, with water rinsing in between stains.
6. Wash in running tap water until excess stain stops leaching from tissue. Rinse with distilled water.
7. Dehydrate through graded alcohols, clear with xylene and coverslip using a synthetic resinous mountant.

TIMINGS

- | | |
|----------------------------|-------|
| a) Deparaffinise in xylene | 3 min |
| b) Deparaffinise in xylene | 3 min |
| c) Clear in alcohol 100 % | 2 min |
| d) Clear in alcohol 100 % | 2 min |

e) Hydrate in alcohol 96 %	2 min
f) Hydrate in alcohol 90 %	2 min
g) Hydrate in alcohol 80 %	2 min
h) Hydrate in alcohol 80 %	2 min
i) Hydrate in distilled water	2 min
j) Hydrate in distilled water	2 min
k) Place in acetic acid	2 min
l) Stain in Alcian blue	30 min
m) Wash in running tap water	2 min
n) Stain in Mayer's haematoxylin	5 min
o) Wash in running tap water	10 min
p) Stain in yellowish eosin	5 min
q) Dehydrate in alcohol 96 %	quick dip
r) Dehydrate in alcohol 100 %	2 min
s) Dehydrate in alcohol 100 %	2 min
t) Dehydrate in alcohol 100 %	2 min
u) Clear in xylene	3 min
v) Clear in xylene	3 min
w) Clear in xylene	3 min

RESULTS

Bright turquoise blue: acid mucopolysaccharides.

Dark bluish violet: nuclei and other basophilic structures.

Lighter pink: collagen.

Deep pink to red: cytoplasm, muscle fibrils, connective tissue fibers and other acidophilic structures.

HAEMATOXYLIN & EOSIN (H&E)

PRINCIPAL

Mayer's haematoxylin is an alum haematoxylin which is chemically ripened with sodium iodate, particularly useful in situations where a nuclear counterstain is needed to emphasise a cytoplasmic component which has been demonstrated by a special stain, and where the acid alcohol differentiation might destroy or decolour the stained cytoplasmic component.

Eosin is the most suitable stain to combine with an alum haematoxylin to demonstrate the general histological architecture of a tissue. Its particular value is its ability, with proper differentiation, to distinguish between the cytoplasm of different types of cells, and between the different types of connective tissue fibres and matrices, by staining them differing

shades of red and pink.

PROCEDURE

1. Deparaffinise the sections in xylene and hydrate them through graded alcohols up to distilled water.
2. Stain in Mayer's haematoxylin.
3. Wash in running tap water until excess stain stops leaching from tissue. Rinse with distilled water.
4. Differentiate in 1 % acid alcohol.
5. Wash in running tap water until excess stain stops leaching from tissue. Rinse with distilled water.
6. Counterstain in 1 % yellowish eosin.
7. Wash in running tap water until excess stain stops leaching from tissue. Rinse with distilled water.
8. Dehydrate through graded alcohols, clear with xylene and coverslip using a synthetic resinous mountant.

TIMINGS

a) Deparaffinise in xylene	5 min
b) Deparaffinise in xylene	2 min
c) Clear in alcohol 100 %	2 min
d) Clear in alcohol 100 %	2 min
e) Hydrate in methylated Spirit	1½ min
f) Hydrate in distilled water	4 min
g) Stain in Mayer's haematoxylin	30 min
h) Wash in running tap water	2 min
i) Place in acid alcohol	3 quick dips
j) Wash in running tap water	4 min
k) Scott's tap water substitute	1 min
l) Wash in running tap water	2 min
m) Stain in yellowish eosin	5 min
n) Wash in running tap water	1 min
o) Dehydrate in methylated spirit	30 sec
p) Clear in alcohol 100 %	2 min
q) Clear in alcohol 100 %	30 sec
r) Clear in xylene	5 min

RESULTS

Blue-black: nuclei.

Varying shades of pink: cytoplasm.

Deep pink: fibrin.

Deep pinky red: muscle fibres.

Orange / red: red blood cells and eosinophil granules.

ASTRA BLUE (BLAIES & WILKINS, 1981)

PROCEDURE & TIMINGS

a) Deparaffinise in xylene	8 min
b) Deparaffinise in xylene	5 min
c) Clear in alcohol 100 %	4 min
d) Clear in alcohol 100 %	4 min
e) Hydrate in alcohol 96 %	4 min
f) Hydrate in alcohol 96 %	4 min
g) Hydrate in alcohol 80 %	4 min
h) Hydrate in distilled water	5 min
i) Hydrate in distilled water	5 min
j) Stain in 1 % Astra blue	30 min
k) Place in 0.7 M HCl	5 min
l) Wash in running tap water	2 min
m) Stain in eosin-Astra	2 quick dips
n) Wash in alcohol 95 %	1 min
o) Clear in alcohol 100 %	2 min
p) Clear in alcohol 100 %	30 sec
q) Clear in xylene	5 min

RESULTS

Bright blue: mammalian mast cells.

AZUR A (HUGHESDON, 1949)

PROCEDURE & TIMINGS

a) Deparaffinise in xylene	3 min
b) Deparaffinise in xylene	3 min
c) Clear in alcohol 100 %	2 min
d) Clear in alcohol 100 %	2 min
e) Hydrate in alcohol 96 %	2 min
f) Hydrate in alcohol 90 %	2 min

g) Hydrate in alcohol 80 %	2 min
h) Hydrate in alcohol 80 %	2 min
i) Hydrate in distilled water	2 min
j) Hydrate in distilled water	2 min
k) Oxidise in 1% potassium permanganate	5 min
l) Rinse in distilled water	5 min
m) Decolourise with 2% oxalic acid	1 min
n) Wash in running tap water	3 min
o) Rinse in distilled water	1 min
p) Stain in azur A	5 min
q) Differentiate in 1% zinc sulphate until the section is macroscopically pale blue.	
r) Rinse in distilled water	5 min
s) Blot, and allow to completely dry.	
t) Clear in xylene	3 min
u) Clear in xylene	5 min

RESULTS

Purple: mammalian mast cell granules, sulphated and carboxylated mucins.

Blue: nuclei.

Pale-blue: background.

HAEMATOXYLIN-ERYTHROSIN-SAFRAN (HES)**PROCEDURE & TIMINGS**

a) Deparaffinise in xylene	8 min
b) Deparaffinise in xylene	5 min
c) Clear in alcohol 100 %	4 min
d) Clear in alcohol 100 %	4 min
e) Hydrate in alcohol 96 %	4 min
f) Hydrate in alcohol 96 %	4 min
g) Hydrate in alcohol 80 %	4 min
h) Hydrate in distilled water	5 min
i) Hydrate in distilled water	5 min
j) Stain in haematoxylin	2 min
k) Stain in haematoxylin	3 min
l) Wash in running tap water	14 min
m) Rinse in 0.2 % ammonia	30 sec
n) Stain in erythrosine B	4 min

o) Place in PBS	3 min
p) Clear in alcohol 100 %	3 quick dips
q) Stain in safran	30 sec
r) Stain in safran	3 min
s) Clear in alcohol 100 %	2 min
t) Clear in alcohol 100 %	30 sec
u) Clear in xylene	5 min

RESULTS

Blue: nuclei.

Red shades: cytoplasm.

Pink: muscle and elastic fibres.

Orange-yellow: collagen.

MAY-GRÜNWARD-GIEMSA (MAY & MAY, 1902; GIEMSA, 1902)

PROCEDURE

1. Fix the air-dried slides in absolute methyl alcohol for 10-20 min.
2. Rinse in Sorensen's phosphate buffer solution, pH 6.8.
3. Stain in freshly prepared May-Grünwald for 8 min.
4. Drain off the excess stain and stain in freshly prepared Giemsa for 10 min.
5. Differentiate in Sorensen's phosphate buffer pH 6.8.
6. Allow smears to dry, and if necessary they can be gently blotted before mounting.

TIMINGS

a) Fix in methanol 100 %	2 min
b) Rinse in Sorensen's buffer	3 min
c) Stain in May-Grünwald	8 min
d) Tap off excess stain	
e) Stain in Giemsa	10 min
f) Place in Sorensen's buffer	5 min

RESULTS

Purple: mammalian mast cell granules, sulphated and carboxylated mucins.

Blue: nuclei.

Pale-blue: background.

PERIODIC-ACID-SCHIFF-HAEMATOXYLIN

PROCEDURE & TIMINGS

a) Deparaffinise in xylene	3 min
b) Deparaffinise in xylene	3 min
c) Clear in alcohol 100 %	2 min
d) Clear in alcohol 100 %	2 min
e) Hydrate in alcohol 96 %	2 min
f) Hydrate in alcohol 90 %	2 min
g) Hydrate in alcohol 80 %	2 min
h) Hydrate in alcohol 80 %	2 min
i) Hydrate in distilled water	2 min
j) Hydrate in distilled water	2 min
k) Oxidise in 0.5 % periodic acid	5 min
l) Rinse in distilled water	2 min
m) Place in Schiff reagent	15 min
n) Wash in lukewarm tap water	5 min
o) Stain in Mayer's hematoxylin	1 min
p) Wash in running tap water	5 min
q) Clear in xylene	3 min
r) Clear in xylene	5 min

RESULTS

Red / purple: glycogen, mucin and some basement membranes.

Blue: background.

PERIODIC-ACID-SCHIFF-ALCIAN-BLUE (MOWRY & WINKLER, 1956)

PROCEDURE & TIMINGS

a) Deparaffinise in xylene	3 min
b) Deparaffinise in xylene	3 min
c) Clear in alcohol 100 %	2 min
d) Clear in alcohol 100 %	2 min
e) Hydrate in alcohol 96 %	2 min
f) Hydrate in alcohol 90 %	2 min
g) Hydrate in alcohol 80 %	2 min
h) Hydrate in alcohol 80 %	2 min
i) Hydrate in distilled water	2 min

j) Hydrate in distilled water	2 min
k) Stain in Alcian blue	15 min
l) Wash in running tap water	2 min
m) Rinse in distilled water	3 min
n) Place in periodic acid	5 min
o) Wash in distilled water	10 min
p) Stain in Schiff's reagent	10 min
q) Wash in running tap water	5 min
r) Stain in Mayer's haematoxylin	1 min
s) Wash in running tap water	2 min
t) Differentiate with acid alcohol	3 quick dips
u) Clear in alcohol 100 %	2 min
v) Clear in alcohol 100 %	30 sec
w) Clear in xylene	5 min

RESULTS

Blue: acidic mucins.

Magenta: neutral mucins.

Blue / purple: mixtures of above.

Deep blue: nuclei.

THIONIN (COOK, 1961)

PROCEDURE & TIMINGS

a) Deparaffinise in xylene	3 min
b) Deparaffinise in xylene	3 min
c) Clear in alcohol 100 %	2 min
d) Clear in alcohol 100 %	2 min
e) Hydrate in alcohol 96 %	2 min
f) Hydrate in alcohol 90 %	2 min
g) Hydrate in alcohol 80 %	2 min
h) Hydrate in alcohol 80 %	2 min
i) Hydrate in distilled water	2 min
j) Hydrate in distilled water	2 min
k) Stain in thionin	20 min
l) Distilled water	3-5 min
m) Distilled water	3-5 min
n) Dehydrate in 70 % ethanol	5 min

- | | |
|-------------------------------|-------|
| o) Dehydrate in 70 % ethanol | 3 min |
| p) Dehydrate in 95 % ethanol | 3 min |
| q) Dehydrate in 100 % ethanol | 3 min |
| r) Clear in xylene | 3 min |
| s) Clear in xylene | 5 min |

RESULTS

Deep blue with distinct chromatin: nuclei.

Light blue: cytoplasm.

Green: erythrocytes.

Red purple to violet: mucus.

Red purple to violet: cartilage matrix.

Deep violet: mammalian mast cell granules.

TOLUIDINE BLUE (SCHUBERT & HAMMERMAN, 1956)

PROCEDURE & TIMINGS

- | | |
|-------------------------------|-------|
| a) Deparaffinise in xylene | 3 min |
| b) Deparaffinise in xylene | 3 min |
| c) Clear in alcohol 100 % | 2 min |
| d) Clear in alcohol 100 % | 2 min |
| e) Hydrate in alcohol 96 % | 2 min |
| f) Hydrate in alcohol 90 % | 2 min |
| g) Hydrate in alcohol 80 % | 2 min |
| h) Hydrate in alcohol 80 % | 2 min |
| i) Hydrate in distilled water | 2 min |
| j) Hydrate in distilled water | 2 min |
| k) Stain in toluidine blue | 3 min |
| l) Wash in running tap water | 3 min |
| m) Rinse in distilled water | 5 min |
| n) Clear in xylene | 3 min |
| o) Clear in xylene | 5 min |

RESULTS

Violet / red purple: mammalian mast cells.

Blue: background.

URANYL ACETATE & REYNOLD'S LEAD CITRATE

PROCEDURE

1. Cut two pieces of 2 × 2" of ParafilmM™ and place a small Petri dish over each piece. Under the second dish, place several pellets of sodium hydroxide around the edge as to allow the absorption of CO₂ in the chamber, giving a CO₂ free area for staining.
2. Centrifuge at 3000 × g for 10 min equal volumes of uranyl acetate and lead citrate.
3. Place 1 drop of uranyl acetate for each grid onto the first parafilm piece. Float section-side-down the grid on the drop of stain for 4 min. Cover with aluminium foil a large Petri dish lid to serve a cover and avoid photosensitive contamination of the uranyl acetate solution.
4. Carefully remove the grid and vigorously rinse it for 15 sec each in 3 successive changes of 50 % ethanol, in 1 change of 25 % ethanol and in 3 successive changes of distilled water.
5. Blot the grid and forceps on a paper towel (or wick out the water between the tongs of the forceps with filter paper) and place the grid in an inverted position, on 1 drop of lead citrate under the second Petri dish and cover to avoid CO₂ contamination. Stain with citrate for 7 min.
6. Carefully remove the grid and vigorously rinse it for 15 sec each in 4 successive changed of distilled water.
7. Blot the grid and the forceps, and place it in a small appropriated labelled Petri dish.
8. Allow the grid to dry at room temperature for at least 20 min before viewing on the electron microscope.

TIMINGS

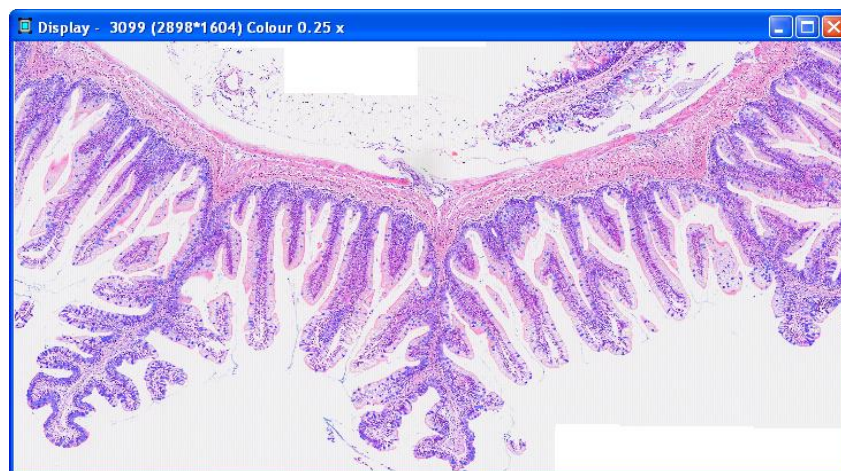
a) Uranyl Acetate	4 min
b) Ethanol 50 %	15 sec
c) Ethanol 50 %	15 sec
d) Ethanol 50 %	15 sec
e) Ethanol 25 %	15 sec
f) Distilled water	15 sec
g) Distilled water	15 sec
h) Distilled water	15 sec
i) Reynold's Lead Citrate	7 min
j) Distilled water	15 sec
k) Distilled water	15 sec
l) Distilled water	15 sec

REFERENCES

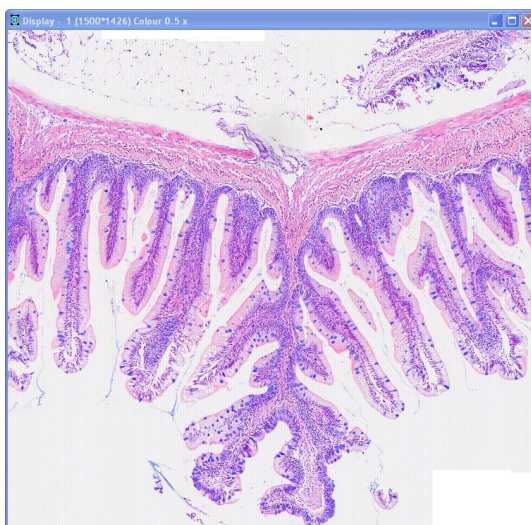
- BANCROFT, J.D. and STEVENS, A. 1982. Theory and Practice of Histological Techniques. 2nd Edition, Churchill-Livingstone, New York, USA, pp. 436.
- BLAIES, D.M. and WILLIAMS, J.F., 1981. A simplified method for staining mast cells with astra blue. *Biotechnic & Histochemistry*, **56**(2), pp. 91-94.
- COOK, H.C., 1961. A modified thionin technique for mast cells in tissue sections. *The Journal of Medical Laboratory Technology*, **18**, pp. 188-189.
- GIEMSA, G., 1902. Färbemethoden für malariaparasiten. *Zentralbl Bakteriol*, **31**:429-430.
- HAYAT, M., 1986. *Basic techniques for transmission electron microscopy*. Academic Press, California, USA, pp. 411.
- HUGHESDON, P., 1949. Two uses of uranyl nitrate. *Journal of the Royal Microscopical Society*, **69**(1), pp. 1-8.
- LEV, R. and SPICER, S.S. 1964. Specific staining of sulphated groups with alcian blue at low pH. *Journal of Histochemistry and Cytochemistry*, **12**: pp. 309.
- MAY, R. and MAY, G.L., 1902. Grünwald stain. *Zentralbl Für Innere Med*, **23**, pp. 265.
- MOWRY, R. and WINKLER, C.H., 1956. The coloration of acidic carbohydrates of bacteria and fungi in tissue sections with special reference to capsules of *Cryptococcus neoformans*, pneumococci, and staphylococci. *American Journal of Pathology*, **32**, pp. 628-629.
- SCHUBERT, M. and HAMMERMAN, D., 1956. Metachromasia; chemical theory and histochemical use. *Journal of Histochemistry & Cytochemistry*, **4**(2), pp. 159-189.
- SHEEHAN, D.C. and HRAPCHAK, B.B. 1980. Theory and Practice of Histotechnology. 2nd Edition, Mosby Company, St. Louis, USA, pp. 481.
- STEEDMAN, H.F. 1950. Alcian blue 8GS; a new stain for mucin. *Quarterly Journal of Microscopic Science*, **91**, pp. 477-479.

REPRESENTATIVE IMAGE SEQUENCE GENERATED BY THE GUT HEALTH IMAGE PROCESSING AND ANALYSIS SEMI-AUTOMATED SYSTEM

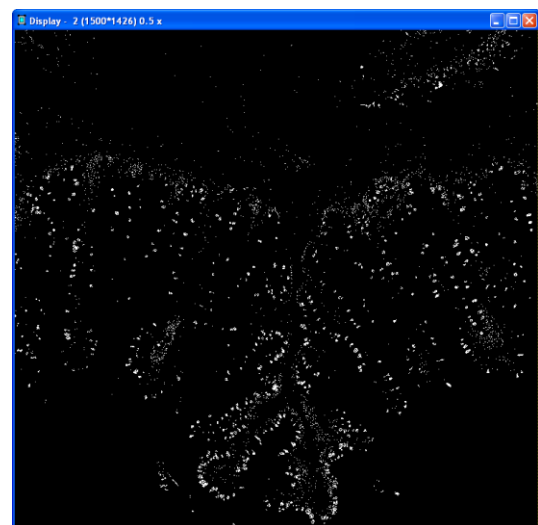
A sequence of images representative of a single run of the gut health imaging processing and analysis system is presented below in order to provide a better understanding of the image processing, segmentation and analysis system referenced throughout this thesis. It comprises an overview of the images (□) generated by the described pipeline (for a more complete description, please see Technical Notes A and B).



□ Image 1



□ Image 1A



□ Image 2

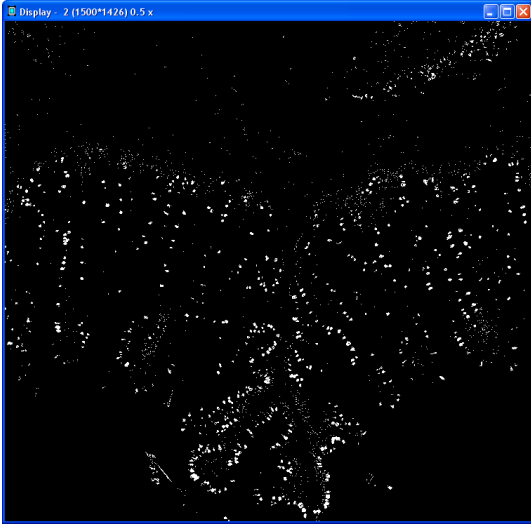


Image 2A

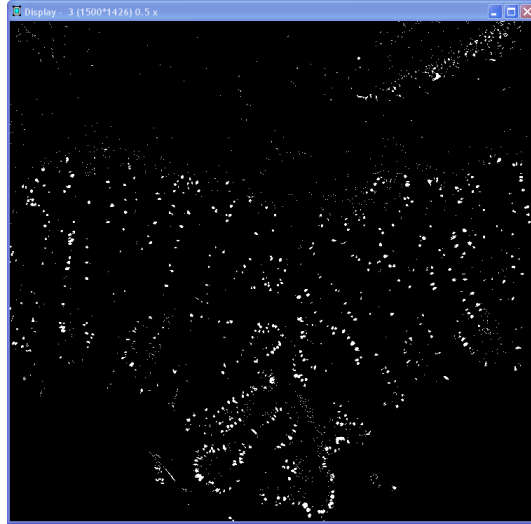


Image 2B

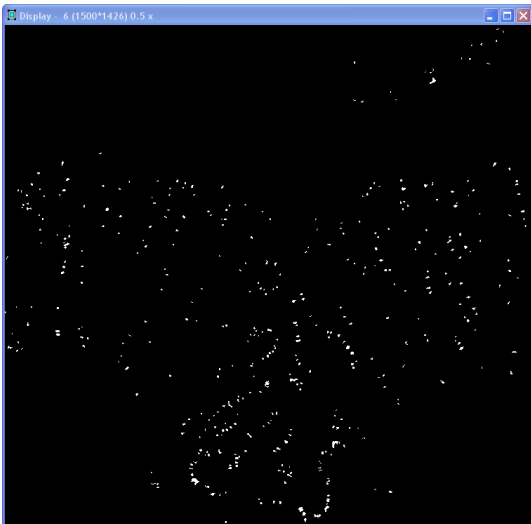


Image 2C



Image 2D

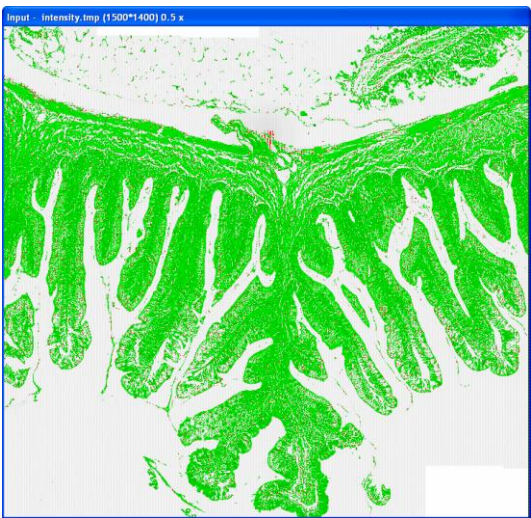


Image 3



Image 3A

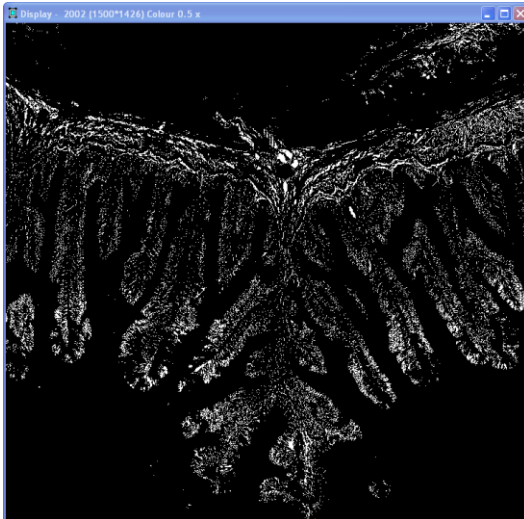


Image 3B

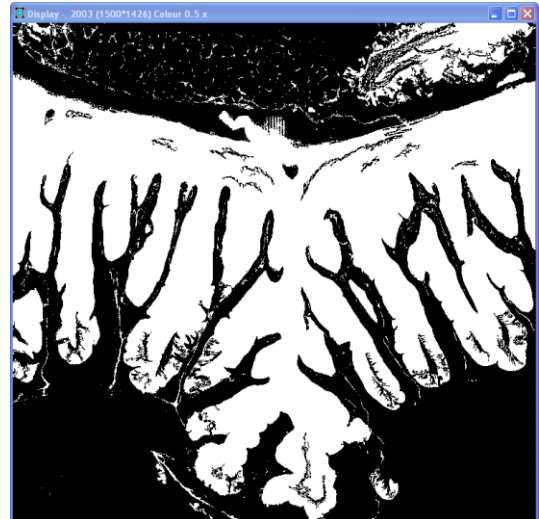


Image 3C

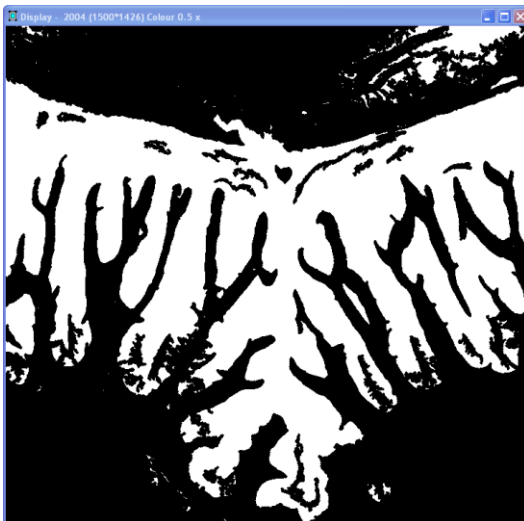


Image 3D



Image 3E

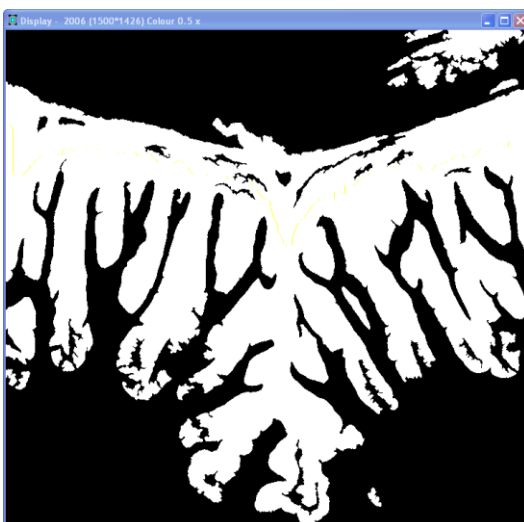


Image 3F

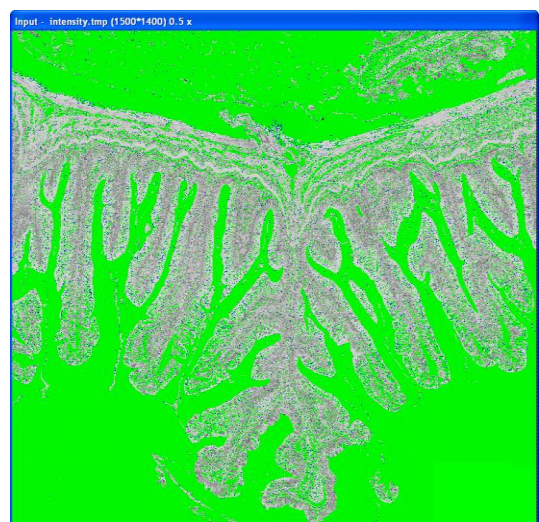


Image 4



Image 4A

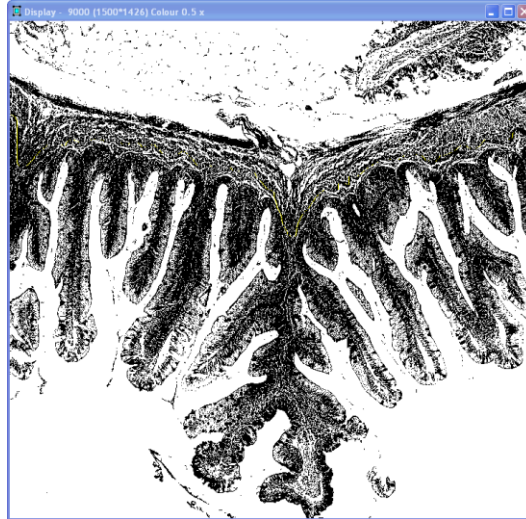


Image 4B

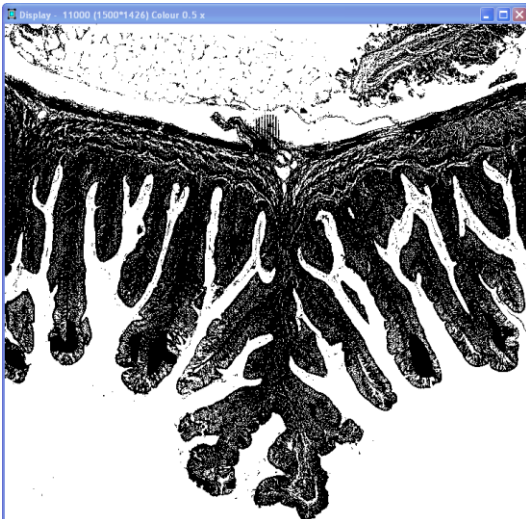


Image 4C

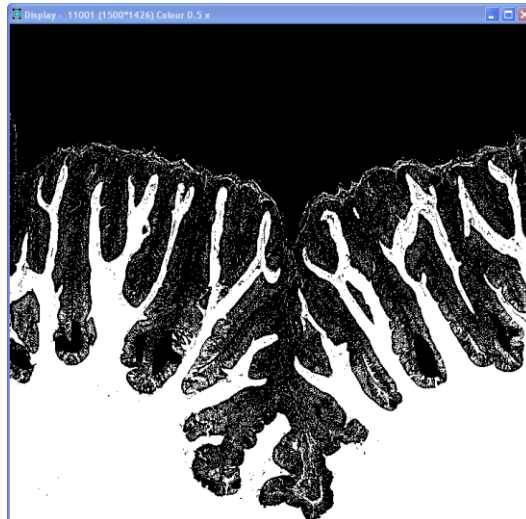


Image 4D

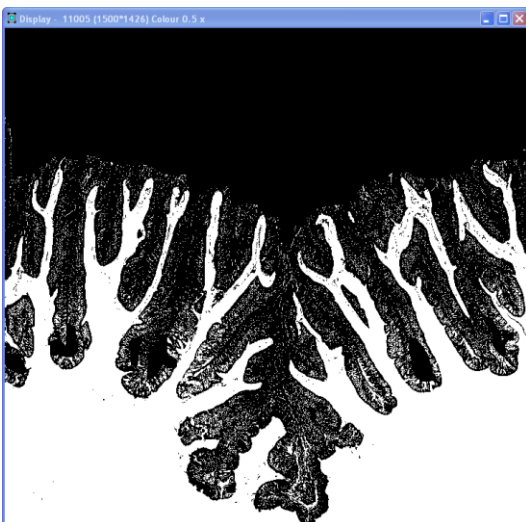


Image 4E

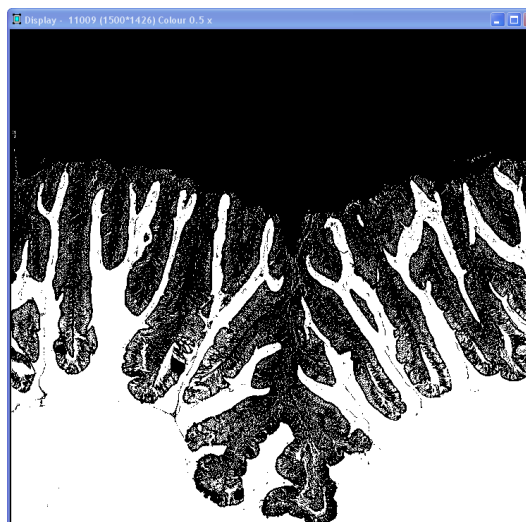


Image 4F

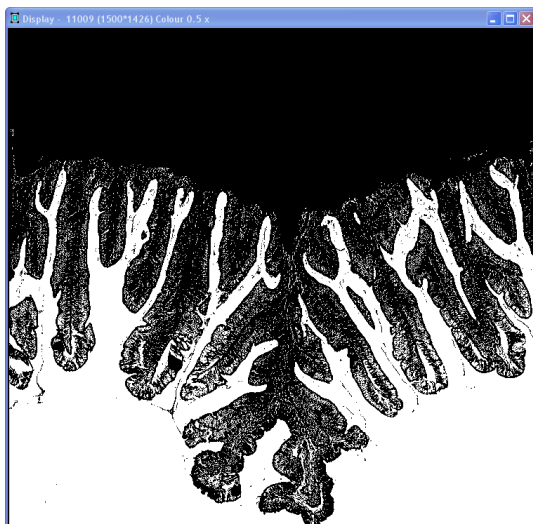


Image 4G

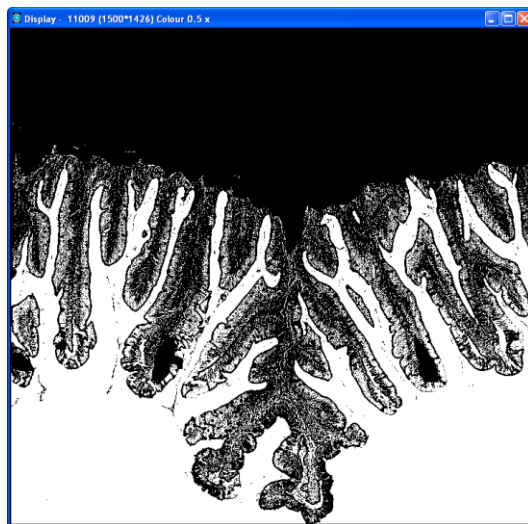


Image 4H

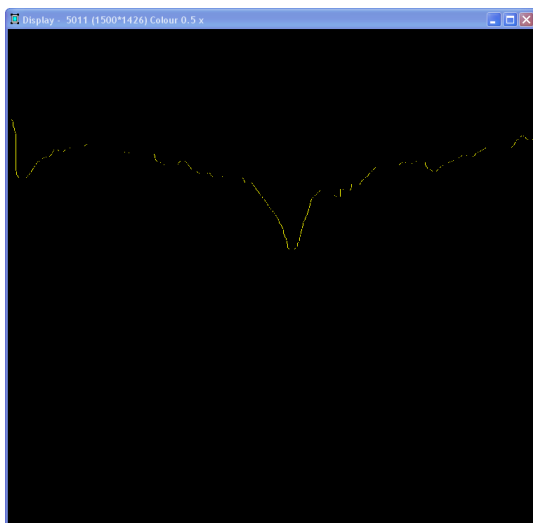


Image 5

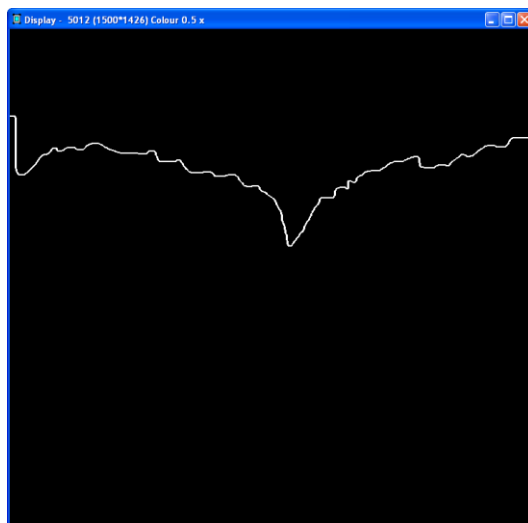


Image 5A

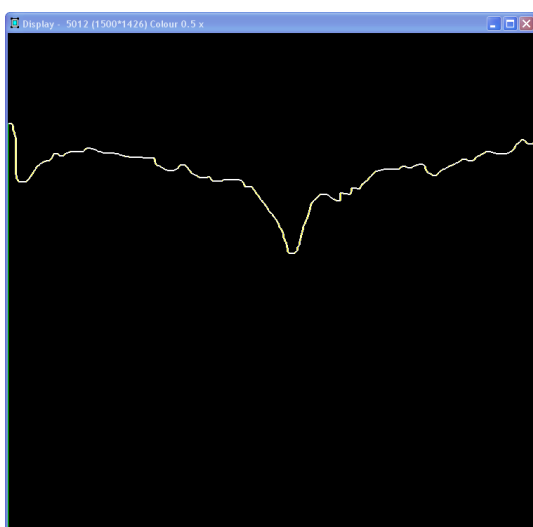


Image 6

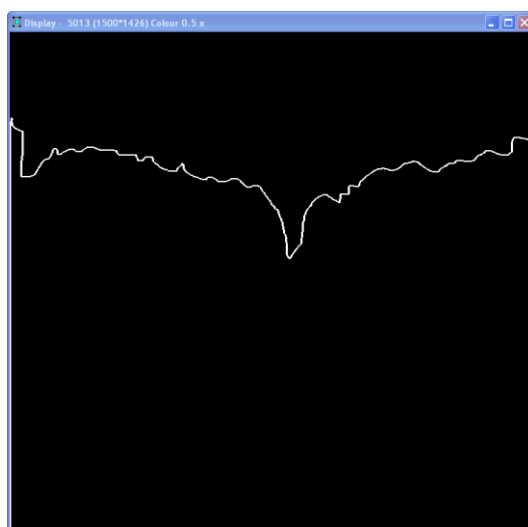


Image 6A

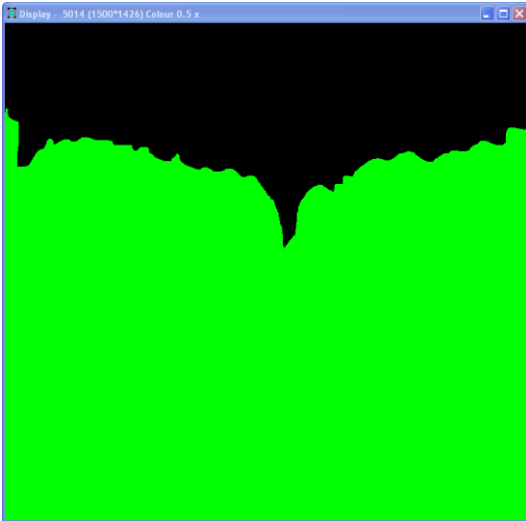


Image 6B



Image 6C



Image 6D

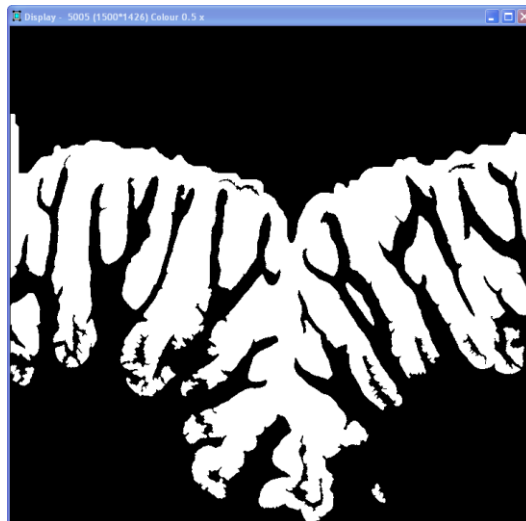


Image 6E

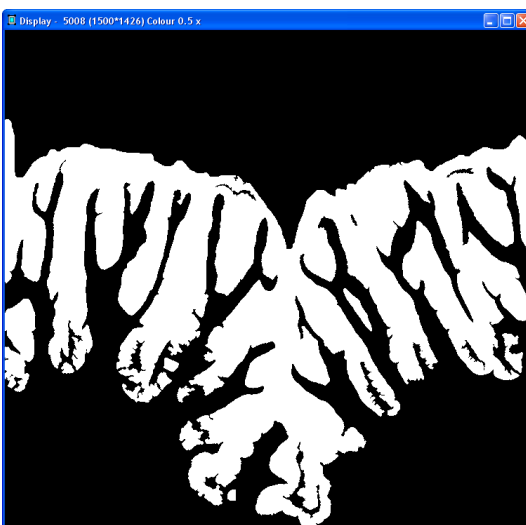


Image 6F

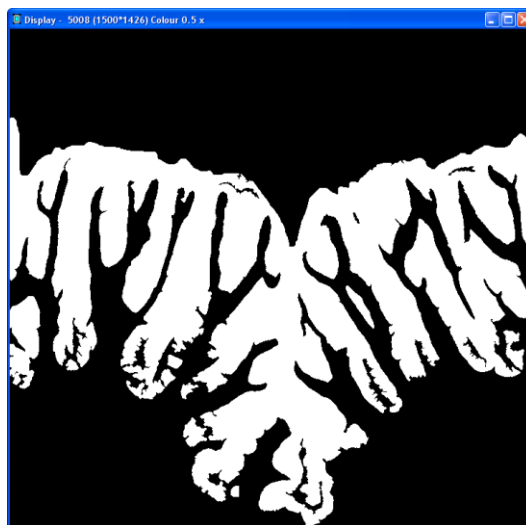


Image 6G

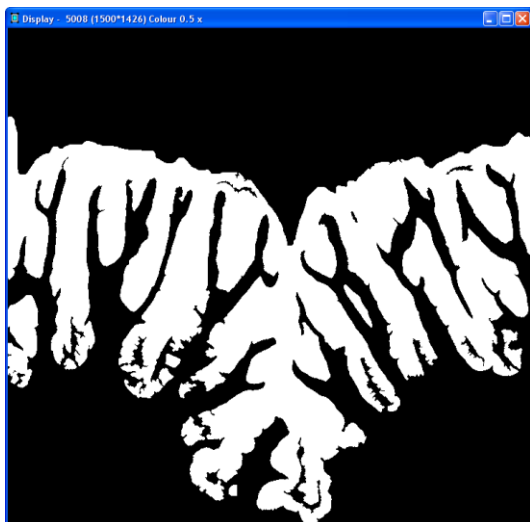


Image 6H_b

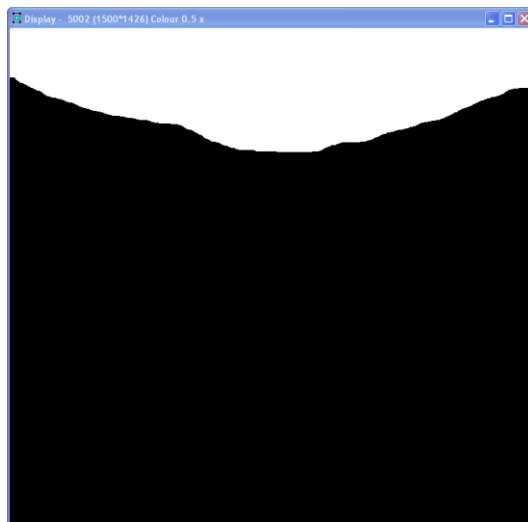


Image 7

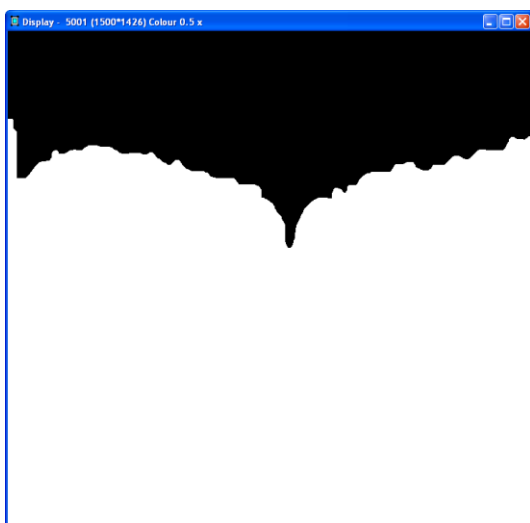


Image 7aa



Image 7aaa



Image 8

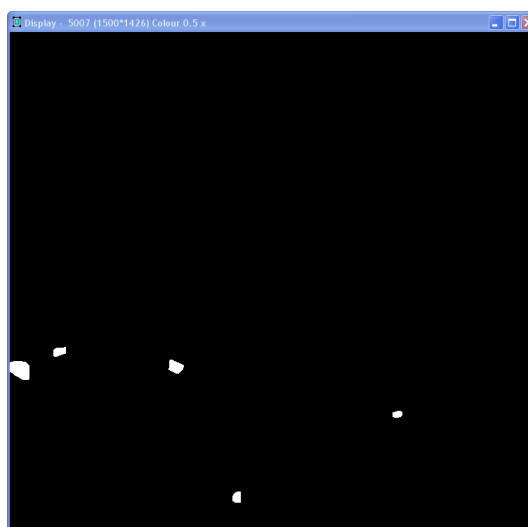


Image 8A

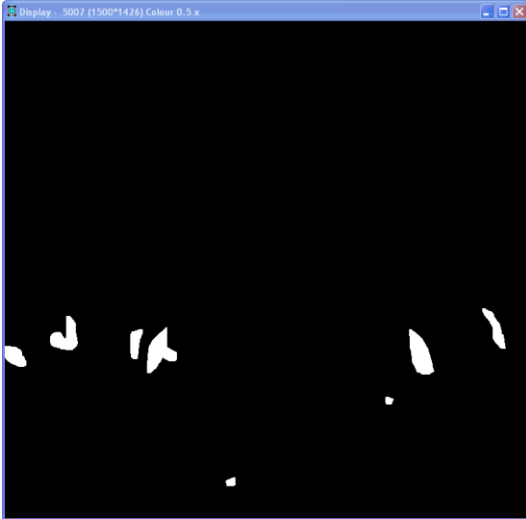


Image 9

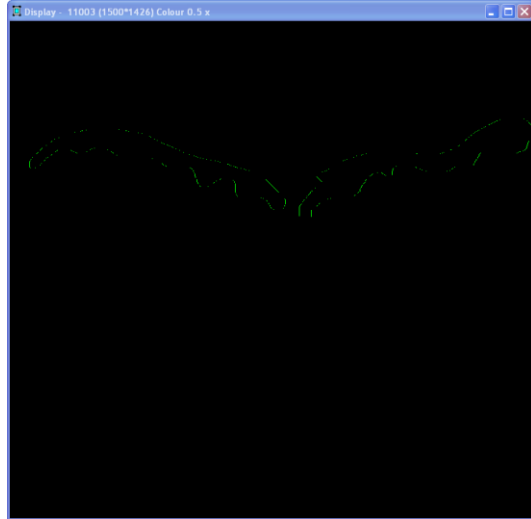


Image 10

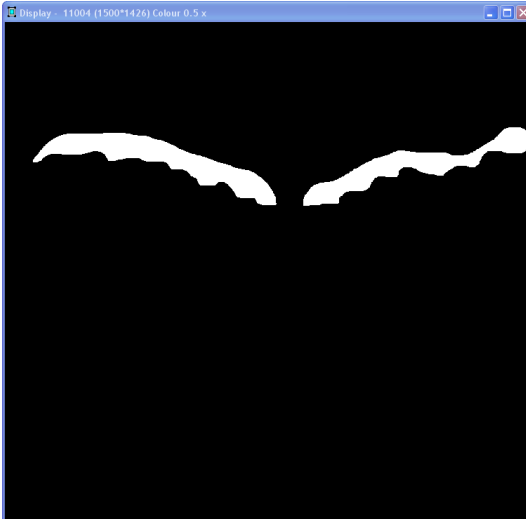


Image 10A

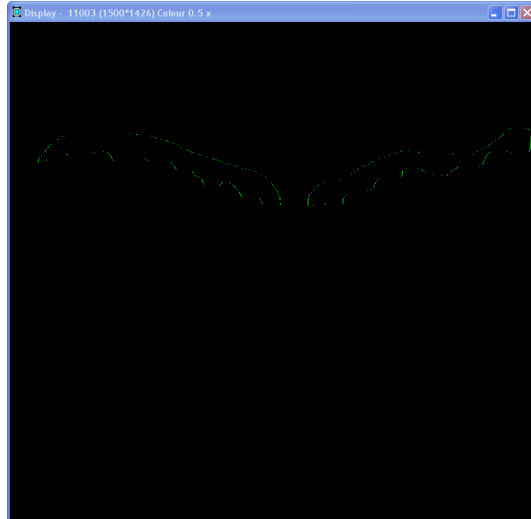


Image 11

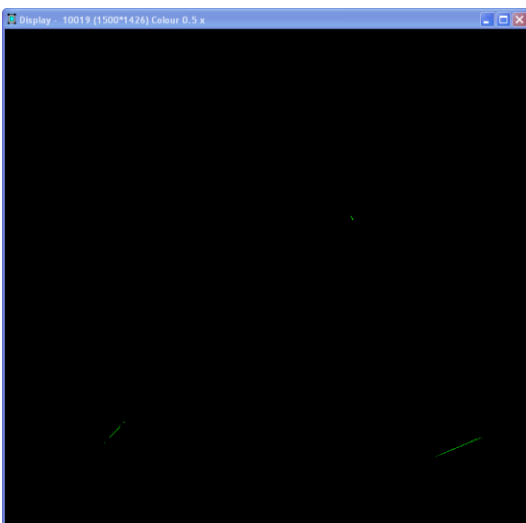


Image 12

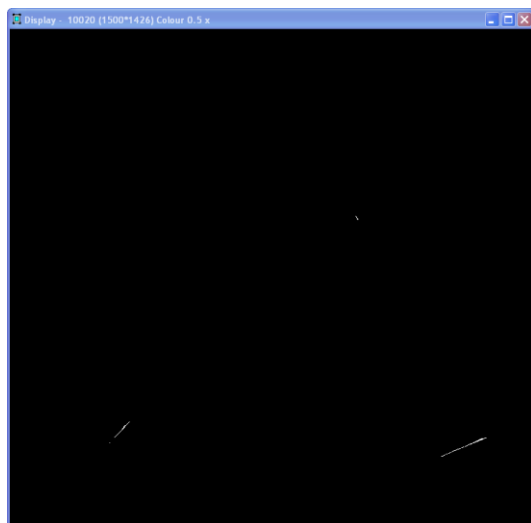


Image 12A



Image 12B

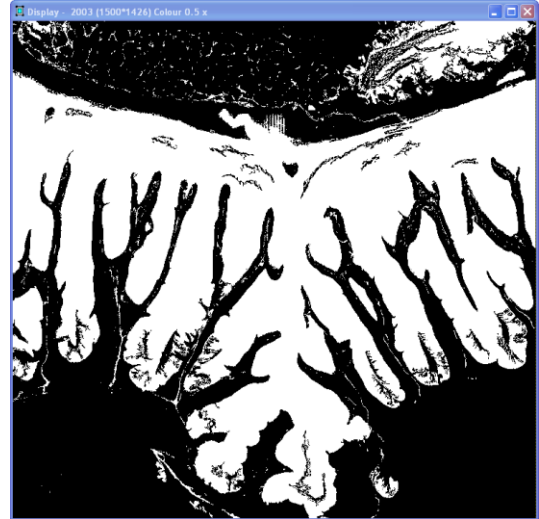


Image 13

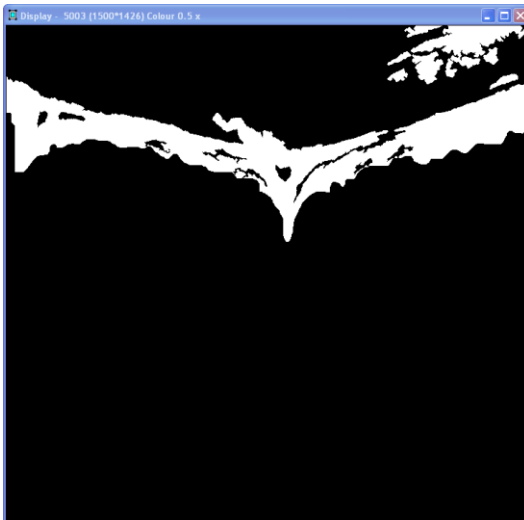


Image 14

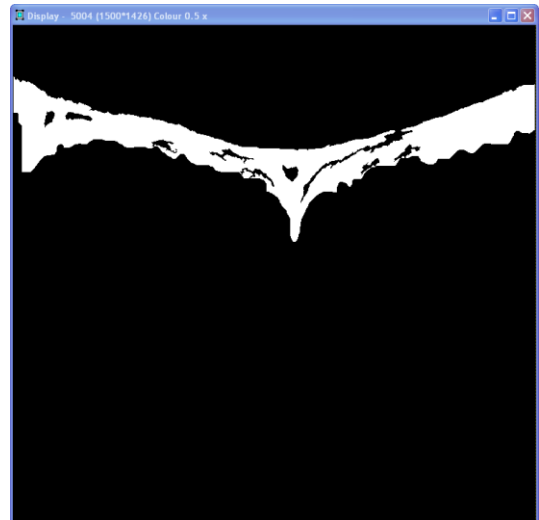


Image 14A



Image 15

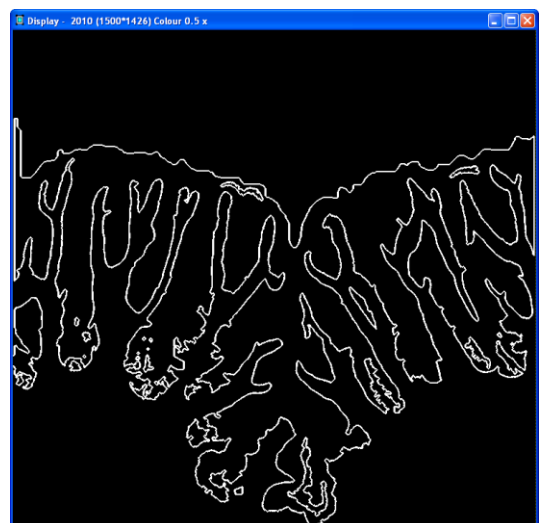


Image 15A



Image 16

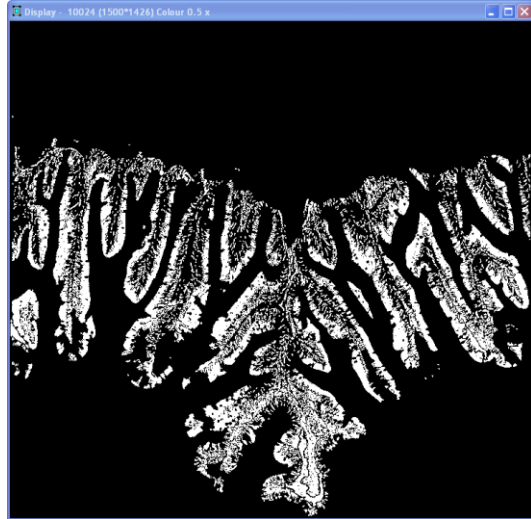


Image 16A

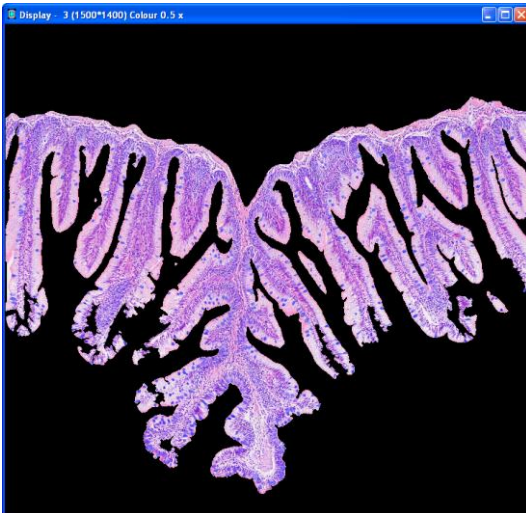


Image A

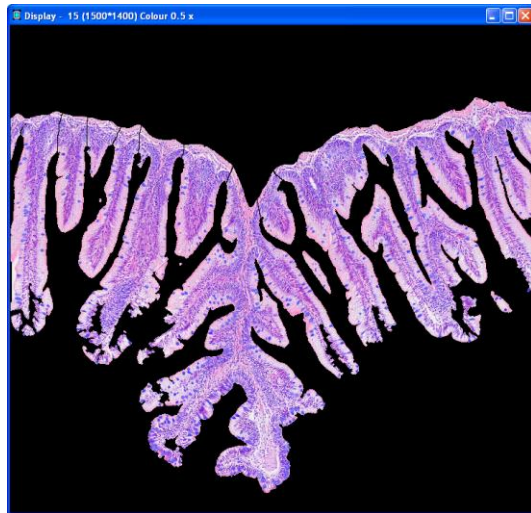


Image A1



Image A2

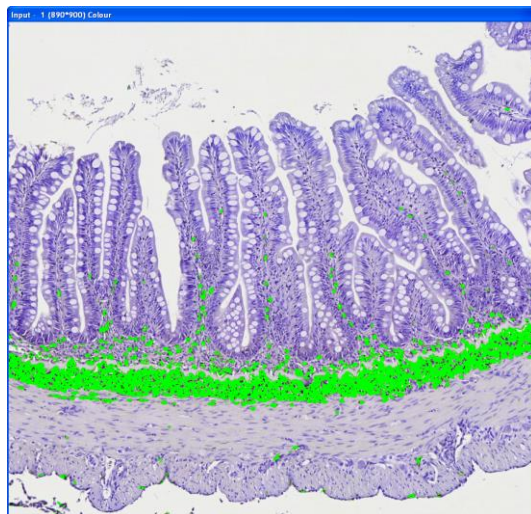


Image I-1

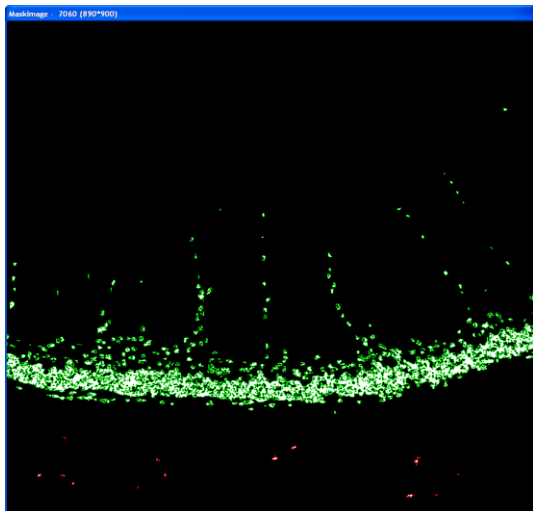


Image I-2

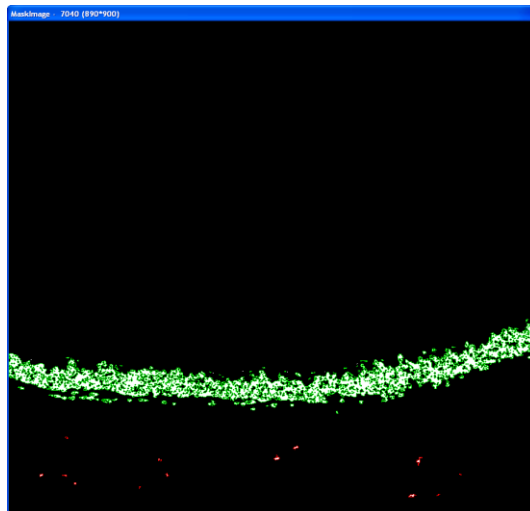


Image II

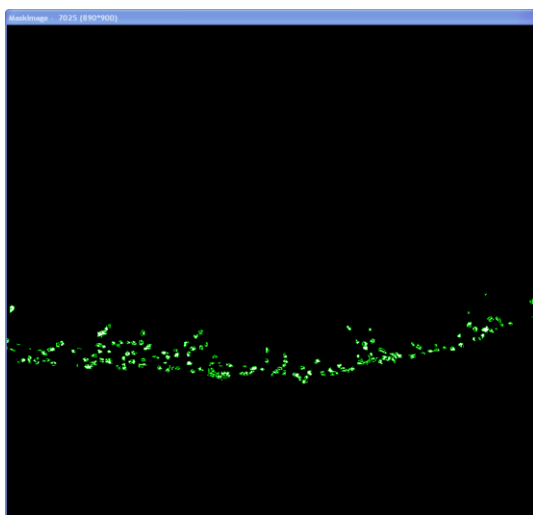


Image III

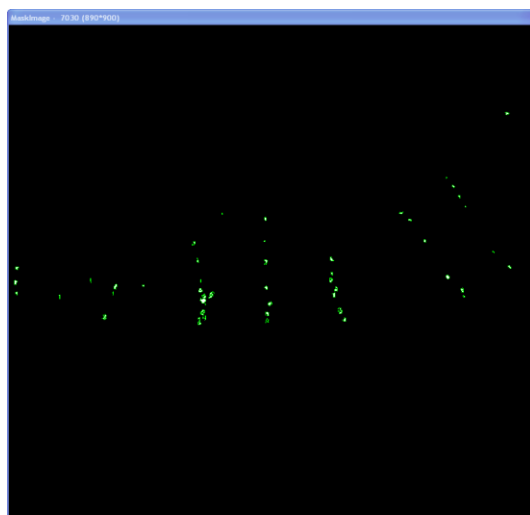


Image IV